Reconstruction of volcanic and hydrothermal settings and mineralization of the ABM deposit, Finlayson Lake district, Yukon, Canada

by

© Nikola Denisová

A thesis submitted to the School of Graduate Studies in partial fulfillment of the requirements for the degree of

Doctor of Philosophy

Department of Earth Sciences

Memorial University of Newfoundland

April 2023

St. John's, Newfoundland and Labrador

Abstract

The ABM deposit is a bimodal-felsic, replacement-style volcanogenic massive sulfide (VMS) deposit located in the Finlayson Lake district, Yukon, Canada. In this dissertation, detailed core mapping, petrography, lithogeochemistry, and microanalytical methods are used to reconstruct the tectonostratigraphic framework for the deposit, the hydrothermal footprint, mineral chemical composition of the mineralization, and to integrate these to understand the genesis of the ABM deposit. The deposit is hosted by Late Devonian continental back-arc-related volcano-sedimentary rocks of the Kudz Ze Kayah formation. The distribution and character of coherent felsic and mafic rocks suggest that the rocks were deposited in a back-arc basin proximal to a volcanic center, and the chemostratigraphy shows three sequences with distinct geochemical signatures. Reconstruction of the basin architecture has identified two sets of synvolcanic faults, and an argillite lens at the contact between the sequence hosting the mineralization and the hanging wall sequence that documents a period of volcanic inactivity during which the hydrothermal system was active. Hydrothermal alteration assemblages extend for 100s-1000s of meters laterally and into the footwall and hanging wall. The main alteration processes are feldspar destruction and formation of white mica and chlorite. The earliest and most extensive alteration assemblage is moderate white mica ± chlorite that formed at ~215±30 °C. It is overprinted by a pervasive white mica assemblage that formed at ~250±15 °C. A pervasive chlorite assemblage formed at ~320±10 °C (temperatures were determined by illite and chlorite thermometry) and overprints the white mica-rich assemblages. The massive sulfide mineralization occurs as a series of stacked and stratabound lenses subparallel to the volcanic stratigraphy, overprinting the pervasive alteration assemblages. Three major mineralization assemblages occur: (1) a pyrite-sphalerite assemblage enriched in Zn-Pb-As-Sb-Ag-Au that formed at temperatures ~200-270 °C; (2) a pyrite-chalcopyrite-magnetite-pyrrhotite assemblage enriched in Cu-Bi-Se-Co that formed at temperatures ~300-350 °C and occurs at the center of the mineralization lenses; and (3) a minor chalcopyrite-pyrrhotite-pyrite stringer assemblage that occurs at the margins of the lenses and formed at temperatures >300 °C. The mineralization formed by mixing of seawater infiltrated in the subsurface with hot reduced acidic hydrothermal fluids and consequent zone refining.

General summary

The ABM deposit is a volcanogenic massive sulfide (VMS) deposit that formed ~360 Ma in an extensional back-arc basin similar to the modern Japan Sea/Okinawa Trough through replacement processes in the subsurface. The deposit is located in the Finlayson Lake district, Yukon, Canada. This dissertation presents a detailed model of basin stratigraphy and the large-scale processes affecting that basin deduced from fieldwork, microscopy, and rock geochemistry to provide insight into how the deposit formed. Volcanogenic massive sulfide deposits form at or below the seafloor from hot seawater heated by volcanic activity and are associated with undersea volcanic eruptive sequences and faults, which both influence the localization of the mineralization. Volcanic rocks hosting the ABM deposit have distinct features that reflect the temperatures and settings in which they formed. The ancient environment of the ABM deposit comprised thick sequences of volcanic- and volcano-sedimentary rocks that formed proximal to an active volcanic centre that was associated with two sets of faults that controlled the emplacement of volcanic rocks and the fluids that generated the massive sulfide mineralization. These fluids first reacted with the host rocks and generated a footprint documenting this interaction. This work demonstrates that the footprint at the ABM deposit has characteristic mineral and bulk rock chemical signatures that can be used to find other deposits in the larger area of the Finlayson Lake district or in similar back-arc environments worldwide. The massive sulfide mineralization contains zinc, lead, copper, silver, and gold, and is zoned according to the temperature of formation. Mineralization with abundant zinc and lead formed at temperatures between ~200-270 °C and occurs on the outer edges of the mineralized lenses, whereas mineralization with abundant copper formed at temperatures ~300-350 °C and occurs in the centre of the mineralized lenses. The deposit formation processes were similar to modern seafloor massive sulfide deposits, and the ABM deposit had a distinct source of metals, and hydrothermal fluids, which comprises dominantly of leaching of igneous rocks. Integration of field and laboratory studies in this work provided distinct insights into ore formation and exploration criteria that can be used to find new resources.

Acknowledgments

I want to thank my supervisor, Steve Piercey, for choosing me to work on this project. I am very grateful for his support and guidance throughout it, and for giving me space to pursue research ideas and to figure out the science in my own way. I really appreciate the time that Steve spent editing my manuscripts and his thoroughness, his thoughtful comments made me a better writer and researcher. I also want to commend Steve on how he picks the members of his research group, because these graduate students and post-docs, past and present, are amazing people, and their company has always been stimulating on both a scientific and a personal level. I also want to thank my PhD. committee members, Dr. Graham Layne and Dr. Luke Beranek, for their guidance throughout the project.

I also want to thank BMC Minerals (No. 1) Ltd. and their personnel, namely Dr. Neil Martin, Robin Black, and Robert Burke. Without the company's commitment to research and science, and their financial and operational support, this project would not be possible. I was able to spend two summers at the Kudz Ze Kayah exploration camp, and thanks to the support of the company geologists and the Equity Exploration Consultants staff, I was able to gather all the samples and complete all the drill logs I needed very efficiently.

I am also very grateful to the staff at the Hibernia Electron Beam Facility and CREAIT labs at Memorial University for all their help when gathering analytical data, sometimes under complicated conditions due to health and safety restrictions. Many thanks go to Wanda Aylward for her help with the SEM and EPMA at the Hibernia Electron Beam facility, to Markus Wälle for his help with the LA-ICP-MS and to Dylan Goudie for his help with the SEM-EDX and sample preparation, both at the Micro Analysis Facility at MUN, and to Matt Crocker, who helped me with sample preparation.

I am extremely grateful to those of my friends who read through and commented on my drafts: Dr. Andrew Martin, Dr. Anne-Sophie Tabaud, and Rosie Cobbett. Thank you for all your comments and thank you especially for all the great times! I would not be able to do this without the help of my friends who have been such great company throughout. I am grateful to my friends Carly

Mueller, Caroline Gini, Daniela Mendoza Marín, Dorota Pietruszka, Kei Quinn, Laura Mateo, Maciej Pawlukiewicz, Marko Szmihelsky, Phil X. Breville, Regan Jacobson, Robert King, and everyone in the Piercey Research Group and at MUN.

I want to single out one person (in a good way), Dr. Matthew J. Manor. Matt has been a great colleague and collaborator and has become a really good friend. Having someone there that is dealing with similar problems, and getting through them, figuring the science and the geology out has been a great example and motivation. Thank you for listening to my rants, all your edits and comments, and for your and Lauren's company, especially during the pandemic days. I am glad I found another coffee and chicken nugget appreciator.

I am very grateful I was able to come to Canada to work on this project, and a big reason I was able to do it is my family. They have always trusted me and supported all my outlandish ideas, and even though we are an ocean apart most of the year, they have always been there for me. My biggest thanks go out to my mom and dad, Lucie and Lubomír, to my brother and sister-in-law, Tadeáš and Tereza, to my sweet, not so little anymore nephew, Theo, and to my grandmother, Marcela. I care for you all deeply.

Financial support for this project was provided by grants from the NSERC Discovery Grant, the NSERC Collaborative Research Development Grant – Project (CRDPJ) program, and by BMC Minerals Ltd. Additional funding was provided by a Student Research Grant from the Society of Economic Geologist Canada Foundation awarded to Nikola Denisová.

First one to find the ninja turtle wins.

Table of contents

List of figures

List of tables

List of appendices

Co-authorship statement

This study was conceptualized and designed by Dr. Stephen Piercey, who acted as the supervisor of this thesis project. Nikola Denisová carried out the field work and the research presented in this dissertation. Field work, consisting of core logging and sampling, was performed by the author in 2018-2019 and was supported by BMC Minerals Ltd. The company also provided access to their assay and lithogeochemistry, core logging, photography, and other available databases.

The manuscript presented in Chapter 2 titled "Lithostratigraphy, lithogeochemistry and tectono-magmatic framework of the ABM replacement-style volcanogenic massive sulfide (VMS) deposit, Finlayson Lake District, Yukon, Canada" has been published in the journal Economic Geology (2022), volume 117, pages 1299-1326. The paper is co-authored by Dr. Stephen J. Piercey, who provided editorial guidance. Whole rock lithogeochemistry was completed at ALS Laboratories (Sudbury, North Vancouver) and Geoscience Laboratories (Ontario Geological Survey, Sudbury). Pre-submission, the manuscript benefited from comments by Dr. Matthew Manor, Rosie Cobbett, and Carly Mueller (MUN). Formal peer review was completed by Dr. Michelle DeWolfe (Mount Royal University) and Dr. Steve Hollis (University of Edinburgh), the editorial handing was by Dr. Jonathan Cloutier (University of Tasmania).

The manuscript presented in Chapter 3 titled "Evolution of the hydrothermal system associated with the ABM replacement-style volcanogenic massive sulfide deposit, Finlayson Lake district, Yukon, Canada" is currently in press in the journal Economic Geology in November 2022. The paper is co-authored by Dr. Stephen J. Piercey, who provided editorial guidance. Whole rock lithogeochemistry was completed at ALS Laboratories (Sudbury, North Vancouver) and Geoscience Laboratories (Ontario Geological Survey, Sudbury). Electron microprobe analysis was completed at Memorial University under the supervision of Dr. Wanda Aylward (CREAIT-MUN), short wave infrared spectroscopy was completed at MUN. Pre-submission, the manuscript benefited from comments by Dr. Matthew Manor, Rosie Cobbett (MUN) and Dr. Neil Martin (BMC Minerals Ltd.). Formal peer review was completed by Dr. Stefanie Brueckner (University of Manitoba) and Dr. Nils Jansson (Technical University of Lulea), the editorial handing was by Dr. Jonathan

Cloutier (University of Tasmania).

The manuscript presented in Chapter 4 is titled "Mineralogy and mineral chemistry of the mineralization at the ABM replacement-style volcanogenic massive sulfide deposit, Finlayson Lake district, Yukon, Canada" and has been submitted to the journal Mineralium Deposita. The paper is co-authored by Dr. Stephen J. Piercey, who provided editorial guidance, and by Dr. Markus Wälle, who provided guidance with the collection of laser ablation ICP-MS data. Electron microprobe analysis was completed at Memorial University under the guidance of Dr. Wanda Aylward (CREAIT-MUN). Imaging using scanning electron microscopy coupled with energy-dispersive X-ray spectroscopy (SEM-EDX) was performed at Memorial University under the guidance of Dylan Goudie (CREAIT-MUN). Pre-submission, the manuscript benefited from comments by Dr. Stefanie Brueckner, Dr. Andrew J. Martin, Dr. Anne-Sophie Tabaud, and Dr. Matthew Manor.

Chapter 1

Introduction

1.1 Introduction

Volcanogenic massive sulfide (VMS) deposits form near or at the sea floor, in spatial, temporal, and genetic association with volcanism (Franklin et al., 2005) and are significant sources of base (Zn, Cu, Pb) and precious (Au, Ag) metals and other critical metals and metalloids (Co, Sn, Se, Mn, In, Bi, Te, Ga and Ge; Franklin et al., 1981; Galley et al., 2007). The polymetallic nature of VMS deposits makes them attractive targets for exploration and mining. Previous studies have defined the parameters for the formation of anomalously rich or large VMS deposits (Sangster, 1980; Galley et al., 2007; Mercier-Langevin et al., 2011; Piercey et al., 2015), and what factors contribute to the formation of large tonnages (Peter and Scott, 1997; Barrie et al., 1999; Goodfellow and McCutcheon, 2003; Tornos, 2006), high grades (Bergman Weihed et al., 1996; Sherlock et al., 1999; McClenaghan et al., 2009), and/or anomalous metal assemblages (Hannington et al., 1999; Relvas et al., 2006) in VMS deposits. These factors are strongly dependent on the type of extensional geodynamic setting that hosts the deposits (Barrie and Hannington, 1999; Franklin et al., 2005; Piercey, 2011).

Seafloor massive sulfide (SMS) deposits are modern analogs of VMS deposits forming on the modern seafloor (Hannington et al., 2005) and have also been helpful in enhancing our understanding of ancient VMS deposits from similar settings. Our understanding of the controls on VMS deposits, from the stratigraphic and tectonomagmatic scale through to the nanoscale, are still incomplete.

The thesis study area is in the Finlayson Lake district in south-central Yukon (Fig. 1.1) that contains >40 Mt of polymetallic VMS mineralization in varying deposit styles hosted by arc and back-arc rocks of the Yukon-Tanana and Slide Mountain terranes (Peter et al., 2007) and formed in the

Figure 1.1. Regional setting of the Finlayson Lake district. (A) Regional geologic map of the Finlayson Lake district, Yukon-Tanana, and Slide Mountain terranes (modified after Murphy et al., 2006). Numbers mark the positions of known VMS deposits in the region. BCT = Big Campbell thrust; CLT = Cleaver Lake thrust; JCF = Jules Creek fault; MCT = Money Creek thrust; NRF = North River thrust. (B) Composite chronostratigraphic column for the Finlayson Lake district showing stratigraphic and structural relationships. Locations of VMS deposits, petrogenetic affinities of volcanic rocks and U-Pb and fossil ages displayed on diagram (modified after Murphy et al., 2006; Piercey et al., 2016; Manor and Piercey, 2018).

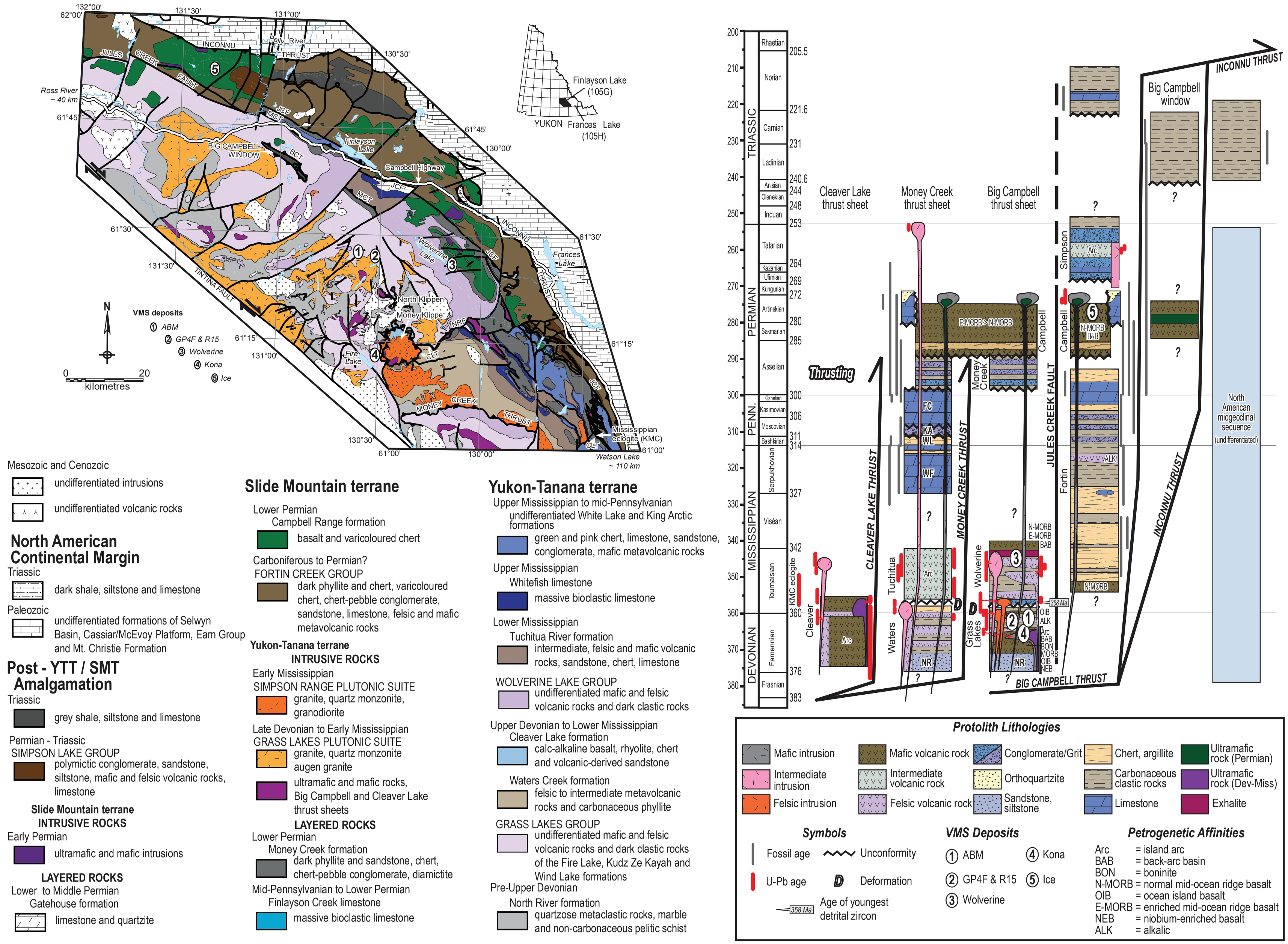

Ross River ~ 40 km
Watson Lake ~ 110 km
Finlayson Lake (105G)
YUKON
Frances Lake (105H)
JULES CREEK FAULT
INCONNU THRUST
TINTINA FAULT
BIG CAMPBELL WINDOW
Campbell Highway
Finlayson Lake
Frances Lake
Wolverine Lake
Fire Lake
North Klippen
Money Klippe
MONEY CREEK THRUST
Pelly River
Mississippian eclogite (KMC)
VMS deposits
1 ABM
2 GP4F & R15
3 Wolverine
4 Kona
5 Ice
kilometres
Mesozoic and Cenozoic
undifferentiated intrusions
undifferentiated volcanic rocks
North American Continental Margin
Triassic
dark shale, siltstone and limestone
Paleozoic
undifferentiated formations of Selwyn Basin, Cassiar/McEvoy Platform, Earn Group and Mt. Christie Formation
Post - YTT / SMT Amalgamation
Triassic
grey shale, siltstone and limestone
Permian - Triassic
SIMPSON LAKE GROUP
polymictic conglomerate, sandstone, siltstone, mafic and felsic volcanic rocks, limestone
Slide Mountain terrane
INTRUSIVE ROCKS
Early Permian
ultramafic and mafic intrusions
LAYERED ROCKS
Lower to Middle Permian
Gatehouse formation
limestone and quartzite
Slide Mountain terrane
Lower Permian
Campbell Range formation
basalt and varicoloured chert
Carboniferous to Permian?
FORTIN CREEK GROUP
dark phyllite and chert, varicoloured chert, chert-pebble conglomerate, sandstone, limestone, felsic and mafic metavolcanic rocks
Yukon-Tanana terrane
INTRUSIVE ROCKS
Early Mississippian
SIMPSON RANGE PLUTONIC SUITE
granite, quartz monzonite, granodiorite
Late Devonian to Early Mississippian
GRASS LAKES PLUTONIC SUITE
granite, quartz monzonite
augen granite
ultramafic and mafic rocks, Big Campbell and Cleaver Lake thrust sheets
LAYERED ROCKS
Lower Permian
Money Creek formation
dark phyllite and sandstone, chert, chert-pebble conglomerate, diamictite
Mid-Pennsylvanian to Lower Permian
Finlayson Creek limestone
massive bioclastic limestone
Yukon-Tanana terrane
Upper Mississippian to mid-Pennsylvanian
undifferentiated White Lake and King Arctic formations
green and pink chert, limestone, sandstone, conglomerate, mafic metavolcanic rocks
Upper Mississippian
Whitefish limestone
massive bioclastic limestone
Lower Mississippian
Tuchitua River formation
intermediate, felsic and mafic volcanic rocks, sandstone, chert, limestone
WOLVERINE LAKE GROUP
undifferentiated mafic and felsic volcanic rocks and dark clastic rocks
Upper Devonian to Lower Mississippian
Cleaver Lake formation
calc-alkaline basalt, rhyolite, chert and volcanic-derived sandstone
Waters Creek formation
felsic to intermediate metavolcanic rocks and carbonaceous phyllite
GRASS LAKES GROUP
undifferentiated mafic and felsic volcanic rocks and dark clastic rocks of the Fire Lake, Kudz Ze Kayah and Wind Lake formations
Pre-Upper Devonian
North River formation
quartzose metaclastic rocks, marble and non-carbonaceous pelitic schist
TRIASSIC
PERMIAN
PENN.
MISSISSIPPIAN
DEVONIAN
Rhaetian
Norian
Carnian
Ladinian
Anisian
Olenekian
Induan
Tatarian
Kazanian
Ufimian
Kungurian
Artinskian
Sakmarian
Asselian
Gzhelian
Kasimovian
Moscovian
Bashkirian
Serpukhovian
Viséan
Tournaisian
Famennian
Frasnian
Cleaver Lake thrust sheet
Money Creek thrust sheet
Big Campbell thrust sheet
Big Campbell window
Thrusting
CLEAVER LAKE THRUST
MONEY CREEK THRUST
JULES CREEK FAULT
INCONNU THRUST
BIG CAMPBELL THRUST
KMC eclogite
Cleaver
Tuchitua
Waters
Wolverine
Grass Lakes
Campbell
Simpson
Fortin
Money Creek
North American miogeoclinal sequence (undifferentiated)
Protolith Lithologies
Mafic intrusion
Intermediate intrusion
Felsic intrusion
Mafic volcanic rock
Intermediate volcanic rock
Felsic volcanic rock
Conglomerate/Grit
Orthoquartzite
Sandstone, siltstone
Chert, argillite
Carbonaceous clastic rocks
Limestone
Ultramafic rock (Permian)
Ultramafic rock (Dev-Miss)
Exhalite
Symbols
Fossil age
Unconformity
U-Pb age
Deformation
Age of youngest detrital zircon
VMS Deposits
1 ABM
2 GP4F & R15
3 Wolverine
4 Kona
5 Ice
Petrogenetic Affinities
Arc = island arc
BAB = back-arc basin
BON = boninite
N-MORB = normal mid-ocean ridge basalt
OIB = ocean island basalt
E-MORB = enriched mid-ocean ridge basalt
NEB = niobium-enriched basalt
ALK = alkalic

Middle to Upper Devonian (Murphy et al., 2006; Cohen et al., 2013; Manor et al., 2022b; Walker et al., 2022). This dissertation focuses on the ABM deposit, a bimodal-felsic replacement-style VMS deposit with zinciferous (>6.1 % Zn; Piercey et al., 2015) Zn grades (6.4 % Zn), as well as significant Ag, Pb, Au, and Cu grades (Table 1.1; van Olden et al. 2020). No comprehensive research focusing on the detailed stratigraphy, volcanic facies, hydrothermal alteration, and ore mineralogy and chemistry characteristics of the ABM deposit has been undertaken; thus, our understanding of the deposit formation and the evolution of its hydrothermal system and mineralization is incomplete. The Kudz Ze Kayah project (including the ABM deposit) has a defined Inferred and Indicated Resource (Table 1.1; van Olden et al. 2020) and the project is currently in development by BMC Minerals (No.1) Ltd. and has reached the mine permitting stage. This dissertation is a detailed study of the geological characteristics, tectonostratigraphic setting, and hydrothermal evolution of the ABM deposit. The conclusions of this dissertation will be used to develop a genetic model that can be applied in exploration for similar style VMS mineralization in the Finlayson Lake district and global analogues, and the presented research will also be used to study some of the more ambiguous aspects of replacement-style VMS deposit formation.

Table 1.1.The Indicated and Inferred Resource at the ABM deposit (van Olden et al. 2020).

ABM deposit Resource Indicated & Inferred								
Zone	Category	Tonne [Mt]	NSR [CAD$/t]	Cu [%]	Pb[%]	Zn [%]	Au [g/t]	Ag [g/t]
ABM (OP)	Indicated	14.6	358	1.0	1.6	6.1	1.3	132
	Inferred	0.3	334	1.5	1.5	4.5	1.1	115
KKT (OP)	Indicated	3.5	443	0.6	3.2	7.2	1.8	213
	Inferred	0.1	347	0.6	2.3	6.3	1.3	142
KKT (UG)	Indicated	0.2	397	1.0	2.0	6.1	1.7	170
	Inferred	0.4	447	0.8	1.6	9.5	1.2	165

OP = open pit, UG = underground, Mt = million tonnes, NSR = net smelter return

The following section in this introductory chapter outlines the main features of the formation of VMS deposits in the terms of tectono-magmatic and stratigraphic framework, replacement-style mineralization and preservation of primary features in the ancient rock record. The next section covers what the main objectives of the dissertation are and how the dissertation contributes to the ongoing research on replacement-style VMS deposits. Following it is a section covering the methods utilized in research, and a brief overview of the organization of the dissertation.

1.1.1 Overview of the general model of VMS deposit formation

Volcanogenic massive sulfide deposits occur in extensional geodynamic environments, ranging from mid-ocean ridges to various arc-associated settings (Allen et al., 2002; Franklin et al., 2005); however, very few VMS deposits that formed at mid-ocean ridges have been preserved in the ancient record, mainly due to subduction of oceanic crust (Huston et al., 2010). Ancient VMS deposits are generally preserved along convergent margins where accreted back-arcs, rifted arcs, and fore-arcs represent previously extensional environments (Huston et al., 2010). Overprinting by metamorphism and deformation is common in convergent regimes and makes recognizing small-scale features of VMS-style mineralization in the ancient rock record challenging (Lafrance et al., 2020).

In the general genetic model of VMS deposits, a heat source at depth, such as a subvolcanic intrusion or an elevated heat gradient in thinned crust, generates high heat flow in a subseafloor environment (Cathles et al., 1997; Barrie et al., 1999; Piercey, 2011). This heat source generates hydrothermal convection cells (Fig. 1.2) where seawater is drawn down along faults and fractures, heats up and reacts with the surrounding rocks, and causes a breakdown of primary minerals and their replacement with alteration minerals (Galley, 2003; Franklin et al., 2005; Hannington, 2013). A reaction zone forms in the volcanic and/or sedimentary rocks at depth (~2000 m depth below the seafloor; Galley 1993; Galley et al. 2007) as the hydrothermal system evolves with rising temperatures (Fig. 1.2), and acts as a reservoir where metals are leached by fluids that evolved from the downdrawn seawater, with potential contributions of magmatic fluids from the underlying subvolcanic intrusions (Galley, 1993; Hannington et al., 2003b). Once the fluids reach temperatures >400 °C, they become buoyant, and ascend through zones of high permeability (e.g., synvolcanic faults, fractures, and unconsolidated sediments and volcaniclastic material near the seafloor; Franklin et al., 2005; Mumin et al., 2007). Sulfide precipitation occurs at or near the seafloor due to the interaction between the high temperature acidic hydrothermal fluids with cold pH-circumneutral seawater (Haymon, 1983; Lydon, 1988) and long-lived hydrothermal activity leads to the formation of massive sulfide mounds or lenses (Franklin et al., 2005). In general, this process leads to massive sulfide deposits that form either by exhalative processes through chimney and mound formation on the seafloor (Lydon, 1984; Lydon, 1988), and/or through replacement of porous and permeable units below the seafloor (Doyle and Allen, 2003; Piercey, 2015; Nozaki et al., 2021).

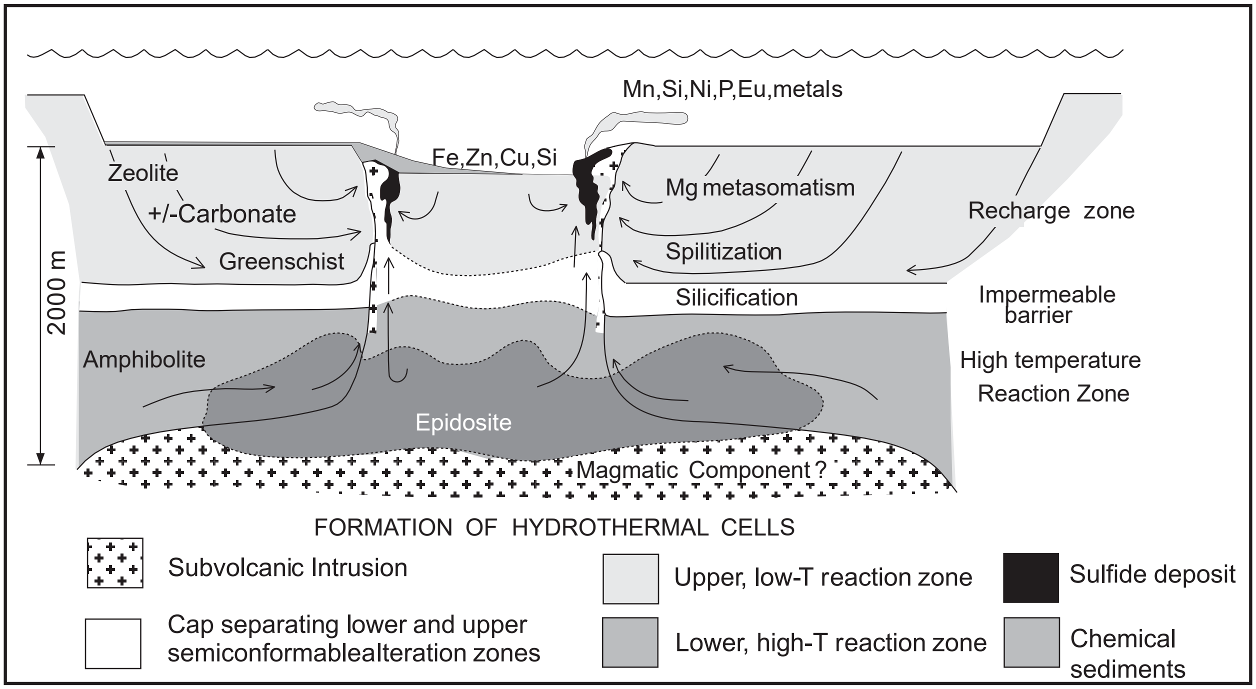

Figure 1.2. Generalized schematic cross-section showing the formation of a high temperature hydrothermal system displaying the alteration and mineralization assemblages. Adapted from Galley (1993), Franklin et al. (2005) and Galley et al. (2007).

The character and genesis of a VMS deposit is controlled by the type of extensional environment that hosts the deposit because the extensional environment controls the tectonic regime and the character of tectonic activity, the character of magmatism and volcanism, basin architecture, and the lithofacies present (Franklin et al., 1981; Gibson et al., 1999). Host rock assemblages are a useful basis for a classification of VMS deposits (Barrie and Hannington, 1999; Franklin et al., 2005; Piercey, 2011) and divide the VMS deposit type into five groups: 1) mafic, commonly associated with ophiolite-hosted or mature intra-oceanic back-arcs (e.g., deposits in Oman, Cyprus; modern mid-ocean ridges); 2) bimodal-mafic, mafic-dominated settings with up to 25 % felsic rocks, occurring in intra-arc rifts above intra-oceanic subduction zones (e.g., the Noranda Camp, Flin Flon-Snow Lake, Canada); 3) pelitic mafic, containing subequal proportions of mafic and siliciclastic rocks, in juvenile and accreted arc assemblages (e.g., Besshi district, Japan; Windy Craggy, Canada; Guyamas basin, Gulf of California; Middle Valley and Escanaba Trough, northeast Pacific Ocean); 4) bimodal-felsic, comprising subequal portions of felsic and mafic volcanic rocks with around 10% sediments, these occur within continental margin arcs and related back-arcs (e.g., Skellefte district, Sweden; Tasman orogen, Australia; Eskay Creek, Canada; Hokuroku district, Japan; Okinawa Trough); 5) siliciclastic-felsic, dominantly siliciclastic rocks, minor mafic and felsic volcanics, these occur in mature epicontinental back-arcs (e.g., Iberian Pyrite Belt, Spain and Portugal; Bathurst district, Canada).

An elevated geothermal gradient is necessary for the existence of sustained hydrothermal circulation that could sustain the formation of any significant VMS deposit (Cathles et al., 1997; Hart et al., 2004; Piercey, 2011). Mantle decompression and the subsequent attenuation of the crust (either oceanic or continental) in extensional basins in the fore-arc/intra-arc/back-arc regions cause basaltic magma to underplate the crust (Galley, 2003; Piercey, 2011). In this type of setting, large volumes of basaltic magma are generated through anatexis at shallow levels in the mantle (<50-100 km depth) and rise rapidly through to the crust without losing considerable amounts of heat that is needed for the formation the VMS deposits and the associated host rocks (Lentz, 1998; Galley, 2003; Piercey, 2011). As the basaltic magma rises and interacts with the crust, felsic magmas form, generating bimodal-type volcanism in the extensional basin (Galley, 2003). Extensional stresses result in the development of fault systems, which can then accommodate rising magmas and form calderas, grabens, and other features typical in extensional basins (Franklin et al., 1981; Piercey, 2011); such faults can reach depths of >5 km (Lentz, 1998). High level intrusions of any composition (Gibson et al., 1999) are general indicators of a heightened geothermal gradient in an extensional basin and have been considered as the motors for hydrothermal circulation forming VMS deposits (Cathles et al., 1997). This has since been questioned, however, as the emplacement of subvolcanic intrusions can post-date VMS formation (Galley, 2003; Piercey, 2011; Manor et al., 2022a). Physiochemical properties of the ascending magmas, such as composition, temperature, density, viscosity, and volatile content, determine the eruption type, which in turn affects which lithofacies will be present and whether the environment will be suitable for VMS deposit formation (Cas and Wright, 1987; McPhie et al., 1993).

VMS deposits are commonly associated with felsic volcanism, even if felsic volcanism constitutes only a minor portion of the total volume of the volcanic rocks (Franklin et al., 2005). Felsic magmas associated with VMS systems are commonly characterized by high temperatures of formation and take the form of dacitic/rhyolitic volcanism or as high level (1-3 km deep beneath the surface) subvolcanic intrusions (Lesher et al., 1986; Hart et al., 2004). Felsic volcanic rocks occur within bimodal or felsic-siliciclastic sequences with compositions between rhyolite and dacite and contain distinct textures (Lentz, 1998), including felsic lavas occurring as lobe-hyaloclastite flows, blocky subaqueous lavas and domes, cryptodomes, sills, or dykes (McPhie et al., 1993; Allen et al., 1996b; Gibson et al., 1999), commonly with distinct petrochemistry related to the substrate that was partially melted (Piercey, 2011). The coherent volcanic rocks are commonly spatially associated with synvolcanic dykes that are feeders to the near-surface to surface lithofacies (McPhie et al., 1993; Allen et al., 1996b; Gibson et al., 1999). These flows, domes, cryptodomes, and high-level synvolcanic dykes and sills are coherent rocks, which are on the surface commonly covered by hyaloclastite-rich breccias with jigsaw-fit textures, and massive volcanic breccias at distance from the centres of the flows (McPhie et al., 1993). Felsic volcanism is commonly accompanied by the generation of large volumes of volcaniclastic rocks through explosive magmatic and phreatomagmatic eruptions and related mass-flow re-sedimentation and reworking (Cas and Wright, 1987; McPhie et al., 1993). Presence of voluminous volcaniclastic rocks together with composite volcanoes can indicate the occurrence of calderas or subsidence structures, such as grabens, where thickest accumulations of volcaniclastic rocks occur at or near the caldera faults (Gibson et al., 1999; Stix et al., 2003; Franklin et al., 2005).

Generally, VMS deposits are associated with the waning stages of volcanism, or they occur close to transitions between consecutive volcanic cycles or caldera stages (Allen et al., 1996b; Allen et al., 1996a; Stix et al., 2003; Mumin et al., 2007; Thurston et al., 2008; Belford et al., 2015). During these breaks in volcanism, the fault systems that served as conduits for ascending magmas can be exploited by the circulating hydrothermal fluids instead (Franklin et al., 2005). Thus, examination of volcanic facies and reconstructions of basin stratigraphy and architecture are essential tools for identifying and following the commonly narrow stratigraphic intervals associated with episodes of rifting or with waning volcanic cycles during which VMS deposits form (Genna et al., 2014; DeWolfe et al., 2018; Friesen et al., 2020). Linking lithofacies and lithofacies assemblages requires detailed facies mapping of outcrops and drill core. Establishing the continuity through facies analysis, petrochemistry, and chemostratigraphy also helps to identify crosscutting and offsetting structures such as synvolcanic and synsedimentary faults (McPhie and Allen, 1992; Doyle and Allen, 2003; Mumin et al., 2007; Pilote et al., 2019). Further, research focused on reconstructing the basin architecture of extensional basins helps to illuminate the more cryptic aspects of replacement-style mineralization, such as the geometry of hydrothermal up-flow zones, the role of synvolcanic faults, and the timing of VMS mineralization in relation to volcanism and processes in underlying magma chambers, such as recharge or magma-mixing.

Although many deposits show evidence of deposition on the seafloor by exhalative processes, a subset of deposits forms via subseafloor replacement of existing volcanic and sedimentary rocks (Doyle and Allen, 2003; Piercey, 2015). As hydrothermal fluids ascend along faults, they may encounter porous and permeable layers and infiltrate pore spaces and voids; fluids may precipitate sulfide minerals in these voids or replace the existing material (Doyle and Allen, 2003). These processes typically take place at depths down to 200 m below the seafloor in wet, porous and unconsolidated to poorly consolidated facies that accumulate at fast rates indicating rapid burial (e.g., glass-rich or pumice-rich lithofacies, breccias, hyaloclastites; Gibson et al., 1999; Doyle and Allen, 2003). Relics of host rocks or their textures (e.g., bedding, preserved clasts) occur within the massive sulfides, and the massive sulfide lenses locally transition into un-mineralized host rock (Doyle and Allen, 2003). Replacement-style VMS deposits have a higher likelihood of preservation (Doyle and Allen, 2003) and commonly have higher tonnages and/or higher grades than mound-style VMS deposits due to a more effective trapping mechanism of upwelling VMS hydrothermal fluids (Doyle and Allen, 2003; Piercey, 2015). Sub-seafloor replacement has been described in a number of ancient VMS (Ansil deposit, Canada, Galley et al., 1995; Highway-Reward, Australia, Doyle and Huston, 1999; Rosebery, Australia, Large et al., 2001; Perseverance and Bracemac-McLeod deposits, Canada; Genna et al., 2014; Boundary deposit, Canada, Piercey et al., 2014) and modern SMS (Anderson et al., 2019; Nozaki et al., 2021) deposits, and appears to be one of the processes that contributes to the formation of large tonnage deposits (e.g. Kidd Creek or Neves Corvo deposits; Barrie et al., 1999; Rosa et al., 2008).

Preservation of primary mineralization and alteration textures in ancient VMS deposits is uncommon and depends predominantly on the degree of metamorphism and deformation (Lafrance et al., 2020). Small-scale features such as fragments of black smoker chimneys (Maslennikov et al., 2017), textures resulting from mechanical erosion of massive sulfide mounds (Goodfellow and McCutcheon, 2003), and replacement textures (Larocque and Hodgson, 1995) are preserved, but not as commonly as deposit-scale features, such as the metal zonation within the mineralization (Knuckey et al., 1983), hydrothermal alteration assemblages and their zonation (Gemmell and Large, 1992; Gemmell and Fulton, 2001; Large et al., 2001), or typical element and/or mineral assemblages (Eldridge et al., 1983; Craig and Vokes, 1992; Vikentyev et al., 2017). However, the limit for preserving the original textures and mineral chemistry in massive sulfide mineralization is commonly greenschist metamorphic facies because at higher temperatures and pressures, partial to full sulfide anatexis may occur (Tomkins et al., 2007). Mineral chemistry of the minerals that originated through hydrothermal alteration processes, however, remains intact up to upper greenschist facies (Riverin and Hodgson, 1980; Urabe et al., 1983; Hannington et al., 2003a; Genna and Gaboury, 2015). Further, lithogeochemical signatures of the hydrothermal footprints of VMS deposits generally withstand metamorphism and represent original fluid flow and fluid-rock interactions processes (Barrett and MacLean, 1994).

1.1.2 Objectives

The key output of this dissertation is a comprehensive description and interpretation of the ABM deposit that is used to constrain the tectonostratigraphic evolution and the volcanic, sedimentary, and hydrothermal processes within the extensional basin formed in the Late Devonian (Piercey et al., 2001; Murphy et al., 2006; Manor et al., 2022b; Manor et al., 2022a). The goal of this study was to connect the deposit evolution with the larger scale tectonomagmatic evolution of the Finlayson Lake district and add new perspectives to VMS prospectivity and exploration methods in the Finlayson Lake district with applications to the broader northern Cordillera, and to ancient bimodal-felsic VMS districts globally. This dissertation brings further insights on replacement-style VMS deposits by constraining and defining: 1) what features of the back-arc tectonic setting were essential for the formation of replacement-style mineralization; 2) the physicochemical characteristics, distribution, and zonation of hydrothermal alteration assemblages in the hanging wall and the footwall of the mineralization and how these were affected by the hosting lithostratigraphy; and 3) the characteristics (e.g., temperature, pH, oxidation state) and sources of hydrothermal fluids, and the processes that formed the mineralization.

This dissertation summarizes a detailed study of the tectono-stratigraphic setting and genesis of the ABM replacement-style VMS deposit. Specific objectives of this study that focus on the ABM deposit were to:

1. Reconstruct the lithostratigraphy of the back-arc basin hosting the ABM deposit and create a comprehensive 2D-3D model of the deposit. The 2D-3D model was used to reconstruct lithostratigraphic units, their depositional environment, the volcanic and volcano-sedimentary processes that occurred in the active back-arc basin, and the basin architecture and structural framework.

2. Describe the hydrothermal alteration assemblages, their zonation, mineralogy, and elemental distribution at the ABM deposit and determine how the hydrothermal system evolved. Detailed petrographic observations, lithogeochemical data, mass balance calculations, phyllosilicate mineral chemistry, and short-wave infrared features of phyllosilicate minerals were used to characterize the hydrothermal alteration assemblages, their zonation, and their distribution in relation to the basin architecture, and to assess the evolution of the hydrothermal system.

3. Describe the replacement-style mineralization at the ABM deposit and investigate what factors

were important in the development of the high tonnages and grades. Detailed petrographic and drill core observations, together with assay data, were used to characterize element and mineralization assemblages, their distribution, and zonation at the ABM deposit. Detailed study of mineral chemistry characteristics of the different mineralization assemblages was used to determine what processes contributed to their formation and what were the sources of metals for the massive sulfide mineralization.

1.2 Methodology

1.2.1 Core logging and sampling

The basis for this dissertation is the data collected from logging and sampling of drill core from the ABM deposit. BMC Minerals (No.1) Ltd. generously provided access to their modern and historic drill core archive covering the Kudz Ze Kayah project (the larger area of the ABM deposit). The purpose of the core logging was to map the different lithostratigraphic units, to map the distribution of alteration minerals in relation to the mineralization and the different lithologies, to describe the different styles of mineralization and their distribution, and to document the textures in both altered and unaltered, and mineralized and barren rocks, and note major structures within the ABM deposit footprint.

During the summer field seasons in 2018 and 2019, graphic logs documenting 56 drill holes (over 11500 m) were produced and 553 hand samples for geochemical analysis and thin sections were collected. Lithology, grain size, type, and intensity of alteration based on occurrence of different mineral (quartz, white mica, chlorite, biotite, carbonate, and sulfide minerals) were recorded in graphic logs and each unit was characterized briefly in the comments section. The logs were digitized into a MS Excel sheet (Electronic Appendix 1). The sampling strategy aimed to create a comprehensive collection of the most common lithologies and alteration styles distributed throughout the ABM deposit footprint. The objective for the sampling of the mineralization was to capture different ore types throughout the mineralized bodies of the ABM deposit and document replacement-style textures.

1.2.2 2D-3D modelling

Digital models of the lithologic units, mineralized lenses and major structures, and numeric models of element distribution were created using the Leapfrog Geo 5.0 software using "Geological Models" and "Numeric Models" tools. Digital models of the lithologic units and mineralized lenses help to visualize the spatial and temporal relationships between the different lithologies and mineralization and give context to the relationship observed in drill core. Visualization of the geometries and changing thickness of the sedimentary, volcaniclastic, volcanic, and subvolcanic units helped determine the mechanism of their deposition/formation. Evaluating the distribution of different elements in relation to the lithological units sheds light on trends in geochemical, mineralogical, short-wave infrared or other data. The basis for the models of the lithostratigraphic units are the digitized graphic logs generated by the author supplemented with company drill logs, photographs of core boxes, and sample photos. BMC Minerals (No.1) Ltd. generously provided their drill log database together with core photographs and assay and geochemistry results. Assay tables of elements used for numeric models have been reviewed for overlapping intervals, negative or non-numeric values and errors. The quality assurance and quality control (QA/QC) procedures used to collect the data are described in van Olden et al. (2020). The Numeric Models tool in Leapfrog 3D was used to construct isosurfaces of element distribution. The linear radial basis function (RBF) interpolation was chosen to mitigate the irregular distribution of the datapoints. The trend was set to the local stratigraphy with the ellipsoid ratios at 3:3:1 to reflect the dip and dip direction of the mineralized lenses. The threshold value for the elements at the deposit were chosen using methods outlined in Reimann et al. (2005) and the grades present in the block model (van Olden et al., 2020).

1.2.3 Short-wave infrared spectroscopy

Spectral features of some minerals within the visible and infrared spectra are caused by electronic and vibrational processes linked to their composition and molecular structure (Hunt, 1977). Reflectance spectra can be used to identify minerals with specific groups (H_2O, OH^-, CO_3^{2-}, SO_4^{2-}) and to determine their chemistry, occurrence and relative abundance. The composition of minerals that occur commonly in alteration halos surrounding VMS deposits (white mica, chlorite and carbonate minerals) changes depending on the temperature of the fluids that deposited them and can thus be used to determine their position relative to the high temperature interior of the hydrothermal system (Herrmann et al., 2001; Jones et al., 2005; Yang et al., 2011; Buschette and Piercey, 2016).

Hyperspectral measurements were collected at Memorial University using a Terraspec™ Infrared Spectrometer with a Hi-Brite Muglight. To monitor the accuracy and precision of the acquired data, an internal reference sample (pyrophyllite) was measured after each white reference optimization, which occurred every 20 samples or every 20 minutes during the run of the instrument. The monitoring confirmed that the instrument yielded absorption hulls that were consistently within 3 nm of accepted values for the internal standard. Data were processed using The Spectral Geologist 7.1 software. Hyperspectral scalars were calculated for the 2200 nm (2,185-2,225 nm) and 2250 nm (2,245-2,265 nm) absorption wavelengths features using a fourth-order polynomial fitting curve, with hull correction and background noise filters applied to the spectra. The diagnostic absorption feature for white mica occurs between 2,180-2,225 nm and is caused by the variation in composition due to the Tschermak substitution ($Al^{VI} + Al^{IV} \leftrightarrow (Fe, Mg, Mn)^{VI} + Si^{IV}$), and by the interlayer cation substitution between K and Na (Velde, 1978; Herrmann et al., 2001; Yang et al., 2011). Values of the 2200 nm feature between 2,180 and 2,195 nm are attributed to Na-bearing muscovite, between 2,200-2,208 nm are considered to be muscovite, wavelengths of 2,216-2,228 nm have a phengite composition, and values between 2,208-2,216 nm are considered to be mixtures of two or more mica phases, or to have an intermediate composition (Herrmann et al., 2001; Jones et al., 2005; Yang et al., 2011). For chlorite, the 2250 nm absorption feature between 2,235-2,255 nm is controlled by the Fe content (relative to Mg), with higher absorption values indicating higher Fe content (relative to Mg) of the chlorite (Herrmann et al., 2001; Cloutier et al., 2021).

1.2.4 Optical microscopy and scanning electron microscopy

Polished thin sections were prepared for two sample suites: one suite comprises mineralized samples covering the different mineralization assemblages; the other suite covers different lithofacies and hydrothermal alteration styles. Traditional transmitted and reflected light petrography was used to further investigate rock types, minerals, and textures observed in core, and to make detailed observations of minerals, textures, and paragenesis not visible in hand sample. The Hibernia Electron Beam Facility, MUN, in-house scanning electron microscopy instrument, a JEOL JSM 7100F scanning electron microscope (SEM) using back scatter electron (BSE) imaging operating at an accelerated voltage of 15 kV, was used to identify minerals that were not recognized during the optical microscopy work and to investigate in detail the hydrothermal alteration and replacement mineralization textures. Selected polished thin sections of massive sulfide mineralization were imaged using SEM coupled with energy-dispersive X-ray spectroscopy (EDX) using a FEI MLA 650FEG equipped with dual Bruker 5th generation XFlash SDD X-ray detectors at the Micro Analysis Facility at MUN-CREAIT, to show the distribution of selected elements in areas with complex textures.

1.2.5 Electron probe microanalysis

The in-house electron probe microanalysis (EPMA) instrument at the Hibernia Electron Beam Facility, MUN, was used for quantitative mineral composition analysis. The JEOL JXA-8230 SuperProbe is equipped with 5 wavelength dispersive spectrometers (WDS), a Thermo energy dispersive spectrometer (EDS), and W electron gun. The electron microprobe was used to quantify the composition of white mica, chlorite, and carbonate minerals that formed during hydrothermal alteration; it was also used to analyze the composition of pyrite, pyrrhotite, arsenopyrite, chalcopyrite, sphalerite, galena, and tetrahedrite group minerals from the different mineralization assemblages observed in the ABM deposit. Natural and synthetic standards were used for calibration of the instrument.

1.2.6 Laser ablation inductively coupled plasma mass spectrometry

In situ laser ablation inductively coupled plasma mass spectrometry (LA-ICP-MS) spot analyses were performed using a geoLas 193 nm Excimer laser (Coherent) coupled to a Thermo-Finnigan Element XR ICP-MS instrument at Memorial University on six polished blocks representing the main mineralization assemblages. The polished blocks were prepared from offcuts from selected thin sections that were previously analyzed using the SEM and EPMA. The ICP-MS was tuned for high sensitivity and a ThO/Th of <0.3 %. Abundances of selected elements were determined by spot analysis for pyrite, pyrrhotite, sphalerite, galena, chalcopyrite, arsenopyrite, and tennantite. Periodically, every 15-20 analyses, the standards NIST 610 (synthetic glass) and MASS-1 (pressed powder pellet) were measured. NIST 610 was used for drift correction and MASS-1 was used for calibration/matrix correction. Data reduction and the subtraction of gas blanks was performed using Iolite v. 3.72, the program was used for data treatment, to inspect the time-resolved signals and to exclude sections of the signal representing micro-inclusions of other minerals. Average values determined using the EPMA were used as internal standards (Fe for pyrite, pyrrhotite, and arsenopyrite, Zn for sphalerite, Cu for chalcopyrite and tennantite, and Pb for galena).

1.2.7 Whole-rock major and trace element lithogeochemistry methods

Eighty-three of the collected samples were analyzed for major and trace elements. Three separate lithogeochemical analytical packages (ME-MS81d, IMC-100, IML-101) were used to analyze the samples, to cover all elements necessary to study the lithostratigraphy, hydrothermal alteration, and mineralization. Sample preparation and measurement of major and trace element data (method PREP-31, PUL-42, ME-MS81d) was performed at ALS Laboratories, North Vancouver, British Columbia. Rock samples were crushed and pulverized using steel plates and agate mills, respectively. Sample powders (~0.2 g) were fused with a lithium metaborate flux (0.9 g) at 1000°C. The fused beads were cooled and digested using 100 mL of a 4% HNO_3-2% HCl mixture. Analyses of the sample solutions were carried out using inductively coupled plasma-atomic emission spectrometry (ICP-AES) for major elements and inductively coupled plasma-mass spectrometry (ICP-MS) for trace elements (full list of analyzed elements available in Appendix 1 and 2). Sub-samples of the returned pulps were sent to Geo Labs in Sudbury, where additional trace element measurements were completed on the same sample suites to obtain transition metals, base metals, and semi-metals (e.g., Li, Be, Co, Cu, Zn, Mo, Cd, In, Sb, W, Bi, Pb, Sc, Ta; full list of analyzed elements available in Appendix 2). Samples were digested on hot plates using a mixture of HF-HCl-$HClO_4$ in closed screwcap Savillex© Teflon© bombs for seven days. The resultant solution was dried and fluxed with a dilute HCl-$HClO_4$ mixture and re-heated. Samples were again dried and fluxed with a final mixture of concentrated HNO_3-HCl, were heated, and finally diluted with HNO_3. Solutions were analyzed for metals on a Perkin-Elmer Elan 9000 ICP-MS (method IMC-100) following the methodology of Burnham and Schweyer (2004) and Burnham (2008). Additionally, the same sample suite was further analyzed using an aqua regia (3:1 HCl and HNO_3) extraction method (method IML-101) with an analytical finish using a Perkin-Elmer Elan 9000 ICP-MS, to obtain minor and trace elements (e.g., Sb, As, Bi, Cd, Co, Cu, Au, In, Ir, Pb, Hg, Mo, Ni, Pd, Pt, Se, Ag, Te, Tl, Sn, Zn; full list of analyzed elements available in Appendix 2). The methodologies from Ontario GeoLabs (OGL) outlined above are detailed in Burnham and Schweyer (2004) and Burnham (2008).

1.3 Presentation of dissertation

This dissertation is presented in five chapters. Chapter 1 serves as an introduction to the dissertation and gives a brief overview of VMS deposits, the main research topics, and the different methods used in the research. Chapters 2, 3, and 4 are individual manuscripts intended for publication in peer-reviewed scientific journals. Chapter 5 presents the conclusions of this dissertation and recommendations for future research.

Chapter 2 ("Lithostratigraphy, lithogeochemistry and tectono-magmatic framework of the ABM replacement-style volcanogenic massive sulfide (VMS) deposit, Finlayson Lake District, Yukon, Canada") employs insights from detailed core logging, petrographic observations, 3D modelling, and the results from whole-rock lithogeochemical analyses to reconstruct the lithostratigraphy, chemostratigraphy, and architecture of the back-arc basin environment hosting the ABM deposit. The reconstructed lithofacies were used to map a volcanic centre within the extensional back-arc basin and to interpret likely synvolcanic faults that were active within the basin and during the genesis of the ABM deposit. The chemostratigraphy, distribution of the volcanic rocks, argillite lenses, and immobile element signatures of the main lithologies were used to constrain the timing and sequence of events and processes that formed the mineralization at the ABM deposit. The manuscript has been published in Economic Geology in 2022, volume 117 (6), pages 1299-1326.

Chapter 3 ("Evolution of the hydrothermal system associated with the ABM replacement-style volcanogenic massive sulfide deposit, Finlayson Lake district, Yukon, Canada") uses insights from hydrothermal alteration-focused core logging, petrographic observations, and lithogeochemical data to determine the major hydrothermal alteration assemblages, their distribution, relationships and paragenesis at the ABM deposit. The phyllosilicate minerals common in the hydrothermal alteration assemblages (white mica and chlorite) were studied using EPMA to determine any differences in their mineral chemistry between different assemblages, and their composition was used to calculate approximate formation temperatures (illite and chlorite geothermometry). The results from the EPMA were compared to approximate mineral composition determined using SWIR methods, and the SWIR data was used to determine the lateral continuity of hydrothermal alteration assemblages across the lithostratigraphic framework presented in Chapter 2. The collected observations and datasets were used to assess the effects of metamorphism and deformation on the hydrothermal alteration assemblages and to describe the evolution of the hydrothermal system from the early low temperature stage to its peak associated with massive sulfide mineralization. A simplified model showing the trends and magnitudes of different alteration indices, minor and trace metal indicators, mass balance changes, and mineral chemistry, in relation to the distribution of hydrothermal alteration assemblages and major lithostratigraphic units is presented and it is transferable to other parts of the Finlayson Lake district and to other similar ancient environments globally.

Chapter 4 ("Mineralogy and mineral chemistry of the mineralization at the ABM replacement-style volcanogenic massive sulfide deposit, Finlayson Lake district, Yukon, Canada") focuses on the massive sulfide mineralization at the ABM deposit. Core logging and petrographic observations, together with assay data were used to determine and describe the major mineralization and element assemblages, their distribution, zonation, and relationships, mineral parageneses and mineral textures. Assay data were also used to develop 3D numerical models of the elements of interest to show the element distribution relative to each other and to the interpreted mineralization assemblages, major lithostratigraphic units, and synvolcanic faults. Based on the petrographic observations, representative samples of the different mineralization assemblages were chosen to determine the sulfide mineral chemistry and investigate rare textures observed locally using EPMA and LA-ICP-MS. These results were used to assess the effects of post-VMS metamorphism and deformation on the massive sulfide mineralization, and to determine and compare the physiochemical conditions at which the different assemblages formed relative to each other.

1.4 References

Allen, R. L., Lundström, I., Ripa, M., Simeonov, A., and Christofferson, H., 1996a, Facies analysis of a 1.9 Ga, continental margin, back-arc, felsic caldera province with diverse Zn-Pb-Ag-(Cu-Au) sulfide and Fe oxide deposits, Bergslagen Region, Sweden: Economic Geology, v. 91, p. 979–1006.

Allen, R. L., Weihed, P., and Svenson, S. A., 1996b, Setting of Zn-Cu-Au-Ag massive sulfide deposits in the evolution and facies architecture of a 1.9 Ga marine volcanic arc, Skellefte district, Sweden: Economic Geology, v. 91, p. 1022–1053.

Allen, R. L., Weihed, P., Blundell, D., Crawford, T., Davidson, G., Galley, A. G., Gibson, H. L., Hannington, M. D., Herrington, R. J., Herzig, P. M., Large, R. R., Lentz, D. R., Maslennikov, V. V., McCutcheon, S. R., Peter, J. M., Tornos, F., 2002, Global comparisons of volcanic-associated massive sulphide districts, in Blundell, D. J., Neubauer, F., and von Quadt, A. eds., The Timing and Location of Major Ore Deposits in an Evolving Orogen. Geological Society, London, Special Publications, 204:, p. 13–37.

Anderson, M. O., Hannington, M. D., McConachy, T. F., Jamieson, J. W., Anders, M., Wienkenjohann, H., Strauss, H., Hansteen, T., and Petersen, S., 2019, Mineralization and alteration of a modern seafloor massive sulfide deposit hosted in mafic volcaniclastic rocks: Economic Geology, v. 114, p. 857–896.

Barrett, T. J., and MacLean, W. H., 1994, Chemostratigraphy and hydrothermal alteration in exploration for VHMS deposits in greenstones and younger volcanic rocks, in Lentz, D. R. ed., Alteration and Alteration Processes Associated with Ore-Forming Systems: Geological Association of Canada, Short Course Notes, v. 11, p. 433–467.

Barrie, C. T., and Hannington, M. D., 1999, Classification of volcanic-associated massive sulfide deposits based on host-rock composition, in Barrie, C. T. and Hannington, M. D. eds, Volcanic-associated massive sulfide deposits: Processes and examples in modern and ancient settings, p. 1–11.

Barrie, C. T., Hannington, M. D., and Bleeker, W., 1999, The giant Kidd Creek volcanic-associated massive sulfide deposit, Abitibi subprovince, Canada: Reviews in Economic Geology, v. 8, p. 247–259.

Belford, S. M., Davidson, G. J., McPhie, J., and Large, R. R., 2015, Architecture of the Neoarchaean Jaguar VHMS deposit, Western Australia: Implications for prospectivity and the presence of depositional breaks: Precambrian Research, v. 260, p. 136–160.

Bergman Weihed, J., Bergstrom, U., Billstrom, K., and Weihed, P., 1996, Geology, tectonic setting, and origin of the Paleoproterozoic Boliden Au-Cu-As deposit, Skellefte district, northern Sweden: Economic Geology, v. 91, p. 1073–1097.

Burnham, O. M., 2008, Trace element analysis of geological samples by inductively coupled plasma mass spectrometry (ICP - MS) at the Geoscience Laboratories: Revised capabilities due to method improvements: Summary of Field Work and Other Activities. Ontario Geological Survey, Open File Report, v. 6226, p. 1–10.

Burnham, O. M., and Schweyer, J., 2004, Trace element analysis of geological samples by inductively coupled plasma mass spectrometry at the Geoscience Laboratories: Revised capabilities due to improvements to instrumentation: Summary of Field Work and Other Activities 2004, Ontario Geological Survey. Open File Report, v. 6145, p. 1–20.

Buschette, M. J., and Piercey, S. J., 2016, Hydrothermal alteration and lithogeochemistry of the Boundary volcanogenic massive sulphide deposit, central Newfoundland, Canada: Canadian Journal of Earth Sciences, v. 53, p. 506–527.

Cas, R. A. F., and Wright, J. V., 1987, Volcanic Successions: Modern and Ancient: A Geological Approach to Processes, Products and Successions: London, Allen & Unwin (Publishers) Ltd, 528 p.

Cathles, L. M., Erendi, A. H. J., and Barrie, C. T., 1997, How long can a hydrothermal system be sustained by a single intrusive event? Economic Geology, v. 92, p. 766–771.

Cloutier, J., Piercey, S. J., and Huntington, J., 2021, Mineralogy, mineral chemistry and SWIR spectral reflectance of chlorite and white mica: Minerals, v. 11, p. 1–16.

Cohen, K.M., Finney, S.C., Gibbard, P.L. & Fan, J.-X. (2013; updated). The ICS International Chronostratigraphic Chart. Episodes 36: 199-204.

Craig, J. R., and Vokes, F. M., 1992, Ore mineralogy of the Appalachian-Caledonian stratabound sulfide deposits: Ore Geology Reviews, v. 7, p. 77–123.

DeWolfe, Y. M., Gibson, H. L., and Richardson, D., 2018, 3D reconstruction of volcanic and ore-forming environments of a giant VMS system: A case study from the Kidd Creek mine, Canada: Ore Geology Reviews, v. 101, p. 532–555.

Doyle, M. G., and Allen, R. L., 2003, Subsea-floor replacement in volcanic-hosted massive sulfide deposits: Ore Geology Reviews, v. 23, p. 183–222.

Doyle, M. G., and Huston, D. L., 1999, The subsea-floor replacement origin of the Ordovician Highway-Reward volcanic-associated massive sulfide deposit, Mount Windsor subprovince, Australia: Economic Geology, v. 94, p. 825–844.

Eldridge, C. S., Barton, P. B., and Ohmoto, H., 1983, Mineral textures and their bearing on formation of the Kuroko orebodies: Economic Geology Monograph 5, p. 241–281.

Franklin, J. M., Lydon, J. W., and Sangster, D. F., 1981, Volcanic-associated massive sulfide deposits: Economic Geology 75th Anniversary Volume, p. 485–627.

Franklin, J. M., Gibson, H. L., Jonasson, I. R., and Galley, A. G., 2005, Volcanogenic massive sulfide deposits, in Economic Geology 100th Anniversary Volume:, p. 523–560.

Friesen, V. C., DeWolfe, Y. M., and Gibson, H. L., 2020, Volcanic reconstruction and geochemistry of the Powderhouse formation in the Paleoproterozoic VMS-hosting Chisel sequence, Snow Lake, Manitoba, Canada: Canadian Journal of Earth Sciences, v. 21, p. 1–21.

Galley, A. G., 1993, Characteristics of semi-conformable alteration zones associated with volcanogenic massive sulphide districts: Journal of Geochemical Exploration, v. 48, p. 175–200.

Galley, A. G., 2003, Composite synvolcanic intrusions associated with Precambrian VMS-related hydrothermal systems: Mineralium Deposita, v. 38, p. 443–473.

Galley, A. G., Watkinson, D. H., Jonasson, I. R., and Riverin, G., 1995, The subsea-floor formation of volcanic-hosted massive sulfide: Evidence from the Ansil deposit, Rouyn-Noranda, Canada: Economic Geology, v. 90, p. 2006–2017.

Galley, A. G., Hannington, M. D., and Jonasson, I. R., 2007, Volcanogenic massive sulphide deposits, in Goodfellow, W. D. ed., Mineral Deposits of Canada: A Synthesis of Major Deposit-Types, District Metallogeny, the Evolution of Geological Provinces, and Exploration Methods: Geological Association of Canada, Mineral Deposits Division, Special Publication No. 5:, p. 141–161.

Gemmell, J. B., and Fulton, R., 2001, Geology, genesis, and exploration implications of the footwall and hanging-wall alteration associated with the Hellyer volcanic-hosted massive sulfide deposit, Tasmania, Australia: Economic Geology, v. 96, p. 1003–1035.

Gemmell, J. B., and Large, R. R., 1992, Stringer system and alteration zones underlying the Hellyer volcanic-hosted massive sulfide deposit, Tasmania, Australia: Economic Geology, v. 87, p. 620–649.

Genna, D., and Gaboury, D., 2015, Deciphering the hydrothermal evolution of a VMS system by LA-ICP-MS using trace elements in pyrite: An example from the Bracemac-McLeod deposits, Abitibi, Canada, and implications for exploration: Economic Geology, v. 110, p. 2087–2108.

Genna, D., Gaboury, D., and Roy, G., 2014, The Key Tuffite, Matagami Camp, Abitibi Greenstone Belt, Canada: petrogenesis and implications for VMS formation and exploration: Mineralium Deposita, v. 49, p. 489–512.

Gibson, H. L., Morton, R. L., and Hudak, G. J., 1999, Submarine volcanic processes, deposits, and environments favourable for the location of volcanic-associated massive sulfide deposits, in Barrie, C. T. and Hannington, M. D. eds., Volcanic Associated Massive Sulfide Deposits: Processes and Examples in Modern and Ancient Settings, p. 15–51.

Goodfellow, W. D., and McCutcheon, S. R., 2003, Geologic and genetic attributes of volcanic sediment-hosted massive sulfide deposits of the Bathurst Mining Camp , northern New Brunswick — A synthesis, in Economic Geology Monograph 11:, p. 245–301.

Hannington, M. D., 2013, Volcanogenic Massive Sulfide Deposits, in Treatise on Geochemistry: Second Edition: Elsevier Ltd., p. 463–488.

Hannington, M. D., Bleeker, W., and Kjarsgaard, I. M., 1999, Sulfide mineralogy, geochemistry, and ore genesis of the Kidd Creek deposit: Part I. North, Central, and South orebodies (M. D. Hannington & C. T. Barrie, Eds.): Economic Geology Monograph 10, p. 225–266.

Hannington, M. D., Kjarsgaard, I. M., Galley, A. G., and Taylor, B., 2003a, Mineral-chemical studies of metamorphosed hydrothermal alteration in the Kristineberg volcanogenic massive sulfide district, Sweden: Mineralium Deposita, v. 38, p. 423–442.

Hannington, M. D., Santaguida, F., Kjarsgaard, I. M., and Cathles, L. M., 2003b, Regional-scale hydrothermal alteration in the Central Blake River Group, western Abitibi subprovince, Canada: Implications for VMS prospectivity: Mineralium Deposita, v. 38, p. 393–422.

Hannington, M. D., De Ronde, C. E. J., and Petersen, S., 2005, Sea-floor tectonics and submarine hydrothermal systems: Economic Geology 100th Anniversary Volume, p. 111–141.

Hart, T. R., Gibson, H. L., and Lesher, C. M., 2004, Trace element geochemistry and petrogenesis of felsic volcanic rocks associated with massive Cu-Zn-Pb sulfide deposits: Economic Geology, v. 99, p. 1003–1013.

Haymon, R. M., 1983, Growth history of hydrothermal black smoker chimneys: Nature, v. 301, p. 695–698.

Herrmann, W., Blake, M., Doyle, M. G., Huston, D. L., Kamprad, J., Merry, N., and Pontual, S., 2001, Short wavelength infrared (SWIR) spectral analysis of hydrothermal alteration zones associated with base metal sulfide deposits at Rosebery and Western Tharsis, Tasmania, and Highway-Reward, Queensland: Economic Geology, v. 96, p. 939–955.

Hunt, G. R., 1977, Spectral signatures of particulate minerals in the visible and infrared: Geophysics, v. 42, p. 501–513.

Huston, D. L., Pehrsson, S., Eglington, B. M., and Zaw, K., 2010, The geology and metallogeny of volcanic-hosted massive sulfide deposits: Variations through geologic time and with tectonic setting: Economic Geology, v. 105, p. 571–591.

Jones, S., Herrmann, W., and Gemmell, J. B., 2005, Short wavelength infrared spectral characteristics of the HW horizon: Implications for exploration in the Myra Falls volcanic-hosted massive sulfide camp, Vancouver Island, British Columbia, Canada: Economic Geology, v. 100, p. 273–294.

Knuckey, M. J., Comba, C. D. A., and Riverin, G., 1983, Structure, metal zoning and alteration at the Millenbach deposit, Noranda, Quebec, in Hutchinson, R. W., Spence, C. D., and Franklin, J. M., eds.: Geological Association of Canada Special Paper 25, p. 255–295.

Lafrance, B., Gibson, H. L., and Stewart, M. S., 2020, Internal and external deformation and modification of volcanogenic massive sulfide deposits, in Rowland, J. V. and Rhys, D. A. eds., Reviews in Economic Geology 21:, p. 147–171.

Large, R. R., McPhie, J., Gemmell, J. B., Herrmann, W., and Davidson, G. J., 2001, The spectrum of ore deposit types, volcanic environments, alteration halos, and related exploration vectors in submarine volcanic successions: Some examples from Australia: Economic Geology, v. 96, p. 913–938.

Larocque, A. C. L., and Hodgson, C. J., 1995, Effects of greenschist-facies metamorphism and related deformation on the Mobrun massive sulfide deposit, Quebec, Canada: Mineralium Deposita, v. 30, p. 439–448.

Lentz, D. R., 1998, Petrogenetic evolution of felsic volcanic sequences associated with Phanerozoic volcanic-hosted massive sulphide systems: the role of extensional geodynamics: Ore Geology Reviews, v. 12, p. 289–327.

Lesher, C. M. M., Goodwin, A. M., Campbell, I. H. I. H., and Gorton, M. P., 1986, Trace-element geochemistry of ore-associated and barren, felsic metavolcanic rocks in the Superior Province, Canada: Reply: Canadian Journal of Earth Sciences, v. 23, p. 222–237.

Lydon, J. W., 1984, Volcanogenic massive sulphide deposits Part 1: A descriptive model: Geoscience Canada, v. 11, p. 195–202.

Lydon, J. W., 1988, Volcanogenic massive sulphide deposits Part 2: Genetic models, in Ore Deposit Models: Geoscience Canada, v. 15, p. 155–181.

Manor, M. J., Piercey, S. J., Murphy, D. C., and Wall, C. J., 2022a, Age and Chemostratigraphy of the Finlayson Lake District , Yukon : Implications for Volcanogenic Massive Sulfide (VMS) Mineralization and Tectonics along the Western Laurentian Continental Margin: Lithosphere, v. 2022, p. 45.

Manor, M. J., Piercey, S. J., Wall, C. J., and Denisová, N., 2022b, High precision CA-ID-TIMS U-Pb zircon geochronology of felsic rocks in the Finlayson Lake VMS district, Yukon: Linking Paleozoic basin-scale accumulation rates to the occurrence of subseafloor replacement-style mineralization: Economic Geology, v. 117, p. 1173–1201.

Maslennikov, V. V., Maslennikova, S. P., Large, R. R., Danyushevsky, L. V., Herrington, R. J., Ayupova, N. R., Zaykov, V. V., Lein, A. Y., Tseluyko, A. S., Melekestseva, I. Y., and Tessalina, S. G., 2017, Chimneys in Paleozoic massive sulfide mounds of the Urals VMS deposits: Mineral and trace element comparison with modern black, grey, white and clear smokers: Ore Geology Reviews, v. 85, p. 64–106.

McClenaghan, S. H., Lentz, D. R., Martin, J., and Diegor, W. G., 2009, Gold in the Brunswick No. 12 volcanogenic massive sulfide deposit, Bathurst Mining Camp, Canada: Evidence from bulk ore analysis and laser ablation ICP-MS data on sulfide phases: Mineralium Deposita, v. 44, p. 523–557.

McPhie, J., and Allen, R. L., 1992, Facies Architecture of Mineralized Submarine Volcanic Sequences Central Volcanic Complex: Economic Geology, v. 87, p. 587–596.

McPhie, J., Doyle, M. G., and Allen, R. L., 1993, Volcanic Textures: A Guide to Interpretation of Textures in Volcanic Rocks: Hobart, Australia, University of Tasmania, 198 p.

Mercier-Langevin, P., Hannington, M. D., Dubé, B., and Bécu, V., 2011, The gold content of volcanogenic massive sulfide deposits: Mineralium Deposita, v. 46, p. 509–539.

Mumin, A. H., Scott, S. D., Somarin, A. K., and Oran, K. S., 2007, Structural controls on massive sulfide deposition and hydrothermal alteration in the South Sturgeon Lake Caldera, northwestern Ontario: Exploration and Mining Geology, v. 16, p. 83–107.

Murphy, D. C., Mortensen, J. K., Piercey, S. J., Orchard, M. J., and Gehrels, G. E., 2006, Mid-Paleozoic to early Mesozoic tectonostratigraphic evolution of Yukon-Tanana and Slide Mountain terranes and affiliated overlap assemblages, Finlayson Lake massive sulphide district, southeastern Yukon, in Colpron, M. and Nelson, J. L. eds., Paleozoic Evolution and Metallogeny of Pericratonic Terranes at the Ancient Pacific Margin of North America, Canadian and Alaskan Cordillera: Geologic Association of Canada, Special Paper 45, p. 75–106.

Nozaki, T., Nagase, T., Takaya, Y., Yamasaki, T., and Otake, T., 2021, Subseafloor sulphide deposit formed by pumice replacement mineralisation: Scientific Reports, v. 11, p. 1–11.

van Olden, K., Green, A., and Davidson, G., 2020, NI 43-101 Feasibility Study Technical Report Kudz Ze Kayah Property, Yukon, Canada CSA Global Report n. R173.2019: CSA Global, 376 p.

Peter, J. M., and Scott, S. D., 1997, Windy Craggy, northwestern British Columbia: The world's biggest Besshi-type deposit (C. T. Barrie & M. D. Hannington, Eds.): Reviews in Economic Geology 8, p. 261–295.

Peter, J. M., Layton-Matthews, D., Piercey, S. J., Bradshaw, G. D., Paradis, S., and Bolton, A., 2007, Volcanogenic-hosted massive sulphide deposits of the Finlayson Lake district, Yukon (W. D. Goodfellow, Ed.): Mineral Deposits of Canada: A Synthesis of Major Deposit-Types, District Metallogeny, the Evolution of Geological Provinces, and Exploration Methods: Geological Association of Canada, Mineral Deposits Division, Special Publication No. 5, p. 471–508.

Piercey, S. J., 2011, The setting, style, and role of magmatism in the formation of volcanogenic massive sulfide deposits: Mineralium Deposita, v. 46, p. 449–471.

Piercey, S. J., 2015, A semipermeable interface model for the genesis of subseafloor replacement-type volcanogenic massive sulfide (VMS) deposits: Economic Geology, v. 110, p. 1655–1660.

Piercey, S. J., Paradis, S., Murphy, D. C., and Mortensen, J. K., 2001, Geochemistry and paleotectonic setting of felsic volcanic rocks in the Finlayson Lake volcanic-hosted massive sulfide district, Yukon, Canada: Economic Geology, v. 96, p. 1877–1905.

Piercey, S. J., Squires, G. C., and Brace, T. D., 2014, Lithostratigraphic, hydrothermal, and tectonic setting of the Boundary volcanogenic massive sulfide deposit, Newfoundland Appalachians, Canada: Formation by subseafloor replacement in a Cambrian rifted arc: Economic Geology, v. 109, p. 661–687.

Piercey, S. J., Peter, J. M., and Herrington, R. J., 2015, Zn-rich volcanogenic massive sulphide (VMS) deposits, in Current Perspectives on Zinc Deposits: Irish Association for Economic Geology, p. 37–57.

Pilote, J. L., Piercey, S. J., and Mercier-Langevin, P., 2019, Evolution of the subseafloor hydrothermal system associated with the Ming VMS deposit, Newfoundland Appalachians, and its controls on base and precious metal distribution: Mineralium Deposita, v. 55, p. 913–936.

Relvas, J. M. R. S., Barriga, F. J. A. S., Ferreira, A., Noiva, P. C., Pacheco, N., and Barriga, G., 2006, Hydrothermal alteration and mineralization in the Neves-Corvo volcanic-hosted massive sulfide deposit, Portugal. I. Geology, mineralogy, and geochemistry: Economic Geology, v. 101, p. 1325.

Riverin, G., and Hodgson, C. J., 1980, Wall-rock alteration at the Millenbach Cu-Zn mine, Noranda, Quebec: Economic Geology, v. 75, p. 424–444.

Rosa, C. J. P., McPhie, J., Relvas, J. M. R. S., Pereira, Z., Oliveira, T., and Pacheco, N., 2008, Facies analyses and volcanic setting of the giant Neves Corvo massive sulfide deposit, Iberian Pyrite Belt, Portugal: Mineralium Deposita, v. 43, p. 449–466.

Sangster, D. F., 1980, Quantitative characteristics of volcanogenic massive sulphide deposits - Metal content and size distribution of massive sulphide deposits in volcanic centers: CIM Bulletin, v. 73, p. 74–81.

Sherlock, R. L., Roth, T., Spooner, E. T. C., and Bray, C. J., 1999, Origin of the Eskay Creek precious metal-rich volcanogenic massive sulfide deposit: Fluid inclusion and stable isotope evidence: Economic Geology, v. 94, p. 803–824.

Stix, J., Kennedy, B., Hannington, M. D., Gibson, H. L., Fiske, R., Mueller, W., and Franklin, J. M., 2003, Caldera-forming processes and the origin of submarine volcanogenic massive sulfide deposits: Geology, v. 31, p. 375–378.

Thurston, P. C., Ayer, J. A., Goutier, J., and Hamilton, M. A., 2008, Depositional gaps in Abitibi greenstone belt stratigraphy: A key to exploration for syngenetic mineralization: Economic Geology, v. 103, p. 1097–1134.

Tomkins, A. G., Pattison, D. R. M., and Frost, B. R., 2007, On the initiation of metamorphic sulfide anatexis: Journal of Petrology, v. 48, p. 511–535.

Tornos, F., 2006, Environment of formation and styles of volcanogenic massive sulfides: The Iberian Pyrite Belt: Ore Geology Reviews, v. 28, p. 259–307.

Urabe, T., Scott, S. D., and Hattori, K., 1983, A comparison of footwall-rock alteration and geothermal systems beneath some Japanese and Canadian volcanogenic massive sulfide deposits (H. Ohmoto & B. J. Skinner, Eds.): Economic Geology Monograph 5, p. 345–364.

Velde, B., 1978, Infrared spectra of synthetic micas in the series muscovite-MgAl celadonite: American Journal of Science, v. 63, p. 343–349.

Vikentyev, I. V., Belogub, E. V., Novoselov, K. A., and Moloshag, V. P., 2017, Metamorphism of volcanogenic massive sulphide deposits in the Urals. Ore geology: Ore Geology Reviews, v. 85, p. 30–63.

Walker, J.D., and Geissman, J.W., compilers, 2022, Geologic Time Scale v. 6.0: Geological Society of America

Yang, K., Huntington, J. F., Gemmell, J. B., and Scott, K. M., 2011, Variations in composition and abundance of white mica in the hydrothermal alteration system at Hellyer, Tasmania, as revealed by infrared reflectance spectroscopy: Journal of Geochemical Exploration, v. 108, p. 143–156.

Chapter 2

Lithostratigraphy, lithogeochemistry and tectono-magmatic framework of the ABM replacement-style volcanogenic massive sulfide (VMS) deposit, Finlayson Lake District, Yukon, Canada

2.1 Abstract

The Late Devonian ABM deposit is a bimodal-felsic, replacement-style volcanogenic massive sulfide (VMS) deposit within the Finlayson Lake district in Yukon, Canada. The deposit is hosted by predominantly felsic volcanic rocks of the upper Kudz Ze Kayah formation that were deposited in an active back-arc basin in three stratigraphic sequences consisting of interbedded felsic volcaniclastic rocks and argillites, felsic lava flows and domes, and felsic and mafic sills. The felsic rocks fall into two groups, Felsic A and Felsic B (FA and FB), based on immobile element abundances and their ratios. Relative to the FB group, the FA group has high Zr abundances (>550 ppm) and generally higher contents of high field strength elements. The FA/FB chemostratigraphy roughly coincides with the lithostratigraphic sequences. Sequence 2 hosting the mineralization consists of FB felsic rocks; the hanging-wall Sequence 3 and footwall Sequence 1 felsic rocks have FA signatures. An argillite lens, recording a period of volcanic quiescence, occurs at the upper contact of Sequence 2.

From reconstruction of the basin architecture, two sets of synvolcanic faults are inferred. The synvolcanic faults were interpreted based on thickness changes of volcanosedimentary units and the distribution of coherent rocks. During breaks in volcanism, synvolcanic faults acted as conduits for upwelling hydrothermal fluids, which were diverted laterally into unconsolidated volcaniclastic rocks and formed the replacement-style VMS mineralization. Although the mineralized lenses are hosted by FB felsic rocks, their replacement-style nature implies that the mineralizing processes occurred during the break in volcanism and were genetically associated with the overlying FA felsic volcanic rocks.

2.2 Introduction

Volcanogenic massive sulfide (VMS) deposits generally form in extensional environments at or near the sea floor by the mixing of cold seawater with hot hydrothermal fluids (± magmatic volatiles; Franklin et al., 1981, 2005; Tornos et al., 2015). The efficiency of the mineralizing process is highest where the mixing of metal-rich hydrothermal fluids with seawater occurs in the subsurface, which results in relatively larger tonnages and higher grades of replacement-style VMS deposits compared to mound-style (exhalative) deposits that formed on the sea floor (Allen et al., 2002; Doyle and Allen, 2003; Piercey, 2015). Despite the challenge of replacement texture identification in deformed and metamorphosed rocks, many deposits have lower strain zones where these features can be recognized (Doyle and Allen, 2003; Piercey, 2015; Lafrance et al., 2020), and when integrated with the stratigraphic reconstruction, architecture, and tectonic framework of basins (Allen et al., 1996a, b; Winter et al., 2004; Thurston et al., 2008; Belford et al., 2015; DeWolfe et al., 2018; Friesen et al., 2020) and lithogeochemistry of the host rocks (Barrett and MacLean, 1994; Barrett et al., 2001), an enhanced understanding of both ancient VMS deposits and their modern analogues, seafloor massive sulfide deposits (SMS), and their emplacement mechanisms can be achieved. Variations to this approach utilizing detailed stratigraphic facies analysis and lithostratigraphic reconstruction have been applied to numerous replacement-style VMS deposits of various ages globally, including the Abitibi district (Ansil deposit; Galley et al., 1995), the Mount Read Volcanics in Tasmania (South Hercules deposit; Zaw and Large, 1992), the Mount Windsor subprovince in Australia (Highway Reward deposit; Doyle and Huston, 1999), the Appalachians in Canada (Boundary deposit; Piercey et al., 2014), the Skellefte district in Sweden (Allen et al., 1996b), and the Iberian Pyrite Belt in Spain and Portugal (Tornos, 2006). Further research focusing on reconstructing the basin architecture of deposit-hosting extensional basins will help to illuminate the more cryptic aspects of replacement-style mineralization, such as the geometry of hydrothermal up-flow zones, the role of synvolcanic faults, and the timing of VMS mineralization in relation to volcanism and processes in underlying magma chambers.

The Finlayson Lake district, Yukon, Canada, consists of arc and back-arc rocks of the Yukon-Tanana and Slide Mountain terranes and hosts various styles of VMS deposits with >40 Mt of reported polymetallic VMS mineralization. The ABM deposit is a bimodal-felsic, replacement-style VMS deposit that contains a mineral resource of 19.1 Mt at 6.6 wt % Zn, 0.9 wt % Cu, 2.0 wt % Pb, 1.4 g/t Au, and 156 g/t Ag (van Olden et al., 2020). The ABM deposit is one of five polymetallic VMS deposits discovered in the district in the 1990s that initiated a number of regional-scale (Murphy, 1998; Piercey, 2001; Piercey et al., 2001, 2003; Murphy et al., 2006; Manor and Piercey, 2019) and deposit-scale studies (Boulton, 2002; Sebert et al., 2004; Peter et al., 2007; Layton-Matthews et al., 2013; McDonald et al., 2018), with particular attention paid to the Zn-enriched Wolverine deposit (Bradshaw et al., 2008; Piercey et al., 2008, 2016; Piercey and Kamber, 2019). In 2015, an extensive drilling campaign (BMC Minerals Ltd.) further delineated the ABM deposit and led to the discovery of the Krakatoa mineralized zone in the immediate vicinity of the ABM deposit (van Olden et al., 2020). This discovery renewed interest in the mineralization potential of the host rocks in the Finlayson Lake district, as much of the area remains underexplored. The new discovery and the recently reinterpreted replacement-style nature of the massive sulfide mineralization (van Olden et al., 2020; Manor et al., 2022) call for further study and re-evaluation of the lithostratigraphic and tectonic framework of the ABM deposit. The relatively low degree of metamorphism (greenschist facies) and deformation together with abundant available drill core from the deposit and its vicinity make the ABM deposit an ideal site to study a Late Devonian back-arc basin environment that hosts replacement-style VMS mineralization. This study uses detailed core logging, lithofacies analysis, and lithogeochemistry to: 1) create a reconstruction of the ABM deposit with respect to its lithostratigraphy and tectonic framework, 2) determine what specific characteristics of the reconstructed environment are linked to the replacement-style VMS mineralization at the ABM deposit, and 3) compare our results with previous larger-scale petrogenetic and metallogenic studies in the Finlayson Lake district to evaluate how our interpretations fit with previous ones. The collected data and derived interpretations are presented in this paper in the form of long sections and cross sections through the deposit. Our results highlight the Late Devonian back-arc basin architecture during which the bimodal, but mostly felsic, volcanism and associated VMS mineralization occurred. The diagnostic features of VMS mineralization in the ABM deposit, including the lithostratigraphy, lithogeochemistry, and structure, are defined in this study and have potential to be utilized in further exploration in the Finlayson Lake district, the northern Cordillera, and analogous ancient environments worldwide.

2.3 Regional Geology

The Finlayson Lake district in southeastern Yukon is a dismembered block of the Yukon-Tanana and Slide Mountain terranes that developed along the western margin of Laurentia throughout the Mid-Paleozoic to the Permo-Triassic (Fig. 2.1; Colpron et al., 2006; Nelson et al., 2006; Piercey et al., 2006). The Yukon-Tanana terrane is an allochthonous peri-Laurentian package that consists of distinct arc–back-arc assemblages that underlie parts of the Yukon, Alaska, and northern British Columbia (Nelson et al., 2006). It comprises a poly-deformed and metamorphosed pre-Late Devonian continental margin assemblage (Snowcap assemblage; Piercey and Colpron, 2009) that is overlain by three unconformity-bound Late Devonian to Middle to Late Permian continental arc, back-arc, and ocean basin-related volcano-sedimentary sequences that underwent variable degrees of metamorphism and deformation (Mortensen and Jilson, 1985; Mortensen, 1992; Colpron et al., 2006; Murphy et al., 2006). The pre-Late Devonian basement of the Yukon-Tanana terrane is not exposed in the Finlayson Lake district, but is characterized as Laurentian-derived, pericontinental crustal material (Piercey et al., 2001, 2003, 2017; Piercey and Colpron, 2009). In the Eocene, the Finlayson Lake district was displaced from its original location approximately 430 km along the dextral strike-slip Tintina fault (Gabrielse et al., 2006).

The Finlayson Lake district is composed of Late Devonian to Permian metasedimentary, metavolcanic, and plutonic rocks that have undergone variable degrees of deformation (Murphy et al., 2006). The core of the Finlayson Lake district reached amphibolite facies metamorphic grade, which transitions to lower greenschist facies further from the center of the district (Murphy et al., 2006). The rocks of the Yukon-Tanana terrane in the Finlayson Lake district occur in three structurally bounded stratigraphic sequences: the Big Campbell, Money Creek, and Cleaver Lake thrust sheets (Fig. 2.2). The largest of these blocks by volume is the structurally deepest Big Campbell

Figure 2.1. Regional geologic setting of the Finlayson Lake district, Yukon-Tanana, and Slide Mountain terranes (modified after Murphy et al., 2006). Numbers mark the positions of known VMS deposits in the region. BCT = Big Campbell thrust; CLT = Cleaver Lake thrust; JCF = Jules Creek fault; MCT = Money Creek thrust; NRF = North River thrust.

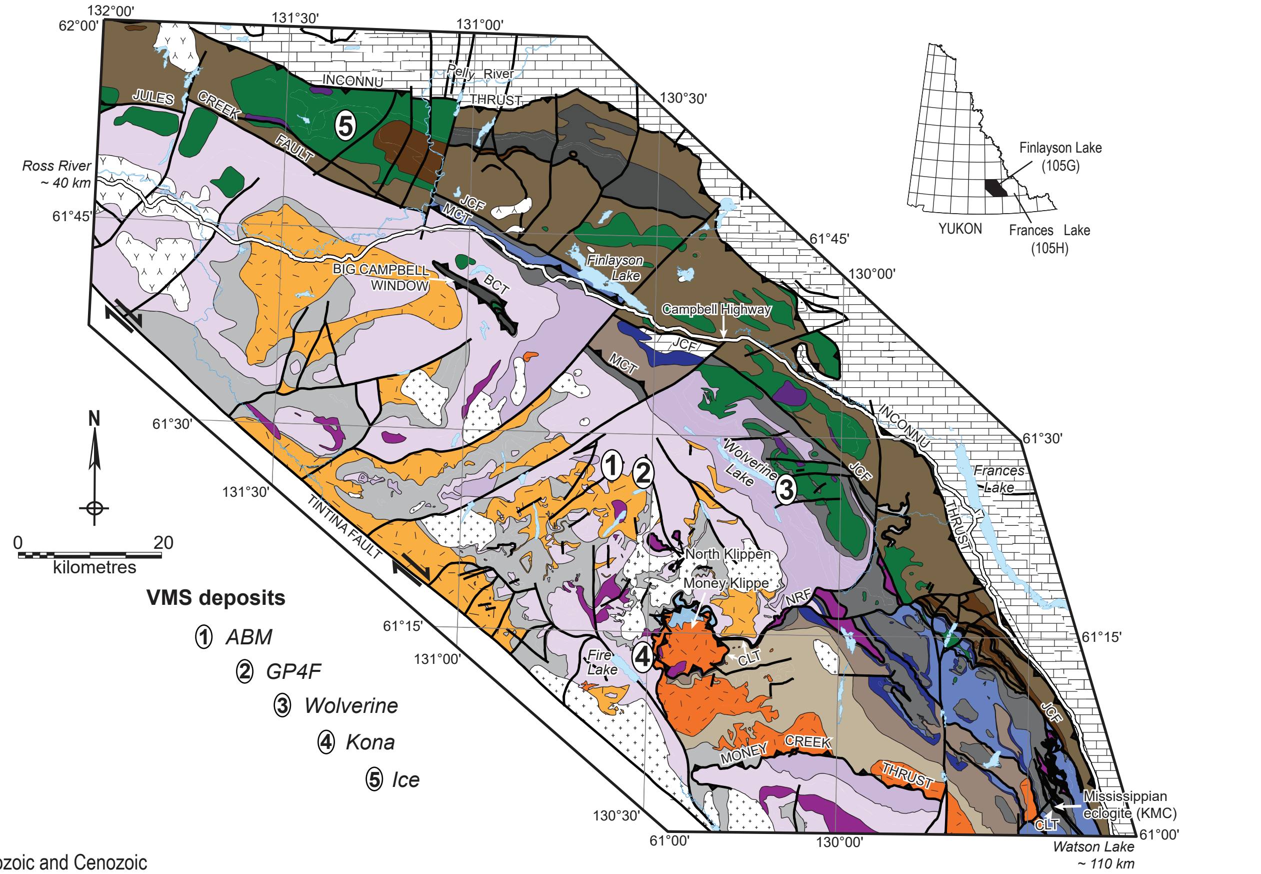

Mesozoic and Cenozoic

- undifferentiated intrusions
- undifferentiated volcanic rocks

North American Continental Margin

Triassic

- dark shale, siltstone and limestone

Paleozoic

- undifferentiated formations of Selwyn Basin, Cassiar/McEvoy Platform, Earn Group and Mt. Christie Formation

Post - YTT / SMT Amalgamation

Triassic

- grey shale, siltstone and limestone

Permian - Triassic

SIMPSON LAKE GROUP

- polymictic conglomerate, sandstone, siltstone, mafic and felsic volcanic rocks, limestone

Slide Mountain terrane

INTRUSIVE ROCKS

Early Permian

- ultramafic and mafic intrusions

LAYERED ROCKS

Lower to Middle Permian

Gatehouse formation

- limestone and quartzite

Slide Mountain terrane

Lower Permian

Campbell Range formation

- basalt and varicoloured chert

Carboniferous to Permian?

FORTIN CREEK GROUP

- dark phyllite and chert, varicoloured chert, chert-pebble conglomerate, sandstone, limestone, felsic and mafic metavolcanic rocks

Yukon-Tanana terrane

INTRUSIVE ROCKS

Early Mississippian

SIMPSON RANGE PLUTONIC SUITE

- granite, quartz monzonite, granodiorite

Late Devonian to Early Mississippian

GRASS LAKES PLUTONIC SUITE

- granite, quartz monzonite augen granite
- ultramafic and mafic rocks, Big Campbell and Cleaver Lake thrust sheets

LAYERED ROCKS

Lower Permian

Money Creek formation

- dark phyllite and sandstone, chert, chert-pebble conglomerate, diamictite

Mid-Pennsylvanian to Lower Permian

Finlayson Creek limestone

- massive bioclastic limestone

Yukon-Tanana terrane

Upper Mississippian to mid-Pennsylvanian

undifferentiated White Lake and King Arctic formations

- green and pink chert, limestone, sandstone, conglomerate, mafic metavolcanic rocks

Upper Mississippian

Whitefish limestone

- massive bioclastic limestone

Lower Mississippian

Tuchitua River formation

- intermediate, felsic and mafic volcanic rocks, sandstone, chert, limestone

WOLVERINE LAKE GROUP

- undifferentiated mafic and felsic volcanic rocks and dark clastic rocks

Upper Devonian to Lower Mississippian

Cleaver Lake formation

- calc-alkaline basalt, rhyolite, chert and volcanic-derived sandstone

Waters Creek formation

- felsic to intermediate metavolcanic rocks and carbonaceous phyllite

GRASS LAKES GROUP

- undifferentiated mafic and felsic volcanic rocks and dark clastic rocks of the Fire Lake, Kudz Ze Kayah and Wind Lake formations

Pre-Upper Devonian

North River formation

- quartzose metaclastic rocks, marble and non-carbonaceous pelitic schist

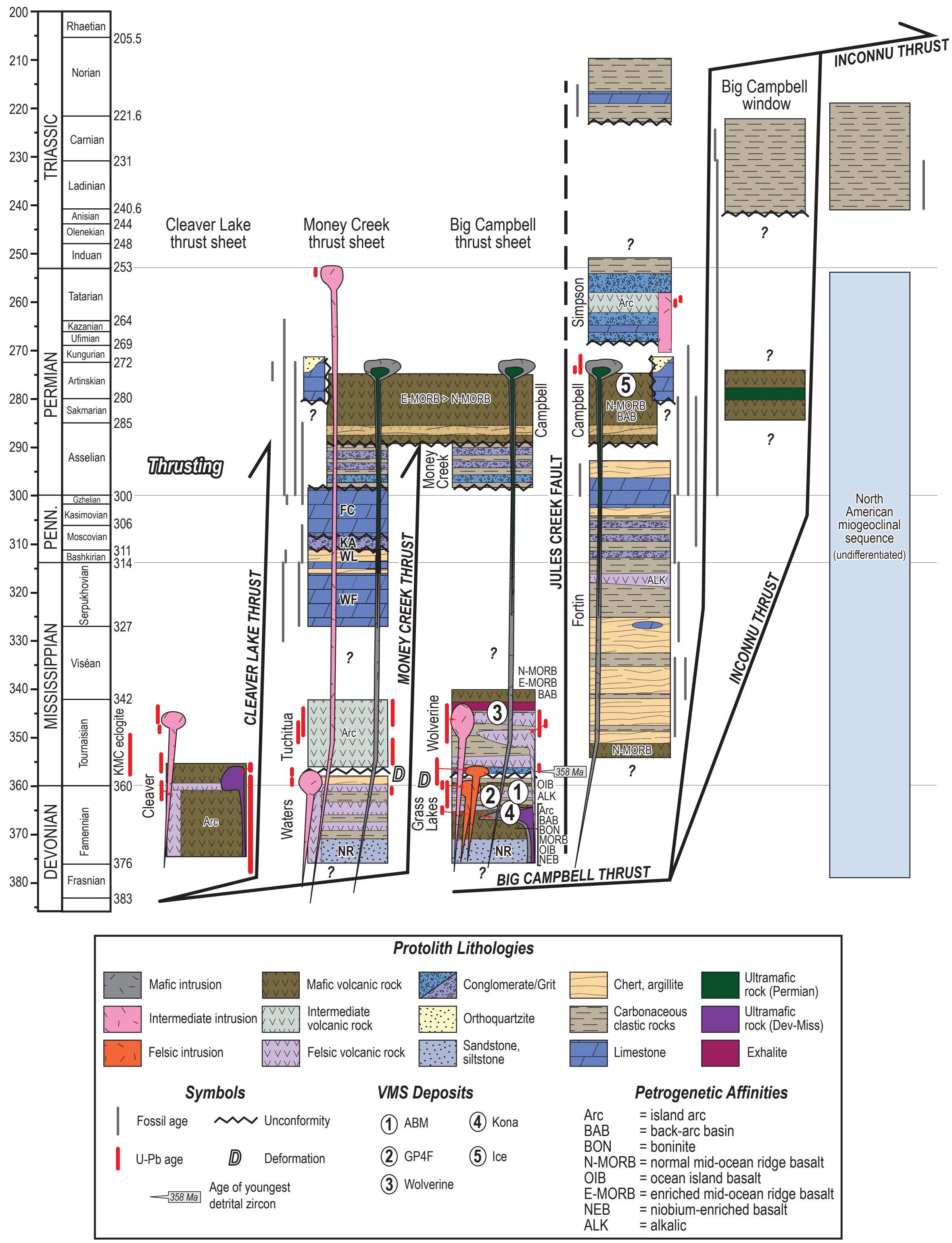

Figure 2.2. Composite chronostratigraphic column for the Finlayson Lake district showing stratigraphic and structural relationships. Locations of VMS deposits, petrogenetic affinities of volcanic rocks and U-Pb and fossil ages are displayed on the diagram (modified after Murphy et al., 2006; Piercey et al., 2016; Manor and Piercey, 2018).

thrust sheet, which consists of Upper Devonian metaclastic rocks of the North River formation, the Upper Devonian Grass Lakes group, and the Lower Mississippian Wolverine Lake group (Fig. 2.2; Murphy et al., 2006). The Grass Lakes group comprises three rock units: the Fire Lake, Kudz Ze Kayah, and Wind Lake formations (Fig. 2.2). The Fire Lake formation comprises mafic metavolcanic and lesser amounts of mafic and ultramafic meta-subvolcanic rocks (Piercey et al., 2002a; Murphy et al., 2006), and hosts the Kona Cu-Au VMS deposit (Sebert et al., 2004; Peter et al., 2007) containing a geologic resource of 10.5 Mt at 1.6 wt % Cu, 0.63 g/t Au, and 4 g/t Ag (BMC Minerals). The Kudz Ze Kayah formation is interpreted to be stratigraphically above the Fire Lake formation and is characterized by dominantly felsic volcanic and sedimentary rocks with back-arc geochemical affinities (Piercey et al., 2001; Murphy et al., 2006). The Wind Lake formation sits conformably on top of the Kudz Ze Kayah formation and consists of interlayered carbonaceous sedimentary rocks and alkalic mafic volcanic rocks with minor quartzite (Piercey et al., 2002b). All rocks in the Grass Lakes group are intruded by the Grass Lakes plutonic suite at ca. 361 Ma (Piercey et al., 2001, 2003; Manor et al., 2022). The Wolverine Lake group unconformably overlies the Grass Lakes group and contains basal conglomerates, sandstones, felsic volcanic rocks, carbonaceous phyllite/shale, ironstones, and basaltic rocks (Murphy and Piercey, 1999; Bradshaw et al., 2001). The Wolverine felsic-siliciclastic type VMS deposit lies on the contact between carbonaceous phyllite and felsic volcanic rocks and contains a geologic resource of 6.2 Mt at 12.9 wt % Zn, 1.5 wt % Pb, 1.4 wt % Cu, 1.81 g/t Au, and 359 g/t Ag (Bradshaw et al., 2008). Structurally above the Big Campbell thrust sheet sits the Money Creek thrust sheet, which is made up of rocks of the same age but formed primarily in an arc environment (Murphy et al., 2006). The Cleaver Lake thrust sheet comprises Late Devonian through Early Mississippian and Early Permian rocks formed in an arc environment and is the uppermost structural panel (Murphy et al., 2006).

2.3.1 VMS mineralization in the Kudz Ze Kayah formation

The ABM and the GP4F VMS deposits are located about 25 km south of Finlayson Lake and the Robert Campbell Highway (Fig. 2.1). The deposits were discovered in the early 1990s by Cominco, following surficial geochemical surveys, and subsequently drilled between 1994 and 1998 (Peter et al., 2007). The GP4F deposit is located roughly 5 km southeast of the ABM deposit (Fig. 2.1) and sits 500 to 600 m stratigraphically below the ABM deposit (Peter et al., 2007; Manor et al., 2022), which itself sits about 150 to 250 m below the contact between the Kudz Ze Kayah and Wind Lake formations. Subseafloor replacement is interpreted to be the primary mineralization style in both deposits (Peter et al., 2007; van Olden et al., 2020; Manor et al., in press), with the most common ore minerals being pyrite, pyrrhotite, sphalerite, chalcopyrite, and galena, and the most common gangue minerals being barite, carbonate minerals, chlorite, quartz, white mica, and Fe carbonate minerals. The GP4F deposit has a geologic resource of 1.5 Mt at 6.4% Zn, 3.1% Pb, 0.1% Cu, 2.0 g/t Au, and 81.7 g/t Ag (MacRobbie and Holroyd, unpub. data) and was described by Boulton (2002). Previous studies of the ABM deposit defined the deposit as an isoclinally folded massive sulfide lens (Peter et al., 2007; Layton-Matthews et al., 2008, 2013); however, more recent (2015–2018) extensive drilling in the deposit area shows replacement-style textures within the orebodies and does not show any evidence of significant folding. A chronostratigraphic study by Manor et al. (2022) dated the rocks hosting the GP4F deposit at 363.254 ± 0.098 Ma, and showed that the ABM deposit is hosted by rocks formed at 362.82 ± 0.12 Ma. Manor et al. (2022) have also suggested that the volcanic activity responsible for the deposition of the Kudz Ze Kayah formation lasted approximately 0.65 to 1.0 m.y., which indicates that rapid deposition and emplacement of volcano-sedimentary rocks played an important role in the formation of both VMS deposits.

2.4 Geology, Lithofacies, Mineralization, and Alteration of the ABM Deposit

2.4.1 Observations and sampling methodology

Fifty-one drill holes and ~10 km of core were logged at 1:400 scale. Lithology, primary textures, grain size, mineralogy, and alteration type and intensity based on mineral occurrence (quartz, white mica, chlorite, biotite, carbonate minerals, and sulfide minerals) were recorded in graphic logs for each unit. Hydrothermal alteration associated with VMS mineralization and greenschist facies metamorphism affected the Kudz Ze Kayah formation in the area of the deposit, but distinguishable primary textures and relationships between units are preserved in mapable sections of the stratigraphy (Piercey et al., 2001; this study). All rock names are presented without metamorphic prefixes, and primary volcanic and sedimentary terminology is used to highlight the remnant primary features observed in the rocks. Volcaniclastic rocks are classified using the nomenclatures outlined in White and Houghton (2006) and Fisher (1966). These classification schemes are based on clast size and abundance and are used with no genetic implications. Sampling aimed to acquire a comprehensive collection of the most common lithofacies and alteration styles distributed in the ABM deposit. Overall, 478 samples were collected. Petrographic studies of 82 samples representing the major lithostratigraphic facies are incorporated in the descriptions below. Presented stratigraphic sections and 3-D digital models of lithostratigraphic units, lenses of mineralization, and faults are based primarily on the detailed drill logs of this study. To further constrain the modeled units, core photographs, logs, and assays provided by BMC Minerals Ltd. were utilized. Company data sets were only used as supportive, not principal, sources of data, apart from the wholerock Ba values. All models and interpretations carry a higher degree of uncertainty due to the limited extent of the drilling below the mineralized horizon. Digital models were created using Leapfrog Geo 5.0 software developed by Seequent.

2.4.2 Geology of the upper Kudz Ze Kayah formation

Rocks that host the ABM deposit occupy the top ~350 m of the >500-m-thick Kudz Ze Kayah formation. The stratigraphy dips between 20° and 30° to the north-northeast and is relatively intact, as field observations and stratigraphic reconstructions do not indicate any fault repetition or major folding, as was suggested by previous studies (van Olden et al., 2020). The East fault is a regional-scale fault and divides the deposit area into two zones: the ABM zone and the Krakatoa zone (Fig. 2.3). The ABM deposit occurs 200 ± 50 m below the transitional contact between the Kudz Ze Kayah and Wind Lake formations. The Wind Lake formation consists of interbedded mafic tuff and argillite near and at the contact with the Kudz Ze Kayah formation. Primary bedding (S_0) is recognized in argillite and mafic tuff of the Wind Lake formation, with S_1 subparallel to S_0; this is observed in argillite and strongly altered units with abundant mica and chlorite (van Olden et al., 2020). Minor S_2 folds and crenulation occur within argillites and rocks with a higher degree of alteration in both formations, but these are not indicative of any large-scale patterns on a deposit scale (van Olden et al., 2020). Lithostratigraphic units are commonly continuous over hundreds of meters, but several of them, such as the mafic sills, argillite lenses, and some felsic sills can be traced up to 500 to 1,000 m throughout the ABM or Krakatoa zones. The upper portion of the Kudz Ze Kayah formation can be informally divided into three sequences based on the graphic drill logs (Fig. 2.4), from stratigraphically oldest to youngest: Sequence 1, Sequence 2, and Sequence 3. The Krakatoa zone generally corresponds stratigraphically to the ABM zone but contains more voluminous volcanic and subvolcanic rocks.

Each sequence consists of interbedded felsic volcaniclastic rocks and minor sedimentary rocks and domes and flows that were intruded by felsic sills and mafic sills and dikes. The lithofacies are described in detail below. Sequence 1 is the lowermost stratigraphic sequence and consists of interbedded felsic tuff, lapilli tuff, felsic subvolcanic rocks, and rare argillite lenses. Its lower contact is unknown due to minimal drilling below the mineralized horizon but extends at least a minimum of 100 m below the contact between Sequence 1 and Sequence 2. Sequence 2 hosts the mineralization and consists of interbedded felsic tuff and lapilli tuff and minor argillite lenses and contains felsic lava flows, two mafic sills, and abundant felsic sills. In the ABM zone, Sequence 2 varies in thickness between 45 and 120 m (average ~100 m), and generally thins down-dip towards the north-northeast. Its lower boundary is defined by the lower contact of the deepest mafic sill; the upper boundary is located at the laterally most extensive argillite lens. Sequence 2 in the Krakatoa zone consists predominantly of felsic volcanic and subvolcanic rocks and mafic sills. At the upper contact, there is a single lens of argillite, defining the boundary with Sequence 3. Sequence 3 sits on top of Sequence 2 and is composed of interbedded lapilli tuff, crystal-rich tuff, tuff, argillite lenses, and felsic lava flows and sills. In the Krakatoa zone within Sequence 3, flows and sills are more common than in the ABM zone. Thin, fine-grained mafic sills commonly intrude Sequence 3.

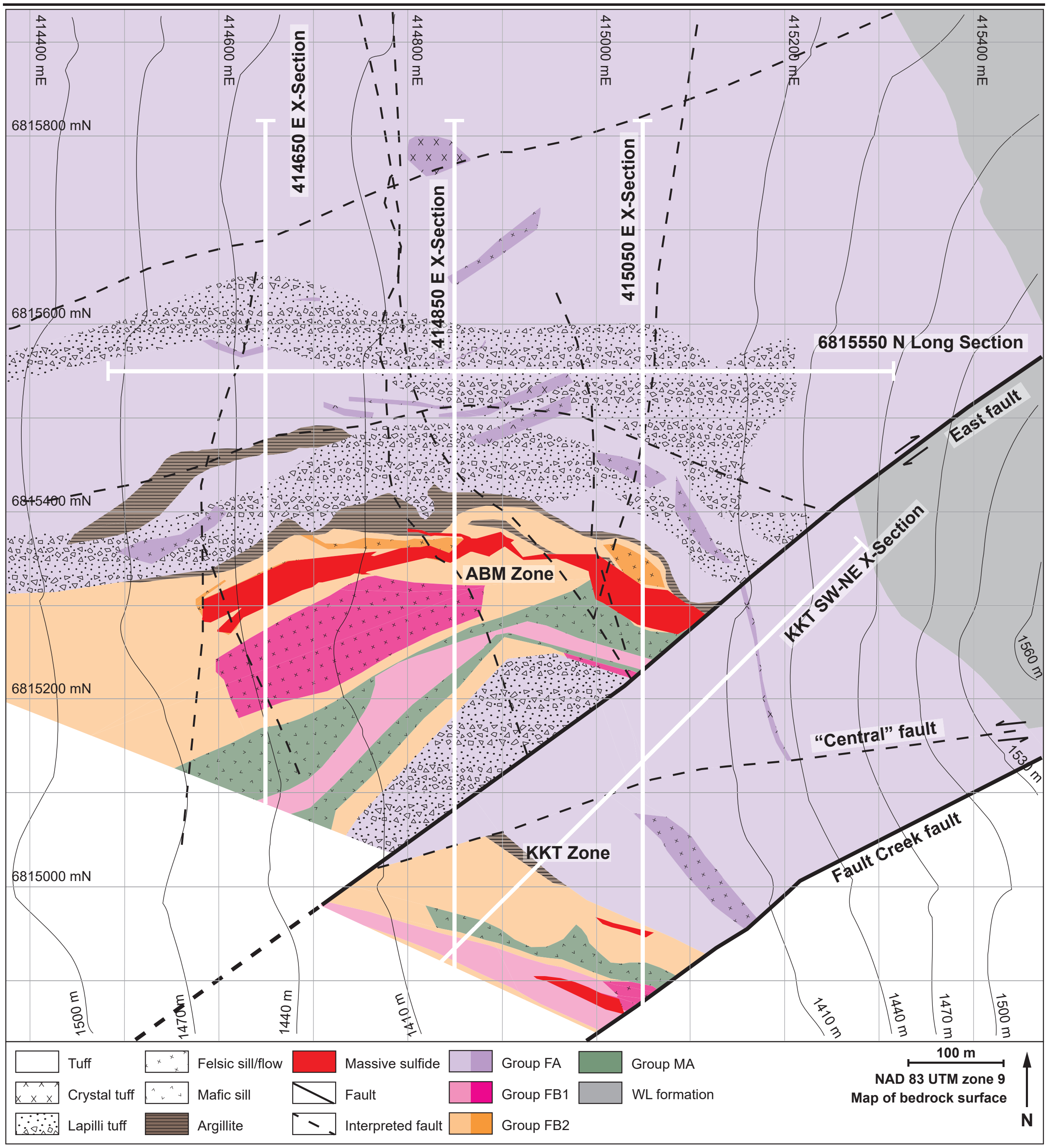

Figure 2.3. Local geology of the ABM deposit. Map units constructed using drilling data and 3D models of litho-stratigraphic units, massive sulfide lenses, and interpreted faults. Displayed lines refer to long section in Figure 2.4 and cross sections in Figures 2.11 and 2.12. Note that lithofacies are displayed using patterns and geochemical groups using colors.

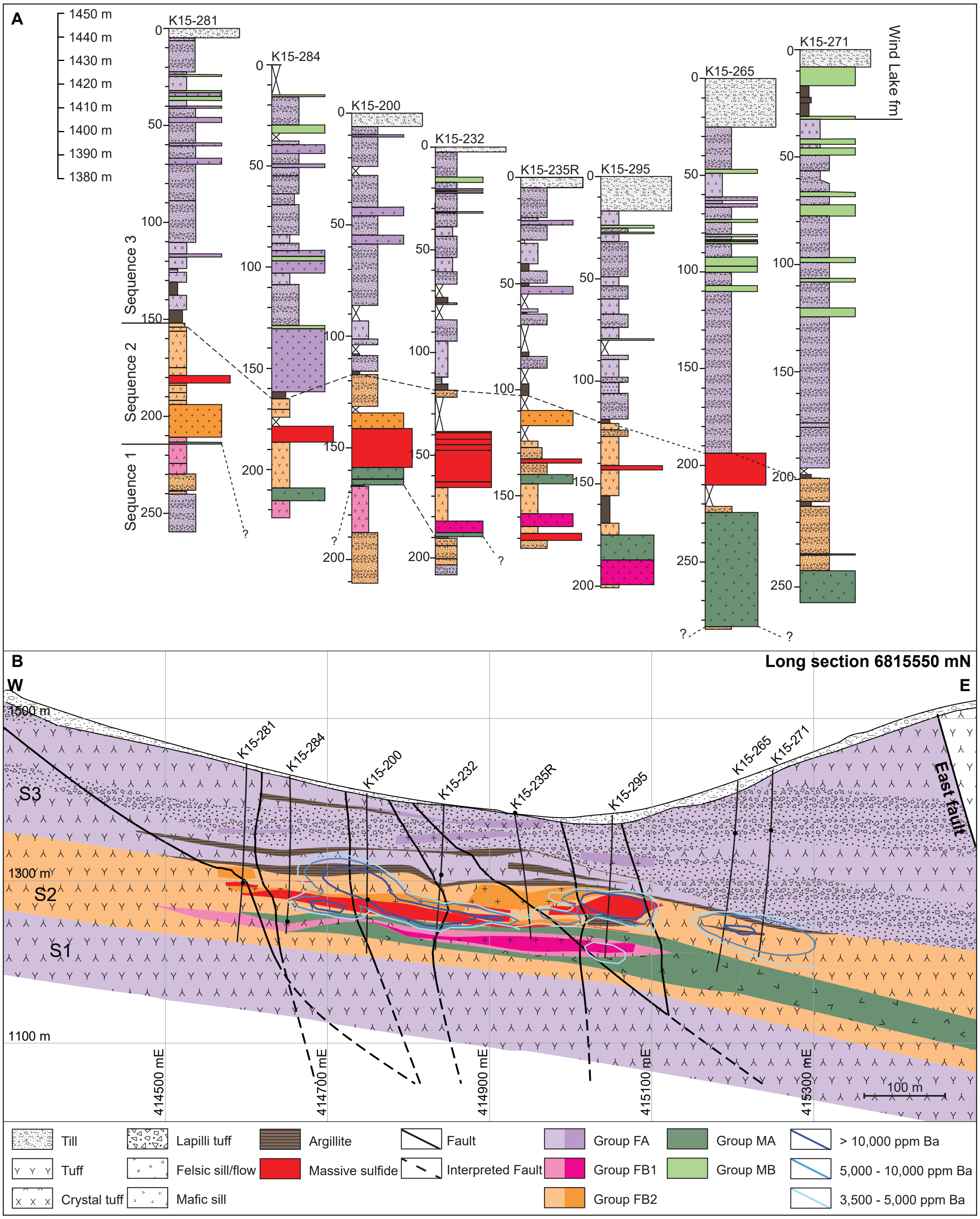

Figure 2.4. Simplified long section through the ABM zone of the ABM deposit with representative graphic logs. Section line position shown in Figure 2.3. Lighter hues of colors representing felsic rocks indicate volcaniclastic rocks. (A) Drill hole collars are arranged according to elevation, drill hole depth adjusted for dip. (B) Long section running W-E, looking north. Drill holes were drilled dipping between -50° and -70° towards the south and their traces are not clipped to section, pierce points through section plane are marked. S1 = Sequence 1, S2 = Sequence 2, S3 = Sequence 3.

2.4.2.1 Felsic volcaniclastic facies

Rocks of rhyolitic/dacitic composition occur within the volcano-sedimentary pile hosting the ABM deposit. Fabric in felsic volcaniclastic rocks is commonly defined by thin micaceous layers that are composed of thin white mica blades. These micaceous layers are up to 1 to 3 mm thick. Petrographic observations from less altered parts of the deposit suggest that the micaceous bands were at least partially formed by pervasive replacement of feldspar phenocrysts and subsequent recrystallization and deformation (Fig. 2.5A). Volcaniclastic rocks have transitional contacts between the different facies; graded bedding within tuffaceous layers is rare (Fig. 2.6A). Individual lapilli tuff lenses can be up to 70 m thick. Volumetrically minor sections of volcaniclastic rock show undulating foliation with minor scale folding (<0.5 m wavelength), commonly in association with argillite lenses or where the rocks are strongly altered. In the text below, the felsic volcaniclastic lithofacies are further divided into subfacies.

2.4.2.1.1 Tuff

Felsic tuffs are fine-grained to very fine-grained with abundant thin white mica-rich layers that define the major fabric of the rock. Tuffs are typically moderately to poorly sorted and locally thinly to very thinly bedded (Fig. 2.6B) with only minor lapilli or feldspar crystals (Fig. 2.6C) occurring locally within the tuffs. The facies predominantly contains quartz, white mica, minor K-feldspar and plagioclase, minor carbonate minerals, and trace disseminated pyrite. In thin section, quartz grains occur in lenses of similar grain size (Fig. 2.5B), with only minor mica and carbonate minerals within these lenses/patches; white mica occurs between these lenses in bands that define the rock fabric.

2.4.2.1.2 Crystal-rich tuff

Felsic crystal-rich tuffs contain quartz and/or K-feldspar crystals within a tuffaceous matrix (Fig. 2.5C) that is fine-grained to very fine-grained and contains quartz, white mica, minor K-feldspar and/or plagioclase, and minor carbonate minerals. Quartz crystals are commonly rounded or subrounded, bluish, locally gray, up to 7 mm in diameter, and can compose up to 10 modal % of the rock (Fig. 2.6D). K-feldspar crystals are subhedral to euhedral, up to 30 mm, and can compose up to 40 modal % of the rock (Fig. 2.6E). Crystal-rich tuffs are commonly poorly sorted and transition gradually to non-crystal–rich tuffs, and lapilli tuffs locally transition to crystal-rich tuffs.

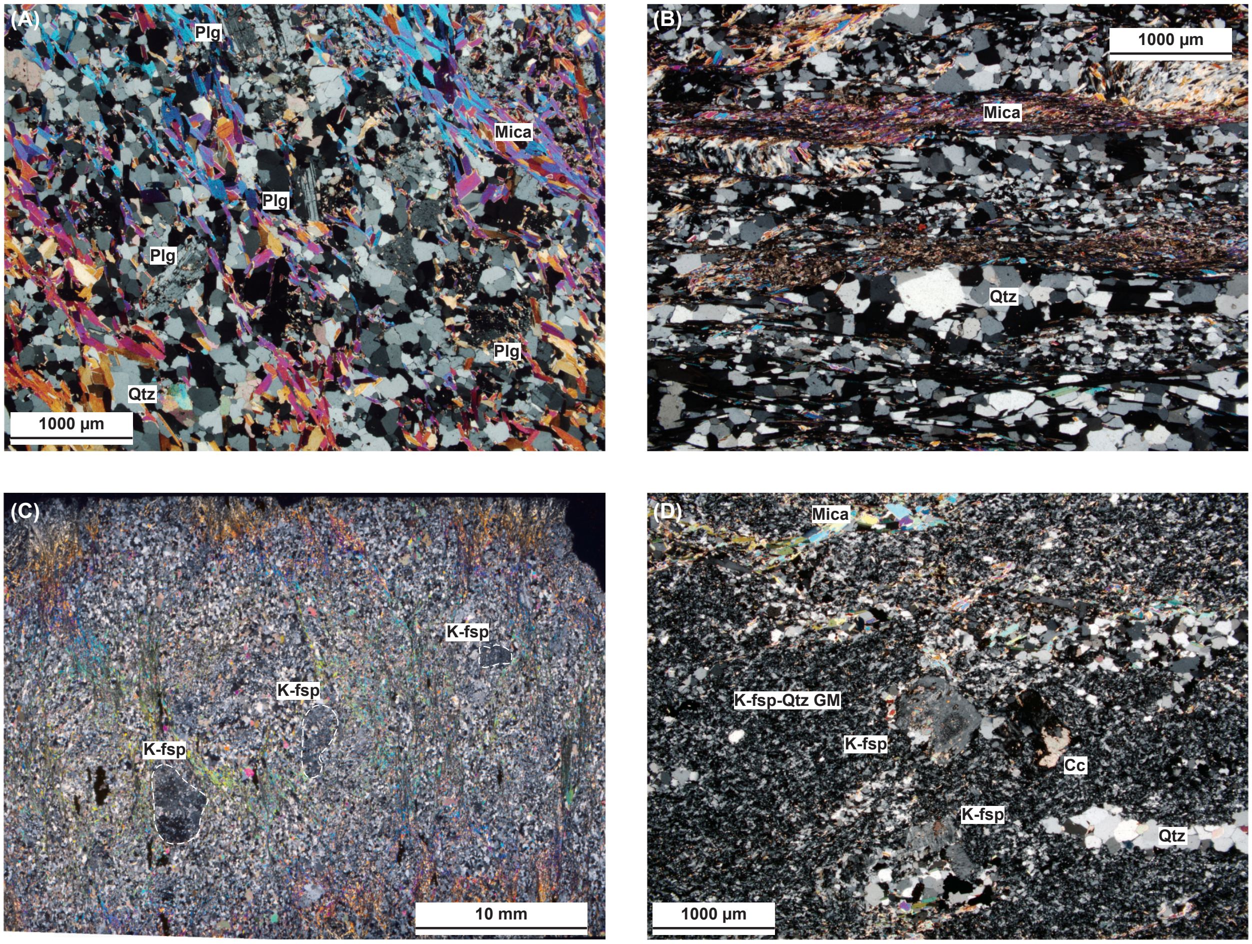

Figure 2.5. Microscopic textures preserved in host rocks from the ABM VMS deposit. (A) Groundmass of crystal-rich tuff, plagioclase grains are weakly to moderately sericitized and overprinted by later white mica fabric; K15-233, 108.1 m downhole. (B) Matrix of lapilli tuff; lenses composed of quartz grains of varying grain size, fine-grained mica fabric in between lenses; K16-370, 277 m down hole. (C) Large K-feldspar crystals, partially sericitized in fine-grained quartz-K-feldspar matrix, later white mica bands overprinting matrix; K15-260, 57.1 m downhole. (D) Felsic lava flow with preserved very fine-grained groundmass consisting of quartz-K-feldspar with preserved K-feldspar phenocrysts that are moderately sericitized and overprinted by calcite, minor later white mica replacing coarser quartz and K-feldspar grains; K15-315, 151.65 m downhole. Cc = calcite, K-fsp = K-feldspar, Mica = white mica, Qtz = quartz, Plg = plagioclase.

2.4.2.1.3 Lapilli tuff

Felsic lapilli tuffs consist of up to 60 to 80 modal % lapilli that are contained within a fine-grained to very fine-grained tuffaceous matrix. White mica, quartz, minor K-feldspar and/or plagioclase, and local, trace disseminated sulfide minerals (pyrite, pyrrhotite) compose the matrix. Lapilli fragments and the matrix are commonly flattened, exhibiting a well-defined structural fabric with the matrix consisting of very fine-grained, white mica-rich layers (Fig. 2.6F). The rock fabric is locally gently to strongly folded. Lapilli fragments that are not flattened are commonly subangular. The lapilli are typically felsic and have a similar composition to the matrix (quartz-white mica). Locally, the lapilli are more altered than the matrix and are inferred to have originally been more porous, possibly even pumice clasts. The lapilli are locally altered to Fe carbonate, quartz, pyrite and white mica. In some units, the lapilli tuffs contain lithic fragments/clasts with abundant chlorite-biotite and quartz patches, and minor Fe carbonate minerals (Fig. 2.6G). Lapilli tuff units are commonly poorly sorted and massive but can grade into tuffs or crystal-rich tuffs.

2.4.2.2 Coherent felsic lithofacies

These lithofacies consist of aphyric rhyolite/dacite with only minor phenocrysts and are very fine-grained. The lithofacies consist predominantly of quartz, minor white mica, K-feldspar, plagioclase, chlorite, and trace sulfide minerals (pyrite, pyrrhotite). Rarely, K-feldspar porphyritic textures are present, with euhedral K-feldspar phenocrysts up to 30 mm comprising up to 5 modal % of rock. The rocks are gray-white to beige-buff, but are locally orange, and rarely pink (Fig. 2.6H). Locally, aphyric rhyolite/dacite display flow banding (Fig. 2.6I) or contains quartz-filled amygdales. Contacts with surrounding rocks can be sharp, but commonly the margins consist of flattened hyaloclastite (Fig. 2.6K). Locally, perlitic fracturing (Fig. 2.6J) occurs on contacts. Units with hyaloclastite or brecciation on contacts, and/or with flow banding and amygdales, indicate deposition on the sea floor or at very shallow depths below the sea floor as individual flows (McPhie et al., 1993). We interpret these units as flows; they have aspect ratios between 1:2.5 and 1:4 and occur within all three sequences. The units with mostly sharp contacts and coherent interiors are interpreted to have been emplaced as subvolcanic sills (Gibson et al., 1999) and have aspect ratios

~1:1.5. The coherent interior of the sills is typically fractured with quartz veinlets with associated carbonate minerals, biotite, and/or sulfide minerals (pyrite, pyrrhotite).

2.4.2.3 Mafic sills

2.4.2.3.1 Sills in Sequence 2

In the ABM zone, mafic subvolcanic rocks are present as two main sills with a relatively uniform thickness (~10 m) that increases towards the east of the ABM zone (max. thickness 40 m). The Krakatoa zone contains one main sill with varying thickness (20–100 m) and three minor sills protruding from the main body. In both zones, the mafic sills occur in Sequence 2, where they intrude the volcano-sedimentary pile and are emplaced along contacts of a pre-existing felsic sill. In the eastern part of the ABM zone, the lower mafic sill crosscuts the pre-existing felsic sill. The mafic sills have chilled margins that are fine- to medium-grained (Fig. 2.6L) and gradually transition to coarser grain sizes in the interior of the sills, where clumps of amphibole occur within the fine-grained groundmass (Fig. 2.6M). The sills consist of minor primary pyroxene and plagioclase and contain alteration minerals including amphibole, biotite, chlorite, carbonate minerals, epidote, K-feldspar, white mica, and minor quartz that replace 90 to 95% of the primary minerals. The finer-grained contacts of the sills are more strongly altered relative to the interiors of the sills where chlorite-carbonate alteration occurs with disseminated biotite. Euhedral-subhedral pyrrhotite-pyrite composite grains up to 2.5 cm occur within the coarse-grained parts of the sills.

2.4.2.3.2 Sills in Sequence 3

Thin mafic sills occur predominantly in the hanging wall of the massive sulfide lenses, commonly in Sequence 3 below the lower Wind Lake formation contact. The sills have sharp contacts and are commonly emplaced bedding-parallel to the felsic volcaniclastic rocks (Fig. 2.6N). Locally, the sills crosscut the bedding at a low angle. Sills are dark green or buff and are commonly fine- to very fine-grained and massive. Their thickness is commonly between 10 cm and 1 m, but can be up to 2.5 m and locally, in rare cases, can be up to 8.5 m. Chlorite and biotite alteration is common, as are overprinting carbonate minerals, quartz, and quartz-carbonate veins.

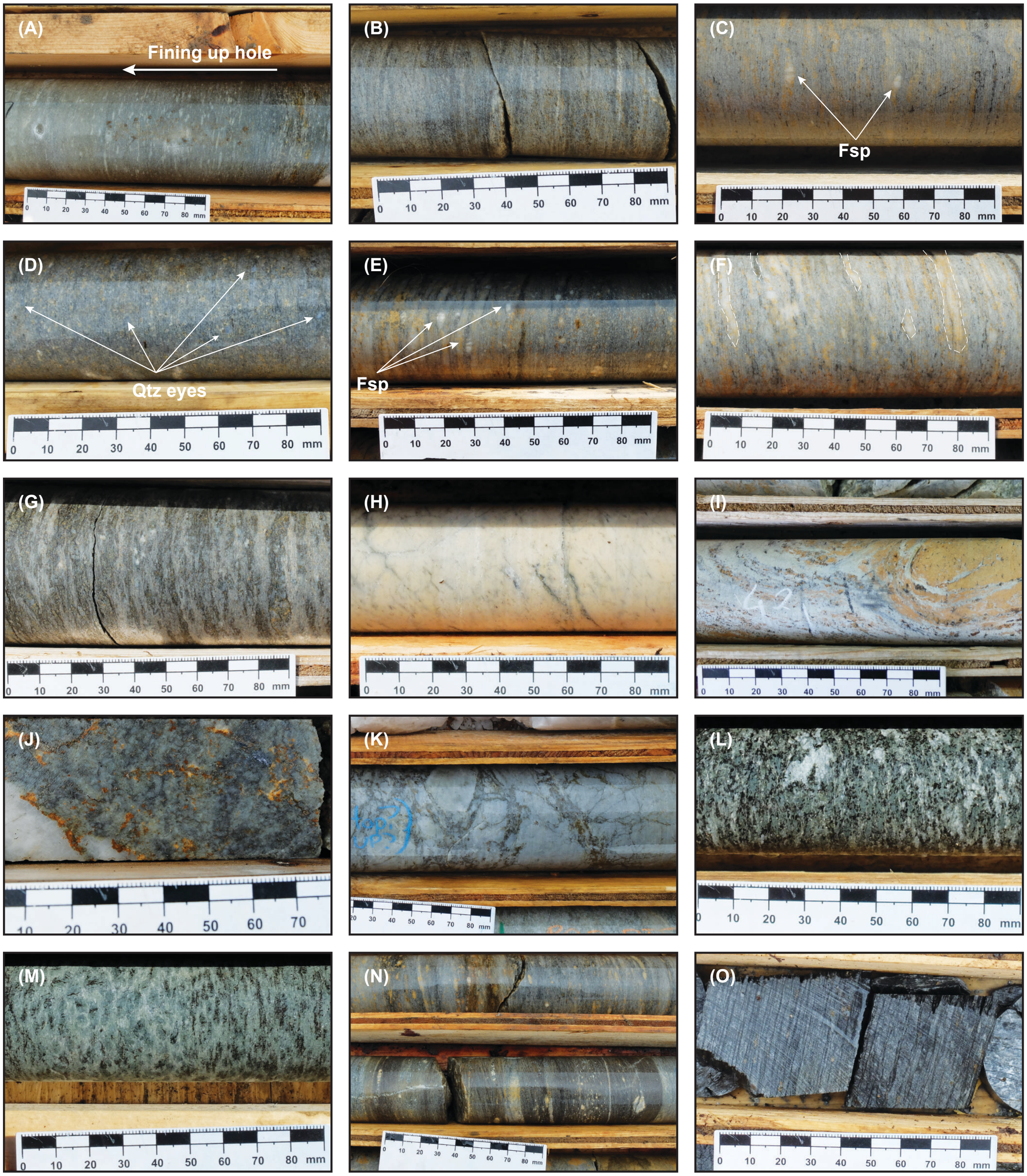

Figure 2.6. Lithofacies present at the ABM deposit. (A). Graded bedding in felsic tuff, arrow showing direction of fining - up hole; K18-484, 37 m down hole. (B) Felsic tuff; K15-291, 41 m down hole. Bedding marked by dashed line (C) Felsic tuff with minor feldspar crystals, arrows pointing to feldspar grains; K15-216, 72 m downhole. (D) Crystal-rich tuff with blue quartz eyes, arrows point to examples of the quartz eyes; K15-206, 62 m down hole. (E) Crystal-rich tuff with feldspar crystals, arrows point to examples of feldspar crystals; K15-233, 81 m downhole. (F) Lapilli tuff, examples of lapilli highlighted by dashed line K15-260, 58 m downhole. (G) Lapilli tuff, fragments with

blue quartz eyes, minor feldspar crystals and biotite-Fe-carbonate alteration; K15-260, 204 m downhole. (H) Aphyric rhyolite; K15-251, 63 m downhole. (I) Flow banding in aphyric rhyolite; K15-231, 42 m downhole. (J) Perlitic fracturing in rhyolite; K15-236, 94 m downhole. (K) Jigsaw breccia on top of rhyolite flow; K16-358, 85 m downhole. (L) Fine-grained and strongly altered lower contact of a MA mafic sill from Sequence 2; K15-265, 267 m downhole. (M) Coarse-grained interior of MA mafic sill from Sequence 2; K15-265, 254 m downhole. (N) Thin MB mafic sill from Sequence 3; K15-232, 61 m downhole. (O) Argillite; K15-301, 70 m downhole. Fsp = feldspar, Qtz = quartz.

2.4.2.4 Sedimentary facies

2.4.2.4.1 Argillite

Carbonaceous argillite lenses are very fine-grained and thinly bedded (Fig. 2.6O). Dark gray to black argillite beds are intercalated with minor tuffaceous or carbonate mineral-rich beds. Locally, minor pyrite and/or pyrrhotite occur. Argillite lenses up to 1 m thick are interbedded with tuff, lapilli tuff, or crystal-rich tuff. The argillite units are commonly strongly foliated, locally crenulated, and/or pervasively quartz altered. Strong foliation and crenulation are likely due to different rheological behavior of the argillite compared to the volcaniclastic and volcanic rocks. Folded quartz and/or quartz-carbonate veins that overprint the argillite fabric are common.

2.4.2.5 Faults

A set of NE-SW–striking (azimuth 050°–060°) subvertical to vertical regional faults cuts the stratigraphy in the deposit area. The two major faults crosscutting the ABM deposit are the East fault and the Fault Creek fault (Fig. 2.3); these two faults define the Krakatoa block. Movement on the East fault was dextral-oblique with roughly 200 m of apparent offset; van Olden et al. (2020) interpreted the Krakatoa block as dropped to the northwest and rotated. Fault rock within both the major fault zones contains angular sulfide clasts along with clay-sized fault gouge, indicating the movement and offset on the faults occurred post-mineralization. A lesser order fault, running east-northeast–west-southwest (~080°) and terminating on the East and Fault Creek faults, bisects the Krakatoa block (“Central” fault; Fig. 2.3). The "Central" fault is subvertical and dextral and accommodated a lateral offset of ~100 m after the formation of the mineralization, as it does not contain any sign of replacement or vein mineralization within the fault fabric. The thickening of subvolcanic units in the Krakatoa zone and their relative abundance compared to the ABM deposit suggests that the East fault or its predecessor was likely present and acted as a feeder/ conduit for the ascending magmas. The mafic sills present at Krakatoa coalesce into a single body and considerably thicken (up to 150 m) north of the "Central" fault. The single body takes on a more dike-like morphology and it parallels the East fault (van Olden et al., 2020). The East fault was later reactivated and facilitated the offset of the Krakatoa zone. The Fault Creek fault and the lower order fault with lateral offset ("Central" fault) do not appear to have controlled coherent rock emplacement or unit thickness.

2.4.3 Mineralization

The ABM VMS deposit consists of two mineralized zones: the ABM zone and the Krakatoa zone (Fig. 2.3). The mineralization is stratabound in both zones, sub-crops at the bedrock surface below the till cover, and dips subparallel to the stratigraphy (20°–30°). The ABM zone extends 700 m along strike and goes from the bedrock surface downdip for 600 m. The Krakatoa zone measures 170 m along strike and extends from the bedrock surface downdip for 600 m and remains open downdip. In both zones, the mineralization occurs as a series of stacked lenses within Sequence 2 rocks and ranges in thickness from 5 to 55 m in the ABM zone and from 15 to 100 m in the Krakatoa zone. Mineralization in the ABM zone tapers off downdip to the north-northeast, laterally to the west, and is cut off by the East fault to the east. In the Krakatoa zone, mineralization thins out downdip to the northeast and is cut off by post-mineralization faults in other directions.

In both the ABM and Krakatoa zones, massive sulfide mineralization is composed of pyrite, sphalerite, and pyrrhotite, with lesser chalcopyrite, magnetite, and galena and minor tennantite-tetrahedrite and freibergite. The most common gangue minerals are barite, carbonate minerals, quartz, chlorite, and white mica. Three main mineralization assemblages compose the massive sulfide lenses: (1) pyrite-sphalerite-galena with lesser chalcopyrite, tennantite-tetrahedrite, and freibergite, with carbonate, barite, quartz, and white mica (Fig. 2.7A-D); (2) magnetite-chalcopyrite-pyrrhotite-pyrite-sphalerite, minor tennantite-tetrahedrite and freibergite, and minor carbonate minerals and chlorite (Fig. 2.7E); (3) chalcopyrite-pyrrhotite-pyrite stringers associated with pervasive chlorite alteration, minor carbonate, and quartz (Fig. 2.7F). The massive sulfide lenses are primarily composed of the first two assemblages. The third assemblage is not as common and typically only present at the upper and lower contacts of the massive sulfide lenses. The latter two assemblages are richer in chalcopyrite, magnetite, and chlorite, are indicative of higher temperatures of emplacement (>300°C; e.g., Lydon, 1988), and are interpreted to have formed later than the pyrite-sphalerite-galena assemblage.

Mineralization at the ABM deposit has generally sharp contacts, but locally grades into unmineralized but altered rocks over the distance of 1 to 2 m. In the ABM zone, massive sulfide mineralization is associated primarily with felsic volcanic and volcaniclastic rocks. In the Krakatoa zone, the majority of massive sulfide mineralization is localized on contacts between the mafic sills and volcaniclastic rocks or, locally, within the mafic sills themselves. Throughout the ABM deposit, features such as preserved lapilli and other clasts (Fig. 2.7A-B), remnant bedding (Fig. 2.7D), and massive sulfides replacing likely glassy groundmass within perlitic and brecciated textures on unit contacts (Fig. 2.7C) are observed within the massive sulfide lenses and on their contacts and suggest that the mineralization formed by replacement (Doyle and Allen, 2003).

Thin, discontinuous stratiform bands (<30 cm thick) of massive sulfide occur in the footwall of the major massive sulfide lenses within the volcaniclastic rocks of Sequence 2 and at the top of Sequence 1. In the hanging wall of the massive sulfide lenses, rare subrounded to subangular clasts (up to 30 cm in size) composed of pyrite-pyrrhotite-carbonate occur within the felsic volcaniclastic rocks of Sequence 2 and Sequence 3.

2.4.4 Alteration

Hydrothermal alteration is widespread both in the hanging wall and footwall of the massive sulfide mineralization in the ABM and Krakatoa zones. The extent and zonation of alteration assemblages is irregular, although the intensity of alteration increases with proximity to the mineralized lenses. Alteration assemblages can vary within a single unit; however, white mica ± quartz ± chlorite alteration is the most widespread assemblage in felsic rocks. Felsic volcaniclastic rocks and flows commonly display pervasive white mica alteration at the contacts of massive sulfide lenses, but locally, pervasive chlorite ± carbonate mineral alteration occurs. Carbonate minerals (i.e., calcite,

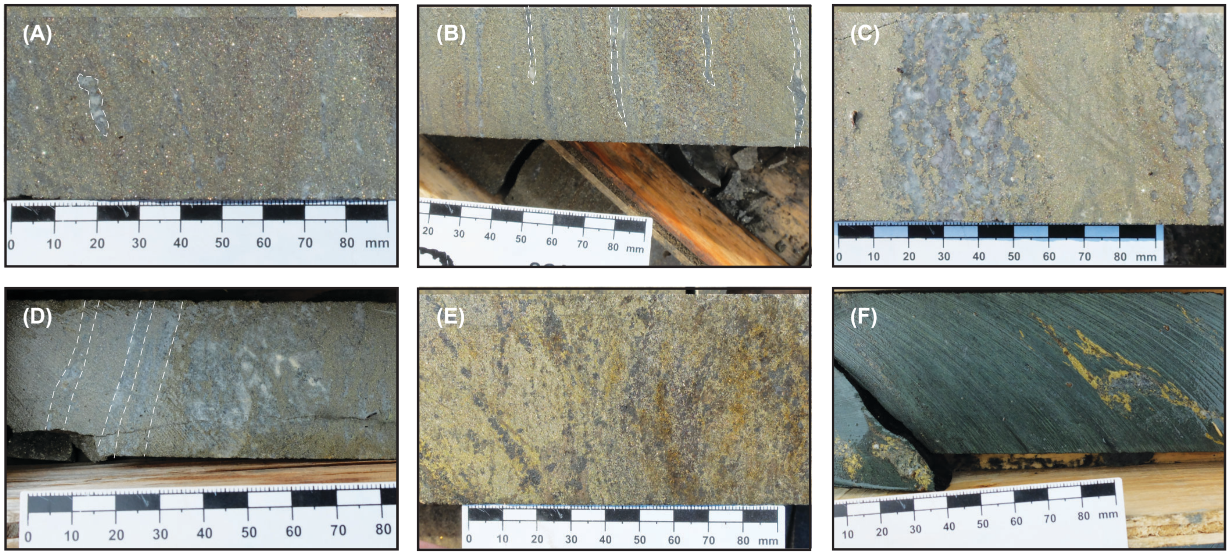

Figure 2.7. Mineralization textures present at the ABM deposit. (A) Massive py ± sph with remnant clasts, clast highlighted with dashed line; K15-265, 185 m downhole. (B) Massive py-sph with remnant lapilli clasts with quartz crystals, clasts are white mica-chlorite altered and highlighted with dashed line; K15-274, 92 m downhole. (C) Massive py ± sph ± cpy replacing felsic flow along perlitic fractures; K15-200, 143 m downhole. (D) Massive py-bar with remnant bedding visible, bedding highlighted with dashed line; K15-286, 139 m downhole. (E) Massive py-po-mgt-cpy mineralization; K12-200, 149 m downhole. (G) Pervasive chlorite alteration with cpy-po stringers; K17-422, 153 m downhole. Py = pyrite, sph = sphalerite, cpy = chalcopyrite, bar = barite, po = pyrrhotite, mgt = magnetite.

dolomite, and ankerite) are a common constituent of alteration assemblages at both the ABM and Krakatoa zones, and occur within the massive sulfides, in proximity to mineralization, or in more distal parts of the deposit. Calcite, dolomite, and Fe carbonate alteration is widespread in Sequences 2 and 3, and commonly presents as patches or veins with an orange tint. Carbonate minerals commonly overprint the primary fabric and/or the mineralization. Amphibole-chlorite-carbonate-biotite-epidote-quartz are common alteration minerals in the altered mafic subvolcanic sills in Sequence 2, where amphibole and chlorite replace the primary pyroxene and biotite locally overprints the chlorite. Post-mineralization carbonate, carbonate-quartz, quartz, quartz-tourmaline, and tourmaline veins occur throughout the deposit and crosscut the rock fabric defined by the primary features in the volcaniclastic rocks and the mineralization.

2.5 Lithogeochemistry

2.5.1 Whole-rock major and trace element lithogeochemistry methods

Eighty-three of the collected samples were analyzed for major and trace elements; the full results are available in Appendix 1.1. Sample preparation and measurement of major and trace element data was performed at ALS Laboratories, North Vancouver, British Columbia. Rock samples were crushed and pulverized using steel plates and agate mills, respectively. Sample powders (~0.2 g) were fused with a lithium metaborate flux (0.9 g) at 1,000°C. The fused beads were cooled and digested using 100 mL of a 4% HNO_3-2% HCl mixture. Analyses of the sample solutions were carried out using inductively coupled plasma-atomic emission spectrometry (ICP-AES) for major elements and inductively coupled plasma-mass spectrometry (ICP-MS) for trace elements. Additional trace element measurements were completed on the same sample suites at Ontario Geoscience Laboratories in Sudbury, Ontario, to obtain transition metals, base metals, and semimetals (e.g., Li, Be, Co, Cu, Zn, Mo, Cd, In, Sb, W, Bi, Pb, Sc, Ta; full list of analyzed elements available in Appendix 1.1). Samples were digested on hot plates using a mixture of HF-HCl-$HClO_4$ in closed screwcap Savillex® Teflon™ bombs for seven days. The resultant solution was dried and fluxed with a dilute HCl-$HClO_4$ mixture and reheated. Samples were again dried and fluxed with a final mixture of concentrated HNO_3-HCl, heated, and finally diluted with HNO_3. Solutions were analyzed for metals on a Perkin-Elmer Elan 9000 ICP-MS following the methodology of Burnham and Schweyer (2004) and Burnham (2008).

Over the course of this study, eight in-house reference materials (SLV-MC basalt and WP-1; Appendix 1.2) and five lab-chosen duplicates were analyzed at ALS and Ontario Geoscience Laboratories during the run to monitor analytical accuracy and reproducibility (Appendix 1.3). The SLV-MC basalt and WP-1 dacite (Watts Point, Coast Plutonic Complex) samples were reproducible to <5% for major elements, except for <10% MnO in the WP-1 dacite. Trace element abundances overall gave relative standard deviation (RSD) values <10%, with many elements below 5%, except for Hf and Lu (<12%) in both reference materials, and Cs and V in SLV-MC (<25 %; Appendix 1.2). The results for both reference materials overlap with published values

(WP-1; Piercey et al., 2001; Manor and Piercey, 2019) and unpublished in-house data for both SLV-MC (n = 44) and WP-1 (n = 19) with reproducibility better than 15% for most trace elements and major element oxides, with the exceptions of Cs and Tl in SLV-MC basalt, which show percent relative differences <61%, and Be, Co, Cs, Mo, Ni, Sb, Sc, Sn, and Tl in the WP-1 dacite, which show percent relative differences >100%. The high percent relative difference values for the trace elements in the WP-1 dacite standard are likely due to a low number of analyses available for the analytes in question for the analytical method used in this paper (n = 4). The lab duplicates show relatively higher RSD values but are generally <15% for most major and trace elements.

2.5.2 Lithogeochemical results

The 83 analyzed samples cover the stratigraphic interval hosting the ABM deposit and encompass rocks from Sequence 1 approximately 60 m below the massive sulfide mineralization to rocks from Sequence 3 below the contact with the Wind Lake formation (Fig. 2.4). Samples commonly contain alteration minerals such as white mica, chlorite, carbonate, quartz, and Fe sulfides (pyrite and pyrrhotite). Examination of the major element data shows that the majority of the sampled rocks were affected by hydrothermal alteration (Fig. 2.8B; Spitz and Darling, 1977; Barrett and MacLean, 1994; Large et al., 2001b; Ruks et al., 2006). Most felsic samples have elevated loss on ignition (LOI) values (>2 wt %) and Al_2O_3/Na_2O values (2.2–401, n = 64) indicative of feldspar destruction or replacement by white mica (Spitz and Darling, 1977; Ruks et al., 2006). Iron carbonate and carbonate alteration can lead to the distortion of expected CaO behavior. In these rocks, the majority of primary CaO is likely lost due to destruction of plagioclase and its replacement by white mica and chlorite, but strongly carbonate-altered samples show significant additions of CaO. The high degree of hydrothermal alteration (Fig. 2.8B) precludes the use of the mobile major elements for characterization of lithological units. Rare earth elements (REEs), high field strength elements (HFSEs), Al_2O_3, and TiO_2 are generally immobile under most VMS conditions (Kranidiotis and MacLean, 1987; MacLean, 1988; MacLean and Barrett, 1993). The immobile behavior of REE-HFSE-Al_2O_3-TiO_2 was assessed and confirmed using methods outlined in MacLean (1988) and MacLean and Barrett (1993) by plotting immobile element pairs and assessing the linear trends between them. Immobile elements (Zr, TiO_2, Al_2O_3, REEs, Cr, Hf, Nb, Sc, Ta, Th, V, and Y) and their ratios are thus used to determine and characterize distinct lithogeochemical groups within the ABM deposit stratigraphy. Values for representative samples and median values for each group in both the ABM and Krakatoa zones are presented in Table 2.1. Lithogeochemical results confirm the bimodal nature of the volcanic rocks; these are visible on the Zr/Ti vs. Nb/Y plot, where all samples plot either as basalt or rhyolite/dacite/trachyte (Fig. 2.8A).

2.5.2.1 Felsic rocks

Immobile element ratios illustrate there are two distinct groups of felsic rocks, FA, and FB, in the ABM deposit stratigraphy (Fig. 2.8D). Both groups occur both as coherent and volcaniclastic lithofacies, which indicates the immobile element signatures are not controlled by lithofacies alone. Groups FA and FB plot on the same linear array in the Zr-TiO_2 space (Fig. 2.8C), but plot on distinctly different linear arrays that pass through the origin in the Al_2O_3/TiO_2-Zr/Al_2O_3 space (Fig. 2.8D).

2.5.2.2 Group FA

In Nb/Y-Zr/Ti space (Fig. 2.8A), group FA rocks plot in the trachyte field with a minor portion overlapping into the dacite-rhyolite field. Group FA rocks have relatively high absolute values of Zr (Zr > 548 ppm, n = 20) compared to the other felsic rocks in the Kudz Ze Kayah formation and overall higher values of HFSEs like Hf, Nb, Sc, V, and Y compared to other felsic rocks (Table 2.1). The Zr/TiO_2 value varies between 1,046 and 1,367, and Zr/Al_2O_3 is between 40.6 and 52.9. The Zr/Y value for all samples of group FA are >10 (10.8–16.4; Fig. 2.8E), indicative of calc-alkaline affinity (Ross and Bédard, 2009). In the Nb-Y plot, the group FA rocks fall into the within-plate affinity field (Fig. 2.8F; Pearce et al., 1984). The primitive mantle (PM) normalized La/Yb value ($(La/Yb)_{PM}$) is between 9.4 and 15.9, indicating steep REE pattern slopes where light rare earth elements (LREEs) are enriched relative to the heavy rare earth elements (HREEs) and the HREEs display a relatively flat pattern (Fig. 2.9B). The mean Eu anomaly (Eu/Eu*; $Eu/Eu^* = Eu_{pm}/(Gd_{pm} \times Sm_{pm})^{0.5}$) for group FA rocks is around 0.53 (n = 20). In extended PM-normalized plots, Nb and Ti show negative anomalies compared to Th and La and Eu and Gd, respectively

Table 2.1 Summary of geochemical characteristics of the rock groups of the upper Kudz Ze Kayah formation

	FA			FB1			FB2			MA			MB		
	N	Mean	2σ	N	Mean	2σ	N	Mean	2σ	N	Mean	2σ	N	Mean	2σ
SiO_2 (wt. %)	20	65.22	2.27	15	72.09	3.53	23	68.84	13.07	16	44.73	1.99	6	47.12	4.78
Al_2O_3	20	14.89	1.16	15	13.58	1.97	23	13.45	2.86	16	14.93	0.65	6	13.29	1.38
Fe2O3	20	4.50	1.45	15	2.18	1.12	23	3.67	5.33	16	9.53	0.59	6	10.87	0.84
CaO	20	2.41	0.96	15	1.37	0.95	23	1.76	2.50	16	9.52	1.32	6	7.40	2.34
MgO	20	1.57	0.45	15	0.50	0.36	23	2.69	3.32	16	7.76	0.84	6	3.09	0.37
Na_2O	20	0.88	0.93	15	0.90	1.05	23	0.52	1.10	16	1.90	1.23	6	1.05	1.31
K_2O	20	4.42	0.86	15	6.36	2.64	23	4.19	1.80	16	2.04	1.65	6	4.02	1.93
TiO_2	20	0.58	0.07	15	0.32	0.05	23	0.24	0.06	16	1.23	0.10	6	2.36	0.28
MnO	20	0.09	0.04	15	0.03	0.02	23	0.05	0.05	16	0.14	0.01	6	0.17	0.02
P_2O_5	20	0.18	0.02	15	0.04	0.01	23	0.04	0.02	16	0.13	0.02	6	0.35	0.03
LOI	20	4.66	1.00	15	2.62	0.98	23	4.62	4.06	16	7.24	3.02	6	8.67	2.50
Total	20	99.41	1.02	15	99.98	1.02	23	100.1	1.1	16	99.22	0.88	6	98.38	0.85
Cr (ppm)	20	12.5	4.3	15	10.7	2.5	23	9.6	1.4	16	339.4	27.7	6	45.0	38.2
Ni	13	4.7	2.3	11	3.3	1.3	16	1.3	1.3	5	91.3	10.7	2	15.1	11.5
Co	13	4.6	1.8	11	2.7	0.9	16	4.9	8.2	5	42.1	2.4	2	28.3	4.0
Sc	13	11.4	1.4	11	5.3	1.5	16	4.2	0.8	5	29.7	1.3	2	31.6	1.7
V	20	29.1	4.8	15	17.9	4.5	23	12.3	5.2	16	219.8	14.4	6	307.7	19.2
Cu	13	19.6	25.7	11	7.4	4.0	16	51.5	82.1	5	42.0	27.5	2	10.1	10.1
Pb	13	25.8	45.8	11	47.1	29.8	16	145.5	226.2	5	120.9	209.9	2	10.2	3.9
Zn	13	175.9	200.6	11	196.1	277.2	16	420.3	443.1	5	190.9	137.6	2	185.8	68.7
Bi	13	0.3	0.3	11	0.4	0.4	16	1.6	3.4	5	0.2	0.4	2	0.1	0.0
In	13	0.1	0.0	11	0.0	0.0	16	0.0	0.0	5	0.1	0.0	2	0.1	0.0
Sn	20	4.8	2.1	15	8.2	2.9	23	7.7	3.1	16	0.9	0.2	6	2.2	0.4
Ag	13	0.6	1.5	11	0.7	1.3	16	0.8	0.9	5	0.2	0.2	2	0.1	0.0
Rb	20	136.1	33.7	15	168.4	73.9	23	141.5	46.6	16	70.8	60.4	6	139.2	73.9
Cs	20	2.9	0.9	15	1.9	0.9	23	2.6	1.1	16	4.3	5.1	6	6.1	3.7
Ba	20	1516	623	15	3557	2594	23	1632	1889	16	1725	1717	6	1582	800
Sr	20	59.7	22.3	15	70.6	39.1	23	43.2	38.7	16	201.8	77.7	6	146.1	24.3
Ga	20	25.7	2.4	15	20.9	4.0	23	22.8	5.6	16	16.0	1.4	6	22.7	2.8
Ta	13	2.5	0.2	11	2.1	0.8	16	1.9	0.3	5	0.5	0.0	2	1.2	0.1
Nb	20	43.6	4.2	15	25.3	4.5	23	23.7	4.4	16	9.2	0.7	6	20.6	3.3
Hf	20	16.7	1.7	15	10.6	1.7	23	7.6	2.0	16	2.5	0.3	6	6.2	1.2
Zr	20	714.1	80.3	15	399.7	67.7	23	259.4	79.5	16	91.1	7.5	6	246.3	48.5
Y	20	53.9	6.1	15	40.4	6.5	23	41.5	12.3	16	20.3	2.0	6	32.5	3.7
Th	20	30.6	3.6	15	27.9	4.5	23	28.8	6.3	16	1.5	0.2	6	8.0	2.7
U	20	4.2	0.4	15	7.4	1.8	23	7.2	2.9	16	0.4	0.1	6	2.1	0.8
La	20	92.9	10.1	15	50.6	6.8	23	52.7	15.3	16	10.0	1.3	6	33.9	9.7
Ce	20	189.1	20.3	15	103.4	15.9	23	107.9	29.7	16	21.9	2.8	6	72.7	19.9
Pr	20	21.8	2.3	15	11.5	1.8	23	12.1	3.3	16	2.9	0.4	6	9.1	2.4
Nd	20	82.1	8.4	15	41.6	6.9	23	43.5	12.6	16	13.1	1.5	6	36.7	8.6
Sm	20	15.5	1.5	15	8.0	1.4	23	8.8	2.8	16	3.5	0.4	6	8.0	1.4
Eu	20	2.4	0.3	15	0.6	0.1	23	0.5	0.1	16	1.1	0.2	6	1.9	0.3
Gd	20	12.3	1.2	15	6.6	1.1	23	7.1	2.1	16	3.7	0.4	6	7.2	0.9
Tb	20	1.8	0.2	15	1.1	0.1	23	1.2	0.4	16	0.6	0.1	6	1.1	0.1
Dy	20	10.2	1.1	15	6.8	1.0	23	7.5	2.2	16	3.9	0.4	6	6.2	0.4
Ho	20	2.0	0.2	15	1.4	0.2	23	1.5	0.4	16	0.8	0.1	6	1.2	0.1
Er	20	5.6	0.6	15	4.2	0.6	23	4.3	1.2	16	2.3	0.3	6	3.5	0.3
Tm	20	0.8	0.1	15	0.6	0.1	23	0.6	0.2	16	0.3	0.0	6	0.5	0.0
Yb	20	5.1	0.5	15	4.1	0.6	23	4.0	0.9	16	2.1	0.2	6	3.2	0.1
Lu	20	0.8	0.1	15	0.6	0.1	23	0.6	0.1	16	0.3	0.0	6	0.5	0.0
Al_2O_3/Na_2O	20	69.3	66.1	15	49.4	43.6	23	98.0	89.8	16	41.0	68.3	6	82.6	64.9
Zr/TiO_2	20	0.1	0.0	15	0.1	0.0	23	0.1	0.0	16	0.0	0.0	6	0.0	0.0
Zr/Al_2O_3	20	48.0	3.7	15	29.3	1.1	23	19.1	2.9	16	6.1	0.5	6	18.4	1.6
Al_2O_3/TiO_2	20	25.7	2.2	15	42.1	1.4	23	57.5	9.2	16	12.2	0.9	6	5.6	0.2
Zr/Y	20	13.3	1.5	15	9.9	1.0	23	6.6	2.1	16	4.5	0.4	6	7.9	2.8
Zr/Nb	20	16.4	1.1	15	15.9	0.7	23	10.9	2.1	16	9.9	0.3	6	11.9	1.0
Zr/Ti	20	0.2	0.0	15	0.2	0.0	23	0.2	0.0	16	0.0	0.0	6	0.0	0.0
Nb/Y	20	0.8	0.1	15	0.6	0.1	23	0.6	0.1	16	0.5	0.0	6	0.7	0.2
La/Yb (cn)	20	12.4	1.6	15	8.3	0.8	23	8.9	2.5	16	3.2	0.2	6	7.0	2.0
Eu/Eu*	20	0.5	0.1	15	0.3	0.0	23	0.2	0.0	16	0.9	0.1	6	0.8	0.0
Nb/Nb*	20	0.3	0.0	15	0.2	0.0	23	0.2	0.1	16	0.8	0.1	6	0.5	0.2
Nb/Ta	13	17.6	0.8	11	12.7	2.1	16	12.0	0.9	5	16.3	0.6	2	15.9	0.6
Ti/Sc	13	308.0	19.7	11	394.5	72.3	16	371.6	57.4	5	231.6	2.6	2	403.9	2.9

(Fig. 2.9A); the mean Nb/Ta value is 17.56 (n = 13). In felsic volcanic fertility diagrams (Fig. 2.9D), group FA rocks plot mostly outside of the designated field for FII rhyolites.

2.5.2.3 Group FB

In the Nb/Y-Zr/Ti discrimination diagram, group FB rocks plot in the rhyolite-dacite field, and a small portion overlaps into the trachyte field (Fig. 2.8A). Group FB rocks have absolute Zr abundances between 157 and 507 ppm (n = 38), relatively lower values of HFSEs compared to the FA group (Table 2.1), and the Zr/TiO_2 and Zr/Al_2O_3 values range from 907 to 1,340 and 12.7 to 31.4, respectively. The Zr/Y values for all samples of group FB are slightly lower than group FA rocks and vary between 2.6 and 16.1 (mean = 7.3; Fig. 2.8E), indicative of a transitional affinity (Ross and Bédard, 2009). In the Nb vs. Y diagram, the rocks of group FB fall into the within-plate affinity field (Fig. 2.8F), but some samples plot close to the syn-collisional and volcanic arc fields. The FB group can be further divided into subgroups FB1 and FB2 based on immobile elements and their ratios. The FB1 subgroup has the higher average Zr (400 ppm, n = 15) and TiO_2 (0.32 wt %, n = 15) values than the FB2 group. The FB group typically contains tuffaceous or sill lithofacies; lapilli or crystal-rich tuffs are rare. Subgroup FB1 typically occurs associated with group MA mafic subvolcanic sills. The FB2 subgroup is the most common lithogeochemical signature in the ABM sample suite and encompasses all observed lithofacies. The $(La/Yb)_{PM}$ of the FB group falls between 4.4 and 14.1, indicating a similar to slightly flatter REE slopes than group FA, and samples from both subgroups have similar chondrite-normalized REE patterns (Fig 2.9B). The LREEs are enriched relative to the HREEs, and the HREEs have relatively flat patterns, similar to group FA but with relatively lower abundances (Fig. 2.9B). The mean Eu anomaly (Eu/Eu*) for subgroup FB1 rocks is 0.25 (n = 15) and 0.19 (n = 23) for subgroup FB2. The FB group rocks show negative Nb and Ti anomalies (Fig. 2.9A) similar to the FA group but have a lower mean Nb/Ta value, 12.40 (N = 27). In the felsic volcanic fertility diagram (Fig. 2.9D), group FB rocks plot within the FII rhyolite field.

2.5.2.4 Mafic rocks

Mafic rocks in the uppermost 350 m of the Kudz Ze Kayah formation occur in two distinct geochemical groups: (1) group Mafic A (MA), which comprises the mafic sills in Sequence 2; and (2) group Mafic B (MB), which consists of the sills in Sequence 3. The two groups differ not only in their stratigraphic position, but also in their immobile and trace element signatures.

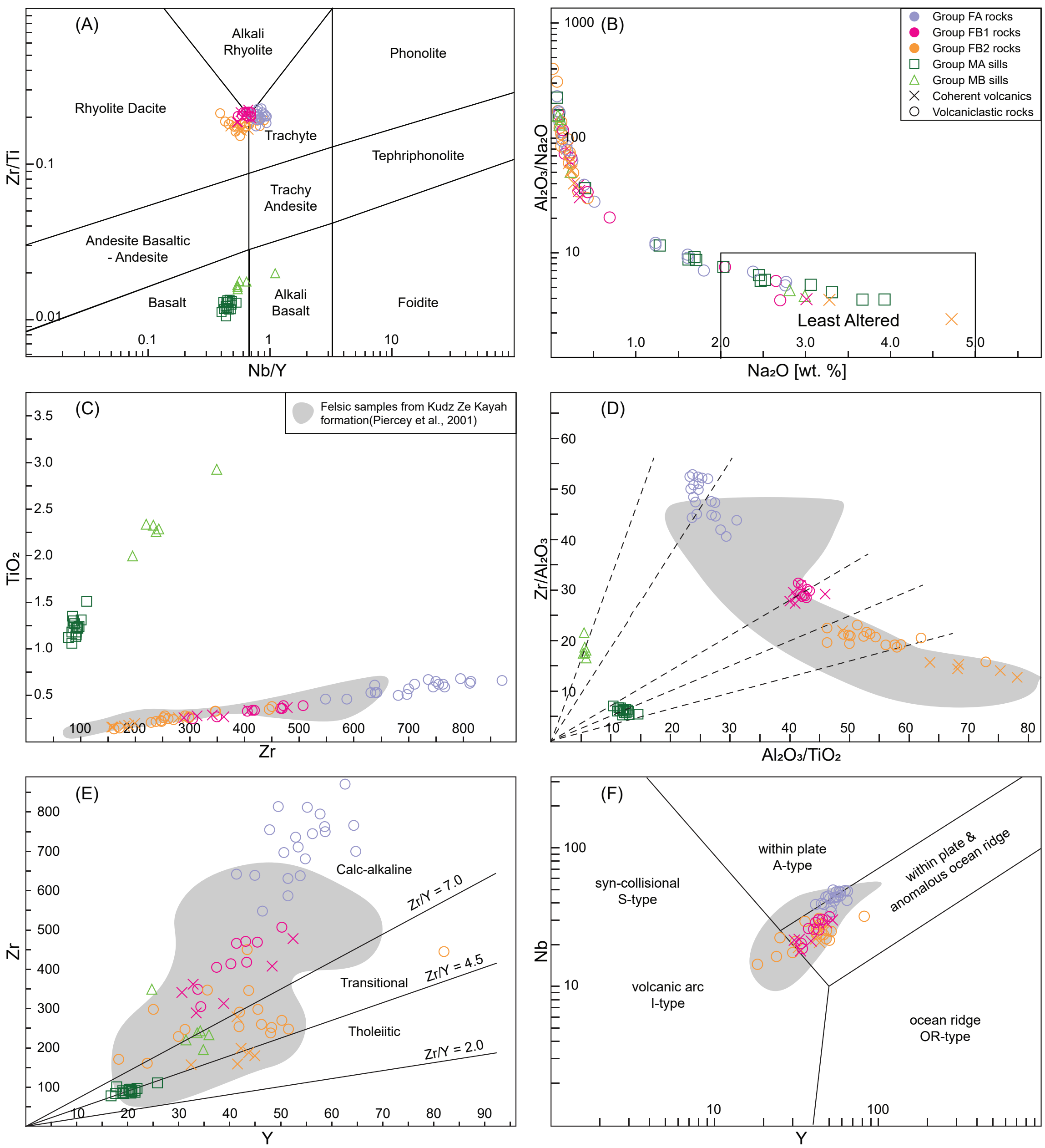

Figure 2.8. Trace and major element discrimination plots for felsic and mafic rocks in the ABM deposit. (A) Volcanic rocks discrimination diagram, Nb/Y vs Zr/Ti (Pearce, 1996). (B) Na_2O vs Al_2O_3/Na_2O showing least altered rocks (Ruks et al., 2006). (C) Zr vs TiO_2. (D) Al_2O_3/TiO_2 vs Zr/Al₂O₃ (Barrett et al., 2001). (E) Y vs Zr (Ross and Bédard, 2009). (F) Y vs Nb (Pearce et al., 1984). Grey shaded areas represent felsic samples from the Kudz Ze Kayah formation presented in Piercey et al. (2001).

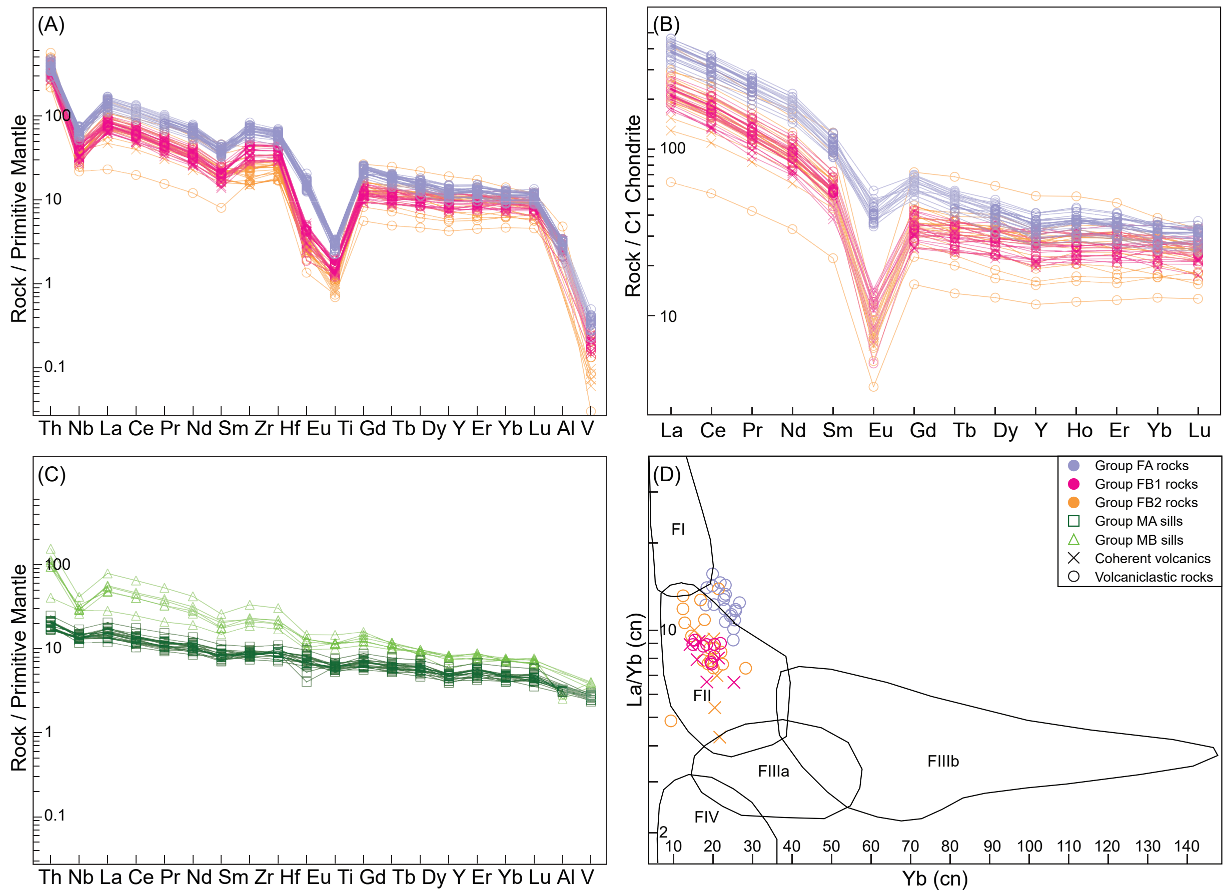

Figure 2.9. Normalized plots of immobile and rare earth elements of the rocks from the ABM deposit. (A) Immobile elements of felsic samples normalized to primitive mantle (McDonough and Sun, 1995). (B) Rare earth elements of felsic samples normalized by C1 chondrite (McDonough and Sun, 1995). (C) Immobile elements of mafic samples normalized by primitive mantle (McDonough and Sun, 1995). (D) Chondrite-normalized felsic samples in plot distinguishing FI-FIV geochemical groups (Lesher et al., 1986; Hart et al., 2004). Symbols same as in Figure 2.8.

2.5.2.5 Group MA

Group MA rocks plot in the basalt field in Nb/Y-Zr/Ti space (Fig. 2.8A). Values of Zr are between 78 and 111 ppm (n = 16), TiO_2 falls between 1.06 and 1.51 wt % (n = 16), and P_2O_5 values are between 0.11 and 0.17 wt % (n = 16). The Zr/TiO_2 values fall between 63.0 and 80.5 (n = 16), and the Zr/Y values are between 4.0 and 5.6 (Fig. 2.8E), straddling the line between transitional and calc-alkaline affinity (Ross and Bédard, 2009). The mean Nb/Ta value is 16.49 (N = 5). In several discrimination diagrams (Pearce and Cann, 1973; Pearce, 1996, 2008), group MA plots in the fields designated for enriched mid-ocean ridge basalts (E-MORBs) and within-plate tholeiites (WPT; Fig. 2.10B-D), for MORB (Fig. 2.10A), or near the within-plate basalt (WPB)/calc-alkali basalt (CAB) field (Fig. 2.10B). In a PM-normalized plot, group MA has a relatively smooth downward sloping curve with a slight negative Nb anomaly in comparison to Th and La (Fig. 2.9C; Nb/Nb* average 0.81, $n = 16$). The $(La/Yb)_{PM}$ ratio is between 2.83 and 3.72 and indicates a relatively flat REE slope (Fig. 2.9C).

2.5.2.6 Group MB

In Nb/Y-Zr/Ti space, the group MB samples plot in the basalt field (Fig. 2.8A). Values of Zr are between 195 and 349 ppm ($n = 6$), TiO_2 is between 2.00 and 2.93 wt % ($n = 6$), and P_2O_5 values are between 0.28 and 0.39 wt % ($n = 6$). The Zr/TiO_2 value falls between 94.0 and 119.1 ($n = 6$); the Zr/Y value is between 5.6 and 14.0 and plots in the calc-alkaline affinity field (Ross and Bédard,

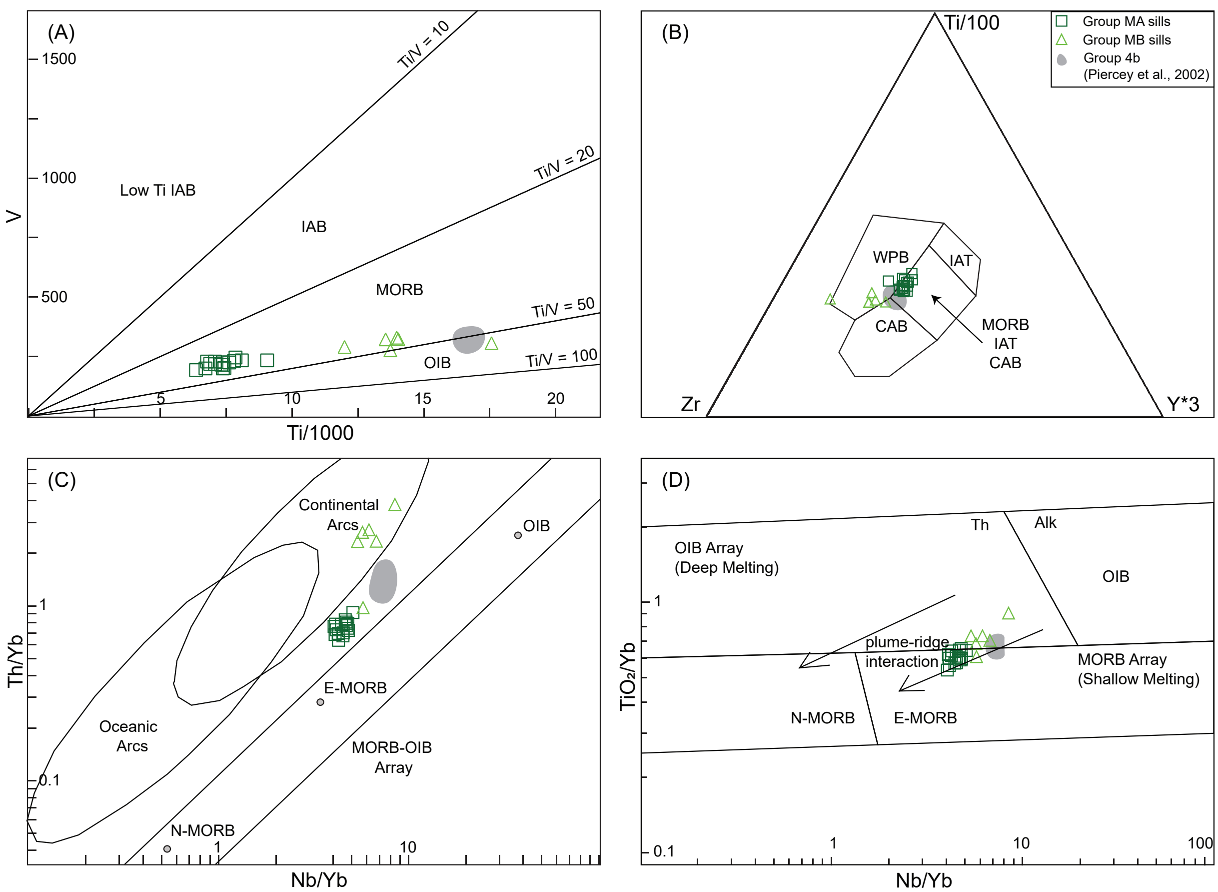

Figure 2.10. Trace element discrimination plots for mafic rocks in the ABM deposit. (A) Ti*1000 vs V (Shervais, 1982). (B) Zr - Y*3 - Ti/100 (Pearce, 1996). (C) Nb/Yb vs TiO2/Yb (Pearce, 2008). (D) Nb/Yb vs TiO2/Yb (Pearce, 2008). Symbols same as in Figure 2.8. Grey shaded areas represent group 4b of the Wind Lake formation described by Piercey et al., (2002b).

2009; Fig. 2.8E). The mean Nb/Ta value is 15.90 (N = 2). In several discrimination diagrams (Pearce and Cann, 1973; Pearce, 1996, 2008), group MB plots in the fields designated for WPBs and volcanic arc basalts (VABs) and CABs (Fig. 2.10B-D) or straddles the line between MORB and ocean island basalt (OIB) (Ti/V = 41.3–57.4, n = 6; Fig. 2.10A). In a PM-normalized plot, group MB curves are downward sloping with a significant negative Nb (Nb/Nb* avg 0.48, n = 6; Fig. 2.9C) and a slight Ti anomaly, whereas the $(La/Yb)_{PM}$ value falls between 3.78 and 10.74. Group MB has similar geochemical characteristics to group 4b in Piercey et al. (2002b) and to the Wind Lake formation mafic rocks presented in Manor and Piercey (2019; Fig. 2.10).

2.5.3 Chemostratigraphy

Distribution of the various lithogeochemical groups in the upper Kudz Ze Kayah formation is described below from stratigraphically lowest to highest based on representative sections of the ABM and Krakatoa zones. In the 6815550 mN long section (Fig. 2.4), the 414650 mE, 414850 mE, and the 414050 mE cross sections through the ABM zone (Fig. 2.11), and the presented Krakatoa cross section (Fig. 2.12), the chemostratigraphy is similar between the two zones. However, the Krakatoa zone shows minor differences compared to the ABM zone, which are described below. Where geochemical sampling is lacking, units are inferred based on spatial extent of defined lithogeochemical groups. The lithogeochemical database of BMC Minerals Ltd. was also utilized, but only as a secondary source of major and trace element data.

2.5.3.1 Sequence 1

At the top of Sequence 1, a felsic volcanic unit with thickness varying between 3 and 25 m sits below the lower mafic sill and comprises felsic tuffs and volcanic rocks with FB1 signatures (Fig. 2.4). The felsic volcanic and volcaniclastic rocks sitting below the FB1 unit make up the majority of the stratigraphy in Sequence 1 and belong to the FA lithogeochemical group.

2.5.3.2 Sequence 2

Close to the lower contact of Sequence 2, the felsic subvolcanic sills, domes, and minor associated tuffs have group FB1 signatures. The two mafic sills occurring at the lower contact of Sequence 2 belong to the MA lithogeochemical group. Felsic rocks occurring in Sequence 2 below the

Sequence 3-Sequence 2 boundary belong to the FB2 group. The boundary between Sequence 3 and Sequence 2 is sharp and coincides with the transition between FA rocks and underlying FB rocks. The laterally most extensive argillite lens separates the two lithofacies domains, where volcaniclastic rocks are more abundant in Sequence 3, in contrast with voluminous subvolcanic and volcanic rocks in Sequence 2. No crosscutting subvolcanic units with the FA signature are present in Sequence 2.

2.5.3.3 Sequence 3

The felsic volcanic and volcaniclastic rocks that are a part of Sequence 3 consistently have group FA signatures. The volcanic and volcaniclastic rocks likely have a common magma source. Thin mafic sills of the MB group intrude FA felsic volcanic and volcaniclastic rocks. The MB group of mafic rocks has similar signatures to the mafic rocks of the Wind Lake formation (Piercey et al., 2002b; Manor and Piercey, 2019) that occur in the immediate hanging wall of Sequence 3. Thus, the MB sills in Sequence 3 are likely coeval with the mafic rocks of the Wind Lake formation and likely acted as feeders.

2.5.3.4 Krakatoa zone

The Krakatoa zone exhibits the same distribution of geochemical groups as the ABM zone (Fig. 2.12). In Sequence 2, the FB1 group felsic sills are surrounded by group MA mafic sills; felsic rocks in the hanging wall and footwall of the thickest mafic sill have group FB2 signatures. Within Sequence 3, most of the felsic rocks are group FA, except for minor felsic lava flows approximately 50 m below the Kudz Ze Kayah-Wind Lake formation contact that have FB signatures.

2.5.4 Barium distribution

The majority of presented Ba values (N = 8989) are sourced from the assay database of BMC Minerals Ltd. The quality assurance and quality control procedures for assays are presented in van Olden et al. (2020). The Numeric Models tool in Leapfrog 3D was used to construct isosurfaces of Ba distribution (Figs. 2.4, 2.11, and 2.12). The linear radial basis function (RBF) interpolation was chosen to mitigate the irregular distribution of the almost 9,000 Ba datapoints. The linear RBF interpolant was run with a sill value of 5000, base range of 50, nugget of 0, and accuracy of

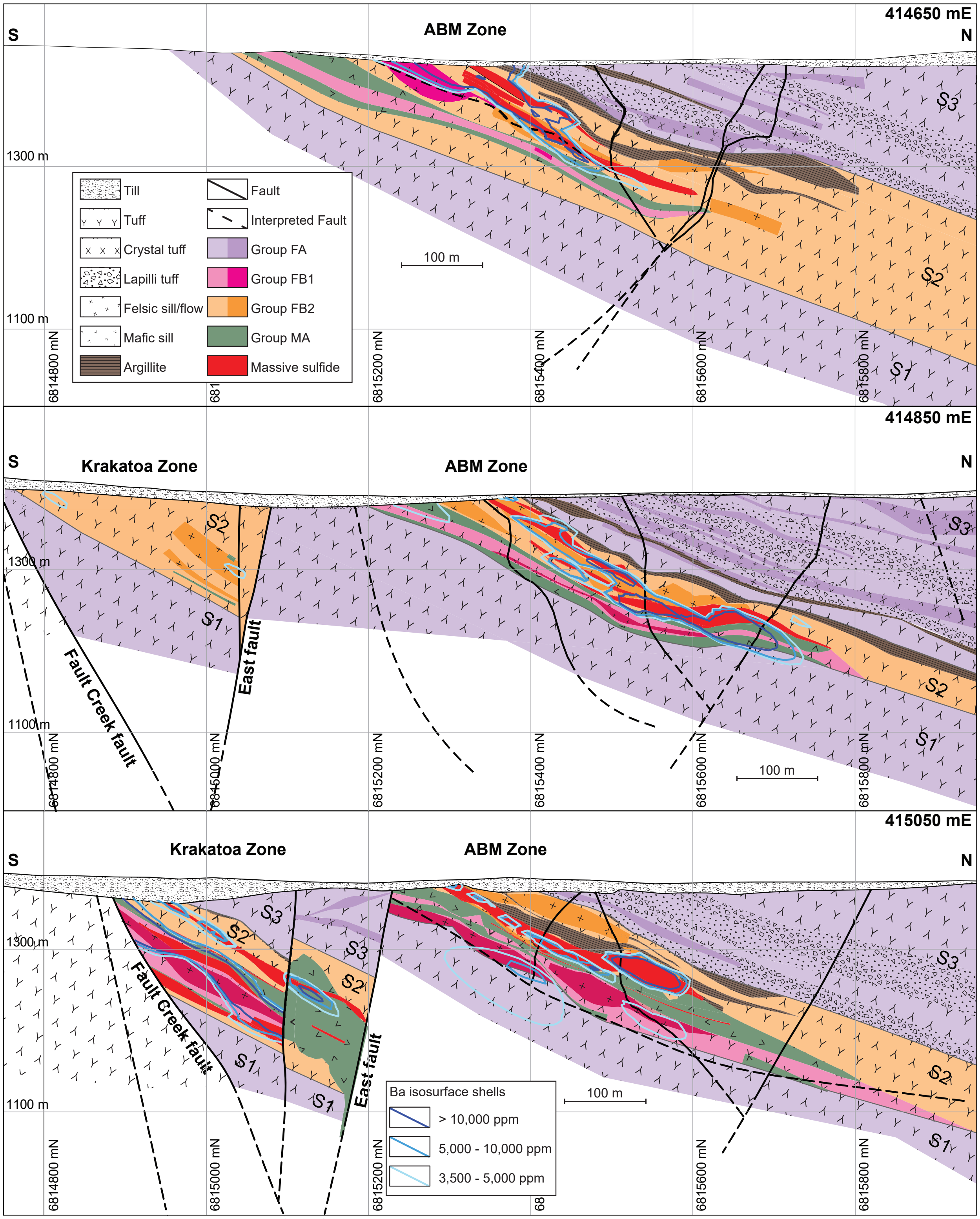

Figure 2.11. Cross sections through the ABM zone of the ABM deposit, cross sections are looking west. Positions of section lines shown in Figure 2.3. S1 = Sequence 1, S2 = Sequence 2, S3 = Sequence 3.

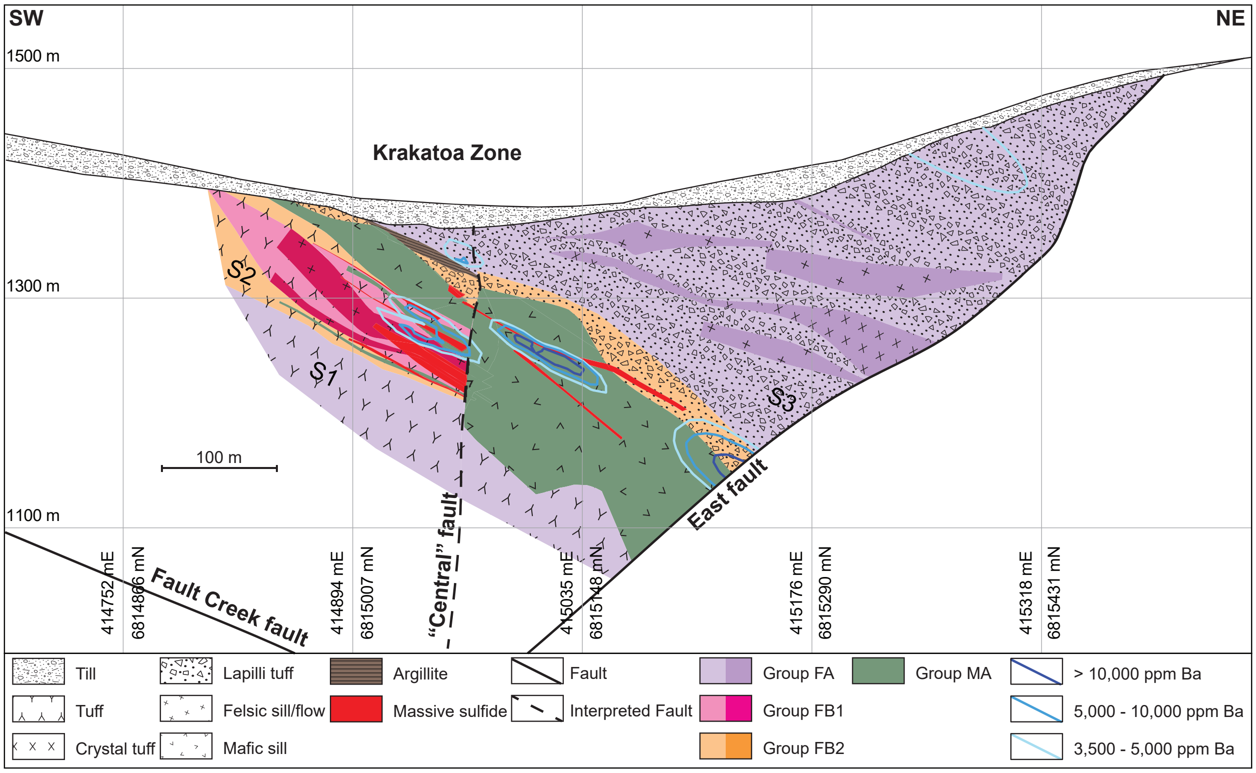

Figure 2.12. Cross section through the Krakatoa zone of the ABM deposit, cross section is looking NW. Position of section line shown in Figure 2.3. S1 = Sequence 1, S2 = Sequence 2, S3 = Sequence 3.

20. The trend was set to the local stratigraphy (dip 30° with dip azimuth of 20° and pitch of 115°) and the ellipsoid ratios were set to 3:3:1. The threshold value for Ba at the deposit was chosen at 3,500 ppm using methods outlined in Reimann et al. (2005). Values above the threshold are considered anomalous and reflect Ba enrichment, as felsic volcanic rocks not associated with VMS deposits commonly show Ba values around 1229 ± 781 ppm (average value for felsic volcanic rocks reported for the Kudz Ze Kayah formation; Piercey et al., 2001). Anomalous Ba values occur in the vicinity of the massive sulfide mineralization at the ABM deposit and are associated with strongly altered rocks. Barite is a common gangue mineral at the ABM deposit; it is associated with the pyrite-sphalerite-galena assemblage (Fig. 2.7D), and minor Ba-rich feldspar (hyalophane, celsian) and Ba-rich white mica occur within the massive sulfide mineralization and the enveloping alteration zones (van Olden et al., 2020).

2.6 Discussion

Ancient VMS and modern SMS deposits occur in numerous tectonic settings but are generally associated with extensional environments (Lentz, 1998; Franklin et al., 2005; Piercey, 2011). Extensional back-arc basins that host VMS deposits have characteristic features in the rock record, including distinctive lithofacies associations (lobe-hyaloclastite flows, cryptodomes, Cas and Wright, 1987; McPhie et al., 1993), specific geochemical signatures (FII-FIII-FIV rhyolites, Lesher et al., 1986; Hart et al., 2004; Piercey, 2011), structures accommodating extension (synvolcanic faults, drape folds, Gibson et al., 1999; Mumin et al., 2007), and alteration haloes and zones around deposits (feldspar destruction, white mica and chlorite formation, Gemmell and Large, 1992; Large et al., 2001a). Recognizing these features is important for regional and local exploration targeting in known (and unknown) VMS districts, and for decoding the conditions and circumstances that governed the formation of VMS mineralization. In newly identified prospective districts, identifying key features of prospective horizons enables more efficient assessment of the stratigraphy and helps focus more targeted exploration efforts. These themes will be further examined below.

2.6.1 Basin reconstruction

In some subduction environments, back-arc basins are generated due to extension of the upper plate, where crustal thinning is accommodated by synvolcanic and/or synsedimentary normal faulting (Uyeda and Kanamori, 1979; Sdrolias and Müller, 2006). In modern rift settings, extension can be accommodated by pull-apart basins, a series of half-graben subbasins with horsetail mesh structures or similar structural arrangements (Parson and Wright, 1996; Sibson, 2000, and references therein), and similar configurations can be expected in ancient back-arc basins. In such ancient environments, VMS deposits are commonly associated with volcanic centers in low order basins (Allen et al., 2002). Synvolcanic faults in these basins typically control the rates of subsidence and the seafloor topography and can also act as conduits for magmas and hydrothermal fluids (Gibson et al., 1999). Movement along normal synvolcanic faults can be reversed during basin inversion, which allows for some of these deeply penetrating structures to be preserved, albeit as thrust or transform faults (e.g., East fault; Fig. 2.3; Nelson, 1997; Lafrance et al., 2020). Lithofacies associations can be used to identify important features of the basin, such as proximity to a volcanic center, rapid burial rates, periods of volcanic quiescence, or structural features. The host rocks of the ABM deposit display features typical for an active and proximal volcanic center in a lower-order subsidence basin; several features also point to the presence of active synvolcanic faults. Chemostratigraphy and lithofacies analysis further constrain the relative timing of the different processes that contributed to the formation of the ABM deposit.

Features within the Kudz Ze Kayah formation indicate that the rocks were deposited in a submarine basin at depths between 500 and 2,000 m below sea level, like modern VMS analogues in back-arc settings (Monecke et al., 2014). These features include lack of diagnostic sedimentary textures, such as evidence for storm beds with hummocky cross-stratification suggesting deposition at depths below the storm base (shallow water environments <500 m; Gibson et al., 1999). Further, no evidence of hydrothermal fluid boiling or phase separation has been observed within the mineralization, which suggests a water depth of at least 500 to 1,000 m (Monecke et al., 2014). The presence of primary Cu-rich mineralization indicates water depths of at least 750 m, as fluids that carried Cu would require temperatures of at least 300°C (Franklin et al., 2005; Hannington et al., 2005) and these fluids are only stable at water depths >750 m (Bischoff and Rosenbauer, 1987; Hannington et al., 2005). So, although the water depth is commonly difficult to interpret in ancient basins, a rough estimate is beneficial for understanding of the volcanic and sedimentary processes active in the basin, and our arguments suggest formation at least 750 m below sea level (or deeper).

A common feature of VMS deposits, regardless of water depth, is the temporal and spatial association of VMS mineralization with active volcanic centers, commonly marked by the occurrence of felsic lava flows and/or domes reflecting proximity to volcanic vents and synvolcanic structures that facilitated hydrothermal venting during periods of volcanic quiescence (McPhie et al., 1993; Gibson et al., 1999; Franklin et al., 2005). The occurrence of abundant primary crystal-rich tuff units in the stratigraphy at the ABM deposit, and their chemical similarities and interlayering with coeval coherent rocks (Figs. 2.4, 2.1, and 2.12), is consistent with emplacement proximal to a volcanic center (e.g., Cas and Wright, 1987). The coeval emplacement of flows and sills with the volcaniclastic rocks is also indicative of a relatively dynamic volcanic environment of magma/volcaniclastic emplacement (e.g., Head and Wilson, 2003). Further, the abundance of coherent volcanic rocks interlayered with crystal-rich volcaniclastic rocks proximal to the ABM deposit suggests that the association of these facies with mineralization at ABM is not coincidental and that the deposit area was proximal to a volcanic center during the deposition of all three sequences of the upper Kudz Ze Kayah formation. The relative abundance of coherent volcanic rocks, and relatively minor volcaniclastic rocks, in the Krakatoa zone compared to the ABM zone suggests that the Krakatoa zone was closer to a potential volcanic center than the ABM zone.

Normal movement on synvolcanic faults accommodates crustal extension in back-arc basins, deepens the basins, and can cause significant changes in topography within lower-order basins; synvolcanic faults also act as conduits for magmas erupting in volcanic centres in the back-arc basins (Halbach et al., 1993; Kerr and Gibson, 1993). Synvolcanic faults are commonly responsible for abrupt changes in thickness or terminations of units in their footwall, whereas units in their hanging wall are commonly not affected (Gibson et al., 1999), and in some cases, synvolcanic faulting segments the basin topography, which results in features such as drape folds (Mumin et al., 2007). Stratigraphic reconstruction of the upper Kudz Ze Kayah formation has identified numerous units of volcanic, volcaniclastic, and sedimentary rocks that can be traced up to 1.4 km along strike through the footprint of the ABM zone. The thickness of the identified volcaniclastic and sedimentary units varies significantly in as little as 50 m strike distance (Figs. 2.4, 2.11). We interpret that the changes in thickness were caused by deposition in a fault-bound basin, where synvolcanic faults created abrupt changes in the topography of the sea floor that resulted in thinning of the units in the footwall of the fault and thickening and accumulation of volcaniclastic and sedimentary material in the hanging wall of the fault. The changes in thickness are most easily observed in argillite lenses, which are locally strongly reminiscent of drape-folds (Figs. 2.4, 2.11; Mumin et al., 2007), typical of a basin with active synvolcanic faults. Minor later modification of the units by the active synvolcanic faults was also likely. The interpreted fault planes of the synvolcanic faults are irregular at the deposit scale, which is typical for a heterogenous environment in a extensional basin (Rissmann et al., 2011). It is notable that the effects of normal movement along the synvolcanic faults can be observed up to the Kudz Ze Kayah-Wind Lake formation contact (Fig. 2.3), which suggests that the synvolcanic faults were active throughout the deposition of the entire Kudz Ze Kayah formation.

Synvolcanic faults are also known to act as magma conduits and to control emplacement of sills, dikes, felsic flows, domes, or cryptodomes (Sibuet et al., 1998; Gibson et al., 1999; Winter et al., 2004; Franklin et al., 2005), and the alignment of such rocks can also be used for reconstructing synvolcanic faults. In the ABM zone, felsic sills and flows thicken in proximity to certain faults, but thin out laterally or terminate in proximity to other faults (Figs. 2.4, 2.11), which suggests that the interpreted synvolcanic faults acted intermittently as conduits for the ascending felsic magmas. The mafic subvolcanic sills also show systematic changes in unit thickness and alteration, indicating their emplacement was also controlled by synvolcanic faulting (Figs. 2.4, 2.11). Further, the occurrence of volcanic units with varying signatures (FB, MA) proximal to one another near the same interpreted synvolcanic faults also implies that these faults acted as conduits for magmas throughout the duration of volcanic activity in the basin.

Synvolcanic faults in the ABM zone occur in two dip directions (Fig. 2.3): 1) 075° to 105° with dips between 60° and 85°, and 2) 150° to 180°, with dips 75° to subvertical. The faults are interpreted to be splays of and subordinate to the regional East fault, which was likely one of the major faults controlling subsidence in the basin. The fault arrangement in the ABM zone (Fig. 2.4) is reminiscent of either a set of listric faults subordinate to the East fault, a pull-apart basin, or a series of half-graben subbasins with horsetail mesh structures; any of these configurations can occur in a modern subsiding basin (Parson and Wright, 1996; Wright et al., 1996). The orientation of the above-described drape folds, the thickening of the volcaniclastic and sedimentary units toward the southeast and the East fault, and the general thickening of Sequence 2 toward the East fault implies the that the basin hosting the ABM deposit was deepening in that direction (i.e., deepening toward the southeast).

2.6.2 Precipitation mechanisms for mineralization

Ore and gangue minerals in VMS deposits precipitate due to fluid mixing between hot, acidic, reducing metal-rich hydrothermal fluids (T = 200°–350°C, pH ~2–5; Hannington et al., 2005 and references therein) and cold, oxidizing pH-neutral seawater (~ 2°C; Haymon, 1983). The earliest estimates of depositional efficiency suggested that up to 90% of the metals within the hydrothermal fluids vented into the ocean and were lost if the mixing occurs at the sea floor (Converse et al., 1984); however, more recent investigations have shown that depositional efficiency of seafloor hydrothermal vents varies between 5 and 30 % (Endeavour vent field and TAG active mound, respectively; Humphris and Cann, 2000; Jamieson et al., 2014). Even so, if the hydrothermal fluids are introduced to water-saturated facies beneath the sea floor, fluid mixing, sulfide precipitation, and zone refining can be as efficient or even more so at forming massive sulfide deposits (Doyle and Allen, 2003; Piercey, 2015). Replacement-style VMS deposits can form anywhere between 0 m depth down to 200 m below the seafloor, where volcaniclastic facies remain porous and permeable (Doyle and Allen, 2003) and lateral fluid flow is possible (Piercey, 2015); they also require the presence of nonpermeable to semipermeable units (sills, lava flows, argillites) within the stratigraphy that act as barriers for fluid flow, and rapid burial rates for most effective sulfide mineral precipitation and preservation (Doyle and Allen, 2003). At the ABM deposit, felsic volcaniclastic rocks comprise a significant portion of the deposit-hosting stratigraphy. Felsic lapilli tuffs in the upper Kudz Ze Kayah formation display features typical for subaqueous mass flows or eruption-fed density currents (Cas and Wright, 1987; McPhie et al., 1993; White, 2000). The lapilli tuffs are generally massive, unsorted to poorly sorted (Fig. 2.6F-G) with singular units that can be spatially extensive (>0.5 km^2) compared to the felsic coherent units (maximum of 0.12 km^2 in the ABM zone), and over 50 m thick, which implies rapid accumulation and burial (McPhie et al., 1993; White, 2000). The thickest units occur in Sequence 3, but lapilli tuffs occur throughout the upper Kudz Ze Kayah formation, indicating that the style of volcanism remained relatively unchanged throughout the deposition of the upper Kudz Ze Kayah formation. Interpreted porous and permeable lithofacies (e.g., lapilli tuffs, crystal-rich tuffs, and brecciated contacts of sills and flows) that were likely saturated with seawater in the shallow subsurface were interbedded with relatively impermeable lithofacies (e.g., coherent volcanic facies and possibly lithified mudstones/argillites) that likely acted as barriers to fluid flow. Moreover, it is possible that coherent portions of volcanic units and possibly semipermeable argillite lenses acted as aquitards that prevented upward flow of fluids along the synvolcanic faults (e.g., Mumin et al., 2007), diverting hydrothermal fluids laterally into the water-saturated, unconsolidated volcaniclastic or brecciated rocks. This diversion would have resulted in fluid mixing between hot hydrothermal fluids and infiltrated seawater in the volcaniclastic rocks and formation of replacement fronts comprising sulfide mineralization and irregular alteration zones; these features are observed in drill core emanating outwards from inferred synvolcanic faults (Figs. 2.4, 2.11). The lateral flow of the hydrothermal fluids within porous and water-saturated units also resulted in the formation of laterally continuous massive sulfide lenses that parallel stratigraphy. Thus, this juxtaposition of lithofacies with varying porosity and permeability proximal to synvolcanic faults controlled the hydrothermal fluid flow, mineralization, and distribution of the alteration within the upper Kudz Ze Kayah formation.

Subseafloor replacement also creates distinctive hydrothermal alteration patterns. In the ABM deposit, replacement-style mineralization is closely associated with pervasive white mica alteration; however, unlike in exhalative mineralization, pervasive white mica alteration occurs in both the hanging wall and footwall to mineralization. The occurrence of hydrothermal alteration in the hanging wall can be explained in two different ways, both of which are consistent with subseafloor replacement. One possible explanation is that the hanging wall to the mineralization was present during hydrothermal activity and sulfide formation, and that the mineralized interval was within 200 m of the sea floor and not diagenetically sealed, because hydrothermal alteration is documented all the way to the contact with the Wind Lake formation. The alternative explanation is that the extended hanging wall to the mineralization (Sequence 3) was absent during the main mineralizing event, but lower-temperature hydrothermal activity continued intermittently during its later deposition. The absence of significant mineralization in Sequence 3 rocks is consistent with the second possibility and indicates that the hydrothermal activity continued throughout the basin evolution, albeit at temperatures lower than those necessary to precipitate mineralization.

The alteration and replacement fronts outlined above are also reflected in the distribution of Ba in the ABM deposit. Barium is a common component of hydrothermal fluids and precipitates as Ba minerals due to mixing of the hydrothermal fluids with seawater (Von Damm, 1990; Averyt and Paytan, 2003). Barium-rich minerals such as barite, Ba-rich white mica (Large et al., 2001a; Soltani Dehnavi et al., 2019), and Ba-rich feldspar are commonly associated with massive sulfide mineralization (Lydon, 1984; Franklin et al., 2005). At the ABM deposit, the highest Ba values occur nearest to the 075°-105° set of synvolcanic faults, suggesting that the hydrothermal fluids upwelled along these faults. The decrease of Ba values along and within sills and flows indicates these units had low permeability and acted as local fluid barriers (Fig. 2.4). In addition, Ba distribution (Figs. 2.4, 2.11) suggests that the immediate hanging wall of the massive sulfide mineralization, comprising the proximal overlying argillite lenses and the volcaniclastic rocks in between, acted as a semipermeable barrier/aquitard for upwelling hydrothermal fluids and were consequently altered by Ba-rich hydrothermal fluids during the mineralization stage. Moreover, the lateral distribution of Ba into units away from synvolcanic faults is also supportive of the Ba- and metal-rich fluids having infiltrated laterally away from synvolcanic structures into the unconsolidated volcaniclastic rocks. In the Krakatoa zone, the mafic sills acted as a partial aquitard for the hydrothermal fluids, as anomalous Ba values occur predominantly at the contacts of the mafic sills or are associated with the mineralized lenses (Fig. 2.12).

We suggest that the distribution of anomalous Ba values is not caused by a later hydrothermal or metamorphic overprint but represents the original fluid pathways and extent of the hydrothermal system that formed the massive sulfide mineralization and associated alteration zones. We base this on the close association of Ba-rich minerals and anomalous Ba values with massive sulfide mineralization (Figs. 2.4, 2.11, and 2.12) and the presence of hanging-wall alteration that exhibits minor Ba enrichment. The presence of argillite in the hanging wall, together with the Ba distribution, suggest that mineralization coincides with a break in volcanism, which is also reflected by the change in chemistry from FB rocks in Sequence 2 to FA rocks in Sequence 3, indicating that mineralization formed during the waning stages of the FB cycle or during the commencement of the second FA cycle.

The period of volcanic inactivity between Sequence 2 and Sequence 3 was likely at minimum 75 k.y., based on estimates of settling rates of argillites from the Middle Devonian (e.g., Goodfellow and Turner, 1989). Estimates calculated from the maximum thickness (adjusted for the drill hole dip) of the thickest argillite lens (9.85 m, not corrected for thickness changes due to diagenesis) and average shale deposition rates (13 cm/1,000 y) from a similar sediment-hosted deposit type (e.g., Goodfellow and Turner, 1989) yield a minimum age of 75,000 years. These rates are similar to the timeframes of modern SMS deposits (Jamieson et al., 2014) and those recently calculated for deposits in the Finlayson Lake district (e.g., Manor et al., in press).

The ABM deposit has zinciferous Zn grades (6.6 wt %), and above average tonnage for VMS deposits globally (19.1 Mt; Piercey et al., 2015). We suggest that the grade and tonnage in the ABM deposit was partly controlled by the basin architecture and magmatic activity. In particular, the permeability contrasts between various lithofacies coupled with fluid flow controlled by synvolcanic faults allowed for replacement-style mineralization, which we suggest enhanced both the amount of metal precipitated from the hydrothermal fluids and increased the efficiency of zone refining, which led to increases of the Zn grade (e.g., Piercey, 2015). These results demonstrate the critical importance of understanding basin architecture and sulfide emplacement processes and its potential influence on grade and tonnage in ancient VMS deposits. By understanding such features and developing criteria for recognizing them, it may be possible to determine similar geologic environments globally that have similar potential for high value deposits.

2.6.3 Relationship between ABM and Krakatoa zones

Although the distribution of lithogeochemical groups and lithofacies is similar in both zones, the transition between the ABM and Krakatoa zones is unclear due to the dextral-oblique offset on the East fault (Fig. 2.3). For example, the mineralization in the eastern part of the ABM zone occurs as a single massive sulfide lens with argillite and tuff in its hanging wall that terminates on the East fault. The corresponding mineralization in the Krakatoa zone, however, comprises several massive sulfide lenses located on the upper and lower contacts and within the MA mafic sill. This suggests that the hydrothermal system in the two zones was likely active during a similar period, after the emplacement of MA sills and the emplacement and deposition of Sequence 1 and 2 felsic rocks, but it is unclear whether the alteration and mineralization in the two zones are part of the same hydrothermal system, with the transition between the ABM and Krakatoa portions eroded from the Krakatoa block due to the offset and rotation of the block, or the two hydrothermal systems formed in separate lower-order basins on each side of the East fault and tapped the same source of hydrothermal fluids, likely along the East fault itself. Further studies of the hydrothermal alteration and ore assemblages in both zones are necessary to determine whether the two zones are part of one hydrothermal system or if they represent two distinct deposits in separate lower-order basins.

2.6.4 Petrogenesis of felsic and mafic rocks

Results of this study echo previous regional-scale research (Piercey et al., 2001, 2002b, 2003; Murphy et al., 2006; Manor and Piercey, 2019) but provide further details on the petrogenesis of the felsic and mafic volcanic rocks that host the ABM deposit. Piercey et al. (2001, 2003) noted anomalously high contents of high field strength elements (HFSEs) and rare earth elements (REEs) in the felsic rocks of the Kudz Ze Kayah formation. Our study further refines the lithostratigraphy and has identified two distinct lithogeochemical groups of felsic rocks within the upper Kudz Ze Kayah formation: 1) the FA group, which has relatively high Zr values compared to felsic rocks occurring in sequences hosting similar felsic-hosted VMS deposits in the geologic record (e.g., Lentz, 1998), and 2) the FB group, which has lower HFSE-REE contents compared to the FA group. Both groups have calc-alkaline affinities and plot as within-plate and A-type felsic rocks (Fig. 2.8; Pearce et al., 1984; Whalen et al., 1987; Ross and Bédard, 2009), and their PM-normalized patterns are alike (Fig. 2.9). Even though chondrite-normalized plots show distinct differences in the intensity of the negative Eu anomaly, the similarities between the two lithogeochemical groups and their close spatial association suggest that the two groups have likely partially melted a common source, most likely continental crust (Piercey et al., 2001, 2003) at relatively low pressures and high temperatures (e.g., Hart et al., 2004 and references therein). However, the differences in absolute

Zr and REE contents, Eu-anomalies, and some immobile element ratios (i.e., Zr/Al_2O_3, Al_2O_3/TiO_2, Zr/Y, Ti/Sc) indicate that the two groups formed under differing conditions, likely forming from melts that were generated at varying temperatures (Piercey et al., 2003). The magmas that formed the FA group felsic rocks likely formed at higher temperatures than the rocks of the FB group, as melting temperatures can control the HFSE-REE budget of continental crust-derived melts (Harrison and Watson, 1983; Watson and Harrison, 1983; Bea, 1996; Lentz, 1998; Piercey et al., 2003, 2008; Hart et al., 2004). Both felsic groups have LREE enrichment and display negative Nb and Ti anomalies in PM-normalized plots, features similar to felsic magmas generated from the remelting of continental arc crust and/or continental crust in general (Morris et al., 2000), which fits with the general continental back-arc setting for these rocks (Piercey et al., 2001). Past studies also suggested mantle-crustal mixing due to juvenile basaltic underplating (Piercey et al., 2001, 2008), which would impart some mantle-like trace element signatures onto the felsic rocks. One of these proxies that identifies such inputs is the Nb/Ta value that is commonly used to distinguish between mantle (Nb/Ta ~17) and upper continental crustal sources (Nb/Ta ~12; Green, 1995; Barth et al., 2000; McLennan et al., 2003). Group FA rocks show higher average values of the Nb/Ta than rocks of group FB (FA ~17.8 vs. FB ~12.0), indicative of a higher juvenile mantle input into the FA group magmas, a consequence of upwelling of basaltic magmas and crustal underplating in an extensional back-arc basin (Piercey et al., 2008; Piercey, 2011). Another possible explanation for the higher Nb/Ta values could be the fractionation of a Ti phase during the ascent of the magma, such as titanite and rutile, that favors Ta over Nb (Green and Pearson, 1987; Green, 1995). This is unlikely, however, as the FA group has higher Ti values than the FB group, and Ti minerals such as rutile were observed in thin section in both felsic rock groups. Comparing the Ti/Sc values for the felsic groups, the FB2 group has higher average values (FA ~308 vs. FB2 ~370), which are lower than typical upper crust values (~445; Wedepohl, 1995) and indicative of a lesser input from juvenile sources to the FB2 group than to the FA group (Wedepohl, 1995; McLennan et al., 2003; Piercey et al., 2008). The trace element signatures (Nb/Ta, Ti/Sc) indicate that both groups display evidence of mixing with juvenile basaltic material, but the FA group rocks have a greater juvenile component compared to the FB group rocks.

The spatial association of the FB1 felsic rocks with the MA mafic sills confirms bimodal magmatism in the upper Kudz Ze Kayah formation. The FB1 felsic sills and tuffs were emplaced and deposited early in the evolution of the ABM basin, given that the MA mafic sills intruded along the contacts of the FB1 felsic sills, and both are hydrothermally altered (Fig. 2.13A, B). The felsic rocks of the upper Kudz Ze Kayah formation (FA and FB groups) are interpreted to be products of crustal melting due to basaltic underplating, and it is likely that the associated mafic rocks formed by modification of upwelling basaltic magmas along synvolcanic conduits. These MA group mafic rocks have transitional to calc-alkaline signatures (Fig. 2.8) and plot in to the MORB, E-MORB, and WPB fields (Fig. 2.10). These signatures are common for mafic rocks within evolved continental to back-arc environments (Piercey, 2011) and point to an enriched mantle source and/or a source/magmas that were contaminated by continental crust (Pearce, 1996). Relative to the overlying Wind Lake formation mafic rocks, the MA mafic rocks have lower degrees of crustal contamination, as demonstrated by the Th/Yb-Nb/Yb and Th/Nb-Zr diagrams (Fig. 2.10C), possibly due to shorter residence times in the crust and/or due to faster rates of magma ascent (Gamble et al., 1995; Piercey et al., 2002a), although having a similar mantle source as the Wind Lake formation mafic rocks. This argument is supported by the similar Nb/Ta for both groups, ~16, indicating a mantle of either lithospheric or asthenospheric origin (Piercey et al., 2001, 2008). Although the mafic sills with MA signatures occur throughout Sequence 2 in the deposit area, their volume is relatively minor compared to the Wind Lake formation mafic rocks regionally. The MB mafic rocks, occurring as relatively thin mafic sills intruding mostly Sequence 3 rocks, have geochemical signatures similar to those of the mafic tuffs in the Wind Lake formation, specifically to the "4b" groups of Piercey et al. (2002b; Fig. 2.10). The occurrence of mafic sills with MB signatures at the top of Sequence 3 (Fig. 2.4) suggests that the mafic tuffs at the base of the Wind Lake and the MB mafic sills have a common source and formed roughly at a similar time, after the deposition of Sequence 3 (Fig. 2.13E).

Most known VMS deposits are interpreted to be associated with hot, shallow synvolcanic intrusions that are comagmatic with rhyolitic volcanism and they are interpreted to have acted as heat sources for the developing VMS hydrothermal systems (Galley, 2003; Franklin et al., 2005). In some cases, spatially associated subvolcanic intrusions postdate the VMS mineralization (Galley, 2003; Barrote et al., 2020) and are viewed as indicators of elevated heat gradients in the rift environment, due to their crystallization ages being younger than the VMS deposits, rather than the immediate drivers of VMS hydrothermal circulation (Hart et al., 2004; Piercey, 2011). Volcanic rocks in the Kudz Ze Kayah formation have similar compositions to the Grass Lakes Plutonic Suite intrusive rocks (Piercey et al., 2003; Murphy et al., 2006; Manor and Piercey, 2019), and the latter have been hypothesized as the heat source for the ABM hydrothermal system (Piercey et al., 2003). However, recent U-Pb geochronology in the district has shown that the plutonic suite postdates the deposition of the upper Kudz Ze Kayah formation by ~900 k.y. (Manor et al., 2022); thus, these granitoids did not directly contribute to the heat flow regime that generated the ABM deposit, but they are likely the upper crustal manifestations of elevated geothermal gradients within a rift environment at a regional scale (e.g., Piercey et al., 2008; Piercey, 2011). The occurrence of multiple magmatic and volcanic events of varying composition ranging from mafic to felsic within the back-arc basin implies an enduring elevated heat gradient and, by extension, the likely presence of a heat corridor underlying the back-arc basin (e.g., Galley, 2003; Piercey, 2011).

This heat corridor also underwent heat gradient fluctuations as recorded by the litho- and chemo-stratigraphy of the upper Kudz Ze Kayah formation, which suggests potential heating and cooling cycles during its evolution. For example, the FA group REE-HFSE signatures show that they

Figure 2.13. Series of schematic diagrams of idealized stratigraphy of 6815400 mN long section though time showing the deposition of the upper Kudz Ze Kayah formation and the massive sulfide mineralization. (A) Deposition of Sequence 2 rocks with FB signatures on top of Sequence 1 rocks with FA signatures. In Sequence 2, rocks with FB2 signatures deposited first, followed by deposition of FB1 tuffs, emplacement of FB1 sills and continued deposition of FB2 volcaniclastic rocks, flows and sills. (B) Emplacement of MA mafic sills along the contacts of pre-existing FB1 felsic sills. (C) Break in volcanism, argillite lenses deposited on top of Sequence 2, massive sulfide mineralization formed in the subsurface. (D) Deposition of Sequence 3 volcaniclastic and volcanic rocks with FA signatures. (E) Switch to mafic alkaline volcanism, deposition of Wind Lake formation rocks. (F) Current erosion level pictured without overlying till. HT = hydrothermal.

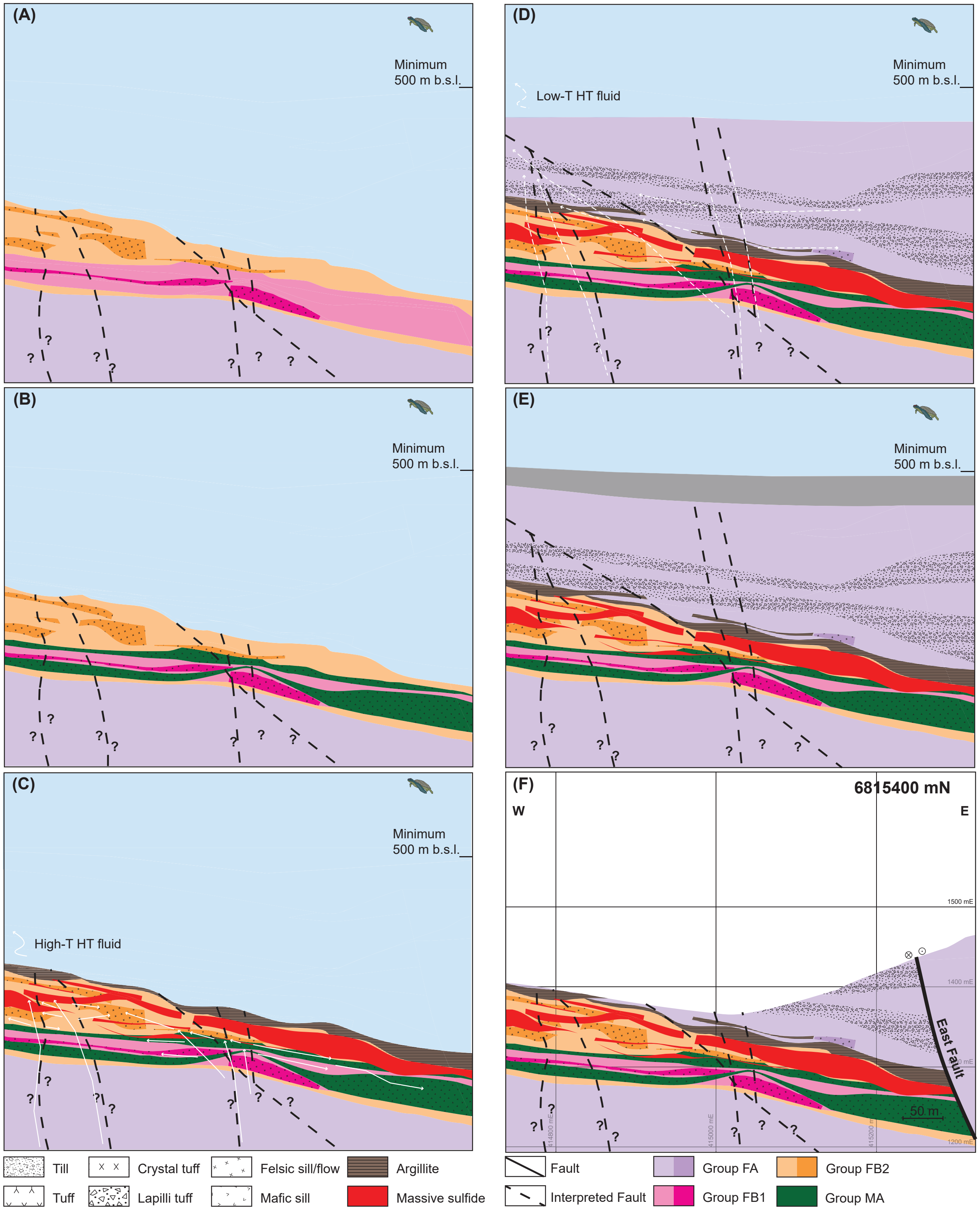
(A)
Minimum
500 m b.s.l.
(B)
Minimum
500 m b.s.l.
(C)
Minimum
500 m b.s.l.
High-T HT fluid
(D)
Minimum
500 m b.s.l.
Low-T HT fluid
(E)
Minimum
500 m b.s.l.
(F)
6815400 mN
W
E
1500 mE
1400 mE
East Fault
50 m
1200 mE
Till
Crystal tuff
Felsic sill/flow
Argillite
Tuff
Lapilli tuff
Mafic sill
Massive sulfide
Fault
Interpreted Fault
Group FA
Group FB1
Group FB2
Group MA

were likely generated at relatively higher temperatures relative to the FB group rocks, reflecting a high- to low-temperature cooling cycle (Piercey et al., 2001, 2003). It would be expected that the FA rocks should be associated with the VMS mineralization, given their high-temperature origin (Piercey et al., 2008; Piercey, 2011), yet the FA rocks are not directly associated with the massive sulfide mineralization, which is instead hosted by Sequence 2 rocks with FB signatures (Figs. 2.4, 2.11, and 2.12). Rather, the mineralization occurs in FB rocks in in the upper portions of Sequence 2 associated with argillite lenses at the transition from Sequence 2 to Sequence 3, indicating that the massive sulfide mineralization occurred during the waning stages of lower-temperature FB volcanic activity or during a period of volcanic quiescence before the restart of a second cycle of higher-temperature FA felsic volcanism (Fig. 2.13). During such a period of quiescence, the influx of FA magma into the chamber at depth could have acted as a heat source that sustained the mineralizing hydrothermal system (e.g., Cathles et al., 1997; Cathles, 2011). The duration of the period of volcanic inactivity at the transition from Sequence 2 to Sequence 3 was at minimum 75 k.y., as evidenced by the thickness of the argillite lenses, which fits within the timeframe of ~400 k.y. for the deposition of 250 m of stratigraphy in the upper part of the Kudz Ze Kayah formation (Manor et al., 2022) and is typical for the lifespan of VMS districts in the ancient record (<2 m.y.; Cathles et al., 1997; Franklin et al., 2005). The evidence for multiple heating cycles within the ABM stratigraphy implies that the mineralizing processes were associated with high-temperature magmatic pulses and input of juvenile material in the magma chamber, possibly during a high-temperature part of a magmatic cycle, similar to what is observed in continental arcs (De Silva et al., 2015). This suggests that the source for the heat that induced the hydrothermal system was prolonged and associated with a deep-seated magma chamber that elevated the crustal-level geothermal gradient, creating a thermal corridor that could sustain robust hydrothermal activity that led to VMS mineralization. Thus, in the Finlayson Lake district, shallow subvolcanic intrusions (and spatially associated mineralization) were a product of elevated geothermal gradient of the environment, but the subvolcanic intrusions themselves were not responsible for driving VMS hydrothermal circulation and deposit formation.

2.7 Conclusions

Reconstruction of the basin architecture of the Upper Devonian Kudz Ze Kayah formation shows that the rocks hosting the ABM VMS deposit were deposited in a back-arc basin at least 750 m deep with an active volcanic center and associated with synvolcanic faults. The identification of significant and systematic changes of the thickness of the sedimentary and volcaniclastic units, together with the distribution of coherent volcanic and subvolcanic rocks, allowed for the reconstruction of two sets of synvolcanic faults that were active during the deposition and emplacement of the lithostratigraphic units. Argillite lenses acted as semipermeable barriers at the top of the volcanosedimentary pile, trapping the hydrothermal fluids that ascended along synvolcanic faults and forcing them to permeate laterally into the subsurface, which likely resulted in more efficient sulfide precipitation and greater abundance of metals preserved and enhanced zone refining, and generated the elevated Zn tonnages and grades in the ABM deposit. The distribution of Ba can be used to map out areas with the most intense fluid flow, and in the ABM deposit, these coincide with synvolcanic faults, zones of pervasive alteration, and lenses of massive sulfide mineralization. The main argillite lens marks a period of volcanic quiescence that coincides with a change in the geochemistry of the footwall and hanging-wall felsic volcanic rocks and during which period the massive sulfide mineralization formed.

The reconstructed litho- and chemo-stratigraphy demonstrates that the ABM and Krakatoa zones were likely part of the same basin, but possibly in separate subbasins, with the Krakatoa zone likely closer to the volcanic center due to the higher relative abundance of coherent rocks. Mineralized lenses in both zones occur at roughly the same stratigraphic position and were either connected and part of the same hydrothermal system or they represent two separate systems but tap the same fluid source at depth.

Although they are not directly associated with the mineralization, FA group volcanic rocks at the ABM deposit serve as an important indicator of the elevated geothermal gradient in the basin, which is a key factor in the formation of VMS mineralization. High Zr values (>550 ppm), together with elevated HFSEs, REEs, and higher Nb/Ta values associated with the FA felsic volcanic rocks, reflect much higher temperatures and a higher degree of mixing of crustal melts with juvenile material compared to the FB felsic rocks. The cyclicity of the magma output represented by the systematic changes in geochemical signatures and the bimodal character of volcanism in the upper Kudz Ze Kayah formation suggest an elevated geothermal gradient within the back-arc basin due to the presence of a magmatically-driven thermal corridor underlying the basin. This elevated geothermal gradient was critical for driving hydrothermal circulation that formed the VMS mineralization at the ABM deposit.

The lithostratigraphic and geochemical features of the host rocks of the ABM deposit outlined in this study can be used as guidance for identifying prospective horizons and sequences in similar environments globally that formed within continental back-arc basins with associated bimodal volcanism.

2.8 Acknowledgments

This paper represents a part of the Ph.D. thesis by the first author. We would like to thank BMC Minerals Ltd. for their generous financial, field, and logistical support. Support for the project was provided by an NSERC Discovery Grant to Dr. Stephen Piercey, an NSERC Collaborative Research Development Grant – Project (CRDPJ) between Dr. Stephen Piercey and BMC Minerals Ltd., a Student Research Grant from the Society of Economic Geologists Canada Foundation, and funding from Memorial University of Newfoundland. We would like to thank Dr. Michelle DeWolfe, Dr. Steven Hollis, and Dr. Jonathan Cloutier for their detailed and constructive reviews of an earlier version of this manuscript that have greatly improved it. The senior author would like to thank Matthew Manor, Carly Mueller, and Rose Cobbett for constructive comments on the manuscript, Neil Martin, Robin Black, and Robert Burke from BMC Minerals and Dillon Hume from Equity Exploration for comments and conversations beneficial to this paper, and the BMC Minerals and Equity Exploration staff at the Kudz Ze Kayah exploration camp for their help during the 2018 and 2019 field seasons.

2.9 References

Allen, R.L., Lundström, I., Ripa, M., Simeonov, A., and Christofferson, H., 1996a, Facies analysis of a 1.9 Ga, continental margin, back-arc, felsic caldera province with diverse Zn-Pb-Ag-(Cu-Au) sulfide and Fe oxide deposits, Bergslagen region, Sweden: Economic Geology, v. 91, p. 979–

Allen, R.L., Weihed, P., and Svenson, S.A., 1996b, Setting of Zn-Cu-Au-Ag massive sulfide deposits in the evolution and facies architecture of a 1.9 ga marine volcanic arc, Skellefte district, Sweden: Economic Geology, v. 91, p. 1022–1053.

Allen, R.L., Weihed, P., Blundell, D., Crawford, T., Davidson, G., et al, 2002, Global comparisons of volcanic-associated massive sulphide districts: Geological Society of London, Special Publications, v. 204, p. 13–37.

Averyt, K.B., and Paytan, A., 2003, Empirical partition coefficients for Sr and Ca in marine barite: Implications for reconstructing seawater Sr and Ca concentrations: Geochemistry, Geophysics, Geosystems, v. 4, p. 1–14.

Barrett, T.J., and MacLean, W.H., 1994, Chemostratigraphy and hydrothermal alteration in exploration for VHMS deposits in greenstones and younger volcanic rocks: Geological Association of Canada, Short Course Notes, v. 11, p. 433–466.

Barrett, T.J., MacLean, W.H., and Tennant, S.C., 2001, Volcanic sequence and alteration at the Parys Mountain volcanic-hosted massive sulfide deposit, Wales, United Kingdom: Applications of immobile element lithogeochemistry: Economic Geology, v. 96, p. 1279–1305.

Barrote, V.R., McNaughton, N.J., Tessalina, S.G., Evans, N.J., Talavera, C., Zi, J.W., and McDonald, B.J., 2020, The 4D evolution of the Teutonic Bore Camp VHMS deposits, Yilgarn Craton, Western Australia: Ore Geology Reviews, v. 120, article 103448, p.1–12.

Barth, M.G., McDonough, W.F., and Rudnick, R.L., 2000, Tracking the budget of Nb and Ta in the continental crust: Chemical Geology, v. 165, p. 197–213.

Bea, F., 1996, Controls on the trace element composition of crustal melts: Transactions of the Royal Society of Edinburgh-Earth Sciences, v. 87, p. 33–41.

Belford, S.M., Davidson, G.J., McPhie, J., and Large, R.R., 2015, Architecture of the Neoarchaean

Jaguar VHMS deposit, Western Australia: Implications for prospectivity and the presence of depositional breaks: Precambrian Research, v. 260, p. 136–160.

Bischoff, J.L., and Rosenbauer, R.J., 1984, The critical point and two-phase boundary of seawater, 200–500 °C: Earth and Planetary Sciences, v. 68, p. 172–180.

Bischoff, J.L., and Rosenbauer, R.J., 1987, Phase separation in seafloor geothermal systems: American Journal of Science, v. 287, p. 953–973.

Boulton, A., 2002, GP4F polymetallic volcanic-hosted massive sulphide (VHMS) deposit, Finlayson Lake District, Yukon Territory: B.Sc. thesis (Honors), Victoria, Canada, University of Victoria, 47 p.

Bradshaw, G.D., Tucker, T.L., Peter, J.M., Paradis, S., and Rowins, S.M., 2001, Geology of the Wolverine polymetallic volcanic-hosted massive sulphide deposit, Finlayson Lake district, Yukon Territory, Canada, in Emond, D.S. and Weston, L.H. eds., Yukon exploration and geology 2000: Exploration and Geological Services Division, Yukon, Indian and Northern Affairs Canada, p. 269–287.

Bradshaw, G.D., Rowins, S.M., Peter, J.M., and Taylor, B.E., 2008, Genesis of the Wolverine volcanic sediment-hosted massive sulfide deposit, Finlayson Lake district, Yukon, Canada: Mineralogical, mineral chemical, fluid inclusion, and sulfur isotope evidence: Economic Geology, v. 103, p. 35–60.

Burnham, O.M., 2008, Trace element analysis of geological samples by inductively coupled plasma mass spectrometry (ICP-MS) at the Geoscience Laboratories: Revised capabilities due to method improvements: Summary of Field Work and Other Activities 2008: Ontario Geological Survey, Open File Report, v. 6226, p. 1–10.

Burnham, O.M., and Schweyer, J., 2004, Trace element analysis of geological samples by inductively coupled plasma mass spectrometry at the Geoscience Laboratories: Revised capabilities due to improvements to instrumentation: Summary of Field Work and Other Activities 2004: Ontario Geological Survey, Open File Report, v. 6145, p. 1–20.

Cas, R.A.F., and Wright, J.V., 1987, Volcanic successions: Modern and ancient: A geological approach to processes, products and successions: London, Allen & Unwin Ltd., 528 p.

Cathles, L.M., 2011, What processes at mid-ocean ridges tell us about volcanogenic massive sulfide deposits: Mineralium Deposita, v. 46, p. 639–657.

Cathles, L.M., Erendi, A.H.J., and Barrie, C.T., 1997, How long can a hydrothermal system be sustained by a single intrusive event?: Economic Geology, v. 92, p. 766–771.

Colpron, M., Nelson, J.L., and Murphy, D.C., 2006, A tectonostratigraphic framework for the pericratonic terranes of the Northern Canadian Cordillera: Geological Association of Canada, Special Paper 45, p. 1–23.

Converse, D.R., Holland, H.D., and Edmond, J.M., 1984, Flow rates in the axial hot springs of the East Pacific Rise (21°N): Implications for the heat budget and the formation of massive sulfide deposits: Earth and Planetary Science Letters, v. 69, p. 159–175.

DeWolfe, Y.M., Gibson, H.L., and Richardson, D., 2018, 3D reconstruction of volcanic and ore-forming environments of a giant VMS system: A case study from the Kidd Creek mine, Canada: Ore Geology Reviews, v. 101, p. 532–555.

Doyle, M.G., and Allen, R.L., 2003, Subsea-floor replacement in volcanic-hosted massive sulfide deposits: Ore Geology Reviews, v. 23, p. 183–222.

Doyle, M.G., and Huston, D.L., 1999, The subsea-floor replacement origin of the Ordovician Highway-Reward volcanic-associated massive sulfide deposit, Mount Windsor Subprovince, Australia: Economic Geology, v. 94, p. 825–844.

Fisher, R.V., 1966, Rocks composed of volcanic fragments and their classification: Earth Science Reviews, v. 1, p. 287–298.

Franklin, J.M., Lydon, J.W., and Sangster, D.F., 1981, Volcanic-associated massive sulfide deposits: Economic Geology, 75th Anniversary Volume, p. 485–627.

Franklin, J.M., Gibson, H.L., Jonasson, I.R., and Galley, A.G., 2005, Volcanogenic massive sulfide deposits: Economic Geology, 100th Anniversary Volume, p. 523–560.

Friesen, V.C., DeWolfe, Y.M., and Gibson, H.L., 2020, Volcanic reconstruction and geochemistry of the Powderhouse formation in the Paleoproterozoic VMS-hosting Chisel sequence, Snow Lake, Manitoba, Canada: Canadian Journal of Earth Sciences, v. 21, p. 1–21.

Gabrielse, H., Murphy, D.C., and Mortensen, J.K., 2006, Cretaceous and Cenozoic dextral orogen-parallel displacements, magmatism, and paleogeography, north-central Canadian Cordillera: Geological Association of Canada, Special Paper no. 46, p. 255–276.

Galley, A.G., 2003, Composite synvolcanic intrusions associated with precambrian VMS-related hydrothermal systems: Mineralium Deposita, v. 38, p. 443–473.

Galley, A.G., Watkinson, D.H., Jonasson, I.R., and Riverin, G., 1995, The subsea-floor formation of volcanic-hosted massive sulfide: Evidence from the Ansil, Rouyn-Noranda, Canada: Economic Geology, v. 90, p. 2006–2017.

Gamble, J.A., Wright, I.C., Woodhead, J.D., and McCulloch, M.T., 1995, Arc and back-arc geochemistry in the southern Kermadec arc-Ngatoro Basin and offshore Taupo volcanic zone, SW Pacific: Geological Society, London, Special Publication no. 81, p. 193–212.

Gemmell, B.J., and Large, R.R., 1992, Stringer system and alteration zones underlying the Hellyer volcanic-hosted massive sulfide deposit, Tasmania, Australia: Economic Geology, v. 87, p. 620–649.

Gibson, H.L., Morton, R.L., and Hudak, G.J., 1999, Submarine volcanic processes, deposits, and environments favourable for the location of volcanic-associated massive sulfide deposits: Reviews in Economic Geology, v. 8, p. 15–51.

Goodfellow, W.D., and Turner, R.J.W., 1989, Sulfur isotope variability in sediment-hosted massive sulfide deposits determined using the ion microprobe SHRIMP: 1. An example from the Rammelsberg orebody - A discussion: Economic Geology, v. 84, p. 451–452.

Green, T.H., 1995, Significance of Nb/Ta as an indicator of geochemical processes in the crust-mantle system: Chemical Geology, v. 120, p. 347–359.

Green, T.H., and Pearson, N.J., 1987, An experimental study of Nb and Ta partitioning between Ti-rich minerals and silicate liquids at high pressure and temperature: Geochimica et Cosmochimica Acta, v. 51, p. 55–62.

Halbach, P., Pracejus, B., and Marten, A., 1993, Geology and mineralogy of massive sulfide ores from the central Okinawa Trough, Japan: Economic Geology, v. 88, p. 2210–2225.

Hannington, M.D., de Ronde, C.E.J., and Petersen, S., 2005, Sea-floor tectonics and submarine hydrothermal systems: Economic Geology, 100th Anniversary Volume, p. 111–141.

Harrison, T.M., and Watson, E.B., 1983, Kinetics of zircon dissolution and zirconium diffusion in granitic melts of variable water content: Contributions to Mineralogy and Petrology, v. 84, p. 66–72.

Hart, T.R., Gibson, H.L., and Lesher, C.M., 2004, Trace element geochemistry and petrogenesis of felsic volcanic rocks associated with volcanogenic massive Cu-Zn-Pb sulfide deposits: Economic Geology, v. 99, p. 1003–1013.

Haymon, R.M., 1983, Growth history of hydrothermal black smoker chimneys: Nature, v. 301, p. 695–698.

Head, J.W., and Wilson, L., 2003, Deep submarine pyroclastic eruptions: Theory and predicted landforms and deposits: Journal of Volcanology and Geothermal Research, v. 121, p. 155–193.

Humphris, S.E., and Cann, J.R., 2000, Constraints on the energy and chemical balances of the modern TAG and ancient Cyprus seafloor sulfide deposits: Journal of Geophysical Research, v.105, p. 28,477–28,488.

Jamieson, J.W., Clague, D.A., and Hannington, M.D., 2014, Hydrothermal sulfide accumulation along the Endeavour Segment, Juan de Fuca Ridge: Earth and Planetary Science Letters, v. 395, p. 136–148.

Kerr, D.J., and Gibson, H.L., 1993, A comparison of the Horne volcanogenic massive sulfide deposit and intracauldron deposits of the Mine Sequence, Noranda, Quebec: Economic Geology, v. 88, p. 1419–1442.

Kranidiotis, P., and MacLean, W.H., 1987, Immobile elements as monitors of mass transfer in hydrothermal alteration: Phelps Dodge massive sulfide deposit, Matagami, Quebec: Economic Geology, v. 82, p. 951–962.

Lafrance, B., Gibson, H.L., and Stewart, M.S., 2020, Internal and external deformation and modification of volcanogenic massive sulfide deposits hydrothermal escape precipitation site discharge heat source: Reviews in Economic Geology, v. 21, p. 147–171.

Large, R.R., Allen, R.L., Blake, M.D., and Herrmann, W., 2001a, Hydrothermal alteration and volatile element halos for the Rosebery K Lens volcanic-hosted massive sulfide deposit, western Tasmania: Economic Geology, v. 96, p. 1055–1072.

Large, R.R., Gemmell, B.J., Paulick, H., and Huston, D.L., 2001b, The alternation box plot: A simple approach to understanding the relationship between alteration mineralogy and lithogeochemistry associated with volcanic-hosted massive sulfide deposits: Economic Geology, v. 96, p. 957–971.

Layton-Matthews, D., Peter, J.M., Scott, S.D., and Leybourne, M.I., 2008, Distribution, mineralogy, and geochemistry of selenium in felsic volcanic-hosted massive sulfide deposits of the Finlayson Lake district, Yukon Territory, Canada: Economic Geology, v. 103, p. 61–88.

Layton-Matthews, D., Leybourne, M.I., Peter, J.M., Scott, S.D., Cousens, B., and Eglington, B.M., 2013, Multiple sources of selenium in ancient seafloor hydrothermal systems: Compositional and Se, S, and Pb isotopic evidence from volcanic-hosted and volcanic-sediment-hosted massive sulfide deposits of the Finlayson Lake district, Yukon, Canada: Geochimica et Cosmochimica Acta, v. 117, p. 313–331.

Le Maitre, R.W., Bateman, P., Dudek, A., Keller, J., Lameyre, J., Le Bas, M.J., Sabine, P.A., Schmid, R., Sorensen, H., and Streckeisen, A., 1989, Igneous rocks: A classification of igneous rocks and glossary of terms: London, Blackwell Scientific Publications, 256 p.

Lentz, D.R., 1998, Petrogenetic evolution of felsic volcanic sequences associated with Phanerozoic volcanic-hosted massive sulphide systems: The role of extensional geodynamics: Ore Geology Reviews, v. 12, p. 289–327.

Lesher, C.M., Goodwin, A.M., Campbell, I.H., and Gorton, M.P., 1986, Trace-element geochemistry of ore-associated and barren, felsic metavolcanic rocks in the Superior Province, Canada: Canadian Journal of Earth Sciences, v. 23, p. 222–237.

Lydon, J.W., 1984, Volcanogenic massive sulphide deposits Part 1: A descriptive model: Geoscience Canada, v. 11, p. 195–202.

Lydon, J.W., 1988, Volcanogenic massive sulphide deposits Part 2: Genetic models: Geoscience Canada Reprint Series, v. 3, p. 1–29.

MacLean, W.H., 1988, Rare earth element mobility at constant inter-REE ratios in the alteration zone at the Phelps Dodge massive sulphide deposit, Matagami, Quebec: Mineralium Deposita, v. 23, p. 231–238.

MacLean, W.H., and Barrett, T.J., 1993, Lithogeochemical techniques using immobile elements: Journal of Geochemical Exploration, v. 48, p. 109–133.

Manor, M.J., and Piercey, S.J., 2018, Re-evaluating the chronostratigraphic framework for felsic volcanic and intrusive rocks of the Finlayson Lake region, Yukon-Tanana terrane, Yukon, in MacFarlane, K.E., ed., Yukon exploration and geology 2017: Yukon Geological Survey, p. 111–127.

Manor, M.J., and Piercey, S.J., 2019, Geochemistry of Devono-Mississippian volcanic and intrusive rocks of the Finlayson Lake district, Yukon-Tanana terrane, Yukon, in Mac-Farlane, K.E., ed., Yukon exploration and geology 2018: Yukon Geological Survey, p. 91–110.

Manor, M.J., Piercey, S.J., Wall, C.J., and Denisová, N., 2022, High-precision CA-ID-TIMS U-Pb zircon geochronology of felsic rocks in the Finlayson Lake VMS district, Yukon: Linking Paleozoic basin-scale accumulation rates to the occurrence of subseafloor replacement-style mineralization: Economic Geology, v. 117, p. 1173–1201 .

McDonald, M., Piercey, S.J., Layne, G., Pigage, L., and Piercey, G., 2018, Mineral assemblages, textures and in situ sulphur isotope geochemistry of sulphide mineralization from the Cyprus-type Ice volcanogenic massive sulphide (VMS) deposit, Yukon, Canada: Minerals, v. 8, p. 25.

McDonough, W.F., and Sun, S.S., 1995, The composition of the Earth: Chemical Geology, v. 120, p. 223–253.

McLennan, S.M., Bock, B., Hemming, S.R., Hurowitz, J.A., Lev, S.M., and McDaniel, D.K., 2003, The roles of provenance and sedimentary processes in the geochemistry of sedimentary rocks: Geological Association of Canada, GeoText 4, p. 7–38.

McPhie, J., Doyle, M.G., and Allen, R.L., 1993, Volcanic textures: A guide to interpretation of textures in volcanic rocks: Hobart, Australia, University of Tasmania, 198 p.

Monecke, T., Petersen, S., and Hannington, M.D., 2014, Constraints on water depth of massive sulfide formation: Evidence from modern seafloor hydrothermal systems in arc-related settings: Economic Geology, v. 109, p. 2079–2101.

Morris, G.A., Larson, P.B., and Hooper, P.R., 2000, "Subduction style" magmatism in a non-subduction setting: The Colville igneous complex, NE Washington State, USA: Journal of Petrology, v. 41, p. 43–67.

Mortensen, J.K., 1992, Pre-mid-Mesozoic tectonic evolution of the Yukon-Tanana terrane, Yukon and Alaska: Tectonics, v. 11, p. 836–853.

Mortensen, J.K., and Jilson, G.A., 1985, Evolution of the Yukon-Tanana terrane: Evidence from southeastern Yukon Territory: Geology, v. 13, p. 806–810.

Mumin, A.H., Scott, S.D., Somarin, A.K., and Oran, K.S., 2007, Structural controls on massive sulfide deposition and hydrothermal alteration in the south Sturgeon Lake Caldera, northwestern Ontario: Exploration and Mining Geology, v. 16, p. 83–107.

Murphy, D.C., 1998, Stratigraphic framework for syngenetic mineral occurrences, Yukon-Tanana terrane south of Finlayson Lake: A Progress Report, in Roots, C.F., ed., Yukon Exploration and Geology 1997: Exploration and Geological Services Division, Yukon, Indian and Northern Affairs Canada, p. 51–58.

Murphy, D.C., and Piercey, S.J., 1999, Finlayson project: Geological evolution of Yukon-Tanana terrane and its relationship to Campbell Range Belt, northern Wolverine Lake map area, southeastern

Yukon, in Roots, C.F., and Emond, D.S., eds., Yukon exploration and geology 1998: Exploration and Geological Services Division, Yukon, Indian and Northern Affairs Canada, p. 47–62.

Murphy, D.C., Mortensen, J.K., Piercey, S.J., Orchard, M.J., and Gehrels, G.E., 2006, Mid-Paleozoic to early Mesozoic tectonostratigraphic evolution of Yukon-Tanana and Slide Mountain terranes and affiliated overlap assemblages, Finlayson Lake massive sulphide district, southeastern Yukon: Geological Association of Canada, Special Paper no. 45, p. 75–106.

Nelson, J., 1997, The quiet counter-revolution: structural control of syngenetic deposits: Geoscience Canada, v. 24, p. 91–98.

Nelson, J.L., Piercey, S.J., Murphy, D.C., and Geological Survey, B.C., 2006, Paleozoic tectonic and metallogenetic evolution of pericratonic terranes in Yukon, northern British Columbia and eastern Alaska: Geological Association of Canada, Special Paper no. 45, p. 323–360.

van Olden, K., Green, A., and Davidson, G., 2020, NI 43-101 feasibility study technical report Kudz Ze Kayah property, Yukon, Canada CSA Global Report n. R375.2020: CSA Global, 376 p.

Parson, L.M., and Wright, I.C., 1996, The Lau-Havre-Taupo back-arc basin: A southward-propagating, multi-stage evolution from rifting to spreading: Tectonophysics, v. 263, p. 1–22.

Pearce, J.A., 1996, A user's guide to basalt discrimination diagrams: Geological Association of Canada, Short Course Notes, v. 12, p. 79–113.

Pearce, J.A., 2008, Geochemical fingerprinting of oceanic basalts with applications to ophiolite classification and the search for Archean oceanic crust: Lithos, v. 100, p. 14–48.

Pearce, J.A., and Cann, J.R., 1973, Tectonic setting of basic volcanic rocks determined using trace element analyses: Earth and Planetary Science Letters, v. 19, p. 290–300.

Pearce, J.A., Harris, N.B.W., and Tindle, A.G., 1984, Trace element discrimination diagrams for the tectonic interpretation of granitic rocks: Journal of Petrology, v. 25, p. 956–983.

Peter, J.M., Layton-Matthews, D., Piercey, S.J., Bradshaw, G.D., Paradis, S., and Bolton, A., 2007, Volcanogenic-hosted massive sulphide deposits of the Finlayson Lake district, Yukon: Geological Association of Canada, Mineral Deposits Division, Special Publication no. 5, p. 471–508.

Piercey, S.J., 2001, Petrology and tectonic setting of mafic and felsic volcanic and intrusive rocks from the Finlayson Lake volcanic-hosted massive sulphide (VHMS) district: A record of mid-Paleozoic arc and back-arc magmatism and metallogeny: Ph.D. Thesis, Vancouver, Canada, University of British Columbia, 305 p.

Piercey, S.J., 2011, The setting, style, and role of magmatism in the formation of volcanogenic massive sulfide deposits: Mineralium Deposita, v. 46, p. 449–471.

Piercey, S.J., 2015, A semipermeable interface model for the genesis of subseafloor replacement-type volcanogenic massive sulphide (VMS) deposits: Economic Geology, v. 110, p. 1655–1660.

Piercey, S.J., and Colpron, M., 2009, Composition and provenance of the Snowcap assemblage, basement to the Yukon-Tanana terrane, Northern Cordillera: Implications for Cordilleran crustal growth: Geosphere, v. 5, p. 439–464.

Piercey, S.J., and Kamber, B.S., 2019, Lead isotope geochemistry of shales from the Wolverine volcanogenic massive sulfide deposit, Yukon: Implications for Pb isotope vectoring in exhalative ore systems: Economic Geology, v. 114, p. 47–66.

Piercey, S.J., Paradis, S., Murphy, D.C., and Mortensen, J.K., 2001, Geochemistry and paleotectonic setting of felsic volcanic rocks in the Finlayson Lake volcanic-hosted massive sulfide district, Yukon, Canada: Economic Geology, v. 96, p. 1877–1905.

Piercey, S.J., Murphy, D.C., Mortensen, J.K., and Paradis, S., 2002a, Boninitic magmatism in a continental margin setting, Yukon-Tanana terrane, southeastern Yukon, Canada: Geology, v. 29, p. 731–734.

Piercey, S.J., Mortensen, J.K., Murphy, D.C., Paradis, S., and Creaser, R.A., 2002b, Geochemistry and tectonic significance of alkalic mafic magmatism in the Yukon-Tanana terrane, Finlayson Lake region, Yukon: Canadian Journal of Earth Sciences, v. 39, p. 1729–1744.

Piercey, S.J., Mortensen, J.K., and Creaser, R.A., 2003, Neodymium isotope geochemistry of felsic volcanic and intrusive rocks from the Yukon-Tanana terrane in the Finlayson Lake region, Yukon, Canada: Canadian Journal of Earth Sciences, v. 40, p. 77–97.

Piercey, S.J., Nelson, J.L., Colpron, M., Dusel-Bacon, C., Simard, R.-L.L., and Roots, C.F., 2006, Paleozoic magmatism and crustal recycling along the ancient Pacific margin of North America, Northern Cordillera: Geological Association of Canada, Special Paper no. 45, p. 281–322.

Piercey, S.J., Peter, J.M., Mortensen, J.K., Paradis, S., Murphy, D.C., and Tucker, T.L., 2008, Petrology and U-Pb geochronology of footwall porphyritic rhyolites from the Wolverine volcanogenic massive sulfide deposit, Yukon, Canada: Implications for the genesis of massive sulfide deposits in continental margin environments: Economic Geology, v. 103, p. 5–33.

Piercey, S.J., Squires, G.C., and Brace, T.D., 2014, Lithostratigraphic, hydrothermal, and tectonic setting of the Boundary volcanogenic massive sulfide deposit, Newfoundland Appalachians, Canada: Formation by subseafloor replacement in a Cambrian rifted arc: Economic Geology, v. 109, p. 661–687.

Piercey, S.J., Peter, J.M., and Herrington, R.J., 2015, Zn-rich volcanogenic massive sulphide (VMS) deposits, in Current Perspectives on Zinc Deposits: Irish Association for Economic Geology, p. 37–57.

Piercey, S.J., Gibson, H.L., Tardif, N., and Kamber, B.S., 2016, Ambient redox and hydrothermal environment of the Wolverine volcanogenic massive sulfide deposit, Yukon: Insights from lithofacies and lithogeochemistry of Mississippian host shales: Economic Geology, v. 111, p. 1439–1463.

Piercey, S.J., Beranek, L.P., and Hanchar, J.M., 2017, Mapping magma prospectivity for Cordilleran volcanogenic massive sulphide (VMS) deposits using Nd-Hf isotopes: Preliminary results, in MacFarlane, K.E., and Weston, L.H., eds., Yukon exploration and geology 2016: Yukon Geological Survey, p. 197–205.

Reimann, C., Filzmoser, P., and Garrett, R.G., 2005, Background and threshold: Critical comparison of methods of determination: Science of the Total Environment, v. 346, p. 1–16.

Rissmann, C., Nicol, A., Cole, J., Kennedy, B., Fairley, J., Christenson, B., Leybourne, M., Milicich, S., Ring, U., and Gravley, D., 2011, Fluid flow associated with silicic lava domes and faults, Ohaaki hydrothermal field, New Zealand: Journal of Volcanology and Geothermal Research, v. 204, p. 12–26.

Ross, P.-S., and Bédard, J.H., 2009, Magmatic affinity of modern and ancient subalkaline volcanic rocks determined from trace element discriminant: Canadian Journal of Earth Sciences, v. 46, p. 823–839.

Ruks, T.W., Piercey, S.J., Road, L., Pe, O., Ryan, J.J., Villeneuve, M.E., and Creaser, R.A., 2006, Mid- to late Paleozoic K-feldspar augen granitoids of the Yukon-Tanana terrane, Yukon, Canada: Implications for crustal growth and tectonic evolution of the Northern Cordillera: Bulletin of the Geological Society of America, v. 118, p. 1212–1231.

Sdrolias, M., and Müller, R.D., 2006, Controls on back-arc basin formation: Geochemistry, Geophysics, Geosystems, v. 7, p. 1–40.

Sebert, C., Hunt, J.A., and Foreman, I.J., 2004, Geology and lithogeochemistry of the Fyre Lake copper-cobalt-gold sulphide-magnetite deposit, southeastern Yukon: Open File 17, p. 46.

Shervais, J.W., 1982, Ti-V plots and the petrogenesis of modern and ophiolitic lavas: Earth and Planetary Science Letters, v. 59, p. 101–118.

Sibson, R.H., 2000, Fluid involvement in normal faulting: Journal of Geodynamics, v. 29, p. 469–499.

Sibuet, J.-C., Deffontaines, B., Hsu, S.-K., Thareau, N., Le Formal, J.-P., and Liu, C.-S., 1998, Okinawa Trough back-arc basin: Early tectonic and magmatic evolution: Journal of Geophysical Research: Solid Earth, v. 103, p. 30,245–30,267.

De Silva, S.L., Riggs, N.R., and Barth, A.P., 2015, Quickening the pulse: Fractal tempos in continental arc magmatism: Elements, v. 11, p. 113–118.

Soltani Dehnavi, A., McFarlane, C., Lentz, D.R., McClenaghan, S., and Walker, J., 2019, Chlorite-white mica pairs' composition as a micro-chemical guide to fingerprint massive sulfide deposits of the Bathurst mining camp, Canada: Minerals, v. 9, p. 1–31.

Spitz, G., and Darling, R., 1977, Major and minor element lithogeochemical anomalies surrounding the Louvem copper deposit, Val d'Or, Quebec: Canadian Journal of Earth Sciences, v. 15, p. 1161–1169.

Thurston, P.C., Ayer, J.A., Goutier, J., and Hamilton, M.A., 2008, Depositional gaps in Abitibi greenstone belt stratigraphy: A key to exploration for syngenetic mineralization: Economic Geology, v. 103, p. 1097–1134.

Tornos, F., 2006, Environment of formation and styles of volcanogenic massive sulfides: The Iberian Pyrite Belt: Ore Geology Reviews, v. 28, p. 259–307.

Tornos, F., Peter, J.M., Allen, R.L., and Conde, C., 2015, Controls on the siting and style of volcanogenic massive sulphide deposits: Ore Geology Reviews, v. 68, p. 142–163.

Uyeda, S., and Kanamori, H., 1979, Back-arc opening and the mode of subduction: Journal of Geophysical Research, v. 84, p. 1049–1061.

Von Damm, K.L., 1990, Seafloor hydrothermal activity: Black smoker chemistry and chimneys: Annual Review of Earth and Planetary Sciences, v. 18, p. 173–204.

Watson, E.B., and Harrison, T.M., 1983, Zircon saturation revisited: Temperature and composition effects in a variety of crustal magma types: Earth and Planetary Science Letters, v. 64, p. 295–304.

Wedepohl, K.H., 1995, The composition of the continental crust: Geochemica et Cosmochimica Acta, v. 59, p. 1217–1232.

Whalen, J.B., Currie, K.L., and Chappell, B.W., 1987, A-type granites: Geochemical characteristics, discrimination and petrogenesis: Contributions to Mineralogy and Petrology, v. 95, p. 407–419.

White, J.D.L., 2000, Subaqueous eruption-fed density currents and their deposits: Precambrian Research, v. 101, p. 87–109.

White, J.D.L., and Houghton, B.F., 2006, Primary volcaniclastic rocks: Geology, v. 34, p. 677–680.

Winter, L.S., Tosdal, R.M., Franklin, J.M., and Tegart, P., 2004, A reconstructed Cretaceous depositional setting for giant volcanogenic massive sulfide deposits at Tambogrande, northwestern Peru: Society of Economic Geologists, Special Publication 11, p. 319–340.

Wright, I.C., Parson, L.M., and Gamble, J.A., 1996, Evolution and interaction of migrating cross-arc volcanism and back-arc rifting: An example from the southern Havre Trough (35°20′-37°S): Journal of Geophysical Research: Solid Earth, v. 101, p. 22,071–22,086.

Zaw, K., and Large, R.R., 1992, The precious metal-rich South Hercules mineralization, western Tasmania: A possible subsea-floor replacement volcanic-hosted massive sulfide deposit: Economic Geology, v. 87, p. 931–952.

Chapter 3

Evolution of the hydrothermal system associated with the ABM replacement-style volcanogenic massive sulfide deposit, Finlayson Lake district, Yukon, Canada

3.1 Abstract

The ABM deposit, Finlayson Lake district, Yukon, Canada, is a bimodal-felsic, replacement-style volcanogenic massive sulfide (VMS) deposit (19.1 Mt at 6.6 wt. % Zn, 0.9 wt. % Cu, 2.0 wt. % Pb, 1.4 g/t Au and 156 g/t Ag) hosted by Late Devonian continental back-arc-related volcano-sedimentary rocks of the Kudz Ze Kayah formation. The VMS-related hydrothermal alteration associated with the deposit extends >1 km beyond the mineralization. Zones of pervasive white mica and chlorite alteration occur proximal to the massive sulfide lenses (<50 m) both in the hanging wall and the footwall, and zones of pervasive white mica and moderate white mica ± chlorite alteration extend laterally from the mineralization and into the hanging wall and footwall for 100s-1000s of meters. Geochemical data and petrographic observations indicate that feldspar destruction and formation of white mica and chlorite were the main alteration processes. In both the hanging wall and footwall to the mineralization, base (Zn, Cu, Pb) and trace metals and metaloids (e.g., Sb, Tl, Mo) form halos with anomalous values (compared to more distal host rocks) up to 100 m and 200 m, respectively.

The paragenesis and the formation conditions of the hydrothermal alteration were determined through petrography of hydrothermal alteration assemblages and their cross-cutting relationships, electron microprobe analyses of the compositions of white mica, chlorite, and carbonate, and illite-chlorite-geothermometry. These data suggest that the white mica ± chlorite assemblage was the earliest and most extensive phase of the hydrothermal alteration that formed at temperatures around 215±30 °C. Overprinting the white mica-chlorite assemblage is the pervasive white mica assemblage that formed at temperatures around 250±15 °C. The pervasive chlorite assemblage formed at temperatures around 320±10 °C and overprints the preceding white mica-rich assemblages. Microprobe analyses of white mica and chlorite generally show that Mg-rich varieties are more common proximal to mineralization and formed earlier in the deposit paragenesis than Fe-rich varieties. Mineralogy derived from short wave infrared data for mica and chlorite; however, shows no clear spatial trends across the deposit due to complex overprinting relationships between alteration minerals.

3.2 Introduction

Hydrothermal alteration in volcanogenic massive sulfide (VMS) deposits reflects the interaction of upwelling fluids with footwall (and hanging wall) lithofacies (Franklin et al., 1981). The nature of fluid-rock interactions is heavily influenced by the temperature and composition of both fluids and host rocks, the porosity and permeability of the deposit-hosting sequence, and subsequent post-alteration overprinting from deformation and metamorphism (Franklin et al., 2005; Lafrance et al., 2020). In coherent volcanic flow-dominated sequences where fluids were interpreted to have exhaled on the seafloor, alteration commonly has distinct geometry, composition, and in many cases restricted distribution due to low permeability and porosity of coherent host rocks (Riverin and Hodgson, 1980; Knuckey et al., 1983; Gemmell and Large, 1992; Gemmell and Fulton, 2001). In sequences with abundant volcaniclastic and sedimentary rocks and associated with sub-seafloor replacement, the alteration can be more complex due to the variability in permeable stratigraphy, which commonly results in more extensive interaction between the ascending hydrothermal fluids and host rocks, which in turn creates complex alteration geometries (Doyle and Allen, 2003; Franklin et al., 2005; Piercey, 2015).

Alteration processes cause geochemical and mineralogical changes in the host rocks and result in zoned geochemical and mineralogical alteration halos that surround VMS mineralization. Further, new and/or improved analytical methods have allowed for recent studies to test more subtle or previously undetectable hydrothermal alteration associated with VMS deposits (Yang et al., 2011; Genna and Gaboury, 2015; Buschette and Piercey, 2016; Soltani Dehnavi et al., 2018; Pilote et al., 2019; Soltani Dehnavi et al., 2019; Brueckner et al., 2021). Despite an abundance of studies focusing on ancient VMS and modern seafloor massive sulfide (SMS) deposits, understanding the evolution of ancient hydrothermal systems and alteration footprints related to replacement-style VMS deposits in variously deformed and metamorphosed sequences is incomplete.

The Finlayson Lake district in southeastern Yukon, Canada, hosts >40 Mt of polymetallic VMS mineralization in six deposits (Kona, ABM, GP4F, R15, Wolverine, and Ice) within arc and back-arc rocks of the Yukon-Tanana and Slide Mountain terranes (Peter et al., 2007). The ABM deposit is a bimodal-felsic, replacement-style VMS deposit and contains a total (geological) mineral resource of 19.1 Mt at 6.6 wt.% Zn, 0.9 wt. % Cu, 2.0 wt. % Pb, 1.4 g/t Au and 156 g/t Ag (van Olden et al., 2020). In 2015, drilling at the ABM deposit discovered a new mineralized zone (Krakatoa zone), which contributed to the re-interpretation of the mineralization as replacement-style (van Olden et al., 2020). Despite the new interpretations, there has been little documentation of the hydrothermal alteration and its relationship to replacement-style processes and mineralization. Further, the relatively low degree of metamorphism (greenschist facies predominantly) and deformation at the ABM deposit makes it ideal for studying the evolution of a hydrothermal system associated with an ancient replacement-style VMS deposit in a back-arc environment. Numerous workers have shown that greenschist metamorphism does not significantly affect the geochemical and mineral-chemical signatures produced by hydrothermal alteration and that recrystallized alteration-related phyllosilicate minerals preserve their original pre-metamorphic compositions (Riverin and Hodgson, 1980; Urabe et al., 1983; Hannington et al., 2003; Genna and Gaboury, 2015).

Considering the above, this study utilizes detailed alteration mineral assemblage observations, whole rock geochemistry, alteration mineral chemistry, and short-wave infrared spectroscopy (SWIR) methods to provide a descriptive and genetic framework for hydrothermal alteration in the ABM replacement-style VMS deposit. The relationships between the different alteration assemblages are used to interpret the temporal and spatial evolution of the hydrothermal system and the geochemical and mineralogical footprint associated with the formation of the ABM deposit. Our research provides insights into processes active in sub-seafloor replacement in VMS deposits and into geochemical and mineralogical vectors towards mineralization and the hydrothermal footprint of VMS deposits. This has implications not only for VMS exploration in the Finlayson Lake district, but also for the study and exploration for replacement-style VMS deposits in similar environments around the world.

3.3 Regional geology

The Finlayson Lake district is a dismembered block of the Yukon-Tanana and Slide Mountain terranes that developed along the western margin of Laurentia throughout the mid-Paleozoic to the Permo-Triassic (Fig. 3.1; Colpron et al., 2006; Nelson et al., 2006; Piercey et al., 2006). In the Eocene, it was displaced from its original location approximately 430 km along the dextral strike-slip Tintina Fault (Gabrielse et al., 2006). The Yukon-Tanana terrane comprises a poly-deformed and metamorphosed pre-Late Devonian continental margin assemblage (Snowcap assemblage; Piercey and Colpron, 2009) that is overlain by three unconformity-bound Late Devonian to Middle to Late Permian continental arc, back-arc, and ocean basin-related volcano-sedimentary sequences (Big Campbell, Money Creek, and Cleaver Lake thrust sheets; Mortensen and Jilson, 1985; Mortensen, 1992; Colpron et al., 2006; Murphy et al., 2006). The core of the Finlayson Lake district reached amphibolite facies metamorphic grade, which transitions to lower greenschist facies further from the centre of the district (Murphy et al., 2006). The Big Campbell thrust sheet is by volume the largest and the structurally deepest of stratigraphically discrete blocks in the Finlayson Lake district (Fig. 3.1). It consists of Upper Devonian metaclastic rocks of the North River formation, the Upper Devonian Grass Lakes group, and the Lower Mississippian Wolverine Lake group, and hosts five VMS deposits (Fig. 3.1; Murphy et al., 2006; Peter et al., 2007). The Grass Lake group comprises three units: the Fire Lake, the Kudz Ze Kayah and the Wind Lake formations (Fig. 3.1). The Fire Lake formation hosts the Kona Cu-Co-Au VMS deposit within mafic metavolcanic and lesser amounts of mafic and ultramafic meta-subvolcanic rocks (Piercey et al., 2001a; Sebert et al., 2004; Murphy et al., 2006; Peter et al., 2007). The Kudz Ze Kayah formation formed in a continental back-arc setting juxtaposed adjacent to the Fire Lake formation (Manor et al., 2022a) and hosts the ABM, GP4F, and R15 deposits. It comprises dominantly felsic volcanic and sedimentary rocks with back-arc geochemical affinities (Piercey et al., 2001b; Murphy et al., 2006; Manor et al., 2022a, b). The Wind Lake formation is conformable atop the Kudz Ze Kayah formation and consists of interlayered carbonaceous sedimentary rocks and alkalic mafic volcanic rocks (Piercey et al., 2002). All rocks in the Grass Lakes group are intruded by the Grass Lakes plutonic suite at ca. 361 Ma (Piercey et al., 2001b; 2003; Manor et al., 2002b). The Wolverine Lake group unconformably overlies the Grass Lakes group and contains basal conglomerates, sandstones, felsic volcanic rocks, carbonaceous phyllites/shales, iron formations, and basaltic rocks, which host the Wolverine felsic-siliciclastic type VMS deposit (Murphy and Piercey, 1998; Bradshaw et al., 2001; Bradshaw et al., 2008).

The Kudz Ze Kayah formation hosts three known VMS deposits: the ABM deposit, the GP4F deposit and the R15 deposit. They are located about 25 km south of Finlayson Lake and the Robert Campbell Highway (Fig. 3.1). The GP4F deposit (Boulton, 2002) is situated roughly 5 km SE from the ABM deposit (Fig. 3.1) and sits ~500-600 m stratigraphically below the ABM deposit (Peter et al., 2007; Manor et al., 2022b). The R15 deposit occurs immediately along strike east of the GP4F deposit and occupies the same stratigraphic position (MacRobbie and Holroyd, unpub. data). The ABM deposit sits roughly 150-250 m below the contact between the Kudz Ze Kayah and Wind Lake formations (Manor et al., 2022b). Subseafloor replacement is interpreted to be the primary mineralization style in all deposits (Peter et al., 2007; van Olden et al., 2020; Denisová and Piercey, 2022; Manor et al., 2022b). The formation of rocks hosting the GP4F deposit was dated at ca. 363.254±0.098 Ma, whereas the ABM deposit is hosted by rocks dated at ca. 362.82±0.12 Ma (Manor et al. 2022b). The volcanic activity responsible for the deposition of the entire Kudz Ze Kayah formation is interpreted to have lasted approximately 0.65-1.0 Myr, indicating that rapid deposition and emplacement of volcano-sedimentary rocks played an important role in the formation of both VMS deposits (Manor et al., 2022b).

Figure 3.1. Regional setting of the Finlayson Lake district. (A) Regional geologic map of the Finlayson Lake district, Yukon-Tanana, and Slide Mountain terranes (modified after Murphy et al., 2006). Numbers mark the positions of known VMS deposits in the region. BCT = Big Campbell thrust; CLT = Cleaver Lake thrust; JCF = Jules Creek fault; MCT = Money Creek thrust; NRF = North River thrust. (B) Composite chronostratigraphic column for the Finlayson Lake district showing stratigraphic and structural relationships. Locations of VMS deposits, petrogenetic affinities of volcanic rocks and U-Pb and fossil ages displayed on diagram (modified after Murphy et al., 2006; Piercey et al., 2016; Manor and Piercey, 2018).

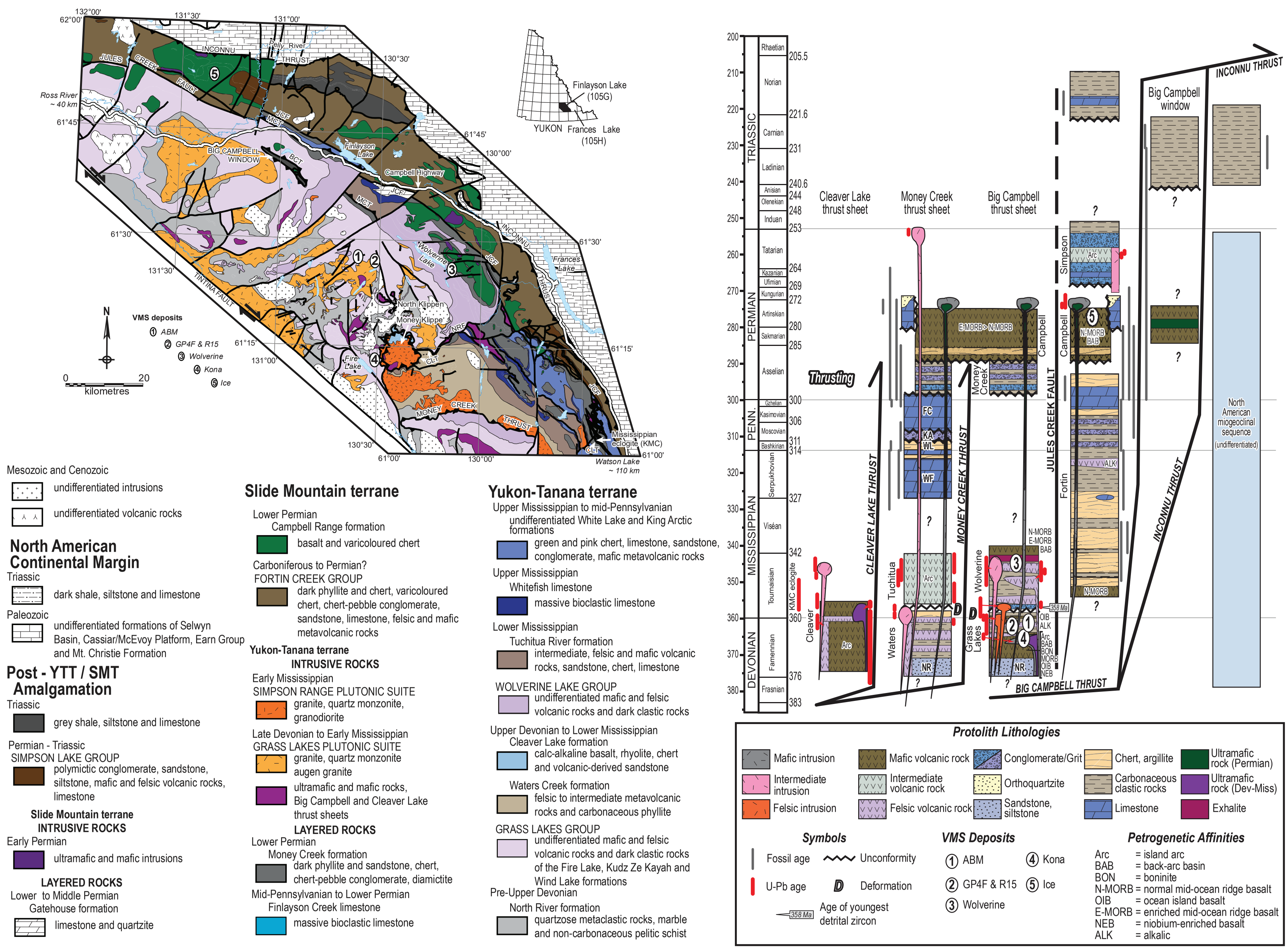
VMS deposits
1 ABM
2 GP4F & R15
3 Wolverine
4 Kona
5 Ice
kilometres
YUKON
Finlayson Lake (105G)
Frances Lake (105H)
Ross River ~ 40 km
Watson Lake ~ 110 km
Mississippian eclogite (KMC)
BIG CAMPBELL WINDOW
TINTINA FAULT
JULES CREEK FAULT
INCONNU THRUST
MONEY CREEK THRUST
Campbell Highway
Finlayson Lake
Frances Lake
Wolverine Lake
Fire Lake
North Klippen
Money Klippe
Mesozoic and Cenozoic
undifferentiated intrusions
undifferentiated volcanic rocks
North American Continental Margin
Triassic
dark shale, siltstone and limestone
Paleozoic
undifferentiated formations of Selwyn Basin, Cassiar/McEvoy Platform, Earn Group and Mt. Christie Formation
Post - YTT / SMT Amalgamation
Triassic
grey shale, siltstone and limestone
Permian - Triassic
SIMPSON LAKE GROUP
polymictic conglomerate, sandstone, siltstone, mafic and felsic volcanic rocks, limestone
Slide Mountain terrane
INTRUSIVE ROCKS
Early Permian
ultramafic and mafic intrusions
LAYERED ROCKS
Lower to Middle Permian
Gatehouse formation
limestone and quartzite
Slide Mountain terrane
Lower Permian
Campbell Range formation
basalt and varicoloured chert
Carboniferous to Permian?
FORTIN CREEK GROUP
dark phyllite and chert, varicoloured chert, chert-pebble conglomerate, sandstone, limestone, felsic and mafic metavolcanic rocks
Yukon-Tanana terrane
INTRUSIVE ROCKS
Early Mississippian
SIMPSON RANGE PLUTONIC SUITE
granite, quartz monzonite, granodiorite
Late Devonian to Early Mississippian
GRASS LAKES PLUTONIC SUITE
granite, quartz monzonite
augen granite
ultramafic and mafic rocks, Big Campbell and Cleaver Lake thrust sheets
LAYERED ROCKS
Lower Permian
Money Creek formation
dark phyllite and sandstone, chert, chert-pebble conglomerate, diamictite
Mid-Pennsylvanian to Lower Permian
Finlayson Creek limestone
massive bioclastic limestone
Yukon-Tanana terrane
Upper Mississippian to mid-Pennsylvanian
undifferentiated White Lake and King Arctic formations
green and pink chert, limestone, sandstone, conglomerate, mafic metavolcanic rocks
Upper Mississippian
Whitefish limestone
massive bioclastic limestone
Lower Mississippian
Tuchitua River formation
intermediate, felsic and mafic volcanic rocks, sandstone, chert, limestone
WOLVERINE LAKE GROUP
undifferentiated mafic and felsic volcanic rocks and dark clastic rocks
Upper Devonian to Lower Mississippian
Cleaver Lake formation
calc-alkaline basalt, rhyolite, chert and volcanic-derived sandstone
Waters Creek formation
felsic to intermediate metavolcanic rocks and carbonaceous phyllite
GRASS LAKES GROUP
undifferentiated mafic and felsic volcanic rocks and dark clastic rocks of the Fire Lake, Kudz Ze Kayah and Wind Lake formations
Pre-Upper Devonian
North River formation
quartzose metaclastic rocks, marble and non-carbonaceous pelitic schist
TRIASSIC
PERMIAN
PENN.
MISSISSIPPIAN
DEVONIAN
Rhaetian
Norian
Carnian
Ladinian
Anisian
Olenekian
Induan
Tatarian
Kazanian
Ufimian
Kungurian
Artinskian
Sakmarian
Asselian
Gzhelian
Kasimovian
Moscovian
Bashkirian
Serpukhovian
Viséan
Tournaisian
Famennian
Frasnian
205.5
221.6
231
240.6
244
248
253
264
269
272
280
285
300
306
311
314
327
342
360
376
383
Cleaver Lake thrust sheet
Money Creek thrust sheet
Big Campbell thrust sheet
Big Campbell window
Thrusting
CLEAVER LAKE THRUST
MONEY CREEK THRUST
JULES CREEK FAULT
BIG CAMPBELL THRUST
INCONNU THRUST
KMC eclogite
Cleaver
Waters
Tuchitua
Grass Lakes
Wolverine
Money Creek
Campbell
Simpson
Fortin
North American miogeoclinal sequence (undifferentiated)
Protolith Lithologies
Mafic intrusion
Intermediate intrusion
Felsic intrusion
Mafic volcanic rock
Intermediate volcanic rock
Felsic volcanic rock
Conglomerate/Grit
Orthoquartzite
Sandstone, siltstone
Chert, argillite
Carbonaceous clastic rocks
Limestone
Ultramafic rock (Permian)
Ultramafic rock (Dev-Miss)
Exhalite
Symbols
Fossil age
U-Pb age
Unconformity
Deformation
Age of youngest detrital zircon
VMS Deposits
1 ABM
2 GP4F & R15
3 Wolverine
4 Kona
5 Ice
Petrogenetic Affinities
Arc = island arc
BAB = back-arc basin
BON = boninite
N-MORB = normal mid-ocean ridge basalt
OIB = ocean island basalt
E-MORB = enriched mid-ocean ridge basalt
NEB = niobium-enriched basalt
ALK = alkalic

3.4 Local geology

The rocks of the Kudz Ze Kayah formation have been interpreted to have formed in a back-arc environment based on their geochemical signatures and tectonostratigraphic setting (Piercey et al., 2001b; 2002). The upper Kudz Ze Kayah formation, which hosts the ABM deposit in the top ~350 m is interpreted to have been deposited in an extensional basin (Denisová and Piercey, 2022; Manor et al., 2022b) and the volcanosedimentary package consists of abundant felsic volcaniclastic and coherent rocks, and lesser mafic sills and argillite lenses. The stratigraphy dips between 20°-30° to the NNE and field observations and stratigraphic reconstructions do not indicate any fault repetition or major folding (van Olden et al., 2020; Denisová and Piercey, 2022; Manor et al., 2022b). The distribution of abundant coherent felsic facies (e.g., sills, flows, domes) and mafic sills, together with abundant volcaniclastic rocks that are typically proximal to active volcanic sites (crystal-rich tuffs, lapilli tuffs) suggests that the ABM deposit formed at a site of an active volcanic centre (Denisová and Piercey, 2022). Denisová and Piercey (2022) also note that the East fault (Fig. 3.2), previously interpreted to be a re-activated transform fault (van Olden et al., 2020), was originally a part of a set of interconnected synvolcanic normal faults. The synvolcanic faults accommodated the subsidence in the back-arc basin, served as conduits for ascending magmas, controlled the emplacement of coherent volcanic units and locally the thickness of volcaniclastic and sedimentary units, and were important in controlling the upwelling VMS-related hydrothermal fluids (Fig. 3.2).

The upper Kudz Ze Kayah formation can be divided into three distinct sequences with different geochemical characteristics; Sequence 1 is the stratigraphically lowest and Sequence 3 is the stratigraphically highest. Sequence 1 consists of felsic volcaniclastic rocks, sills, and rare argillite lenses. Sequence 2 hosts the massive sulfide mineralization and comprises felsic volcaniclastic rocks, coherent flows, sills, domes, and two mafic sills that extend throughout the deposit footprint. Sequence 3 contains abundant felsic volcaniclastic rocks, felsic flows and sills, and argillite lenses. The boundary between Sequence 2 and Sequence 3 consists of an extensive argillite lens that marks a protracted period of volcanic quiescence. Other, lesser argillite lenses in its hanging wall mark later minor breaks in volcanism during the deposition of Sequence 3.

3.5 Mineralization at the ABM deposit

The ABM deposit consists of two mineralized zones: the ABM zone and the Krakatoa zone (Fig. 3.2), that were offset along the East fault post-mineralization. The mineralization in each zone consists of a series of stacked stratabound massive sulfide lenses enveloped by pervasive alteration that dip subparallel to the stratigraphy (20°-30°; Fig. 3.3). The ABM zone is 700 m wide and extends from the bedrock surface down dip for 600 m. Mineralization in the ABM zone tapers off down dip to the NNE, along strike to the W, and is cut off by the East fault. The Krakatoa zone is 170 m wide and extends from the bedrock surface down dip for 600 m and remains open down dip, whereas along strike, the mineralized lenses are cut off by post-mineralization faults.

In both the ABM and Krakatoa zones, three main ore assemblages comprise the massive sulfide lenses (Denisová and Piercey, 2022): (1) a pyrite-sphalerite-galena ± chalcopyrite-tetrahedrite group sulfosalts assemblage with associated carbonate minerals, barite, quartz, and white mica; (2) an assemblage comprising pyrite-chalcopyrite-pyrrhotite-magnetite-sphalerite ± galena-tetrahedrite group sulfosalts, with minor associated carbonate minerals and chlorite that occurs commonly in the core of the sulfide lenses; (3) chalcopyrite-pyrrhotite-pyrite stringers associated with pervasive chlorite alteration, with minor associated carbonate minerals, and quartz. The massive sulfide lenses are primarily composed of the first two assemblages. The third assemblage is not as common and is typically only present at the upper and lower contacts of the massive sulfide lenses.

Figure 3.2. Local geology of the ABM deposit. (A) Geological map with units constructed using drilling data and 3D models. Cross section and long section lines displayed. Note that lithofacies are displayed using patterns and geochemical groups using colors. (B) Upward projections of maximum extent of modeled alteration zones and mineralization. (C) Upward projection of mineralization and maximum extent of numerically modeled Ba isosurfaces. Alt = alteration. Chl = chlorite. DDH = diamond drill hole. FA = felsic A, FB = felsic B, MA = mafic A, Mod = moderate. Perv = pervasive. wm = white mica. WL = Wind Lake.

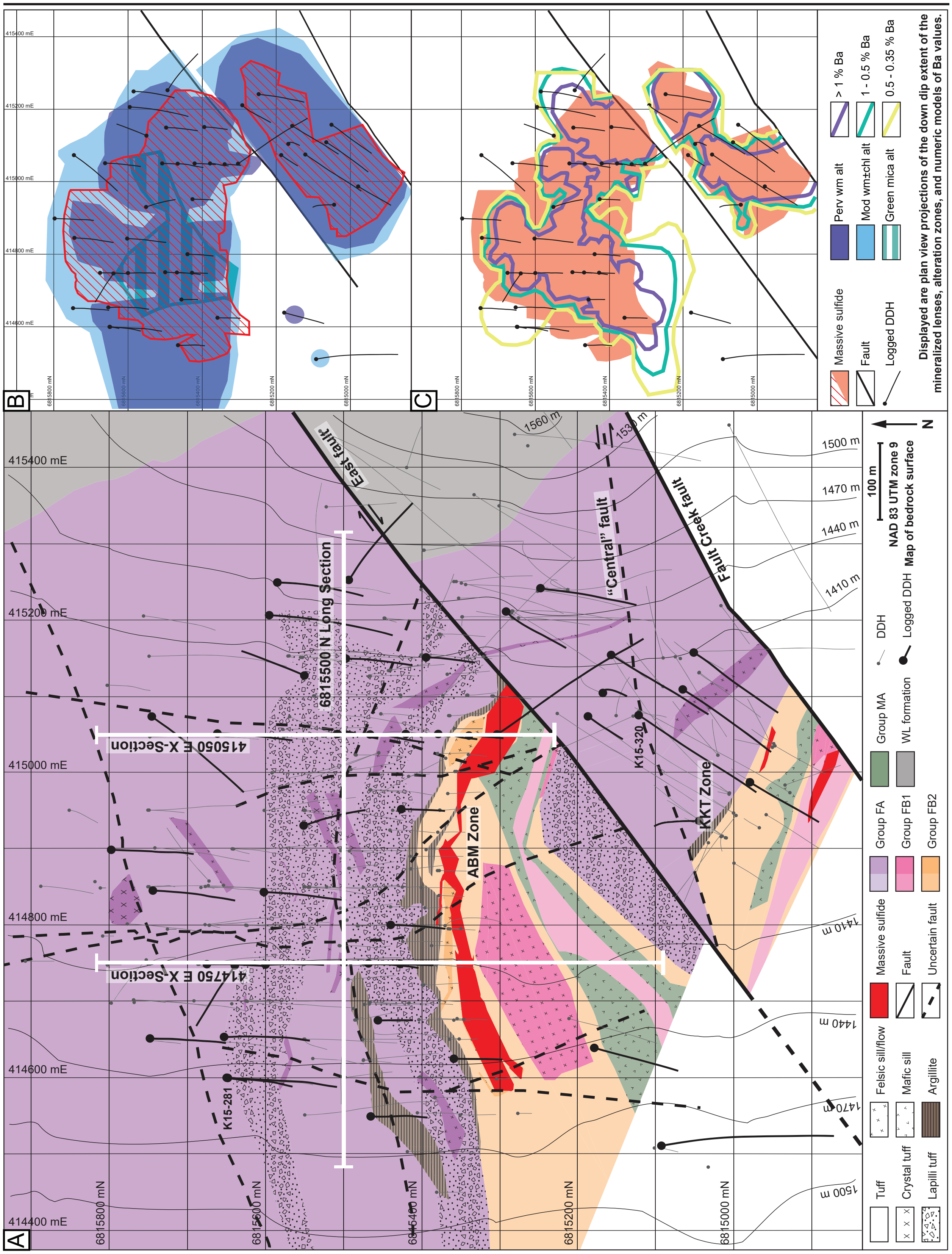
A
B
C
414400 mE
414600 mE
414800 mE
415000 mE
415200 mE
415400 mE
6815800 mN
6815600 mN
6815400 mN
6815200 mN
6815000 mN
1410 m
1440 m
1470 m
1500 m
1530 m
1560 m
East fault
"Central" fault
Fault Creek fault
ABM Zone
KKT Zone
6815500 N Long Section
415050 E X-Section
414750 E X-Section
K15-281
K15-320
Tuff
Crystal tuff
Lapilli tuff
Felsic sill/flow
Mafic sill
Argillite
Massive sulfide
Fault
Uncertain fault
Group FA
Group FB1
Group FB2
Group MA
WL formation
DDH
Logged DDH
100 m
NAD 83 UTM zone 9
Map of bedrock surface
N
Massive sulfide
Fault
Logged DDH
Perv wm alt
Mod wm±chl alt
Green mica alt
> 1 % Ba
1 - 0.5 % Ba
0.5 - 0.35 % Ba
Displayed are plan view projections of the down dip extent of the mineralized lenses, alteration zones, and numeric models of Ba values.

In the ABM zone, massive sulfide mineralization is associated with felsic volcanic and volcaniclastic rocks. In the Krakatoa zone, most of the massive sulfide mineralization is localized on mafic sill contacts or within the mafic sills themselves. In recent years, the ABM deposit has been re-interpreted as a replacement-style VMS deposit (van Olden et al., 2020; Denisová and Piercey, 2022; Manor et al., 2022b). Features such as preserved lapilli and other clasts, remnant bedding, massive sulfides replacing glassy groundmass within perlitic and brecciated textures on unit contacts occur within the massive sulfide lenses and on their contacts and suggest that the mineralization formed by replacement (Doyle and Allen, 2003).

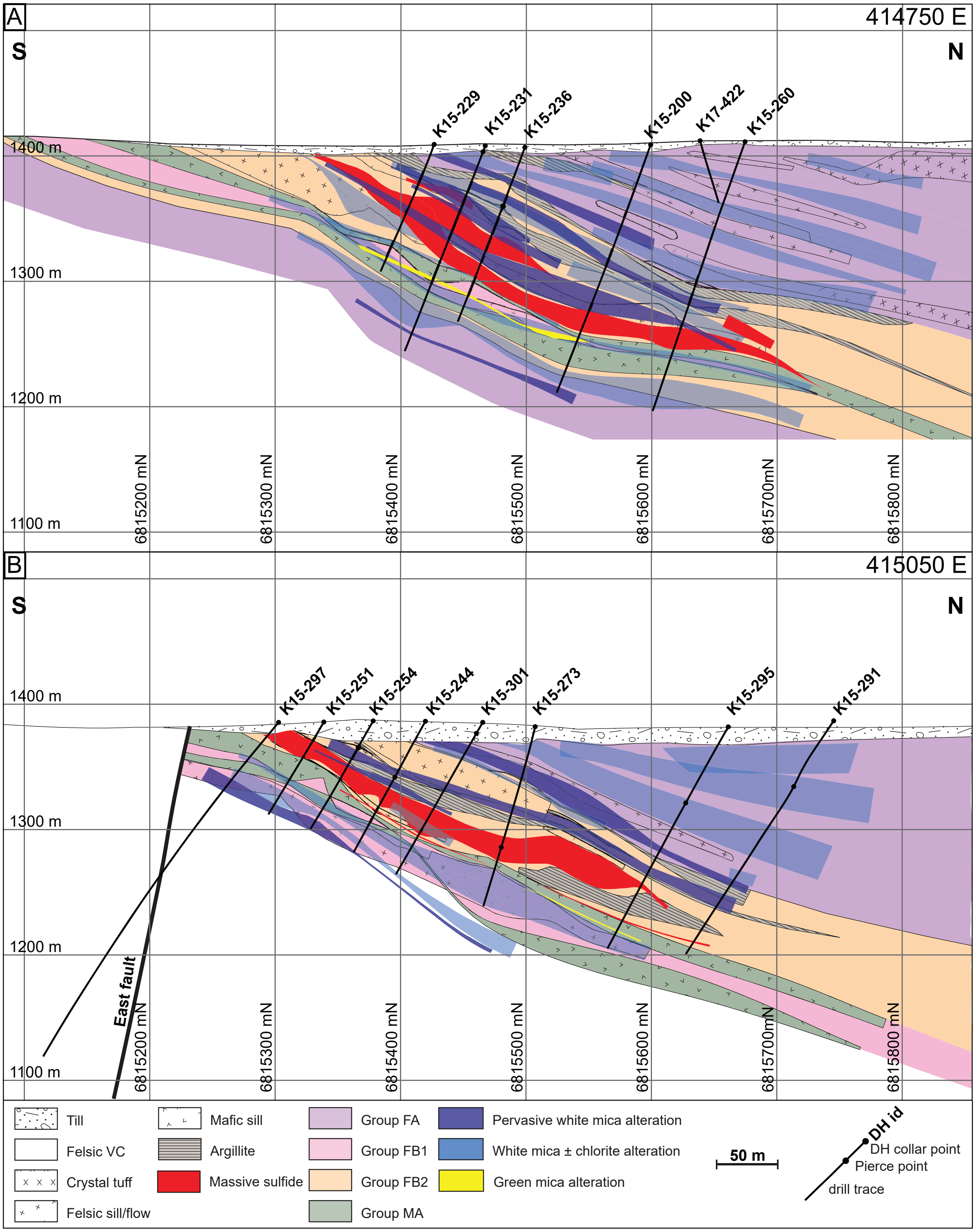

Figure 3.3. Cross sections through the ABM zone of the ABM deposit, cross sections are running N-S, looking west. Positions of section lines shown in Figure 3.2.

3.6 Methods

This study builds on the work presented in Denisová and Piercey (2022); the same sample set is used to describe and investigate the hydrothermal system at the ABM deposit; the existing lithogeochemical dataset was extended beyond immobile elements to supplement them with mobile elements acquired using different digestions and analytical methods. Over ~10 km of drill core from 51 drill holes was logged and lithology, primary textures, grain size, mineralogy, and alteration type and intensity based on mineral occurrence (quartz, white mica, chlorite, biotite, carbonate minerals, and sulfide minerals) were recorded in graphic core logs. Out of 478 collected samples, 83 were analyzed for lithogeochemistry to characterize the host rocks and alteration, and 82 representative samples were studied petrographically. In addition, alteration minerals and their paragenesis were studied in 51 samples representing the main types of mineralization. Petrography was undertaken using standard petrographic microscopy and a JEOL JSM 7100F scanning electron microscope (SEM) at Memorial University using back scatter electron (BSE) imaging operating at an accelerated voltage of 15 kV. Datasets provided by BMC Minerals Ltd., including core photos, drill logs, and geochemical data, were used as additional resources to document the macro-scale alteration in the deposit; the quality assurance and quality control procedures for the company analytical datasets are described in van Olden et al. (2020). Presented cross sections displaying modelled alteration zones are based primarily on detailed graphic drill logs; company drill logs and drill core photos were used to populate gaps between the acquired data and to refine the model. All models and interpretations carry a higher degree of uncertainty in the footwall of the mineralization due to limited drilling below the ore horizon. Digital models of alteration zones and mineralized lenses were created using the Leapfrog Geo 6.0 software developed by Seequent. Isosurfaces of Ba distribution (Fig. 3.2 and 3.4) were modelled using the Numeric Models tool in Leapfrog 3D. The linear radial basis function (RBF) interpolation was chosen to mitigate the irregular distribution of the almost 9,000 Ba datapoints from the assay database of BMC Minerals Ltd. The linear RBF interpolant was run with a sill value of 5,000, base range of 50, nugget of 0 and accuracy of 20. The trend was set to the local stratigraphy (dip 30° with dip azimuth of 20° and pitch of 115°) and the ellipsoid ratios were set to 3:3:1. The threshold value for Ba at the deposit was chosen at 3,500 ppm using methods outlined in Reimann et al. (2005). Throughout this study, we will refer to micaceous material observed in drill core and hand samples as white mica, and where its composition has been determined using the EMPA, the correct mineral name will be used (muscovite, illite, illite/smectite).

3.6.1 Major and trace element lithogeochemistry methods

Three separate lithogeochemical analytical packages (ME-MS81d, IMC-100, IML-101) were used to analyze the data, to cover all elements necessary to study hydrothermal alteration. The full dataset is available in Appendix 2.1. Sample preparation and analysis methods, together with the quality assurance and quality control procedures for the major and trace element data for the first two packages given below were presented in detail in Denisová and Piercey (2022). Sample preparation and measurement of major and trace element data (including immobile elements, e.g., Zr, Th, REE; ME-MS81d) were performed at ALS Laboratories, North Vancouver, British Columbia. Sample powders were fused with a lithium metaborate flux, the fused beads were then cooled and digested using 4% HNO_3-2% HCl mixture. Analyses of the sample solutions were conducted using inductively coupled plasma-atomic emission spectrometry (ICP-AES) for major elements and inductively coupled plasma-mass spectrometry (ICP-MS) for immobile trace elements (e.g., Zr, Hf, Nb, Ta, Th, U, REE). The sample suite was also analyzed at Ontario Geoscience Laboratories in Sudbury, Ontario (OGL) to obtain transition metals, base metals, and semi-metals (e.g., Li, Be, Co, Cu, Zn, Mo, Cd, In, Sb, W, Bi, Pb, Sc, Ta; full list of analyzed elements available in Appendix 2.1) using a closed beaker HF-HCl-$HClO_4$ digest followed by an analytical finish using a Perkin-Elmer Elan 9000 inductively coupled plasma-mass spectrometer (ICP-MS, method IMC-100). Additionally, the same sample suite was further analyzed using an aqua regia extraction method at the same lab, also with an analytical finish using a Perkin-Elmer Elan 9000 ICP-MS, to obtain minor and trace elements (e.g., Sb, As, Bi, Cd, Co, Cu, Au, In, Ir, Pb, Hg, Mo, Ni, Pd, Pt, Se, Ag, Te, Tl, Sn, Zn; method IML-101). The methodologies from OGL outlined above are detailed in Burnham and Schweyer (2004) and Burnham (2008).

Over the course of this study, eight in-house reference material samples (SLV-MC basalt and WP-1 dacite), and several lab duplicates were analyzed at OGL to monitor analytical accuracy and reproducibility (Appendix 2.2). For the IMC-100 method, trace element abundances overall gave RSD values <10%, except for Tl (<19 %) in both WP-1 and SLV-MC. The results for both reference materials overlap with published values (WP-1; Piercey et al., 2001b; Manor and Piercey, 2019) and unpublished in-house data for both SLV-MC and WP-1 with reproducibility better than 10 % for most trace elements, with exception of Cd and Cu in the WP-1 dacite that show the percent relative differences <17 %. The blind and lab-chosen duplicates show relatively higher relative standard deviation (RSD) values but are generally <15% for most major and trace elements. For the IML-101 method, trace element abundances overall gave RSD values <10%, except for Mo and In (< 16 %), and Tl (< 30 %) in WP-1 and Cd (< 11 %) in SLV-MC. The results for both reference materials overlap with unpublished in-house data for both SLV-MC and WP-1 with reproducibility better than 10 % for most trace elements, with exception of Tl (<51 %) in the WP-1 dacite and Cd (<17 %) in SLV-MC basalt. The blind and lab-chosen duplicates show relatively higher RSD values but are generally <15% for most major and trace elements. The aqua regia digestion is devised to leach only elements bound loosely in less resistant mineral phases like sulfide minerals, Fe- and Mn-oxide minerals, sulfate minerals, carbonate minerals, and clay-sized silicate minerals, whereas the HF-HCl-$HClO_4$ digestion dissolves all but the most resistant minerals like zircons and chromites. The two different digestion methods were chosen to better understand the relative distribution of elements like Cd, Cu, In, Mo, Pb, Sb, Tl, and Zn and elucidate whether these elements are bound in the more resistant silicates, or whether they occur in sulfides or adsorbed on to clays and would therefore be released by the less aggressive aqua regia digest.

3.6.2 Electron Probe Microanalysis

The composition of white mica, chlorite, and carbonate minerals in 9 polished thin sections was analysed at Memorial University using the JEOL JXA-8230 SuperProbe electron probe microanalyzer (EPMA) equipped with five wavelength dispersive spectrometers (WDS), a Thermo energy dispersive spectrometer (EDS), and a W electron gun. Natural and synthetic standards were used for calibration of the instrument, where standards and X-ray lines were used on five respective crystals (spectrometers) and average detection limits for each element are in brackets: 1) LDE1: apatite (FKα; 275 ppm); 2) LIFL: almandine (FeKα; 70 ppm), vanadium (VKα; 39), rutile (TiKα; 54 ppm), $BaSO_4$ (BaLα; 155 ppm); 3) PETL: tugtupite (ClKα; 26 ppm), orthoclase (KKα; 30 ppm), diopside (CaKα; 39 ppm), celestite (SrLα; 106 ppm); 4) TAP: albite (NaKα; 68 ppm), albite (AlKα; 38 ppm), diopside (SiKα; 79 ppm), diopside (MgKα; 72 ppm); 5) LIFH: chromium oxide (CrKα; 40 ppm), rhodonite (MnKα; 52 ppm), willemite (ZnKα; 92 ppm). Counting times for calibration are 10 seconds on peaks and 5 seconds on background. Analyses on unknowns were performed using the same crystals as the calibration. White mica was analyzed for 14 elements (Si, Al, Sr, Ba, Zn, Fe, Mg, Mn, Ca, Na, K, Ti, F, and Cl), chlorite grains were analysed for 16 elements (Si, Al, Fe, Ba, Sr, Cr, V, Zn, Mg, Mn, Ca, Na, K, Ti, F, and Cl), and carbonate minerals were analyzed for 7 elements (Fe, Ba, Ca, Sr, Mg, Mn, and Zn). Silicate minerals were analyzed using an accelerating voltage of 15 kV, a 20 nA beam current, focused to 3-5 µm, with elemental counting times between 5-60 seconds. Carbonate minerals were analyzed using an accelerating voltage of 20 kV, a 5 nA beam current, defocused to 8-15 µm, with elemental counting times between 5-30 seconds. Internal standards were measured periodically and showed no inconsistencies. Samples with totals falling outside of typical range of mineral composition minus H_2O were rejected; in the case of micas this was for totals <85 %, in the case of chlorite <82 %, and in the case of carbonate minerals where the back-calculated CO_2 values were >60 %. Mineral formulas of white mica were calculated based on 11 O; chlorite formulas were calculated based on 14 O.

3.6.3 Short-wave Infrared Spectroscopy

Hyperspectral measurements of the samples from the original sample suite, together with additional samples, 576 analyses in total, were collected at Memorial University using the Terraspec™ Infrared Spectrometer with a Hi-Brite Muglight. To monitor the accuracy and precision of the acquired data, an internal reference sample (pyrophyllite) was measured after each white reference optimization, which occurred every 20 samples or every 20 minutes during the run of the instrument (Appendix 6.2). The monitoring confirmed that the instrument yielded absorption hulls that were consistently within 3 nm of accepted values for the internal standard. Data were processed using The Spectral Geologist 7.1 software. Hyperspectral scalars were calculated for the 2200 nm (2,185-2,225 nm) and 2250 nm (2,245-2,265 nm) absorption wavelengths features using a fourth-order polynomial fitting curve, with hull correction and background noise filters applied to the spectra. The diagnostic absorption feature for white mica occurs between 2,180-2,225 nm and is caused by the variation in composition due to the Tschermak substitution ($Al^{VI} + Al^{IV} \leftrightarrow (Fe, Mg, Mn)^{VI} + Si^{IV}$), and by the interlayer cation substitution between K and Na (Velde, 1978; Herrmann et al., 2001; Yang et al., 2011). Values of the 2200 nm feature between 2,180 and 2,195 nm are attributed to Na-bearing muscovite, between 2,200-2,208 nm are considered to be muscovite, wavelengths of 2,216-2,228 nm have a phengite composition, and values in between 2,208-2,216 nm are considered to be mixtures of two or more mica phases, or to have an intermediate composition (Herrmann et al., 2001; Jones et al., 2005; Yang et al., 2011). For chlorite, the 2250 nm absorption feature between 2,235-2,255 nm is controlled by the Fe content with higher absorption values indicating higher Fe content of the chlorite (Herrmann et al., 2001; Cloutier et al., 2021). Most of the samples from the ABM deposit are mixed samples, therefore the depth of the above-described absorption features to determine relative mineral abundance is of limited use, but in general, the deeper the absorption feature, the higher the relative abundance of the mineral (Cloutier and Piercey, 2020).

3.7 Observations and Results

3.7.1 Hydrothermal alteration at the ABM deposit

The descriptions presented in this section are based on drill core and petrographic observations. Alteration in the ABM deposit occurs both in the hanging wall and footwall of the massive sulfide lenses (Fig. 3.3, 3.4) and consists of five main assemblages: pervasive white mica, pervasive chlorite, moderate to weak white mica ± chlorite, chlorite-calcite-actinolite, and Fe-carbonate. Pervasive alteration assemblages contain >15 modal % of the mineral in question. The alteration assemblages and their intensity do not differ significantly between the hanging wall and footwall and no alteration assemblage is bound to a particular stratigraphic unit or position, except for

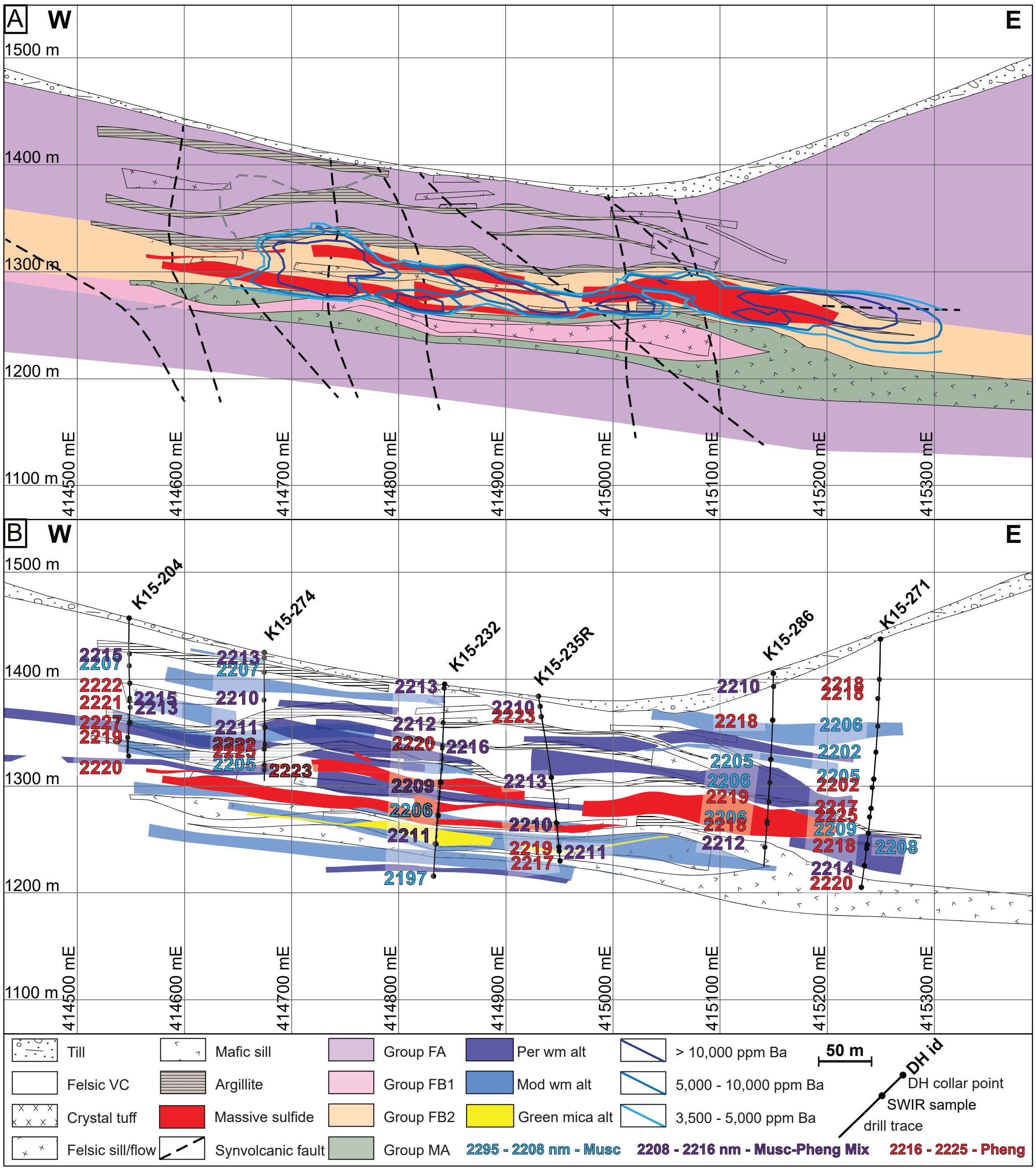

Figure 3.4. Long section through the ABM zone of the ABM deposit running W-E, looking north. Drill holes are not clipped to section, entire extent of drill hole displayed. Section line position shown in Figure 3.2. (A) Lithostratigraphy and Ba content contours shown. (B) Mineralization, modelled alteration zones and 2200 nm feature SWIR values displayed.

those restricted to a specific rock type (e.g., chlorite-calcite-actinolite assemblage in mafic sills in Sequence 2). Alteration zones are generally stratabound (Fig. 3.3, 3.4), but in rare cases they cross lithological boundaries, and there are mostly gradual transitions between the different assemblages. Locally, sharp contacts occur between pervasive chlorite alteration and paragenetically earlier alteration assemblages. The pervasive white mica and chlorite alteration assemblages occur in proximity to the mineralization, commonly within 100 m of mineralization into the hanging wall or footwall. Less pervasive alteration assemblages extend up to 1400 m west along strike and 500 m down dip, and typically these assemblages are weak white mica ± chlorite assemblages; however, even in these weakly altered areas there are some localized zones of pervasive alteration implying that there are other possible mineralized zones in the area (Fig. 3.2). The following sections will describe the distribution, extent, mineralogy, textures present of each major alteration assemblage, and their relationship to the mineralization.

3.7.1.1 Pervasive white mica alteration assemblage

Zones of pervasive white mica alteration occur in all felsic lithologies in the ABM deposit in both the hanging wall and footwall to the mineralization (Fig. 3.3, 3.4). The alteration zones are stratabound, up to ~25 m thick, and extend along strike and down dip. Contacts with surrounding zones of moderate white mica ± chlorite alteration are gradual. Locally, individual lapilli, quartz or feldspar crystals are preserved (Fig. 3.5A). The assemblage is dominated by white mica comprising between 15-45 modal %. Tabular white mica grains have roughly similar size (100-200 μm), replace the matrix, and their alignment defines the fabric, which is oriented subparallel to the lapilli or other preserved features within the felsic rocks (Fig. 3.5B, C). White mica commonly overprints remnant primary minerals including K-feldspar or plagioclase, and locally minor early alteration minerals like dolomite. Carbonate minerals, chlorite, and biotite are minor (commonly ≤5 modal %) and paragenetically contemporaneous or later than the white mica. Minor (<1 volume %) disseminated fine- to medium-grained sulfide grains (pyrite and pyrrhotite) are present and locally, discontinuous sulfide stringers or rare diffuse bands of sulfide minerals occur in this assemblage. In proximity to the massive sulfide mineralization, some pervasively white mica altered intervals are locally fissile and extensively fractured, likely due to the abundance of white mica (Fig. 3.5D). Locally, these fractured intervals also contain irregular milky white quartz veins with minor associated carbonate minerals, sulfide sulfides and/or rare tourmaline or biotite. These veins are paragenetically late (post-deformation) but formed before the extensive fracturing.

3.7.1.2 Pervasive chlorite alteration assemblage

Zones of pervasive chlorite alteration are stratabound and on average ~2 m thick and affect both felsic and mafic lithofacies. This alteration assemblage occurs commonly on the hanging wall or footwall contacts of massive sulfide lenses, and/or within the lenses themselves, and also on the contacts of the mafic subvolcanic sills in Sequence 2. Contacts with mineralization are gradual, whereas with pervasive white mica and moderate white mica ± chlorite alteration zones they are sharp (Fig. 3.5E). The rocks are dark green due to pervasive replacement by very fine-grained to fine-grained green chlorite and primary igneous textures are rarely preserved. The assemblage contains two subtypes: one that is barren of mineralization (Fig. 3.5F), and a second spatially associated with sulfide and magnetite mineralization (Fig. 3.5G). The two subtypes most commonly occur separately but locally gradually transition into each other. The first barren subtype of the assemblage contains between 15-60 modal % chlorite (Fig. 3.5F, H), bands of bladed chlorite define the fabric and overprint the primary minerals and minor biotite has replaced chlorite (Fig. 3.5H). In the second, mineralization-associated subtype, chlorite is the dominant phase (locally with black chlorite grains up to 5 cm) but comprises only up to 30 modal %; white mica, biotite, and carbonate minerals occur at higher proportions than in the barren subtype (Fig. 3.5I). Both white mica and chlorite define the fabric in the mineralized subtype of this alteration assemblage. Sulfide minerals are one of the paragenetically latest phases in the mineralized subtype occurring as stringers, irregular patches, or disseminated grains. Chalcopyrite-pyrrhotite-pyrite veinlets and stringers are the most common sulfide occurrences (Fig. 3.5J) with lesser magnetite, sphalerite, galena, and sulfosalts. The proportion of sulfide minerals increases with proximity to the massive sulfide lenses.

3.7.1.3 Moderate to weak white mica ± chlorite alteration assemblage

The moderate to weak white mica ± chlorite alteration assemblage is the most widespread assemblage in the ABM deposit and consists of white mica and lesser chlorite, with minor carbonate minerals, sulfide minerals, and biotite. This assemblage is ubiquitous across the volcanosedimentary package and occurs up to the conformable contact with the Wind Lake formation. It occurs in felsic volcaniclastic and volcanic rocks and commonly varies from moderate to weak in intensity, with gradual transitions in between. The rocks are greenish due to the abundance of yellow-green white mica. Primary textures are preserved in the host rocks and the alteration affects the groundmass/ matrix predominantly, the orientation of the alteration mineral grains roughly aligns with the fabric defined by the remnant primary igneous features (Fig. 3.5K). Locally, the lapilli in volcaniclastic rocks are affected by a different alteration assemblage than the matrix and contain chlorite, biotite, carbonate minerals and/or sulfide minerals, typically pyrite or pyrrhotite (Fig. 3.5L). In thin section, white mica comprises between 5-15 modal % and bladed white mica grains occur most commonly in bands that define the fabric (Fig. 3.5M); relict feldspar grains are partly to fully replaced by fine white mica (Fig. 3.5N). Chlorite is less common than white mica in this assemblage, commonly <10 modal % where it occurs, and in most cases overprints the mica-defined fabric. Minor biotite locally overprints or replaces chlorite. Fine-grained disseminated sulfide minerals (dominantly pyrite) and carbonate minerals are commonly the paragenetically latest phases (Fig. 3.5O). Where the alteration assemblage affects coherent felsic rocks, minor carbonate-sulfide veinlets with random orientations occur. In the central part of the ABM zone within Sequence 2 (Fig. 3.4), white mica-altered intervals contain light green mica. The green mica-white mica assemblage is limited to the contacts of the mafic sills with other rocks and to the contacts of the felsic sill that is enclosed between the two mafic sills (Fig. 3.4). Green mica is very fine-grained and green mica-altered intervals gradually transition into white mica-rich intervals. Carbonate bands up to 30 cm thick occur in the green mica-rich intervals and are commonly associated with lesser red sphalerite and minor galena and pyrite/pyrrhotite (Fig. 3.5P). The green mica-altered intervals of felsic volcanic rocks have elevated Cr content (~600 ppm Cr in one sample) compared to felsic rocks of the Kudz

Ze Kayah formation affected by different alteration assemblages (<30 ppm Cr); mafic sills with MA signatures (see "Key immobile elements" section) contain high Cr values (>290 ppm Cr; Denisová and Piercey, 2022).

3.7.1.4 Fe-carbonate alteration

Carbonate with significant Fe content, in addition to Ca and Mg, typically occurs as the paragenetically latest mineral phase in drill core. It occurs as dispersed euhedral grains or as coatings on grains, lapilli, or other heterogeneities and has an orange color in older (>2 years) weathered drill core surfaces (Fig. 3.5Q). It occurs across the stratigraphy and affects all lithological units in the upper Kudz Ze Kayah formation and the argillites and mafic tuffs in the lower Wind Lake formation.

3.7.1.5 Chlorite-calcite-actinolite assemblage

The chlorite-carbonate-actinolite assemblage occurs only in the mafic sills in Sequence 2; no unaltered or less altered mafic sills exist in the ABM deposit footprint. Contacts of the mafic sills are commonly finer-grained and more intensely altered with carbonate and locally biotite, compared to the inner portions of the sills, which have a dark green fine-grained groundmass with aligned darker biotite-chlorite-rich patches, assumed to be replaced primary mafic mineral phenocrysts (Fig. 3.6A, B). The assemblage replaces most of the primary igneous minerals, yet primary igneous textures are partially preserved and overprinted by the alteration minerals (Fig. 3.6A). The assemblage consists of abundant chlorite (10-35 modal %), calcite (5-20 modal %), biotite (5-20 modal %), actinolite (20-25 modal % if present) and paragenetically late epidote (5-15 modal %). Calcite, chlorite, and minor white mica replace the groundmass (Fig. 3.6C), and white mica and calcite commonly replace K-feldspar and plagioclase, respectively. Corroded euhedral to subhedral equant actinolite grains are commonly replaced by chlorite and/or biotite (Fig. 3.6D), although late amphibole needles are observed locally. Barium-rich K-feldspar (hyalophane) occurs along biotite cleavage planes (Fig. 3.6E). The paragenetically youngest mineral phase is commonly euhedral fine-grained epidote (Fig. 3.6F).

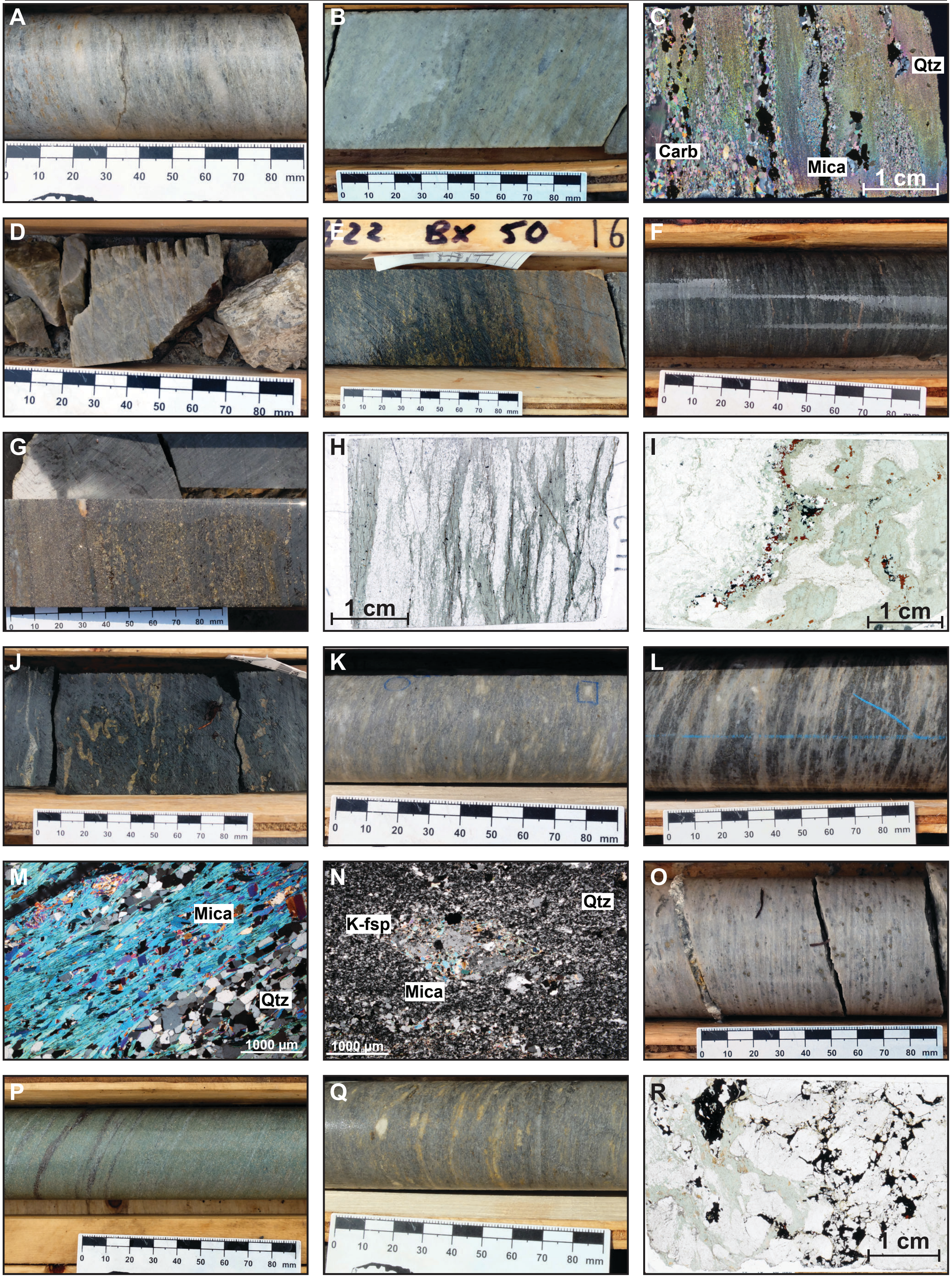
A
B
C
Qtz
Carb
Mica
1 cm
D
E
22 BX 50
16
F
G
H
1 cm
I
1 cm
J
K
L
M
Mica
Qtz
1000 µm
N
K-fsp
Qtz
Mica
1000 µm
O
P
Q
R
1 cm

Figure 3.5. Alteration assemblages present at the ABM deposit. (A) Pervasive white mica alteration in lapilli tuff; K15-290 m, 59 m down hole. (B) Fabric preserved in pervasively white mica altered tuff; K15-320, 200 m down hole. (C) Pervasive white mica alteration in thin section, white mica bands, later coarser carbonate alteration with associated sulfides; B370151; K15-295, 188.3 m down hole. (D) Fissile pervasively white mica altered drill core; K15-287, 31 m down hole. (E) Sharp contact of pervasive chlorite alteration over pervasive white mica alteration; K17-422, 165 m down hole. (F) Barren pervasive chlorite alteration; K15-287, 118 m down hole. (G) Mineralized pervasive chlorite alteration; K15-235R, 140 m down hole. (H) Barren pervasive chlorite alteration in thin section; Q721071; K15-287, 118.45 m down hole. (I) Mineralized pervasive chlorite alteration in thin section; Q930216; K15-232; 142.1 m down hole. (J) Sulfide stringers in pervasive chlorite alteration; K14-281, 197 m down hole. (K) Moderate white mica ± chlorite alteration in crystal-lapilli tuff; K15-271, 40 m down hole. (L) White mica ± chlorite alteration in matrix; K15-260, 204 m downhole. (M) Bands of illite in thin section of white mica ± chlorite alteration; B370159; K15-301, 91.3 m down hole. (N) K-feldspar in K-feldspar-quartz clot replaced by mica; Q930295; K15-315, 151.65 m downhole. (O) Disseminated pyrite in moderate white mica ± chlorite altered tuff; K15-320, 261 m down hole. (P) Green mica alteration with bands of sphalerite and carbonate; K15-232, 175 m down hole. (Q) Fe-carbonate alteration in white mica ± chlorite tuff; K15-271, 60 m down hole. (R) Euhedral albite overprinted by chlorite and chalcopyrite-pyrrhotite-sphalerite; K7-422, 160.9 m down hole. Carb = carbonate, K-fsp = K-feldspar, Mica = white mica, Qtz = quartz.

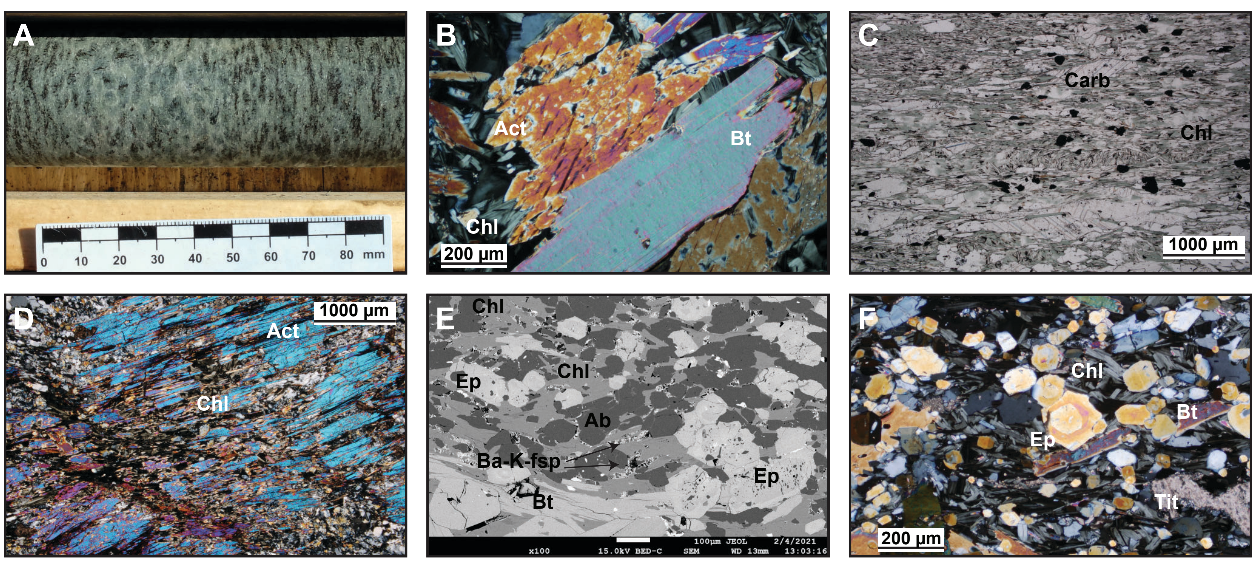

Figure 3.6. Alteration assemblages in mafic sills with MA signatures. (A) Coarse grained interior of mafic sill in Sequence 2 with amphibole-biotite clots; K15-265, 245 m down hole. (B) Biotite overgrowing amphibole, core of mafic sill; AA00348399; K15-290, 117.4 m down hole. (C) Barren chlorite alteration in thin section, margin of mafic sill; AA00348398; K15- 290, 90.8 m down hole. (D) Chlorite replacing amphibole, core of mafic sill; K15-290, 117.4 m down hole. (E) Ba-rich K-feldspar along fractures and grain boundaries in chlorite, late zoned epidote grains overgrowing; Q930290; K15-315, 121 m down hole. (F) Late zoned epidote grains overgrowing biotite and chlorite; Q930291, K15-315, 122 m down hole. Ab = albite, Act = actinolite, Ba-K-fsp = Ba-K-feldspar, Bt = biotite, Carb = carbonate, Chl = chlorite, Ep = epidote, Tit = titanite.

3.7.1.6 Paragenesis

Cross-cutting relationships determined from drill core and thin sections are used to establish the paragenesis of the different alteration assemblages in the ABM deposit (Fig. 3.7). The moderate white mica ± chlorite assemblage is interpreted to be the paragenetically oldest one preserved in the ABM deposit. It has the widest extent within the upper Kudz Ze Kayah formation (Fig. 3.2B) and is overprinted by both pervasive assemblages. The contacts between moderate white mica ± chlorite and pervasive white mica alteration zones are commonly gradual. Pervasive chlorite alteration overprints the pervasive white mica assemblage and commonly has sharp contacts (Fig. 3.5F). Sulfide mineralization crosscuts both pervasive assemblages. Contacts with mineralization are sharp (Fig. 3.8); rarely they are gradational over 10-20 cm. The paragenetically youngest observed phase is fine-grained diffuse Fe-rich carbonate or calcite, with minor euhedral Fe-carbonate and calcite grains overprinting all other assemblages (Fig. 3.5Q, R).

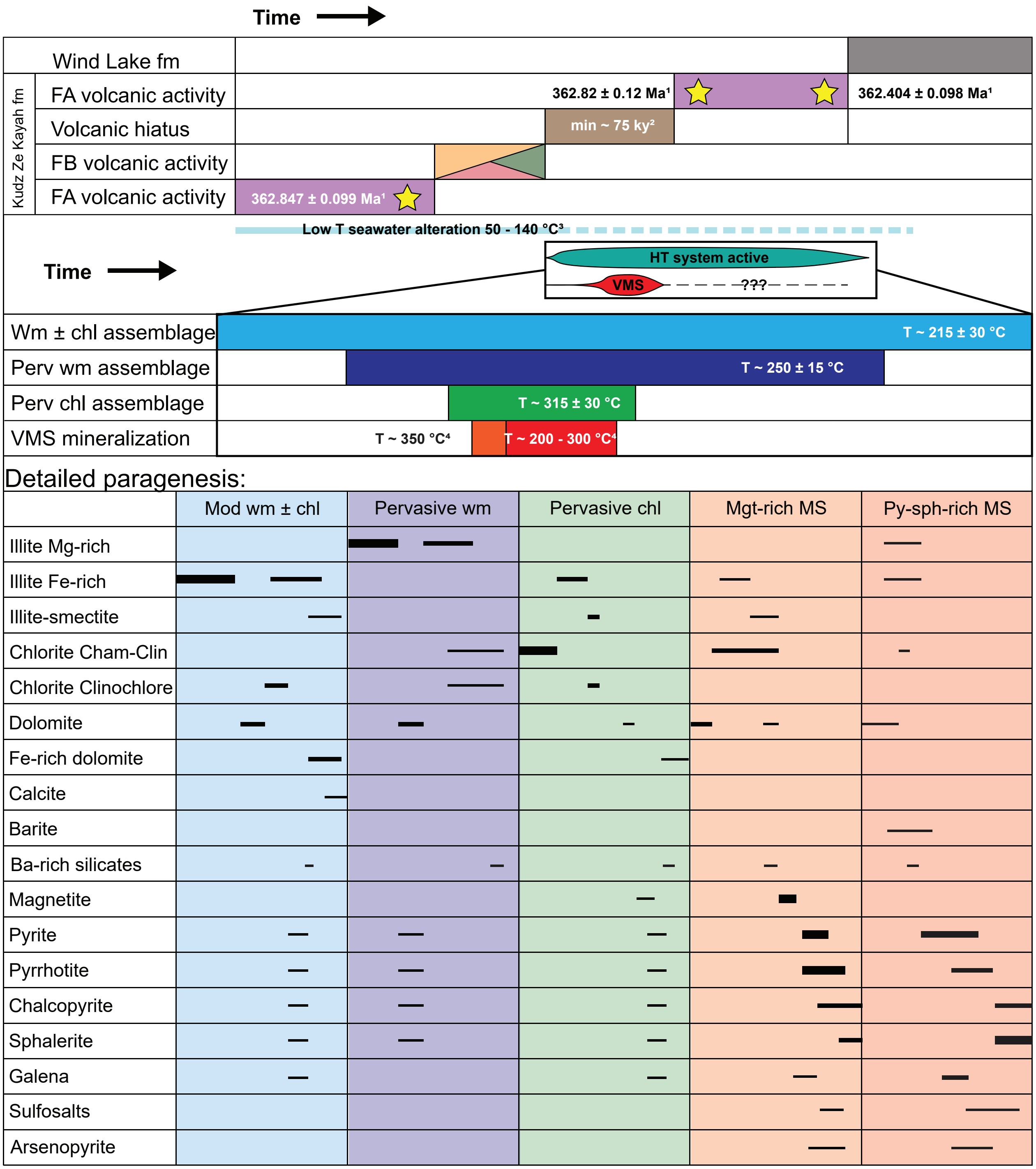

Figure 3.7. Paragenesis at the ABM deposit. [1]Manor et al. (2022b); [2]Denisová and Piercey (2022); [3]Gifkins and Allen (2001); [4]Franklin et al. (2005). Colors correspond to previous figures. Cham = chamosite. Clin = clinochlore.

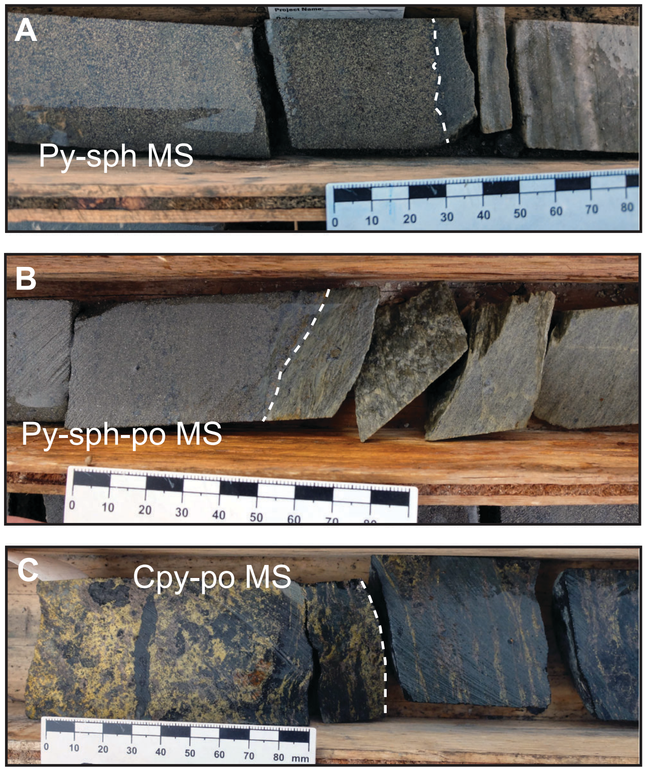

Figure 3.8. Examples of mineralization overprinting alteration assemblages. Dashed lines mark the contact. (A) Sharp contact between pyrite-sphalerite mineralization and moderate white mica ± chlorite altered tuff; K15-240, 54.5 m down hole. (B) Sharp contact between pyrite-sphalerite-pyrrhotite mineralization and pervasively white mica altered tuff; K15-287, 47 m down hole. (C) Chalcopyrite-pyrrhotite mineralization overprinting pervasive chlorite alteration; K17-422, 149.5 m down hole. Cpy = chalcopyrite, Py = pyrite, Po = Pyrrhotite, Sph = sphalerite, MS = massive sulfide mineralization.

3.7.2 Key immobile elements characteristics of host rocks

Denisová and Piercey (2022) described the immobile element systematics of the volcanic rocks of the upper Kudz Ze Kayah formation. Immobile behaviour of HFSE-REE-Al_2O_3-TiO_2 was assessed and confirmed using methods defined by MacLean (1988) and MacLean and Barrett (1993). Felsic rocks of the upper Kudz Ze Kayah formation plot on a single linear array in the Zr-TiO_2 space (Fig. 3.9A); therefore, immobile element ratios have been employed to further differentiate between the rock types and chemostratigraphic units. In the Al_2O_3/TiO_2-Zr/Al_2O_3 space three distinct groupings of felsic volcanic rocks exist (Fig. 3.9B). Group Felsic A (FA) has high Zr abundances (722 ± 118 ppm, n=33) and generally higher contents of high field strength elements (HFSE) relative to the group Felsic B (FB). The FB group is further divided into subgroups FB1 and FB2, based on differences between immobile elements and their ratios, with group FB1 having a higher average Zr value (419 ± 101 ppm, n=16) than the subgroup FB2 (267 ± 91 ppm, n=26). Felsic rocks belonging to the FB group occur in Sequence 2 and host the massive sulfide mineralization. Sequences 1 and 3 comprise felsic volcanic rocks of group FA. Mafic rocks of the upper Kudz Ze Kayah formation fall into two distinct groups based on their immobile element compositions (Fig. 3.9A, B): group Mafic A (MA) comprises mafic sills in Sequence 2, whereas group Mafic B (MB) represents younger mafic sills present in Sequence 3.

3.7.3 Major and mobile trace elements

Using major oxides to trace hydrothermal alteration is a simple but an effective technique utilized in VMS environments to track alteration processes such as feldspar destruction and subsequent white mica (Na_2O, CaO, K_2O) and chlorite and pyrite formation (MgO, Fe_2O_3; Spitz and Darling, 1978; Riverin and Hodgson, 1980; Date et al., 1983; Large et al., 2001c; Mathieu, 2018).

In the alteration box plot (Fig. 3.9C; Large et al., 2001b), samples identified by other methods as least altered (Fig. 3.9D; the Na_2O-Na_2O/Al_2O_3 diagram; Ruks et al., 2006) plot within the least altered rhyolite and dacite fields. Most of the felsic samples follow the white mica alteration path with data plotting on a trend from the least altered fields towards the illite node (trend 2 in Figure 3.9C). Rocks with FB signatures from Sequence 2 (proximal to the mineralization) show a more significant shift towards white mica than the FA rocks that are more distal from the massive sulfide mineralization. Samples that follow the chlorite-pyrite and white mica-chlorite-pyrite trends are strongly to pervasively altered by white mica and/or chlorite (trend 1 in Figure 3.9C). A minor subset of the felsic samples follows a diagenetic trend towards the albite node, indicating they experienced diagenetic alteration that is locally preserved (trend 3 in Figure 3.9C). Observed textures show euhedral albite grains locally overprinted by chlorite and sulfide mineralization (Fig. 3.5R) or minor white mica. Feldspar destruction and common white mica alteration are also easily distinguishable in molar ratio plots of K_2O and Na_2O (Davies and Whitehead, 2006), where FB felsic rocks show strong feldspar destruction and white mica alteration (Fig. 3.9E). Large ion lithophile elements (LILE) such as Rb and Sr correlate with the behaviour of their geochemical twins, K and Ca, respectively (Fig. 3.9F, G).

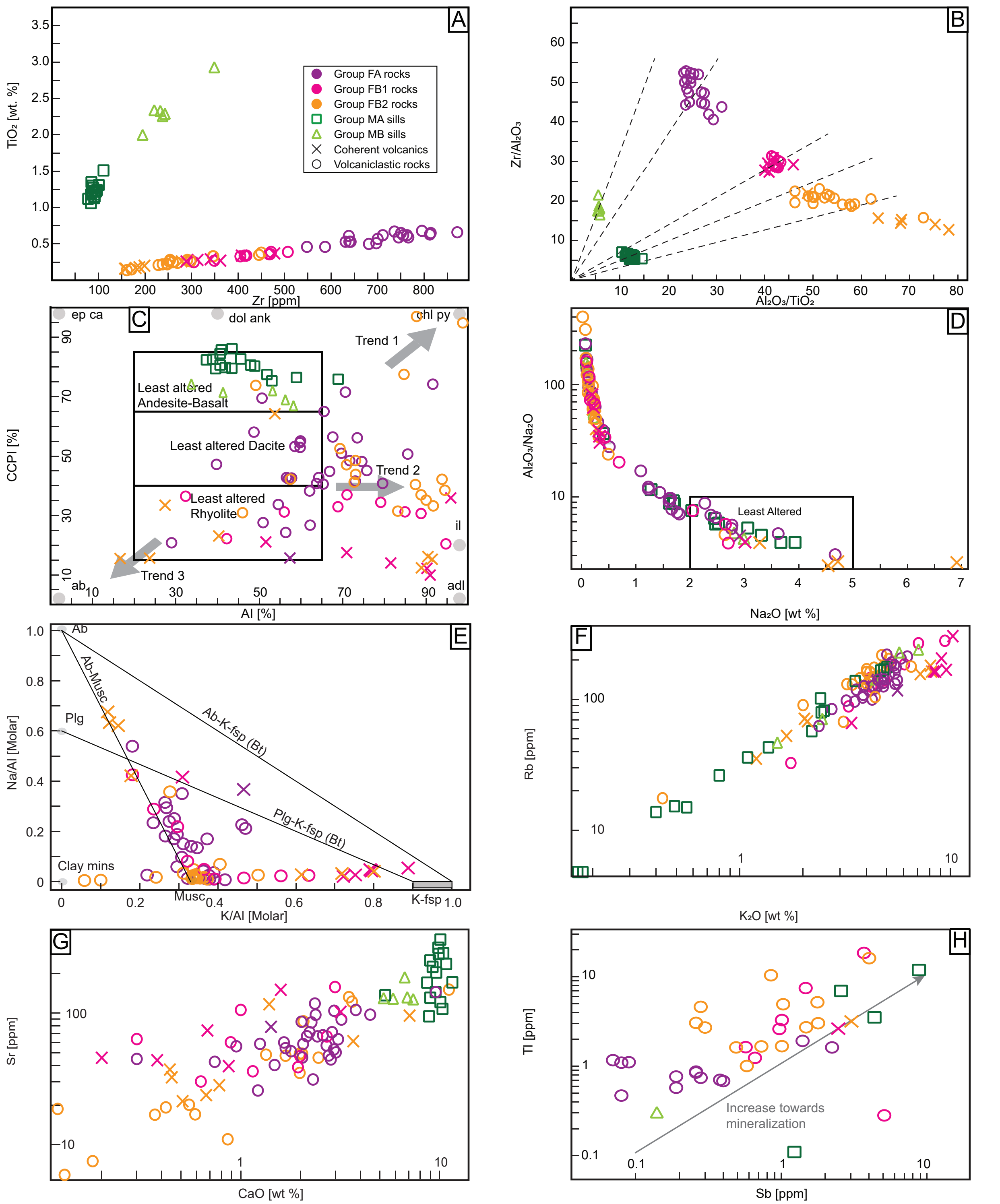

Figure 3.9. Major and trace element plots. (A) Plot of Zr vs. TiO_2. (B) Plot of Al_2O_3/TiO_2 vs. Zr/Al_2O_3. (C) Alteration box plot after Large et al. (2001b). (D) Na_2O vs Al_2O_3/Na_2O (Spitz-Darling index) showing least altered rocks. Diagram after Ruks et al. (2006). (E) K/Al vs. Na/Al molar ratio plot of mobile/immobile element after Davies and Whitehead (2006). (F) Plot of K_2O vs Rb. (G) Plot of CaO vs Sr. (H) Plot of Sb vs Tl after Large et al. (2001a).

In different types of VMS deposits, mobile metallic and metalloid trace elements (Sb, Tl, Mn) form halos of varying magnitude around the massive sulfide lenses (Large et al., 2001a; Large et al., 2001c). At the ABM deposit, some of these elements increase proximal to mineralization (Fig. 3.10). Thallium and Sb, both volatile elements, show elevated values (approximately >1 ppm) in proximity to massive sulfide mineralization (Fig. 3.9H). Anomalous values of Tl and Sb in felsic rocks occur up to 300 m from the massive sulfide lenses in all directions. Arsenic, Bi, Cd, Mo, and Sn values have higher abundances within Sequence 2 rocks compared to other sequences but do not show consistent increases with proximity to mineralization (Fig. 3.10, Appendix 2.1); base metals abundant in the mineralization (Zn, Cu, Pb) and Au and Ag follow a similar pattern: they are slightly increased within Sequence 2 rocks compared to other sequences (Appendix 3.1). Manganese and In display relatively higher values in Sequence 3 rocks compared to Sequence 2 rocks (Fig. 3.10), although rare anomalous values occur associated with massive sulfide mineralization (Fig. 3.10).

Figure 3.10. Down hole profiles of drill holes in the ABM deposit. (A) Drill hole K15-281, in the western part of the ABM Zone, position of the drill hole is highlighted in the map in Figure 3.2A. Colored circles highlighted samples that are part of the EMPA dataset. (B) Drill hole K15-301 in the east part of the ABM Zone, 415050 mE cross section. (C) Drill hole K15-320, in the Krakatoa Zone, position of the drill hole is highlighted in the map in Figure 3.2A.

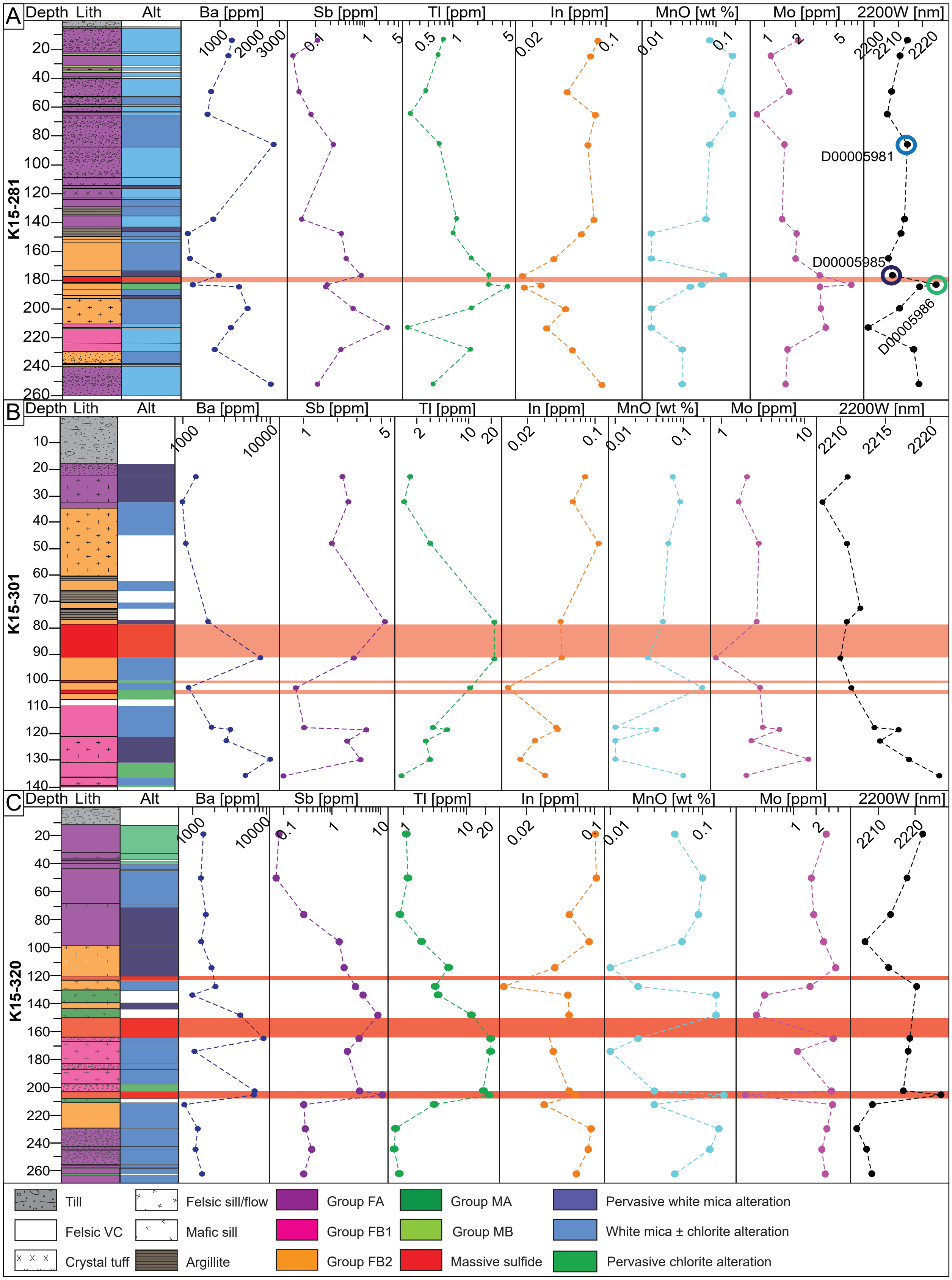
A
Depth Lith Alt Ba [ppm] Sb [ppm] Tl [ppm] In [ppm] MnO [wt %] Mo [ppm] 2200W [nm]
K15-281
D00005981
D00005985
D00005986
B
K15-301
C
K15-320
Till
Felsic VC
Crystal tuff
Felsic sill/flow
Mafic sill
Argillite
Group FA
Group FB1
Group FB2
Group MA
Group MB
Massive sulfide
Pervasive white mica alteration
White mica ± chlorite alteration
Pervasive chlorite alteration

3.7.4 Mass balance

Mass balance calculations for felsic volcanic rocks were performed using the single precursor method outlined in MacLean and Barrett (1993) and Barrett et al. (2008). No unaltered samples of mafic volcanic rocks were identified from hand samples or from geochemical data; therefore, mass balance calculations were not performed for mafic rocks in the ABM deposit footprint. Samples of the FA and FB felsic geochemical groups plot on separate linear arrays in Al_2O_3/TiO_2-Zr/TiO_2 space (Fig. 3.9B), which indicates they belong to two distinct homogenous volcanic units (Barrett et al., 2008). Least-altered samples from the felsic geochemical groups (FA, FB1, and FB2; Appendix 4.1) were selected based on low loss on ignition (LOI) values (<2.5 %), low base metal values (Zn+Pb+Cu<500 ppm), relatively high Na_2O content (>2 %), and low Spitz-Darling index (Al_2O_3/Na_2O<10; Spitz and Darling, 1978; Ruks et al. 2006). The least-altered values were averaged to establish a precursor composition for each geochemical group, with Al_2O_3 used as the monitor of mass change (Barrett et al., 2008). Least-altered samples were chosen from both the project dataset (this study) and the BMC lithogeochemical database. The company dataset contains an incomplete and inconsistent suite of elements compared to new results presented in this study, particularly for minor LILE (Cs, Rb, Sr) and other trace elements for non-mineralized samples (Sr, Sc, Rb, Tl, Sb, Hg); therefore, mass balance calculations were performed only for the major mobile elements, base metals, and Ba, as these are universal across our new data and legacy data from the company dataset. Calculated values of mass change for felsic samples are presented in Appendix 4.2. Most samples show depletions in Na_2O, typical for the destruction of feldspar (Fig. 3.11A). Commonly, plagioclase destruction can be monitored using both Na_2O and CaO mass changes (MacLean, 1990; Barrett et al., 1993; MacLean and Barrett, 1993), but late carbonate mineral overprints prevent this at the ABM deposit. Samples with $\Delta Na_2O<-1.5$ wt. % generally have values of AI>60. Samples with additions of Na_2O (Fig. 3.11A) coincide with the diagenetic trend in the alteration box plot (Fig. 3.9C). A minority of FB group samples shows significant additions of K_2O (>3 %; Fig. 3.11B) indicative of pervasive white mica alteration; these samples also show AI>60. Minor samples from groups FB2 and FA show Fe_2O_3+MgO gains between 7-20 % and also display mass losses of SiO_2, which is indicative of pervasive chlorite alteration (Fig. 3.11C). These samples generally have chlorite-calcite-pyrite index (CCPI) values >65. Samples closest to the mineralization (i.e., FB rocks) show the highest degree of feldspar destruction and locally significant mass gains of Ba (Fig. 3.11D). Most samples with significant Fe_2O_3+MgO gains show mass changes of Ba lower than 1000 ppm. Samples with mass gains of base metals (Zn + Pb + Cu >500 ppm) display losses of Na_2O and locally Fe_2O_3+MgO gains (Fig. 3.11E, F). Representative downhole profiles with mass change values are available in Appendix 3.1.

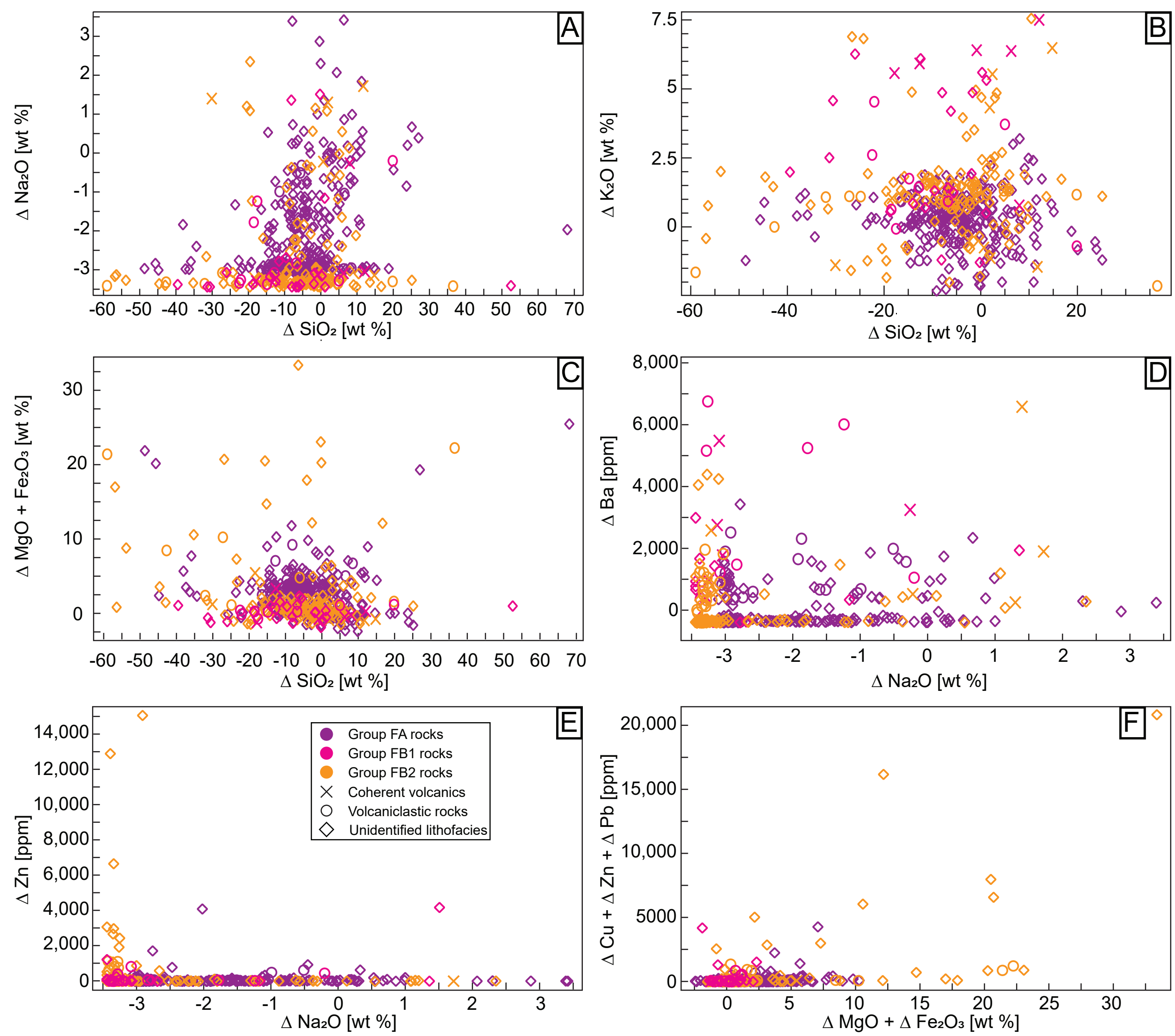

Figure 3.11. Mass balance plots of selected elements. (A) Δ SiO_2 vs Δ Na_2O. (B) Δ SiO_2 vs Δ K_2O. (C) Δ SiO_2 vs (Δ MgO + Δ Fe_2O_3). (D) Δ Na_2O vs Δ Ba. (E) Δ Na_2O vs Δ Zn. (F) (Δ MgO + Δ Fe_2O_3) vs (Δ Cu + Δ Zn + Δ Pb).

3.7.5 Mineral Chemistry

Nine samples were selected for the study of the mineral composition of the major alteration minerals (white mica, carbonate, and chlorite). The samples were chosen to be representative of the major alteration types (pervasive white mica - D00005985, pervasive chlorite – D00005986, Q721071, Q721080. Q930216, moderate white mica ± chlorite – D00005981, Q930221, Q931973, Q931984) and to determine the compositional variety of the minerals based on their position in the stratigraphy, alteration intensity and proximity to massive sulfide mineralization. Full results of the EMPA analyses are given in Appendix 5.1-5.3.

3.7.5.1 White Mica

White mica composition has been calculated based on 11 oxygens with all iron assumed to be Fe^{2+}. The composition of the 152 analyzed grains ranges between $(K_{0.187\text{-}0.904}Na_{0.003\text{-}0.129}Ba_{0.003\text{-}0.047})_{\sum 0.21\text{-}0.93}$ $(Al_{0.102\text{-}2.082}Fe_{0.038\text{-}1.938}Mg_{0.053\text{-}1.742})_{\sum 2.01\text{-}3.12}$ $(Si_{2.417\text{-}3.563}Al_{0.437\text{-}1.582})_{\sum 4}$ O_{10} $(OH)_2$ (Appendix 5.1). The majority of analyzed white mica grains have compositions typical for illite (Fig. 3.12B) with the sum of interlayer cations (I) between 0.75-0.93 apfu and illite/smectite I between 0.21-0.75 apfu. The main interlayer cation is K (0.19-0.90 apfu), with only minor Na (~0.04 apfu) and negligible Ca and Sr. Barium content in the interlayer deficient mica is locally between 0.035-0.047 apfu, with an average value of 0.01 apfu. Based on their Fe, Mg, and K content, the interlayer-deficient micas can be divided into three groups (Fig. 3.12A). The first group (group 1) is illite with a high proportion of Mg compared to Fe (Fe# between 15-30 %). The second group (group 2) is illite and illite/smectite with a higher proportion of Fe compared to Mg (Fe# ~35-60 %). The third group (group 3) is illite/smectite due to its lower cation sum (between 0.2-0.5 apfu), although it has a similar range of Fe# as group 2 micas. The group 1 illite with higher Mg are present in pervasively white mica-altered felsic rocks proximal to the massive sulfide mineralization, whereas group 2 illites with higher Fe are much more widespread across different alteration types in the sample suite. The group 3 illite/smectite are associated with group 2 illites but appear to post-date them. A subset of the group 2 illites shows slightly elevated Ba values compared to the rest of the sample set with Ba between 0.0313-0.029 apfu with rare values up to 0.047 apfu. The occurrence of the Ba-enriched illites is limited to the samples from Sequence 2 in the immediate proximity of mineralization.

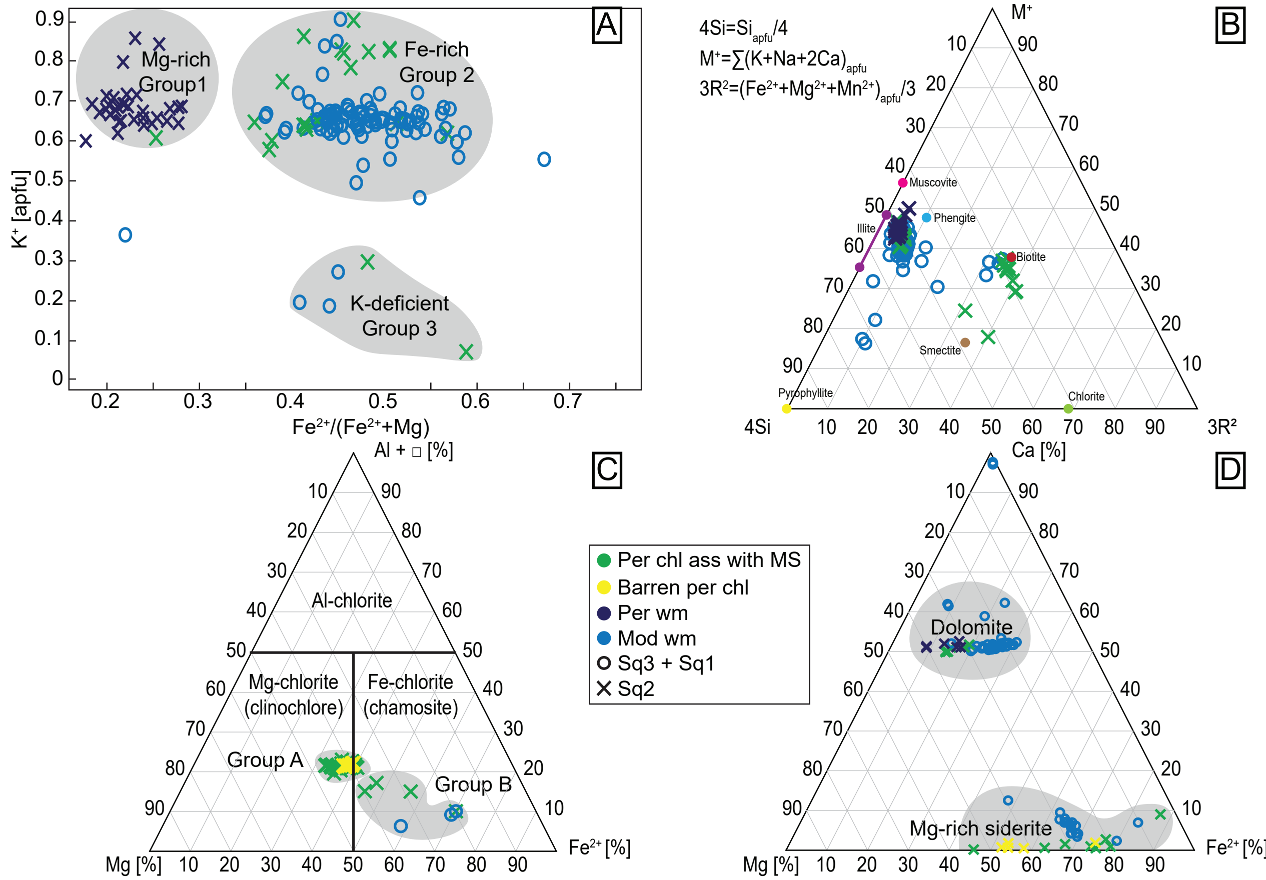

Figure 3.12. Results of EMPA analyses. (A) Plot of $Fe^{2+}/(Fe^{2+}+Mg)$ vs K^+ in atoms per formula unit (apfu) in white mica. (B) $4Si\text{-}M^{+}3R^{2}$ diagram after Aja (2020) showing analyzed illite composition and ideal composition of phyllosilicates (Deer et al., 2013). (C) Chlorite discrimination diagram after Zane and Weiss (1998). (D) Discrimination diagram for carbonate minerals.

3.7.5.2 Illite Geothermometry

Temperatures were calculated for 152 of the analyzed illite and illite/smectite grains using the equation proposed by Battaglia (2004). This method is based on calibrated empirical data from several geothermal fields and quantifies the relationship between illite composition (K, Fe, Mg) and temperature (Cathelineau, 1988; Battaglia, 2004). Results from illite and illite/smectite grains at ABM adhere to the trends described by Battaglia (2004): the calculated temperature rises with higher K content (Appendix 5.1). The highest temperatures 249.3±14.9 °C are in illite with low

Fe# (group 1) that occurs in the pervasively white mica altered zone (D00005985). Illite grains with higher Fe# (group 2) from samples from moderate white mica ± chlorite alteration zones have lower temperatures: 219.5±10.2 °C (sample D0005981), 223.2±31.8 °C (sample Q930221), 204.6±10.8 °C (sample Q931973), and 217.8±17.5 °C (sample Q931984). In a sample from a pervasively chlorite altered zone (sample D00005986), the illite with high Fe# (group 2) has a temperature of 215.3±4.3 °C.

3.7.5.3 Carbonate minerals

Most of the analyzed carbonate minerals have compositions between dolomite ($(Ca,Mg)CO_3$) and ankerite ($(Ca,Fe)CO_3$) (Fig. 3.12C, Appendix 5.2). The group classified as dolomite has the following compositional range: $(Ca_{0.48\text{-}0.60}Mg_{0.15\text{-}0.39}Fe_{0.08\text{-}0.29})_{\Sigma 0.95\text{-}1.23}$ CO_3. Another group is Ca-poor and is classified as Mg-rich siderite: $(Ca_{0\text{-}0.11}Mg_{0.04\text{-}0.45}Fe_{0.23\text{-}0.73})_{\Sigma 0.87\text{-}0.99}$ CO_3. Minor Mn (0.015-0.060 apfu) occurs in dolomite and Mg-rich siderite and occurs proximal to the mineralization (in Sequence 2 rocks), although some carbonates in this setting show Mn contents below the detection limit or near zero abundances. Calcite is the least common of the observed carbonate phases in the analyzed felsic rocks.

3.7.5.4 Chlorite

Chlorite composition was calculated on the basis of 14 oxygens and assuming all iron to be Fe^{2+}. All analyzed chlorite grains are from samples of the altered felsic lithofacies. The compositional range of the 56 analyzed grains is $(Al_{1.18\text{-}2.76}Fe_{1.01\text{-}2.97}Mg_{0.61\text{-}2.72})_{\Sigma 4.96\text{-}6.04}$ $(Si_{2.60\text{-}3.89}Al_{0.11\text{-}1.38})_{\Sigma 4.00}$ O_{10} $(OH)_8$ (Appendix 5.3). The chlorites fall into two distinct groups based on the Si, Fe, and Mg content (Zane and Weiss, 1998). The more abundant group A occurs on the chamosite-clinochlore boundary; group B has a clinochlore composition (Fig. 3.12C). The chlorites of group A are relatively homogenous except for a minor subset that has elevated Mn content (~0.03-0.04 apfu) compared to the group B. The Mn-rich samples occur within pervasive chlorite alteration that is not associated with massive sulfide mineralization.

Chlorite geothermometry: Geothermometry calculations were performed using the composition of the 56 analyzed chlorite grains. Four methods were tested (Kranidiotis and MacLean, 1987;

Cathelineau, 1988; Jowett, unpub. data; Zang and Fyfe, 1995), all based on calibrated empirical data and investigating the link between the contents of Al, Si, Fe, and Mg in chlorite in relation to temperature. All methods show that the calculated temperatures fall into two groups: the chlorites with compositions on the chamosite-clinochlore boundary formed at higher temperatures than the chlorites with the clinochlore compositions (Appendix 5.3). Three of the methods (Kranidiotis and MacLean, 1987; Cathelineau, 1988; Jowett, unpub. data) report similar ranges of temperatures with the lower temperature group between 200-300 °C and the higher temperature group ranging between 300-400 °C (Appendix 5.3). The last method (Zang and Fyfe, 1995) shows lower temperatures for both groups that are shifted approximately 100 °C lower, but the method has not accounted for possible effects of pressure, whereas the other methods were developed using data from low pressure environments, like the one presumed at the ABM deposit during its formation. We chose to report temperatures calculated according to Kranidiotis and MacLean (1987), because the ranges of calculated temperatures are closest to those expected based on the observed mineralization assemblages (chalcopyrite-pyrrhotite-pyrite-magnetite associated with chlorite ~350 °C; Franklin et al., 2005; Hannington et al., 2005). Higher temperatures 322.0±8.8 °C (max 345 °C; n=49) characterize group A chlorites in the pervasive chlorite assemblage, whereas the lower temperature chlorites occur in moderately white mica altered felsic rocks (samples Q931984, Q930221; 134.2 °C, n=4) or as late minor chlorites occurring on sulfide grain boundaries in pervasively chlorite altered rocks (sample Q721080; 243.4 °C, n=3).

3.7.6 Hyperspectral data

Results of the hyperspectral analyses of the samples (Appendix 6.1) show that the measured values of the 2200 nm feature (referred to herein as 2200W) span a wide range between 2197 and 2227 nm, largely independent of lithology (Fig. 3.4B). Felsic rocks with varying degrees of predominantly white mica alteration (pervasive to weak), both coherent and volcaniclastic, show a single population (Fig. 3.13A). The relative abundance of values in the 2208-2216 nm range indicates the common occurrence of mixtures of the two white mica compositions - muscovite and phengite - within the alteration footprint. Only felsic samples with ΔK_2O>3 % show 2200W feature values typical for phengite (2215.5-2224 nm). Mineralized or pervasively chlorite-altered samples (n=54) show a bimodal distribution, with a gap in the 2212-2217 nm range (Fig 3.13B). Proximal to the mineralization, values from the opposite sides of the 2200W feature spectrum commonly occur adjacent to each other over a few meters (Fig. 3.4, 3.10) regardless of lithology.

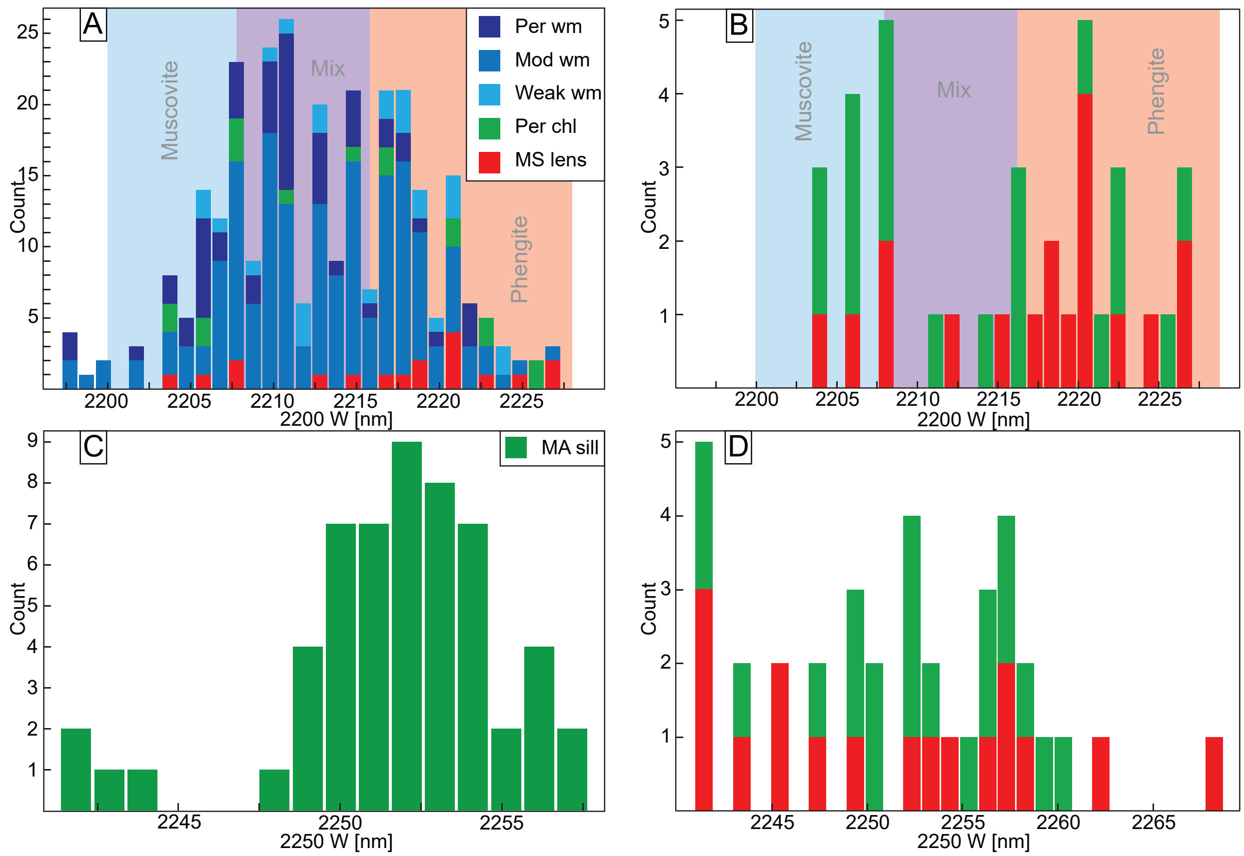

Figure 3.13. Histograms showing results of SWIR analyses. (A) Values of 2200 nm feature in felsic rocks. (B) Values of 2200 nm feature in pervasively chlorite altered and mineralized rocks. (C) Values of 2250 nm feature in mafic rocks with MA signature. (D) Values of 2250 nm feature in pervasively chlorite altered and mineralized rocks.

The values of the depth of the 2200W feature are generally higher for felsic samples than for the mafic samples, indicative of more abundant white mica in the felsic rocks (Yang et al., 2011).

Values for the 2250 nm feature (referred to herein as 2250W) vary between 2240 and 2260 nm and do not correlate to any specific lithology. Felsic samples with no to low chlorite contents, as recognized from drill core, commonly show values below 2245 nm, which confirms the absence of chlorite in the rock (Herrmann et al., 2001). Mafic sill samples skew towards the 2250 nm feature values that are indicative of chlorite compositions with a higher #Fe compared to the other analyzed chlorites because most of samples show values above 2250 nm (Fig. 3.13C). Mafic sills with MA signatures show higher values for the depth of the 2250W feature, reflecting the abundant chlorite observed in thin sections compared to the sills with MB signatures that more commonly display lower abundances of chlorite and higher contents of biotite in thin section. Felsic samples displaying strong to pervasive chlorite alteration show a wide spread of values (Fig. 3.13D).

Compared with geochemical data, hyperspectral data for white mica-rich samples with longer 2200W feature wavelength values correspond to rocks with higher Al_2O_3/Na_2O index and a higher K_2O content (Appendix 2.1, 6.1). The 2200W feature values do not correlate with AI, CCPI, or the Ba/Sr value. The 2250W feature correlates negatively with SiO_2 values in accordance with more abundant chlorite proportions observed in mafic and pervasively chlorite altered rocks. Comparing values of the 2200W feature with averaged compositions of white mica analyzed by the EMPA shows two groupings: samples with longer 2200W wavelengths (>2213 nm) that represent the moderate white mica ± chlorite assemblage and have lower sum of interlayer cations (I) values (<0.7 apfu), higher Si/Al, and higher Fe# (>40 %); and samples with shorter 2200W wavelengths (<2208 nm) that have higher I and lower Si/Al values. One of the samples with shorter 2200W wavelengths represents the pervasive white mica assemblage (D00005985) and has a low Fe# (<25 %), the other sample (Q930221) represents the moderate white mica ± chlorite assemblage and has similar Fe# values (>40 %). A possible reason for the shorter 2200W values in the latter sample is the presence of minor biotite in the sample. Samples representing the pervasive chlorite assemblage containing >40 modal % chlorite all have 2200W values >2213 nm, illite from these samples has Fe# values >40 %.

3.8 Discussion

In replacement-style VMS deposits, the contrasts in porosity and permeability within the subseafloor lithologies control hydrothermal fluid flow leading to irregular but mostly conformable alteration zones in the footwall and hanging wall of massive sulfide mineralization (Doyle and Huston, 1999; Doyle and Allen, 2003; Anderson et al., 2019; Nozaki et al., 2021). Despite past work in the

Finlayson Lake district, there has been no study of the hydrothermal alteration footprint that has integrated field observations, mineralogical, spectral, and lithogeochemical data, and that relates the hydrothermal alteration to the emplacement mechanisms of the mineralization. Following brief remarks on the effects of greenschist facies metamorphism on hydrothermally altered rocks at the ABM deposit, the discussion will address two major topics: 1) how the hydrothermal system associated with the ABM deposit developed in time and space and its relation to the mineralization; and 2) do any alteration vectors exist and at what scales are they most useful to target a replacement-style VMS deposit in a dominantly felsic volcanosedimentary sequence.

Metamorphism in this part of the Finlayson Lake district reached a maximum of greenschist facies (Murphy et al., 2006). Generally, this metamorphic facies does not significantly affect the geochemical and mineral-chemical signatures produced by hydrothermal alteration and recrystallized alteration-related phyllosilicates preserve their original pre-metamorphic compositions (Riverin and Hodgson, 1980; Urabe et al., 1983; Hannington et al., 2003; Genna and Gaboury, 2015). This appears to be the case at the ABM deposit; however, under contemporaneous deformation, the hydrothermally altered rocks at the ABM deposit recrystallized, which partially obscured the primary paragenetic relationships at the microscopic scale. The relationships between the different alteration assemblages at the deposit scale remain unaffected, as no major folding has been documented in the deposit footprint, the major deformation fabric is subparallel to primary bedding (van Olden et al., 2020), and the observed crosscutting relationships between alteration assemblages are not significantly affected by deformation. The effects of greenschist facies metamorpism are most apparent in the mafic sills in Sequence 2. The chlorite-calcite-actinolite assemblage that occurs throughout this lithofacies contains locally abundant actinolite (Fig. 3.6A, B, D), which suggests it is of a regional metamorphic origin (Arghe et al., 2011). Other overprinting minerals in the mafic sills are also linked to metamorphic processes (biotite, chlorite, zoned epidote; Fig. 3.6E, F). The effects of metamorphism on the mafic sills were likely isochemical, as samples of mafic sills affected by the chlorite-calcite-actinolite assemblage plot mostly in the least altered mafic rocks field in the alteration boxplot (Fig. 3.9C). Despite greenschist facies metamorphism and associated deformation in the ABM deposit, it does not significantly affect macro- and mesoscale relationships between hydrothermal alteration assemblages and/or host rocks, and the different mineral-chemical signatures of phyllosilicate and carbonate minerals in hydrothermal alteration assemblages are also preserved. Thus, despite post-VMS metamorphism and deformation, the original footprint of VMS-related alteration and mineralization is still preserved and reflects the original evolution of the ABM deposit hydrothermal system and not subsequent post-VMS tectonothermal activity.

3.8.1 Hydrothermal system extent and evolution

Prior to VMS-related hydrothermal alteration (200-350 °C), the felsic volcanic rocks hosting the ABM deposit were likely affected by diagenetic alteration (<150 °C) similar to the alteration processes described by Munhá et al. (1980) and Gifkins and Allen (2001). Evidence of these low temperature (<200 °C) pre-hydrothermal processes in the ABM deposit footprint is scarce and these assemblages were predominantly overprinted by younger, higher temperature hydrothermal alteration and post-VMS metamorphic assemblages. The paragenetically oldest observed alteration assemblage is recorded by the diagenetic trend in the felsic volcanic rocks on the alteration boxplot (Fig. 3.9C). This assemblage has a limited spatial distribution and comprises large (~0.5 cm) euhedral feldspar, most commonly albite. Similar zones of Na-enrichment were described by Date et al. (1983) in the Kuroko district and recently by Pilote et al. (2019) in the Ming deposit, where this alteration assemblage was interpreted to form from late fluids generated by plagioclase breakdown or due to late influx of unmodified cold, Na-rich seawater. Even though these zones of Na-enrichment are locally associated with massive sulfide lenses at the ABM deposit, the euhedral feldspar crystals appear to be one of the earliest preserved phases, and locally, the feldspar is overprinted by white mica, chlorite, and/or carbonate minerals along grain boundaries and fractures, implying its formation preceded pervasive VMS alteration. In the deposit area, the Na-rich alteration would have taken place during and after the deposition of Sequence 2 rocks and was succeeded by the higher temperature VMS hydrothermal alteration (T >230 °C; Fig. 3.7).

The moderate white mica ± chlorite assemblage is the most spatially extensive hydrothermal alteration assemblage at the ABM deposit (Fig. 3.2, 3.3, 3.4) and it is the earliest of the higher temperature assemblages as it is crosscut by all other VMS-related hydrothermal assemblages. The extent of the moderate white mica ± chlorite alteration assemblage, together with only rare later overprints further away from the core of the deposit (Fig. 3.2B), suggest that it formed as the initial phase of the hydrothermal fluid flow that infiltrated porous and permeable units where the hydrothermal fluids interacted with the host rocks saturated in cold seawater. The mapped moderate white mica ± chlorite alteration zones are stratabound, and commonly flanked by units with lower porosities and permeabilities, such as coherent volcanic rocks or mudstones (Fig. 3.3, 3.4). For such a widespread alteration halo to form away from the core of the hydrothermal system and the major synvolcanic faults, hydrothermal fluids must have circulated laterally through the units with high porosity and permeability (Large et al., 2001a; Genna et al., 2014; Piercey et al., 2014), similar to what has been described in some modern-day SMS deposits (Anderson et al., 2019; Nozaki et al., 2021). Lateral flow of hydrothermal fluids within volcaniclastic units is further supported by the similarity of mica compositions along the extent of the moderate white mica ± chlorite alteration zones, which have 2200W feature spectral values that generally fall within the same range throughout the interpreted alteration lenses (Fig. 3.4). Commonly, the moderate white mica ± chlorite assemblage has 2200W values in the same range as the assemblage samples analyzed by EMPA that contain predominantly group 2 illite (2200W>2212 nm).

Mineral-chemical data from samples in the moderate white mica ± chlorite alteration zone show there was voluminous early illite in this assemblage. Temperatures calculated using illite compositions from moderately white mica ± chlorite altered zones average 214.5±33.0 °C (n=110 from 4 samples). In hydrothermal systems, illite commonly forms in the early stages at lower temperature and/or at lower pH (Iijima, 1974; Schardt et al., 2001). Under such conditions, illite forms preferentially over chlorite (Schardt et al., 2001), which would explain the relative scarcity of chlorite in the most widespread alteration assemblage in the ABM deposit. Where chlorite is more abundant in the moderate white mica ± chlorite assemblage (~10 modal % and above), it is likely due to more extensive mixing of hydrothermal fluids with the seawater present in the water saturated porous and permeable units, which would have raised the pH of the fluid, added Mg, and would have allowed chlorite to precipitate (Schardt et al., 2001). Proximal to zones of pervasive white mica alteration, disseminated sulfide minerals occur within the moderate white mica ± chlorite assemblage. In other VMS deposits, pyrite is a common component of white mica alteration assemblages forming at temperatures below 250 °C (Schardt et al., 2001), which correlates with the proposed temperatures at which the alteration minerals comprising this alteration assemblage formed.

In VMS deposits, zones of pervasive alteration are interpreted to be the pathways of the most intense fluid flow with highest fluid:rock ratios and highest fluid temperatures (e.g., Holk et al., 2008). The centre of the ABM deposit comprises zones of pervasive alteration that surround the mineralized bodies and overprint the moderate white mica ± chlorite alteration assemblage. The temperatures recorded by group 1 illite in pervasive white mica altered zones here are 248.9±14.9 °C, similar to temperatures recorded in pervasive white mica zones in other VMS deposits (Schardt et al., 2001). A lens of moderately to pervasively green mica-white mica altered felsic volcaniclastic rocks occurs between the two mafic sills in Sequence 2 (Fig. 3.4). This alteration assemblage has elevated Cr content (~600 ppm) compared to other felsic volcanic rocks (<30 ppm Cr) and occurs at or in proximity to mafic sill contacts, which are inferred to be the source of Cr for the green mica, as mafic sills with MA signatures contain high Cr values (>290 ppm Cr; Denisová and Piercey, 2022). Intense fuchsite-carbonate-barite alteration has been described in basalts directly in the hanging wall of the Hellyer deposit, Tasmania, and the source of Cr in fuchsite was determined to be the breakdown of Cr-rich pyroxenes in the basalt (Gemmell and Large, 1992; Large et al., 2001c); mafic rocks were likely the source of Cr in the green mica-white mica altered zones in the ABM deposit as well. At the ABM deposit, the lens of green mica altered rocks is interpreted to mark a zone of maximum fluid flow in the restricted space below the massive sulfide lenses and between the mafic sills. Temperatures calculated for mica in the pervasive white mica alteration zones at the ABM deposit (248.9±14.9 °C) are in a similar range as those reported for the fuchsite alteration zone at Hellyer (~250 °C; Gemmell and Fulton, 2001). Proximal to the mineralization, temperatures calculated from chlorite compositions in pervasively chlorite altered zones, both mineralized and barren, are ~315±30 °C, which are typical for chlorite alteration in VMS deposits globally (Kranidiotis and MacLean, 1987; Mercier-Langevin et al., 2014). Textural relationships show that pervasive chlorite alteration overprints pervasive white mica alteration (Fig. 3.5F), and that sulfide mineralization overprints all types of pervasive alteration (Fig. 3.8), although locally massive sulfide mineralization is interpreted to be contemporaneous with the pervasive chlorite alteration. Additionally, in the pervasive chlorite alteration associated with the massive sulfide lenses, one of the earliest occurring ore minerals is magnetite, which commonly occurs spatially associated with chalcopyrite and pyrrhotite, indicative of formation from >350 °C high temperature fluids (Franklin et al., 2005; Hannington et al., 2005), which is consistent with the formation temperature calculated for chlorite above. These relationships between alteration and ore mineral assemblages suggest a steady rise in temperatures of the hydrothermal fluids culminating in the precipitation of massive sulfide mineralization in Sequence 2.

The occurrence of pervasive white mica and moderate white mica ± chlorite assemblages in Sequence 3 in the hanging wall of the massive sulfide lenses (Fig. 3.3, 3.4) indicates that the hydrothermal system remained active after the main mineralization phase ended in Sequence 2. These hanging wall alteration zones likely formed during the shorter breaks in volcanic activity recorded by lesser argillite lenses present throughout Sequence 3 (Denisová and Piercey, 2022) and are not associated with significant mineralization (Fig. 3.3, 3.4). The lack of overprinting of the mineralization by further pervasive hydrothermal alteration suggests that the hydrothermal fluids responsible for the alteration assemblages in the hanging wall exploited a different part of the synvolcanic fault/conduit network. These pathways were still relatively proximal to the mineralized part of the hydrothermal system due to the occurrence of the pervasive white mica assemblage in the hanging wall but their more limited extent down dip (Fig. 3.3) suggests that their source could have occurred to the south of the current outcrop of the massive sulfide mineralization at the bedrock surface. Further, alteration intensity of the white mica ± chlorite assemblage in Sequence 3 varies from moderate to weak with increasing distance from the mineralization, suggesting a decrease in intensity of hydrothermal fluid flow distal from the upflow zones.

The hanging wall in Sequence 3 also contains the greatest abundance of K-deficient illite/smectite (group 3) in the deposit. Within Sequence 3, the group 1 and group 2 illites in the pervasive and moderate assemblages are overgrown by minor K-deficient illite/smectite (group 3). These group 3 illite/smectite grains also overprint the Sequence 2 mineralized and pervasively chlorite altered zones, implying that they are very late in the evolution of the ABM hydrothermal system. The group 3 illite/smectite has average calculated formation temperatures of 110.4±14.6 °C (n=4 from 2 samples) implying a further cooling of the hydrothermal system as it evolved.

These assemblages are also cross-cut by widespread Mg-rich siderite (vs diagenetic dolomite), which occurs as coatings and overprints on other alteration phases throughout the upper Kudz Ze Kayah formation and up into the Wind Lake formation. This late Fe-carbonate mineral overprint is interpreted to reflect a very late, low temperature phase of the hydrothermal system, likely formed through low temperature diffuse circulation, similar to the Wolverine deposit (Bradshaw et al., 2008).

The complexity of the observed overprinting of alteration and mineralization assemblages in the ABM deposit and the upper Kudz Ze Kayah formation demonstrates the deposit formed via an evolving hydrothermal system that comprised multiple pulses of fluids. This is not unique to the ABM deposit as similar style alteration assemblages and mineralization have been discovered at the base of the Kudz Ze Kayah formation in the GP4F deposit (Boulton, 2002), the R15 deposit (MacRobbie and Holroyd, unpub. data), and several anomalous showings across the stratigraphy (van Olden et al., 2020). This suggests that hydrothermal activity was ongoing throughout the deposition of the Kudz Ze Kayah formation and that conditions favourable for the precipitation of sulfide mineralization were not limited to a single horizon within the Kudz Ze Kayah formation, implying that there is potential for mineralization in other portions of the stratigraphy.

3.8.2 VMS mineralization vectoring

The hydrothermal alteration footprint of VMS mineralization is relatively small on the scale of a VMS district (100s-low 1000s of meters; Sangster, 1980). Therefore, successful exploration for VMS deposits requires the use of complimentary geological, geochemical, and mineralogical vectors to track the footprint of hydrothermal processes involved in formation of massive sulfide mineralization (Hannington et al., 2003; Gibson et al., 2007). Further, hydrothermal alteration in replacement-style VMS deposits is complex, in large part due to the more widespread infiltration of the hydrothermal fluids into host rocks in the subseafloor environment (Gibson et al., 1999; Doyle and Allen, 2003). In the following section, we will describe geochemical and mineralogical vectors within the ABM deposit from distal to proximal to the mineralization and link them to the VMS-related hydrothermal processes, utilizing whole rock mobile major and trace mobile elements, and mineral chemistry, to determine alteration intensity variations with proximity to massive sulfide mineralization.

The most widespread hydrothermal alteration assemblages at the ABM deposit are the weak to moderate intensity hydrothermal alteration zones in the upper Kudz Ze Kayah formation that envelop the ABM and Krakatoa mineralized zones and several prospective base metal anomalies. The combination of alteration and overprinting sulfide mineralization result in distinctive chemical and mineral-chemical changes. As with most VMS deposits, feldspar destruction and subsequent formation of phyllosilicate minerals (white mica ± chlorite) resulted in very low absolute abundances and mass losses of Na_2O (Fig. 3.11A), and high Spitz-Darling index values (Fig. 3.9D; Spitz and Darling, 1978; MacLean and Barrett, 1993; Barrett and MacLean, 1994a) across the ABM deposit footprint. The lateral continuity of the zones affected by weak to moderate intensity alteration can be tracked through the mineral chemistry of the phyllosilicate minerals. Similar conditions (pH, redox, temperature) within these zones produced illite with homogenous compositions that can be monitored using mineral chemistry or the 2200W feature (Fig. 3.4, 3.12A, C).

Barium is also a district- to deposit- scale vector towards massive sulfide mineralization. Denisová and Piercey (2022) noted that Ba>3,500 ppm is indicative of pervasive white mica alteration assemblages proximal to mineralization and extending into the hanging wall and was useful in mapping the likely lateral flow in the deposit (Fig. 3.4). White mica in these Ba-rich zones also exhibits minor but elevated Ba content including in the hanging wall of the mineralization. Given that these Ba-rich micas are contemporaneous to slightly after sulfide formation (Fig. 3.7) it is possible they received Ba via dissolution of barite during the precipitation of early high temperature sulfide mineralization (e.g., Magnall et al., 2020). Equally viable, however, is that they could be related to upwelling Ba-rich hydrothermal fluids that have been recognized in other VMS districts (e.g., Lentz et al., 1997). The Ba-bearing micas are restricted to the ABM deposit and have limited extent within the deposit footprint (e.g., 10s to 100s of meters), unlike other VMS districts (Hannington et al., 2003), but using absolute Ba values can be used for district scale vectoring.

Although Ba and Na_2O variations are useful for both regional and deposit-scale vectoring, other elements are more spatially sensitive and enriched closer to the mineralization. In areas proximal to the massive sulfide mineralization (<200 m), zones of pervasive white mica alteration assemblages with extensive formation of white mica translate to mass gains of K_2O (Fig. 3.11B) and elevated Ishikawa alteration index values (Fig. 3.9C). Increasing absolute values and mass gains of K_2O reflect progressively more pervasive white mica alteration and can be used to vector towards zones of highest intensity alteration. In most VMS environments, high Ba/Sr and Rb/Sr indices are also useful vectors for white mica alteration and Ba-enrichment (Large et al., 2001a; McNulty et al., 2020), because they monitor both feldspar destruction and phyllosilicate formation in a similar way to K_2O-Na_2O-CaO systematics. Strontium substitutes for Ca, and Ba or Rb substitute for K in various primary and alteration phases (Large et al., 2001a). At the ABM deposit Ba increases with proximity to mineralization (Denisová and Piercey, 2022) but it is not accompanied by coincident low Sr values, due to the presence of overprinting carbonate alteration, which leads to Sr enrichment and mixed Ba/Sr values throughout the deposit. In contrast, the Ba/Na_2O value tracks similar processes as the Ba/Sr value and correlates well with AI, Al_2O_3/Na_2O, and other monitors of hydrothermal alteration discussed below, and can be used on a district scale (km-scale) to delineate VMS-prospective rocks.

Proximal to the mineralization (<200 m), elevated values of base and trace metals occur in the host rocks. Mass balance calculations show mass gains of Zn, Pb, Cu, and Ba with proximity to the mineralization (Fig. 3.11 D-F). Additionally, elements commonly enriched in sulfide minerals, such as Tl, Sb, As, Ag, Cd, Mo, Bi, and Se, have anomalous values in altered felsic rocks and increase in concentration with proximity to the mineralized lenses (Fig. 3.10), whereas Co and Ni decrease. The altered rocks commonly contain disseminated sulfide minerals, and it is likely they carry some of these trace metals proximal to the massive sulfide mineralization. Soltani Dehnavi et al. (2018) have also shown that semi-volatile metals like Tl, Sb, Sn, Hg, and In, can exhibit lithophile behaviour and be hosted in phyllosilicates like mica and chlorite. Whole rock data for felsic rocks shows correlation between Rb (substituting for K) and Tl, Sn, In, and Sb (Fig. 3.14), suggesting that at least distal from the mineralization in Sequence 1 and 3 in moderately altered felsic rocks these semi-volatile metals likely occur in micas, which extends the trace element halo further away from the massive sulfide mineralization. This is further supported by comparing the results from different digestion methods (HF-HCl-$HClO_4$ digest vs aqua regia digest) used for geochemical analysis of the felsic samples (Fig. 3.15). The aqua regia digestion dissolves sulfide minerals and other weakly resistant minerals, whereas the HF-HCl-$HClO_4$ solution digests the majority of silicate minerals present in the sample. In the case of semi-volatile metals (Tl and Sb), if values from the different digests match, the metals likely occur in sulfide minerals. If the results are higher for the HF-HCl-$HClO_4$ digest, it is likely that the metals are occurring in silicate minerals, most likely phyllosilicates, like white mica or chlorite. The results demonstrate that Tl is likely hosted by silicate minerals, as the analyses of felsic samples skew towards higher abundances in the HF-HCl-$HClO_4$ digest (Fig. 3.15). Based on this, Tl, either as absolute values or in a ratio with Co (Genna and Gaboury, 2019), can be used to map white mica alteration and its intensity in felsic lithofacies of the upper Kudz Ze Kayah formation (Fig. 3.9, 3.10, 3.15).

The most proximal alteration in the ABM deposit is the pervasive chlorite alteration that is closely associated with massive sulfide mineralization (<50 m) and is characterized by high values of the chlorite-carbonate-pyrite and Ishikawa alteration indices (Fig. 3.9C) and by mass gains of MgO and FeO and mass losses of K_2O and SiO_2 (Fig. 3.11B, C). Such features are typical for chlorite formation at the expense of feldspar and white mica (Barrett and MacLean, 1994b; Schardt et al., 2001). In contrast to zones of strong to pervasive white mica alteration, zones of pervasive chlorite alteration at the ABM deposit show Ba values below the 3,500 ppm threshold. This likely indicates that the hydrothermal fluids associated with zones of pervasive chlorite alteration were reduced, acidic and high temperature (~320 °C) and dissolved any barite present and/or remobilized any Ba present into feldspars and micas (±carbonates; Fig. 3.16; Cooke et al., 2000). Chlorite in mineralized or mineralization-proximal pervasive alteration zones is more Mg-rich than chlorite from distal moderately white mica ± chlorite altered zones (Fig 3.12C). In these

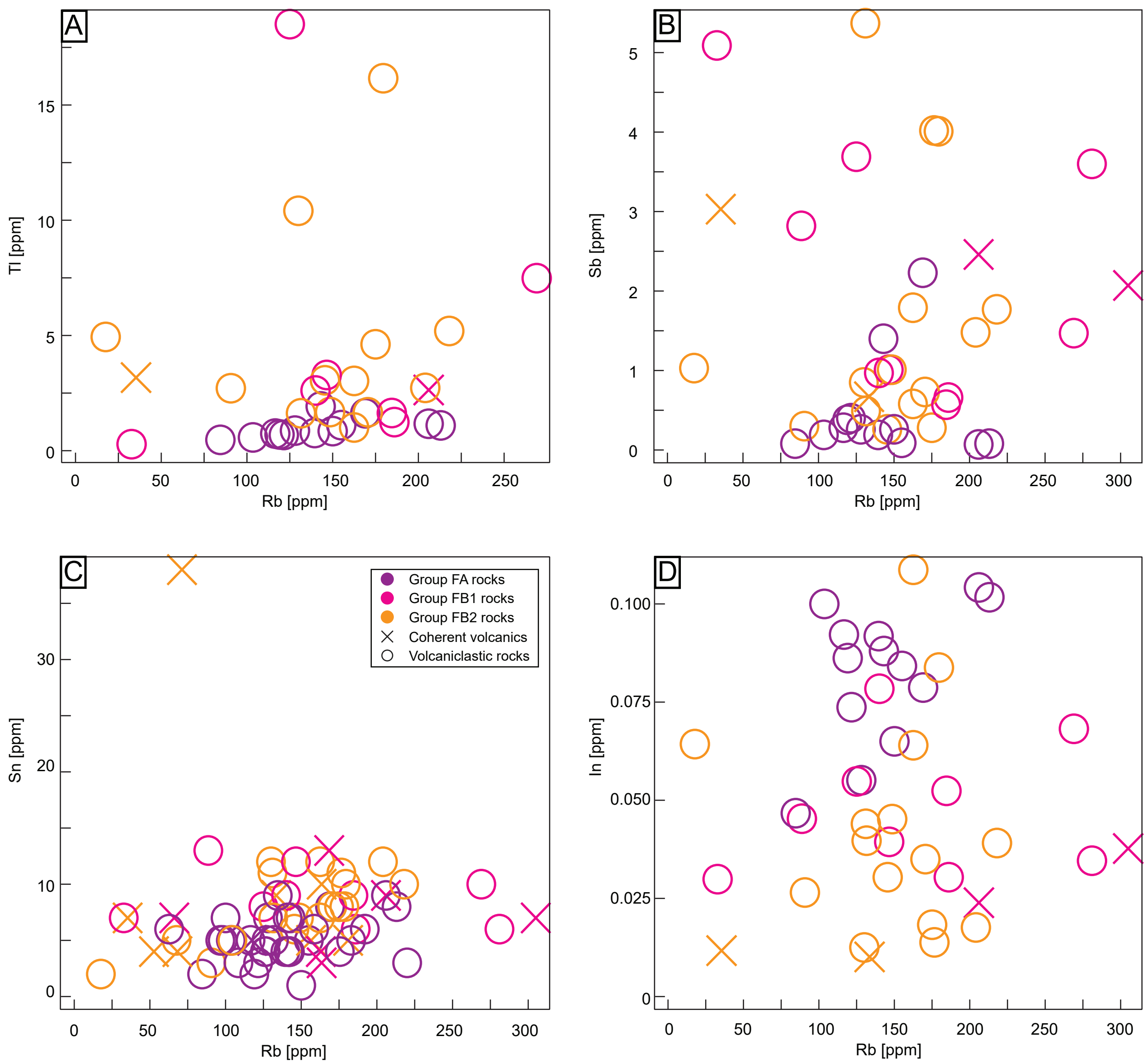

Figure 3.14. Plots of Rb versus trace elements in felsic rocks, Rb stands in for K_2O, samples digested using HF-HCl-$HClO_4$. (A) Rb vs Tl. (B) Rb vs Sb. (C) Rb vs Sn. (D) Rb vs In.

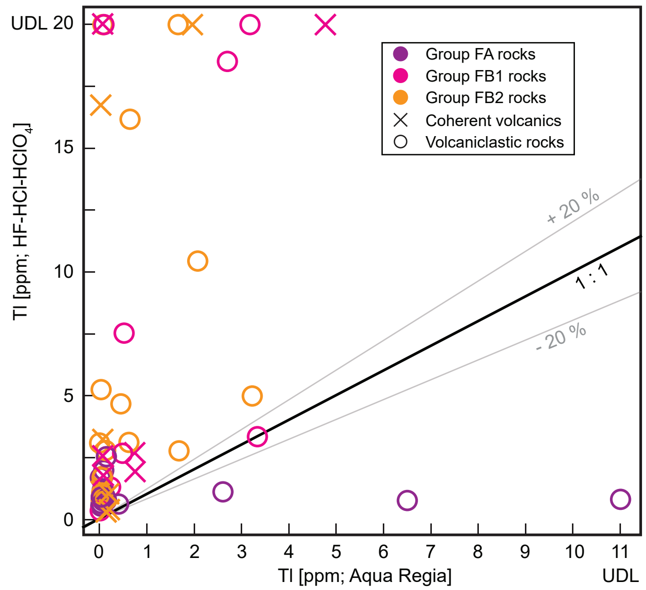

Figure 3.15. Comparison of trace element results in felsic rocks using the aqua regia and HF-HCl-$HClO_4$ digests in sample analysis. The HF-HCl-$HClO_4$ digests the majority of minerals, whereas aqua regia leaches loosely bound elements and digests sulfide minerals, Fe- and Mn-oxide minerals, sulfate minerals, carbonate minerals, and some silicate minerals. Comparison of digestions for Tl, Tl likely more prevalent in silicates. Detection range of Tl in aqua regia is between 0.0006-11 ppm, in HF-HCl-$HClO_4$ it is between 0.002-20 ppm.

proximal Mg-chlorite-rich zones, the illite composition behaves similarly, and illite is enriched in Mg proximal to mineralization (Fig. 3.12A), which has been observed in some VMS districts (e.g., Skellefte district; Hannington et al., 2003a; Chmielowski et al., 2016). This Mg-enrichment has been interpreted to be due to abundant entrained Mg-rich seawater mixing with the hydrothermal fluids, whereas the sulfide minerals precipitated later without significant input of seawater and Mg-enrichment (Hannington et al., 2003; Chmielowski et al., 2016). Another possible explanation is that early in the evolution of the hydrothermal system, Fe from the hydrothermal fluids was consumed by precipitation of Fe-rich sulfide minerals or magnetite, whereas the consequently more Mg-rich fluid precipitated the more Mg-rich phyllosilicate minerals (Richards et al., 1989; Saccocia and Seyfried, 1994), or that changes in sulfur and oxygen fugacity resulted in the formation of Mg-rich chlorite (Bryndzia and Scott, 1987). Given the strong association of Mg-rich chlorite with proximity to mineralization, the latter explanations are more plausible for Mg-rich chlorite formation.

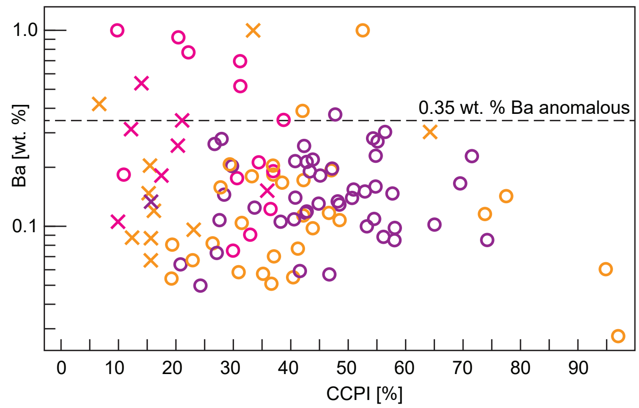

Figure 3.16. Plot of CCPI vs Ba in felsic rocks, the threshold for anomalous Ba values (0.35 wt. %) marked in plot.

At the ABM deposit gradients in lithogeochemical and mineral-chemical data are observed on a deposit scale (<2 km), including those reflecting feldspar destruction (e.g., Na_2O, mass changes of Na_2O, K_2O, Spitz-Darling index) and enrichments in elements hosted by alteration minerals and sulfides (e.g., Ba, base metals, gradients in Fe-Mg contents of phyllosilicates). To delineate and vector towards zones proximal to mineralization, tracking of coincident geochemical indicators (AI>80, CCPI>65, Ba/Na_2O>1), changes in mass balance of major elements (mass gains of K_2O, MgO, FeO, Ba, mass losses of Na_2O) and base metals (mass gains of Zn, Cu, Pb), mineral chemistry of phyllosilicates (Mg-rich compositions, enrichments in Ba and/or trace metals proximal to VMS), increase in base (Zn, Cu, Pb) and trace metal (Sb, Tl, Mn, In, Sn, Mo) values, and SWIR features typical for certain phyllosilicate compositions (specific illite composition in white mica-bearing alteration assemblages) should accompany detailed field mapping of alteration and alteration intensity (Fig. 3.17).

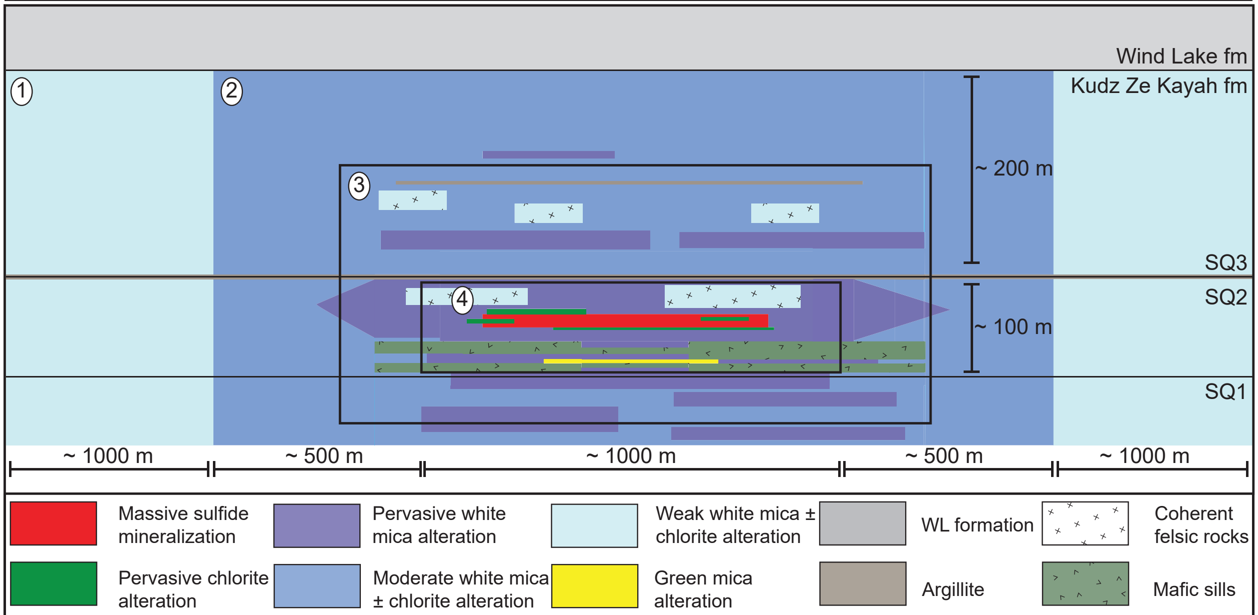

	Distal weak (1)	Distal moderate (2)	Proximal (3)	Proximal MS (4)
Spitz-Darling	> 5	> 10	> 20	> 20
AI	n/a	> 65 %	> 80 %	> 80 %
CCPI	n/a	n/a	n/a	> 65 %
Mass balance	Δ Na_2O << 0, Δ K_2O > 0	Δ K_2O >> 0, Δ Na_2O << 0	Δ K_2O >> 0, Δ Na_2O << 0	Δ K_2O, Δ MgO, Δ FeO >> 0
Ba/Na_2O	n/a	> 0.5	>1	n/a
Ba [wt %]	~ 0.15 %	~ 0.15 %	> 0.35 %	> 0.35 %
Rb [ppm]	n/a	> 100	> 150	> 150
Fe# mica	> 0.3	> 0.3	< 0.3	< 0.3
Fe# chlorite	n/a	> 0.5	> 0.5	< 0.5
Base metals	n/a	Cu < 30 ppm, Pb < 20 ppm, Zn < 100 ppm	Cu >30 ppm, Pb > 70 ppm, Zn > 200 ppm	n/a
Tl [ppm]	n/a	>1	>1	>>1
Sb [ppm]	n/a	>1	>1	>>1
Mn [ppm]	n/a	> 0.075	< 0.075	n/a
In [ppm]	n/a	> 0.06	< 0.06	n/a
2200W [nm]	< 2208	< 2208	> 2216	< 2208 & > 2216

Figure 3.17. Simplified stratigraphy of the upper Kudz Ze Kayah formation showing schematic distribution of the hydrothermal alteration assemblages at the ABM massive sulfide deposit. Approximate values of key alteration indices and minor and trace elements characteristic for the main hydrothermal alteration assemblages are shown in the table below the legend. MS = Massive sulfide mineralization, n/a = not applicable.

3.9 Conclusions

At least two major alteration episodes are recorded in the host rocks of the ABM deposit. Early diagenesis-related alteration is preserved locally in Sequence 2, whereas extensive hydrothermal alteration affected most of the rocks in the ABM deposit footprint with the distribution of alteration zones being controlled by the porosity and permeability contrasts between coherent and volcaniclastic/sedimentary units. Within the core of the hydrothermal alteration at the ABM deposit, there are zones of pervasive alteration that envelop lenses of massive sulfide mineralization, with lower temperature assemblages (pervasive white mica or moderate white mica ± chlorite alteration) overprinted by higher temperature assemblages (pervasive chlorite alteration). The hydrothermal system that formed the ABM deposit was at its peak during the volcanic hiatus between the deposition of Sequence 2 and Sequence 3; this hiatus was also when mineralization and pervasive alteration in Sequence 2 were formed. The hydrothermal system continued post-VMS formation and involved pervasive white mica and moderate to weak white mica ± chlorite alteration extending up to 300 m into the hanging wall of the massive sulfide mineralization implying that the hydrothermal system was active during the deposition of the volcanic rocks of Sequence 3.

The most extensive zones of hydrothermal alteration at the ABM deposit extend laterally up to 1000 m along strike from mineralization and are concentrated along originally porous and permeable units within the volcanosedimentary package. Quantifying feldspar destruction identifies these broad zones of weak to moderate alteration. Precipitation of minor disseminated sulfides within zones of moderate and pervasive alteration also resulted in enrichment in base and trace metals (Zn, Cu, Pb, Ag, Au, Mo, Sb, Tl, As, Hg) in proximity to massive sulfide mineralization (<200 m). The composition of phyllosilicate minerals characteristic for the moderate and pervasive alteration assemblages is dependant on the temperature at which they formed, and they are more Mg-rich and K-rich proximal to massive sulfide mineralization where the hydrothermal fluids had the highest temperatures. They can also be enriched in minor and trace metals (Ba, Rb, Tl, Sb). Mineral chemistry and SWIR spectroscopy can both be used to identify compositional vectors from the distal parts of the alteration footprint towards massive sulfide mineralization and to track the lateral continuity of the zones affected by different hydrothermal alteration assemblages. Notably, there are complex overprinting alteration mineral relationships reflecting the evolution of the dynamic hydrothermal system at the ABM deposit, demonstrating that SWIR spectral signals are challenging to interpret in such dynamic systems and sound interpretation of such data requires good control on alteration mineral paragenesis and relationships to mineralization.

3.10 Acknowledgments

We thank BMC Minerals Ltd. for their generous financial, field, and logistical support. Support for the project was provided by a NSERC Discovery Grant, a NSERC Collaborative Research Development Grant (CRDPJ), and funding from BMC Minerals Ltd. (Piercey), and a Student Research Grant from the Society of Economic Geologists Canada Foundation, and by financial assistance from Memorial University of Newfoundland (Denisová). We thank Wanda Aylward for her assistance with analytical work. We thank Stefanie Brueckner, Nils Jansson, and Associate Editor Jonathan Cloutier for their thorough reviews of the manuscript, which greatly improved the manuscript. The corresponding author would like to thank Matthew Manor and Rosie Cobbett for constructive comments on an earlier draft of the manuscript, Neil Martin and Robin Black from BMC Minerals, Dillon Hume from Equity Exploration, and Robert Burke for helpful comments and conversations beneficial to this paper. We thank BMC Minerals and Equity Exploration staff at the Kudz Ze Kayah exploration camp for their help during the 2018 and 2019 field seasons.

3.11 References

Aja, S. U., 2020, On the thermodynamic stability of illite and I-S minerals: Clays and Clay Minerals, v. 67, p. 518–536.

Anderson, M. O., Hannington, M. D., McConachy, T. F., Jamieson, J. W., Anders, M., Wienkenjohann, H., Strauss, H., Hansteen, T., and Petersen, S., 2019, Mineralization and alteration of a modern seafloor massive sulfide deposit hosted in mafic volcaniclastic rocks: Economic Geology, v. 114, p. 857–896.

Arghe, F., Skelton, A., and Pitcairn, I., 2011, Spatial coupling between spilitization and carbonation of basaltic sills in SW Scottish Highlands: evidence of a mineralogical control of metamorphic fluid flow: Geofluids, v. 11, p. 245–259.

Barrett, T. J., and MacLean, W. H., 1994a, Chemostratigraphy and hydrothermal alteration in exploration for VHMS deposits in greenstones and younger volcanic rocks, in Lentz, D. R. ed., Alteration and Alteration Processes Associated with Ore-Forming Systems: Geological Association of Canada, Short Course Notes, v. 11, p. 433–467.

Barrett, T. J., and MacLean, W. H., 1994b, Mass changes in hydrothermal alteration zones associated with VMS deposits of the Noranda area: Exploration and Mining Geology, v. 3, p. 131–160.

Barrett, T. J., Cattalani, S., and MacLean, W. H., 1993, Volcanic lithogeochemistry and alteration at the Delbridge massive sulfide deposit, Noranda, Quebec: Journal of Geochemical Exploration, v. 48, p. 135–173.

Barrett, T. J., Dawson, G. L., and MacLean, W. H., 2008, Volcanic stratigraphy, alteration, and sea-floor setting of the Paleozoic Feitais massive sulfide deposit, Aljustrel, Portugal: Economic Geology, v. 103, p. 215–239.

Battaglia, S., 2004, Variations in the chemical composition of illite from five geothermal fields: a possible geothermometer: Clay Minerals, v. 39, p. 501–510.

Boulton, A., 2002, GP4F polymetallic volcanic-hosted massive sulphide (VHMS) deposit, Finlayson Lake District, Yukon Territory: B.Sc. thesis (Honors), Victoria, Canada, University of Victoria, 47 p.

Bradshaw, G. D., Peter, J. M., Paradis, S., and Rowins, S., 2001, Geological characteristics of the Wolverine volcanic-hosted massive sulphide deposit, Finlayson Lake district, Yukon Territory, Canada (D. S. Emond & L. H. Weston, Eds.): Yukon Exploration and Geology, p. 269–288.

Bradshaw, G. D., Rowins, S. M., Peter, J. M., and Taylor, B. E., 2008, Genesis of the Wolverine volcanic sediment-hosted massive sulfide deposit, Finlayson Lake district, Yukon, Canada: Mineralogical, mineral chemical, fluid inclusion, and sulfur isotope evidence: Economic Geology, v. 103, p. 35–60.

Brueckner, S. M., Johnson, G., Wafforn, S., Gibson, H. L., Sherlock, R., Anstey, C., and Mcnaughton, K., 2021, Potential for volcanogenic massive sulfide mineralization at the A6 Anomaly, north-west British Columbia, Canada: Stratigraphy, lithogeochemistry, and alteration mineralogy and chemistry: Minerals, v. 11, 50 p.

Burnham, O. M., 2008, Trace element analysis of geological samples by inductively coupled plasma mass spectrometry (ICP - MS) at the Geoscience Laboratories: Revised capabilities due to method improvements: Summary of Field Work and Other Activities. Ontario Geological Survey, Open File Report, v. 6226, p. 1–10.

Burnham, O. M., and Schweyer, J., 2004, Trace element analysis of geological samples by inductively coupled plasma mass spectrometry at the Geoscience Laboratories: Revised capabilities due to improvements to instrumentation: Summary of Field Work and Other Activities 2004, Ontario Geological Survey. Open File Report, v. 6145, p. 1–20.

Buschette, M. J., and Piercey, S. J., 2016, Hydrothermal alteration and lithogeochemistry of the Boundary volcanogenic massive sulphide deposit, central Newfoundland, Canada: Canadian Journal of Earth Sciences, v. 53, p. 506–527.

Bryndzia, L. T., Scott, S. D., 1987, The composition of chlorite as a function of sulfur and oxygen fugacity: An experimental study: American journal of Science, v. 287, p. 50–76.

Cathelineau, M., 1988, Cation site occupancy in chlorites and illites as a function of temperature: Clay Minerals, v. 23, p. 471–485.

Chmielowski, R. M., Jansson, N. F., Persson, M. F., and Fagerström, P., 2016, 3D modelling of hydrothermal alteration associated with VHMS deposits in the Kristineberg area, Skellefte district, northern Sweden: Mineralium Deposita, v. 51, p. 113–130.

Cloutier, J., and Piercey, S. J., 2020, Tracing mineralogy and alteration intensity using the spectral alteration index and depth ratios at the Northwest Zone of the Lemarchant volcanogenic massive sulfide deposit, Newfoundland, Canada: Economic Geology, v. 115, p. 1055–1078.

Cloutier, J., Piercey, S. J., and Huntington, J., 2021, Mineralogy, mineral chemistry and SWIR spectral reflectance of chlorite and white mica: Minerals, v. 11, 16 p.

Colpron, M., Nelson, J. L., and Murphy, D. C., 2006, A tectonostratigraphic framework for the pericratonic terranes of the northern Canadian Cordillera, in Colpron, M. and Nelson, J. L. eds., Paleozoic Evolution and Metallogeny of Pericratonic Terranes at the Ancient Pacific Margin of North America, Canadian and Alaskan Cordillera: Geological Association of Canada, Special Paper 45, p. 1–23.

Cooke, D. R., Bull, S. W., Large, R. R., and McGoldrick, P. J.. 2000, The importance of oxidized brines for the formation of Australian Proterozoic stratiform sediment-hosted Pb-Zn (Sedex) deposits: Economic Geology, v. 95, p. 1–18.

Date, J., Watanabe, Y., and Saeki, Y., 1983, Zonal alteration around the Fukazawa Kuroko deposits, Akita prefecture, northern Japan: Economic Geology Monograph 5, p. 365–386.

Davies, J. F., and Whitehead, R. E., 2006, Alkali-alumina and MgO-alumina molar ratios of altered and unaltered rhyolites: Exploration and Mining Geology, v. 15, p. 75–88.

Deer, W. A., Howie, R. A., and Zussman, J., 2013, An Introduction to the Rock-Forming Minerals Third Edition: Mineralogical Society of Great Britain and Ireland, London, UK, 498 p.

Denisová, N., and Piercey, S. J., 2022, Lithostratigraphy, lithogeochemistry and tectono-magmatic framework of the ABM replacement-style volcanogenic massive sulfide (VMS) deposit, Finlayson Lake District, Yukon, Canada: Economic Geology, v. 117, p. 1299–1326.

Doyle, M. G., and Allen, R. L., 2003, Subsea-floor replacement in volcanic-hosted massive sulfide deposits: Ore Geology Reviews, v. 23, p. 183–222.

Doyle, M. G., and Huston, D. L., 1999, The subsea-floor replacement origin of the Ordovician Highway-Reward volcanic-associated massive sulfide deposit, Mount Windsor subprovince, Australia: Economic Geology, v. 94, p. 825–844.

Franklin, J. M., Lydon, J. W., and Sangster, D. F., 1981, Volcanic-associated massive sulfide deposits, Economic Geology 75th Anniversary Volume, p. 485–627.

Franklin, J. M., Gibson, H. L., Jonasson, I. R., and Galley, A. G., 2005, Volcanogenic massive sulfide deposits, Economic Geology 100th Anniversary Volume, p. 523–560.

Gabrielse, H., Murphy, D. C., and Mortensen, J. K., 2006, Cretaceous and Cenozoic dextral orogen-parallel displacements, magmatism, and paleogeography, north-central Canadian Cordillera, in

Haggart, J. W., Enkin, R. J., and Monger, J. W. H. eds., Paleogeography of the North American Cordillera: Evidence For and Against Large-Scale Displacements: Geological Association of Canada Special Paper, v. 46, p. 255–276.

Gemmell, J. B., and Fulton, R., 2001, Geology, genesis, and exploration implications of the footwall and hanging-wall alteration associated with the Hellyer volcanic-hosted massive sulfide deposit, Tasmania, Australia: Economic Geology, v. 96, p. 1003–1035.

Gemmell, J. B., and Large, R. R., 1992, Stringer system and alteration zones underlying the Hellyer volcanic-hosted massive sulfide deposit, Tasmania, Australia: Economic Geology, v. 87, p. 620–649.

Genna, D., and Gaboury, D., 2015, Deciphering the hydrothermal evolution of a VMS system by LA-ICP-MS using trace elements in pyrite: An example from the Bracemac-McLeod deposits, Abitibi, Canada, and implications for exploration: Economic Geology, v. 110, p. 2087–2108.

Genna, D., and Gaboury, D., 2019, Use of semi-volatile metals as a new vectoring tool for VMS exploration : Example from the Zn-rich McLeod deposit, Abitibi, Canada Bracemac: Journal of Geochemical Exploration, v. 207, 106358.

Genna, D., Gaboury, D., and Roy, G., 2014, The Key Tuffite, Matagami Camp, Abitibi Greenstone Belt, Canada: petrogenesis and implications for VMS formation and exploration: Mineralium Deposita, v. 49, p. 489–512.

Gibson, H. L., Morton, R. L., and Hudak, G. J., 1999, Submarine volcanic processes, deposits, and environments favourable for the location of volcanic-associated massive sulfide deposits: Reviews in Economic Geology, v. 8, p. 15–51.

Gibson, H. L., Allen, R. L., Riverin, G., and Lane, T. E., 2007, The VMS model : Advances and application to exploration targeting: Fifth Decennial International Conference on Mineral Exploration - Ore Deposits and Exploration Technology, Toronto, Canada, p. 713–730.

Gifkins, C. C., and Allen, R. L., 2001, Textural and chemical characteristics of diagenetic and hydrothermal alteration in glassy volcanic rocks: Examples from the Mount Read volcanics, Tasmania: Economic Geology, v. 96, p. 973–1002.

Hannington, M. D., Kjarsgaard, I. M., Galley, A. G., and Taylor, B., 2003, Mineral-chemical studies of metamorphosed hydrothermal alteration in the Kristineberg volcanogenic massive sulfide district, Sweden: Mineralium Deposita, v. 38, p. 423–442.

Hannington, M. D., De Ronde, C. E. J., and Petersen, S., 2005, Sea-floor tectonics and submarine hydrothermal systems: Economic Geology 100th Anniversary Volume, p. 111–141.

Herrmann, W., Blake, M., Doyle, M. G., Huston, D. L., Kamprad, J., Merry, N., and Pontual, S., 2001, Short wavelength infrared (SWIR) spectral analysis of hydrothermal alteration zones associated with base metal sulfide deposits at Rosebery and Western Tharsis, Tasmania, and Highway-Reward, Queensland: Economic Geology, v. 96, p. 939–955.

Holk, G. J., Taylor, B. E., and Galley, A. G., 2008, Oxygen isotope mapping of the Archean Sturgeon Lake caldera complex and VMS-related hydrothermal system, Northwestern Ontario, Canada: Mineralium Deposita, v. 43, p. 623–640.

Iijima, A., 1974, Clay and zeolite alteration zones surrounding Kuroko deposits in the Hokuroku district, Northern Akita, as submarine hydrothermal-diagenetic alteration products, in Ishihara, S. ed., Geology of Kuroko Deposits Mining Geology Special Issue, No. 6, p. 267–289.

Jones, S., Herrmann, W., and Gemmell, J. B., 2005, Short wavelength infrared spectral characteristics of the HW horizon: Implications for exploration in the Myra Falls volcanic-hosted massive sulfide camp, Vancouver Island, British Columbia, Canada: Economic Geology, v. 100, p. 273–294.

Knuckey, M. J., Comba, C. D. A., and Riverin, G., 1983, Structure, metal zoning and alteration at the Millenbach deposit, Noranda, Quebec: Geological Association of Canada Special Paper, v. 25, p. 255–295.

Kranidiotis, P., and MacLean, W. H., 1987, Systematics of chlorite alteration at the Phelps Dodge massive sulfide deposit, Matagami, Quebec: Economic Geology, v. 82, p. 1898–1911.

Lafrance, B., Gibson, H. L., and Stewart, M. S., 2020, Internal and external deformation and modification of volcanogenic massive sulfide deposits: Reviews in Economic Geology v. 21, v.

21, p. 147–171.

Large, R. R., Allen, R. L., Blake, M. D., and Herrmann, W., 2001a, Hydrothermal alteration and volatile element halos for the Rosebery K lens volcanic-hosted massive sulfide deposit, western Tasmania: Economic Geology, v. 96, p. 1055–1072.

Large, R. R., Gemmell, J. B., Paulick, H., and Huston, D. L., 2001b, The alternation box plot: A simple approach to understanding the relationship between alteration mineralogy and lithogeochemistry associated with volcanic-hosted massive sulfide deposits: Economic Geology, v. 96, p. 957–971.

Large, R. R., McPhie, J., Gemmell, J. B., Herrmann, W., and Davidson, G. J., 2001c, The spectrum of ore deposit types, volcanic environments, alteration halos, and related exploration vectors in submarine volcanic successions: Some examples from Australia: Economic Geology, v. 96, p. 913–938.

Lentz, D. R., Hall, D. C., and Hoy, L. D., 1997, Chemostratigraphic, alteration, and oxygen isotopic trends in a profile through the stratigraphic sequence hosting the Heath Steele B zone massive sulfide deposit, New Brunswick: Canadian Mineralogist, v. 35, p. 841–874.

MacLean, W. H., 1988, Rare earth element mobility at constant inter-REE ratios in the alteration zone at the Phelps Dodge massive sulphide deposit, Matagami, Quebec: Mineralium Deposita, v. 23, p. 231–238.

MacLean, W. H., 1990, Mass change calcualtions in altered rock series: Mineralium Deposita, v. 25, p. 44–49.

MacLean, W. H., and Barrett, T. J., 1993, Lithogeochemical techniques using immobile elements: Journal of Geochemical Exploration, v. 48, p. 109–133.

Magnall, J. M., Gleeson, S. A., Creaser, R. A., Paradis, S., Glodny, J., and Kyle, J. R., 2020, The mineralogical evolution of the clastic dominant-type Zn-Pb ± Ba deposits at Macmillan Pass (Yukon, Canada) - Tracing subseafloor barite replacement in the layered mineralization: Economic Geology, v. 115, p. 961–979.

Manor, M. J., and Piercey, S. J., 2018, Re-evaluating the chronostratigraphic framework for felsic volcanic and intrusive rocks of the Finlayson Lake region, Yukon-Tanana terrane, Yukon, in MacFarlane, K. E. ed., Yukon Exploration and Geology 2017: Yukon Geological Survey, p. 111–127.

Manor, M. J., and Piercey, S. J., 2019, Geochemistry of Devono–Mississippian volcanic and intrusive rocks of the Finlayson Lake district, Yukon-Tanana Terrane, Yukon (MacFarlane, K. E. Ed.): Yukon Exploration and Geology, p. 91–110.

Manor, M. J., Piercey, S. J., Murphy, D. C., and Wall, C. J., 2022a, High-precision CA-ID-TIMS U-Pb zircon geochronology, chemostratigraphy, and tectono-magmatic framework of the Finlayson Lake volcanogenic massive sulfide district, Yukon-Tanana terrane, Yukon: Geosphere.

Manor, M. J., Piercey, S. J., Wall, C. J., and Denisová, N., 2022b, High precision CA-ID-TIMS U-Pb zircon geochronology of felsic rocks in the Finlayson Lake VMS district, Yukon: Linking Paleozoic basin-scale accumulation rates to the occurrence of subseafloor replacement-style mineralization: Economic Geology, v. 117, p. 1173–1201.

Mathieu, L., 2018, Quantifying hydrothermal alteration: A review of methods: Geosciences, v. 8, 27 p.

McNulty, B. A., Fox, N., and Bruce Gemmell, J., 2020, Assessing hydrothermal alteration intensity in volcanic-hosted massive sulfide systems using portable X-ray fluorescence analysis of drill core: An example from Myra Falls, Canada: Economic Geology, v. 115, p. 443–453.

Mercier-Langevin, P., Lafrance, B., Bécu, V., Dubé, B., Kjarsgaard, I., and Guha, J., 2014, The Lemoine auriferous volcanogenic massive sulfide deposit, Chibougamau camp, Abitibi greenstone belt, Quebec, Canada: Geology and genesis: Economic Geology, v. 109, p. 231–269.

Mortensen, J. K., 1992, Pre-mid-Mesozoic tectonic evolution of the Yukon-Tanana terrane, Yukon and Alaska: Tectonics, v. 11, p. 836–853.

Mortensen, J. K., and Jilson, G. A., 1985, Evolution of the Yukon-Tanana terrane: Evidence from southeastern Yukon territory: Geology, v. 13, p. 806–810.

Munhá, J., Fyfe, W. S., and Kerrich, R., 1980, Adularia, the characteristic mineral of felsic spilites:

Contributions to Mineralogy and Petrology, v. 75, p. 15–19.

Murphy, D. C., and Piercey, S. J., 1998, Finlayson project : Geological evolution of Yukon-Tanana terrane and its relationship to Campbell Range belt, northern Wolverine Lake map area, southeastern Yukon (C. F. Roots & D. S. Emond, Eds.): Yukon Exploration and Geology, p. 47–62.

Murphy, D. C., Mortensen, J. K., Piercey, S. J., Orchard, M. J., and Gehrels, G. E., 2006, Mid-Paleozoic to early Mesozoic tectonostratigraphic evolution of Yukon-Tanana and Slide Mountain terranes and affiliated overlap assemblages, Finlayson Lake massive sulphide district, southeastern Yukon, in Colpron, M. and Nelson, J. L. eds., Paleozoic Evolution and Metallogeny of Pericratonic Terranes at the Ancient Pacific Margin of North America, Canadian and Alaskan Cordillera: Geologic Association of Canada, Special Paper, v. 45, p. 75–106.

Nelson, J. L., Piercey, S. J., Murphy, D. C., Colpron, M., Dusel-Bacon, C., and Roots, C. F., 2006, Paleozoic tectonic and metallogenetic evolution of pericratonic terranes in Yukon, northern British Columbia and eastern Alaska, in Colpron, M. and Nelson, J. L. eds., Paleozoic Evolution and Metallogeny of Pericratonic Terranes at the Ancient Pacific Margin of North America, Canadian and Alaskan Cordillera: Geologic Association of Canada, Special Paper, v. 45, p. 323–360.

Nozaki, T., Nagase, T., Takaya, Y., Yamasaki, T., and Otake, T., 2021, Subseafloor sulphide deposit formed by pumice replacement mineralisation: Scientific Reports, v. 11, p. 1–11.

van Olden, K., Green, A., and Davidson, G., 2020, NI 43-101 Feasibility Study Technical Report Kudz Ze Kayah Property , Yukon , Canada CSA Global Report n. R173.2019: CSA Global, 376 p.

Peter, J. M., Layton-Matthews, D., Piercey, S. J., Bradshaw, G. D., Paradis, S., and Bolton, A., 2007, Volcanogenic-hosted massive sulphide deposits of the Finlayson Lake district, Yukon, in Goodfellow W. D. ed., Mineral Deposits of Canada: A Synthesis of Major Deposit-Types, District Metallogeny, the Evolution of Geological Provinces, and Exploration Methods: Geological Association of Canada, Mineral Deposits Division, Special Publication No. 5, p. 471–508.

Piercey, S. J., 2015, A semipermeable interface model for the genesis of subseafloor replacement-type volcanogenic massive sulfide (VMS) deposits: Economic Geology, v. 110, p. 1655–1660.

Piercey, S. J., and Colpron, M., 2009, Composition and provenance of the Snowcap assemblage, basement to the Yukon-Tanana terrane, northern Cordillera: Implications for Cordilleran crustal growth: Geosphere, v. 5, p. 439–464.

Piercey, S. J., Murphy, D. C., Mortensen, J. K., and Paradis, S., 2001a, Boninitic magmatism in a continental margin setting, Yukon-Tanana terrane, southeastern Yukon, Canada: Geology, v. 29, p. 731–734.

Piercey, S. J., Paradis, S., Murphy, D. C., and Mortensen, J. K., 2001b, Geochemistry and paleotectonic setting of felsic volcanic rocks in the Finlayson Lake volcanic-hosted massive sulfide district, Yukon, Canada: Economic Geology, v. 96, p. 1877–1905.

Piercey, S. J., Mortensen, J. K., Murphy, D. C., Paradis, S., and Creaser, R. A., 2002, Geochemistry and tectonic significance of alkalic mafic magmatism in the Yukon-Tanana terrane, Finlayson Lake region, Yukon: Canadian Journal of Earth Sciences, v. 39, p. 1729–1744.

Piercey, S. J., Mortensen, J. K., and Creaser, R. A., 2003, Neodymium isotope geochemistry of felsic volcanic and intrusive rocks from the Yukon-Tanana terrane in the Finlayson Lake region, Yukon, Canada: Canadian Journal of Earth Sciences, v. 40, p. 77–97.

Piercey, S. J., Nelson, J. L., Colpron, M., Dusel-Bacon, C., Simard, R.-L. L., and Roots, C. F., 2006, Paleozoic magmatism and crustal recycling along the ancient Pacific margin of North America, northern Cordillera, in Colpron, M. and Nelson, J. L. eds., Paleozoic Evolution and Metallogeny of Pericratonic Terranes at the Ancient Pacific Margin of North America, Canadian and Alaskan Cordillera: Geological Association of Canada, Special Paper 45, p. 281–322.

Piercey, S. J., Squires, G. C., and Brace, T. D., 2014, Lithostratigraphic, hydrothermal, and tectonic setting of the Boundary volcanogenic massive sulfide deposit, Newfoundland Appalachians, Canada: Formation by subseafloor replacement in a Cambrian rifted arc: Economic Geology, v. 109, p. 661–687.

Piercey, S. J., Gibson, H. L., Tardif, N., and Kamber, B. S., 2016, Ambient redox and hydrothermal environment of the Wolverine volcanogenic massive sulfide deposit, Yukon: Insights from lithofacies and lithogeochemistry of Mississippian host shales: Economic Geology, v. 111, p. 1439–1463.

Pilote, J. L., Piercey, S. J., and Mercier-Langevin, P., 2019, Evolution of the subseafloor hydrothermal system associated with the Ming VMS deposit, Newfoundland Appalachians, and its controls on base and precious metal distribution: Mineralium Deposita, v. 55, p. 913–936.

Reimann, C., Filzmoser, P., and Garrett, R. G., 2005, Background and threshold: critical comparison of methods of determination: Science of the Total Environment, v. 346, p. 1–16.

Richards, H. G., Cann, J. R., and Jensenius, J., 1989, Mineralogical zonation and metasomatism of the alteration pipes of Cyprus sulfide deposits: Economic Geology, v. 84, p. 91–115.

Riverin, G., and Hodgson, C. J., 1980, Wall-rock alteration at the Millenbach Cu-Zn mine, Noranda, Quebec: Economic Geology, v. 75, p. 424–444.

Ruks, T. W., Piercey, S. J., Road, L., Pe, O., Ryan, J. J., Villeneuve, M. E., and Creaser, R. A., 2006, Mid- to late Paleozoic K-feldspar augen granitoids of the Yukon-Tanana terrane, Yukon, Canada: Implications for crustal growth and tectonic evolution of the northern Cordillera: GSA Bulletin, v. 118, p. 1212–1231.

Saccocia, P. J., and Seyfried, W. E., 1994, The solubility of chlorite solid solutions in 3.2 wt% NaCl fluids from 300-400°C, 500 bars: Geochimica et Cosmochimica Acta, v. 58, p. 567–585.

Sangster, D. F., 1980, Quantitative characteristics of volcanogenic massive sulphide deposits - Metal content and size distribution of massive sulphide deposits in volcanic centers: CIM Bulletin, v. 73, p. 74–81.

Schardt, C., Cooke, D. R., Gemmell, J. B., and Large, R. R., 2001, Geochemical modeling of the zoned footwall alteration pipe, Hellyer volcanic-hosted massive sulfide deposit, Western Tasmania, Australia: Economic Geology, v. 96, p. 1037–1054.

Sebert, C., Hunt, J. A., and Foreman, I. J., 2004, Geology and lithogeochemistry of the Fyre Lake copper-cobalt-gold sulphide-magnetite deposit, southeastern Yukon, Yukon Geological Survey. Open File 2004-17, 46 p.

Soltani Dehnavi, A., Lentz, D. R., McFarlane, C. R. M., and Walker, J. A., 2018, Quantification of fluid-mobile elements in white mica by LA-ICP-MS: From chemical composition to a potential micro-chemical vectoring tool in VMS exploration: Journal of Geochemical Exploration, v. 188, p. 290–307.

Soltani Dehnavi, A., McFarlane, C. R. M., Lentz, D. R., McClenaghan, S. H., Walker, J. A., Dehnavi, A. S., McFarlane, C. R. M., Lentz, D. R., McClenaghan, S. H., and Walker, J. A., 2019, Chlorite-white mica pairs' composition as a micro-chemical guide to fingerprint massive sulfide deposits of the Bathurst mining camp, Canada: Minerals, v. 9, 31 p.

Spitz, G., and Darling, R., 1978, Major and minor element lithogeochemical anomalies surrounding the Louvem copper deposit, Val d'Or, Quebec: Canadian Journal of Earth Sciences, v. 15, p. 1161–1169.

Urabe, T., Scott, S. D., and Hattori, K., 1983, A comparison of footwall-rock alteration and geothermal systems beneath some Japanese and Canadian volcanogenic massive sulfide deposits: Economic Geology Monograph, v. 5, p. 345–364.

Velde, B., 1978, Infrared spectra of synthetic micas in the series muscovite-MgAl celadonite: American Journal of Science, v. 63, p. 343–349.

Yang, K., Huntington, J. F., Gemmell, J. B., and Scott, K. M., 2011, Variations in composition and abundance of white mica in the hydrothermal alteration system at Hellyer, Tasmania, as revealed by infrared reflectance spectroscopy: Journal of Geochemical Exploration, v. 108, p. 143–156.

Zane, A., and Weiss, Z., 1998, A procedure for classifying rock-forming chlorites based on microprobe data: Lincei Sci. Fis. Nat., v. 9, 51–56.

Zang, W., and Fyfe, W. S., 1995, Chloritization of the hydrothermally altered bedrock at the Igarapé Bahia gold deposit, Carajás, Brazil: Mineralium Deposita, v. 30, p. 30–38.

Chapter 4

Mineralogy and mineral chemistry of the mineralization at the ABM replacement-style volcanogenic massive sulfide deposit, Finlayson Lake district, Yukon, Canada

4.1 Abstract

The ABM deposit is a bimodal-felsic, replacement-style volcanogenic massive sulfide deposit (VMS) that is hosted by back-arc affinity rocks of the Yukon-Tanana terrane in the Finlayson Lake VMS district, Yukon, Canada. The massive sulfide mineralization occurs as a series of stacked and stratabound lenses subparallel to the volcanic stratigraphy, surrounded by an envelope of pervasive white mica and/or chlorite alteration. Remnant clasts of volcanic rocks and preserved bedding occur locally within the massive sulfide lenses and indicate that mineralization formed through replacement of pre-existing strata below the seafloor. Three major mineral assemblages occur at the ABM deposit: (1) a pyrite-chalcopyrite-magnetite-pyrrhotite assemblage that is associated with Cu-Bi-Se-Co enrichment and occurs at the centre of the massive sulfide lenses; (2) a pyrite-sphalerite assemblage, which occurs more commonly towards lens margins and is enriched in Zn-Pb-Ag-Au-Hg-As-Sb-Ba; (3) a minor assemblage comprising chalcopyrite-pyrrhotite-pyrite stringers associated with pervasive chlorite alteration, which occurs mostly at the sulfide lens margins. Massive sulfide mineralization contains preserved primary, zone refining, and metamorphic textures. This study combines petrographic observations, bulk element distribution and mineral assemblage modelling together with *in situ* mineral geochemical analyses to determine the effects (if any) of greenschist metamorphism on the mineralogy and mineral chemistry at the ABM deposit. The application of in situ mineral chemistry is used to distinguish between original sub-seafloor VMS-related signatures and subsequent metal and sulfur remobilizations that occurred during later metamorphism of the ABM deposit and contribute to the study of effects of greenschist facies metamorphism on ancient replacement-style VMS deposits.

4.2 Introduction

Volcanogenic massive sulfide (VMS) deposits are major sources of base and precious metals, both at present and historically (e.g., Galley et al. 2007); however, what controls the grade and tonnage of the mineralization is still not completely understood. In a subset of VMS deposits, subseafloor replacement is an important process and these types of deposits are interpreted to have had higher precipitation efficiency than exhalative-style deposits, due to greater portion of the dissolved metals being precipitated from the hydrothermal fluids in the subsurface and resulting in higher tonnages and higher grade deposits relative to those precipitated solely on the seafloor (Doyle and Allen, 2003; Piercey, 2015). Further, zone refining, the dissolution of existing mineralization by higher temperature fluids and precipitation of new high temperature mineralization, is a critical mechanism responsible for increasing the grades of base and precious metals in massive sulfide mineralization in both exhalative- and subseafloor replacement-style deposits (Eldridge et al., 1983; Ohmoto, 1996). In many ancient deposits, however, distinguishing textural features are commonly obscured due to post-VMS deposition overprinting, metamorphism, and deformation (Lafrance et al., 2020). This creates a unique challenge in VMS deposit research: recognition of primary exhalative- and replacement-related textures versus those imposed by subsequent post-VMS formation events (e.g., Craig and Vokes 1992; Larocque and Hodgson 1995; Lafrance et al. 2020).

Past studies have been successful at identifying replacement-style VMS mineralization in the ancient record, including documenting the genesis of the mineralization, metal sources, and impact of metamorphic and structural overprinting effects (Larocque and Hodgson, 1995; Genna et al., 2014; Brueckner et al., 2016; Vikentyev et al., 2017). However, the effects of metamorphism on VMS mineralization, even by the relatively low grade greenschist facies have not been yet fully resolved. In particular, primary geochemical signatures are commonly influenced by metamorphic overprints (Lockington et al., 2014; Genna and Gaboury, 2015; George et al., 2016). Correctly interpreting primary versus secondary textures in the field and in ore and gangue minerals is critical for understanding the competing roles of exhalation, replacement, and metamorphic overprinting, and the primary hydrothermal conditions under which the massive sulfide deposits formed versus secondary conditions of metamorphic and structural overprinting (e.g., Brueckner et al. 2014, 2016; Martin et al. 2018). Deciphering these effects is also important for understanding the distribution of economic (e.g., Ag and Au), critical (e.g., Co, Se, or Sn), and deleterious (e.g., As and Cd) metals and the relative roles of primary VMS-related metal zoning and the metamorphic effects (Layton-Matthews et al., 2008; Carvalho et al., 2018; Cugerone et al., 2021).

The ABM deposit is a bimodal-felsic, replacement-style VMS deposit that contains a total (geological) mineral resource of 19.1 Mt at 6.6 wt. % Zn, 0.9 wt. % Cu, 2.0 wt. % Pb, 1.4 g/t Au and 156 g/t Ag (van Olden et al., 2020). The deposit is located in the Finlayson Lake VMS district, which contains >40 Mt of polymetallic VMS mineralization in varying styles of deposits hosted by arc and back-arc rocks of the Yukon-Tanana and Slide Mountain terranes (Peter et al., 2007). Following an extensive drilling program in 2015, the massive sulfide mineralization at the ABM deposit was re-interpreted as replacement style on the basis of lithofacies, textural, and structural studies (van Olden et al., 2020; Denisová and Piercey, 2022; Manor et al., 2022b). Previous work on the massive sulfide mineralization at the ABM deposit focused on the distribution and sources of Se (Layton-Matthews et al., 2008; Layton-Matthews et al., 2013) but no comprehensive research has been presented on the genesis of the massive sulfide mineralization at the ABM VMS deposit.

This study presents results of detailed textural and mineralogical studies based on drill core observations, assay results, 3D modelling, detailed petrography and paragenetic studies, electron probe microanalysis (EPMA), and laser ablation-inductively coupled plasma-mass spectrometry (LA-ICP-MS). We discuss the timing and evolution of the mineralization at the ABM deposit and the characteristics and potential sources of mineralizing fluids. Further, we distinguish primary subseafloor VMS-related mineralogical and geochemical signatures from those related to greenschist-facies metamorphic overprinting. The results herein contribute to our understanding of massive sulfide mineralization in ancient, metamorphosed replacement-style VMS deposits.

4.3 Regional geology

The Finlayson Lake VMS district is a dismembered block of the Yukon-Tanana and Slide Mountain terranes that developed along the western margin of Laurentia from the Devonian to the Permo-Triassic (Fig. 4.1; Colpron et al., 2006; Nelson et al., 2006; Piercey et al., 2006). The district was displaced from its original location ~430 km along the dextral strike-slip Tintina Fault in the Eocene (Gabrielse et al., 2006). The Yukon-Tanana terrane in the district comprises a poly-deformed and metamorphosed pre-Late Devonian continental margin assemblage (Piercey and Colpron, 2009) that is overlain by three unconformity-bound Late Devonian to Middle to Late Permian continental arc, back-arc, and ocean basin-related volcanic-sedimentary sequences (Big Campbell, Money Creek, and Cleaver Lake thrust sheets; Mortensen and Jilson, 1985; Mortensen, 1992; Colpron et al., 2006a; Murphy et al., 2006). Metamorphism and deformation in the district are interpreted to be a result of a Middle Jurassic-Early Cretaceous mid-crustal tectonometamorphic event, which comprised ductile deformation and moderate temperature-high pressure metamorphism (Staples et al., 2014). The core of the Finlayson Lake district reached amphibolite facies metamorphic grade, which transitions to lower greenschist facies further from the centre of the district (Murphy et al., 2006). The Big Campbell thrust sheet is by volume the largest and structurally deepest block in the Finlayson Lake district (Fig. 4.1) and contains Upper Devonian metaclastic rocks of the North River formation, the Upper Devonian Grass Lakes group, and the Lower Mississippian Wolverine Lake group; these lithological units host four VMS deposits (Fig. 4.1; Murphy et al., 2006; Peter et al., 2007). The Grass Lake group is composed of three units: the Fire Lake, Kudz Ze Kayah and Wind Lake formations (Fig. 4.1). The Fire Lake formation hosts the Kona Cu-Co-Au mafic-siliciclastic VMS deposit (Piercey et al., 2001a; Sebert et al., 2004; Murphy et al., 2006; Peter et al., 2007). The Kudz Ze Kayah formation is interpreted to be coeval to the Fire Lake formation, but structurally separated and stratigraphically distinct (Manor et al., 2022a); it comprises dominantly felsic volcanic and sedimentary rocks with back-arc geochemical affinities (Piercey et al., 2001b; Murphy et al., 2006; Denisová and Piercey, 2022; Manor et al., 2022b). The Wind Lake formation sits conformably atop the Kudz Ze Kayah formation (Piercey et al., 2002). All rocks in the Grass Lakes group are intruded by the Grass Lakes plutonic suite at ca. 361 Ma (Piercey et al., 2001b; Piercey et al., 2003; Manor et al., 2022a). The Wolverine Lake group unconformably overlies the Grass Lakes group and hosts the Wolverine felsic-siliciclastic VMS deposit (Murphy and Piercey, 1998; Bradshaw et al., 2001; Bradshaw et al., 2008; Manor et al., 2022b).

Figure 4.1. Regional setting of the Finlayson Lake district. (A) Regional geologic map of the Finlayson Lake district, Yukon-Tanana, and Slide Mountain terranes (modified after Murphy et al., 2006). Numbers mark the positions of known VMS deposits in the region. BCT = Big Campbell thrust; CLT = Cleaver Lake thrust; JCF = Jules Creek fault; MCT = Money Creek thrust; NRF = North River thrust. (B) Composite chronostratigraphic column for the Finlayson Lake district showing stratigraphic and structural relationships. Locations of VMS deposits, petrogenetic affinities of volcanic rocks and U-Pb and fossil ages displayed on diagram (modified after Murphy et al., 2006; Piercey et al., 2016; Manor and Piercey, 2018).

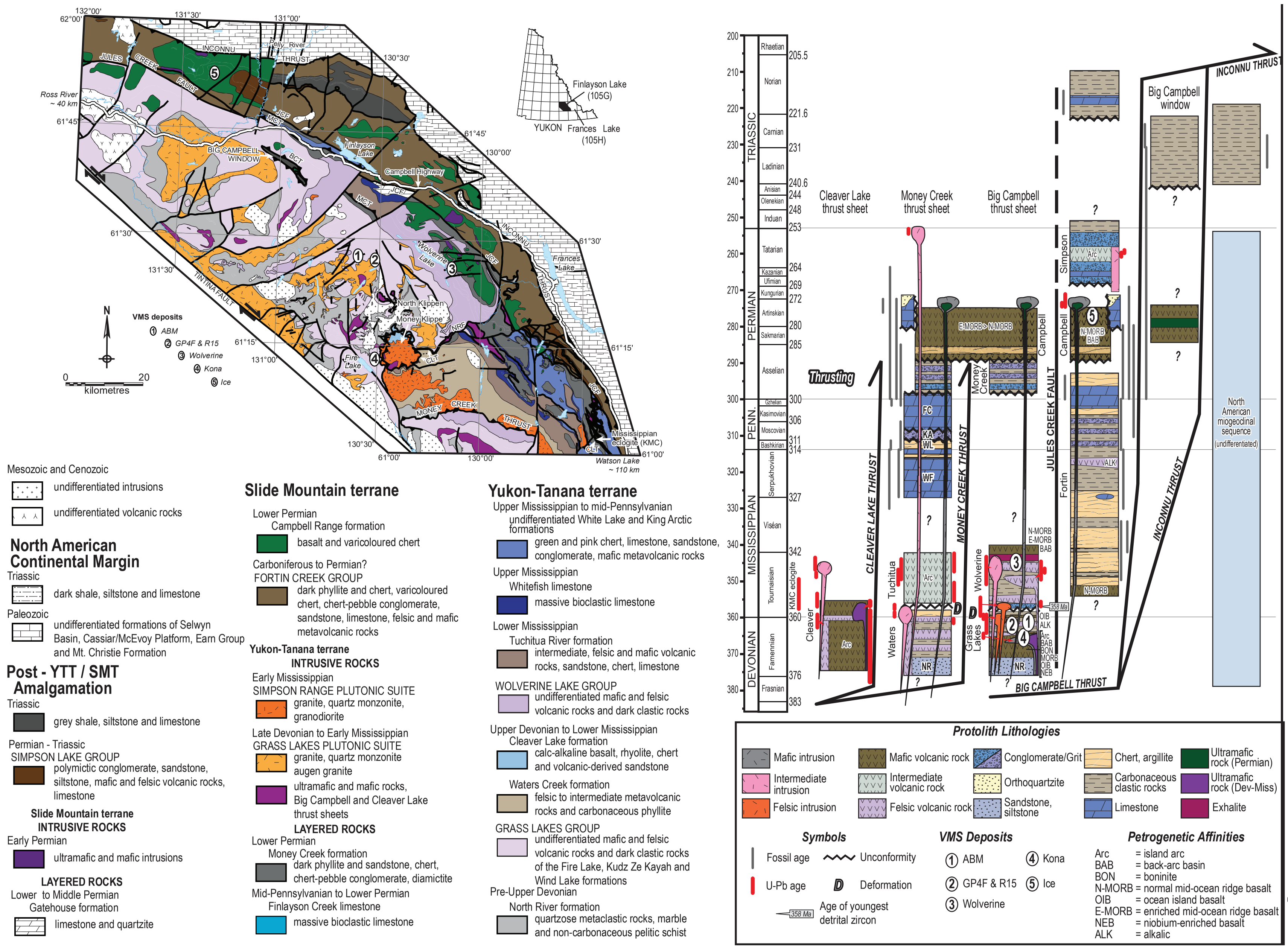
Ross River ~ 40 km
Watson Lake ~ 110 km
JULES CREEK FAULT
INCONNU THRUST
Pelly River
BIG CAMPBELL WINDOW
Finlayson Lake
Campbell Highway
TINTINA FAULT
Wolverine Lake
Frances Lake
North Klippen
Money Klippe
Fire Lake
MONEY CREEK THRUST
Mississippian eclogite (KMC)
YUKON
Finlayson Lake (105G)
Frances Lake (105H)
VMS deposits
1 ABM
2 GP4F & R15
3 Wolverine
4 Kona
5 Ice
kilometres
Mesozoic and Cenozoic
undifferentiated intrusions
undifferentiated volcanic rocks
North American Continental Margin
Triassic
dark shale, siltstone and limestone
Paleozoic
undifferentiated formations of Selwyn Basin, Cassiar/McEvoy Platform, Earn Group and Mt. Christie Formation
Post - YTT / SMT Amalgamation
Triassic
grey shale, siltstone and limestone
Permian - Triassic
SIMPSON LAKE GROUP
polymictic conglomerate, sandstone, siltstone, mafic and felsic volcanic rocks, limestone
Slide Mountain terrane
INTRUSIVE ROCKS
Early Permian
ultramafic and mafic intrusions
LAYERED ROCKS
Lower to Middle Permian
Gatehouse formation
limestone and quartzite
Slide Mountain terrane
Lower Permian
Campbell Range formation
basalt and varicoloured chert
Carboniferous to Permian?
FORTIN CREEK GROUP
dark phyllite and chert, varicoloured chert, chert-pebble conglomerate, sandstone, limestone, felsic and mafic metavolcanic rocks
Yukon-Tanana terrane
INTRUSIVE ROCKS
Early Mississippian
SIMPSON RANGE PLUTONIC SUITE
granite, quartz monzonite, granodiorite
Late Devonian to Early Mississippian
GRASS LAKES PLUTONIC SUITE
granite, quartz monzonite augen granite
ultramafic and mafic rocks, Big Campbell and Cleaver Lake thrust sheets
LAYERED ROCKS
Lower Permian
Money Creek formation
dark phyllite and sandstone, chert, chert-pebble conglomerate, diamictite
Mid-Pennsylvanian to Lower Permian
Finlayson Creek limestone
massive bioclastic limestone
Yukon-Tanana terrane
Upper Mississippian to mid-Pennsylvanian
undifferentiated White Lake and King Arctic formations
green and pink chert, limestone, sandstone, conglomerate, mafic metavolcanic rocks
Upper Mississippian
Whitefish limestone
massive bioclastic limestone
Lower Mississippian
Tuchitua River formation
intermediate, felsic and mafic volcanic rocks, sandstone, chert, limestone
WOLVERINE LAKE GROUP
undifferentiated mafic and felsic volcanic rocks and dark clastic rocks
Upper Devonian to Lower Mississippian
Cleaver Lake formation
calc-alkaline basalt, rhyolite, chert and volcanic-derived sandstone
Waters Creek formation
felsic to intermediate metavolcanic rocks and carbonaceous phyllite
GRASS LAKES GROUP
undifferentiated mafic and felsic volcanic rocks and dark clastic rocks of the Fire Lake, Kudz Ze Kayah and Wind Lake formations
Pre-Upper Devonian
North River formation
quartzose metaclastic rocks, marble and non-carbonaceous pelitic schist
TRIASSIC
PERMIAN
PENN.
MISSISSIPPIAN
DEVONIAN
Rhaetian
Norian
Carnian
Ladinian
Anisian
Olenekian
Induan
Tatarian
Kazanian
Ufimian
Kungurian
Artinskian
Sakmarian
Asselian
Gzhelian
Kasimovian
Moscovian
Bashkirian
Serpukhovian
Viséan
Tournaisian
Famennian
Frasnian
KMC eclogite
Cleaver Lake thrust sheet
Money Creek thrust sheet
Big Campbell thrust sheet
Big Campbell window
Thrusting
CLEAVER LAKE THRUST
MONEY CREEK THRUST
JULES CREEK FAULT
BIG CAMPBELL THRUST
INCONNU THRUST
Cleaver
Waters
Tuchitua
Grass Lakes
Wolverine
Money Creek
Campbell
Fortin
Simpson
North American miogeodinal sequence (undifferentiated)
Protolith Lithologies
Mafic intrusion
Intermediate intrusion
Felsic intrusion
Mafic volcanic rock
Intermediate volcanic rock
Felsic volcanic rock
Conglomerate/Grit
Orthoquartzite
Sandstone, siltstone
Chert, argillite
Carbonaceous clastic rocks
Limestone
Ultramafic rock (Permian)
Ultramafic rock (Dev-Miss)
Exhalite
Symbols
Fossil age
Unconformity
U-Pb age
Deformation
Age of youngest detrital zircon
VMS Deposits
1 ABM
2 GP4F & R15
3 Wolverine
4 Kona
5 Ice
Petrogenetic Affinities
Arc = island arc
BAB = back-arc basin
BON = boninite
N-MORB = normal mid-ocean ridge basalt
OIB = ocean island basalt
E-MORB = enriched mid-ocean ridge basalt
NEB = niobium-enriched basalt
ALK = alkalic

Three known VMS deposits are hosted within the Kudz Ze Kayah formation: the ABM, GP4F, and R15 deposits. The ABM deposit is located about 25 km south of Finlayson Lake and the Robert Campbell Highway (Fig. 4.1). The GP4F deposit is situated roughly 5 km SE from the ABM deposit (Fig. 4.1) and sits ~500-600 m stratigraphically below the ABM deposit (Peter et al., 2007; Manor et al., 2022b). The R15 deposit occurs immediately along strike east of the GP4F deposit and occupies the same stratigraphic position (MacRobbie and Holroyd, unpub. data). The mineralization style at the R15 deposit (MacRobbie and Holroyd, unpub. data) is described as similar to the GP4F deposit (Boulton, 2002). Subseafloor replacement is interpreted to be the primary mineralization style in all three deposits (Peter et al., 2007; van Olden et al., 2020; Denisová and Piercey, 2022; Manor et al., 2022b). The rocks hosting the GP4F deposit formed at ca. 363.254±0.098 Ma, whereas the ABM deposit is hosted by rocks formed at ca. 362.82±0.12 Ma (Manor et al., 2022b).

4.4 Local geology

The geochemical signatures and tectonostratigraphic setting of the upper Kudz Ze Kayah formation suggest that the rocks were deposited in a back-arc environment (Piercey et al., 2001b; Piercey et al., 2002) in a lower order basin with an active volcanic centre (Denisová and Piercey, 2022). The ABM deposit is hosted within a volcanosedimentary package that occupies the upper ~350 m of the Kudz Ze Kayah formation and comprises felsic volcanic and volcaniclastic rocks, and lesser mafic sills and argillite lenses. The stratigraphy dips between 20°-30° to the NNE and field observations and stratigraphic reconstructions do not indicate any fault repetition or major folding (van Olden et al., 2020; Denisová and Piercey, 2022; Manor et al., 2022b). The East fault is interpreted to be a re-activated transform fault (Fig. 4.2A; van Olden et al. 2020) that was originally part of a set of interconnected synvolcanic normal faults that accommodated extension within the basin and acted as magma conduits (Denisová and Piercey, 2022).

The upper Kudz Ze Kayah formation can be divided into three sequences (Fig. 4.2B) with different geochemical characteristics based on immobile element values and their ratios (Zr/

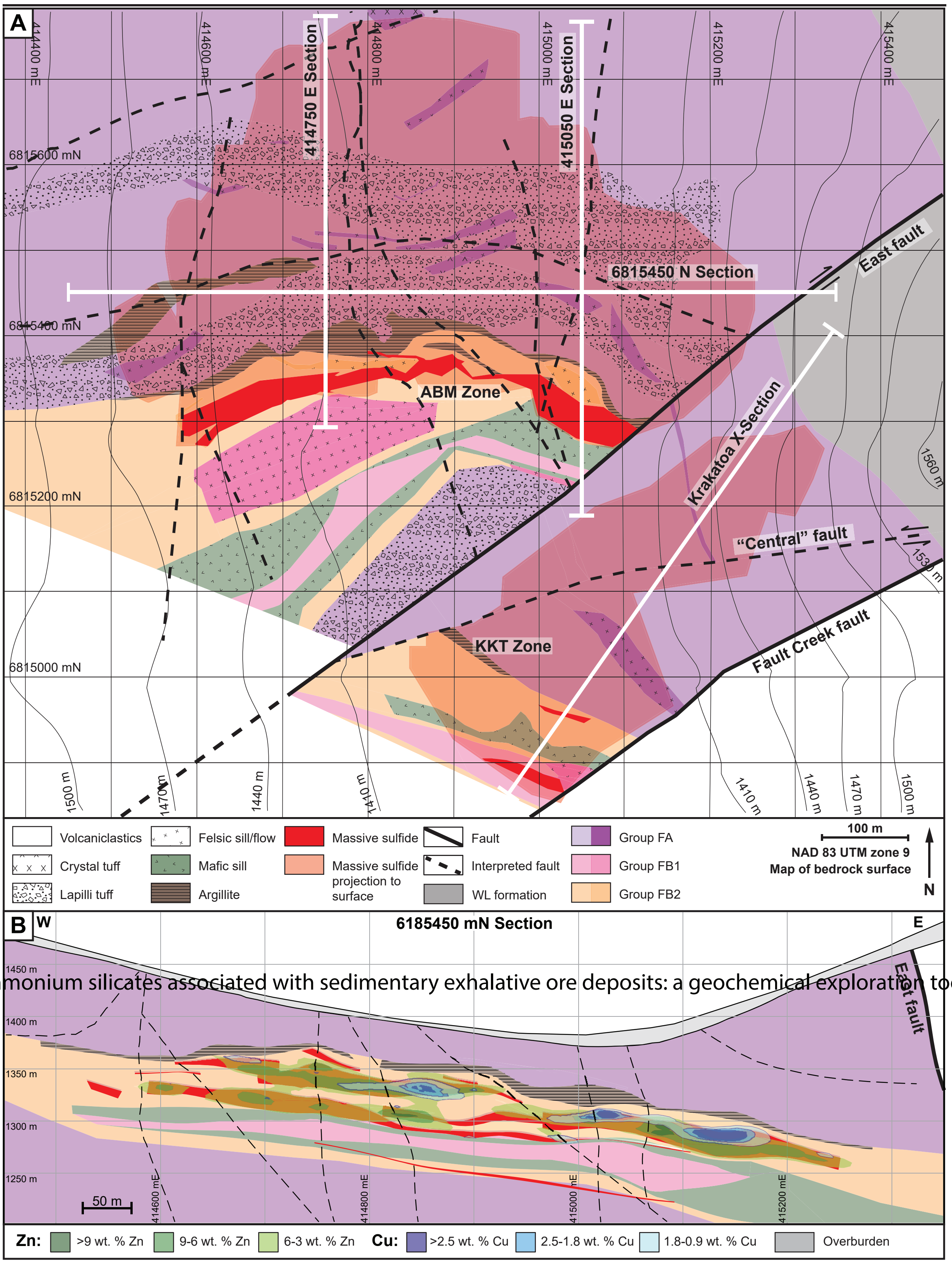

.., 1987, Ammonium silicates associated with sedimentary exhalative ore deposits: a geochemical exploration tool: Journ

Figure 4.2. Local geology of the ABM deposit. (A) Geological map with units constructed using drilling data and 3D models. Section lines displayed. Upward projections of maximum known extent of mineralization displayed. Note that lithofacies are displayed using patterns and geochemical groups using colors. (B) Section through the ABM zone of the ABM deposit running W-E, looking north with simplified lithofacies and lithogeochemistry displayed. Contours of Zn and Cu content are overlayed on the simplified stratigraphy.

Al_2O_3, Al_2O_3/TiO_2, Nb/Ta; Denisová and Piercey 2022). The hanging wall and footwall sequences comprise felsic volcanic rocks (FA signatures, Zr >550 ppm). The sequence hosting the massive sulfide mineralization varies in thickness between 45 to 120 m (average ~100 m) and comprises interbedded felsic (FB1 and FB2 signatures, Zr <500 ppm) volcaniclastic rocks, coherent flows, sills, domes, and two mafic sills that extend through the deposit footprint. The upper boundary of the mineralized zone is an argillite lens that marks a protracted period of volcanic quiescence (minimum ~75,000 years; Denisová and Piercey, 2022).

Hydrothermal alteration affects most of the rocks in the ABM deposit footprint (~1 km radius surrounding the deposit) and these assemblages affect predominantly felsic lithofacies (Denisová and Piercey, in press). The distribution of hydrothermal alteration zones in the volcanosedimentary stratigraphy was controlled by the porosity and permeability contrasts between coherent, volcaniclastic and sedimentary units (Denisová and Piercey, 2022). Proximal to massive sulfide mineralization, high temperature pervasive chlorite assemblages (~315 °C) overprint lower temperature pervasive white mica assemblages (~250 °C) or moderate white mica ± chlorite assemblages (~215 °C; Denisova and Piercey in press). Textural relationships show that sulfide mineralization overprints all types of pervasive alteration, although locally massive sulfide mineralization is contemporaneous with pervasive chlorite alteration. Sulfide mineralization is locally associated with white mica, chlorite, and/or K-Ba feldspars. Pervasive alteration and mineralization formed when the hydrothermal system at the ABM deposit was at its thermal peak during a protracted break in volcanism. Pervasive white mica and moderate to weak white mica ± chlorite alteration extends up to 300 m stratigraphically into the hanging wall of the massive sulfide mineralization indicating that the hydrothermal system continued during periods of volcanic quiescence after the main mineralizing period (Denisová and Piercey, in press).

4.5 Methods

Over 10 km of drill core from 50 drill holes were logged for this study. Lithology, primary textures, grain size, mineralogy, and alteration type and intensity based on mineral occurrence (quartz, white mica, chlorite, biotite, carbonate minerals, and sulfide minerals) was recorded in graphic core logs (scale 1:400); attention was paid to all intervals with sulfide content >1 vol % to document the sulfide mineralogy, textures, and relationships to host rock. Fifty-one samples representative of massive sulfide assemblages distributed across the ABM deposit were collected and studied with a transmitted and reflected light petrographic microscope and with a JEOL JSM 7100F scanning electron microscope (SEM) with back scatter electron (BSE) imaging operating at an acceleratingvoltage of 15 kV at the Hibernia Electron Beam Facility at MUN. Selected polished thin sections of massive sulfide mineralization were imaged using SEM coupled with energy-dispersive X-ray spectroscopy (EDX) using a FEI Mineral Liberation Analysis (MLA) 650 field emission gun (FEG) instrument equipped with dual Bruker 5th generation XFlash Silicon Drift Detector (SDD) X-ray detectors at the Micro Analysis Facility at MUN-CREAIT, to show the distribution of elements in areas with complex textures. A dataset of all available assay data in the ABM deposit and surrounding areas was provided by BMC Minerals Ltd.; quality assurance and quality control (QA/QC) procedures for the company datasets are described in van Olden et al. (2020). Additional datasets provided by BMC Minerals Ltd., including core photos and drill logs, were used as secondary resources.

Digital models of mineralized lenses, alteration zones and lithostratigraphic units displayed in the sections from the ABM deposit herein were created using the Leapfrog 2021.2 software developed by Seequent. Isosurfaces representing the distribution of elements of interest were created using the assay database provided by BMC Minerals Ltd. and modelled using the Numeric Models tool in Leapfrog 3D. The linear radial basis function (RBF) interpolation was chosen to mitigate the irregular distribution of the datapoints, and it was run with a base range of 60, nugget of 0, and varying total sill and accuracy (Appendix 7.1) for all the modelled isosurfaces. The trend for the numeric models was set to the local stratigraphy (dip 30° with dip azimuth of 20° and pitch of

115°), the ellipsoid ratios were set to 3:3:1.

4.5.1 Electron probe microanalyzer

The composition of pyrite, pyrrhotite, arsenopyrite, chalcopyrite, sphalerite, galena, and tennantite-tetrahedrite-freibergite in 15 polished thin sections was analysed at Memorial University using the JEOL JXA-8230 SuperProbe electron probe microanalyzer (EPMA) equipped with five wavelength dispersive spectrometers (WDS) and a tungsten filament electron gun. Natural and synthetic standards were used for calibration of the instrument, where the following standards and X-ray lines were used on five respective crystals (spectrometers) and average detection limits for each element are given in parentheses: 1) LIF: sphalerite (ZnKα; 283 ppm), rhodonite (MnKα; 150 ppm), pentlandite (NiKα; 231 ppm); 2) PETL: stibnite (SbLα; 50 ppm), silver (AgLα; 47 ppm), cadmium (CdLα; 31 ppm), cinnabar (HgMα; 65 ppm), bismuth (BiMα; 115 ppm), galena (PbMα; 151 ppm), pyrite (SKα; 32 ppm); 3) TAP: arsenopyrite (AsLα; 105 ppm), selenium (SeLα; 110 ppm); 4) LIFH: cuprite (CuKα; 46 ppm), cobalt (CoKα; 28 ppm), pyrite (FeKα; 41 ppm). Counting times for calibration were between 10-30 seconds on peaks and 5-15 seconds on background. Analyses of unknown minerals were performed using the same crystals as the calibration. Pyrite, pyrrhotite, and arsenopyrite were analyzed for 9 elements (Zn, Sb, Ag, Pb, S, As, Cu, C, and Fe), sphalerite was analysed for 6 elements (Zn, Mn, Cd, Hg, S, Fe), chalcopyrite was analyzed for 8 elements (Zn, Ag, Hg, Bi, Pb, S, Cu, and Fe), galena was analyzed for 10 elements (Zn, Sb, Ag, Hg, Bi, Pb, S, Se, Cu, Fe) and tennantite-tetrahedrite-freibergite were analyzed for 11 elements (Zn, Ni, Sb, As, Hg, Pb, S, As, Cu, Co, and Fe). The sulfide minerals were analyzed using an accelerating voltage of 25 kV, a 2 nA beam current, focused to 1 µm, with elemental counting times between 5–30 seconds. Internal standards were measured periodically to demonstrate reproducibility. Sulfide mineral analyses with totals falling outside 100 ± 2 wt. % range were rejected. For galena, pyrite, and sulfosalts, due to the irregular surface of some of the grains, analyses with totals falling outside 100 ± 3 wt. % range were rejected. All analyses, calculated atoms per formula unit (apfu) values, and QA/QC data are available in Appendix 8.

4.5.2 Laser ablation inductively coupled plasma mass spectrometry

In situ LA-ICP-MS spot analyses (n=127) were performed using a geoLas 193 nm Excimer laser (Coherent) coupled to a Thermo-Finnigan Element XR ICP-MS instrument at Memorial University on six polished blocks with single samples representing the main mineralization assemblages. The ICP-MS was tuned for high sensitivity and a ThO/Th of <0.3 %. Abundances of selected elements using analyte masses of ^{34}S, ^{55}Mn, ^{57}Fe, ^{59}Co, ^{60}Ni, ^{65}Cu, ^{66}Zn, ^{69}Ga, ^{72}Ge, ^{75}As, ^{77}Se, ^{107}Ag, ^{111}Cd, ^{115}In, ^{118}Sn, ^{121}Sb, ^{125}Te, ^{197}Au, ^{202}Hg, ^{205}Tl, ^{206}Pb, and ^{209}Bi were determined for pyrite, pyrrhotite, sphalerite, galena, chalcopyrite, arsenopyrite, and tennantite. Ablation employed a spot diameter of 20 µm for galena and 30 µm for all other sulfide minerals at a repetition rate of 5 Hz with an energy density of 3 J/cm^2. For each spot, a gas blank was analyzed for 30 s, followed by 40 s of ablation. Periodically, the standards NIST 610 (synthetic glass) and MASS-1 (pressed powder pellet) were measured. NIST 610 was used for drift correction and MASS-1 was used for calibration/matrix correction. Data reduction and the subtraction of gas blanks was performed using Iolite v. 3.72 (Paton et al., 2011); this program was used for data treatment, to inspect the time-resolved signals and to exclude time-resolved sections of the signal representing micro-inclusions. Detection limits and standard deviations for all analyzed elements, together with the collected data are available in Appendix 9. Average values for a reference element in each mineral as determined using EPMA were used as internal ratio standards (Fe for pyrite, pyrrhotite, and arsenopyrite, Zn for sphalerite, Cu for chalcopyrite and tennantite, and Pb for galena). The mass ^{115}In (natural abundance 95.72 %) can show interference from ^{115}Sn (natural abundance 0.34 %) but in cases where In concentrations are greater than or similar to Sn concentrations, the interference effect is negligible.

4.6 Observations and results

4.6.1 Mineralization lenses extent, distribution, and morphology

The ABM deposit contains two main mineralized zones - ABM and Krakatoa (Fig. 4.2A) - that were offset from each other ~200 m by the East fault post-mineralization. The mineralization in both zones consists of a series of stacked stratabound massive sulfide lenses that dip subparallel to the stratigraphy (20°-30°; Fig. 4.2B, 4.3). The ABM zone is 700 m across and extends from the bedrock surface down dip for 600 m. Mineralization in the ABM zone tapers off down dip to the NNE, along strike to the west, and is truncated by the East fault in the east; the thickness of the mineralized stack varies from 5 to 55 m true thickness. The western portion of the ABM zone is characterized by several thinner and less extensive massive sulfide lenses (at least seven lenses varying in thickness from <1-10 m true thickness), some of which merge towards the east. In the eastern portion of the ABM zone, a single thick (up to 20 m true thickness) massive sulfide lens occurs. The Krakatoa mineralized zone is 170 m wide, 15 to 100 m thick, and extends from the bedrock surface down dip for 600 m and remains open down dip, whereas mineralized lenses are cut off by post-mineralization movement on bounding faults along strike in both directions (i.e., East fault and Fault Creek fault; Fig. 4.2A). The Krakatoa zone is bisected by the post-mineralization "Central" fault, which offset the two blocks dextrally by at least a 100 m. The northern block generally contains thin massive sulfide lenses associated with a mafic sill, whereas the southern block contains most of the known mineralized lenses in the Krakatoa zone with true thickness varying up to 16 m (Fig. 4.3). In the Krakatoa zone, reactivated faults (e.g., "Central" fault) have cut through the mineralized zones and samples proximal to the fault show evidence of ductile deformation (durchbewegung textures in mineralization).

The ABM deposit is hosted by hydrothermally altered volcaniclastic and volcanic rocks. In the ABM zone, massive sulfide mineralization is associated primarily with felsic coherent and volcaniclastic rocks (Fig. 4.2B). In the Krakatoa zone, massive sulfide mineralization is localized on contacts between the mafic sills and felsic volcaniclastic rocks or locally, within the mafic sills themselves (Fig. 4.3). Massive sulfide lenses in both zones generally have sharp contacts, although rarely they grade into altered rocks over a distance of 1-2 m. Features such as preserved lapilli and other clasts (Fig. 4.4A), remnant bedding (Fig. 4.4B), massive sulfides replacing glassy groundmass within perlitic and brecciated textures at unit contacts (Fig. 4.4C) occur within the massive sulfide lenses and on their contacts and suggest that the mineralization formed by replacement (van Olden et al., 2020; Denisová and Piercey, 2022; Manor et al., 2022b).

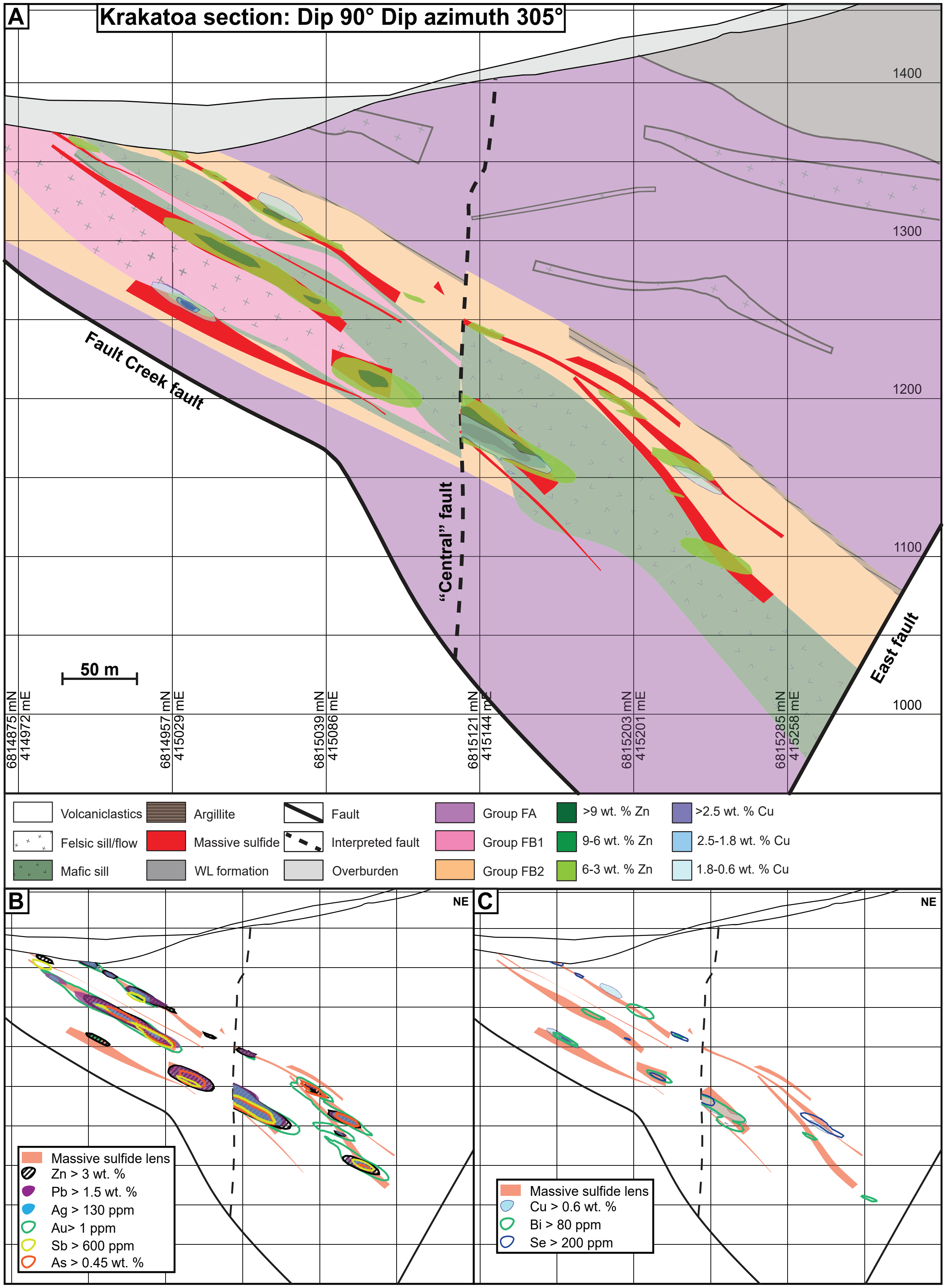
A
Krakatoa section: Dip 90° Dip azimuth 305°
1400
1300
1200
1100
1000
Fault Creek fault
"Central" fault
East fault
50 m
6814875 mN 414972 mE
6814957 mN 415029 mE
6815039 mN 415086 mE
6815121 mN 415144 mE
6815203 mN 415201 mE
6815285 mN 415258 mE
Volcaniclastics
Felsic sill/flow
Mafic sill
Argillite
Massive sulfide
WL formation
Fault
Interpreted fault
Overburden
Group FA
Group FB1
Group FB2
>9 wt. % Zn
9-6 wt. % Zn
6-3 wt. % Zn
>2.5 wt. % Cu
2.5-1.8 wt. % Cu
1.8-0.6 wt. % Cu
B
NE
Massive sulfide lens
Zn > 3 wt. %
Pb > 1.5 wt. %
Ag > 130 ppm
Au> 1 ppm
Sb > 600 ppm
As > 0.45 wt. %
C
NE
Massive sulfide lens
Cu > 0.6 wt. %
Bi > 80 ppm
Se > 200 ppm

Figure 4.3. Cross section of the Krakatoa zone looking northwest. (A) Simplified lithostratigraphy of the Krakatoa zone with an overlay showing the distribution of elevated Zn and Cu. (B) Distribution of the Zn-Pb-Ag-Au-Sb-As element assemblage in the Krakatoa zone. (C) Distribution of the Cu-Bi-Se element assemblage in the Krakatoa zone.

4.6.2 Mineralization assemblages

In both the ABM and Krakatoa zones, massive sulfide mineralization consists of pyrite, locally abundant sphalerite and/or chalcopyrite, and lesser pyrrhotite, magnetite, galena and minor tetrahedrite group minerals and other rare sulfosalts. The most common non-sulfide gangue minerals are barite, carbonate minerals, quartz, chlorite, and white mica. Massive sulfide assemblages contain >50 modal % sulfide minerals. The three main mineralization assemblages are: (1) pyrite-sphalerite with lesser galena, chalcopyrite, and tetrahedrite group minerals, with carbonate, barite, quartz, and white mica; (2) pyrite-chalcopyrite-magnetite-pyrrhotite with lesser sphalerite, minor tetrahedrite group minerals, and minor carbonate and chlorite; and (3) chalcopyrite-pyrrhotite-pyrite stringers associated with pervasive chlorite alteration, minor carbonate, and quartz.

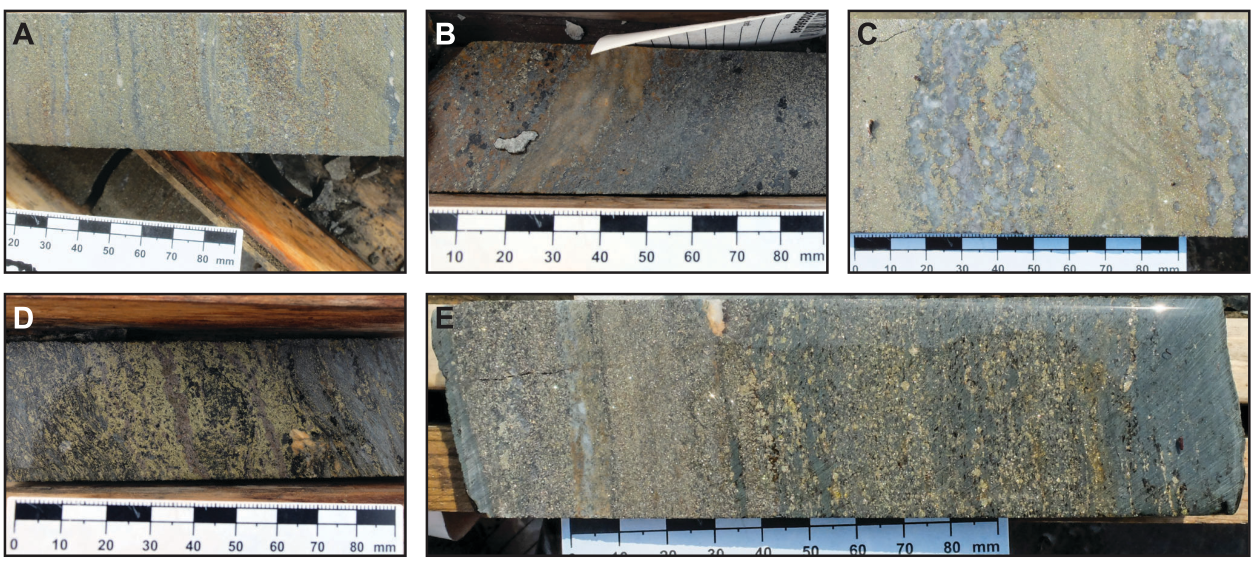

Figure 4.4. Replacement textures in massive sulfide mineralization at the ABM deposit. (A) Massive pyrite-sphalerite mineralization with remnant lapilli clasts with quartz crystals; clasts are white mica-chlorite altered; K15-274, 92 m downhole. (B) Pyrite replacing white mica-altered contact of felsic flow; K15-236, 97 m downhole. (C) Massive pyrite-sphalerite and minor chalcopyrite replacing a felsic flow along perlitic fractures; K15-200, 143 m downhole. (D) Banded pyrite-chalcopyrite-pyrrhotite mineralization with associated black chlorite replacing white mica-chlorite altered felsic volcaniclastic rocks; K15-286, 127 m downhole. (E) Pyrite-sphalerite mineralization with minor chalcopyrite replacing chlorite altered felsic volcaniclastic rocks; K15-235R, 140 m downhole. Scale in all photos is in millimetres.

4.6.2.1 Pyrite-sphalerite assemblage (Assemblage 1)

The pyrite-sphalerite assemblage is most common in the massive sulfide lenses and comprises ~45-50 vol. % of the total massive sulfide mineralization at the ABM deposit. The assemblage typically occurs on the lens margins (Fig. 4.5) and has sharp contacts with the surrounding altered rocks. Contacts with other mineralization assemblages are commonly gradational, although sharp contacts with pyrrhotite-rich intervals occur locally (Fig. 4.6A). Pyrite-sphalerite assemblages are commonly banded, with centimeter to decimeter scale bands that vary in composition (dominantly pyrite, sphalerite, barite, or carbonate mineral bands) and/or grain size (Fig. 4.6B). Pyrite is the dominant sulfide in this assemblage, locally occurs in massive intervals and is very fine- to relatively coarse-grained (up to millimetre scale) and locally has buckshot textures (Fig. 4.6B). Sphalerite is commonly dark red to brown and fine-grained. Other sulfide minerals (galena, chalcopyrite, arsenopyrite, tennantite-tetrahedrite) and rare magnetite occur in medium to coarse-grained patches, locally associated with gangue minerals or remnant clasts, and/or in bands with sphalerite. Barite is the most common gangue mineral and is present as diffuse layers within the mineralization (Fig. 4.6C). Locally, euhedral grains of Ba-rich feldspar occur (Fig. 4.6D); hyalophane (K-Ba-feldspar) is more common than celsian (Ba-feldspar), however, celsian can be replaced by hyalophane along fractures, or rarely, both Ba-rich feldspars replace and/or overgrow K-feldspar. Rare cassiterite occurs as very fine-grained (<10 μm) anhedral grains that are replaced along contacts by stannite (Fig. 4.6E). Remnant white mica and/or chlorite-altered lapilli-sized clasts (Fig. 4.4A) that are locally quartz-rich or replaced by carbonate occur within this assemblage. Clasts are aligned in bands concordant with the sulfide-defined banding where most abundant (Fig. 4.4A, D-E).

4.6.2.2 Pyrite-chalcopyrite-magnetite-pyrrhotite assemblage (Assemblage 2)

This assemblage comprises roughly 35-40 % of the total massive sulfide mineralization at the ABM deposit. Within individual massive sulfide lenses, the assemblage commonly occurs in the centre of the lenses, surrounded by assemblages 1 and 3 (Fig. 4.5). Contacts between the assemblages are typically gradational over 10-50 cm, with a modal increase in chalcopyrite and/or magnetite towards assemblage 2. The assemblage is commonly banded, with centimetre to

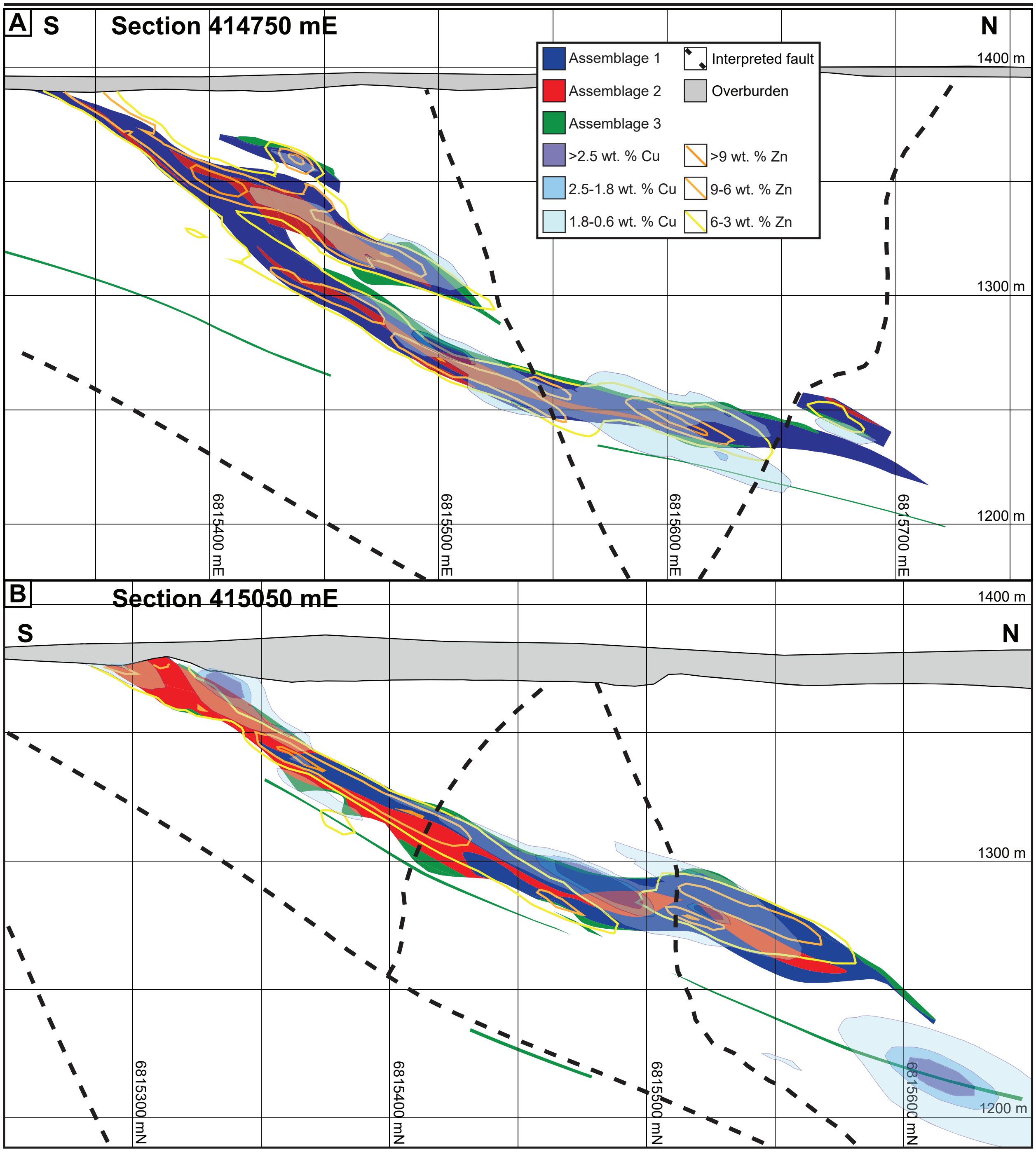

Figure 4.5. Cross sections through the eastern part of the ABM zone showing the distribution of mineralization assemblages and of Cu and Zn values. (A) Section along the line 414750 mE looking west. (B) Section along the line 415050 mE looking west.

decimetre-scale bands of pyrite, chalcopyrite, sphalerite, pyrrhotite, and locally magnetite (Fig. 4.6F). There are also intervals with abundant chalcopyrite and/or pyrrhotite that are commonly massive (Fig. 4.6G). The bands vary in grain size, but where coarse, pyrite commonly displays a buckshot texture. Anhedral fine-grained chalcopyrite commonly occurs as patches and stringers, or in bands with pyrite and pyrrhotite. Magnetite is euhedral to subhedral, up to 0.5 cm in size and occurs as patches or centimetre-scale bands of individual magnetite grains. Fine-grained to very fine-grained pyrrhotite occurs in bands and patches, commonly associated with chalcopyrite. Relict clasts are typically quartz-rich and relatively less common than in assemblage 1. Chlorite is the most common gangue mineral that replaces remnant clasts within the assemblage and occurs as euhedral black grains, likely pseudomorphs after cordierite or earlier alteration minerals (Fig. 4.6H).

4.6.2.3 Chalcopyrite-pyrrhotite-pyrite stringer assemblage (Assemblage 3)

Chalcopyrite-pyrrhotite-pyrite stringers occur within intervals of pervasive chlorite alteration and comprise ~10-15 % of the total mineralization. The most common sulfide minerals are chalcopyrite, pyrite and pyrrhotite, with minor sphalerite or galena, and rare discrete magnetite grains or patches. Carbonate minerals and quartz are associated locally with the sulfide minerals in bands and patches. In places where chalcopyrite is most abundant, singular grains or clusters of coarse-grained euhedral cordierite occur; in thin section, cordierite is replaced by a mixture fine-grained calcite and chlorite. This mineralization assemblage occurs at the contacts of the massive sulfide lenses (Fig. 4.5), or, less commonly, it transitions gradually into the pyrite-chalcopyrite-magnetite-pyrrhotite assemblage with decreasing chlorite content. The assemblage can also transition gradually to background pervasive chlorite alteration distal from the massive sulfide lenses. Assemblage intervals are commonly under 1.5 m thick, but locally, in the absence of other mineralization assemblages, they extend up to 4 m in true thickness. The matrix comprises very fine-grained chlorite, whereas sulfide minerals associated with lesser gangue minerals (carbonate minerals, quartz) occur as bands or stringers on a centimetre to decimetre scale (Fig. 4.6I).

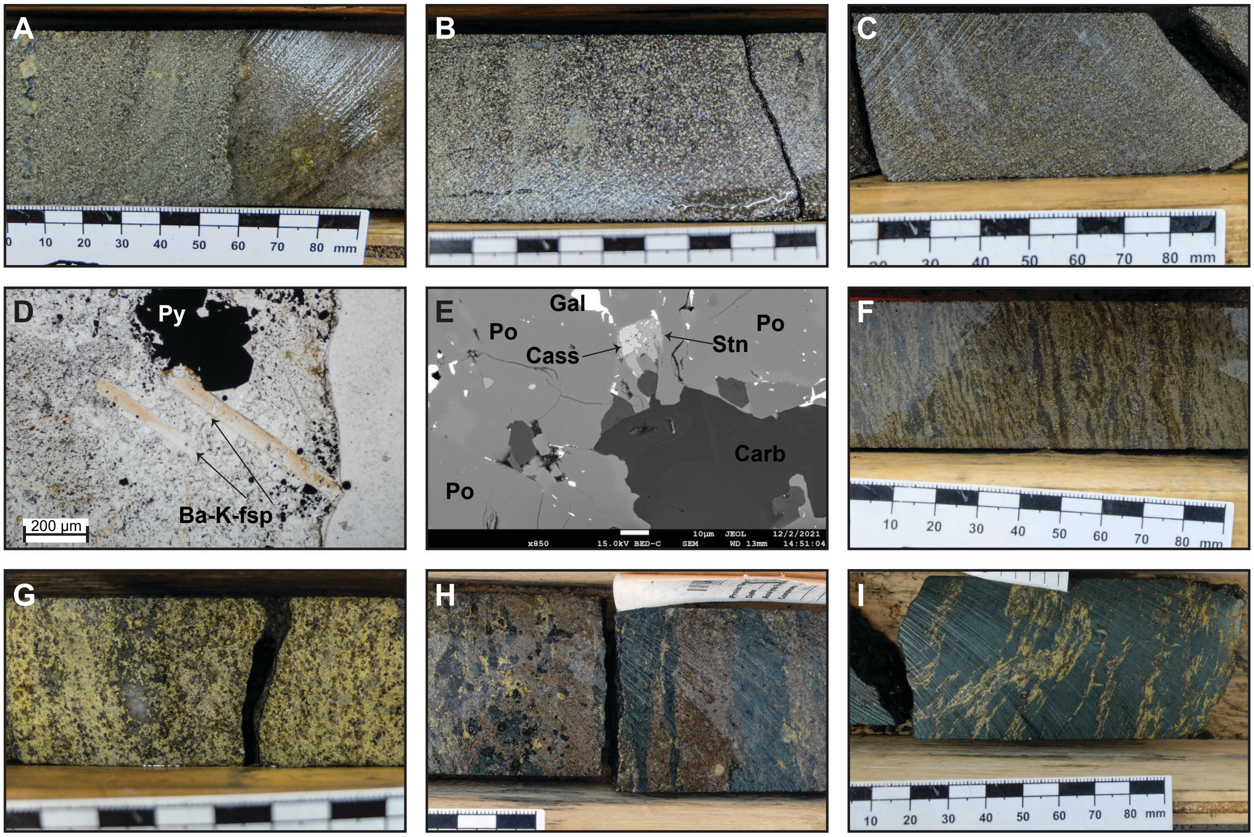

Figure 4.6. Mineralization assemblages at the ABM deposit. (A) Pyrite-sphalerite with minor chalcopyrite overprinting fine-grained section with massive pyrrhotite; K15-229, ~75 m downhole. (B) Buckshot pyrite texture in pyrite-sphalerite mineralization with abundant galena; K15-260, ~169 m downhole. (C) Pyrite-sphalerite assemblage with abundant associated barite; K15-232, 161 m downhole. (D) Elongated prismatic crystals of Ba-rich feldspar in carbonate-barite matrix with disseminated fine-grained sulfides and clusters of euhedral pyrite grains; K15-236, 86.35 m downhole. (E) Rare cassiterite with mantle of stannite enclosed in pyrrhotite, in pyrite-sphalerite assemblage; K15-339, 165.3 m downhole. (F) Banded pyrite-chalcopyrite-magnetite-pyrrhotite assemblage, magnetite appears as dark discontinuous lenses within pyrite-pyrrhotite bands, chalcopyrite minor; K15-274, 62 m downhole. (G) Massive pyrite-chalcopyrite-magnetite-pyrrhotite assemblage, minor associated black chlorite in matrix, rare quartz patch; K15-273, ~92 m downhole. (H) Pyrrhotite-chalcopyrite bands with black chlorite pseudomorphs replacing pervasively chlorite altered felsic volcaniclastic rocks; K17-422, 150 m downhole. (I) Chalcopyrite-pyrite stringers in pervasively chlorite altered felsic volcaniclastic rocks; K17-422, 159 m downhole. Scale in all photos except for (D) and (E) is in millimetres. Ba-K-fsp = Ba-K-feldspar, Carb = carbonate, Cass = cassiterite, Gal = galena, Po = pyrrhotite, Stn = stannite.

4.6.3 Mineral textures

Minerals listed in the previous section (except for barite, Ba-rich silicate minerals, Sn-minerals, and less common sulfosalts) occur across all mineralization assemblages, even though they might be too fine-grained and/or occur in abundances too low to be observed in drill core. In the following section, mineral textures will be described based on their assumed origin (and through literature comparison), including those that reflect: (1) relict primary textures, (2) replacement features, (3) modified textures due to post-VMS metamorphism and deformation, or (4) mixed or unknown origin.

4.6.3.1 Relict primary textures

Numerous primary textures preserved in the ABM deposit have features that are similar to modern SMS deposits (Ames et al., 1993; Grant et al., 2018) and those in well-preserved and relatively undeformed ancient VMS deposits (Eldridge et al., 1983; Martin et al., 2021). In assemblage 1, banding and finer-grained laminations interpreted to be primary occur as millimetre to centimeter layers defined by varying sulfide mineralogy and grain size (Fig. 4.7A). Within these layers, fine-grained pyrite and to a lesser extent arsenopyrite and sphalerite show relict primary textures, including rare round clusters of fine-grained to very fine-grained pyrite and arsenopyrite resembling framboids that are up to 50 µm across (Fig. 4.7B) and are associated with galena and/or sphalerite. Similarly, fine-grained pyrite grains commonly constitute the cores of atoll textures (Fig. 4.7C). In these atolls, very fine-grained pyrite and/or arsenopyrite at the core is replaced/surrounded by galena and/or tennantite-tetrahedrite, which is surrounded by sphalerite with only minor very fine-grained pyrite, and with a rim composed of coarse euhedral pyrite grains. These atolls locally fuse together or with spongiform pyrite and/or arsenopyrite or are surrounded by gangue minerals in sulfide-poor bands or patches. Spongiform pyrite and arsenopyrite most commonly contain interstitial galena, sphalerite, and minor chalcopyrite and/or tennantite-tetrahedrite, and locally form bands or nodules within the massive mineralization (Fig. 4.7D). The spongiform pyrite-arsenopyrite bands commonly have margins where the spongiform sulfide minerals are overgrown by coarser euhedral pyrite (Fig. 4.7E). Locally, very fine-grained elongated arsenopyrite grains occur as skeletal intergrowths in sphalerite (Fig. 4.7F).

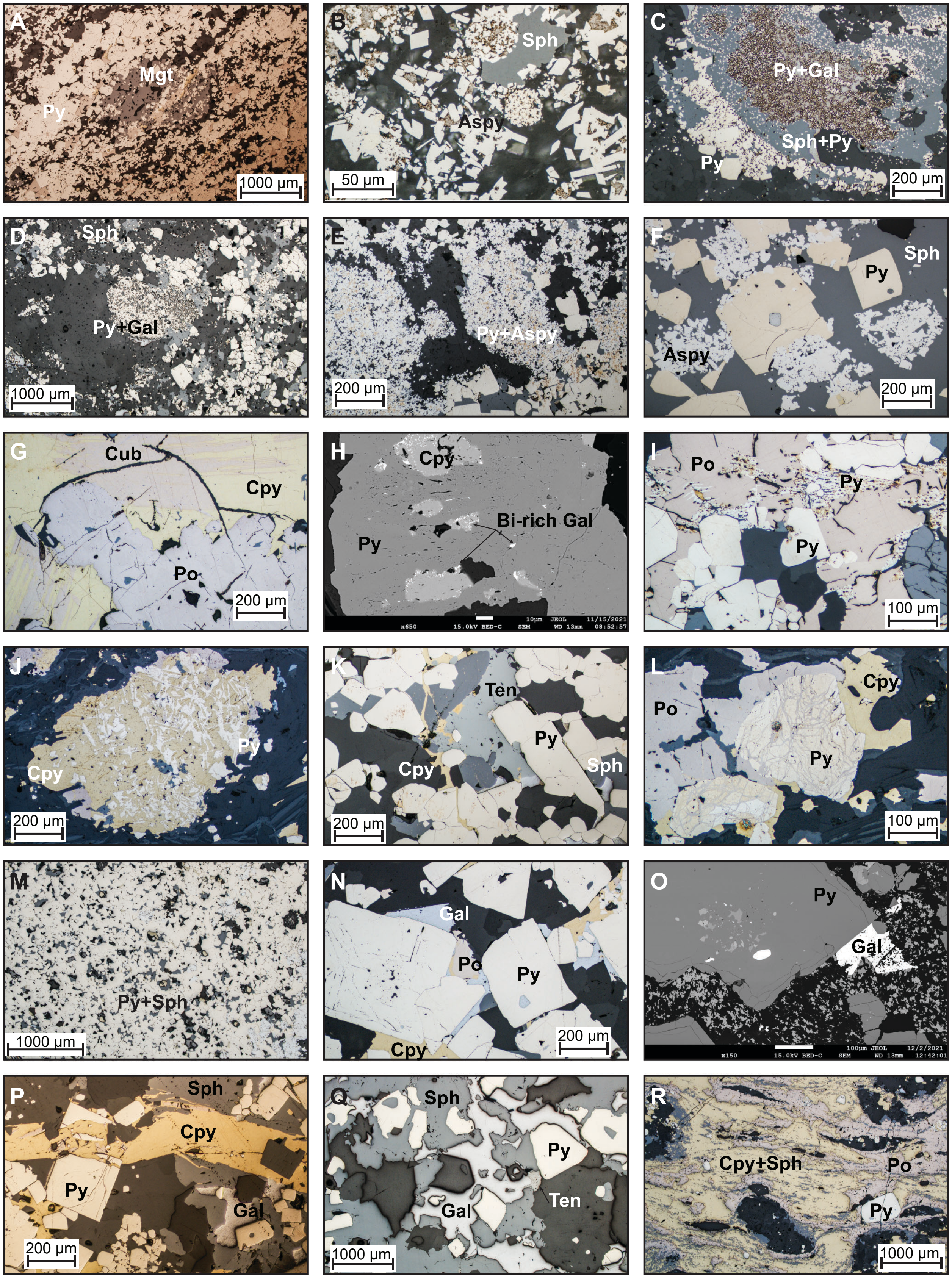
A
Mgt
Py
1000 µm
B
Sph
Aspy
50 µm
C
Py+Gal
Sph+Py
Py
200 µm
D
Sph
Py+Gal
1000 µm
E
Py+Aspy
200 µm
F
Sph
Py
Aspy
200 µm
G
Cub
Cpy
Po
200 µm
H
Cpy
Bi-rich Gal
Py
I
Po
Py
Py
100 µm
J
Py
Cpy
200 µm
K
Ten
Py
Cpy
Sph
200 µm
L
Cpy
Po
Py
100 µm
M
Py+Sph
1000 µm
N
Gal
Po
Py
Cpy
200 µm
O
Py
Gal
P
Sph
Cpy
Py
Gal
200 µm
Q
Sph
Py
Ten
Gal
1000 µm
R
Cpy+Sph
Po
Py
1000 µm

Figure 4.7. Mineral textures occurring at the ABM deposit. (A) Bands with varying grain size of pyrite, minor pyrrhotite, chalcopyrite, and magnetite present; K15-260, 155.8 m downhole. (B) Incipiently recrystallized framboids comprising euhedral to subhedral arsenopyrite grains, infilled by galena; K15-321, 237.9 m downhole. (C) Atoll texture, pyrite at the core of the atolls is engulfed by galena, surrounded by sphalerite with only minor very fine-grained pyrite the rim comprises euhedral pyrite grains coarsening outwards; K15-236; 86.4 m downhole. (D) Spongiform pyrite with minor associated galena and sphalerite; K15-216, 167.2 m downhole. (E) Spongiform pyrite and arsenopyrite, minor associated sphalerite, overgrown euhedral to subhedral pyrite; K15-231. 71 m downhole. (F) Skeletal arsenopyrite in sphalerite locally overgrowing euhedral pyrite; K15-290, 79 m downhole. (G) Exsolution lamellae of cubanite in chalcopyrite, earlier pyrrhotite with minor sphalerite; K15-236, 82.4 m downhole. (H) Minute Bi-rich galena exsolutions in chalcopyrite replacing pyrite; K15-204, 122.6 m downhole. (I) Fine-grained "ribbed" pyrite containing minute inclusions of Fe-oxides and Fe-carbonates replaces pyrrhotite, overprinted by euhedral pyrite; K15-231, 63.1 m downhole. (J) Skeletal pyrite replaced by chalcopyrite; K15-286, 127.1 m downhole. (K) Chalcopyrite disease in sphalerite; K15-229, 63.6 m downhole. (L) Pyrite replaced along fractures by pyrrhotite, K15-286, 127.1 m downhole. (M) Foam texture, euhedral to subhedral fused pyrite grains, minor arsenopyrite, sphalerite, chalcopyrite, and interstitial galena; K15-290, 79 m downhole. (N) Euhedral pyrite grains with fine-grained non-sulfide inclusions in the cores; K15-339, 171 m downhole. (O) Fine-grained non-sulfide inclusion in the core of euhedral pyrite; K15-299, 116 m downhole. (P) Fractured euhedral pyrite grain partly replaced by chalcopyrite; K15-339, 171 m downhole. (Q) Subhedral pyrite grains engulfed by sphalerite, galena and minor tennantite-tetrahedrite; K15-260, 171.8 m downhole. (R) Rounded euhedral grains of pyrite in massive chalcopyrite with sphalerite and pyrrhotite schlieren; K15-292, 239.7 m downhole. Aspy = arsenopyrite, Cpy = Chalcopyrite, Cub = Cubanite, Gal = Galena, Po = Pyrrhotite, Py = Pyrite, Sph = Sphalerite, Ten = Tennantite.

In assemblages 2 and 3, relict primary textures are more subtle than in the pyrite-sphalerite assemblage. Rarely, exsolution lamellae of cubanite are preserved in chalcopyrite (Fig. 4.7G). Locally, chalcopyrite overprints large subhedral pyrite grains (>500 μm) and contains minute (<2 μm) Bi-Se-bearing galena inclusions on the contacts with pyrite (Fig. 4.7H), similar to what has been observed in chalcopyrite-rich chimneys in SMS deposits and which are interpreted to have formed due to rapid quenching of hydrothermal fluids (Berkenbosch et al., 2012).

4.6.3.2 Replacement textures

Replacement textures interpreted to be from zone refining and primary VMS hydrothermal processes are ubiquitous in assemblages 1 and 2. During continued zone refining, grain size coarsens (Eldridge et al., 1983). Similarly, in all assemblages, fine-grained anhedral pyrite is overgrown by coarser euhedral pyrite grains. Common throughout all the assemblages is the conversion of pyrrhotite into pyrite along cleavage planes, fractures, and grain boundaries (Fig. 4.7I). A previous study documented that fine-grained pyrite replacing pyrrhotite commonly contains minute inclusions of Fe-oxides and Fe-carbonates (Murowchick 1992). In assemblage 2, pyrite replaced by chalcopyrite commonly displays skeletal texture (Fig. 4.7J). Locally, minute chalcopyrite inclusions occur in anhedral sphalerite and in places they are aligned (Fig. 4.7K), which is indicative of chalcopyrite disease, a replacement feature common during the primary stages of VMS-deposits (Barton and Bethke, 1987). Also, in assemblage 2 samples, networks of meandering fractures occur in euhedral to subhedral pyrite grains (>200 μm) and are filled by pyrrhotite (Fig. 4.7L), similar textures have been observed in Kuroko-type deposits (Eldridge et al., 1983).

4.6.3.3 Metamorphic textures

The ABM deposit has reached greenschist facies metamorphic grade and was also affected by deformation locally associated with the reactivation of synvolcanic faults (van Olden et al., 2020). In all assemblages, bands and pyrite-rich zones commonly exhibit foam textures with 120° angles between the euhedral grains, where pyrite grains are annealed (Fig. 4.7M) interpreted to be from the impacts of increasing temperature and pressure (Craig and Vokes, 1992). Other sulfide minerals, originally surrounding the pyrite grains, occur as inclusions within the annealed mass, here interpreted to have been trapped during metamorphic pyrite growth (Fig. 4.7M). In all assemblages, coarser euhedral pyrite grains (>100 μm) locally display inclusion-free rims and inclusion-rich cores (Fig. 4.7N, O) that were likely originally spongiform and were overgrown and filled during continued hydrothermal activity and/or metamorphism. Locally, pyrite displays a cataclastic texture with other sulfide minerals filling the cracks in the pyrite grains. Magnetite grains are commonly fractured as well but are not infilled by other sulfide minerals as commonly as fractured pyrite; minor finer pyrite grains locally overgrow magnetite. Euhedral pyrite grains and to a lesser degree other sulfides (pyrrhotite, sphalerite) are commonly fractured, and the fractures are filled by chalcopyrite (Fig. 4.7P). In the Krakatoa zone, in proximity to reactivated faults, euhedral to subhedral grains of pyrite and carbonate clasts are interpreted to have rotated in massive chalcopyrite with sphalerite and pyrrhotite schlieren, or in massive sphalerite with galena schlieren (Fig. 4.Q, R).

4.6.3.4 Textures of unknown origin

In assemblages 1 and 2, there are 100-300 µm (up to 1 mm) clusters of intergrown minerals that have uncommon mineral associations and are of uncertain origin.

In assemblage 1, the clusters have two mineral associations: (1) galena-tennantite-tetrahedrite; and (2) chalcopyrite-tennantite-tetrahedrite. The first association occurs as anhedral patches of galena with irregular patches of tennantite-tetrahedrite and other lesser sulfosalts (e.g., boulangerite). These intergrowths have a “symplectite-like” appearance, and the patches commonly appear to be later than or filling the surrounding pyrite and sphalerite grains (Fig. 4.8A). The second association displays anhedral patches of chalcopyrite in tennantite-tetrahedrite (Fig. 4.8B). These occur where chalcopyrite and tennantite-tetrahedrite coexist, associated with galena, and fractured euhedral pyrite. Previous authors (Bortnikov et al., 1993; Cook, 1996) described similar textures and attributed them to decomposition due to changing As/Sb activities in the hydrothermal fluid, although the occurrence of these textures locally associated with fractured pyrite grains at the ABM deposit suggests the possibility of metamorphic origin (Miller and Craig, 1983; Brueckner et al., 2016).

In assemblage 2, clusters of intergrown minerals consist of galena (Se- and/or Bi-rich), pyrrhotite, Bi minerals (native Bi, bismuthinite), minor tetrahedrite-freibergite, Pb-rich sulfosalts (bournonite, boulangerite, meneghinite), Sb-rich sulfosalts (gudmundite, ullmannite), and rare Ag-Hg-Sb minerals (dyscrasite). The sulfosalts that are not tetrahedrite group are fine- to very fine-grained and occur as anhedral grains within galena and/or pyrrhotite. Locally, the sulfosalts are intergrown with the sulfides, but have a less distinct “symplectite-like’ appearance (Fig. 4.8D-I). In clusters larger than 100 µm, parallel bands of sulfosalts, likely crystallographically oriented, occur within galena (Fig. 4.8C), and some clusters show a mineralogical zonation (Fig. 4.8J-P). The more complex of these intergrowths occur in the Krakatoa zone (Fig. 4.8C, G-P), although they show lower contents of Se and Bi than the clusters in the ABM zone (Fig. 4.8D-I).

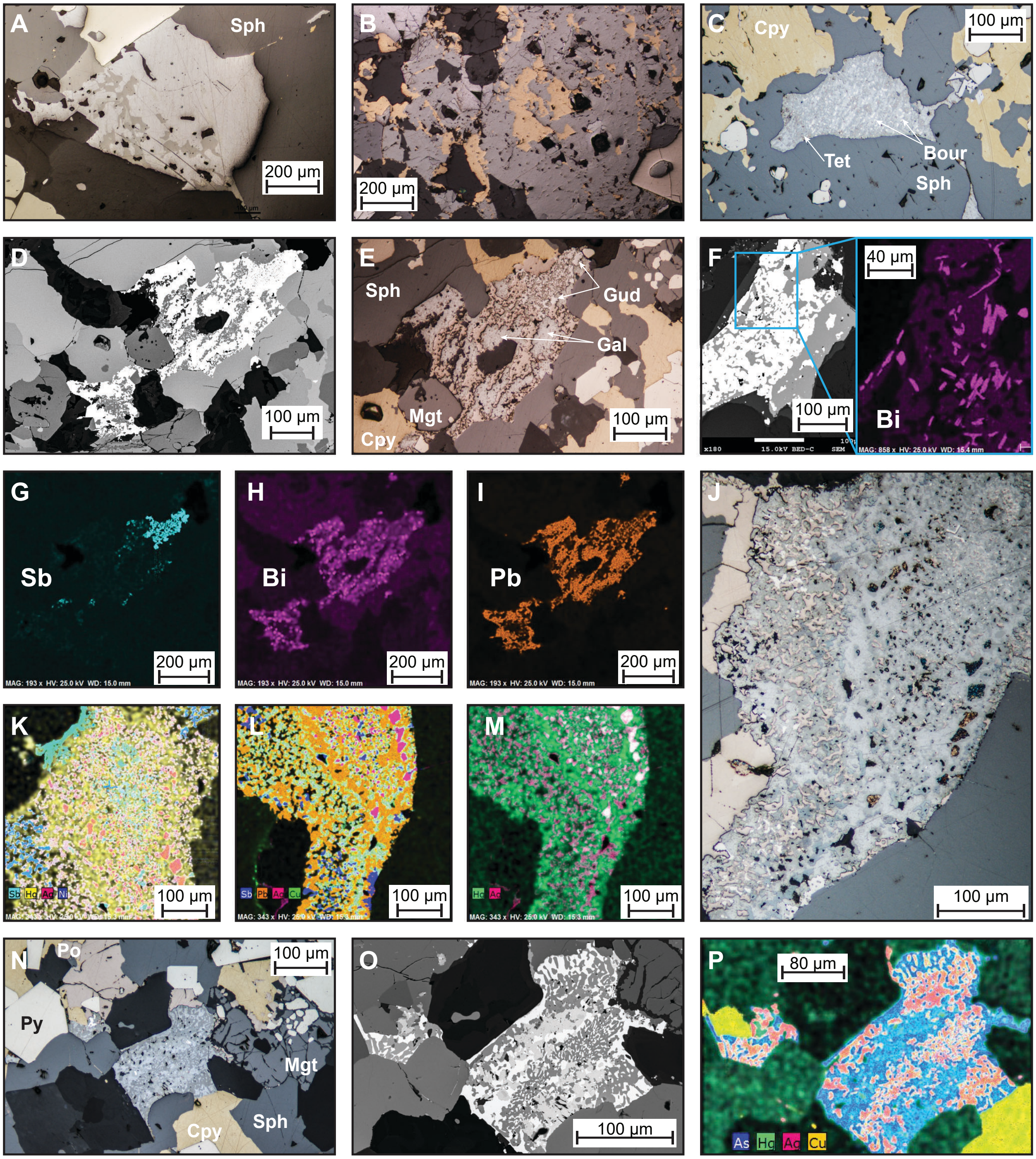

Figure 4.8. Symplectic intergrowths of unknown origin in the mineralization at the ABM deposit. (A) Galena with associated tennantite and tetrahedrite; K15-303, 212.8 m downhole. (B) Anhedral chalcopyrite in tennantite, minor associated galena; K15-231, 56. 1 m downhole. (C) Semi-parallel bands of meneghinite, bournonite, and tetrahedrite in myrmekitic intergrowth; K15-292, 239.7 m downhole. (D) Back-scatter electron (BSE) image of symplectic intergrowth comprising pyrrhotite, Bi- and Se-enriched galena and gudmundite; K15-231, 63.1 m downhole. (E) Reflected light image of (D). (F) BSE image of a symplectic intergrowth comprising Se- and Bi-enriched galena and pyrrhotite,

with a close up of an EDX elemental map showing the distribution of Bi as discrete patches within the intergrowth; K15-204, 112.6 m down hole. (G, H, I) EDX elemental maps showing the distribution of Sb, Bi, and Pb, respectively, in the symplectic intergrowth pictured in (D) and (E). (J) Symplectic intergrowth showing mineralogical and elemental zonation comprising pyrrhotite, galena, freibergite, dyscrasite, meneghinite, and gudmundite; K15-292, 239.7 m downhole. (K) Composite image of EDX elemental maps of Sb, Hg, Ag, and Ni for the top portion of (J). (L) Composite image of EDX elemental maps of Sb, Pb, Ag, and Cu for the bottom portion of (J). (M) Composite image of EDX elemental maps of Hg and Ag for the bottom portion of (J). (N) Symplectic intergrowth comprising freibergite, meneghinite, boulangerite, and galena; K15-339, 171 m downhole. (O) BSE image of (N). (P) Composite image of EDX element maps of As, Hg, Ag and Cu for (N). Bou = bournonite, Cpy = Chalcopyrite, Gal = Galena, Gud = Gudmundite, Po = Pyrrhotite, Py = Pyrite, Sph = Sphalerite, Tet = Tetrahedrite.

4.6.3.5 Paragenesis

Despite overprinting relationships, an apparent mineral paragenesis can be determined from preserved primary and replacement textures and their inter-relationships (Fig. 4.9). Assemblages 2 and 3 display similar relationships between the most abundant minerals and based on the observations from drill core, assemblage 2 overprints assemblage 1. The “apparent” paragenesis presented here is consistent across the ABM deposit.

In assemblage 1 (Fig. 4.9A), major pyrite formation (fine-grained, commonly with atoll and spongiform textures) is followed by galena and arsenopyrite precipitation, formation of barite and Ba-rich feldspar, tetrahedrite group minerals, and co-precipitation of abundant sphalerite with lesser chalcopyrite. The latest minerals to form are calcite and Fe-rich carbonate. In assemblages 2 and 3 (Fig. 4.9B), the earliest observed mineral accompanying the silicate gangue minerals is magnetite. Magnetite grains are commonly sub- to euhedral with fractures filled by gangue minerals and overgrown by fine grained pyrite (Fig. 4.7A). The early formed sulfide minerals are dominated by pyrite and pyrrhotite, followed by the precipitation of galena, and abundant chalcopyrite with lesser coprecipitated sphalerite.

Figure 4.9. Mineralization paragenesis at the ABM deposit. (A) Paragenesis for assemblage 1. (B) Combined paragenesis of assemblages 2 and 3. Black color of bars indicates modal abundances >30 %, dark grey indicates modal abundances between 30-10 %, and light grey indicates modal abundaces <10 %.

4.6.4 Metal distribution and zonation in massive sulfide mineralization

Economically significant metals at the ABM deposit are Zn, Pb, Cu, Ag, and Au. Other metals and metalloids occurring at elevated concentrations within the mineralized zones are Fe, As, Sb, Se, Bi, Hg, Co, Ni, Mo, Tl, Cd, Sn, In, and Mn. The distribution and abundances of these elements reflect which sulfide minerals occur within the massive sulfide lenses. Although the above-described assemblages control the lens-scale enrichment of these metals, all assemblages may carry economic abundances of Cu, Zn, and Pb (van Olden et al., 2020).

Within the massive sulfide mineralization in the ABM zone, Cu-rich zones (>0.9 wt. % Cu) are at the centre of the mineralized lenses and commonly extend to the upper contacts of the lenses (Fig. 4.2B, 4.3, 4.10). Even where Cu-rich zones overlap with elevated Zn (>6 wt. % Zn), the Zn-rich zones occur at the base of the mineralized lenses and extend further along the lenses (Fig. 4.2B, 4.10). In the Krakatoa zone, the Cu-rich zones are vertically more limited than in the ABM zone and do not reach the upper contacts of the lenses (Fig. 4.3). Across both zones, Pb is strongly associated with Zn but there is no distinguishable zonation developed between the two elements on a deposit scale (Fig. 4.3, 4.10). Zones with elevated Ba (>1 wt. % Ba) locally overlap with and

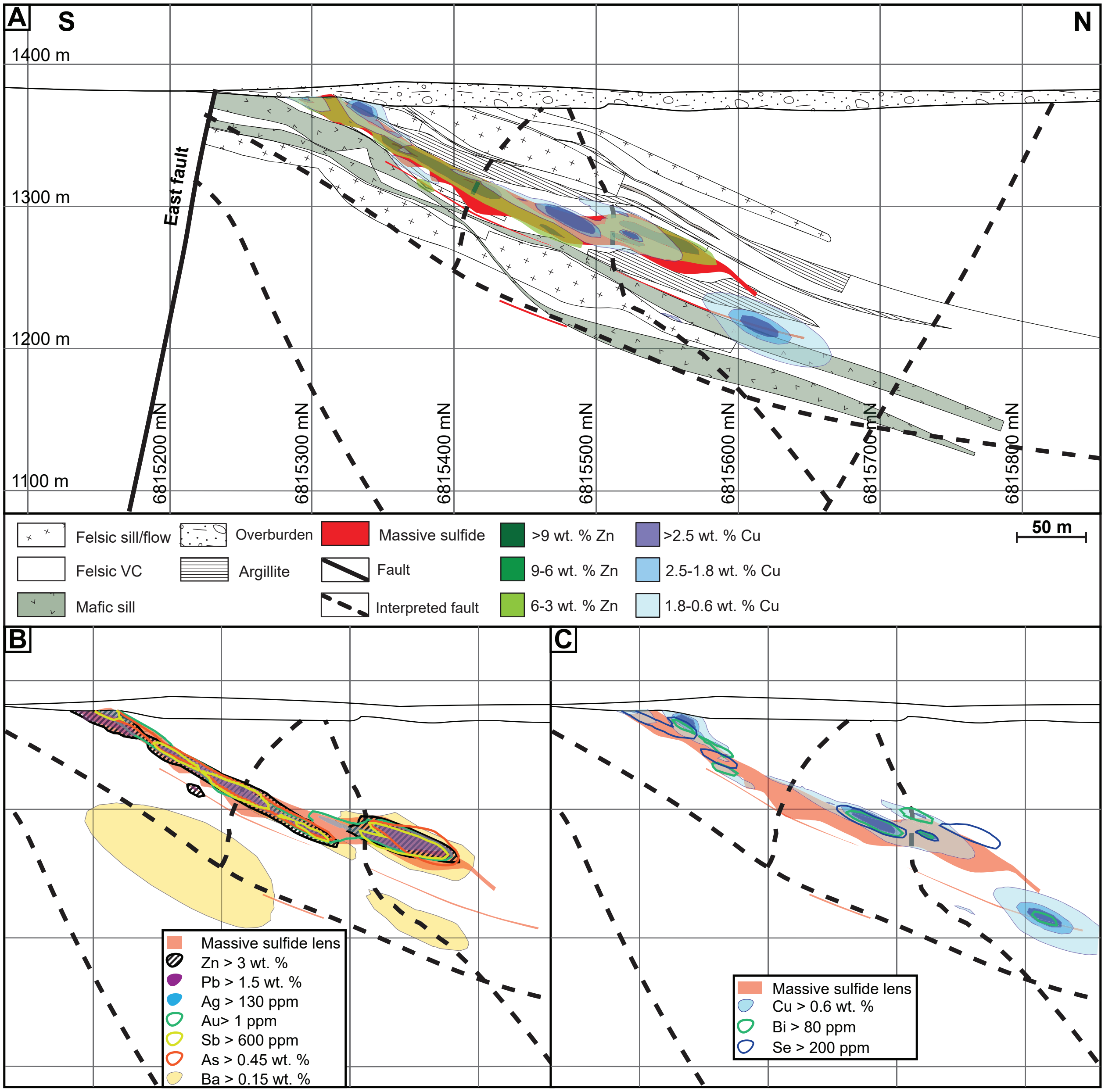

Figure 4.10. Cross section through the eastern part of the ABM zone along the line 415050 mE looking west. (A) Simplified lithostratigraphy of the ABM zone with an overlay showing the distribution of elevated Zn and Cu. (B) Distribution of the Zn-Pb-Ag-Au-Sb-As element assemblage. (C) Distribution of the Cu-Bi-Se element assemblage.

extend beyond the limits of Zn-Pb-rich zones (Fig. 4.10), with anomalous Ba values (>0.15 wt. % Ba) extending beyond the massive sulfide mineralization into the altered host rocks (Denisová and Piercey, 2022).

In assemblage 1, sphalerite is the prevalent Zn-bearing mineral. Cadmium and Hg commonly substitute in sphalerite and positively correlate with Zn in assay data (Fig. 4.11A, B). Zinc and Pb also have a broad positive correlation (Fig. 4.11C). Galena is the primary Pb-bearing mineral and occurs in significant amounts within assemblage 1 and only Ag shows a significant positive correlation with Pb (Fig. 4.11D) in this assemblage. These correlations are reflected in the spatial distribution of the elements within the massive sulfide lenses, where numeric models representative of elevated values of Zn, Pb, and Ag overlap (Fig. 4.3, 10). Arsenic, Sb, and Ba show a spatial correlation with elevated Zn, Pb, and Ag (Fig. 4.3, 10), but not a distinct correlation in the assay dataset. Variations in sample mineralogy can explain the observed distribution of As, Sb, and Ba within assemblage 1, which contains greater amounts of arsenopyrite, tennantite-tetrahedrite and barite, which preferentially host these elements, compared to the other mineralization assemblages.

In assemblage 2, chalcopyrite is the dominant residence site of Cu. Bismuth, Co, and Se show a positive correlation with Cu in the assay data (Fig. 4.11E-G), and models representing elevated values of Cu, Se, and Bi overlap across the ABM deposit (Fig. 4.3, 4.10). Magnetite occurs in minor amounts within the assemblage (<10 modal %) and pyrrhotite is locally more abundant than pyrite. Both are magnetic, which suggests that pyrrhotite is monoclinic (Kissin and Scott, 1982). Numeric models of magnetic susceptibility values ($>30 \times 10^{-3}$SI units) that represent mineralization with minimum 5 modal % magnetite and/or pyrrhotite combined overlap with modelled lenses based on visual logging of magnetite content (Fig. 4.12). These units commonly occur in the cores of individual massive sulfide lenses.

Assemblage 3 shows overall higher contents of Cu, Bi, and Se, compared to the other two assemblages, and contains lower Ba, Pb, Zn, Ag, Au, Hg, and As values.

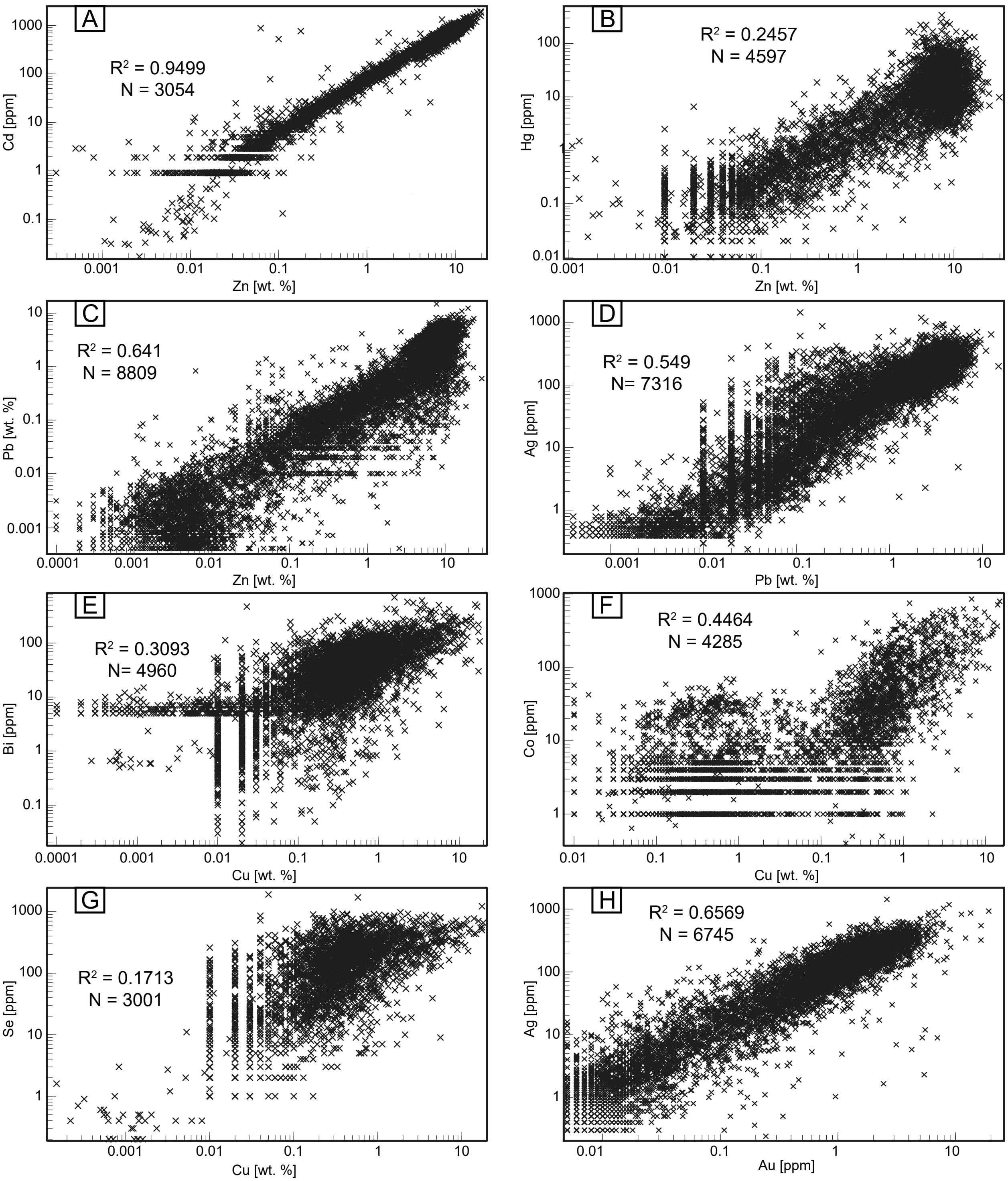

Figure 4.11. Plots showing correlations between metals at the ABM deposit. “Streak” artifacts at low abundances result from different dection limits and decimal point rounding as values approach detection limits. Data sourced from BMC Minerals assay database. (A) Zn vs. Cd. (B) Zn vs. Hg. (C) Zn vs. Pb. (D) Pb vs. Ag. (E) Cu vs. Bi. (F) Cu vs. Co. (G) Cu vs. Se. (H) Au vs. Ag.

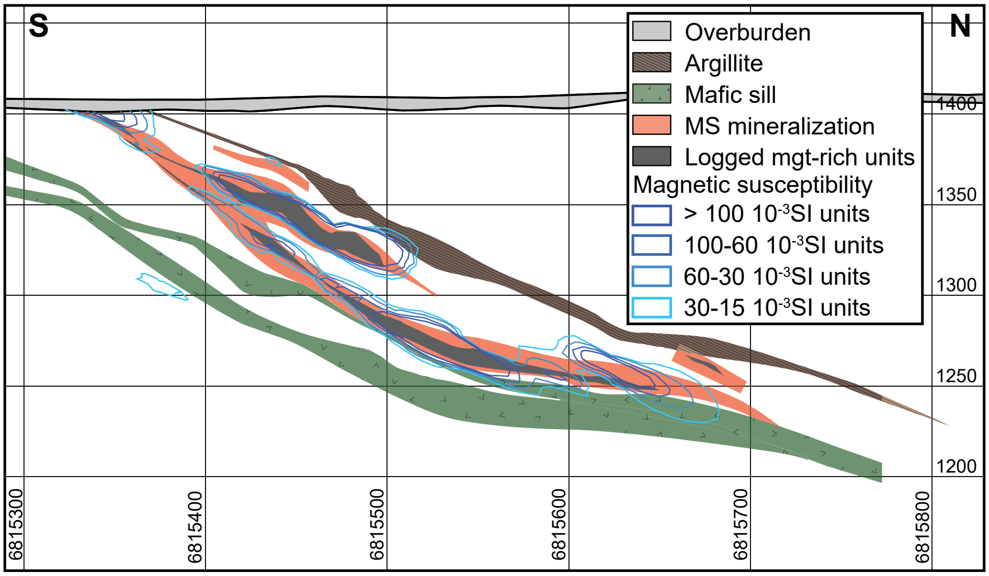

Figure 4.12. Cross section through the western part of the ABM zone along the line 414750 mE looking west, showing simplified lithostratigraphy with an overlay of modelled units with visually logged magnetite and the distribution of magnetic susceptibility.

4.6.4.1 Element associations

Principal component analysis (PCA) using a correlation matrix performed on log-normalized bulk data shows two major element associations. The first association comprises Zn-Pb-Ag-Au-Hg-As-Sb-Ba and has positive loadings of component 1 and negative loadings on component 2, whereas the second association, Cu-Bi-Se, has positive loadings on component 2 (Table 4.1). These associations correspond to the spatial distribution of the elements within the massive sulfide lenses (Fig. 4.3, 4.10). These element associations remain the same across the ABM and Krakatoa zones. An element association that correlates well spatially is Ag-Au-As-Sb. However, of these four elements, only Ag correlates with base metals (Zn, Pb) in the bulk data. The ratio of Ag to Au is ~100:1 (Fig. 4.11H), which is comparable to other VMS deposits (Mercier-Langevin et al., 2011). Numeric models representing elevated Ag and Au overlap together, and with zones representing elevated As, Sb, Zn and Pb values (Fig. 4.3, 4.10).

Table 4.1 Results of principal component analysis of available assay data (1732 samples).

	Component 1	Component 2	Component 3	Component 4
Eigenvalue	3.74	2.17	1.27	0.85
Variance %	34.00	19.72	11.55	7.71
Cumulative %	34.00	53.73	65.28	72.99
Zn (wt %)	0.64	0.28	0.58	0.15
Pb (wt %)	0.74	-0.06	0.45	0.35
Ag (ppm)	0.88	0.05	-0.15	0.26
Au (ppm)	0.77	0.15	-0.45	0.15
Hg (ppm)	0.62	-0.15	0.14	-0.46
As (ppm)	0.62	-0.11	0.10	-0.52
Sb (ppm)	0.70	-0.19	-0.42	0.04
Ba (wt %)	0.39	-0.40	-0.17	-0.25
Cu (wt %)	0.07	0.73	-0.47	0.00
Bi (ppm)	0.03	0.83	-0.01	-0.14
Se (ppm)	0.10	0.78	0.21	-0.21

4.6.5 Electron microprobe analysis results

The complete EPMA results are available in Appendix 8. The composition of the analyzed sulfide minerals is generally stoichiometric, but there is systematic variation in major and trace element composition of some minerals depending on their mineralization assemblage, paragenesis, or spatial distribution (ABM zone vs Krakatoa zone) that are described below.

4.6.5.1 Pyrite

The Fe and S content in pyrite varies between 43.9-47.9 wt. %, and 52.4-54.3 wt. %, respectively (Appendix 8.2). Elevated Co values in pyrite (>0.1 wt. % Co) occur in samples from assemblage 2 in the ABM zone (Fig. 4.13C). Samples with elevated As (>0.15 wt. % As) occur mostly in assemblage 1 in the ABM zone.

4.6.5.2 Arsenopyrite

Arsenic, Fe, and S content in arsenopyrite vary between 40.3-44.3 wt. % As, 34.3-37.0 wt. % Fe, and 19.1-22.7 wt. % S, respectively (Appendix 8.3). The highest values of Co (max 2.27 wt. %) occur in samples from assemblage 2 where arsenopyrite is relatively rare (Fig. 4.13E). Antimony (0.13-2.12 wt. %) and Zn (0.5-2.35 wt. %) are elevated in samples from assemblage 1. Arsenopyrite from assemblage 2 generally has low trace element contents, except for Co.

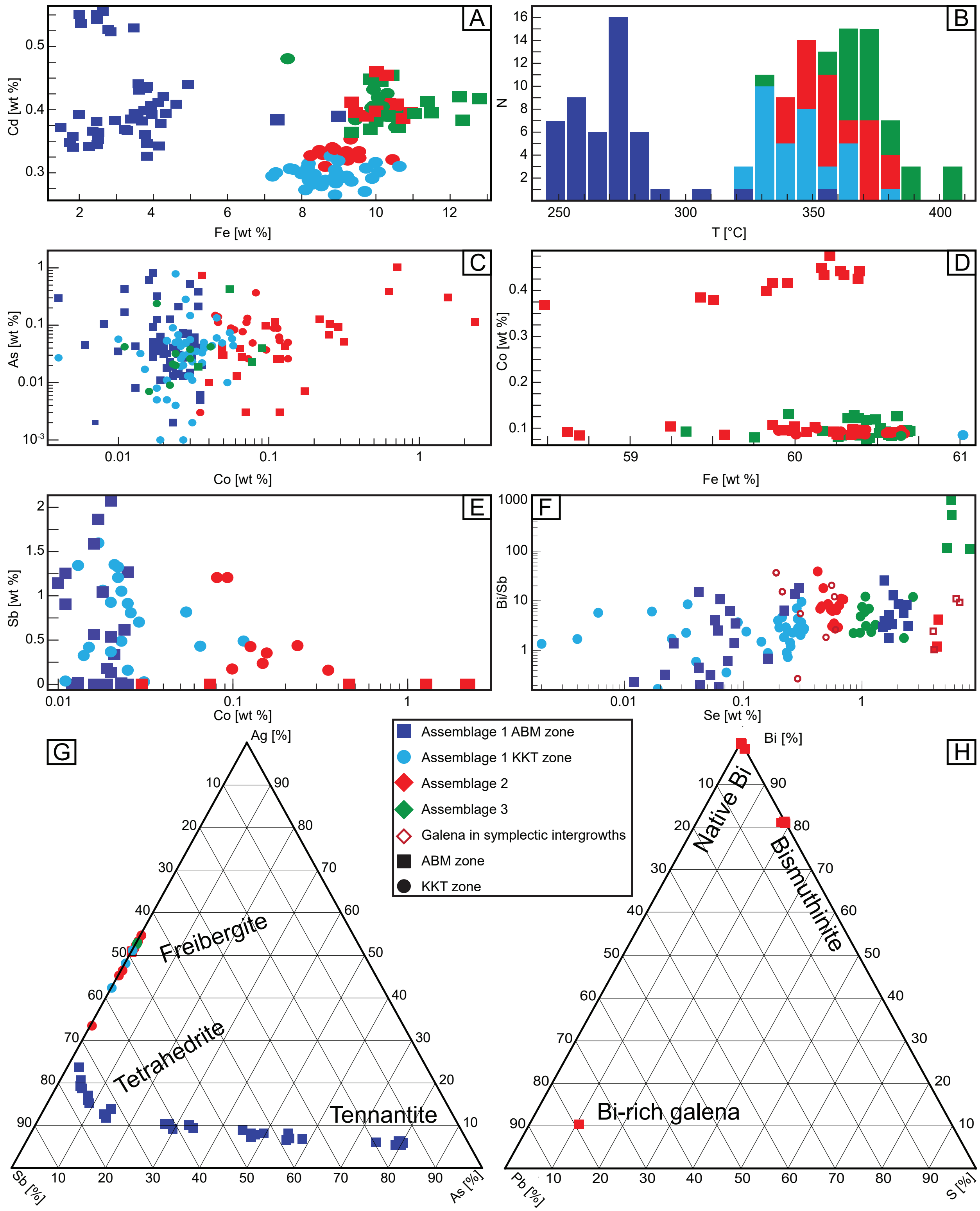

A
Cd [wt %]
Fe [wt %]
B
N
T [°C]
C
As [wt %]
Co [wt %]
D
Co [wt %]
Fe [wt %]
E
Sb [wt %]
Co [wt %]
F
Bi/Sb
Se [wt %]
G
Ag [%]
Sb [%]
As [%]
Freibergite
Tetrahedrite
Tennantite
Assemblage 1 ABM zone
Assemblage 1 KKT zone
Assemblage 2
Assemblage 3
Galena in symplectic intergrowths
ABM zone
KKT zone
H
Bi [%]
Pb [%]
S [%]
Native Bi
Bismuthinite
Bi-rich galena

Figure 4.13. Results of EPMA analyses. (A) Fe vs Cd (both in wt. %) in sphalerite. (B) Histogram showing the distribution of calculated temperatures of sphalerite precipitation using Fe/Zn ratios in a linear equation from Keith et al. (2014). (C) Co vs As (both in wt. %) in pyrite. (D) Fe vs Co (both in wt. %) in pyrrhotite. (E) Co vs Sb (both in wt. %) in arsenopyrite. (F) Se vs Bi/Sb (Se in wt. %) in galena. (G) Ternary diagram showing Ag, Sb and As distribution in tetrahedrite group minerals. (H) Ternary diagram showing Bi, Pb, and S distribution in Bi-rich minerals.

4.6.5.3 Pyrrhotite

The Fe and S content in pyrrhotite is between 58.7-60.3 wt. %, and 39.5-40.7 wt. %, respectively (Appendix 8.4). This range of compositions corresponds to monoclinic pyrrhotite (<46.9 at % Fe; Kissin and Scott 1982) and explains the weak magnetic properties of pyrrhotite from the ABM deposit. Pyrrhotite from sample Q721151 has significantly higher Co values (between 0.35-0.50 wt. % Co) similar to the pyrite from the same sample. All pyrrhotite has Co >0.05 wt. % (Fig. 4.13D).

4.6.5.4 Sphalerite

The Zn and S content in sphalerite varies between 53.3-65.4 wt. %, and 32.6-37.1 wt. %, respectively (Appendix 8.5). Iron content in sphalerite classifies it into two groups: low (<5 wt. % Fe), and high (>7 wt. % Fe) Fe content. Low Fe values dominantly occur in samples from assemblage 1 in the ABM zone, whereas high Fe values occur in samples of assemblage 2 (Fig. 4.13A). Cadmium content in sphalerite is between 0.25–0.58 wt. %, but there is no correlation with other elements (Fig. 4.13A).

Using the linear equation of Keith et al. (2014), which uses Fe/Zn values in sphalerite to calculate likely temperatures at which the sphalerite precipitated, sphalerite from the low Fe group yields an average temperature (±1 standard deviation) of 266 ± 11 °C (n=45), and the average temperature (±1 standard deviation) for the high Fe group is 357 ± 19 °C (n=93). The highest calculated temperatures correspond to the samples occurring in assemblage 2 (Fig. 4.13B).

4.6.5.5 Chalcopyrite

Copper, Fe, and S contents in chalcopyrite vary between 30.8-34.8 wt. % Cu, 29.8-32.5 wt. % Fe, and 34.5-36.4 wt. % S (Appendix 8.6). The highest Bi contents (between 0.1-0.2 wt. %) occur in chalcopyrite from assemblage 2. Silver is enriched (between 0.06-0.15 wt. %) in samples from assemblage 3 and assemblage 2 from the Krakatoa zone.

4.6.5.6 Galena

The Pb and S content of galena varies between 61.1-86.4 wt. %, and 1.9-21.2 wt. %, respectively (Appendix 8.7). Selenium contents are up to 8.9 wt. % and vary systematically with the type of mineralization assemblage in which the galena occurs (Fig. 4.13F). The highest Se content (>3 wt. %) occurs in samples from assemblage 3 and assemblage 2 from the ABM zone. The same samples show elevated Ag (0.2-1.65 wt. %) and Bi (0.75-4.5 wt. %) that correlate with each other. In rare cases, galena in these assemblages contains up to 10 wt. % Bi substituting for Pb (Fig. 4.13H). In the Krakatoa zone, the highest Se content is 2.75 wt. % , and samples from assemblage 1 have Se contents in galena below 0.35 wt. % (Fig. 4.13F).

4.6.5.7 Sulfosalts

The most common sulfosalts occurring within the mineralization are the members of the tetrahedrite group (tetrahedrite, tennantite, freibergite). In assemblage 1 in the ABM zone, tetrahedrite group minerals have up to 8.6 wt. % Ag (Fig. 4.13G), and significant Fe (ranging between 2.6-7.8 wt. %) and Zn (between 2.0-4.8 wt. %) that inversely correlate. Freibergite contains minimal As (less than 0.16 wt. %) but contains significant Pb (0.5-20.1 wt. %), Fe (4.5-9.8 wt. %), and lesser Zn (0.4-1.4 wt. %).

Other sulfosalts that have been identified in the mineralization at the ABM deposit are rare and commonly very fine-grained. These are bournonite, boulangerite, meneghinite, gudmundite, ullmannite, and dyscrasite (Appendix 8.8).

4.6.5.8 Bismuth minerals

In assemblage 2, rare (<< 1 modal %) minerals rich in Bi occur (Fig. 4.13H). Very fine-grained native bismuth grains can occur (>90 wt. % Bi) and have minor Sb (between 1-3 wt. %) and trace Fe (<1 wt. %) . Bismuthinite (Bi_2S_3) also occurs, its Bi and S content varies between 81-84 wt. %, and 7.8-19.1 wt. %, respectively. Minor Fe (between 1.3-3.3 wt. %) occurs in the bismuthinite.

4.6.6 LA-ICP-MS results

The complete LA-ICP-MS results are available in Appendix 9.1. Observations stemming from these results are generally in accordance with the EPMA analyses, but the results are at lower detection limits and document a more diverse suite of elements. Overall, Au contents range between 0.007-17.1 ppm, and the highest values (>1 ppm Au) occur in arsenopyrite (max 17.1 ppm), galena (max 6.7 ppm), chalcopyrite (max 2.5 ppm), and pyrite (max 2.5 ppm). The highest values of Hg occur in tennantite-tetrahedrite (>50 ppm), and sphalerite (8-25 ppm). Highest values of Tl occur in galena (~30-350 ppm, locally up to 1224 ppm).

4.6.6.1 Sphalerite

Sphalerite grains from assemblage 1 have enriched Ga contents (Fig. 4.14A), and Hg in samples from the ABM zone. Sphalerite grains from samples of assemblage 2 and 3 in the ABM zone show enrichments of Se, and Bi (Se>100 ppm, Bi>0.09 ppm; Appendix 9.1). Using the Frenzel et al. (2016) trace element thermometer for sphalerite yields temperatures between 300-380 °C for samples from the assemblages 2 and 3 (n=8), and temperatures between 223-281 °C for grains (n=7) from assemblage 1 (Appendix 9.1).

4.6.6.2 Pyrite

Pyrite grains from assemblages 2 and 3 have elevated contents of Se, Co, Ni, and As (Fig. 4.13C). Pyrite from assemblage 1 show higher average Tl and Hg than in toher assemblages. Zoned pyrite grains commonly occur in all assemblages. The cores display very fine-grained inclusions of other sulfide minerals and have a higher trace metal content compared to the inclusion free rims, regardless of the mineralization assemblage (Fig. 4.14C).

4.6.6.3 Chalcopyrite

Chalcopyrite grains from assemblages 2 and 3 have elevated Se and Ag contents compared to chalcopyrite analyzed in assemblage 1. Samples in all assemblages in the Krakatoa zone are enriched in Ag compared to those from the ABM zone.

4.6.6.4 Galena

Galena grains from the assemblage 2 and 3 are relatively enriched in Bi, Ag, and Se (Fig. 4.14E). Galena grains in assemblage 1 show elevated As, Fe, Tl and Cd. Analyzed galena grains from the Krakatoa zone show enrichments in In and Sn regardless of mineralization assemblage (Fig. 4.14D).

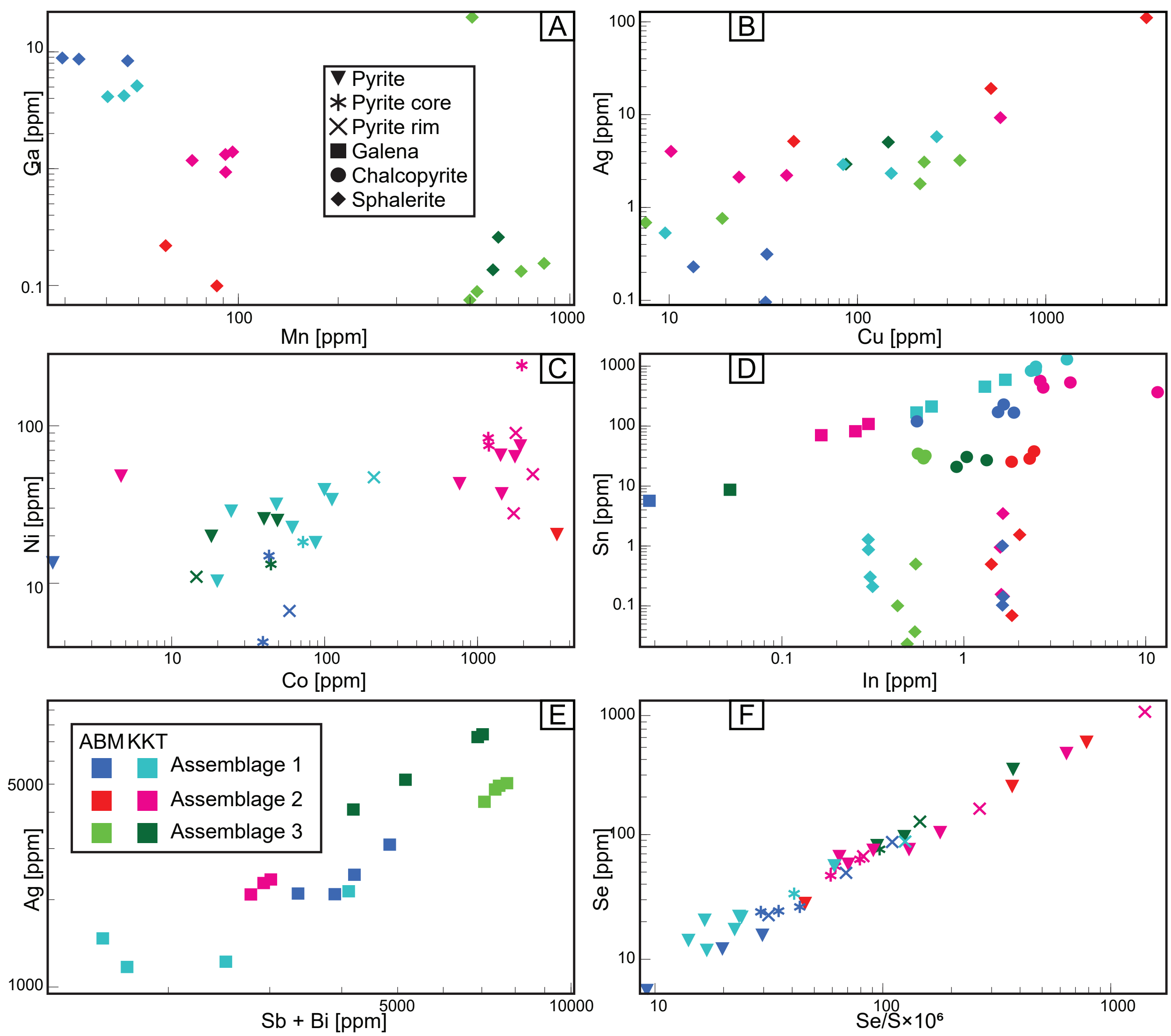

Figure 4.14. Results of LA-ICP-MS analyses. (A) Mn vs Ga in sphalerite. (B) Cu vs Ag in sphalerite. (C) Co vs Ni in pyrite. (D) In vs Sn in chalcopyrite, galena, and sphalerite. (E) Sum of Sb and Bi vs Ag in galena. (F) Se/S×10⁶ vs Se in pyrite.

4.7 Discussion

Although primary features, such as remnant clasts and bedding in massive sulfide mineralization, or the hydrothermal alteration of host rocks, are commonly preserved at the ABM deposit (Denisová and Piercey, 2022; Denisová and Piercey, in press), metamorphism and deformation affected the massive sulfide mineralization. In the following sections, the role of metamorphic overprinting and how it has affected the primary geochemistry and mineralogy of the ABM deposit is evaluated. This is then contrasted with the delineation of features that are likely primary and the potential conditions of deposition during the formation of the replacement-style VMS mineralization. We also compare the mineralization at the ABM zone and the Krakatoa zone to determine whether they belong to the same mineralizing system. Lastly, we discuss the potential sources of metals and their enrichment in the ABM replacement-style VMS deposit.

4.7.1 Effects of metamorphism and deformation

Previous studies at the ABM deposit by Denisová and Piercey (2022, in press) have documented primary textures and lithogeochemical and hydrothermal alteration signatures in the variably hydrothermally altered host rocks. Despite primary features, distal from mineralization the minerals present in the host rocks (e.g., chlorite, actinolite, epidote, carbonate minerals) are consistent with greenschist facies metamorphism (Murphy et al., 2006). Recrystallization is a common metamorphic process (Lafrance et al., 2020), and does not significantly affect the mineral chemistry of metamorphosed hydrothermal phyllosilicate minerals (Riverin and Hodgson, 1980; Urabe et al., 1983; Hannington et al., 2003), but it can affect the mineralogy and mineral chemistry of sulfide minerals (Barton and Bethke, 1987; Lockington et al., 2014; Kampmann et al., 2018). The scale on which these processes operate, however, varies depending on the intensity of the metamorphism and deformation (Marshall et al., 1998). Further, similar to silicate-rich rocks, sulfide orebodies respond to deformation based on their mineralogy and the rheological properties of the contained minerals (Marshall and Gilligan, 1987).

Arsenopyrite can provide insight into the metamorphic conditions using arsenopyrite geothermometry, which is based on As content in arsenopyrite in equilibrium with other Fe sulfide minerals and that contains <1 wt. % Sb+Co+Ni (Kretschmar and Scott, 1976; Sharp et al., 1985). In most cases, arsenopyrite in the ABM deposit occurs intergrown with recrystallized pyrite (Fig. 4.7E, F), which suggests it has been affected by metamorphism. Where re-crystallized with pyrite, the As content in arsenopyrite varies between 29-31.6 at. % (Appendix 8.3), which corresponds to a temperature range of 300-420 °C using the T-X plot of Kretschmar and Scott (1976). This range fits with the temperatures normally reached during greenschist facies metamorphism, although it also overlaps with the upper end of temperatures that can be associated with primary VMS fluids.

4.7.1.1 Effects of metamorphism and deformation on mineral textures at different scales

In the ABM deposit, macro-scale banding displays most of the features characteristic for tectonic banding described by Lafrance et al. (2020), such as monomineralic sulfide and polymineralic modal sulfide bands, and elongation of silicate fragments. The mineralization at the ABM deposit is replacement in style, so where sulfide minerals replaced the volcaniclastic rocks, the S_0 fabric should have been preserved. Previous studies (van Olden et al., 2020) documented that the major S_1 fabric is subparallel to primary bedding S_0; in drill core, the orientation of the fabric does not differ notably between the massive sulfide lenses and host rocks. This suggests that the tectonometamorphic processes likely enhanced already existing macro-scale structures in the massive sulfide mineralization.

On the micro-scale, textures reflective of metamorphism and deformation are even more pronounced. Pyrite is the prevailing sulfide and commonly has fractures filled by chalcopyrite, galena, or sphalerite (Fig. 4.7P). Durchbewegung structures (Marshall and Gilligan, 1989), typical for metamorphism in massive sulfides deposits, are also observed with coarse pyrite grains within a matrix of fabric-defining chalcopyrite and sphalerite (Fig. 4.7Q, R). Because pyrite does not show any evidence of ductile deformation, the sulfide deformation features within the ABM deposit are consistent with greenschist facies metamorphism recorded in silicate mineral assemblages and by the arsenopyrite geothermometry outlined above (Murphy et al., 2006; Denisová and Piercey, in press).

Additional micro-scale features that likely reflect the effect of metamorphism include the symplectite-like clusters of galena and associated sulfosalts within the pyrite-chalcopyrite-magnetite-pyrrhotite assemblage (Fig. 4.8C-P); these features are similar to textures in quenched sulfide melts (Tomkins et al., 2007). Tomkins et al. (2007) suggested that under greenschist facies conditions, if elevated Bi, Hg, Sb and/or As are present and multiple minerals (galena, chalcopyrite, arsenopyrite, sulfosalts) coexist in the mineralization assemblages, sulfide anatexis can occur. In assemblage 2, galena grains analyzed in the symplectic intergrowths have elevated Bi contents, and the grains commonly contain inclusions of bismuthinite and/or native Bi (Fig. 8F, H). Symplectic intergrowths also commonly comprise tetrahedrite, freibergite, and Pb- and Pb-Sb-rich sulfosalts, and rarely, they contain sulfosalts with significant contents of less common elements like Hg, Ni, Tl, and Se. The observed textures, range of sulfosalts, and chemical features of the clusters are consistent with partial melting of sulfide minerals. Compared to other deposits where similar mineral assemblages and textures have been described and where sulfide partial melting has been suggested (e.g., Broken Hill, Lengenbach; Hofmann 1994; Sparks and Mavrogenes 2005), the scale of partial sulfide melting observed at the ABM deposit is much smaller (clusters <1 mm in size) and the intergrowths make up a negligible portion of the mineralization (<<0.1 vol. %). This is likely due to the lower metamorphic grade (greenschist facies) and lower metamorphic temperatures affecting the ABM deposit compared to the other deposits with suggested partial melting (e.g., ~750-800 °C at Broken Hill; Sparks and Mavrogenes 2005). Moreover, symplectic intergrowths that are interpreted to be the products of sulfide mineral partial melting have been observed only in zones of Bi enrichment (ABM zone), or in Cu-enriched zones where maximum deformation/strain has been observed (Krakatoa zone). Therefore, at the ABM zone, Bi enrichment appears to be a key factor for initiating sulfide mineral melting; however, the effects of sulfide mineral anatexis are negligible on the deposit scale and the process only operated on a micrometer- to centimeter-scale and did not affect the mineral and element assemblages at the ABM deposit on the macro- to deposit-scale.

4.7.1.2 Effects of metamorphism and deformation on sulfide mineral chemistry

The following section discuses the effect of metamorphism on the mineral chemistry of sulfide mineral at the ABM deposit. Overall, metamorphic recrystallization and other deformation related changes to the fabric of the massive sulfide mineralization appear to have minimal effect on major elements and mostly affect the trace element distribution within individual ore zones.

The composition and textures of individual grains of some sulfide minerals in the massive sulfide mineralization in the ABM deposit reflect the effects of metamorphism. Pyrite grains that are >100 µm in diameter show inclusion rich cores with higher contents of trace elements that preserve primary fine-grained textures and likely the primary geochemical signatures but the rims that likely resulted from metamorphic recrystallization, are poor in trace elements compared to the cores (Appendix 9.1). Another mineral affected by metamorphism at the ABM deposit is sphalerite. With increasing metamorphic grade, chalcopyrite disease (Barton and Bethke, 1987) typical for primary hydrothermal sphalerite diminishes due to recrystallization, and remobilization of the minute included chalcopyrite blebs (Craig and Vokes, 1992; Lockington et al., 2014). At the ABM deposit, chalcopyrite disease in sphalerite is preserved locally within the mineralization (Fig. 4.7K), but most sphalerite is inclusion-free and the Cu content of sphalerite is generally <600 ppm (Fig. 4.14B), implying elimination of microinclusions as a result of metamorphic recrystallization (Cugerone et al., 2021). A further effect of metamorphism on sphalerite in the ABM deposit is the enrichment of Hg. At the ABM deposit, sphalerite shows the highest enrichment of Hg among the studied sulfide minerals, with the exception of tennantite (Appendix 9.1). Enrichment of Hg in sphalerite is a characteristic effect of metamorphic recrystallization (Lockington et al., 2014), and this also suggests that in the ABM deposit other trace elements in sphalerite have been remobilized during metamorphism.

The Fe content in sphalerite has been used as a geothermometer and a geobarometer (Scott and Barnes, 1971) but recent studies have noted that in VMS deposits determining original fluid temperatures is only possible if the system has not been affected by metamorphism above lower greenschist conditions (Keith et al., 2014) or if the rocks have not been subject to metamorphism above the 310 °C closure temperature of the sphalerite system in the case of the sphalerite trace element geothermometer (Frenzel et al., 2016). Temperatures calculated from sphalerite at the ABM deposit using both methods show two groupings: a lower temperature group (235-290 °C) comprises only samples representing the pyrite-sphalerite assemblage from the ABM zone of the deposit and a higher temperature group encompasses all other mineral assemblages in both zones with temperatures varying between 320-410 °C (Fig. 4.13B). The temperatures calculated for sphalerite from assemblage 1 in the ABM zone appear to be in accordance with the temperature range typical for this assemblage in modern SMS systems. However, the majority of the higher calculated temperatures appears to be either too high for the assemblage where sphalerite occurs (assemblage 1 in the Krakatoa zone; Figure 4.13B), or too high for sphalerite precipitation in general, even though the grains in question occur in assemblages with chalcopyrite and pyrrhotite. In these assemblages in SMS and VMS deposits, sphalerite commonly forms at ~290±50 °C (Pisutha-Arnond and Ohmoto, 1983), however our data suggest sphalerite precipitated between ~340-390 °C (Fig. 4.13B). This implies that at least in some samples, the Fe and Zn content in sphalerite was affected by metamorphism.

During metamorphic recrystallization, if multiple sulfide minerals (galena, sphalerite, and chalcopyrite) co-crystallize or recrystallize simultaneously, they acquire trace element signatures that are distinct from those typical for precipitation from hydrothermal fluids (George et al., 2016; Kampmann et al., 2018). In co-crystallized assemblages, Sn is preferentially enriched in chalcopyrite followed by galena and sphalerite (George et al., 2016; George et al., 2018), and Ga and In prefer chalcopyrite to sphalerite (George et al., 2016; George et al., 2018). The mineral scale distribution of Sn, Ga, and In in the ABM deposit conforms to these trends (Fig. 4.14D), indicating co-crystallization/recrystallization of sulfide minerals occurred. Similarly, if galena is present, Ag content in co-crystallized sphalerite should be significantly lower (Lockington et al., 2014; George et al., 2016), as observed in the ABM deposit (Fig. 4.14B), which further supports trace element redistribution during metamorphism. The above-described distribution of trace elements between minerals is the same across mineral assemblages, but absolute values of the trace element in the minerals vary consistently between the assemblages, e.g., elevated Bi, Se, and Co in assemblages 2 and 3, or enrichment in Sb, As, Cd, In, and Ga in assemblage 1. Regardless, the mineral scale distributions described above all support trace element redistribution during metamorphism.

4.7.2 Conditions during the precipitation of the replacement-style VMS mineralization at the ABM deposit

Although greenschist facies metamorphism affected some textures and also created new textures, and affected trace element distribution in the massive sulfide mineralization at the ABM deposit, windows with lesser effects of strain and metamorphism occur, where primary textures, such as spongiform and atoll textures, cubanite exsolution, and rare framboids, are preserved. In these zones, sulfide mineral chemistry and lens-scale geochemical trends can potentially be used to determine the primary conditions for the formation of the massive sulfide mineralization. In VMS deposits, temperature, redox, and pH control the precipitation of elements from the hydrothermal fluid (Large, 1977; Solomon and Walshe, 1979; Lydon, 1988; Ohmoto, 1996; Franklin et al., 2005) and are recorded in the mineral assemblages and mineral chemistry of the massive sulfide mineralization. The following section provides an interpretation of available data to establish the potential primary depositional conditions during the formation of the ABM deposit, and determines whether they differed significantly between the ABM and Krakatoa zones.

Zone refining, the dissolution and re-precipitation of ore and gangue minerals, generates a temperature-dependent metal zonation in long-lived thermally evolving VMS deposits (Eldridge et al., 1983; Lydon, 1988). In replacement-style deposits, metal zonation follows the same sequence as in exhalative- and mound-style deposits with interiors dominated by Cu and becoming progressively Zn-, Pb-, and Ba-enriched towards the outer parts of the sulfide lenses (Knuckey et al., 1983; Lydon, 1988), however, the geometry is different than in mound-style deposits due to contrasts in porosity and permeability of the host rocks that control the fluid flow in the subsurface. In particular, the metal zonation is commonly more pronounced laterally than vertically in replacement-style mineralization (Bradshaw et al., 2008; Piercey et al., 2014; Nozaki et al., 2021). The metal distribution within the massive sulfide mineralization in the ABM zone has

Cu-rich zones at the centre of the mineralized lenses, overlapping with Zn-enriched zones at the margins of the lenses (Fig. 4.2B, 4.10, 4.15). Zones that are enriched in Cu and associated metals (Bi-Se-Co) generally have a similar trend to some (but not all) of the interpreted synvolcanic faults (Fig. 4.15D; Denisová and Piercey, 2022), suggesting the faults likely acted as conduits for ascending high temperature hydrothermal fluids. As Cu is commonly the metal to precipitate from hydrothermal fluids at the highest temperatures (Pisutha-Arnond and Ohmoto, 1983), this trend in Cu-enrichment is also interpreted to delineate the zones where the fluids infiltrated laterally along synvolcanic faults into the porous and permeable host units (Fig. 4.15).

Compared to Cu, the distribution of Zn-Pb-Ba extends further from the synvolcanic structures and into the surrounding host rocks (Fig. 4.15C). In general, Pb is associated with Zn, and locally zones with elevated Ba (>1 wt. % Ba) overlap with Zn-Pb rich zones and extend into altered host rocks with Ba values >0.15 wt. % (Fig. 4.10B; Denisová and Piercey 2022). Despite the effects of metamorphism and deformation described above, the deposit-scale metal zonation (Cu→Zn-Pb→Ba) at ABM appears to not have been significantly affected by these processes and it is similar to the zonation typical for VMS deposits (Knuckey et al., 1983; Lydon, 1988; Large, 1992). The deposit-scale metal zonation and the character and distribution of mineralization assemblages result from changing temperature, pH and redox conditions, the following sections provide the evidence for the conditions under which specific assemblages formed and the processes that were active during their formation.

4.7.2.1 Evidence for low temperature (<270 °C) fluids and seawater mixing

Generally, in SMS and VMS deposits, assemblages enriched in Zn-Pb-Ba with abundant pyrite, sphalerite, and barite are interpreted to have formed at temperatures of 250 ± 50 °C from mixing of acidic and reduced hydrothermal fluids with infiltrated seawater (Pisutha-Arnond and Ohmoto, 1983). Tennantite-tetrahedrite and barite commonly occur in the low temperature, and more distal parts of VMS and SMS deposits (Grant et al., 2015), whereas pyrrhotite is typical for high temperature assemblages proximal to the centre of the system (Knuckey et al., 1983). Mineral textures in low temperature assemblages are commonly fine-grained, due to rapid nucleation

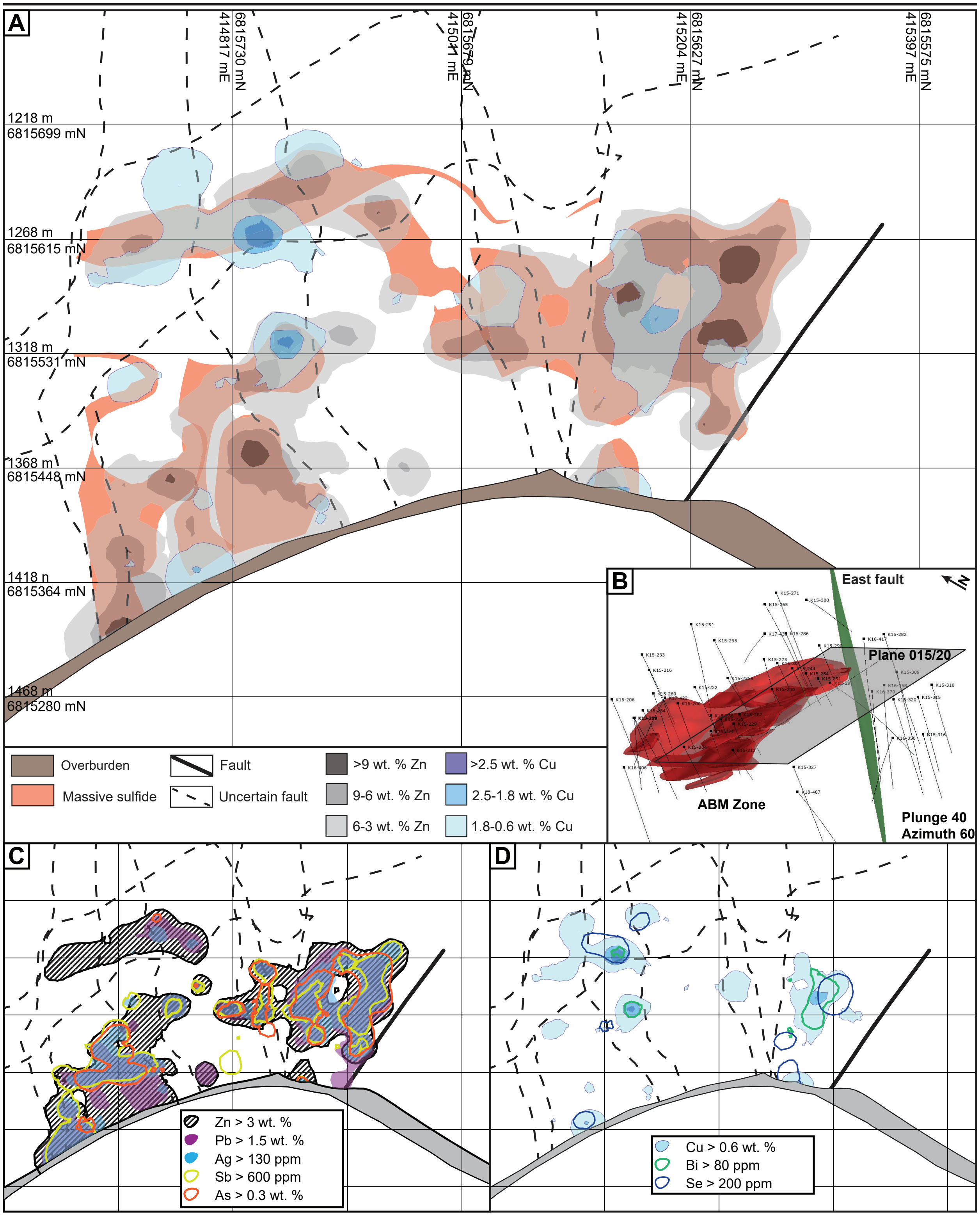

Figure 4.15. View along section parallel to main trend of massive sulfide mineralization (section plane 015/20) in the ABM zone. (A) Plan view of the section showing the cross section of the massive sulfide lenses and distribution of Cu and Zn. (B) Oblique view of the ABM zone showing where the viewing plane cuts the massive sulfide mineralization. (C) Distribution of the Zn-Pb-Ag-Sb-As element assemblage. (D) Distribution of the Cu-Bi-Se element assemblage.

resulting from fluid mixing, and include framboids, colloform, spongiform, and atoll textures (Butler and Rickard, 2000).

At the ABM deposit, assemblage 1 (pyrite-sphalerite) is the most voluminous of the assemblages and commonly occurs at the margins of the massive sulfide lenses. It roughly outlines the extent of the Zn-Pb-As-Sb-Ag-Au-Hg-Ba enrichment zones and represents zones where the majority of arsenopyrite, tennantite-tetrahedrite-freibergite, and barite occur, whereas pyrrhotite is minor. Low temperature (200-270 °C) textures, including rare framboids and relatively common atoll and spongiform textures featuring pyrite and/or arsenopyrite are preserved in this assemblage (Fig. 4.7B, C, D, E). In addition, despite some metamorphic features in these assemblages, the abundance of arsenopyrite in assemblage 1 suggests precipitation from reduced hydrothermal fluids (Heinrich and Eadington, 1986). In contrast, tennantite and tetrahedrite, likely paragenetically younger than arsenopyrite, occur in assemblage 1; however, both require more oxidized conditions to precipitate, tetrahedrite more so than tennantite (Grant et al., 2015). In the ABM deposit, tetrahedrite appears to form later than tennantite and locally replaces it. This sulfosalt overprinting relationship is more prevalent in the Krakatoa zone, where freibergite, which requires even more oxidizing conditions to precipitate than tetrahedrite (Grant et al., 2015), occurs commonly. The decomposition textures locally associated with the tetrahedrite group minerals (Fig. 4.8A, B) possibly document changing conditions, which rendered the tetrahedrite-group minerals unstable.

Sulfide mineral chemistry also provides insights into the depositional conditions of the mineralization. Although metamorphism affected trace element distribution between various mineral phases, the suites of elements that originally substituted the mineral lattice of sulfide/sulfosalt minerals were not affected by greenschist facies metamorphism and reflect primary VMS-related mineral-chemical signatures (Huston et al., 1995). In pyrite, these elements are Co, Ni, Se, and Te (Huston et al., 1995). The Co values for pyrite in assemblage 1 are lower than in the other two assemblages (Fig. 4.13C), which suggests that assemblage 1 formed at lower temperature, and the lower values are consistent with the framboidal, atoll, and spongiform textures noted above (Huston et al., 1995). Similarly, Bi-Sb-As-Se systematics of galena also indicate a lower temperature origin. In particular, for galena to contain more than 0.1 wt. % Ag in solid solution, Bi and/or Sb also have to be present and balance out the coupled substitution of Bi+Sb:Ag ~2:1; Sb is more abundant at lower temperatures than Bi (Amcoff, 1984; Foord and Shawe, 1989). Further, Se in galena is also governed by temperature, with Se substituting for S in the mineral lattice; it is also not affected by greenschist facies metamorphism (Amcoff, 1984; Huston et al., 1996). In both the ABM and Krakatoa zones, galena in assemblage 1 has lower values of Se compared to the other two assemblages and although Ag values in galena can be up to 0.38 wt. % (Fig. 4.14E), Ag substitution is offset by Sb substitution instead of Bi (low Bi/Sb; Fig. 4.13F). These trends in galena composition suggest a lower temperature of galena formation in assemblage 1. These features are also paralleled by the Fe content in sphalerite, which is lower compared to other assemblages and suggests precipitation from lower temperature and less reduced fluids, at least for the ABM zone (1.5-6 wt. % Fe). In the Krakatoa zone, however, the Fe values are in the same range as in the assemblages 2 and 3 (7-11 wt. % Fe). However, arsenopyrite is common in the Krakatoa zone, which suggests a more reducing environment, which could explain the occurrence of Fe-rich sphalerite in that zone. In assemblage 1, the mineralogy, textures, and behaviour of greenschist facies metamorphism-resistate elements contained by the minerals suggest that assemblage 1 formed at relatively lower temperatures than assemblages 2 and 3, and that the redox conditions of the environment varied during the precipitation of the assemblage.

4.7.2.2 Evidence for high temperature (270-350 °C) reducing fluids

In modern and ancient deposits, assemblages containing abundant chalcopyrite and pyrrhotite are interpreted to have formed at temperatures between 300-360 °C (Pisutha-Arnond and Ohmoto, 1983; Hannington et al., 2005). Locally, primary textures that would be indicative of high temperature precipitation and zone refining in other VMS deposits (Eldridge et al., 1983; Craig and Vokes, 1992) such as cubanite exsolution lamellae, chalcopyrite disease in sphalerite, skeletal pyrite, or pyrrhotite replacing pyrite (Fig. 4.7G-L) are also preserved at the ABM deposit, which implies high temperature primary VMS hydrothermal activity.

Pyrrhotite is locally abundant (up to 33 modal %) and occurs early in the paragenesis of assemblages

2 and 3 (Fig. 4.9). Pyrrhotite is commonly replaced along fractures and grain boundaries by fine-grained “ribbed” pyrite (Fig.4.7I) and likely records the influx of later, more oxidized fluids (Murowchick, 1992; Grant et al., 2015). The average pyrrhotite composition (60.32±1.05 wt. % Fe, n=79; Appendix 8.4) indicates that pyrrhotite is monoclinic (Kissin and Scott, 1982), and although monoclinic pyrrhotite can form by direct precipitation from hydrothermal fluids, it commonly occurs at temperatures <258 °C (Lianxing and Vokes, 1996), which is at the lower end of the temperature range suggested by the chlorite thermometer (Denisová and Piercey, in press) and other sulfide minerals common in the assemblage. Locally, pyrrhotite displays annealed textures (Fig. 4.8N), which are typical in metamorphosed deposits (Craig and Vokes, 1992), and suggests that annealing and transformation from hexagonal to monoclinic pyrrhotite was thorough during metamorphism. Thus, it is likely that before undergoing metamorphism, pyrrhotite was originally hexagonal and formed at temperatures higher than 272 °C, which would be typical for this type of its host assemblage, or possibly, the transition from hexagonal to monoclinic occurred because of zone refining during deposit formation.

Other features of the sulfide mineral chemistry of assemblages 2 and 3 also indicate deposition at high temperatures. For example, pyrite from the assemblage 2 has elevated values of Se, Co, and Ni compared to the assemblage 1 (Fig. 4.13C, 4.14C), which is indicative of formation at higher temperatures (Huston et al., 1995; Genna and Gaboury, 2015; Martin et al., 2021). Elevated Se content in pyrite (Fig. 4.14F) and in the minor galena occurring in this assemblage compared to assemblage 1 (Fig. 4.13F) is also an indicator of high (>300 °C) temperatures of precipitation and reduced conditions (Huston et al., 1995; Layton-Matthews et al., 2008). Further, galena in assemblages 2 and 3 has elevated Bi/Sb values (Fig. 4.13F) and Ag values up to 1.25 wt. %., which are indicative of higher temperatures and more reducing conditions compared to assemblage 1 (Amcoff, 1984; Grant et al., 2015). This is also mirrored by the Fe content in sphalerite in assemblage 2 (9-11 wt. %), which is associated with pyrite and similar to the values from assemblage 3, both of which imply that the hydrothermal fluids forming these assemblages were likely more reducing than those forming assemblage 1 (e.g., Scott 1983; Keith et al. 2014).

The stringer assemblage 3 is not extensive and commonly occurs on the margins of the massive sulfide lenses where it transitions into the unmineralized pervasive chlorite alteration assemblage (Fig. 4.5, 4.6I). Formation temperatures calculated for chlorite in both mineralized and barren pervasive chlorite assemblages are ~275-345 °C (Denisová and Piercey, in press). Pyrrhotite and chalcopyrite occur commonly, and minor sphalerite has a relatively high Fe content (~9-13 wt. %) and elevated Mn content (Fig. 4.14A) compared to other assemblages at the ABM deposit, typical of reduced hydrothermal fluids (Scott, 1983; Keith et al., 2014; Frenzel et al., 2016). The recorded temperatures for the pervasive chlorite hydrothermal alteration also correspond to those recorded for similar assemblages in modern SMS and ancient VMS deposits (Pisutha-Arnond and Ohmoto, 1983; Large, 1992; Hannington et al., 2005). The occurrence of assemblage 3 predominantly on the margins of the massive sulfide lenses suggests it formed together with the pervasive chlorite alteration assemblage from reduced fluids with some of the highest temperatures reached in the mineralizing system.

4.7.2.3 Relationship between the ABM and Krakatoa zones

The relationship between massive sulfide mineralization in the ABM and the Krakatoa zones of the ABM deposit is incompletely understood. The mineralization occurs in a similar stratigraphic position in both zones, which would suggest contemporaneous development of the massive sulfide lenses (Denisová and Piercey, 2022), but the post-mineralization offset along the East fault has disrupted the continuity of stratigraphic units. The predecessor of the East fault was a major structure controlling the basin subsidence (Denisová and Piercey, 2022) and likely acted both as a pathway for downwelling seawater and for upwelling hydrothermal fluids.

Reconstruction of the offset along the East fault suggests that the two zones were not connected directly, because the number and characteristics of the mineralized lenses do not match between the two zones (Denisová and Piercey, 2022). In the Krakatoa zone, the mafic sills take up more volume within the lithostratigraphic sequence hosting the mineralization than in the ABM zone and have greater control over the distribution of the massive sulfide mineralization (Fig. 4.2, 4.3). The mafic sills are interpreted to have had significantly lower primary porosity and permeability, in contrast to the surrounding volcaniclastic rocks, and would have likely acted as barriers to hydrothermal fluid flow and limited the influx of seawater into the more porous and permeable lithofacies in their footwall.

The mineralogical and element assemblages are generally very similar between the ABM and Krakatoa zones; however, their distribution and extent vary. Ohmoto (1996) and Hannington et al. (1998) suggested that if zone refining continues to completion in VMS and SMS deposits, lower temperature assemblages will be on the margins of the massive sulfide lenses and the mineralized bodies can eventually become fully pyritized. In the ABM zone, the distribution of assemblage 2 reaches all the way to the hanging wall contact at the centre of the massive sulfide lenses zone (Fig. 4.5, 4.10C). In the Krakatoa zone, assemblage 1 is more extensive and the distribution of assemblage 2 is vertically more limited than in the ABM zone (Fig. 4.3), suggesting that the hydrothermal system was possibly less active than in the ABM zone, either due to barriers to fluid flow, or the hydrothermal fluid flow was active for a shorter period in the Krakatoa zone. The recorded differences in mineralogy and mineral chemistry between the two zones are relatively minor, such as the more common occurrence of freibergite and overall low Ag and Bi contents in galena from assemblage 1 in the Krakatoa zone, which suggests a greater influence of oxidized fluids in the Krakatoa zone, likely due to more mixing with seawater given the possibly less vigorous hydrothermal fluid flow.

Given their very similar mineralogy, mineral chemistry, and element assemblages, the mineralization at the ABM zone and the Krakatoa zone likely formed from the same hydrothermal circulation system but the depositional conditions varied due to differences in host rock facies and their distribution, which controlled the local influx of seawater and availability of high temperature hydrothermal fluid.

4.7.3 Metal sources and genetic interpretation

The formation of the massive sulfide mineralization at the ABM deposit was a continuous process. The earliest mineralization phase in the massive sulfide lenses at the ABM deposit was likely the formation of euhedral magnetite grains that are common in assemblage 2 and rare in assemblage 1

(Fig. 4.9). The grains likely precipitated before the hydrothermal fluid became more reduced and/or rich in H_2S, possibly during the formation of early hydrothermal alteration assemblages. This was followed by continuous and extensive infiltration of hydrothermal fluids that were moderate temperature (200-270 °C), rich in H_2S, acidic and reduced, into the subsurface along porous and permeable units, where the hydrothermal fluids interacted with infiltrated seawater (Denisová and Piercey, 2022; Denisová and Piercey, in press) and precipitated assemblage 1. As the system heated up (>270 °C), higher temperature hydrothermal fluids ascended along the synvolcanic faults, permeated assemblage 1, and through zone refining processes, where the hydrothermal fluids dissolved Zn- and Pb-rich phases, chalcopyrite precipitated, and the now Zn- and Pb-rich fluids reprecipitated sulfide minerals on the margins of the existing sulfide lenses, and thus assemblage 2 formed in the centers of the massive sulfide lenses. With time and continued infiltration of high temperature hydrothermal fluids, assemblage 2 grew outward from the synvolcanic faults, which resulted in the dissolution and reprecipitation of assemblage 1 outward into the host rocks. Zones of assemblage 3 within and on the contacts of the massive sulfide lenses are likely a result of limited high-temperature (>350 °C) pulses of hydrothermal fluids that formed together with the zones of the pervasive chlorite hydrothermal alteration assemblage (Fig. 4.5). The wide distribution of the hydrothermal alteration assemblages (Denisová and Piercey, in press) and the considerable tonnage and grade contained by the deposit (van Olden et al., 2020) suggest that the hydrothermal system that formed the deposit was robust and long-lived, considering that assemblage 2 comprises up to 40 % of the massive sulfide mineralization and formed through zone refining processes.

The mineralization assemblages at the ABM deposit are enriched in specific element suites (As-Sb-Hg-Ag-Au in assemblage 1, Cu-Se-Bi-Co in assemblages 2 and 3) that have been attributed to a magmatic-hydrothermal contributions to the hydrothermal fluids in both VMS and SMS deposits (Sillitoe et al., 1996; Hannington et al., 1999b; Sillitoe and Hedenquist, 2003; de Ronde et al., 2005). In assemblage 1, the As-Sb-Hg-Ag-Au element association, and the locally abundant tetrahedrite group minerals and barite, are consistent with an arc- or intermediate sulfidation-type assemblage (Sillitoe and Hedenquist, 2003). The enrichment of Cu-Se-Bi-Co in assemblage 2 has similar characteristics to other deposits where a magmatic-hydrothermal contribution to the mineralization has been interpreted (e.g., the bornite zone in the Kidd Creek VMS deposit; Hannington et al. 1999b). However, other characteristics typical for magmatic-hydrothermal contributions to the hydrothermal system are lacking at the ABM deposit. The only potential intrusion that could have contributed magmatic-hydrothermal fluids mapped in the area (so far) was emplaced after the formation of the ABM deposit (Manor et al., 2022a). In assemblage 1, minerals that typically form under reducing conditions (arsenopyrite, Fe-rich sphalerite in the Krakatoa zone) occur commonly, and the mineralogy of all assemblages suggests that the hydrothermal fluids that formed them had a low fO_2, which is not typical for magmatic-hydrothermal fluids (Sillitoe and Hedenquist, 2003). The strongly acidic nature of magmatic-hydrothermal fluids would have also formed alteration assemblages with high-Al alteration minerals such as alunite or pyrophyllite that are variably preserved in the ancient record (Hannington et al., 2003; Sillitoe and Hedenquist, 2003), but these hydrothermal alteration assemblages have not been observed at the ABM deposit. Despite this, the presence of abundant illite in the pervasive white mica hydrothermal alteration assemblage (Denisová and Piercey, in press) could have formed as a result of dilution of the extremely acidic magmatic-hydrothermal fluids by mixing with abundant seawater.

At present, the arguments above for a direct magmatic-hydrothermal contribution to the hydrothermal fluids that formed the ABM deposit are permissive, but the evidence is circumstantial. In particular, it is possible that the presence of magmatic-hydrothermal-like element and mineral assemblages may be due to the leaching of rocks with magmatic-hydrothermal metal assemblages similar to those discussed above (Lydon, 1988; Kase et al., 1994; James et al., 2003; Franklin et al., 2005). Previous studies demonstrated that Se in sulfides can be used to track the origin of hydrothermal fluids (Huston et al., 1995; Layton-Matthews et al., 2008; Layton-Matthews et al., 2013). At the ABM deposit, only galena and sulfide minerals from assemblage 1 and 2 in the ABM zone show $Se/S\times10^6$ values >1000 (Appendix 9.1). The majority of the sulfide minerals have signatures that are different than those associated with magmatic-hydrothermal origins (Huston et al., 1995; Layton-Matthews et al., 2008), which coupled with published Se isotope data from

ABM, are consistent with leaching of basement rocks of potentially magmatic or volcanic origin (Layton-Matthews et al., 2013). Layton-Matthews et al. (2013) also suggested that the source of Pb in the massive sulfide mineralization at the ABM deposit was the leaching of basement of Laurentian affinity, and Mortensen et al. (2006) showed from Pb isotopes that basement leaching was important in most VMS deposits along the western Laurentian margin. Moreover, the western margin of Laurentia contains numerous shale basins, including parts of the Finlayson Lake district, and thus it is reasonable to assume that these would be potential sources of metals for VMS hydrothermal systems. Black shales can be enriched in elements like Co, Bi, Se, Cu, Zn, As, Ag, Tl, and Sb, depending on their depositional environment (Vine and Tourtel, 1970; Hatch and Leventhal, 1992; Brumsack, 2006; Paikaray, 2012) and trace elements commonly occur in sulfide minerals or are associated with organic molecules and are available for leaching (Vine and Tourtel, 1970; Paikaray, 2012). Leaching of sedimentary rocks, and black shales in particular, or of volcanic rocks could also account for the enrichment of metals belonging to the more magmatic-hydrothermal association (e.g., As-Sb-Hg-Ag-Au and/or Cu-Se-Bi-Co) occurring at the ABM deposit; however, this requires further study to decipher.

4.8 Conclusions

Textural, mineralogical, and assay data show that the effects of greenschist facies metamorphism at the ABM deposit are limited to recrystallization, small-scale remobilization (<1 m) and trace element redistribution.

Deposit-scale metal zonation Cu→Zn-Pb→Ba, corresponds to the distribution of mineralization and element assemblages and reflects decreasing temperatures and more oxidizing conditions as hot, reduced, metal-rich hydrothermal fluids gradually infiltrated porous substrate, mixed with cold seawater, and precipitated mineralization, which was further modified by zone refining as the deposit matured. The widespread pyrite-sphalerite mineral assemblage zones coincide with the Zn-Pb-Ag-Au-Hg-As-Sb-Ba element association and formed at temperatures ~200-270 °C under fluctuating redox conditions documented by the occurrence of arsenopyrite, tetrahedrite group minerals, and barite. Pyrite-chalcopyrite-magnetite-pyrrhotite assemblage zones occur in the centres of massive sulfide lenses and overlap with zones of Cu-Bi-Se-Co enrichment. The assemblage formed at temperatures ~300-350 °C, which is illustrated by commonly occurring chalcopyrite, pyrrhotite, Fe-rich sphalerite, and rare arsenopyrite. The similarities in mineral textures, mineralogy, and trace metal enrichment signatures, suggest that the ABM and Krakatoa zones were part of the same hydrothermal system, yet the differences in their distribution indicate that the system was more active for longer in the ABM zone.

Element associations characteristic of the observed mineral assemblages are similar to those in other deposits with direct magmatic-hydrothermal contributions to the hydrothermal fluids; however, the hydrothermal alteration assemblages and the sulfide mineral chemistry suggest that leaching of volcanic and/or subvolcanic rocks was the major metal source for the ABM deposit, even though a direct magmatic-hydrothermal contribution cannot be completely excluded.

4.9 Acknowledgements

We would like to thank BMC Minerals Ltd. for their generous financial, field, and logistical support. Support for the project was provided by grants from the NSERC Discovery Grant, the NSERC Collaborative Research Development Grant – Project (CRDPJ) program, and BMC Minerals Ltd. (Piercey) and a Student Research Grant from the Society of Economic Geologist Canada Foundation, and by funding from Memorial University of Newfoundland (Denisová). We thank Dr. Wanda Aylward and Dylan Goudie for their assistance with analytical work. The first author would like to thank Dr. Andrew Martin, Dr. Anne-Sophie Tabaud and Dr. Matthew Manor for their thorough reviews of the early versions of the manuscript, Dr. Stefanie Brueckner for constructive comments, and Neil Martin and Robin Black from BMC Minerals for helpful comments and conversations beneficial to this paper. We thank BMC Minerals and Equity Exploration staff at the Kudz Ze Kayah exploration camp for their help during the 2018 and 2019 field seasons.

4.10 References

Amcoff, O., 1984, Distribution of silver in massive sulfide ores: Mineralium Deposita, v. 19, p. 63–69.

Ames, D. E., Franklin, J. M., and Hannington, M. D., 1993, Mineralogy and geochemistry of active and inactive chimneys and massive sulfide, Middle Valley, northern Juan de Fuca Ridge: An evolving hydrothermal system: Canadian Mineralogist, v. 31, p. 997–1024.

Barton, P. B., and Bethke, P. M., 1987, Chalcopyrite disease in sphalerite: Pathology and epidemiology: American Mineralogist, v. 72, p. 451–467.

Berkenbosch, H. A., De Ronde, C. E. J., Gemmell, J. B., McNeill, A. W., and Goemann, K., 2012, Mineralogy and formation of black smoker chimneys from brothers submarine volcano, Kermadec Arc: Economic Geology, v. 107, p. 1613–1633.

Bortnikov, N. S., Genkin, A. D., and Troneva, N. V., 1993, Tennantite decomposition: Evidence from the Kedabek copper deposit, Azerbaijan: Mineralogy and Petrology, v. 47, p. 171–181.

Boulton, A., 2002, GP4F polymetallic volcanic-hosted massive sulphide (VHMS) deposit, Finlayson Lake District, Yukon Territory: B.Sc. thesis (Honors), University of Victoria, Victoria, British Columbia, Canada: 56 p.

Bradshaw, G. D., Peter, J. M., Paradis, S., and Rowins, S., 2001, Geological characteristics of the Wolverine volcanic-hosted massive sulphide deposit, Finlayson Lake district, Yukon Territory, Canada (D. S. Emond & L. H. Weston, Eds.): Yukon Exploration and Geology, p. 269–288.

Bradshaw, G. D., Rowins, S. M., Peter, J. M., and Taylor, B. E., 2008, Genesis of the Wolverine volcanic sediment-hosted massive sulfide deposit, Finlayson Lake district, Yukon, Canada: Mineralogical, mineral chemical, fluid inclusion, and sulfur isotope evidence: Economic Geology, v. 103, p. 35–60.

Brueckner, S. M., Piercey, S. J., Sylvester, P. J., Maloney, S., and Pilgrim, L., 2014, Evidence for syngenetic precious metal enrichment in an appalachian volcanogenic massive sulfide system: The 1806 Zone, Ming Mine, Newfoundland, Canada: Economic Geology, v. 109, p. 1611–1642.

Brueckner, S. M., Piercey, S. J., Pilote, J. L., Layne, G. D., and Sylvester, P. J., 2016, Mineralogy and mineral chemistry of the metamorphosed and precious metal-bearing Ming deposit, Canada: Ore Geology Reviews, v. 72, p. 914–939.

Brumsack, H. J., 2006, The trace metal content of recent organic carbon-rich sediments: Implications for Cretaceous black shale formation: Palaeogeography, Palaeoclimatology, Palaeoecology, v. 232, p. 344–361.

Butler, I. B., and Rickard, D., 2000, Framboidal pyrite formation via the oxidation of iron (II) monosulfide by hydrogen sulphide: Geochemica et Cosmochimica Acta, v. 64, p. 2665–2672.

Carvalho, J. R. S., Relvas, J. M. R. S., Pinto, A. M. M., Frenzel, M., Krause, J., Gutzmer, J., Pacheco, N., Fonseca, R., Santos, S., Caetano, P., Reis, T., and Gonçalves, M., 2018, Indium and selenium distribution in the Neves-Corvo deposit, Iberian Pyrite Belt, Portugal: Mineralogical Magazine, v. 82, p. S5–S41.

Colpron, M., Nelson, J. L., and Murphy, D. C., 2006, A tectonostratigraphic framework for the pericratonic terranes of the northern Canadian Cordillera, in Colpron, M. and Nelson, J. L. eds., Paleozoic Evolution and Metallogeny of Pericratonic Terranes at the Ancient Pacific Margin of North America, Canadian and Alaskan Cordillera: Geological Association of Canada, Special Paper 45, p. 1–23.

Cook, N. J., 1996, Mineralogy of the sulphide deposits at Sulitjelma, northern Norway: Ore Geology Reviews, v. 11, p. 303–338.

Craig, J. R., and Vokes, F. M., 1992, Ore mineralogy of the Appalachian-Caledonian stratabound sulfide deposits: Ore Geology Reviews, v. 7, p. 77–123.

Cugerone, A., Cenki-tok, B., Muñoz, M., Kouzmanov, K., Oliot, E., Motto-ros, V., and Le Goff, E., 2021, Behavior of critical metals in metamorphosed Pb-Zn ore deposits : example from the Pyrenean Axial Zone: Mineralium Deposita, p. 685–705.

Denisová, N., and Piercey, S. J., 2022, Lithostratigraphy, lithogeochemistry and tectono-magmatic framework of the ABM replacement-style volcanogenic massive sulfide (VMS) deposit, Finlayson

Lake District, Yukon, Canada: Economic Geology, v. 117, p. 1299–1326.

Denisová, N., and Piercey, S. J., in press, Evolution of the hydrothermal system associated with the ABM replacement-style volcanogenic massive sulfide (VMS) deposit, Finlayson Lake district, Yukon, Canada: Economic Geology.

Doyle, M. G., and Allen, R. L., 2003, Subsea-floor replacement in volcanic-hosted massive sulfide deposits: Ore Geology Reviews, v. 23, p. 183–222.

Eldridge, C. S., Barton, P. B., and Ohmoto, H., 1983, Mineral textures and their bearing on formation of the Kuroko orebodies: Economic Geology Monograph 5, p. 241–281.

Foord, E. E., and Shawe, D. R., 1989, Pb-Bi-Ag-Cu-(Hg) chemistry of galena and some associated sulfosalts: A review and some new data from Colorado California and Pennsylvania: Canadian Mineralogist, v. 27, p. 363–382.

Franklin, J. M., Gibson, H. L., Jonasson, I. R., and Galley, A. G., 2005, Volcanogenic massive sulfide deposits, in Economic Geology 100th Anniversary Volume:, p. 523–560.

Frenzel, M., Hirsch, T., and Gutzmer, J., 2016, Gallium, germanium, indium, and other trace and minor elements in sphalerite as a function of deposit type - A meta-analysis: Ore Geology Reviews, v. 76, p. 52–78.

Gabrielse, H., Murphy, D. C., and Mortensen, J. K., 2006, Cretaceous and Cenozoic dextral orogen-parallel displacements, magmatism, and paleogeography, north-central Canadian Cordillera, in Haggart, J. W., Enkin, R. J., and Monger, J. W. H. eds., Paleogeography of the North American Cordillera: Evidence For and Against Large-Scale Displacements: Geological Association of Canada, Special Paper 46, p. 255–276.

Galley, A. G., Hannington, M. D., and Jonasson, I. R., 2007, Volcanogenic massive sulphide deposits, in Goodfellow, W. D. ed., Mineral Deposits of Canada: A Synthesis of Major Deposit-Types, District Metallogeny, the Evolution of Geological Provinces, and Exploration Methods: Geological Association of Canada, Mineral Deposits Division, Special Publication No. 5:, p. 141–161.

Genna, D., and Gaboury, D., 2015, Deciphering the hydrothermal evolution of a VMS system by LA-ICP-MS using trace elements in pyrite: An example from the Bracemac-McLeod deposits, Abitibi, Canada, and implications for exploration: Economic Geology, v. 110, p. 2087–2108.

Genna, D., Gaboury, D., and Roy, G., 2014, The Key Tuffite, Matagami Camp, Abitibi Greenstone Belt, Canada: petrogenesis and implications for VMS formation and exploration: Mineralium Deposita, v. 49, p. 489–512.

George, L. L., Cook, N. J., and Ciobanu, C. L., 2016, Partitioning of trace elements in co-crystallized sphalerite-galena-chalcopyrite hydrothermal ores: Ore Geology Reviews, v. 77, p. 97–116.

George, L. L., Cook, N. J., Crowe, B. B. P., and Ciobanu, C. L., 2018, Trace elements in hydrothermal chalcopyrite: Mineralogical Magazine, v. 82, p. 59–88.

Grant, H. L. J., Layton-Matthews, D., and Peter, J. M., 2015, Distribution and controls on silver mineralization in the Hackett River Main zone, Nunavut, Canada: An Ag- and Pb-enriched Archean volcanogenic massive sulfide deposit: Economic Geology, v. 110, p. 943–982.

Grant, H. L. J., Hannington, M. D., Petersen, S., Frische, M., and Fuchs, S. H., 2018, Constraints on the behavior of trace elements in the actively-forming TAG deposit, Mid-Atlantic Ridge, based on LA-ICP-MS analyses of pyrite: Chemical Geology, v. 498, p. 45–71.

Hannington, M. D., Galley, A. G., Herzig, P. M., Petersen, S., Gerzig, P. M., and Petersen, S., 1998, Comparison of the TAG mound and stockwork complex with Cyprus-type massive sulfide deposits, in Herzig, P. M., Humphris, S. E., Miller, D. J., and Zierenberg, R. A. eds., Proceedings of the Ocean Drilling Program: Scientific Results:, p. 389–415.

Hannington, M. D., Bleeker, W., and Kjarsgaard, I. M., 1999a, Sulfide mineralogy, geochemistry, and ore genesis of the Kidd Creek deposit: Part I. North, Central, and South orebodies (M. D. Hannington & C. T. Barrie, Eds.): Economic Geology Monograph 10, p. 225–266.

Hannington, M. D., Bleeker, W., and Kjarsgaard, I. M., 1999b, Sulfide mineralogy, geochemistry, and ore genesis of the Kidd Creek deposit: Part II. The bornite zone (M. D. Hannington & C. T. Barrie, Eds.): Economic Geology Monograph 10, p. 225–266.

Hannington, M. D., Kjarsgaard, I. M., Galley, A. G., and Taylor, B., 2003, Mineral-chemical studies of metamorphosed hydrothermal alteration in the Kristineberg volcanogenic massive sulfide district, Sweden: Mineralium Deposita, v. 38, p. 423–442.

Hannington, M. D., De Ronde, C. E. J., and Petersen, S., 2005, Sea-floor tectonics and submarine hydrothermal systems: Economic Geology 100th Anniversary Volume, p. 111–141.

Hatch, J. R., and Leventhal, J. S., 1992, Relationship between inferred redox potential of the depositional environment and geochemistry of the Upper Pennsylvanian (Missourian) Stark Shale Member of the Dennis Limestone, Wabaunsee County, Kansas, U.S.A.: Chemical Geology, v. 99, p. 65–82.

Heinrich, C. A., and Eadington, P. J., 1986, Thermodynamic predictions of the hydrothermal chemistry of arsenic, and their significance for the paragenetic sequence of some cassiterite-arsenopyrite-base metal sulfide deposits.: Economic Geology, v. 81, p. 511–529.

Hofmann, B. A., 1994, Formation of a sulfide melt during Alpine metamorphism of the Lengenbach polymetallic sulfide mineralization, Binntal, Switzerland: Mineralium Deposita, v. 29, p. 439–442.

Huston, D. L., Sie, S. H., Suter, G. F., Cooke, D. R., and Both, R. A., 1995, Trace elements in sulfide minerals from eastern Australian volcanic-hosted massive sulfide deposits: Part I. Proton microprobe analyses of pyrite, chalcopyrite, and sphalerite, and Part II. Selenium levels in pyrite: Comparison with d34S values and implic: Economic Geology, v. 90, p. 1167–1196.

Huston, D. L., Jablonski, W., and Sie, S. H., 1996, The distribution and mineral hosts of silver in eastern Australian volcanogenic massive sulfide deposits: Canadian Mineralogist, v. 34, p. 529–546.

James, R. H., Allen, D. E., and Seyfried, J. E., 2003, An experimental study of alteration of oceanic crust and terrigenous sediments at moderate temperatures (51 to 350°C): Insights as to chemical processes in near-shore ridge-flank hydrothermal systems: Geochimica et Cosmochimica Acta, v. 67, p. 681–691.

Kampmann, T. C., Jansson, N. F., Stephens, M. B., Olin, P. H., Gilbert, S., and Wanhainen, C., 2018, Syn-tectonic sulphide remobilization and trace element redistribution at the Falun pyritic Zn-Pb-Cu-(Au-Ag) sulphide deposit, Bergslagen, Sweden: Ore Geology Reviews, v. 96, p. 48–71.

Kase, K., Yamamoto, M., and Mitsuno, C., 1994, Germanium-bearing colusite from the Yanahara mine, Japan, and its significance to ore genesis: Resource Geology, v. 44, p. 33–38.

Keith, M., Haase, K. M., Schwarz-Schampera, U., Klemd, R., Petersen, S., Bach, W., Nordbayern, G., Erlangen-nürnberg, U., and Erlangen, D.-, 2014, Effects of temperature, sulfur, and oxygen fugacity on the composition of sphalerite from submarine hydrothermal vents: Geology, v. 42, p. 699–702.

Kissin, S. A., and Scott, S. D., 1982, Phase relations involving pyrrhotite below 350 C.: Economic Geology, v. 77, p. 1739–1754.

Knuckey, M. J., Comba, C. D. A., and Riverin, G., 1983, Structure, metal zoning and alteration at the Millenbach deposit, Noranda, Quebec: Geological Association of Canada Special Paper 25, p. 255–295.

Kretschmar, U., and Scott, S. D., 1976, Phase relations involving arsenopyrite in the system Fe-As-S and their application: Canadian Mineralogist, v. 14, p. 364–486.

Lafrance, B., Gibson, H. L., and Stewart, M. S., 2020, Internal and external deformation and modification of volcanogenic massive sulfide deposits, in Rowland, J. V. and Rhys, D. A. eds., Reviews in Economic Geology 21:, p. 147–171.

Large, R. R., 1977, Chemical evolution and zonation of massive sulfide deposits in volcanic terrains: Economic Geology, v. 72, p. 549–572.

Large, R. R., 1992, Australian volcanic-hosted massive sulfide deposits: Features, styles, and genetic models: Economic Geology, v. 87, p. 471–510.

Larocque, A. C. L., and Hodgson, C. J., 1995, Effects of greenschist-facies metamorphism and related deformation on the Mobrun massive sulfide deposit, Quebec, Canada: Mineralium Deposita, v. 30, p. 439–448.

Layton-Matthews, D., Peter, J. M., Scott, S. D., and Leybourne, M. I., 2008, Distribution, mineralogy, and geochemistry of selenium in felsic volcanic-hosted massive sulfide deposits of the Finlayson Lake district, Yukon Territory, Canada: Economic Geology, v. 103, p. 61–88.

Layton-Matthews, D., Leybourne, M. I., Peter, J. M., Scott, S. D., Cousens, B., and Eglington, B. M., 2013, Multiple sources of selenium in ancient seafloor hydrothermal systems: Compositional and Se, S, and Pb isotopic evidence from volcanic-hosted and volcanic-sediment-hosted massive sulfide deposits of the Finlayson Lake district, Yukon, Canada: Geochimica et Cosmochimica Acta, v. 117, p. 313–331.

Lianxing, G., and Vokes, F. M., 1996, Intergrowths of hexagonal and monoclinic pyrrhotites in some sulphide ores from norway: Mineralogical Magazine, v. 60, p. 303–316.

Lockington, J. A., Cook, N. J., and Ciobanu, C. L., 2014, Trace and minor elements in sphalerite from metamorphosed sulphide deposits: Mineralogy and Petrology, v. 108, p. 873–890.

Lydon, J. W., 1988, Volcanogenic massive sulphide deposits Part 2: Genetic models, in Ore Deposit Models Geoscience Canada Reprint Series 3:, p. 155–181.

Manor, M. J., Piercey, S. J., Murphy, D. C., and Wall, C. J., 2022a, Age and Chemostratigraphy of the Finlayson Lake District , Yukon : Implications for Volcanogenic Massive Sulfide (VMS) Mineralization and Tectonics along the Western Laurentian Continental Margin: Lithosphere, v. 2022, p. 45.

Manor, M. J., Piercey, S. J., Wall, C. J., and Denisová, N., 2022b, High precision CA-ID-TIMS U-Pb zircon geochronology of felsic rocks in the Finlayson Lake VMS district, Yukon: Linking Paleozoic basin-scale accumulation rates to the occurrence of subseafloor replacement-style mineralization: Economic Geology, v. 117, p. 1173–1201.

Marshall, B., and Gilligan, L. B., 1987, An introduction to remobilization: Information from ore-body geometry and experimental considerations: Ore Geology Reviews, v. 2, p. 87–131.

Marshall, B., and Gilligan, L. B., 1989, Durchbewegung structure, piercment cusps, and piercement veins in massive sulfide deposits: Formation and interpretation: Economic Geology, v. 84, p. 2311–2319.

Marshall, B., Vokes, F. M., and Larocque, A. C. L., 1998, Regional metamorphic remobilization: Upgrading and formation of ore deposits, in Vokes, F. M., Marshall, B., and Spry, P. G. eds., Reviews in Economic Geology 11:, p. 19–38.

Martin, A. J., McDonald, I., MacLeod, C. J., Prichard, H. M., and McFall, K., 2018, Extreme enrichment of selenium in the Apliki Cyprus-type VMS deposit, Troodos, Cyprus: Mineralogical Magazine, v. 82, p. 697–724.

Martin, A. J., McDonald, I., Jamieson, J. W., Jenkin, G. R. T., McFall, K. A., Piercey, G., MacLeod, C. J., and Layne, G. D., 2021, Mineral-scale variation in the trace metal and sulfur isotope composition of pyrite: Implications for metal and sulfur sources in mafic VMS deposits: Mineralium Deposita.

Mercier-Langevin, P., Hannington, M. D., Dubé, B., and Bécu, V., 2011, The gold content of volcanogenic massive sulfide deposits: Mineralium Deposita, v. 46, p. 509–539.

Miller, W. J., and Craig, J. R., 1983, Tetrahedrite-tennantite series compositional variations in the Cofer Deposit, Mineral District, Virginia: American Mineralogist, v. 68, p. 227–234.

Mortensen, J. K., 1992, Pre-mid-Mesozoic tectonic evolution of the Yukon-Tanana terrane, Yukon and Alaska: Tectonics, v. 11, p. 836–853.

Mortensen, J. K., and Jilson, G. A., 1985, Evolution of the Yukon-Tanana terrane: Evidence from southeastern Yukon territory: Geology, v. 13, p. 806–810.

Mortensen, J. K., Dusel-Bacon, C., Hunt, J., and Gabites, J., 2006, Lead isotopic constraints on the metallogeny of middle and late Paleozoic syngenetic base-metal occurences in the Yukon-Tanana and Slide Mountain/Seventymile terranes and adjacent portions of the North American miogeocline, in Colpron, M. and Nelson, J. A. L. eds., Paleozoic evolution and metallogeny of pericratonic terranes at the Ancient Pacific Margin of North America, Canadian and Alaskan Cordillera: Geological Association of Canada, p. 261–279.

Murowchick, J. B., 1992, Marcasite inversion and the petrographic determination of pyrite ancestry: Economic Geology, v. 87, p. 1141–1152.

Murphy, D. C., and Piercey, S. J., 1998, Finlayson project : Geological evolution of Yukon-Tanana terrane and its relationship to Campbell Range belt, northern Wolverine Lake map area, southeastern Yukon (C. F. Roots & D. S. Emond, Eds.): Yukon Exploration and Geology 1998, p. 47–62.

Murphy, D. C., Mortensen, J. K., Piercey, S. J., Orchard, M. J., and Gehrels, G. E., 2006, Mid-Paleozoic to early Mesozoic tectonostratigraphic evolution of Yukon-Tanana and Slide Mountain terranes and affiliated overlap assemblages, Finlayson Lake massive sulphide district, southeastern Yukon, in Colpron, M. and Nelson, J. L. eds., Paleozoic Evolution and Metallogeny of Pericratonic Terranes at the Ancient Pacific Margin of North America, Canadian and Alaskan Cordillera: Geologic Association of Canada, Special Paper 45, p. 75–106.

Nelson, J. L., Piercey, S. J., Murphy, D. C., Colpron, M., Dusel-Bacon, C., Roots, C. F., Geologicalsurvey, B. C., Piercey, S. J., and Murphy, D. C., 2006, Paleozoic tectonic and metallogenetic evolution of pericratonic terranes in Yukon, northern British Columbia and eastern Alaska 1, in Colpron, M. and Nelson, J. L. eds., Paleozoic Evolution and Metallogeny of Pericratonic Terranes at the Ancient Pacific Margin of North America, Canadian and Alaskan Cordillera: Geological Association of Canada, Special Paper 45: Geological Association of Canada, p. 323–360.

Nozaki, T., Nagase, T., Takaya, Y., Yamasaki, T., and Otake, T., 2021, Subseafloor sulphide deposit formed by pumice replacement mineralisation: Scientific Reports, v. 11, p. 1–11.

Ohmoto, H., 1996, Formation of volcanogenic massive sulfide deposits: The Kuroko perspective: Ore Geology Reviews, v. 10, p. 135–177.

van Olden, K., Green, A., and Davidson, G., 2020, NI 43-101 Feasibility Study Technical Report Kudz Ze Kayah Property, Yukon, Canada CSA Global Report n. R173.2019: CSA Global, 376 p.

Paikaray, S., 2012, Environmental hazards of arsenic associated with black shales: A review on geochemistry, enrichment and leaching mechanism: Reviews in Environmental Science and Biotechnology, v. 11, p. 289–303.

Paton, C., Hellstrom, J., Paul, B., Woodhead, J., & Hergt, J., 2011. Iolite: Freeware for the visualisation and processing of mass spectrometric data: Journal of Analytical Atomic Spectrometry, v. 26, p. 2508-2518.

Peter, J. M., Layton-Matthews, D., Piercey, S. J., Bradshaw, G. D., Paradis, S., and Bolton, A., 2007, Volcanogenic-hosted massive sulphide deposits of the Finlayson Lake district, Yukon (W. D. Goodfellow, Ed.): Mineral Deposits of Canada: A Synthesis of Major Deposit-Types, District Metallogeny, the Evolution of Geological Provinces, and Exploration Methods: Geological Association of Canada, Mineral Deposits Division, Special Publication No. 5, p. 471–508.

Piercey, S. J., 2015, A semipermeable interface model for the genesis of subseafloor replacement-type volcanogenic massive sulfide (VMS) deposits: Economic Geology, v. 110, p. 1655–1660.

Piercey, S. J., and Colpron, M., 2009, Composition and provenance of the Snowcap assemblage, basement to the Yukon-Tanana terrane, northern Cordillera: Implications for Cordilleran crustal growth: Geosphere, v. 5, p. 439–464.

Piercey, S. J., Murphy, D. C., Mortensen, J. K., and Paradis, S., 2001a, Boninitic magmatism in a continental margin setting, Yukon-Tanana terrane, southeastern Yukon, Canada: Geology, v. 29, p. 731–734.

Piercey, S. J., Paradis, S., Murphy, D. C., and Mortensen, J. K., 2001b, Geochemistry and paleotectonic setting of felsic volcanic rocks in the Finlayson Lake volcanic-hosted massive sulfide district, Yukon, Canada: Economic Geology, v. 96, p. 1877–1905.

Piercey, S. J., Mortensen, J. K., Murphy, D. C., Paradis, S., and Creaser, R. A., 2002, Geochemistry and tectonic significance of alkalic mafic magmatism in the Yukon-Tanana terrane, Finlayson Lake region, Yukon: Canadian Journal of Earth Sciences, v. 39, p. 1729–1744.

Piercey, S. J., Mortensen, J. K., and Creaser, R. A., 2003, Neodymium isotope geochemistry of felsic volcanic and intrusive rocks from the Yukon-Tanana terrane in the Finlayson Lake region, Yukon, Canada: Canadian Journal of Earth Sciences, v. 40, p. 77–97.

Piercey, S. J., Nelson, J. L., Colpron, M., Dusel-Bacon, C., Roots, C. F., Simard, R.-L. L., Roots, C. F., Road, R. L., Nelson, J. L., Colpron, M., Dusel-Bacon, C., and Roots, C. F., 2006, Paleozoic magmatism and crustal recycling along the ancient Pacific margin of North America, northern Cordillera, in Colpron, M. and Nelson, J. L. eds., Paleozoic Evolution and Metallogeny of Pericratonic Terranes at the Ancient Pacific Margin of North America, Canadian and Alaskan Cordillera: Geological Association of Canada, Special Paper 45, p. 281–322.

Piercey, S. J., Squires, G. C., and Brace, T. D., 2014, Lithostratigraphic, hydrothermal, and tectonic setting of the Boundary volcanogenic massive sulfide deposit, Newfoundland Appalachians, Canada: Formation by subseafloor replacement in a Cambrian rifted arc: Economic Geology, v. 109, p. 661–687.

Pisutha-Arnond, V., and Ohmoto, H., 1983, Thermal history, and chemical and isotopic compositions of the ore-forming fluids responsible for the Kuroko massive sulfide deposits in the Hokuroku district of Japan: Economic Geology Monograph 5, p. 523–558.

Riverin, G., and Hodgson, C. J., 1980, Wall-rock alteration at the Millenbach Cu-Zn mine, Noranda, Quebec: Economic Geology, v. 75, p. 424–444.

de Ronde, C. E. J., Hannington, M. D., Stoffers, P., Wright, I. C., Ditchburn, R. G., Reyes, A. G., Baker, E. T., Massoth, G. J., Lupton, J. E., Walker, S. L., Greene, R. R., Soong, C. W. R., Ishibashi, J., Lebon, G. T., et al., 2005, Evolution of a submarine magmatic-hydrothermal system: Brothers volcano, southern Kermadec arc, New Zealand: Economic Geology, v. 100, p. 1097–1133.

Scott, S. D., 1983, Chemical behaviour of sphalerite and arsenopyrite in hydrothermal and metamorphic environments: Mineralogical Magazine, v. 47, p. 427–435.

Scott, S. D., and Barnes, H. L., 1971, Sphalerite geothermometry and geobarometry: Economic Geology, v. 66, p. 653–669.

Sebert, C., Hunt, J. A., and Foreman, I. J., 2004, Geology and lithogeochemistry of the Fyre Lake copper-cobalt-gold sulphide-magnetite deposit, southeastern Yukon: Yukon Geological Survey, accessed at Open File 2004-17, 46 p.

Sharp, Z. D., Essene, E. J., Kelly, W. C., and Arbor, A., 1985, A re-examination of the arsenopyrite geothermometer: Pressure considerations and applications to natural assemblages: Canadian Mineralogist, v. 23, p. 517–534.

Sillitoe, R. H., and Hedenquist, J. W., 2003, Linkages between volcanotectonic settings, ore-fluid compositions, and epithermal precious metal deposits, in Simmons, S. F. and Graham, I. eds., Volcanic, Geothermal, and Ore-Forming Fluids:Society of Economic Geologists, p. 315–343.

Sillitoe, R. H., Hannington, M. D., and Thompson, J. F. H., 1996, High sulfidation deposits in the volcanogenic massive sulfide environment: Economic Geology, v. 91, p. 204–212.

Solomon, N., and Walshe, J. L., 1979, The formation of massive sulfide deposits on the sea floor: Economic Geology, v. 74, p. 797–813.

Sparks, H. A., and Mavrogenes, J. A., 2005, Sulfide melt inclusions as evidence for the existence of a sulfide partial melt at Broken Hill, Australia: Economic Geology, v. 100, p. 773–779.

Staples, R. D., Murphy, D. C., Gibson, H. D., Colpron, M., Berman, R. G., and Ryan, J. J., 2014, Middle Jurassic to earliest Cretaceous mid-crustal tectono-metamorphism in the northern Canadian Cordillera: Recording foreland-directed migration of an orogenic front: GSA Bulletin, v. 126, p. 1511–1530.

Tomkins, A. G., Pattison, D. R. M., and Frost, B. R., 2007, On the initiation of metamorphic sulfide anatexis: Journal of Petrology, v. 48, p. 511–535.

Urabe, T., Scott, S. D., and Hattori, K., 1983, A comparison of footwall-rock alteration and geothermal systems beneath some Japanese and Canadian volcanogenic massive sulfide deposits (H. Ohmoto & B. J. Skinner, Eds.): Economic Geology Monograph 5, p. 345–364.

Vikentyev, I. V., Belogub, E. V., Novoselov, K. A., and Moloshag, V. P., 2017, Metamorphism of volcanogenic massive sulphide deposits in the Urals. Ore geology: Ore Geology Reviews, v. 85, p. 30–63.

Vine, J. D., and Tourtel, E. B., 1970, Geochemistry of black shale deposits - A summary report: Economic Geology, v. 65, p. 253–272.

Chapter 5

Conclusions and implications for future research

5.1 Summary and conclusions

The research in this dissertation has characterized the lithostratigraphy, hydrothermal alteration, and massive sulfide mineralization at the ABM deposit and this has provided insight into genetic and exploration models for this deposit and similar environments globally. The reconstruction of the lithostratigraphy and basin architecture has been an indispensable research tool in all stages of the project, and it has provided a stratigraphic and paragenetic framework for detailed deposit-scale observations. Summarized below are the key findings of this thesis that focus on the: (1) lithostratigraphy, chemostratigraphy and the tectonomagmatic framework of the ABM deposit; (2) evolution of the hydrothermal system and the hydrothermal footprint of mineralization; and (3) genesis of the massive sulfide mineralization.

The reconstruction of the basin architecture that hosts the ABM deposit has revealed several previously unidentified features in the basin. Lack of storm bed textures in the host rocks, and lack of textures indicative of hydrothermal boiling or fluid separation, together with the occurrence of Cu-rich zones in the mineralization at the ABM deposit suggest that the basin was at least 750 metres deep. The abundance of coherent volcanic rocks, the common occurrence of crystal-rich tuffs, and thick units of lapilli tuffs suggest that the ABM deposit formed proximal to an active volcanic centre in a sub-basin. The systematic changes in the thickness of the sedimentary and volcaniclastic units across different drill holes, combined with the distribution and morphology of coherent volcanic units, have identified two sets of synvolcanic faults, subordinate to the predecessor of East fault. The faults were active during the deposition and emplacement of the lithostratigraphic units comprising the upper Kudz Ze Kayah formation, and acted as conduits for ascending magmas, thus exercising a degree of control over the distribution of the sills, domes, and flows. During periods of volcanic inactivity, the faults also functioned as conduits for the hydrothermal fluids.

The felsic volcanic rocks occur in two major geochemical groups, FA, and FB. Group FA has elevated Zr contents (>550 ppm) and has elevated values of high field strength elements (Hf, Nb, Ta, Th, Ti), rare earth elements, and Nb/Ta ratios compared to the group FB (Zr<500 ppm). The felsic lithofacies in the hanging wall and footwall sequences comprise group FA, whereas the felsic lithofacies in the sequence hosting the massive sulfide mineralization comprise group FB. Although the FA rocks are not directly associated with the replacement-style mineralization at the ABM deposit, they are an important indicator of an elevated heat gradient in the back-arc basin, and the mantle-like Nb/Ta ratio (~17.8) of the FA felsic rocks reflects high temperature magmas in the subsurface and mixing of juvenile material with crustal melts in the magma chamber. The elevated geothermal gradient in the back-arc basin drove the hydrothermal fluid circulation that formed the hydrothermal alteration and the massive sulfide mineralization at the ABM deposit.

The hydrothermal system affected predominantly felsic volcanic rocks in the ABM deposit footprint and the hydrothermal fluids exploited the porosity and permeability contrasts between volcaniclastic and coherent (e.g., sills, domes, flows) units. The main hydrothermal alteration processes were feldspar destruction and formation of phyllosilicate minerals, which suggests that the hydrothermal fluids were hot and acidic. Formation temperatures determined from illite and chlorite geothermometry indicate that the hydrothermal system became progressively hotter. The moderate white mica ± chlorite alteration assemblage is the most extensive and is interpreted to have formed at ~215±30 °C. Overprinting it are zones of pervasive white mica alteration that surround the massive sulfide mineralization that are interpreted to have formed at ~250±15 °C. Directly associated with the massive sulfide mineralization is the pervasive chlorite alteration assemblage that is interpreted to have formed at ~320±10 °C and overprints the pervasive white mica alteration. The VMS-related hydrothermal alteration extends >1 km beyond the mineralization, the hydrothermal system was at its peak during a period of volcanic inactivity, but hydrothermal activity continued during the deposition of the hanging wall sequence, although it is possible that the centre of the hydrothermal system moved elsewhere in the basin, given the lack of the high temperature chlorite-rich assemblages in the hanging wall sequence at the ABM deposit.

The replacement-style massive sulfide mineralization at the ABM deposit occurs as a series of stacked stratabound lenses subparallel to the host rock stratigraphy. Mineralization formed through replacement of pre-existing strata below the seafloor, and remnant clasts of volcanic rocks and preserved bedding occur within the massive sulfide lenses. Mineralogical, textural, and assay data show that the effects of greenschist facies metamorphism and deformation on the ABM massive sulfide mineralization were limited to recrystallization of sulfides, small-scale remobilization (<1 m) and trace element redistribution. Metamorphism did not affect the deposit-scale metal zonation of Cu→Zn-Pb→Ba from interior to exterior of the massive sulfide lenses that reflects lowering temperatures and more oxidizing conditions as hot, reduced, metal-rich hydrothermal fluids gradually infiltrated porous substrate, mixed with cold seawater, and precipitated mineralization, which was further modified by zone refining as the deposit matured. The widespread pyrite-sphalerite mineral assemblage occurs more commonly towards the lens margins and coincides with enrichment of Zn-Pb-Ag-Au-Hg-As-Sb-Ba and is interpreted to have formed at temperatures ~200-270 °C under fluctuating redox conditions documented by the occurrence of arsenopyrite, tetrahedrite group minerals, and barite. The pyrite-chalcopyrite-magnetite-pyrrhotite assemblage occurs in the centres of massive sulfide lenses and overlaps with zones of Cu-Bi-Se-Co enrichment. The assemblage formed from reducing, high temperature (~300-350 °C) fluids, which is illustrated by commonly occurring sphalerite enriched in Fe and rare arsenopyrite. A minor assemblage comprising chalcopyrite-pyrrhotite-pyrite stringers is associated with pervasive chlorite alteration and occurs on the margins and locally within the massive sulfide lenses.

The element assemblages occurring in the massive sulfide mineralization are reminiscent of VMS deposits with an possible magmatic-volatile contribution, however, no other characteristic features such as an advanced argillitic alteration assemblage or a contemporaneous intrusion/magma chamber have been observed at the ABM deposit, and it is possible that leaching from shales could also have contributed to some enrichment in the elements outlined above. Studies of *in situ* mineral chemistry of the sulfides in different assemblages across the ABM deposit have shown values of the $Se/S \times 10^6$ ratio that are consistent with Se (and likely other metals) derived from the leaching of igneous (± other types of) basement rocks.

From an exploration viewpoint, this research presents several features that can be used in camp- and district-scale exploration in bimodal-felsic back-arc environments. The ABM deposit is associated with a volcanic centre, so the abundance of coherent units, crystal-rich tuffs, and thick volcaniclastic units should be considered as prospective features in the stratigraphy that become more prominent with proximity to the centre of volcanic activity. The prospective horizon at the ABM deposit has features that mark a period of volcanic inactivity like the deposition of an argillite unit and the switch from one geochemical signature to another (e.g., FB to FA), so similar stratigraphic markers of major changes in magmatic activity should be investigated for hydrothermal alteration. The effects of hydrothermal alteration at the ABM deposit are quantifiable and track the feldspar destruction and white mica and chlorite formation. In basins with abundant and extensive volcaniclastic units, mineral chemistry of white mica, and to a limited extent of chlorite, can be used to trace prospective horizons. At the ABM deposit, phyllosilicates are enriched in Mg (both white mica and chlorite) and K (white mica only) in proximity to the massive sulfide mineralization, and their composition can be used to vector towards zones of higher temperature hydrothermal alteration. Barium abundances in whole-rock lithogeochemical data can be used on the camp- to deposit-scale to target hydrothermally altered units and the massive sulfide mineralization. On a smaller scale (deposit- and/or camp-scale), element (base metals, Sb, and Tl in whole-rock) and compositional (Sb and Tl in white mica) vectors can be used to target the massive sulfide mineralization.

5.2 Suggestions for future research

This study provides new insights into the lithostratigraphy, tectonomagmatic setting, and the evolution of the hydrothermal system and mineralization at the ABM replacement-style VMS deposit in the Finlayson Lake district, Yukon, Canada that can be applied to understand the formation of replacement-style VMS deposits in back-arc environments globally. Outlined below are suggestions for future research that could answer some of the remaining unresolved questions and add to the understanding of the evolution and prospectivity of the wider area surrounding the ABM deposit.

5.2.1 Extending the basin reconstruction outwards from the ABM deposit

The model of the lithostratigraphy, chemostratigraphy, and basin architecture at present covers the ABM deposit and extends approximately 100 m out along strike and dip, where not cut by post-VMS faults. Investigation of drill holes outside of the immediate deposit footprint has been limited in this study. Expansion of detailed core logging with focus on volcanic textures and hydrothermal alteration assemblages should be combined with an investigation of the structural geology of the area to identify other post-VMS faults that are indicated by locally abundant fault zones in drill core, and that segment the lithostratigraphy into offset blocks like in the case of the Krakatoa zone. Characterizing the lithostratigraphic units in terms of chemostratigraphy and identifying major stratigraphic breaks (e.g., argillite units, possible exhalite units) can then be used to correlate the blocks together and to identify and follow any VMS-prospective horizons, and possibly identify other sub-basin with active volcanic centres like the one hosting the ABM deposit.

5.2.2 Use of portable X-ray fluorescence instruments

The use of portable X-ray fluorescence (pXRF) instruments is becoming more common in exploration as the technology improves and the instruments are able to deliver reliable results for elements from Al to U (Ross et al., 2014; Young et al., 2016; McNulty et al., 2020; Gisbert et al., 2021) that commonly occur in varying quantities in hydrothermal systems and igneous rocks. The use of pXRF at the ABM deposit would help investigate two features of the VMS hydrothermal system at the ABM deposit – the chemostratigraphy of the host rocks and the hydrothermal alteration.

The research presented in this dissertation identified distinct geochemical groups within the felsic and mafic lithofacies that are identifiable using immobile element ratios (e.g., Zr/TiO_2, Al_2O_3/TiO_2, Zr/Al_2O_3, Nb/TiO_2) and mapped out the chemostratigraphy of the upper Kudz Ze Kayah formation. The pXRF instrument could potentially be used to rapidly assess the geochemical composition of the volcanic rocks and help identify VMS-prospective horizons based on the changes in geochemistry.

The restricted range of light elements reliably analyzed by the pXRF (e.g., Na, Mg not analyzed) precludes the use of most of the alteration indices (alteration index, chlorite-carbonate-pyrite index, Spitz-Darling index; Spitz and Darling, 1978; Large et al., 2001; Ruks et al., 2006), and the later low-temperature carbonate overprint at the ABM deposit limits the use of other indices that utilize Ca or Sr (e.g., Rb/Sr; McNulty et al., 2020). However, other elements that can be used as vectors towards the massive sulfide mineralization (e.g., Ba, base metals), either as abundances or in ratios with other elements are within the range of elements analyzed by the pXRF (McNulty et al., 2020; Gisbert et al., 2021). At the ABM deposit, mapping out the distribution of Ba in greater detail could help identify fluid pathways and vector towards zones of more intense hydrothermal alteration. Potential zones with elevated of Ba or other elements of interest can be evaluated using other types of geochemical analysis.

5.2.3 Tracking fluid pathways using O isotope geochemistry

Studies of O isotopes in whole-rock samples in VMS deposits have been used to map out the hydrothermal systems and their architecture, to map the thermal effects of the hydrothermal fluid flow, and to determine the hydrothermal fluids temperatures and fluid to rock ratios, on both district- (Green et al., 1983; Cathles, 1993; Holk et al., 2008) and deposit-scale (Beaudoin et al., 2014; Taylor et al., 2014). A similar study at the ABM deposit could test the interpreted synvolcanic faults and identify previously unknown pathways, and possibly identify large-scale fluid flow trends, and help in identifying potential conduits, or source subvolcanic intrusions. Oxygen isotope geochemistry could also be another independent method for determining the different formation temperatures of hydrothermal alteration assemblages (Taylor, 1997).

5.2.4 Testing ammonium content in micas

Shortwave infra-red analyses performed using Terraspec have identified the occurrence of a 2115W spectral feature in several of the white mica spectra from the samples collected in the ABM deposit footprint. The 2115W spectral feature indicates the presence of NH_4 in the crystal structure of the white mica (Felzer et al., 1994; Yang et al., 2001; Ruiz Cruz and Sanz De Galdeano, 2008). Samples with peaks at the 2115W feature occur proximal to the massive sulfide mineralization and in the hanging wall sequence, in laterally continuous zones. Other studies have shown that NH_4-

enriched micas can form halos surrounding stratiform massive sulfide mineralization (Sterne et al., 1982), but they are commonly associated with argillites (Sterne et al., 1982; Nieto, 2002) or with pyrophyllite deposits or similar hydrothermal alteration assemblages (Higashi, 1982; Kawano and Tomita, 1988). The samples identified at the ABM deposit do not show any systematic association with the known argillite lenses. Determining whether the samples with peaks at the 2115W feature actually contain NH_4 in the mica structure through analytical methods would confirm if the 2115W feature measured by Terraspec is a reliable method of identifying the presence of the ammonium group in white micas. If NH_4-enriched micas occur at the ABM deposit, their relationship to the hydrothermal system and mineralization at the ABM deposit would need to be determined to assess the usefulness of NH_4-enriched micas as indicators of hydrothermal alteration.

5.2.5 Low Te content in the massive sulfide mineralization

Sulfide minerals at the ABM deposit have low Te contents that are rarely above the detection limit (~0.2 ppm). For a deposit enriched in Se, with the As-Sb-Ag-Au-Hg element assemblage present in the major mineralization assemblages, this is unusual. Other VMS deposit that contain similar elemental assemblages are relatively enriched in Te (Brueckner et al., 2016; Martin et al., 2018). The very low Te contents in the ABM deposit are atypical, and further study of this feature of the massive sulfide mineralization could help constrain the underlying sources of metals, especially regarding any magmatic volatile influx.

5.2.6 Detailed examination of symplectic intergrowths

Further investigation of symplectic intergrowths present in the pyrite-chalcopyrite-magnetite-pyrrhotite assemblage, and the effects of metamorphism more widely would enhance our understanding of how sulfide anatexis initiates at relatively low temperatures (300-400 °C) during metamorphism and what features of the massive sulfide mineralization in VMS deposits are needed for the formation of sulfide melts. For example, enrichment of Bi, Sb, Hg, Ag, or other metals and metalloids, the occurrence of two or more minerals (galena, chalcopyrite, sphalerite), or the added deformation from nearby post-VMS faults. Transmitted electron microscopy or atom probe tomography could be used to study the behaviour of Bi and other possible nanoparticles in the symplectic intergrowths.

5.3 References

Beaudoin, G., Mercier-Langevin, P., Dubé, B., and Taylor, B. E., 2014, Low-temperature alteration at the world-class LaRonde Penna Archean Au-rich volcanogenic massive sulfide deposit, Abitibi subprovince, Quebec, Canada: Evidence from whole-rock oxygen isotopes: Economic Geology, v. 109, p. 167–182.

Brueckner, S. M., Piercey, S. J., Pilote, J. L., Layne, G. D., and Sylvester, P. J., 2016, Mineralogy and mineral chemistry of the metamorphosed and precious metal-bearing Ming deposit, Canada: Ore Geology Reviews, v. 72, p. 914–939.

Cathles, L. M., 1993, Oxygen isotope alteration in the Noranda mining district, Abitibi Greenstone Belt, Quebec: Economic Geology, v. 88, p. 1483–1511.

Felzer, B., Hauff, P., and Goetz, A. F. H., 1994, Quantitative reflectance spectroscopy of buddingtonite from the Cuprite mining district, Nevada: Journal of Geophysical Research, v. 99, p. 2887–2895.

Gisbert, G., Tornos, F., Losantos, E., Pons, J. M., and Videira, J. C., 2021, Vectors to ore in replacive volcanogenic massive sulfide (VMS) deposits of the northern Iberian Pyrite Belt: mineral zoning, whole rock geochemistry, and application of portable X-ray fluorescence: Solid Earth, v. 12, p. 1931–1966.

Green, G. R., Ohmoto, H., Date, J., and Takahashi, T., 1983, Whole-rock oxygen isotope distribution in the Fukazawa-Kosaka area, Hokuroku district, Japan, and its potential application to mineral exploration: Economic Geology Monograph 5, p. 395–411.

Higashi, S., 1982, Tobelite, a new ammonium dioctahedral mica: Mineralogical Journal, v. 11, p. 138–146.

Holk, G. J., Taylor, B. E., and Galley, A. G., 2008, Oxygen isotope mapping of the Archean Sturgeon Lake caldera complex and VMS-related hydrothermal system, Northwestern Ontario, Canada: Mineralium Deposita, v. 43, p. 623–640.

Kawano, M., and Tomita, K., 1988, Ammonium-bearing dioctahedral 2M1 mica from Aira district, Kagoshima Prefecture: Clay Science, v. 7, p. 161–169.

Large, R. R., Gemmell, J. B., and Paulick, H., 2001, The alternation box plot: A simple approach to understanding the relationship between alteration mineralogy and lithogeochemistry associated with volcanic-hosted massive sulfide deposits: Economic Geology, v. 96, p. 957–971.

Layton-Matthews, D., Leybourne, M. I., Peter, J. M., Scott, S. D., Cousens, B., and Eglington, B. M., 2013, Multiple sources of selenium in ancient seafloor hydrothermal systems: Compositional and Se, S, and Pb isotopic evidence from volcanic-hosted and volcanic-sediment-hosted massive sulfide deposits of the Finlayson Lake district, Yukon, Canada: Geochimica et Cosmochimica Acta, v. 117, p. 313–331.

Martin, A. J., McDonald, I., MacLeod, C. J., Prichard, H. M., and McFall, K., 2018, Extreme enrichment of selenium in the Apliki Cyprus-type VMS deposit, Troodos, Cyprus: Mineralogical Magazine, v. 82, p. 697–724.

McNulty, B. A., Fox, N., and Bruce Gemmell, J., 2020, Assessing hydrothermal alteration intensity in volcanic-hosted massive sulfide systems using portable X-ray fluorescence analysis of drill core: An example from Myra Falls, Canada: Economic Geology, v. 115, p. 443–453.

Nieto, F., 2002, Characterization of coexisting NH4- and K-micas in very low-grade metapelites: American Mineralogist, v. 87, p. 205–216.

Ross, P. S., Bourke, A., and Fresia, B., 2014, Improving lithological discrimination in exploration drill-cores using portable X-ray fluorescence measurements: (1) testing three Olympus Innov-X analysers on unprepared cores: Geochemistry: Exploration, Environment, Analysis, v. 14, p. 171–185.

Ruiz Cruz, M. D., and Sanz De Galdeano, C., 2008, High-temperature ammonium white mica from the Betic Cordillera (Spain): American Mineralogist, v. 93, p. 977–987.

Ruks, T. W., Piercey, S. J., Road, L., Pe, O., Ryan, J. J., Villeneuve, M. E., and Creaser, R. A., 2006, Mid- to late Paleozoic K-feldspar augen granitoids of the Yukon-Tanana terrane, Yukon, Canada:

Implications for crustal growth and tectonic evolution of the northern Cordillera: Bulletin of the Geological Society of America, v. 118, p. 1212–1231.

Spitz, G., and Darling, R., 1978, Major and minor element lithogeochemical anomalies surrounding the Louvem copper deposit, Val d’Or, Quebec: Canadian Journal of Earth Sciences, v. 15, p. 1161–1169.

Sterne, E. J., Reynolds, R. C., and Zantop, H., 1982, Natural ammonium illites from black shales hosting a stratiform base metal deposit, Delong Mountains, northern Alaska.: Clays & Clay Minerals, v. 30, p. 161–166.

Taylor, B. E., De Kemp, E., Grunsky, E., Martin, L., Maxwell, G., Rigg, D., Goutier, J., Lauzière, K., and Dubé, B., 2014, Three-dimensional visualization of the Archean Horne and Quemont Au-bearing volcanogenic massive sulfide hydrothermal systems, Blake River Group, Quebec: Economic Geology, v. 109, p. 183–203.

Taylor, H. P., 1997, Oxygen and hydorgen isotope relationships in hydrothermal mineral deposits, in Barnes, H. L. ed., Geochemistry of Hydrothermal Ore Deposits: John Wiley and Sons, p. 229–302.

Yang, K., Browne, P. R. L., Huntington, J. F., and Walshe, J. L., 2001, Characterising the hydrothermal alteration of the Broadlands-Ohaaki geothermal system, New Zealand, using short-wave infrared spectroscopy: Journal of Volcanology and Geothermal Research, v. 106, p. 53–65.

Young, K. E., Evans, C. A., Hodges, K. V., Bleacher, J. E., and Graff, T. G., 2016, A review of the handheld X-ray fluorescence spectrometer as a tool for field geologic investigations on Earth and in planetary surface exploration: Applied Geochemistry, v. 72, p. 77–87.

Appendix 1.1 Whole rock lithogeochemistry analyses

Sample	B370156	B370157	B370158	B370159	B370160	B370161	B370162	B370163	B370175	B370176	B370177	B370178	B370179
Rock Type*	LT	LT	TF	TF	TF	TF	VF	TF	TF	TF	TF	TF	TF
DDH_ID	K15-301	K15-301	K15-301	K15-301	K15-301	K15-301	K15-301	K15-301	K15-320	K15-320	K15-320	K15-320	K15-320
DDH_From	22.65	47.9	77.55	91.25	102.55	117.6	122.7	135.85	18.85	50.3	76.45	95.85	114.45
DDH_To	22.8	48.05	77.65	91.4	102.7	117.7	122.8	136	18.95	50.4	76.55	95.95	114.55
Major elements (wt%)													
SiO_2	68.7	71.6	76.9	69	41.8	76.2	73.1	74.4	63.8	61.4	64.6	70.8	76.3
TiO_2	0.57	0.26	0.14	0.36	0.21	0.33	0.27	0.27	0.59	0.66	0.51	0.46	0.26
Al_2O_3	15.7	13	10.2	15.1	11	14.05	12.4	11.7	16.2	16.7	13.4	13.5	13.75
Fe_2O_3	2.48	2.59	1.21	0.97	3.23	1.93	1.34	2.62	5.67	4.43	3.27	2.51	1.77
MnO	0.07	0.06	0.05	0.03	0.19	0.01	0.01	0.1	0.05	0.1	0.09	0.06	0.01
MgO	1.31	1.7	1.89	0.82	7.66	0.82	0.1	0.47	1.4	1.6	2.27	1.36	0.8
CaO	1.48	2.04	1.98	2.98	11.15	0.63	0.68	1	1.22	2.84	4.48	2.7	0.42
Na_2O	0.14	0.12	0.12	2.65	0.32	0.69	0.32	0.16	0.07	0.1	0.1	0.12	0.08
K_2O	5	4.16	3.23	3.29	3.43	4.18	9.09	6.07	6.26	5.84	4.54	4.33	4.73
P_2O_5	0.19	0.07	0.02	0.04	0.02	0.03	0.03	0.02	0.17	0.19	0.17	0.15	0.02
Cr_2O_3	<0.002	<0.002	<0.002	<0.002	<0.002	<0.002	<0.002	<0.002	<0.002	<0.002	<0.002	<0.002	<0.002
SrO	<0.01	<0.01	<0.01	0.01	0.02	<0.01	0.01	0.01	<0.01	<0.01	0.01	<0.01	<0.01
BaO	0.15	0.12	0.21	0.83	0.16	0.23	0.34	0.55	0.15	0.14	0.16	0.14	0.19
LOI	3.87	4.08	4.28	4.21	19.25	2.81	1.2	2.2	3.24	5.38	7.46	4.45	2.53
Total	99.66	99.8	100.23	100.29	98.44	101.91	98.89	99.57	98.82	99.38	101.06	100.58	100.86
*Trace elements (ppm)***													
Ba	1400	1075	1930	7720	1155	2120	3130	5190	1395	1290	1505	1305	1800
Be (OGL)	3.13	2.9	1.54	2.32	1.17	3.84	1.06	1.55	3.94	3.48	2.63	2.85	2.91
Bi (OGL)	<0.47	1.03	0.59	<0.47	<0.47	<0.47	0.65	0.69	<0.47	<0.47	<0.47	0.5	<0.47
Ce	203	101	109.5	127	89.9	105	83.3	95.6	157	206	167	175.5	98
Cd (OGL)	0.3	>4	1.856	0.126	0.283	0.113	0.253	1.158	0.074	0.142	0.077	0.49	0.701
Co (OGL)	4.57	3.61	0.85	1.93	0.82	2.32	2.13	1.5	7.58	3.98	5.57	3.59	1.57
Cr	10	10	10	10	10	10	10	10	10	20	10	10	10
Cs	2.12	2.58	4.74	4.12	3.6	3.02	0.97	1.58	3.23	3.22	2.14	2.5	2.11
Cu (OGL)	8.1	59.2	14.3	3.2	<1.4	14.1	5.5	5.5	14.1	<1.4	23.3	6	13.8
Dy	12.2	7.95	4.11	7.81	5.77	6.75	5.42	5.63	11.75	11.45	9.43	8.72	4.63
Er	6.63	4.64	2.5	4.83	3.15	3.93	3.4	3.31	6.52	6.23	5.35	4.61	2.69
Eu	2.39	0.53	0.41	0.74	0.41	0.66	0.46	0.29	2.26	2.55	2.19	1.93	0.37
Ga	27.5	23.9	17.5	23.2	18	23.1	17.6	16.8	27	28.4	22.8	23.3	20.1
Gd	13.95	7.02	4.48	8.06	6.21	6.43	5.08	5.59	11.2	13.3	11.25	10.5	5.48
Hf	16.4	6.9	4.9	12.2	6.5	10.8	9.6	9.4	17.2	19.7	15.9	12.6	8.2
Ho	2.43	1.61	0.88	1.66	1.11	1.34	1.13	1.19	2.38	2.29	1.83	1.65	0.94
In (OGL)	0.0787	0.1087	0.044	0.0453	0.0125	0.0394	0.0239	0.0304	0.1017	0.1042	0.0551	0.088	0.0391
La	98.7	49	53.9	59.9	44.9	51	41.7	46.9	76.5	100	81.6	85.2	48.4
Li (OGL)	12.4	16.9	17.6	18.2	21.2	28.1	4.3	18.2	30.5	22.8	13.9	9.9	22.8
Lu	0.78	0.6	0.45	0.66	0.38	0.57	0.52	0.52	0.85	0.91	0.67	0.62	0.4
Mo (OGL)	2.04	2.82	2.67	0.86	2.92	3.15	2.3	2	2.75	1.73	1.86	2.54	3.71
Nb	48.7	25.2	16.4	30.4	17.5	26.1	21.8	20.4	41.7	49.1	43.1	39	22.4
Nd	89.3	40.3	41.1	52.6	38	43.8	32.7	37.5	68.8	90.5	74.1	75.6	38.5
Ni (OGL)	10.8	5.3	<0.7	2.2	<0.7	2.5	3.3	1.5	5.1	3.4	3.8	3.4	0.9
Pb (OGL)	182.21	9.42	400.53	18.87	17.67	37.73	44.29	90.18	4.13	6.12	12.15	17.97	29.99
Pr	23.4	11.25	11.75	14.15	10.05	11.8	9.14	10.7	18.2	23.9	19.35	20.2	10.7
Rb	169	162.5	131	88.6	130	146.5	206	186	213	206	128	143	218
Sb (OGL)	2.23	1.79	5.37	2.82	0.85	1.01	2.46	0.66	0.08	0.07	0.26	1.4	1.77
Sc (OGL)	11.1	4.8	3.2	5.4	4.8	5.4	4.1	3.8	12.8	12.3	10.9	8.6	4
Sm	17.35	8.11	6.51	10.1	8.3	8.47	5.91	7.36	13.3	17	13.6	14.45	7.3
Sn (OGL)	4.94	8.23	7.2	9.08	7.68	9.38	5.31	3.79	4.4	4.67	3.68	4.13	8.03
Sr	40.3	49.1	49.2	157.5	150.5	30.2	73.7	105.5	25.8	44.4	97.2	56.7	19.2
Ta	2.7	1.9	1.5	2.3	1.4	1.9	1.6	1.7	2.2	2.8	2.4	2.3	1.8
Tb	2.03	1.21	0.72	1.23	0.95	1.08	0.89	0.9	1.88	1.93	1.65	1.52	0.83
Th	34.7	26.6	26.4	33.6	24	29	23.7	25.1	32.9	33.8	27.5	30.7	31.8
Tl (OGL)	1.623	3.028	>20	>20	10.41	3.286	2.634	1.24	1.097	1.169	0.871	1.921	5.194
Tm	0.93	0.68	0.37	0.74	0.43	0.57	0.53	0.49	0.9	0.82	0.71	0.63	0.41
U	4.6	6.98	4.16	8.32	3.88	8.22	5.66	5.59	4.51	4.74	4.01	3.63	6.45
V	31	20	<5	20	11	18	13	14	41	35	27	23	14
W (OGL)	3.36	2.42	2.33	1.97	2.92	3.16	2.24	3.76	2.58	2.14	1.9	2.08	3.6
Y	64.8	48.3	23.9	45.5	30	37.5	32.9	33.8	64.4	62.7	50.7	46.5	25.1
Yb	5.66	4.42	2.74	4.48	2.83	3.87	3.52	3.39	5.53	5.66	4.45	4.06	2.73
Zn (OGL)	131.5	865.8	381.5	51.9	79.4	83.5	62.2	384.1	111.1	91.3	29.1	167.4	179.7
Zr	700	252	161	469	229	405	362	349	766	871	697	548	298

*LT, felsic lapillit tuff; TF, felsic tuff, VF, felsic coherent volcanic rock; MI, mafic intrusive; MD, mafic dike; XT, felsic crystal-rich tuff.

**Trace element analyses were performed at ALS Laboratories, some elements were analyzed for at the Ontario Geoscience Laboratiories and are marked as such (OGL).

B370180	B370181	B370182	B370183	B370184	B370185	B370186	B370187	B370188	B370189	B370190	D00005977	D00005978	D00005979
VF	MI	MI	TF	VF	TF	MI	TF	LT	LT	TF	LT	TF	LT
K15-320	K15-320	K15-320	K15-320	K15-320	K15-320	K15-320	K15-320	K15-320	K15-320	K15-320	K15-281	K15-281	K15-281
127.95	134	148.4	165	174.3	202.65	205.5	212.45	229.65	244.4	262	13.5	24.3	49.1
128.05	134.15	148.5	165.2	174.4	202.75	205.65	212.55	229.8	244.55	262.1	13.8	24.45	49.3
76.2	48.5	43.2	68	70.2	69.4	44.9	74.9	65.7	65.8	66.1	65.8	43	66.5
0.2	1.15	1.13	0.39	0.37	0.36	1.22	0.28	0.5	0.59	0.63	0.67	2	0.53
11.05	14.7	14.15	16.15	15.45	15.45	14.2	12.95	15.55	14.6	15.5	16.35	11.75	12.65
0.68	9.73	8.78	2.45	0.85	2.15	9.79	1.5	3.19	5.29	3.33	2.06	9.8	4.95
0.02	0.14	0.14	0.02	0.01	0.03	0.17	0.03	0.15	0.12	0.05	0.08	0.18	0.12
0.44	8.52	7.28	0.28	0.39	0.91	8.12	1.45	1.39	1.46	1.67	1.47	3.21	1.83
3.68	8.97	9.55	0.3	0.87	1.99	9.86	1.68	2.43	1.79	2.04	2.31	12.4	3.01
4.54	2.52	2.47	0.24	0.19	2.05	1.62	0.26	1.61	1.61	0.18	2.38	0.23	1.8
1.2	1.09	1.37	9.44	10.3	4.23	2.44	3.73	4.13	3.58	4.84	4.16	2.92	2.74
0.01	0.12	0.12	0.05	0.04	0.04	0.13	0.07	0.15	0.19	0.21	0.22	0.28	0.16
<0.002	0.05	0.041	<0.002	<0.002	<0.002	0.044	<0.002	<0.002	<0.002	<0.002	0.002	0.019	0.002
<0.01	0.03	0.01	<0.01	<0.01	<0.01	0.04	<0.01	0.01	<0.01	<0.01	<0.01	0.02	<0.01
0.22	0.11	0.47	0.99	0.12	0.75	0.74	0.08	0.12	0.12	0.15	0.14	0.13	0.09
3.59	3.83	10.2	1.83	1.55	3.58	4.94	4.14	5.1	4.01	5.28	4.57	12.9	5.17
101.83	99.46	98.91	100.14	100.34	100.94	98.21	101.07	100.03	99.16	99.98	100.21	98.84	99.55

2040	986	4440	9210	1055	6960	6820	769	1170	1090	1340	1245	1170	849
0.49	0.79	0.78	1.74	2.77	3.31	0.57	2.71	2.57	2.48	3	2.67	1.93	2
<0.47	<0.47	<0.47	0.95	<0.47	0.85	1	<0.47	<0.47	<0.47	0.66	<0.47	<0.47	<0.47
94.2	20.9	20.2	135.5	119.5	111	23.6	96.2	215	168.5	225	200	41.3	149
0.121	0.224	0.212	0.05	0.023	0.06	1.565	0.089	0.11	0.057	0.064	1.62	0.367	0.167
1.73	42.26	40.74	4.34	2.97	2.9	40.08	0.64	3.06	5.83	6.77	0.84	32.22	1.92
10	380	310	10	10	10	320	10	10	10	10	10	130	10
1.11	1.41	1.41	2.21	1.72	2.35	4.52	2.8	2.72	3.77	2.55	2.8	4.59	1.91
12.6	1.5	61	5.7	4.6	6	80.6	5	6.2	12.3	2.7	2.2	20.2	39.3
5.96	3.77	3.74	7.85	7.91	6.93	3.62	7.26	10.65	10.35	10.55	10.15	6.25	7.63
3.8	2.27	1.96	5.06	4.9	4.34	2.15	4.32	5.5	5.68	5.37	5.37	3.6	4.22
0.57	1.01	1.13	0.77	0.76	0.63	0.99	0.43	2.32	2.29	3.17	2.67	1.5	2.12
11.2	15	14.6	24	22.7	24.6	14.8	20.2	26.9	24.4	25.5	27.7	19.8	20.1
5.76	3.32	3.37	8.47	7.21	6.88	3.49	6.51	12.65	11.6	13.75	12.9	5.97	9.83
7.9	2.3	2.5	13.2	12.6	11.9	2.5	6.9	16.1	16.8	18.4	17.8	4.8	14.8
1.28	0.76	0.7	1.68	1.69	1.43	0.75	1.51	2.04	2.02	2.06	1.98	1.35	1.54
0.0117	0.0532	0.0548	0.0346	0.0377	0.0548	0.0636	0.0304	0.0922	0.0862	0.065	0.0918	0.0783	0.0467
45.8	9.8	8.8	65	56.5	54.1	11	45.3	105	81.5	109	98.4	18.3	73.1
6	24	32.2	13.4	18.8	25.8	26.3	14.4	9.7	15.7	16.2	34.7	36.8	18.6
0.53	0.3	0.27	0.73	0.71	0.58	0.33	0.56	0.71	0.77	0.74	0.71	0.52	0.6
1.66	0.4	0.31	3.44	1.12	3.25	0.22	3.36	2.81	2.4	2.67	2.12	1.15	1.74
21.2	9.1	8.9	31.8	30.1	28.9	9.4	23.8	43.9	44.1	48	49.5	18.9	38.9
38	12.6	12.5	54.8	48.4	43.7	13.4	37.9	94	74.4	98.3	87.7	23.9	65.6
6.1	96.4	80.2	4.7	3.3	4.1	83.6	1.5	2.6	4.8	6.2	1.1	26.6	4.7
59.09	19.53	20.98	46.98	11.49	63.76	540.55	9.97	6.91	15.12	27.38	8.53	14.03	6.07
10.4	2.74	2.69	15.05	13.35	12.55	3.08	10.7	24.6	19.35	26.1	23.2	5.29	17.15
35.3	36.1	43.1	281	305	125	79.8	145.5	116.5	119	150	139.5	105	84.5
3.03	4.36	8.8	3.6	2.07	3.69	10.89	0.26	0.28	0.38	0.26	0.19	0.06	0.08
2.7	30.2	29.5	4.7	4.8	7	31.4	3.9	8.8	12.5	11.1	13.1	29.9	10.6
7.14	3.21	3.4	10.85	8.82	8.32	3.35	7.76	18.2	14.6	18.4	17.05	6.03	13.2
4.86	0.7	0.81	7.04	8.75	9.88	1.22	7.31	4.79	3.15	4.17	4.15	1.46	2.07
61.1	251	144	63.4	39.5	47	313	47.4	66.5	51.3	45.9	31.3	173.5	50.2
1.8	0.6	0.6	4.4	2.3	2	0.6	1.9	2.5	2.4	2.7	2.9	1.1	2.2
1	0.57	0.56	1.34	1.13	0.99	0.59	1.17	1.79	1.58	1.97	1.88	0.96	1.42
25.9	1.64	1.38	34.4	35	32.7	1.69	26.2	37.2	27.5	34.8	30.6	3.22	22.9
3.172	3.525	11.937	>20	>20	18.508	>20	3.054	0.743	0.705	0.849	0.767	0.661	0.47
0.54	0.3	0.29	0.71	0.82	0.71	0.31	0.62	0.78	0.86	0.77	0.78	0.52	0.61
10.05	0.35	0.57	7.94	7.57	9.16	0.51	6.43	4.7	3.64	3.95	3.98	0.93	3.49
13	219	229	19	19	30	216	17	23	30	32	33	290	28
1.1	0.35	0.97	5.03	3.36	2.68	1.12	2.28	1.55	2	1.61	1.84	1.54	1.72
36.3	20.4	19.1	50.3	52.5	41.4	20.7	41.9	54.9	56.3	55.3	53	34.9	41.4
3.63	1.79	1.97	4.82	4.71	4.05	2.03	3.85	4.81	5.09	5.09	5.02	3.29	4
13.4	92.9	205	59.1	26.4	84.9	450.6	34.1	81.1	83.7	53.4	581.7	254.5	112
284	92	91	507	478	466	95	254	681	745	812	736	195	642

D00005980	D00005981	D00005982	D00005983	D00005984	D00005985	D00005986	D00005987	D00005988	D00005989	D00005990	D00005991	Q930095	Q930096
MD	TF	TF	TF	TF	TF	TF	TF	TF	TF	TF	TF	TF	VF
K15-281	K15-281	K15-281	K15-281	K15-281	K15-281	K15-281	K15-281	K15-281	K15-281	K15-281	K15-281	K15-235R	K15-235R
64.9	85.8	137.6	147.5	164.8	176.55	183.05	184.45	199.45	212.75	227.9	251.9	86.15	116.7
65	86	137.7	147.7	165	176.65	183.2	184.65	199.6	212.9	228.05	252.1	86.3	116.95
46.3	62.8	63.4	77.7	76.8	65.6	27.6	50.1	76.1	78.8	68.9	68.5	73.7	57.2
2.26	0.62	0.62	0.25	0.28	0.33	0.35	0.38	0.23	0.25	0.34	0.65	0.27	0.26
12.7	14.4	15.3	12.25	12.95	16.45	21.7	19.5	12.9	10.45	14.4	15.5	15.55	12.7
10.55	5.66	5.73	2.22	1.67	2.21	26.4	8.86	2.02	2.74	1.82	4.49	1.86	3.14
0.18	0.08	0.07	0.01	0.01	0.13	0.06	0.04	0.01	0.01	0.03	0.03	0.04	0.18
3.51	1.83	1.91	0.79	0.76	2.17	14.35	7.71	0.98	0.09	0.97	0.81	1.28	4.6
6.88	2.95	2.15	0.59	0.37	2.46	0.13	1.98	0.18	1.15	2.71	0.74	0.55	7.07
2.99	1.23	0.39	0.1	0.16	0.22	0.07	0.2	0.13	2.7	0.09	2.77	0.22	0.24
1.51	4.41	5.13	4.01	4.01	5.11	2	4.35	4.34	1.75	5.22	3.84	4.82	3.89
0.33	0.21	0.21	0.08	0.07	0.04	0.03	0.06	0.03	0.02	0.04	0.22	0.04	0.04
0.005	0.003	0.002	0.002	0.002	<0.002	0.002	0.002	<0.002	<0.002	<0.002	0.003	0.002	0.002
0.01	0.01	0.01	<0.01	<0.01	<0.01	<0.01	<0.01	<0.01	<0.01	0.01	<0.01	<0.01	0.01
0.09	0.3	0.1	0.06	0.06	0.11	0.06	0.16	0.19	0.14	0.1	0.29	0.21	0.35
10.7	5.8	4.06	2.82	2.69	5.3	8.3	7.32	2.46	2.43	4.06	3.13	2.73	12.05
98.02	100.3	99.08	100.88	99.83	100.13	101.05	100.66	99.57	100.53	98.69	100.97	101.27	101.73

794	2710	883	549	572	977	604	1425	1670	1225	906	2570	1835	3030
1.47	2.87	3.36	2.38	2.71	3.08	0.69	1.56	1.84	1.28	3.54	2.35	2.52	1.48
<0.47	1.13	<0.47	0.71	<0.47	<0.47	13.24	6.57	1.41	<0.47	<0.47	0.73	0.82	<0.47
67	203	186	97.6	102.5	144	155	188	94.4	87.1	101	185.5	114.5	107
0.223	0.178	0.107	0.484	0.039	>4	0.16	0.126	1.208	1.051	0.07	>4	>4	0.317
24.31	5.98	5.14	2	2.16	2.41	34.58	11.88	3.49	2.21	1.93	4.93	1.57	0.7
30	20	20	10	10	10	10	10	10	10	10	10	10	10
1.52	2.54	3.87	2.27	2.38	3.91	2.88	4.31	2.25	0.54	2.04	1.84	3.61	3.93
<1.4	99.5	9.3	8.3	6.3	172.6	323.2	7.4	51.7	11.7	2.9	31.6	86.7	17
5.86	8.86	10.8	8.03	6.89	6.4	14.8	7.88	5.61	5.74	7.11	10.5	7.1	7.39
3.25	4.63	5.54	4.61	4.06	3.76	7.6	4.49	2.84	3.64	4.05	5.79	4.77	4.11
1.86	2.83	2.63	0.51	0.5	0.66	0.68	0.6	0.3	0.59	0.65	2.24	0.45	0.64
22.2	25.5	28	22.3	23.6	28.6	41.4	32.2	21.1	18.2	23.3	27.7	26.5	22
6.74	11.45	12.45	6.76	6.7	7.98	14.45	9.13	5.14	5.68	6.59	12.75	5.83	6.37
6.2	17.8	18	7.4	8	9.8	12.3	12.6	7.4	8.4	11.7	17.9	9.1	8.1
1.24	1.81	2.1	1.63	1.46	1.22	2.84	1.49	1.12	1.26	1.41	2.18	1.65	1.38
0.0867	0.0737	0.0842	0.064	0.035	0.0176	0.0265	0.0183	0.0452	0.0299	0.0524	0.1	0.0838	0.0101
31.3	102.5	91	47.2	49.9	70.6	68.8	97.9	45.9	43.8	49.8	90	56.4	53.8
20.1	38	40.6	32.6	17.6	30.2	58.3	34.5	18.2	1.6	27.8	14	18.9	23.7
0.45	0.65	0.79	0.62	0.59	0.52	0.82	0.65	0.44	0.5	0.69	0.8	0.67	0.53
0.84	1.56	1.48	2.05	2	3.44	7	3.45	3.53	3.94	1.67	1.6	3.31	2.85
21.6	44.1	47.6	23.6	26.3	29.4	32	30.9	21.1	18.7	25.5	45.1	28.4	22
35.2	87.1	82.1	40	40.9	57.3	79.2	70.8	38	34.1	41.3	82.6	42.3	41.3
3.6	7.4	4.2	1.1	1	0.7	1.3	1.2	1.2	3.2	2.4	3.8	1.3	<0.7
6.27	13.97	6.9	66.13	11.15	>700	150.36	27.33	64.87	107.44	14.77	28.3	681.58	22.15
8.29	22.8	21.4	11.05	11.7	16.15	19.25	20.4	10.5	9.75	11.3	21.6	12.35	11.75
46.9	121.5	155	162.5	170.5	204	90.6	175	148.5	32.7	184.5	103.5	179.5	133.5
0.14	0.4	0.09	0.58	0.73	1.48	0.3	0.28	1.01	5.09	0.57	0.19	4.01	0.67
33.3	11.8	11.9	4	4.5	4.5	4.8	5.1	3.7	3.6	4.8	13	4.7	4.1
8.26	16.25	15.65	8.65	8.38	10.85	18.6	14.1	7.16	6.7	8.21	15.9	8.07	8.14
1.57	2.85	4.6	6.45	6.92	11.64	1.53	6.76	7.85	6.86	8.51	3.65	11.13	9.55
131.5	104	66.7	17	16.9	45.8	5.9	35.1	7.5	36.1	66.4	42.6	20.1	95.5
1.3	2.6	2.7	1.9	2.1	2.4	2.5	2.6	1.9	1.5	1.9	2.7	2.5	1.8
1.01	1.66	1.89	1.32	1.12	1.13	2.46	1.34	0.87	0.95	1.1	1.8	1.11	1.1
7.51	27.2	28.3	25.6	26.3	37.8	39.4	44.7	26.7	21.6	26.2	27.3	31.4	28
0.305	0.682	1.109	1.006	1.667	2.726	2.71	4.617	1.676	0.282	1.635	0.575	16.161	>20
0.49	0.69	0.87	0.66	0.63	0.57	1.07	0.71	0.46	0.52	0.69	0.85	0.72	0.59
1.61	3.81	4.44	4.92	6.38	8.09	10.95	9.16	7.35	5.62	6.89	3.94	8.8	7.33
322	29	29	14	14	17	21	20	13	13	15	30	11	12
1.5	1.98	2.31	1.93	2.57	3.7	5.53	5.2	3.96	1.87	2.26	1.64	2.89	2.87
33.7	47.9	58.7	46.3	42	35.7	82.1	43.5	31.3	34.4	43.4	58.8	45.6	41.5
3.2	4.38	5.61	4.12	4.25	3.71	6.22	4.71	3.21	3.28	4.3	5.37	4.94	3.87
117.1	55.5	96.4	151	20	1470.1	1108.5	185.4	291.3	386.7	35.9	691.9	966.2	76.7
238	755	763	260	291	347	445	450	247	305	418	750	298	279

Q930097	Q930098	Q930099	Q930100	Q931941	Q931942	Q931943	A00348398	A00348399	Q311613	Q720929	Q720932	Q720934	Q720939
TF	TF	MI	TF	TF	MI	LT	MI	MI	VF	LT	MI	MI	LT
K15-235R	K15-235R	K15-235R	K15-235R	K15-235R	K15-235R	K15-235R	K15-290	K15-290	K16-417	K16-370	K16-370	K16-370	K16-370
133.3	136.1	143.65	149.25	159.05	163.35	173.75	90.7	117.3	96.85	98.3	160.35	189.1	276.95
133.5	136.35	143.95	149.4	159.25	163.6	173.95	90.9	117.45	96.9	98.45	160.5	189.3	277.1
56.5	71.1	43.7	68.5	71.9	43.9	77.2	40.2	46.7	75.7	66.6	46.2	43.6	62.5
0.33	0.15	1.18	0.39	0.34	1.06	0.22	1.23	1.24	0.18	0.46	1.51	1.23	0.68
16.55	8.02	14.85	16.4	14.55	15.45	12.75	13.95	15.05	12.3	12.35	15.7	14.2	15.9
2.71	9.74	9.32	2.34	2.46	8.45	2.36	9.73	9.24	1.3	6.41	11.1	9.02	7.96
0.05	0.12	0.15	0.05	0.03	0.13	<0.01	0.14	0.14	0.02	0.14	0.16	0.15	0.19
3.36	5.85	8.2	1.08	0.91	8.25	0.97	5.47	8.21	0.45	1.65	8.13	6.94	2.79
3.63	0.86	9.63	0.89	1.94	8.98	0.12	11.6	9.9	0.67	2.77	10.1	10.35	0.3
0.12	0.02	1.28	0.14	0.43	3.93	0.21	0.09	3.31	0.24	0.13	2.45	0.09	0.25
5.12	0.43	3.54	7.07	4.9	0.18	4.03	2.52	0.17	8.16	3.86	0.56	4.84	3.21
0.03	0.02	0.13	0.05	0.05	0.12	0.03	0.13	0.13	0.03	0.15	0.17	0.12	0.21
0.002	<0.002	0.05	0.002	0.002	0.051	<0.002	0.044	0.047	<0.002	<0.002	0.055	0.042	<0.002
0.01	<0.01	0.02	0.01	<0.01	0.01	<0.01	0.02	0.03	<0.01	<0.01	0.04	0.01	<0.01
2.43	0.04	0.18	0.2	0.22	0.01	0.12	0.25	0.02	0.13	0.11	0.08	0.17	0.09
8.01	3.73	7.82	2.82	3.57	10.3	2.8	13.15	4.26	1.52	4.58	3.02	7.56	4.21
98.85	100.08	100.05	99.94	101.3	100.82	100.81	98.52	98.45	100.7	99.21	99.28	98.32	98.29

>10000	275	1530	1760	1910	93.4	1135	2410	173	1200	1020	810	1535	851
2.08	0.18	0.72	3.76	2.61	0.34	2.06	-	-	-	-	-	-	-
<0.47	1.11	<0.47	<0.47	0.59	<0.47	0.5	-	-	-	-	-	-	-
128.5	33.2	19.4	100.5	112	19	112	22.4	25.1	123.5	179.5	29.5	20.2	221
0.14	0.864	0.136	0.046	3.213	0.189	0.074	-	-	-	-	-	-	-
1.91	8.04	46.58	3.1	4.1	40.78	2.05	-	-	-	-	-	-	-
10	<10	360	10	10	370	10	300	330	10	10	360	310	20
3.83	1.06	8.62	2.28	2.28	0.57	2.55	2.35	0.32	0.92	3.24	0.87	8.17	1.63
15.9	33.7	42	7.1	14.8	25.1	8.3							
7.32	3.15	3.35	7.14	6.44	3.14	8.33	3.8	4.01	8.01	9.9	4.91	4.12	11.3
4.04	1.98	2	4.2	4.27	1.85	4.89	2.29	2.52	4.95	5.77	2.94	2.34	6.02
0.52	0.21	1.05	0.68	0.68	1.05	0.47	0.62	1.26	0.43	2.05	1.48	1.23	2.64
29.8	18	16.8	27.2	24.6	16.4	22.2	15.6	16.1	20.3	20.4	18.4	13.5	26.5
7.86	3.06	3.37	6.93	6.24	3.33	7.67	3.79	3.92	7.69	11	4.77	3.68	13.85
9.9	4.8	2.3	12.6	10.8	2.1	7.6	2.5	2.6	6.5	14.4	3.1	2.6	18.2
1.55	0.66	0.73	1.5	1.43	0.66	1.79	0.77	0.88	1.66	2.05	1.03	0.75	2.1
0.0138	0.0643	0.0559	0.0682	0.0784	0.0471	0.0397	-	-	-	-	-	-	-
63.9	15	8.6	49.5	54.3	8.8	54.9	10.1	11.3	62.2	89.5	13.3	9.3	109.5
52.6	27.1	41.7	31.2	32.6	26.8	18.7							
0.58	0.31	0.29	0.63	0.65	0.28	0.61	0.31	0.33	0.66	0.77	0.39	0.31	0.82
2.86	1.73	0.39	3.09	2.67	0.56	2.41							
27.9	14.4	8.6	30.2	25.8	8.6	22	9.9	9.6	20.7	34.5	11.2	9.1	48.5
51.4	15.1	12	40.1	45.3	11.7	44.1	13.3	14.6	47.1	75.7	17.1	11.8	93.5
1.6	<0.7	86.8	3.1	6.4	109.7	2.9	-	-	-	-	-	-	-
17.73	38.71	12.43	22.21	60.19	10.82	80.65	-	-	-	-	-	-	-
14.35	3.94	2.55	11.1	12.35	2.45	12.4	2.97	3.31	13.75	20.7	3.91	2.7	25.1
176.5	17.6	138.5	269	140	4.8	131.5	82.1	4.8	163.5	108.5	15	170	98.1
4.02	1.03	2.57	1.47	0.97	1.23	0.49	-	-	-	-	-	-	-
5.3	2.1	30	5.5	9.3	27.5	4.3	-	-	-	-	-	-	-
9.94	3.27	3.35	8.15	8.52	2.96	8.41	3.57	3.94	9.55	14.75	4.54	3.44	17.1
10.14	1.92	0.6	9.79	8.62	0.64	7.39	1	1	10	3	1	1	5
122	11	203	59.9	38.8	130.5	18.7	171	281	23.8	47.6	361	107.5	44.8
2.2	1.2	0.5	2.1	2	0.5	1.9	0.6	1.3	2.3	2.2	1.2	<0.1	3.3
1.24	0.49	0.58	1.25	1.05	0.52	1.33	0.6	0.68	1.34	1.69	0.77	0.62	1.99
33.9	17.3	1.34	31	27.3	1.43	29.1	1.49	1.7	32.3	30.1	1.97	1.36	33.7
>20	4.936	6.961	7.486	2.612	0.11	1.624	-	-	-	-	-	-	-
0.66	0.3	0.29	0.67	0.63	0.28	0.72	0.31	0.35	0.68	0.78	0.41	0.32	0.83
7.02	4.55	0.24	7.99	7.39	0.36	6.09	0.32	0.31	6	3.95	0.4	0.29	4.65
18	7	218	19	24	193	11	200	202	5	19	234	215	34
3.82	0.64	2.32	3.63	2.31	0.26	1.84	7	1	2	3	1	2	4
43.8	18.3	19.3	43.2	40.3	17.7	48.1	20.4	21.9	43.8	51.5	25.9	19.1	57.8
3.93	2.06	1.8	4.33	4.46	1.8	4.23	2.06	2.17	4.45	5.06	2.7	2.02	5.88
148.5	733.5	71.5	10.7	972.2	134.6	33.2	-	-	-	-	-	-	-
346	171	84	471	414	84	238	94	97	188	587	111	86	795

Q720946	Q720949	Q721051	Q721071	Q721073	Q721099	Q721154	Q721155	Q721156	Q721157	Q721158	Q721160	Q721170	Q930221
LT	MI	MS	MD	MD	VF	VF	MI	LT	LT	VF	VF	VF	LT
K15-271	K15-271	K15-309	K15-287	K17-422	K15-290	K15-204	K15-204	K17-448	K17-448	K17-448	K17-448	K15-300	K15-232
174.2	257.35	165.25	118.35	40.3	139.7	135.6	146.4	322.45	334	346.15	358.45	67.95	207.85
174.35	257.55	165.45	118.55	40.5	139.9	135.8	146.6	322.65	334.15	346.3	358.6	68.15	208
65.4	47.9	76.1	71.5	52.5	74	68.4	43.2	60.8	64	76.5	77	77.6	62.5
0.53	1.18	0.22	0.24	2.33	0.28	0.34	1.23	0.93	0.61	0.16	0.17	0.2	0.62
14.25	15.35	12.9	13.05	13.2	11.45	13.8	14.85	14.3	14.4	12.5	12.8	12.7	15
4.48	9.5	1.04	4.2	10.25	1.45	5.83	9.28	8.06	5.35	1.06	1.34	0.95	5.11
0.09	0.15	0.02	0.09	0.14	0.03	0.02	0.12	0.06	0.1	0.03	0.01	0.01	0.08
0.98	9.06	0.52	3.09	2.35	0.11	0.25	6.86	3.73	0.8	0.23	0.41	0.48	1.72
2.94	10.8	0.95	0.45	5.84	1.59	0.2	10.1	3.21	3.79	1.39	0.44	0.51	2.88
0.51	2.03	0.43	0.12	0.1	0.33	0.22	1.71	0.11	2.76	4.72	3.28	0.21	0.19
3.89	0.8	4.22	3.61	4.4	8.36	9.59	2.2	4.26	3.52	1.67	2.1	7.21	4.69
0.18	0.11	<0.01	0.03	0.37	0.02	0.05	0.13	0.21	0.18	0.08	0.09	0.09	0.18
0.002	0.051	0.002	0.002	0.004	0.003	0.002	0.047	0.019	<0.002	<0.002	<0.002	<0.002	<0.002
<0.01	0.03	<0.01	<0.01	0.01	0.02	<0.01	0.01	0.01	0.01	0.01	<0.01	<0.01	0.01
0.11	0.11	0.25	0.14	0.33	0.6	0.17	0.09	0.25	0.22	0.07	0.11	0.16	0.32
4.15	2.54	2.8	3.07	5.66	1.28	3.07	10.65	3.59	3.36	1.6	2.1	1.45	4.77
97.51	99.61	99.45	99.59	97.48	99.52	101.94	100.48	99.54	99.1	100.02	99.85	101.57	98.07

999	954	2300	1255	3060	5370	1520	787	2280	1970	670	960	1475	3030
-	-	-	-	-	-	-	-	-	-	-	-	-	-
-	-	-	-	-	-	-	-	-	-	-	-	-	-
187.5	22.9	125.5	114.5	77.7	97.9	112	22.5	127	171	77.3	66.8	101.5	186
-	-	-	-	-	-	-	-	-	-	-	-	-	-
-	-	-	-	-	-	-	-	-	-	-	-	-	-
20	380	10	10	30	10	20	320	130	10	<10	10	10	10
3.35	0.99	2.28	2.88	7.13	1.04	2.67	3.01	1.96	2.9	0.82	2.3	1.33	4.61
9.19	3.96	9.94	8.48	6.56	6.72	8.97	4.21	8.75	11.25	7.97	8.28	9.54	10.7
4.77	2.46	5.48	5.12	3.75	3.94	5.58	2.48	4.81	6.17	4.67	5.06	4.92	6.19
2.31	1.06	0.39	0.36	1.99	0.39	0.81	1.04	1.86	2.02	0.42	0.43	0.64	2.52
24.4	16.1	17.3	21.2	21.6	14.1	20.8	17.5	23.2	26.3	19.9	22.7	19.8	27.1
11.4	3.67	8.64	7.18	7.91	6.07	8.38	3.84	9.81	13.4	7.14	6.71	8.98	13.5
14.7	2.3	7.6	7.7	5.6	8.1	10.8	2.6	12.7	15.9	5	6	6	16.8
1.7	0.78	1.91	1.69	1.29	1.32	1.8	0.83	1.62	2.01	1.6	1.67	1.71	1.97
-	-	-	-	-	-	-	-	-	-	-	-	-	-
92.9	10.5	61	57.9	36.5	49.7	55.1	10.2	61.4	84	36.4	30.6	48.2	92.1
0.7	0.32	0.64	0.62	0.49	0.53	0.82	0.34	0.61	0.81	0.53	0.63	0.59	0.8
39.6	8.9	24.9	21.5	19.4	21.2	28.7	9.8	31.8	41.3	23.1	25.4	28.2	43.7
77.8	12.9	49.2	42.1	39.4	37.6	46	13.8	59	77.1	33.6	28.3	44.9	81.8
-	-	-	-	-	-	-	-	-	-	-	-	-	-
-	-	-	-	-	-	-	-	-	-	-	-	-	-
21.3	3.03	13.95	12.5	9.92	10.9	12.75	3.11	14.95	20.4	9.14	7.76	11.85	21.7
126.5	26.3	138.5	116.5	142.5	163.5	168.5	57.3	100	96.5	52.7	68.2	156.5	142
-	-	-	-	-	-	-	-	-	-	-	-	-	-
-	-	-	-	-	-	-	-	-	-	-	-	-	-
14.05	3.21	9.57	8.04	8.62	7.56	9.07	3.89	11.45	15.55	7.1	6.54	9.58	15.25
4	1	3	10	2	3	13	1	7	5	4	4	5	4
52.8	236	38.1	18.4	128.5	150	45.7	121	89.2	105.5	116.5	37.2	21.4	71.5
2.2	0.7	1.8	1.8	1.3	2	2.4	0.8	2.5	2.7	2.2	2.3	3.2	3
1.64	0.63	1.5	1.26	1.17	1.06	1.28	0.63	1.37	1.91	1.24	1.19	1.42	1.81
31.3	1.68	33.9	30.4	8.97	24.9	29.5	1.61	19.7	27.3	18.5	20.8	23.9	29.6
-	-	-	-	-	-	-	-	-	-	-	-	-	-
0.72	0.33	0.76	0.75	0.56	0.57	0.8	0.32	0.62	0.81	0.63	0.72	0.69	0.83
4.24	0.32	10.25	7.33	2	5.99	12.55	0.34	3.1	3.85	5.84	4.58	6.22	4.17
27	229	11	17	329	17	19	226	90	30	6	6	7	31
3	1	2	3	4	3	4	2	3	2	2	2	1	3
45	21.5	51.6	50.3	36	38.9	48.4	20.3	41.3	53.9	41.6	45	42.3	53.5
4.37	2.2	4.85	4.47	3.4	3.63	5.57	2.09	4.37	5.55	4.5	4.78	4.62	5.43
-	-	-	-	-	-	-	-	-	-	-	-	-	-
639	92	248	270	233	313	408	92	510	638	159	180	199	711

Q930240	Q930243	Q930244	Q930277	Q930281	Q930282	Q930290	Q930291	Q930292	Q930294	Q931952	Q931973	Q931984	Q931989
VF	MI	VF	MI	MD	VF	MI	MI	MI	VF	MD	XT	XT	MD
K15-236	K15-236	K15-236	K15-286	K15-315	K15-315	K15-315	K15-315	K15-315	K15-315	K15-216	K15-233	K15-282	K15-282
95	113.35	117.15	179.7	11.3	20.95	118.15	121.9	132.1	146.6	31.05	108	165.1	129
95.26	113.65	117.35	179.9	11.5	21.15	118.3	122.15	132.35	146.95	31.2	108.2	165.25	129.2
64.1	43	78.5	46.1	51.1	77.8	44.7	45	44.9	72	50.6	65.3	64.2	39.2
0.3	1.12	0.29	1.31	2.34	0.16	1.35	1.27	1.3	0.26	2.29	0.53	0.65	2.93
17.95	14.65	11.9	15.75	12.55	10.9	16.15	15.55	14.4	10.4	13.4	15.05	15.4	16.15
4.16	9.05	1.67	10	11.05	0.94	10.05	9.69	9.81	2.01	11.1	3.15	4.53	12.45
0.01	0.12	<0.01	0.12	0.16	0.03	0.15	0.15	0.14	0.03	0.14	0.06	0.13	0.21
0.75	8.32	0.21	6.97	2.96	0.33	7.56	8.02	8.17	0.07	3.19	1.33	1.77	3.34
0.45	8.66	0.38	5.33	6.68	0.78	10.45	9.23	8.86	3.18	5.23	2.27	3.09	7.37
6.91	0.4	3.01	0.07	0.08	0.27	3.06	1.69	3.67	0.34	2.81	1.23	0.09	0.11
2.03	4.67	3.4	5.01	5.73	8.06	0.49	2.42	0.4	8.53	2.47	4.82	5.54	7.07
0.04	0.12	0.04	0.13	0.36	0.03	0.14	0.15	0.16	0.03	0.35	0.17	0.18	0.39
<0.002	0.052	<0.002	0.049	0.006	<0.002	0.052	0.048	0.044	<0.002	0.005	0.003	0.002	0.005
<0.01	0.02	<0.01	0.02	0.02	<0.01	0.04	0.03	0.01	0.01	0.01	0.01	0.01	0.01
1.04	0.31	0.38	0.23	0.1	0.11	0.05	0.17	0.03	0.23	0.15	0.24	0.17	0.25
2.36	9.39	1.42	8.78	6.27	1.15	4.68	6.45	8.31	3.25	7.92	4.7	5.95	8.54
100.1	99.88	101.2	99.87	99.41	100.56	98.92	99.87	100.2	100.34	99.67	98.86	101.71	98.03

9990	2850	3470	2060	912	875	416	1505	231	1815	1365	2150	1540	2190
-	-	-	-	-	-	-	-	-	-	-	-	-	-
-	-	-	-	-	-	-	-	-	-	-	-	-	-
172	17.4	82.5	19.8	66.8	101.5	21.6	21.7	23.5	81	74.8	205	191.5	108.5
-	-	-	-	-	-	-	-	-	-	-	-	-	-
-	-	-	-	-	-	-	-	-	-	-	-	-	-
10	340	10	360	30	10	350	350	290	10	30	10	10	20
2.69	14.65	0.95	17.4	13.25	0.82	0.52	3.8	0.59	0.88	3.26	1.7	4.53	6.79
11.75	3.48	5.78	3.67	6.19	7.09	4.14	4.44	4.43	6.13	6.56	10.1	9.42	5.59
7.17	2.08	3.51	2.15	3.39	3.84	2.44	2.43	2.45	3.66	3.88	5.65	5.56	3.01
0.76	0.95	0.48	0.81	1.58	0.37	1.1	1.18	1.27	0.6	1.99	1.99	2.72	2.26
30.2	15.6	19.6	17	21.2	16	16.6	17.8	13.7	13.1	22.9	27.2	27.1	28.6
11.15	3.05	5.03	3.24	6.59	6.44	3.97	4.4	4.06	6.04	7.33	12.55	12.1	8.6
15.6	2	9	2.5	5.6	5.2	2.8	2.5	2.6	8.3	6.1	15.6	19	8.6
2.3	0.7	1.19	0.71	1.17	1.31	0.75	0.83	0.87	1.24	1.35	1.97	1.96	1.01
-	-	-	-	-	-	-	-	-	-	-	-	-	-
84.3	7.8	40.3	8.9	30.8	50.4	9.9	9.7	11.5	41.8	35.5	101.5	95.5	51
0.84	0.24	0.54	0.28	0.44	0.43	0.28	0.3	0.3	0.43	0.46	0.78	0.77	0.5
23.8	7.7	21.5	9.5	17.1	19	9	8.8	8.6	18	19.2	37.1	44.8	27.3
68.3	10.6	33.8	11.3	32.7	39.7	13.3	14.1	14.5	31.8	36.3	84.6	81.6	52.5
-	-	-	-	-	-	-	-	-	-	-	-	-	-
-	-	-	-	-	-	-	-	-	-	-	-	-	-
19.3	2.37	9.77	2.63	8.25	10.55	2.66	3.01	2.84	8.37	9.5	23.5	22.1	13.45
71.2	166.5	66.1	177	229	181	15.3	102	13.8	163	70.9	126	175.5	241
-	-	-	-	-	-	-	-	-	-	-	-	-	-
-	-	-	-	-	-	-	-	-	-	-	-	-	-
13.25	3.24	6.7	2.87	7.11	7.36	3.06	3.5	3.86	5.61	7.24	15.05	14.2	10.5
38	1	7	1	2	5	1	1	1	4	2	4	4	3
32.5	170	43.8	136.5	186.5	28.3	285	224	94.4	102	129.5	84.8	63.2	127
3.7	0.9	1.6	0.4	1.1	2	0.3	0.7	0.6	1.6	1.9	2.8	2.9	2.3
1.7	0.52	0.86	0.54	1.02	0.99	0.58	0.66	0.65	0.99	1.12	1.84	1.75	1.14
81	1.47	23.1	1.64	7.44	27.3	1.34	1.44	1.44	21.3	8.48	36.1	28.4	12.3
-	-	-	-	-	-	-	-	-	-	-	-	-	-
0.98	0.26	0.49	0.31	0.5	0.47	0.31	0.33	0.32	0.51	0.53	0.74	0.8	0.45
36.1	0.41	6.53	0.35	3.44	17.8	0.57	0.68	0.38	5.35	1.81	4.82	4.03	2.8
318	200	17	246	323	8	234	225	231	12	276	23	27	306
6	3	1	4	5	2	1	1	1	3	2	3	3	3
60.5	16.8	30.7	17.9	31.5	32.5	20.7	20.9	21.5	33.5	34.3	51.5	49.6	24.8
7.02	1.87	4.06	2.03	3.18	3.37	2.11	2.07	2.1	3.13	3.11	5.1	5	3.23
-	-	-	-	-	-	-	-	-	-	-	-	-	-
503	78	341	101	220	157	85	89	87	289	243	631	814	349

Appendix 1.2 QA/QC Data

						SLV-MC basalt		
	2018	2018		2019	2019			2018
Sample	B00267984	B00267986	B00267986 lab duplicate	Q311621	Q311623	Mean	σ	% RSD
Rock Type	SLV-MC basalt	SLV-MC basalt	SLV-MC basalt	SLV-MC basalt	SLV-MC basalt			
Major elements (wt%)								
SiO_2	49.9	49.9		48.9	49.4	49.90	0.00	0.00
TiO_2	1.44	1.51		1.5	1.52	1.48	0.05	3.36
Al_2O_3	15.4	15.75		15.45	15.55	15.58	0.25	1.59
Fe_2O_3	12.55	12.9		12.8	12.9	12.73	0.25	1.94
MnO	0.16	0.17		0.16	0.16	0.17	0.01	4.29
MgO	7.42	7.59		7.55	7.61	7.51	0.12	1.60
CaO	8.58	8.37		8.54	8.61	8.48	0.15	1.75
Na_2O	3.44	3.58		3.51	3.54	3.51	0.10	2.82
K_2O	0.5	0.53		0.52	0.52	0.52	0.02	4.12
P_2O_5	0.23	0.24		0.24	0.25	0.24	0.01	3.01
LOI	-0.8	-0.79		-0.81	-0.81	-0.80	0.01	-0.89
Total	98.92	99.85		98.46	99.35	99.39	0.66	0.66
Trace elements (ppm)								
Ba	159	160.5		179	180	159.75	1.06	0.66
Be	0.77	0.77	0.75	-	-	0.76	0.00	0.00
Bi	<0.47	<0.47	<0.47	-	-			
Ce	21.4	21.1		23.3	23.4	21.25	0.21	1.00
Co	49.65	48.62	47.78	-	-	49.135	0.73	1.48
Cr	240	230		210	210	235	7.07	3.01
Cs	0.08	0.06		0.1	0.1	0.07	0.01	20.20
Cu	54.8	52.8	52.30	-	-	53.8	1.41	2.63
Dy	3.64	3.53		3.67	3.71	3.585	0.08	2.17
Er	1.74	1.73		1.84	1.91	1.735	0.01	0.41
Eu	1.2	1.29		1.32	1.34	1.245	0.06	5.11
Ga	21.6	21.6		20.6	20.2	21.6	0.00	0.00
Gd	3.93	3.6		4.28	4.2	3.765	0.23	6.20
Hf	2.4	2.6		2.6	2.6	2.5	0.14	5.66
Ho	0.64	0.67		0.68	0.71	0.655	0.02	3.24
In	0.0682	0.0659	0.0663	-	-	0.06705	0.00	2.43
La	9.3	9.1		10	10.2	9.2	0.14	1.54
Lu	0.22	0.2		0.22	0.24	0.21	0.01	6.73
Mo	3.63	3.59	3.42	-	-	3.61	0.03	0.78
Nb	8.6	8.6		8.9	8.4	8.6	0.00	0.00
Nd	14.3	14.5		15.2	15.2	14.4	0.14	0.98
Ni	153.4	149.5	149.50	-	-	151.45	2.76	1.82
Pb	6.68	5.91	5.59	-	-	6.295	0.54	8.65
Pr	2.96	3.08		3.28	3.29	3.02	0.08	2.81
Rb	5.8	5.5		5.4	5.4	5.65	0.21	3.75
Sb	0.21	0.17	0.18	-	-	0.19	0.03	14.89
Sc	19.8	19.8	19.00	-	-	19.8	0.00	0.00
Sm	3.87	3.81		4.51	4.21	3.84	0.04	1.10
Sn	6	<1		2	1			
Sr	473	467		468	467	470	4.24	0.90
Ta	0.49	0.519		-	-	0.5045	0.02	4.06
Tb	0.61	0.61		0.62	0.64	0.61	0.00	0.00
Th	0.85	0.88		0.88	0.88	0.865	0.02	2.45
Tl	0.016	0.029	0.02	-	-	0.0225	0.01	40.86
Tm	0.24	0.22		0.23	0.22	0.23	0.01	6.15
U	0.28	0.3		0.31	0.3	0.29	0.01	4.88
V	205	191		164	166	198	9.90	5.00
W	1	1		1	1	1	0.00	0.00
Y	17.7	17.3		17.6	17.3	17.5	0.28	1.62
Yb	1.47	1.44		1.5	1.6	1.455	0.02	1.46
Zn	108.8	105.7	103.70	-	-	107.25	2.19	2.04
Zr	104	104		103	104	104	0.00	0.00

* Percent relative difference with average and value of internal standard (SLV-MC basalt and WP-1 dacite)

	2019				ALL				2018	2018	2019
% RD IS*	Mean	σ	% RSD	% RD IS*	Mean	σ	% RSD	% RD IS*	B00267983	B00267985	Q311620
									WP-1 dacite	WP-1 dacite	WP-1 dacite
-0.27	49.15	0.35	0.72	-1.77	49.53	0.48	0.97	-1.02	65.1	65.4	64.7
-1.75	1.51	0.01	0.94	0.58	1.49	0.04	2.41	-0.58	0.47	0.47	0.49
0.58	15.50	0.07	0.46	0.09	15.54	0.15	1.00	0.34	16.3	16.45	16.5
-1.12	12.85	0.07	0.55	-0.15	12.79	0.17	1.29	-0.63	4.18	4.22	4.31
-0.50	0.16	0.00	0.00	-3.52	0.16	0.01	3.08	-2.01	0.07	0.07	0.08
-0.07	7.58	0.04	0.56	0.93	7.54	0.09	1.13	0.43	2.52	2.54	2.62
-1.02	8.58	0.05	0.58	0.15	8.53	0.11	1.26	-0.44	4.82	4.8	4.88
-0.93	3.53	0.02	0.60	-0.51	3.52	0.06	1.68	-0.72	4.19	4.26	4.32
0.41	0.52	0.00	0.00	1.38	0.52	0.01	2.43	0.89	1.53	1.53	1.6
-3.75	0.25	0.01	2.89	0.34	0.24	0.01	3.40	-1.71	0.16	0.17	0.18
9.40	-0.81	0.00	0.00	11.47	-0.80	0.01	-1.19	10.44	0.27	0.1	0.19
	98.91	0.63	0.64		99.15	0.59	0.60		99.77	100.18	100.04
0.50	179.50	0.71	0.39	12.92	169.63	11.43	6.74	6.71	620	622	694
-8.25									0.77	0.77	-
									<0.47	<0.47	-
1.57	23.35	0.07	0.30	11.61	22.30	1.22	5.47	6.59	27.9	29	30.7
-4.26									49.65	48.62	-
0.00	210.00	0.00	0.00		222.50	15.00	6.74	-5.32	70	70	70
1.82	0.10	0.00	0.00		0.09	0.02	22.53	23.64	0.41	0.41	0.49
-7.94									54.8	52.8	-
-1.26	3.69	0.03	0.77	1.63	3.64	0.08	2.12	0.18	2.39	2.3	2.41
-2.98	1.88	0.05	2.64	4.85	1.81	0.09	4.76	0.93	1.25	1.27	1.45
-8.00	1.33	0.01	1.06	-1.72	1.29	0.06	4.80	-4.86	0.87	0.86	0.88
1.25	20.40	0.28	1.39	-4.38	21.00	0.71	3.39	-1.56	19.1	19.4	19
-7.69	4.24	0.06	1.33	3.95	4.00	0.31	7.68	-1.87	2.7	2.54	2.8
-4.00	2.60	0.00	0.00	-0.16	2.55	0.10	3.92	-2.08	3	2.8	3.4
-4.38	0.70	0.02	3.05	1.46	0.68	0.03	4.28	-1.46	0.44	0.44	0.47
-1.51									0.0682	0.0659	-
-1.43	10.10	0.14	1.40	8.21	9.65	0.53	5.52	3.39	13.2	13.7	14.6
-6.67	0.23	0.01	6.15	2.22	0.22	0.02	7.42	-2.22	0.18	0.21	0.24
-5.10									3.63	3.59	
1.23	8.65	0.35	4.09	1.81	8.63	0.21	2.39	1.52	3.8	3.9	3.8
2.61	15.20	0.00	0.00	8.31	14.80	0.47	3.17	5.46	15	16.1	16.1
-4.01									153.4	149.5	-
12.25									6.68	5.91	-
1.46	3.29	0.01	0.22	10.36	3.15	0.16	5.10	5.91	3.64	3.71	3.95
1.73	5.40	0.00	0.00	-2.78	5.53	0.19	3.43	-0.53	22.4	21.5	21.4
3.26									0.21	0.17	-
-11.13									19.8	19.8	-
0.64	4.36	0.21	4.87	14.27	4.10	0.33	7.93	7.46	3.19	3.34	3.5
	1.50	0.71	47.14	-18.18					4	<1	1
1.17	467.50	0.71	0.15	0.64	468.75	2.87	0.61	0.91	761	753	750
1.75					0.50	0.02	4.06	1.75	0.213	0.218	-
-0.54	0.63	0.01	2.24	2.72	0.62	0.01	2.28	1.09	0.38	0.4	0.42
0.92	0.88	0.00	0.00	2.67	0.87	0.02	1.72	1.80	2.08	2.3	2.09
60.71									0.016	0.029	-
-4.00	0.23	0.01	3.14	-6.09	0.23	0.01	4.21	-5.04	0.22	0.2	0.22
-4.00	0.31	0.01	2.32	0.97	0.30	0.01	4.23	-1.52	0.81	0.71	0.84
1.84	165.00	1.41	0.86	-15.13	181.50	19.91	10.97	-6.64	88	88	79
	1.00	0.00	0.00		1.00	0.00	0.00		<1	<1	1
0.72	17.45	0.21	1.22	0.43	17.48	0.21	1.18	0.58	13	12.9	13.1
-5.31	1.55	0.07	4.56	0.87	1.50	0.07	4.62	-2.22	1.28	1.31	1.35
-0.88									108.8	105.7	-
5.09	103.50	0.71	0.68	4.59	103.75	0.50	0.48	4.84	130	129	131

WP-1 Watts Point dacite (Coast Plutonic Complex)												
2019	2018				2019				ALL			
Q311622	Mean	σ	% RSD	% RD IS*	Mean	σ	% RSD	% RD IS*	Mean	σ	% RSD	% RD IS*
WP-1 dacite												
64.9	65.25	0.21	0.33	0.14	64.80	0.14	0.22	-0.55	65.03	0.30	0.46	-0.21
0.49	0.47	0.00	0.00	-2.08	0.49	0.00	0.00	2.08	0.48	0.01	2.41	0.00
16.55	16.375	0.11	0.65	-0.09	16.53	0.04	0.21	0.82	16.45	0.11	0.66	0.37
4.37	4.2	0.03	0.67	-3.36	4.34	0.04	0.98	-0.14	4.27	0.09	2.01	-1.75
0.08	0.07	0.00	0.00	-7.89	0.08	0.00	0.00	5.26	0.08	0.01	7.70	-1.32
2.58	2.53	0.01	0.56	-1.56	2.60	0.03	1.09	1.17	2.57	0.04	1.73	-0.19
4.88	4.81	0.01	0.29	-1.23	4.88	0.00	0.00	0.21	4.85	0.04	0.85	-0.51
4.34	4.225	0.05	1.17	-1.74	4.33	0.01	0.33	0.70	4.28	0.07	1.58	-0.52
1.61	1.53	0.00	0.00	-4.49	1.61	0.01	0.44	0.19	1.57	0.04	2.77	-2.15
0.17	0.165	0.01	4.29	-2.94	0.18	0.01	4.04	2.94	0.17	0.01	4.80	0.00
0.12	0.185	0.12	64.98	26.71	0.16	0.05	31.93	6.16	0.17	0.08	45.31	16.44
100.26	99.975	0.29	0.29		100.15	0.16	0.16		100.06	0.22	0.22	
704	621	1.41	0.23	-1.30	699.00	7.07	1.01	11.09	660.00	45.23	6.85	4.90
-	0.77	0.00	0.00	-29.20								
-												
31	28.45	0.78	2.73	3.08	30.85	0.21	0.69	11.78	29.65	1.46	4.93	7.43
	49.135	0.73	1.48	269.37								
60	70	0.00	0.00	-2.78	65.00	7.07	10.88	-9.72	67.50	5.00	7.41	-6.25
0.48	0.41	0.00	0.00	3.54	0.49	0.01	1.46	22.47	0.45	0.04	9.72	13.01
-	53.8	1.41	2.63	232.10								
2.49	2.345	0.06	2.71	-3.10	2.45	0.06	2.31	1.24	2.40	0.08	3.26	-0.93
1.37	1.26	0.01	1.12	-14.05	1.41	0.06	4.01	-3.82	1.34	0.09	6.96	-8.94
0.88	0.865	0.01	0.82	-2.59	0.88	0.00	0.00	-0.90	0.87	0.01	1.10	-1.75
18.5	19.25	0.21	1.10	-2.48	18.75	0.35	1.89	-5.02	19.00	0.37	1.97	-3.75
2.99	2.62	0.11	4.32	-4.45	2.90	0.13	4.64	5.58	2.76	0.19	6.83	0.57
3.5	2.9	0.14	4.88	-13.17	3.45	0.07	2.05	3.29	3.18	0.33	10.41	-4.94
0.5	0.44	0.00	0.00	-7.56	0.49	0.02	4.37	1.89	0.46	0.03	6.21	-2.84
-	0.06705	0.00	2.43	94.21								
14.5	13.45	0.35	2.63	1.43	14.55	0.07	0.49	9.73	14.00	0.67	4.77	5.58
0.21	0.195	0.02	10.88	-4.41	0.23	0.02	9.43	10.29	0.21	0.02	11.66	2.94
	3.61	0.03	0.78	276.04								
3.7	3.85	0.07	1.84	8.15	3.75	0.07	1.89	5.34	3.80	0.08	2.15	6.74
16.5	15.55	0.78	5.00	5.93	16.30	0.28	1.74	11.04	15.93	0.64	4.05	8.48
-	151.45	2.76	1.82	228.52								
-	6.295	0.54	8.65	-10.39								
3.99	3.675	0.05	1.35	0.91	3.97	0.03	0.71	9.01	3.82	0.17	4.54	4.96
21.2	21.95	0.64	2.90	-0.41	21.30	0.14	0.66	-3.36	21.63	0.53	2.46	-1.88
-	0.19	0.03	14.89	72.73								
-	19.8	0.00	0.00	88.12								
3.54	3.265	0.11	3.25	6.84	3.52	0.03	0.80	15.18	3.39	0.16	4.72	11.01
1					1.00	0.00	0.00	-28.57				
741	757	5.66	0.75	3.59	745.50	6.36	0.85	2.01	751.25	8.26	1.10	2.80
-	0.2155	0.00	1.64	-10.21					0.22	0.00	1.64	-10.21
0.43	0.39	0.01	3.63	-2.50	0.43	0.01	1.66	6.25	0.41	0.02	5.44	1.87
2.13	2.19	0.16	7.10	10.05	2.11	0.03	1.34	6.03	2.15	0.10	4.76	8.04
-	0.0225	0.01	40.86	-83.81								
0.21	0.21	0.01	6.73	11.70	0.22	0.01	3.29	14.36	0.21	0.01	4.51	13.03
0.88	0.76	0.07	9.30	-11.42	0.86	0.03	3.29	0.23	0.81	0.07	8.96	-5.59
79	88	0.00	0.00	-2.00	79.00	0.00	0.00	-12.03	83.50	5.20	6.22	-7.02
1					1.00	0.00	0.00					
13.2	12.95	0.07	0.55	1.65	13.15	0.07	0.54	3.22	13.05	0.13	0.99	2.43
1.37	1.295	0.02	1.64	1.17	1.36	0.01	1.04	6.25	1.33	0.04	3.04	3.71
-	107.25	2.19	2.04	78.97								
131	129.5	0.71	0.55	3.77	131.00	0.00	0.00	4.97	130.25	0.96	0.74	4.37

B370163 (lab duplicate)					Q930096 (lab duplicate)					
B370163	B370163	Mean	σ	% RSD	Q930096	Q930096	Mean	σ	% RSD	D00005979
felsic tuff	felsic tuff				felsic volcanic flow	felsic volcanic flow				felsic lapilli tuff
74.4	74.7	74.55	0.21	0.28						
0.27	0.28	0.275	0.01	2.57						
11.7	12.1	11.9	0.28	2.38						
2.62	2.76	2.69	0.10	3.68						
0.1	0.1	0.1	0.00	0.00						
0.47	0.5	0.485	0.02	4.37						
1	1.01	1.005	0.01	0.70						
0.16	0.16	0.16	0.00	0.00						
6.07	6.25	6.16	0.13	2.07						
0.02	0.03	0.025	0.01	28.28						
-	-									
-	-									
5190	5410	5300	155.56	2.94						
1.58	1.55	1.565	0.02	1.36	1.43	1.48	1.46	0.04	2.43	2.09
0.62	0.69	0.655	0.05	7.56	<0.47	<0.47	-	-	-	<0.47
95.6	108	101.8	8.77	8.61						
1.37	1.5	1.435	0.09	6.41	0.70	0.70	0.70	0.00	0.00	2.12
10	10	10	0.00	0.00						
1.58	1.72	1.65	0.10	6.00						
5.7	5.5	5.6	0.14	2.53	17.30	17.00	17.15	0.21	1.24	41.80
5.63	6.15	5.89	0.37	6.24						
3.31	3.69	3.5	0.27	7.68						
0.29	0.34	0.315	0.04	11.22						
16.8	17.3	17.05	0.35	2.07						
5.59	5.87	5.73	0.20	3.46						
9.4	10	9.7	0.42	4.37						
1.19	1.27	1.23	0.06	4.60						
0.0324	0.0304	0.0314	0.00	4.50	0.0103	0.0101	0.0102	0.000	1.386	0.0484
46.9	52.8	49.85	4.17	8.37						
0.52	0.56	0.54	0.03	5.24						
2.25	2	2.125	0.18	8.32	2.48	2.85	2.67	0.26	9.82	1.81
20.4	20.6	20.5	0.14	0.69						
37.5	43.9	40.7	4.53	11.12						
1.5	1.5	1.5	0.00	0.00	<0.7	<0.7	-	-	-	4.80
81.36	90.18	85.77	6.24	7.27	25.28	22.15	23.72	2.21	9.33	6.01
10.7	11.95	11.325	0.88	7.80						
186	188	187	1.41	0.76						
0.64	0.66	0.65	0.01	2.18	0.66	0.67	0.67	0.01	1.06	0.08
3.9	3.8	3.85	0.07	1.84	4.10	4.10	4.10	0.00	0.00	10.70
7.36	8.22	7.79	0.61	7.81						
6	<1	6								
105.5	105.5	105.5	0.00	0.00						
1.7	1.7	1.7	0.00	0.00						
0.9	0.96	0.93	0.04	4.56						
25.1	26.7	25.9	1.13	4.37						
1.277	1.24	1.2585	0.03	2.08	>20	>20	-	-	-	0.45
0.49	0.57	0.53	0.06	10.67						
5.59	5.65	5.62	0.04	0.75						
14	12	13	1.41	10.88						
4	5	4.5	0.71	15.71						
33.8	36.3	35.05	1.77	5.04						
3.39	3.78	3.585	0.28	7.69						
386.9	384.1	385.5	1.98	0.51	79.70	76.70	78.20	2.12	2.71	118.10
349	363	356	9.90	2.78						

D00005979 (lab duplicate)				D00005989 (lab duplicate)					B370184 (lab d	
D00005979	Mean	σ	% RSD	D00005989	D00005989	Mean	σ	% RSD	B370184	B370184
felsic lapilli tuff				felsic tuff	felsic tuff				felsic volcanic flow	felsic volcanic flow
2.00	2.05	0.06	3.11	1.31	1.28	1.30	0.02	1.64	2.87	2.77
<0.47	-	-	-	<0.47	<0.47	-	-	-	<0.47	<0.47
1.92	2.02	0.14	7.00	2.12	2.21	2.17	0.06	2.94	3.18	2.97
39.30	40.55	1.77	4.36	13.60	11.70	12.65	1.34	10.62	3.80	4.60
0.0467	0.0476	0.0012	2.5280	0.0314	0.0299	0.0307	0.0011	3.4606	0.0384	0.0377
1.74	1.78	0.05	2.79	3.94	3.94	3.94	0.00	0.00	1.28	1.12
4.70	4.75	0.07	1.49	3.00	3.20	3.10	0.14	4.56	3.70	3.30
6.07	6.04	0.04	0.70	112.98	107.44	110.21	3.92	3.55	11.83	11.49
0.08	0.08	0.00	0.00	5.70	5.09	5.40	0.43	8.00	2.15	2.07
10.60	10.65	0.07	0.66	3.50	3.60	3.55	0.07	1.99	5.20	4.80
0.47	0.46	0.01	2.60	0.29	0.28	0.28	0.00	1.00	>20	>20
112.00	115.05	4.31	3.75	390.60	386.70	388.65	2.76	0.71	26.90	26.40

(lab duplicate)			B00267986 (lab duplicate)				
Mean	σ	% RSD	B00267986 SLV-MC basalt	B00267986 SLV-MC basalt	Mean	σ	% RSD
2.82	0.07	2.51	0.75	0.77	0.76	0.01	1.86
-	-	-	<0.47	<0.47	-	-	-
3.08	0.15	4.83	47.78	48.62	48.20	0.59	1.23
4.20	0.57	13.47	52.30	52.80	52.55	0.35	0.67
0.0381	0.0005	1.3009	0.0663	0.0659	0.0661	0.0003	0.4279
1.20	0.11	9.43	3.42	3.59	3.51	0.12	3.43
3.50	0.28	8.08	149.50	149.50	149.50	0.00	0.00
11.66	0.24	2.06	5.59	5.91	5.75	0.23	3.94
2.11	0.06	2.68	0.18	0.17	0.18	0.01	4.04
5.00	0.28	5.66	19.00	19.80	19.40	0.57	2.92
-	-	-	0.02	0.03	0.02	0.01	29.46
26.65	0.35	1.33	103.70	105.70	104.70	1.41	1.35

Appendix 1.1 Certified Reference Materials QA/QC Data

		ALS 2018						
Certified reference material	Analysis method	SRM88B	SY-4	OREAS-105	AMIS0085	AMIS0304	OREAS 146	AMIS0167
Major elements (wt%)								
SiO_2	ME-ICP06	-	50	-	-	-	20.2	94
Al_2O_3	ME-ICP06	-	20.5	-	-	-	2.98	2.43
Fe_2O_3	ME-ICP06	-	5.96	-	-	-	27.6	3.29
CaO	ME-ICP06	-	7.87	-	-	-	17.25	0.12
MgO	ME-ICP06	-	0.5	-	-	-	6.86	0.23
Na_2O	ME-ICP06	-	6.91	-	-	-	0.3	0.08
K_2O	ME-ICP06	-	1.58	-	-	-	1.25	0.48
Cr_2O_3	ME-ICP06	-	<0.002	-	-	-	0.024	0.057
TiO_2	ME-ICP06	-	0.27	-	-	-	1.35	0.14
MnO	ME-ICP06	-	0.1	-	-	-	2.38	0.02
P_2O_5	ME-ICP06	-	0.12	-	-	-	0.52	0.04
SrO	ME-ICP06	-	0.14	-	-	-	0.38	<0.01
BaO	ME-ICP06	-	0.04	-	-	-	1.47	0.01
LOI	OA-GRA05	-	-	-	-	-	-	-
Total	TOT-ICP06	-	98.55	-	-	-	91.91	>102.00
Trace elements (ppm)								
Ba	ME-MS81	11.6	350	696	373	2630	>10000	87.3
Ce	ME-MS81	4	125	113	74.4	8250	4820	46.6
Cr	ME-MS81	<10	10	50	590	90	190	430
Cs	ME-MS81	0.18	1.51	1.97	4.36	0.4	0.56	1.1
Dy	ME-MS81	0.63	18.25	12	10.85	126	219	5.95
Er	ME-MS81	0.31	14.25	7.57	8.13	32.3	81.6	3.05
Eu	ME-MS81	0.15	1.8	1.44	0.87	141.5	122.5	0.75
Ga	ME-MS81	0.5	38.1	29.3	15.8	43.1	21.3	3.3
Gd	ME-MS81	0.58	13.4	12.3	7.11	321	325	4.68
Hf	ME-MS81	0.2	10.9	6.6	4.7	28.1	4	2.5
Ho	ME-MS81	0.13	4.44	2.44	2.56	17.05	35.6	1.1
La	ME-MS81	5.1	58.4	47.1	37.5	3350	2490	23.9
Lu	ME-MS81	0.05	2.03	0.99	1.38	1.99	6.08	0.31
Nb	ME-MS81	0.3	14.5	43.7	11.8	>2500	402	4.8
Nd	ME-MS81	3.3	62.3	64.9	29.5	4090	2340	20.1
Pr	ME-MS81	0.82	15.15	14.8	8.21	>1000	576	5.18
Rb	ME-MS81	2.7	54	105	231	10.7	26.2	16.9
Sm	ME-MS81	0.64	13.75	15.8	7.4	620	460	4.48
Sn	ME-MS81	<1	12	10	3	25	43	<1
Sr	ME-MS81	68.5	1265	91.1	107.5	3460	3220	20.6
Ta	ME-MS81	0.1	0.8	4.6	1.7	13	4	1.7
Tb	ME-MS81	0.08	2.64	2.02	1.53	32.2	43.1	0.92
Th	ME-MS81	0.34	1.17	377	51.2	432	962	50
Tm	ME-MS81	0.05	2.26	1.14	1.32	3.29	9.53	0.39
U	ME-MS81	0.14	0.69	542	250	22.1	2.6	482
V	ME-MS81	<5	8	32	24	365	157	61
W	ME-MS81	<1	<1	3	2	5	29	1
Y	ME-MS81	8	120.5	64.5	71.9	393	942	24.7
Yb	ME-MS81	0.38	14.85	7.14	9.19	16.3	49.9	2.43
Zr	ME-MS81	6	598	237	169	1170	239	104

OREAS-101b	OREAS-101b	SY-4	CDN-W-4	SRM88B	AMIS0085	AMIS0167	AMIS0304	OREAS 146
63	-	49.6	-	1.17	72.1	93.3	-	20.2
10.3	-	20.6	-	0.32	11	2.45	-	3.02
14.95	-	6.2	-	0.28	3.43	3.4	-	28.4
1.59	-	7.89	-	30.2	3.21	0.13	-	17.4
2.03	-	0.51	-	20.9	1.73	0.23	-	7.04
0.08	-	7.21	-	0.03	1.73	0.08	-	0.3
2.81	-	1.66	-	0.1	4.66	0.5	-	1.31
0.005	-	<0.002	-	<0.002	0.08	0.059	-	0.025
0.63	-	0.28	-	0.01	0.21	0.15	-	1.43
0.12	-	0.1	-	0.01	0.06	0.02	-	2.46
0.26	-	0.12	-	<0.01	0.07	0.03	-	0.55
<0.01	-	0.14	-	0.01	0.01	<0.01	-	0.39
0.02	-	0.04	-	<0.01	0.04	0.01	-	1.55
-	-	-	4.34	-	-	-	-	-
95.8	-	98.91		99.73	100.87	101.98	-	93.43
195.5	205	-	-	6.2	382	-	2670	-
1400	1375	-	-	4	75	-	8400	-
40	40	-	-	<10	610	-	100	-
2.57	2.52	-	-	0.14	4.29	-	0.42	-
34.3	33.5	-	-	0.61	12.15	-	140	-
19.75	20.3	-	-	0.4	8.84	-	36.5	-
7.97	8.34	-	-	0.13	1.09	-	156.5	-
25.6	29.1	-	-	0.3	12.7	-	41.9	-
37.8	37.9	-	-	0.55	7.77	-	371	-
11.5	11.5	-	-	<0.2	5.3	-	29.3	-
6.58	6.76	-	-	0.17	2.54	-	18.7	-
817	785	-	-	4.9	38.2	-	3460	-
2.57	2.8	-	-	0.04	1.4	-	2.25	-
62.5	65.2	-	-	0.2	11.5	-	>2500	-
401	382	-	-	3.5	30.8	-	3880	-
129	127	-	-	0.91	8.45	-	>1000	-
193.5	193.5	-	-	3	230	-	11.2	-
52.1	51.1	-	-	0.57	7.19	-	609	-
10	9	-	-	<1	3	-	23	-
22.1	23.8	-	-	62.4	101.5	-	3520	-
3	3.3	-	-	<0.1	1.3	-	13.6	-
5.64	5.74	-	-	0.09	1.55	-	37	-
36.6	37.4	-	-	0.25	53.1	-	444	-
2.74	2.81	-	-	0.05	1.35	-	3.59	-
414	400	-	-	0.23	269	-	23.6	-
85	92	-	-	5	32	-	403	-
22	20	-	-	1	2	-	5	-
170	182	-	-	7.9	68.6	-	419	-
19.15	18.8	-	-	0.23	10.05	-	17.45	-
417	445			5	160	-	1200	-

AMIS0547	AMIS0304	SY-4	SY-4	CDN-W-4	AMIS0547	OREAS 146	AMIS0167	AMIS0167	OREAS-14P
-	12.5	49.5	50.7	-	-	-	91.8	92.6	20.7
-	1.54	20.4	20.7	-	-	-	2.39	2.38	4.63
-	21.4	6.18	6.32	-	-	-	3.35	3.35	52.6
-	28.6	7.82	8.1	-	-	-	0.11	0.13	1.44
-	2.81	0.5	0.58	-	-	-	0.22	0.24	0.5
-	0.1	6.92	7.08	-	-	-	0.07	0.07	0.81
-	0.28	1.62	1.61	-	-	-	0.49	0.47	1.08
-	0.014	<0.002	0.002	-	-	-	0.057	0.058	0.008
-	1.76	0.27	0.28	-	-	-	0.14	0.14	0.42
-	0.45	0.1	0.11	-	-	-	0.02	0.02	0.08
-	18.5	0.12	0.12	-	-	-	0.03	0.03	0.13
-	0.42	0.14	0.15	-	-	-	<0.01	<0.01	0.01
-	0.29	0.04	0.04	-	-	-	0.01	0.01	0.04
38.5	-	-	-	4.32	38.5	-	-	-	-
-	96.4	98.17	100.35	-	-	-	100.31	101.12	97.87
-	2790	354	-	-	-	>10000	87.5	-	-
-	8460	131.5	-	-	-	4890	48	-	-
-	100	10	-	-	-	200	430	-	-
-	0.43	1.65	-	-	-	0.55	1.11	-	-
-	145	19.85	-	-	-	236	6.35	-	-
-	36.8	15.4	-	-	-	86.8	3.28	-	-
-	152.5	2.14	-	-	-	129	0.75	-	-
-	56.6	37.4	-	-	-	18.4	3.1	-	-
-	362	14.35	-	-	-	344	4.8	-	-
-	30.3	11.7	-	-	-	4	2.8	-	-
-	18.45	4.54	-	-	-	37.6	1.15	-	-
-	3470	62.5	-	-	-	2570	24.6	-	-
-	2.02	2.28	-	-	-	6.59	0.33	-	-
-	>2500	13.8	-	-	-	396	4.6	-	-
-	4290	61.9	-	-	-	2310	20	-	-
-	>1000	16.05	-	-	-	581	5.38	-	-
-	10.8	55.2	-	-	-	26.9	16.9	-	-
-	637	13.8	-	-	-	469	4.4	-	-
-	27	8	-	-	-	46	1	-	-
-	3470	1255	-	-	-	3260	20.7	-	-
-	12.9	0.8	-	-	-	4.4	1.7	-	-
-	35.2	2.69	-	-	-	45.4	0.94	-	-
-	434	1.31	-	-	-	916	48.9	-	-
-	3.49	2.43	-	-	-	10.1	0.45	-	-
-	23.9	0.87	-	-	-	2.67	469	-	-
-	380	6	-	-	-	167	60	-	-
-	6	1	-	-	-	30	2	-	-
-	397	124.5	-	-	-	968	25.8	-	-
-	18	16	-	-	-	54.4	2.55	-	-
-	1140	633	-	-	-	234	103	-	-

ALS 2019									
SRM 694	OREAS-101b	CDN-W-4	SRM88B	AMIS0547	AMIS0085	AMIS0304	OREAS-101b	SY-4	SY-4
11.35	62.3	-	1.14	-	70.8	12.15	62.9	-	-
1.87	10.35	-	0.32	-	11.1	1.54	10.5	-	-
0.77	15.2	-	0.29	-	3.45	21.5	15.35	-	-
44.6	1.6	-	30.5	-	3.29	29.3	1.6	-	-
0.35	2.09	-	21.3	-	1.75	2.84	2.11	-	-
0.86	0.07	-	0.03	-	1.74	0.1	0.07	-	-
0.56	2.83	-	0.11	-	4.64	0.28	2.89	-	-
0.119	0.004	-	<0.002	-	0.08	0.013	0.004	-	-
0.12	0.63	-	0.02	-	0.22	1.78	0.65	-	-
0.01	0.11	-	0.01	-	0.06	0.46	0.12	-	-
30.2	0.27	-	<0.01	-	0.06	18.65	0.3	-	-
0.12	<0.01	-	0.01	-	0.01	0.43	<0.01	-	-
0.01	0.02	-	<0.01	-	0.04	0.3	0.02	-	-
-	-	4.26		38.2	-	-	-	-	-
90.94	95.47	-	100.43	-	99.78	97.08	96.51	-	-
-	190.5	-	6.2	-	370	2730	198.5	354	317
-	1375	-	4.2	-	70.3	8490	1425	131.5	122.5
-	30	-	10	-	530	90	40	10	10
-	2.23	-	0.2	-	4.09	0.37	2.55	1.65	1.47
-	33.7	-	0.63	-	11.85	142.5	33.9	19.85	20
-	19.9	-	0.42	-	8.92	35.8	20.2	15.4	15.45
-	7.51	-	0.12	-	0.85	145	7.63	2.14	1.84
-	28.1	-	0.5	-	14.6	52.1	29.7	37.4	36.2
-	37.6	-	0.58	-	7.48	358	38.2	14.35	15.1
-	10.2	-	0.2	-	4.6	27	11.2	11.7	11.2
-	6.35	-	0.13	-	2.47	17.95	6.67	4.54	4.58
-	799	-	4.9	-	35.8	3500	821	62.5	58.1
-	2.55	-	0.05	-	1.45	1.98	2.57	2.28	2.1
-	57.7	-	0.4	-	10.9	>2500	59.9	13.8	13.6
-	381	-	3.4	-	28.8	4240	400	61.9	59.6
-	121.5	-	0.79	-	7.93	>1000	126.5	16.05	14.4
-	182	-	3	-	220	10.5	195	55.2	53.7
-	49.7	-	0.57	-	6.88	630	51.7	13.8	12.6
-	10	-	<1	-	3	25	10	8	8
-	20.4	-	60.8	-	99.7	3520	21.3	1255	1260
-	3	-	0.3	-	1.7	12.6	2.6	0.8	1
-	5.31	-	0.08	-	1.53	34	5.46	2.69	2.7
-	34.3	-	0.3	-	51.5	452	36.5	1.31	1.34
-	2.68	-	0.05	-	1.37	3.49	2.89	2.43	2.31
-	373	-	0.43	-	250	22.6	405	0.87	0.73
-	83	-	6	-	29	375	83	6	8
-	21	-	5	-	2	6	21	1	1
-	166	-	7.6	-	68.5	392	170	124.5	117
-	18.95	-	0.31	-	9.83	17.75	19.3	16	15.85
-	396	-	8	-	154	1170	408	633	558

SY-4	CDN-W-4	SRM88B	AMIS0547	AMIS0304	OREAS 146	AMIS0167	AMIS0167	OREAS 146	AMIS0085
50.7	-	1.18	-	12.3	-	-	92.6	-	72.1
20.7	-	0.33	-	1.5	-	-	2.38	-	11.15
6.32	-	0.31	-	21.6	-	-	3.35	-	3.57
8.1	-	30.5	-	29.1	-	-	0.13	-	3.22
0.58	-	21.4	-	2.85	-	-	0.24	-	1.81
7.08	-	0.03	-	0.1	-	-	0.07	-	1.79
1.61	-	0.11	-	0.29	-	-	0.47	-	4.8
0.002	-	<0.002	-	0.013	-	-	0.058	-	0.08
0.28	-	0.02	-	1.8	-	-	0.14	-	0.22
0.11	-	0.01	-	0.46	-	-	0.02	-	0.06
0.12	-	0.01	-	18.8	-	-	0.03	-	0.07
0.15	-	0.01	-	0.43	-	-	<0.01	-	0.01
0.04	-	<0.01	-	0.29	-	-	0.01	-	0.04
	4.32		38.5	-	-	-		-	-
100.35	-	100.61	-	97.27	-	-	101.12	-	101.46
-	-	6.2	-	2680	>10000	87.5	-	>10000	379
-	-	4.4	-	8430	4890	48	-	5070	71.9
-	-	<10	-	100	200	430	-	190	600
-	-	0.19	-	0.39	0.55	1.11	-	0.57	4
-	-	0.62	-	144.5	236	6.35	-	242	11.85
-	-	0.42	-	36.6	86.8	3.28	-	90	9.22
-	-	0.1	-	146	129	0.75	-	135.5	1.05
-	-	0.4	-	48.2	18.4	3.1	-	37	16.8
-	-	0.69	-	359	344	4.8	-	367	7.72
-	-	<0.2	-	28.7	4	2.8	-	4.5	5
-	-	0.12	-	18.15	37.6	1.15	-	37.6	2.71
-	-	5	-	3460	2570	24.6	-	2670	36.1
-	-	0.05	-	2.03	6.59	0.33	-	6.37	1.39
-	-	0.4	-	>2500	396	4.6	-	403	11.1
-	-	3.3	-	4260	2310	20	-	2360	29.1
-	-	0.85	-	>1000	581	5.38	-	574	8.06
-	-	3	-	10.4	26.9	16.9	-	27.2	236
-	-	0.57	-	632	469	4.4	-	475	7.34
-	-	<1	-	25	46	1	-	44	3
-	-	61.9	-	3510	3260	20.7	-	3330	100
-	-	0.3	-	12.2	4.4	1.7	-	4.3	2.1
-	-	0.12	-	34.1	45.4	0.94	-	46.7	1.51
-	-	0.27	-	458	916	48.9	-	955	54.2
-	-	0.07	-	3.52	10.1	0.45	-	9.94	1.44
-	-	0.4	-	21.8	2.67	469	-	2.66	248
-	-	<5	-	395	167	60	-	161	24
-	-	1	-	6	30	2	-	32	2
-	-	7.8	-	388	968	25.8	-	985	69.5
-	-	0.33	-	18.2	54.4	2.55	-	54.2	9.59
-	-	6	-	1190	234	103	-	238	160

OREAS-14P	SRM 694	SY-4	SY-4	AMIS0286	AMIS0461	OREAS 146	AMIS0167
20.7	11.35	-	49.6	-	-	-	93.6
4.63	1.87	-	20.5	-	-	-	2.55
52.6	0.77	-	6.04	-	-	-	3.5
1.44	44.6	-	7.9	-	-	-	0.15
0.5	0.35	-	0.52	-	-	-	0.25
0.81	0.86	-	6.99	-	-	-	0.1
1.08	0.56	-	1.65	-	-	-	0.56
0.008	0.119	-	0.002	-	-	-	0.063
0.42	0.12	-	0.27	-	-	-	0.16
0.08	0.01	-	0.1	-	-	-	0.03
0.13	30.2	-	0.11	-	-	-	0.01
0.01	0.12	-	0.14	-	-	-	<0.01
0.04	0.01	-	0.04	-	-	-	0.01
-	-	-		7.68	38.9	-	-
97.87	90.94	-	98.42	-	-	-	>102.00
-	-	344	-	-	-	>10000	-
-	-	130	-	-	-	5080	-
-	-	10	-	-	-	180	-
-	-	1.55	-	-	-	0.54	-
-	-	18.55	-	-	-	219	-
-	-	14.75	-	-	-	86.3	-
-	-	1.99	-	-	-	125	-
-	-	39.6	-	-	-	19.7	-
-	-	14.3	-	-	-	337	-
-	-	10.9	-	-	-	4.3	-
-	-	4.49	-	-	-	36.1	-
-	-	61.3	-	-	-	2640	-
-	-	2.22	-	-	-	6.59	-
-	-	13.7	-	-	-	394	-
-	-	60.7	-	-	-	2320	-
-	-	15.85	-	-	-	596	-
-	-	50	-	-	-	25.6	-
-	-	12.55	-	-	-	444	-
-	-	7	-	-	-	43	-
-	-	1145	-	-	-	3060	-
-	-	0.7	-	-	-	3.9	-
-	-	2.69	-	-	-	44.8	-
-	-	1.25	-	-	-	914	-
-	-	2.33	-	-	-	10.15	-
-	-	0.92	-	-	-	2.63	-
-	-	7	-	-	-	146	-
-	-	1	-	-	-	27	-
-	-	114	-	-	-	915	-
-	-	15.3	-	-	-	52.1	-
-	-	611	-	-	-	246	-

	OGL IMC-100 2018							
Certified reference material	MRB-29	MRB-29	MRB-29	GSP-2	AGV-2	BHVO-2	MRB-29	MRB-29
Trace elements (ppm)								
Ba	288.0	290.7	297.3	1379.6	1140.1	134.1	280.8	292
Be	0.94	0.98	0.92	1.32	2.07	0.92	0.97	0.95
Bi	0.03	0.03	0.03	0.03	0.04	0.01	0.03	0.03
Cd	0.102	0.107	0.104	0.097	0.058	0.098	0.114	0.089
Ce	49.54	49.84	49.04	442.97	70.13	37.24	47.11	48.04
Co	54.59	51.27	50.81	7.33	16.04	46.01	48.38	46.99
Cr	297	285	275	21	16	302	279	265
Cs	0.234	0.246	0.233	1.181	1.182	0.090	0.243	0.246
Cu	143.4	133.8	154.4	42.3	50.9	125.1	149.3	139.1
Dy	5.283	5.257	5.383	5.990	3.648	5.406	5.245	5.227
Er	2.871	2.876	2.835	2.376	1.888	2.682	2.85	2.824
Eu	1.9684	1.8877	1.8395	2.4157	1.6048	2.1006	1.9432	1.9536
Ga	19.52	20.22	19.52	22.29	20.60	21.39	19.75	19.42
Gd	6.210	6.064	6.055	12.901	4.720	6.317	6.002	6.06
Hf	4.43	4.67	4.61	12.29	5.62	4.56	4.45	4.64
Ho	1.0587	1.0588	1.0499	0.9698	0.7070	0.9958	1.0547	1.0373
In	0.0803	0.0842	0.0805	0.0529	0.0444	0.0864	0.0782	0.0708
La	21.6	21.8	21.9	186.1	37.8	15.1	20.9	21.6
Li	10.1	10.3	9.7	33.9	10.5	4.0	11.2	9.7
Lu	0.363	0.370	0.360	0.227	0.263	0.288	0.379	0.364
Mo	0.75	0.78	0.71	3.20	1.97	4.12	0.68	0.65
Nb	12.679	12.839	12.531	25.620	13.540	17.454	12.207	12.459
Nd	28.81	27.82	28.06	211.91	31.64	24.98	26.64	28.23
Ni	114.1	104.8	107.5	16.0	17.7	117.7	109.6	105.6
Pb	4.97	4.70	4.83	41.23	12.77	1.79	4.92	4.72
Pr	6.661	6.615	6.666	56.802	8.278	5.420	6.395	6.475
Rb	14.43	14.45	13.76	254.55	70.48	9.56	14.12	14.1
Sb	0.05	0.06	0.05	0.37	0.46	0.09	0.07	0.06
Sc	32.5	31.4	30.6	6.4	11.9	31.9	31.1	31.7
Sm	6.365	6.303	6.487	27.011	5.673	6.257	6.134	6.232
Sn	2.10	2.16	2.35	6.19	1.91	1.46	2.46	2.01
Sr	303.0	304.2	302.8	231.9	652.3	402.5	311.2	302.2
Ta	0.760	0.803	0.802	0.888	0.861	1.143	0.75	0.806
Tb	0.9183	0.9148	0.9083	1.3680	0.6561	0.9696	0.9106	0.8971
Th	2.616	2.670	2.614	110.199	6.000	1.247	2.503	2.426
Ti	12021	11325	11305	4047	6104	16322	11554	11468
Tl	0.089	0.079	0.086	1.391	0.291	0.026	0.072	0.071
Tm	0.3878	0.4067	0.3933	0.2905	0.2684	0.3422	0.3895	0.3994
U	0.631	0.648	0.658	2.537	1.926	0.435	0.654	0.623
V	339.2	313.4	320.5	54.5	119.9	335.8	322.6	315.8
W	0.20	0.22	0.22	0.37	0.52	0.29	0.21	0.21
Y	27.04	26.22	26.83	26.37	18.82	25.98	27.18	26.5
Yb	2.533	2.548	2.554	1.744	1.821	2.071	2.511	2.483
Zn	106.8	103.9	103.8	114.5	90.5	97.7	106.8	106.6
Zr	175	173	177	475	236	181	174	176

OGL IMC-100 2019							
MRB-29	MRB-29	MRB-29	AGV-2	BHVO-2	GSP-2	AGV-2	AGV-2
285.4	281.7	294.4	1127	129.8	1314.7	1095.9	1123.4
0.93	0.98	0.86	1.99	1.03	1.35	2.06	1.97
0.02	0.03	0.02	0.04	0.01	0.08	0.05	0.04
0.122	0.093	0.097	0.071	0.102	0.09	0.07	0.069
47.25	47	48.21	66.08	37.27	429.49	66.02	65.81
45.86	49.31	45.83	15.01	42.96	6.54	15.16	14.3
265	287	256	16	294	19	16	15
0.247	0.239	0.226	1.11	0.103	1.214	1.119	1.133
135.7	143.8	135.2	50.8	125.8	42.2	50	48.1
5.435	5.119	5.56	3.495	5.45	6.004	3.466	3.556
2.895	2.794	2.956	1.932	2.63	2.45	1.89	1.888
1.9481	1.9356	2.0165	1.5825	2.0966	2.3481	1.5948	1.5303
19.42	19.8	19.14	20.46	21.23	22.3	20.6	20.33
6.136	6.113	6.31	4.706	6.378	12.652	4.541	4.592
4.71	4.29	4.77	5.33	4.6	12.47	5.11	5.6
1.0611	1.001	1.0894	0.6956	1.0063	0.9962	0.6787	0.6888
0.0752	0.0756	0.0732	0.0458	0.0826	0.0481	0.0445	0.0435
21.2	20.8	21.5	36.1	14.9	178.4	35.9	36
10	10.4	9.3	10	4.2	34.5	10.3	9.9
0.371	0.352	0.384	0.265	0.279	0.235	0.257	0.268
0.72	0.7	0.72	1.96	4.98	2.25	1.9	1.86
12.314	12.147	11.842	12.593	17.068	24.94	12.877	12.784
27.77	26.75	27.82	29.62	25.14	202.52	29.83	30.05
104.8	108.8	103.3	18.3	119.8	15.8	17.9	17.6
4.99	4.63	4.64	12.96	1.92	39.58	13.12	12.72
6.493	6.382	6.755	8.194	5.505	56.071	8.058	8.29
13.9	14.57	14.99	68.02	8.9	236.6	68.49	65.23
0.05	0.05	0.05	0.44	0.11	0.39	0.45	0.41
30.6	31.6	31.7	12	32.1	6.3	11.9	11.9
6.374	6.044	6.253	5.602	6.105	26.476	5.396	5.492
2.33	1.85	2.13	1.77	1.68	6.17	1.75	1.88
298.3	303.7	310.1	656.6	386.4	229.5	638.7	627.3
0.797	0.739	0.827	0.787	1.124	0.855	0.77	0.825
0.8965	0.8792	0.9274	0.6341	0.9562	1.2893	0.6346	0.6351
2.445	2.583	2.614	6.212	1.168	103.944	6.204	5.831
11404	11860	11118	6172	16287	3832	6120	5946
0.077	0.07	0.073	0.273	0.021	1.328	0.28	0.279
0.4013	0.3872	0.4108	0.2647	0.3378	0.2994	0.2528	0.2693
0.622	0.637	0.655	2.011	0.447	2.38	1.921	1.885
319.7	323.8	313.4	123.6	336.2	52.2	119.5	119.6
0.22	0.21	0.23	0.5	0.24	0.36	0.49	0.52
26.1	26.49	26.9	19.3	25.71	25.84	19.18	18.5
2.502	2.46	2.592	1.735	1.985	1.722	1.631	1.703
107.1	111.1	105.3	90.9	100.8	114.2	89.5	88.3
173	174	178	237	177	471	233	233

	OGL IML-101 2018			OGL IML-101 2019							
Certified reference material	RAFT-2	RAFT-2	LKSD-2	RAFT-2	RAFT-2	RAFT-2	RAFT-2	WPR-1a	SdAR-H1	WPR-1a	SdAR-H1
Trace elements (ppm)											
Ag	1.12	1.15	0.91	1.16	1.13	1.15	1.13	1.09	88	1.05	83.42
As	83.2	89.8	9.6	84.3	82.2	82.1	82.2	9	390.6	9.4	391.6
Au	0.019	0.016	0.002	0.02	0.015	0.017	0.015	0.024	2.68	0.051	6.117
Bi	5.41	5.14	1.11	4.83	4.93	4.98	4.86	0.12	5.1	0.12	4.93
Cd	2.43	2.66	0.71	2.52	2.61	2.59	2.47	0.49	27.18	0.57	25.86
Co	40.0	40.0	14.5	41.4	41.8	42.8	41.5	221.8	56.3	219.2	56.8
Cu	598	603	34	626	629	627	626	3063	1192	3021	1197
Hg	0.2	0.2	0.1	0.2	0.2	0.2	0.2	0.1	7.2	0.1	7.3
In	0.104	0.103	0.062	0.098	0.103	0.103	0.1	0.074	10.067	0.071	10.027
Ir	0.004	0.003	0.001	0.004	0.002	0.003	0.003	0.003	0	0.003	0.001
Mo	2.98	3.07	1.27	3.28	3.18	3.27	3.26	0.8	62.59	0.78	63.17
Ni	848	844	24	883	878	902	883	4505	230	4456	234
Pb	105.3	98.0	37.3	95.6	97	96	94.4	6.9	3957.1	7	3807.7
Pd	0.03	0.05	0.00	0.04	0.05	0.05	0.05	0.6	0.42	0.58	0.41
Pt	0.036	0.032	0.000	0.048	0.036	0.026	0.028	0.192	0.056	0.216	0.079
Rh	0.013	0.012	0.002	-	-	-	-	-	-	-	-
Sb	1.32	1.35	0.64	1.38	1.35	1.39	1.35	1.49	554.69	1.63	542.91
Se	7.8	8.3	1.2	7	7.5	7.3	7.3	5.6	15.3	5.5	14.8
Sn	3.1	3.0	1.4	3	3.1	3.1	3.1	0.7	1.5	0.8	1.5
Te	2.40	2.53	0.09	2.38	2.4	2.37	2.29	1.11	9.99	1.08	10.09
Tl	0.292	0.262	0.267	0.26	0.267	0.268	0.257	0.067	9.568	0.066	9.305
Zn	115	119	189	118	124	122	119	133	3936	129	3926

Appendix 2.1 Whole rock lithogeochemistry analyses full set

Sample	A00348398	A00348399	B370156	B370157	B370158	B370159	B370160	B370161	B370162
Rock Type*	MI	MI	LT	LT	TF	TF	TF	TF	VF
DDH_ID	K15-290	K15-290	K15-301	K15-301	K15-301	K15-301	K15-301	K15-301	K15-301
DDH_From	90.7	117.3	22.65	47.9	77.55	91.25	102.55	117.6	122.7
DDH_To	90.9	117.45	22.8	48.05	77.65	91.4	102.7	117.7	122.8
Major elements (wt%) ALS ME-MS81									
SiO_2	40.2	46.7	68.7	71.6	76.9	69	41.8	76.2	73.1
TiO_2	1.23	1.24	0.57	0.26	0.14	0.36	0.21	0.33	0.27
Al_2O_3	13.95	15.05	15.7	13	10.2	15.1	11	14.05	12.4
Fe_2O_3	9.73	9.24	2.48	2.59	1.21	0.97	3.23	1.93	1.34
MnO	0.14	0.14	0.07	0.06	0.05	0.03	0.19	0.01	0.01
MgO	5.47	8.21	1.31	1.7	1.89	0.82	7.66	0.82	0.1
CaO	11.6	9.9	1.48	2.04	1.98	2.98	11.15	0.63	0.68
Na_2O	0.09	3.31	0.14	0.12	0.12	2.65	0.32	0.69	0.32
K_2O	2.52	0.17	5	4.16	3.23	3.29	3.43	4.18	9.09
P_2O_5	0.13	0.13	0.19	0.07	0.02	0.04	0.02	0.03	0.03
Cr_2O_3	0.044	0.047	<0.002	<0.002	<0.002	<0.002	<0.002	<0.002	<0.002
SrO	0.02	0.03	<0.01	<0.01	<0.01	0.01	0.02	<0.01	0.01
BaO	0.25	0.02	0.15	0.12	0.21	0.83	0.16	0.23	0.34
LOI	13.15	4.26	3.87	4.08	4.28	4.21	19.25	2.81	1.2
Total	98.52	98.45	99.66	99.8	100.23	100.29	98.44	101.91	98.89
Trace elements (ppm) ALS ME-ICP06									
Ba	2410	173	1400	1075	1930	7720	1155	2120	3130
Ce	22.4	25.1	203	101	109.5	127	89.9	105	83.3
Cr	300	330	10	10	10	10	10	10	10
Cs	2.35	0.32	2.12	2.58	4.74	4.12	3.6	3.02	0.97
Dy	3.8	4.01	12.2	7.95	4.11	7.81	5.77	6.75	5.42
Er	2.29	2.52	6.63	4.64	2.5	4.83	3.15	3.93	3.4
Eu	0.62	1.26	2.39	0.53	0.41	0.74	0.41	0.66	0.46
Ga	15.6	16.1	27.5	23.9	17.5	23.2	18	23.1	17.6
Gd	3.79	3.92	13.95	7.02	4.48	8.06	6.21	6.43	5.08
Hf	2.5	2.6	16.4	6.9	4.9	12.2	6.5	10.8	9.6
Ho	0.77	0.88	2.43	1.61	0.88	1.66	1.11	1.34	1.13
La	10.1	11.3	98.7	49	53.9	59.9	44.9	51	41.7
Lu	0.31	0.33	0.78	0.6	0.45	0.66	0.38	0.57	0.52
Nb	9.9	9.6	48.7	25.2	16.4	30.4	17.5	26.1	21.8
Nd	13.3	14.6	89.3	40.3	41.1	52.6	38	43.8	32.7
Pr	2.97	3.31	23.4	11.25	11.75	14.15	10.05	11.8	9.14
Rb	82.1	4.8	169	162.5	131	88.6	130	146.5	206
Sm	3.57	3.94	17.35	8.11	6.51	10.1	8.3	8.47	5.91
Sn	1	1	8	12	11	13	12	12	9
Sr	171	281	40.3	49.1	49.2	157.5	150.5	30.2	73.7
Ta	0.6	1.3	2.7	1.9	1.5	2.3	1.4	1.9	1.6
Tb	0.6	0.68	2.03	1.21	0.72	1.23	0.95	1.08	0.89
Th	1.49	1.7	34.7	26.6	26.4	33.6	24	29	23.7
Tm	0.31	0.35	0.93	0.68	0.37	0.74	0.43	0.57	0.53
U	0.32	0.31	4.6	6.98	4.16	8.32	3.88	8.22	5.66
V	200	202	31	20	<5	20	11	18	13
W	7	1	4	3	2	3	3	4	3
Y	20.4	21.9	64.8	48.3	23.9	45.5	30	37.5	32.9
Yb	2.06	2.17	5.66	4.42	2.74	4.48	2.83	3.87	3.52
Zr	94	97	700	252	161	469	229	405	362

*LT, felsic lapillit tuff; TF, felsic tuff, VF, felsic coherent volcanic rock; MI, mafic intrusive; MD, mafic dike; XT, felsic crystal-rich tuff.

B370163	B370175	B370176	B370177	B370178	B370179	B370180	B370181	B370182	B370183
TF	TF	TF	TF	TF	TF	VF	MI	MI	TF
K15-301	K15-320	K15-320	K15-320	K15-320	K15-320	K15-320	K15-320	K15-320	K15-320
135.85	18.85	50.3	76.45	95.85	114.45	127.95	134	148.4	165
136	18.95	50.4	76.55	95.95	114.55	128.05	134.15	148.5	165.2
74.4	63.8	61.4	64.6	70.8	76.3	76.2	48.5	43.2	68
0.27	0.59	0.66	0.51	0.46	0.26	0.2	1.15	1.13	0.39
11.7	16.2	16.7	13.4	13.5	13.75	11.05	14.7	14.15	16.15
2.62	5.67	4.43	3.27	2.51	1.77	0.68	9.73	8.78	2.45
0.1	0.05	0.1	0.09	0.06	0.01	0.02	0.14	0.14	0.02
0.47	1.4	1.6	2.27	1.36	0.8	0.44	8.52	7.28	0.28
1	1.22	2.84	4.48	2.7	0.42	3.68	8.97	9.55	0.3
0.16	0.07	0.1	0.1	0.12	0.08	4.54	2.52	2.47	0.24
6.07	6.26	5.84	4.54	4.33	4.73	1.2	1.09	1.37	9.44
0.02	0.17	0.19	0.17	0.15	0.02	0.01	0.12	0.12	0.05
<0.002	<0.002	<0.002	<0.002	<0.002	<0.002	<0.002	0.05	0.041	<0.002
0.01	<0.01	<0.01	0.01	<0.01	<0.01	<0.01	0.03	0.01	<0.01
0.55	0.15	0.14	0.16	0.14	0.19	0.22	0.11	0.47	0.99
2.2	3.24	5.38	7.46	4.45	2.53	3.59	3.83	10.2	1.83
99.57	98.82	99.38	101.06	100.58	100.86	101.83	99.46	98.91	100.14
5190	1395	1290	1505	1305	1800	2040	986	4440	9210
95.6	157	206	167	175.5	98	94.2	20.9	20.2	135.5
10	10	20	10	10	10	10	380	310	10
1.58	3.23	3.22	2.14	2.5	2.11	1.11	1.41	1.41	2.21
5.63	11.75	11.45	9.43	8.72	4.63	5.96	3.77	3.74	7.85
3.31	6.52	6.23	5.35	4.61	2.69	3.8	2.27	1.96	5.06
0.29	2.26	2.55	2.19	1.93	0.37	0.57	1.01	1.13	0.77
16.8	27	28.4	22.8	23.3	20.1	11.2	15	14.6	24
5.59	11.2	13.3	11.25	10.5	5.48	5.76	3.32	3.37	8.47
9.4	17.2	19.7	15.9	12.6	8.2	7.9	2.3	2.5	13.2
1.19	2.38	2.29	1.83	1.65	0.94	1.28	0.76	0.7	1.68
46.9	76.5	100	81.6	85.2	48.4	45.8	9.8	8.8	65
0.52	0.85	0.91	0.67	0.62	0.4	0.53	0.3	0.27	0.73
20.4	41.7	49.1	43.1	39	22.4	21.2	9.1	8.9	31.8
37.5	68.8	90.5	74.1	75.6	38.5	38	12.6	12.5	54.8
10.7	18.2	23.9	19.35	20.2	10.7	10.4	2.74	2.69	15.05
186	213	206	128	143	218	35.3	36.1	43.1	281
7.36	13.3	17	13.6	14.45	7.3	7.14	3.21	3.4	10.85
6	8	9	7	7	10	7	1	<1	6
105.5	25.8	44.4	97.2	56.7	19.2	61.1	251	144	63.4
1.7	2.2	2.8	2.4	2.3	1.8	1.8	0.6	0.6	4.4
0.9	1.88	1.93	1.65	1.52	0.83	1	0.57	0.56	1.34
25.1	32.9	33.8	27.5	30.7	31.8	25.9	1.64	1.38	34.4
0.49	0.9	0.82	0.71	0.63	0.41	0.54	0.3	0.29	0.71
5.59	4.51	4.74	4.01	3.63	6.45	10.05	0.35	0.57	7.94
14	41	35	27	23	14	13	219	229	19
4	3	2	2	2	4	2	1	1	5
33.8	64.4	62.7	50.7	46.5	25.1	36.3	20.4	19.1	50.3
3.39	5.53	5.66	4.45	4.06	2.73	3.63	1.79	1.97	4.82
349	766	871	697	548	298	284	92	91	507

B370184	B370185	B370186	B370187	B370188	B370189	B370190	D00005977	D00005978	D00005979
VF	TF	MI	TF	LT	LT	TF	LT	TF	LT
K15-320	K15-320	K15-320	K15-320	K15-320	K15-320	K15-320	K15-281	K15-281	K15-281
174.3	202.65	205.5	212.45	229.65	244.4	262	13.5	24.3	49.1
174.4	202.75	205.65	212.55	229.8	244.55	262.1	13.8	24.45	49.3
70.2	69.4	44.9	74.9	65.7	65.8	66.1	65.8	43	66.5
0.37	0.36	1.22	0.28	0.5	0.59	0.63	0.67	2	0.53
15.45	15.45	14.2	12.95	15.55	14.6	15.5	16.35	11.75	12.65
0.85	2.15	9.79	1.5	3.19	5.29	3.33	2.06	9.8	4.95
0.01	0.03	0.17	0.03	0.15	0.12	0.05	0.08	0.18	0.12
0.39	0.91	8.12	1.45	1.39	1.46	1.67	1.47	3.21	1.83
0.87	1.99	9.86	1.68	2.43	1.79	2.04	2.31	12.4	3.01
0.19	2.05	1.62	0.26	1.61	1.61	0.18	2.38	0.23	1.8
10.3	4.23	2.44	3.73	4.13	3.58	4.84	4.16	2.92	2.74
0.04	0.04	0.13	0.07	0.15	0.19	0.21	0.22	0.28	0.16
<0.002	<0.002	0.044	<0.002	<0.002	<0.002	<0.002	0.002	0.019	0.002
<0.01	<0.01	0.04	<0.01	0.01	<0.01	<0.01	<0.01	0.02	<0.01
0.12	0.75	0.74	0.08	0.12	0.12	0.15	0.14	0.13	0.09
1.55	3.58	4.94	4.14	5.1	4.01	5.28	4.57	12.9	5.17
100.34	100.94	98.21	101.07	100.03	99.16	99.98	100.21	98.84	99.55
1055	6960	6820	769	1170	1090	1340	1245	1170	849
119.5	111	23.6	96.2	215	168.5	225	200	41.3	149
10	10	320	10	10	10	10	10	130	10
1.72	2.35	4.52	2.8	2.72	3.77	2.55	2.8	4.59	1.91
7.91	6.93	3.62	7.26	10.65	10.35	10.55	10.15	6.25	7.63
4.9	4.34	2.15	4.32	5.5	5.68	5.37	5.37	3.6	4.22
0.76	0.63	0.99	0.43	2.32	2.29	3.17	2.67	1.5	2.12
22.7	24.6	14.8	20.2	26.9	24.4	25.5	27.7	19.8	20.1
7.21	6.88	3.49	6.51	12.65	11.6	13.75	12.9	5.97	9.83
12.6	11.9	2.5	6.9	16.1	16.8	18.4	17.8	4.8	14.8
1.69	1.43	0.75	1.51	2.04	2.02	2.06	1.98	1.35	1.54
56.5	54.1	11	45.3	105	81.5	109	98.4	18.3	73.1
0.71	0.58	0.33	0.56	0.71	0.77	0.74	0.71	0.52	0.6
30.1	28.9	9.4	23.8	43.9	44.1	48	49.5	18.9	38.9
48.4	43.7	13.4	37.9	94	74.4	98.3	87.7	23.9	65.6
13.35	12.55	3.08	10.7	24.6	19.35	26.1	23.2	5.29	17.15
305	125	79.8	145.5	116.5	119	150	139.5	105	84.5
8.82	8.32	3.35	7.76	18.2	14.6	18.4	17.05	6.03	13.2
7	8	<1	6	5	2	1	4	2	2
39.5	47	313	47.4	66.5	51.3	45.9	31.3	173.5	50.2
2.3	2	0.6	1.9	2.5	2.4	2.7	2.9	1.1	2.2
1.13	0.99	0.59	1.17	1.79	1.58	1.97	1.88	0.96	1.42
35	32.7	1.69	26.2	37.2	27.5	34.8	30.6	3.22	22.9
0.82	0.71	0.31	0.62	0.78	0.86	0.77	0.78	0.52	0.61
7.57	9.16	0.51	6.43	4.7	3.64	3.95	3.98	0.93	3.49
19	30	216	17	23	30	32	33	290	28
4	3	1	3	2	6	2	3	2	2
52.5	41.4	20.7	41.9	54.9	56.3	55.3	53	34.9	41.4
4.71	4.05	2.03	3.85	4.81	5.09	5.09	5.02	3.29	4
478	466	95	254	681	745	812	736	195	642

D00005980	D00005981	D00005982	D00005983	D00005984	D00005985	D00005986	D00005987	D00005988	D00005989
MD	TF	TF	TF	TF	TF	TF	TF	TF	TF
K15-281	K15-281	K15-281	K15-281	K15-281	K15-281	K15-281	K15-281	K15-281	K15-281
64.9	85.8	137.6	147.5	164.8	176.55	183.05	184.45	199.45	212.75
65	86	137.7	147.7	165	176.65	183.2	184.65	199.6	212.9
46.3	62.8	63.4	77.7	76.8	65.6	27.6	50.1	76.1	78.8
2.26	0.62	0.62	0.25	0.28	0.33	0.35	0.38	0.23	0.25
12.7	14.4	15.3	12.25	12.95	16.45	21.7	19.5	12.9	10.45
10.55	5.66	5.73	2.22	1.67	2.21	26.4	8.86	2.02	2.74
0.18	0.08	0.07	0.01	0.01	0.13	0.06	0.04	0.01	0.01
3.51	1.83	1.91	0.79	0.76	2.17	14.35	7.71	0.98	0.09
6.88	2.95	2.15	0.59	0.37	2.46	0.13	1.98	0.18	1.15
2.99	1.23	0.39	0.1	0.16	0.22	0.07	0.2	0.13	2.7
1.51	4.41	5.13	4.01	4.01	5.11	2	4.35	4.34	1.75
0.33	0.21	0.21	0.08	0.07	0.04	0.03	0.06	0.03	0.02
0.005	0.003	0.002	0.002	0.002	<0.002	0.002	0.002	<0.002	<0.002
0.01	0.01	0.01	<0.01	<0.01	<0.01	<0.01	<0.01	<0.01	<0.01
0.09	0.3	0.1	0.06	0.06	0.11	0.06	0.16	0.19	0.14
10.7	5.8	4.06	2.82	2.69	5.3	8.3	7.32	2.46	2.43
98.02	100.3	99.08	100.88	99.83	100.13	101.05	100.66	99.57	100.53
794	2710	883	549	572	977	604	1425	1670	1225
67	203	186	97.6	102.5	144	155	188	94.4	87.1
30	20	20	10	10	10	10	10	10	10
1.52	2.54	3.87	2.27	2.38	3.91	2.88	4.31	2.25	0.54
5.86	8.86	10.8	8.03	6.89	6.4	14.8	7.88	5.61	5.74
3.25	4.63	5.54	4.61	4.06	3.76	7.6	4.49	2.84	3.64
1.86	2.83	2.63	0.51	0.5	0.66	0.68	0.6	0.3	0.59
22.2	25.5	28	22.3	23.6	28.6	41.4	32.2	21.1	18.2
6.74	11.45	12.45	6.76	6.7	7.98	14.45	9.13	5.14	5.68
6.2	17.8	18	7.4	8	9.8	12.3	12.6	7.4	8.4
1.24	1.81	2.1	1.63	1.46	1.22	2.84	1.49	1.12	1.26
31.3	102.5	91	47.2	49.9	70.6	68.8	97.9	45.9	43.8
0.45	0.65	0.79	0.62	0.59	0.52	0.82	0.65	0.44	0.5
21.6	44.1	47.6	23.6	26.3	29.4	32	30.9	21.1	18.7
35.2	87.1	82.1	40	40.9	57.3	79.2	70.8	38	34.1
8.29	22.8	21.4	11.05	11.7	16.15	19.25	20.4	10.5	9.75
46.9	121.5	155	162.5	170.5	204	90.6	175	148.5	32.7
8.26	16.25	15.65	8.65	8.38	10.85	18.6	14.1	7.16	6.7
2	3	5	7	8	12	3	8	7	7
131.5	104	66.7	17	16.9	45.8	5.9	35.1	7.5	36.1
1.3	2.6	2.7	1.9	2.1	2.4	2.5	2.6	1.9	1.5
1.01	1.66	1.89	1.32	1.12	1.13	2.46	1.34	0.87	0.95
7.51	27.2	28.3	25.6	26.3	37.8	39.4	44.7	26.7	21.6
0.49	0.69	0.87	0.66	0.63	0.57	1.07	0.71	0.46	0.52
1.61	3.81	4.44	4.92	6.38	8.09	10.95	9.16	7.35	5.62
322	29	29	14	14	17	21	20	13	13
2	2	3	2	3	5	6	6	4	4
33.7	47.9	58.7	46.3	42	35.7	82.1	43.5	31.3	34.4
3.2	4.38	5.61	4.12	4.25	3.71	6.22	4.71	3.21	3.28
238	755	763	260	291	347	445	450	247	305

D00005990	D00005991	Q311613	Q720929	Q720932	Q720934	Q720939	Q720946	Q720949	Q721051
TF	TF	VF	LT	MI	MI	LT	LT	MI	LT
K15-281	K15-281	K16-417	K16-370	K16-370	K16-370	K16-370	K15-271	K15-271	K15-309
227.9	251.9	96.85	98.3	160.35	189.1	276.95	174.2	257.35	165.25
228.05	252.1	96.9	98.45	160.5	189.3	277.1	174.35	257.55	165.45
68.9	68.5	75.7	66.6	46.2	43.6	62.5	65.4	47.9	76.1
0.34	0.65	0.18	0.46	1.51	1.23	0.68	0.53	1.18	0.22
14.4	15.5	12.3	12.35	15.7	14.2	15.9	14.25	15.35	12.9
1.82	4.49	1.3	6.41	11.1	9.02	7.96	4.48	9.5	1.04
0.03	0.03	0.02	0.14	0.16	0.15	0.19	0.09	0.15	0.02
0.97	0.81	0.45	1.65	8.13	6.94	2.79	0.98	9.06	0.52
2.71	0.74	0.67	2.77	10.1	10.35	0.3	2.94	10.8	0.95
0.09	2.77	0.24	0.13	2.45	0.09	0.25	0.51	2.03	0.43
5.22	3.84	8.16	3.86	0.56	4.84	3.21	3.89	0.8	4.22
0.04	0.22	0.03	0.15	0.17	0.12	0.21	0.18	0.11	<0.01
<0.002	0.003	<0.002	<0.002	0.055	0.042	<0.002	0.002	0.051	0.002
0.01	<0.01	<0.01	<0.01	0.04	0.01	<0.01	<0.01	0.03	<0.01
0.1	0.29	0.13	0.11	0.08	0.17	0.09	0.11	0.11	0.25
4.06	3.13	1.52	4.58	3.02	7.56	4.21	4.15	2.54	2.8
98.69	100.97	100.7	99.21	99.28	98.32	98.29	97.51	99.61	99.45
906	2570	1200	1020	810	1535	851	999	954	2300
101	185.5	123.5	179.5	29.5	20.2	221	187.5	22.9	125.5
10	10	10	10	360	310	20	20	380	10
2.04	1.84	0.92	3.24	0.87	8.17	1.63	3.35	0.99	2.28
7.11	10.5	8.01	9.9	4.91	4.12	11.3	9.19	3.96	9.94
4.05	5.79	4.95	5.77	2.94	2.34	6.02	4.77	2.46	5.48
0.65	2.24	0.43	2.05	1.48	1.23	2.64	2.31	1.06	0.39
23.3	27.7	20.3	20.4	18.4	13.5	26.5	24.4	16.1	17.3
6.59	12.75	7.69	11	4.77	3.68	13.85	11.4	3.67	8.64
11.7	17.9	6.5	14.4	3.1	2.6	18.2	14.7	2.3	7.6
1.41	2.18	1.66	2.05	1.03	0.75	2.1	1.7	0.78	1.91
49.8	90	62.2	89.5	13.3	9.3	109.5	92.9	10.5	61
0.69	0.8	0.66	0.77	0.39	0.31	0.82	0.7	0.32	0.64
25.5	45.1	20.7	34.5	11.2	9.1	48.5	39.6	8.9	24.9
41.3	82.6	47.1	75.7	17.1	11.8	93.5	77.8	12.9	49.2
11.3	21.6	13.75	20.7	3.91	2.7	25.1	21.3	3.03	13.95
184.5	103.5	163.5	108.5	15	170	98.1	126.5	26.3	138.5
8.21	15.9	9.55	14.75	4.54	3.44	17.1	14.05	3.21	9.57
9	5	10	3	1	1	5	4	1	3
66.4	42.6	23.8	47.6	361	107.5	44.8	52.8	236	38.1
1.9	2.7	2.3	2.2	1.2	<0.1	3.3	2.2	0.7	1.8
1.1	1.8	1.34	1.69	0.77	0.62	1.99	1.64	0.63	1.5
26.2	27.3	32.3	30.1	1.97	1.36	33.7	31.3	1.68	33.9
0.69	0.85	0.68	0.78	0.41	0.32	0.83	0.72	0.33	0.76
6.89	3.94	6	3.95	0.4	0.29	4.65	4.24	0.32	10.25
15	30	5	19	234	215	34	27	229	11
2	3	2	3	1	2	4	3	1	2
43.4	58.8	43.8	51.5	25.9	19.1	57.8	45	21.5	51.6
4.3	5.37	4.45	5.06	2.7	2.02	5.88	4.37	2.2	4.85
418	750	188	587	111	86	795	639	92	248

Q721071	Q721073	Q721099	Q721154	Q721155	Q721156	Q721157	Q721158	Q721160	Q721170
TF	MD	VF	VF	MI	LT	LT	VF	VF	VF
K15-287	K17-422	K15-290	K15-204	K15-204	K17-448	K17-448	K17-448	K17-448	K15-300
118.35	40.3	139.7	135.6	146.4	322.45	334	346.15	358.45	67.95
118.55	40.5	139.9	135.8	146.6	322.65	334.15	346.3	358.6	68.15
71.5	52.5	74	68.4	43.2	60.8	64	76.5	77	77.6
0.24	2.33	0.28	0.34	1.23	0.93	0.61	0.16	0.17	0.2
13.05	13.2	11.45	13.8	14.85	14.3	14.4	12.5	12.8	12.7
4.2	10.25	1.45	5.83	9.28	8.06	5.35	1.06	1.34	0.95
0.09	0.14	0.03	0.02	0.12	0.06	0.1	0.03	0.01	0.01
3.09	2.35	0.11	0.25	6.86	3.73	0.8	0.23	0.41	0.48
0.45	5.84	1.59	0.2	10.1	3.21	3.79	1.39	0.44	0.51
0.12	0.1	0.33	0.22	1.71	0.11	2.76	4.72	3.28	0.21
3.61	4.4	8.36	9.59	2.2	4.26	3.52	1.67	2.1	7.21
0.03	0.37	0.02	0.05	0.13	0.21	0.18	0.08	0.09	0.09
0.002	0.004	0.003	0.002	0.047	0.019	<0.002	<0.002	<0.002	<0.002
<0.01	0.01	0.02	<0.01	0.01	0.01	0.01	0.01	<0.01	<0.01
0.14	0.33	0.6	0.17	0.09	0.25	0.22	0.07	0.11	0.16
3.07	5.66	1.28	3.07	10.65	3.59	3.36	1.6	2.1	1.45
99.59	97.48	99.52	101.94	100.48	99.54	99.1	100.02	99.85	101.57
1255	3060	5370	1520	787	2280	1970	670	960	1475
114.5	77.7	97.9	112	22.5	127	171	77.3	66.8	101.5
10	30	10	20	320	130	10	<10	10	10
2.88	7.13	1.04	2.67	3.01	1.96	2.9	0.82	2.3	1.33
8.48	6.56	6.72	8.97	4.21	8.75	11.25	7.97	8.28	9.54
5.12	3.75	3.94	5.58	2.48	4.81	6.17	4.67	5.06	4.92
0.36	1.99	0.39	0.81	1.04	1.86	2.02	0.42	0.43	0.64
21.2	21.6	14.1	20.8	17.5	23.2	26.3	19.9	22.7	19.8
7.18	7.91	6.07	8.38	3.84	9.81	13.4	7.14	6.71	8.98
7.7	5.6	8.1	10.8	2.6	12.7	15.9	5	6	6
1.69	1.29	1.32	1.8	0.83	1.62	2.01	1.6	1.67	1.71
57.9	36.5	49.7	55.1	10.2	61.4	84	36.4	30.6	48.2
0.62	0.49	0.53	0.82	0.34	0.61	0.81	0.53	0.63	0.59
21.5	19.4	21.2	28.7	9.8	31.8	41.3	23.1	25.4	28.2
42.1	39.4	37.6	46	13.8	59	77.1	33.6	28.3	44.9
12.5	9.92	10.9	12.75	3.11	14.95	20.4	9.14	7.76	11.85
116.5	142.5	163.5	168.5	57.3	100	96.5	52.7	68.2	156.5
8.04	8.62	7.56	9.07	3.89	11.45	15.55	7.1	6.54	9.58
10	2	3	13	1	7	5	4	4	5
18.4	128.5	150	45.7	121	89.2	105.5	116.5	37.2	21.4
1.8	1.3	2	2.4	0.8	2.5	2.7	2.2	2.3	3.2
1.26	1.17	1.06	1.28	0.63	1.37	1.91	1.24	1.19	1.42
30.4	8.97	24.9	29.5	1.61	19.7	27.3	18.5	20.8	23.9
0.75	0.56	0.57	0.8	0.32	0.62	0.81	0.63	0.72	0.69
7.33	2	5.99	12.55	0.34	3.1	3.85	5.84	4.58	6.22
17	329	17	19	226	90	30	6	6	7
3	4	3	4	2	3	2	2	2	1
50.3	36	38.9	48.4	20.3	41.3	53.9	41.6	45	42.3
4.47	3.4	3.63	5.57	2.09	4.37	5.55	4.5	4.78	4.62
270	233	313	408	92	510	638	159	180	199

Q930095	Q930096	Q930097	Q930098	Q930099	Q930100	Q930221	Q930240	Q930243	Q930244
TF	VF	TF	TF	MI	TF	LT	VF	MI	VF
K15-235R	K15-235R	K15-235R	K15-235R	K15-235R	K15-235R	K15-232	K15-236	K15-236	K15-236
86.15	116.7	133.3	136.1	143.65	149.25	207.85	95	113.35	117.15
86.3	116.95	133.5	136.35	143.95	149.4	208	95.26	113.65	117.35
73.7	57.2	56.5	71.1	43.7	68.5	62.5	64.1	43	78.5
0.27	0.26	0.33	0.15	1.18	0.39	0.62	0.3	1.12	0.29
15.55	12.7	16.55	8.02	14.85	16.4	15	17.95	14.65	11.9
1.86	3.14	2.71	9.74	9.32	2.34	5.11	4.16	9.05	1.67
0.04	0.18	0.05	0.12	0.15	0.05	0.08	0.01	0.12	<0.01
1.28	4.6	3.36	5.85	8.2	1.08	1.72	0.75	8.32	0.21
0.55	7.07	3.63	0.86	9.63	0.89	2.88	0.45	8.66	0.38
0.22	0.24	0.12	0.02	1.28	0.14	0.19	6.91	0.4	3.01
4.82	3.89	5.12	0.43	3.54	7.07	4.69	2.03	4.67	3.4
0.04	0.04	0.03	0.02	0.13	0.05	0.18	0.04	0.12	0.04
0.002	0.002	0.002	<0.002	0.05	0.002	<0.002	<0.002	0.052	<0.002
<0.01	0.01	0.01	<0.01	0.02	0.01	0.01	<0.01	0.02	<0.01
0.21	0.35	2.43	0.04	0.18	0.2	0.32	1.04	0.31	0.38
2.73	12.05	8.01	3.73	7.82	2.82	4.77	2.36	9.39	1.42
101.27	101.73	98.85	100.08	100.05	99.94	98.07	100.1	99.88	101.2
1835	3030	>10000	275	1530	1760	3030	9990	2850	3470
114.5	107	128.5	33.2	19.4	100.5	186	172	17.4	82.5
10	10	10	<10	360	10	10	10	340	10
3.61	3.93	3.83	1.06	8.62	2.28	4.61	2.69	14.65	0.95
7.1	7.39	7.32	3.15	3.35	7.14	10.7	11.75	3.48	5.78
4.77	4.11	4.04	1.98	2	4.2	6.19	7.17	2.08	3.51
0.45	0.64	0.52	0.21	1.05	0.68	2.52	0.76	0.95	0.48
26.5	22	29.8	18	16.8	27.2	27.1	30.2	15.6	19.6
5.83	6.37	7.86	3.06	3.37	6.93	13.5	11.15	3.05	5.03
9.1	8.1	9.9	4.8	2.3	12.6	16.8	15.6	2	9
1.65	1.38	1.55	0.66	0.73	1.5	1.97	2.3	0.7	1.19
56.4	53.8	63.9	15	8.6	49.5	92.1	84.3	7.8	40.3
0.67	0.53	0.58	0.31	0.29	0.63	0.8	0.84	0.24	0.54
28.4	22	27.9	14.4	8.6	30.2	43.7	23.8	7.7	21.5
42.3	41.3	51.4	15.1	12	40.1	81.8	68.3	10.6	33.8
12.35	11.75	14.35	3.94	2.55	11.1	21.7	19.3	2.37	9.77
179.5	133.5	176.5	17.6	138.5	269	142	71.2	166.5	66.1
8.07	8.14	9.94	3.27	3.35	8.15	15.25	13.25	3.24	6.7
10	9	11	2	1	10	4	38	1	7
20.1	95.5	122	11	203	59.9	71.5	32.5	170	43.8
2.5	1.8	2.2	1.2	0.5	2.1	3	3.7	0.9	1.6
1.11	1.1	1.24	0.49	0.58	1.25	1.81	1.7	0.52	0.86
31.4	28	33.9	17.3	1.34	31	29.6	81	1.47	23.1
0.72	0.59	0.66	0.3	0.29	0.67	0.83	0.98	0.26	0.49
8.8	7.33	7.02	4.55	0.24	7.99	4.17	36.1	0.41	6.53
11	12	18	7	218	19	31	318	200	17
4	3	5	1	2	4	3	6	3	1
45.6	41.5	43.8	18.3	19.3	43.2	53.5	60.5	16.8	30.7
4.94	3.87	3.93	2.06	1.8	4.33	5.43	7.02	1.87	4.06
298	279	346	171	84	471	711	503	78	341

Q930277	Q930281	Q930282	Q930290	Q930291	Q930292	Q930294	Q931941	Q931942	Q931943
MI	MD	VF	MI	MI	MI	VF	TF	MI	LT
K15-286	K15-315	K15-315	K15-315	K15-315	K15-315	K15-315	K15-235R	K15-235R	K15-235R
179.7	11.3	20.95	118.15	121.9	132.1	146.6	159.05	163.35	173.75
179.9	11.5	21.15	118.3	122.15	132.35	146.95	159.25	163.6	173.95
46.1	51.1	77.8	44.7	45	44.9	72	71.9	43.9	77.2
1.31	2.34	0.16	1.35	1.27	1.3	0.26	0.34	1.06	0.22
15.75	12.55	10.9	16.15	15.55	14.4	10.4	14.55	15.45	12.75
10	11.05	0.94	10.05	9.69	9.81	2.01	2.46	8.45	2.36
0.12	0.16	0.03	0.15	0.15	0.14	0.03	0.03	0.13	<0.01
6.97	2.96	0.33	7.56	8.02	8.17	0.07	0.91	8.25	0.97
5.33	6.68	0.78	10.45	9.23	8.86	3.18	1.94	8.98	0.12
0.07	0.08	0.27	3.06	1.69	3.67	0.34	0.43	3.93	0.21
5.01	5.73	8.06	0.49	2.42	0.4	8.53	4.9	0.18	4.03
0.13	0.36	0.03	0.14	0.15	0.16	0.03	0.05	0.12	0.03
0.049	0.006	<0.002	0.052	0.048	0.044	<0.002	0.002	0.051	<0.002
0.02	0.02	<0.01	0.04	0.03	0.01	0.01	<0.01	0.01	<0.01
0.23	0.1	0.11	0.05	0.17	0.03	0.23	0.22	0.01	0.12
8.78	6.27	1.15	4.68	6.45	8.31	3.25	3.57	10.3	2.8
99.87	99.41	100.56	98.92	99.87	100.2	100.34	101.3	100.82	100.81
2060	912	875	416	1505	231	1815	1910	93.4	1135
19.8	66.8	101.5	21.6	21.7	23.5	81	112	19	112
360	30	10	350	350	290	10	10	370	10
17.4	13.25	0.82	0.52	3.8	0.59	0.88	2.28	0.57	2.55
3.67	6.19	7.09	4.14	4.44	4.43	6.13	6.44	3.14	8.33
2.15	3.39	3.84	2.44	2.43	2.45	3.66	4.27	1.85	4.89
0.81	1.58	0.37	1.1	1.18	1.27	0.6	0.68	1.05	0.47
17	21.2	16	16.6	17.8	13.7	13.1	24.6	16.4	22.2
3.24	6.59	6.44	3.97	4.4	4.06	6.04	6.24	3.33	7.67
2.5	5.6	5.2	2.8	2.5	2.6	8.3	10.8	2.1	7.6
0.71	1.17	1.31	0.75	0.83	0.87	1.24	1.43	0.66	1.79
8.9	30.8	50.4	9.9	9.7	11.5	41.8	54.3	8.8	54.9
0.28	0.44	0.43	0.28	0.3	0.3	0.43	0.65	0.28	0.61
9.5	17.1	19	9	8.8	8.6	18	25.8	8.6	22
11.3	32.7	39.7	13.3	14.1	14.5	31.8	45.3	11.7	44.1
2.63	8.25	10.55	2.66	3.01	2.84	8.37	12.35	2.45	12.4
177	229	181	15.3	102	13.8	163	140	4.8	131.5
2.87	7.11	7.36	3.06	3.5	3.86	5.61	8.52	2.96	8.41
1	2	5	1	1	1	4	9	1	7
136.5	186.5	28.3	285	224	94.4	102	38.8	130.5	18.7
0.4	1.1	2	0.3	0.7	0.6	1.6	2	0.5	1.9
0.54	1.02	0.99	0.58	0.66	0.65	0.99	1.05	0.52	1.33
1.64	7.44	27.3	1.34	1.44	1.44	21.3	27.3	1.43	29.1
0.31	0.5	0.47	0.31	0.33	0.32	0.51	0.63	0.28	0.72
0.35	3.44	17.8	0.57	0.68	0.38	5.35	7.39	0.36	6.09
246	323	8	234	225	231	12	24	193	11
4	5	2	1	1	1	3	3	1	2
17.9	31.5	32.5	20.7	20.9	21.5	33.5	40.3	17.7	48.1
2.03	3.18	3.37	2.11	2.07	2.1	3.13	4.46	1.8	4.23
101	220	157	85	89	87	289	414	84	238

Q931952	Q931973	Q931984	Q931989
MD	XT	XT	MD
K15-216	K15-233	K15-282	K15-282
31.05	108	165.1	129
31.2	108.2	165.25	129.2
50.6	65.3	64.2	39.2
2.29	0.53	0.65	2.93
13.4	15.05	15.4	16.15
11.1	3.15	4.53	12.45
0.14	0.06	0.13	0.21
3.19	1.33	1.77	3.34
5.23	2.27	3.09	7.37
2.81	1.23	0.09	0.11
2.47	4.82	5.54	7.07
0.35	0.17	0.18	0.39
0.005	0.003	0.002	0.005
0.01	0.01	0.01	0.01
0.15	0.24	0.17	0.25
7.92	4.7	5.95	8.54
99.67	98.86	101.71	98.03
1365	2150	1540	2190
74.8	205	191.5	108.5
30	10	10	20
3.26	1.7	4.53	6.79
6.56	10.1	9.42	5.59
3.88	5.65	5.56	3.01
1.99	1.99	2.72	2.26
22.9	27.2	27.1	28.6
7.33	12.55	12.1	8.6
6.1	15.6	19	8.6
1.35	1.97	1.96	1.01
35.5	101.5	95.5	51
0.46	0.78	0.77	0.5
19.2	37.1	44.8	27.3
36.3	84.6	81.6	52.5
9.5	23.5	22.1	13.45
70.9	126	175.5	241
7.24	15.05	14.2	10.5
2	4	4	3
129.5	84.8	63.2	127
1.9	2.8	2.9	2.3
1.12	1.84	1.75	1.14
8.48	36.1	28.4	12.3
0.53	0.74	0.8	0.45
1.81	4.82	4.03	2.8
276	23	27	306
2	3	3	3
34.3	51.5	49.6	24.8
3.11	5.1	5	3.23
243	631	814	349

Sample	A00348398	A00348399	B370156	B370157	B370158	B370159	B370160	B370161	B370162	B370163	B370175
Rock Type*	MI	MI	LT	LT	TF	TF	TF	TF	VF	TF	TF
DDH_ID	K15-290	K15-290	K15-301	K15-301	K15-301	K15-301	K15-301	K15-301	K15-301	K15-301	K15-320
DDH_From	90.7	117.3	22.65	47.9	77.55	91.25	102.55	117.6	122.7	135.85	18.85
DDH_To	90.9	117.45	22.8	48.05	77.65	91.4	102.7	117.7	122.8	136	18.95
Trace elements (ppm) OGL IMC-100											
Ba	2168.7	149.4	1357	1044.9	>1740	>1740	1317.2	>1740	>1740	>1740	1400.2
Be	1.56	0.52	3.13	2.9	1.54	2.32	1.17	3.84	1.06	1.55	3.94
Bi	<0.05	0.05	<0.47	1.03	0.59	<0.47	<0.47	<0.47	0.65	0.69	<0.47
Cd	0.195	0.153	0.3	>4	1.856	0.126	0.283	0.113	0.253	1.158	0.074
Ce	20.39	21.02	145.79	71.41	112.09	131.76	84.76	109.48	87.16	94.58	106.27
Co	35.29	40.39	4.57	3.61	0.85	1.93	0.82	2.32	2.13	1.5	7.58
Cr	307	336	12	6	5	9	3	8	7	9	13
Cs	2.12	0.265	2.226	2.733	5.018	4.381	3.737	3.331	1.071	1.733	3.439
Cu	29.7	28.7	8.1	59.2	14.3	3.2	<1.4	14.1	5.5	5.5	14.1
Dy	3.746	4.117	9.738	6.798	4.349	7.53	6.1	6.374	5.81	5.725	10.55
Er	2.242	2.464	5.24	4.29	2.681	4.453	3.214	4.065	3.585	3.527	5.987
Eu	0.7165	1.2467	1.9117	0.4459	0.4179	0.8581	0.4144	0.7019	0.5874	0.3665	1.7689
Ga	15.36	15.82	26.69	23.11	17.05	23.61	17.53	24.15	16.95	16.44	27.69
Gd	3.669	3.913	10.704	5.739	4.682	8.039	6.516	6.558	5.765	5.891	9.488
Hf	2.33	2.38	9.46	5.77	4.67	10.57	6.44	10.23	8.35	8.64	11.15
Ho	0.7763	0.831	1.894	1.4688	0.8727	1.5331	1.163	1.3338	1.2075	1.1812	2.1273
In	0.0517	0.0561	0.0787	0.1087	0.044	0.0453	0.0125	0.0394	0.0239	0.0304	0.1017
La	9.5	9.6	70	34	55.7	62.9	41.9	53.9	44.1	47.7	52.3
Li	41.1	16.9	12.4	16.9	17.6	18.2	21.2	28.1	4.3	18.2	30.5
Lu	0.302	0.325	0.678	0.57	0.436	0.635	0.432	0.609	0.522	0.505	0.746
Mo	0.46	0.41	2.04	2.82	2.67	0.86	2.92	3.15	2.3	2	2.75
Nb	8.83	8.364	47.49	24.784	17.16	30.842	17.272	24.585	21.665	19.988	41.505
Nd	12.47	12.87	61.96	28.88	39.75	51.77	35.42	42.99	33.55	36.71	46.47
Ni	77.1	87	10.8	5.3	<0.7	2.2	<0.7	2.5	3.3	1.5	5.1
Pb	14.88	15.13	182.21	9.42	400.53	18.87	17.67	37.73	44.29	90.18	4.13
Pr	2.685	2.963	16.679	7.99	12.126	14.781	9.937	12.242	9.663	10.578	12.502
Pb	81.49	4.87	172.28	171.61	150.21	102.23	137.6	164.41	224.71	200.47	229.75
Sb	0.59	2.51	2.23	1.79	5.37	2.82	0.85	1.01	2.46	0.66	0.08
Sc	31	31.1	11.1	4.8	3.2	5.4	4.8	5.4	4.1	3.8	12.8
Sm	3.124	3.306	12.179	5.899	6.318	9.98	7.278	8.297	6.379	7.144	9.052
Sn	0.68	0.71	4.94	8.23	7.2	9.08	7.68	9.38	5.31	3.79	4.4
Sr	162.1	264.3	39.4	49.1	52	163.3	148.6	31.6	75.4	104.3	25.3
Ta	0.56	0.562	2.663	1.883	1.572	2.117	1.418	1.705	1.549	1.664	2.281
Tb	0.5819	0.6635	1.7007	1.077	0.7467	1.2371	1.0401	1.0177	0.9401	0.9301	1.599
Th	1.321	1.442	20.213	17.37	26.858	34.127	23.971	27.955	24.076	26.019	21.61
Ti	7565	7488	3731	1756	1028	2591	1302	2211	1753	1898	3974
Tl	14.812	0.293	1.623	3.028	>20	>20	10.41	3.286	2.634	1.24	1.097
Tm	0.3108	0.3489	0.7352	0.6365	0.4376	0.659	0.4956	0.6176	0.5515	0.5398	0.8319
U	0.288	0.308	4.707	7.212	4.325	8.601	4.232	8.653	5.977	5.854	4.703
V	215.2	221.5	26.1	17.8	4	19.3	10.3	16.3	12.4	13.3	40.8
W	6.39	0.37	3.36	2.42	2.33	1.97	2.92	3.16	2.24	3.76	2.58
Y	20.52	21.6	53.35	43.09	25.21	47.65	32.27	38.8	35.76	34.6	60.2
Yb	2.047	2.223	4.722	4.116	2.965	4.425	3.18	4.245	3.669	3.586	5.268
Zn	102.5	77.4	131.5	865.8	381.5	51.9	79.4	83.5	62.2	384.1	111.1
Zr	89	90	370	213	155	438	228	401	315	314	471
Trace elements (ppm) OGL IML-101											
Ag	<0.4	<0.4	0.43	<0.2	2.96	0.23	<0.2	0.38	0.26	0.22	<0.2
As	57.6	40.2	8.5	0.7	1150.9	26.5	1.6	3.8	16.6	<0.7	<0.7
Au	0.006	<0.003	0.004	<0.002	0.009	0.002	0.002	0.002	0.009	<0.002	<0.002
Bi	0.02	<0.02	0.16	1.25	0.62	0.2	0.06	0.36	0.68	0.68	0.1
Cd	0.23	0.05	0.34	5.98	2.05	0.13	0.3	0.08	0.34	1.53	0.05
Co	34.7	31.8	4.4	3.3	0.8	1.1	0.6	2	2	0.5	6.1
Cu	28	29	9	61	14	2	<0.6	12	5	4	12
Hg	<0.08	<0.08	0.1	0.1	<0.08	<0.08	<0.08	<0.08	<0.08	0.1	<0.08
In	0.012	0.005	0.006	0.06	0.03	0.002	0.003	0.002	0.01	0.008	0.004
Ir	<0.003	<0.003	<0.003	<0.003	<0.003	<0.003	<0.003	<0.003	<0.003	<0.003	<0.003
Mo	0.51	0.36	1.89	1.98	1.65	0.92	1.72	2.65	1.69	1.45	1.79
Ni	59	51	4	5	<2	<2	<2	2	3	<2	4
Pb	12.4	2.6	190	8.1	425.8	18	14.9	37	29.9	60.1	3
Pd	<0.02	<0.02	<0.02	<0.02	<0.02	<0.02	<0.02	<0.02	<0.02	<0.02	<0.02
Pt	<0.005	<0.005	<0.005	<0.005	<0.005	<0.005	<0.005	<0.005	<0.005	<0.005	<0.005
Sb	0.18	0.88	1.92	1.39	5.34	1.6	0.44	0.82	1.6	0.28	0.06
Se	<0.2	<0.2	0.4	0.9	10.4	0.2	0.5	0.6	0.5	0.9	0.3
Sn	<0.06	0.1	0.1	0.6	0.3	0.2	0.2	0.2	0.1	0.1	0.2
Te	<0.04	<0.04	0.06	0.07	0.17	0.12	0.06	0.19	0.9	0.37	0.11
Tl	0.76	0.192	0.073	0.097	2.076	3.335	0.746	0.238	0.071	0.081	0.118
Zn	75	40	86	833	348	10	51	20	49	318	29

*LT, felsic lapillit tuff; TF, felsic tuff, VF, felsic coherent volcanic rock; MI, mafic intrusive; MD, mafic dike; XT, felsic crystal-rich tuff.

B370176	B370177	B370178	B370179	B370180	B370181	B370182	B370183	B370184	B370185	B370186	B370187
TF	TF	TF	TF	VF	MI	MI	TF	VF	TF	MI	TF
K15-320	K15-320	K15-320	K15-320	K15-320	K15-320	K15-320	K15-320	K15-320	K15-320	K15-320	K15-320
50.3	76.45	95.85	114.45	127.95	134	148.4	165	174.3	202.65	205.5	212.45
50.4	76.55	95.95	114.55	128.05	134.15	148.5	165.2	174.4	202.75	205.65	212.55
1242.9	1495.9	1252.2	1737.6	>1740	966.7	>1740	>1740	1065.7	>1740	>1740	766.6
3.48	2.63	2.85	2.91	0.49	0.79	0.78	1.74	2.77	3.31	0.57	2.71
<0.47	<0.47	0.5	<0.47	<0.47	<0.47	<0.47	0.95	<0.47	0.85	1	<0.47
0.142	0.077	0.49	0.701	0.121	0.224	0.212	0.05	0.023	0.06	1.565	0.089
167.72	119.98	122.25	91.31	90.86	20.89	20.33	127.41	123.77	113.81	23.07	91.06
3.98	5.57	3.59	1.57	1.73	42.26	40.74	4.34	2.97	2.9	40.08	0.64
13	12	10	4	4	384	299	10	8	8	313	7
3.203	2.298	2.489	2.161	1.114	1.475	1.409	2.265	1.753	2.395	4.683	3.04
<1.4	23.3	6	13.8	12.6	1.5	61	5.7	4.6	6	80.6	5
9.643	8.604	7.064	5.613	6.302	3.681	3.808	8.371	7.866	7.091	3.796	7.627
4.999	4.535	3.572	3.188	3.994	2.156	2.258	5.321	5.188	4.407	2.303	4.46
2.2775	1.8915	1.6284	0.4227	0.6267	1.0588	1.1558	0.9101	0.8769	0.7388	1.0834	0.477
27.05	22.31	22.15	20.7	10.14	14.12	14.46	22.78	22.27	24.78	14.81	20.75
11.771	9.265	8.647	5.772	6.018	3.608	3.709	8.349	7.639	7.2	3.753	6.948
11.38	9.13	7.84	7.69	7.47	2.18	2.26	12.37	11.53	10.81	2.35	6.46
1.8219	1.6658	1.3319	1.1207	1.2686	0.7487	0.7815	1.7326	1.6964	1.4782	0.8	1.5208
0.1042	0.0551	0.088	0.0391	0.0117	0.0532	0.0548	0.0346	0.0377	0.0548	0.0636	0.0304
82.6	58.8	59.9	45.5	44.9	9.6	9.1	62.2	59.8	57.7	11.2	43.6
22.8	13.9	9.9	22.8	6	24	32.2	13.4	18.8	25.8	26.3	14.4
0.705	0.622	0.487	0.455	0.54	0.294	0.298	0.748	0.769	0.652	0.306	0.562
1.73	1.86	2.54	3.71	1.66	0.4	0.31	3.44	1.12	3.25	0.22	3.36
47.78	43.403	36.787	24.458	19.755	8.801	8.604	31.013	29.228	28.188	9.188	23.69
71.42	51.36	52.72	34.2	36.69	12.12	12.58	51.35	49.16	44.75	13.29	36.86
3.4	3.8	3.4	0.9	6.1	96.4	80.2	4.7	3.3	4.1	83.6	1.5
6.12	12.15	17.97	29.99	59.09	19.53	20.98	46.98	11.49	63.76	540.55	9.97
19.416	14.189	14.268	10.208	10.363	2.75	2.851	14.605	13.927	12.951	3.103	10.554
201.52	136.48	140.76	216.26	33.43	34.01	40.92	274.71	306.86	128.59	77.86	143.74
0.07	0.26	1.4	1.77	3.03	4.36	8.8	3.6	2.07	3.69	10.89	0.26
12.3	10.9	8.6	4	2.7	30.2	29.5	4.7	4.8	7	31.4	3.9
13.616	9.896	10.048	6.682	6.766	3.111	3.237	9.63	8.971	8.505	3.322	7.503
4.67	3.68	4.13	8.03	4.86	0.7	0.81	7.04	8.75	9.88	1.22	7.31
42	96.7	54.7	18.8	56.8	231.9	137.3	60.1	39.1	47.6	292.2	44.4
2.746	2.378	2.236	2.394	1.693	0.512	0.537	4.652	2.214	2.066	0.557	1.818
1.6726	1.4327	1.2764	0.9584	0.9868	0.6143	0.603	1.3986	1.2229	1.1544	0.6	1.2359
26.011	17.328	21.584	33.757	25.63	1.618	1.41	33.708	35.263	34.115	1.716	24.638
4357	3581	3028	1722	1212	7520	7115	2350	2391	2373	7507	1742
1.169	0.871	1.921	5.194	3.172	3.525	11.937	>20	>20	18.508	>20	3.054
0.7174	0.6291	0.5158	0.4935	0.5955	0.313	0.3014	0.7904	0.7912	0.6698	0.3265	0.6348
4.628	3.87	3.549	8.391	10.493	0.339	0.63	8.526	7.777	9.929	0.535	6.673
32.6	27.1	21.4	13.3	11.3	219	220.8	17.6	18.2	29.6	215.1	17
2.14	1.9	2.08	3.6	1.1	0.35	0.97	5.03	3.36	2.68	1.12	2.28
48.81	47.19	36.42	30.62	36.36	20.51	19.65	50.92	52.69	44.95	21.06	43.85
4.641	4.159	3.463	3.175	3.733	1.943	2.023	5.138	5.079	4.45	2.063	3.963
91.3	29.1	167.4	179.7	13.4	92.9	205	59.1	26.4	84.9	450.6	34.1
458	380	323	274	262	88	84	453	428	425	93	239
<0.2	<0.2	<0.2	<0.2	0.53	<0.2	0.36	0.4	0.2	0.8	5.66	<0.2
<0.7	1.2	<0.7	13.1	198.4	94.8	110.5	20.6	7.2	21.4	73.6	<0.7
<0.002	<0.002	<0.002	0.005	0.002	<0.002	0.002	0.018	0.002	0.024	0.021	<0.002
0.16	0.35	0.51	0.45	0.29	0.05	0.09	1.04	0.48	0.85	1.09	0.14
0.18	0.1	0.7	1.03	0.1	0.04	0.25	0.04	0.02	0.07	1.23	0.14
2.5	4.4	3.1	1.4	2.1	37.5	33.6	3.8	2.3	2.7	36.4	0.5
1	21	5	13	11	1	61	4	4	6	78	4
<0.08	<0.08	<0.08	<0.08	<0.08	<0.08	<0.08	<0.08	<0.08	<0.08	<0.08	<0.08
0.008	0.004	0.012	0.006	0.004	0.002	0.034	0.004	0.002	0.004	0.005	0.003
<0.003	<0.003	<0.003	<0.003	<0.003	<0.003	<0.003	<0.003	<0.003	<0.003	<0.003	<0.003
1.43	1.17	2.06	2.95	1.47	0.3	0.28	3.29	1	3.26	0.28	2.54
4	2	3	<2	6	65	58	3	2	3	55	<2
4.5	9.7	14.4	29.1	51.5	3.2	19	15.5	2.8	61.2	552.7	3.8
<0.02	<0.02	<0.02	<0.02	<0.02	<0.02	<0.02	<0.02	<0.02	<0.02	<0.02	<0.02
<0.005	<0.005	<0.005	<0.005	<0.005	<0.005	<0.005	<0.005	<0.005	<0.005	<0.005	<0.005
0.03	0.08	1.07	1.41	2.17	1.09	5.51	1.85	0.77	3.05	5.15	0.09
<0.2	0.2	0.2	1.6	0.4	<0.2	<0.2	0.5	0.4	0.6	0.4	0.3
0.2	0.1	0.1	0.2	0.3	0.2	0.3	0.2	0.3	0.3	0.3	0.2
0.2	0.15	0.53	0.43	0.51	0.1	0.18	0.68	0.6	0.32	0.1	0.21
0.093	0.036	0.072	0.173	0.358	3.178	4.77	2.702	0.711	0.623	>11	0.152
31	12	142	126	7	54	152	8	2	16	290	18

B370188	B370189	B370190	D00005977	D00005978	D00005979	D00005980	D00005981	D00005982	D00005983	D00005984	D00005985
LT	LT	TF	LT	TF	LT	MD	TF	TF	TF	TF	TF
K15-320	K15-320	K15-320	K15-281	K15-281	K15-281	K15-281	K15-281	K15-281	K15-281	K15-281	K15-281
229.65	244.4	262	13.5	24.3	49.1	64.9	85.8	137.6	147.5	164.8	176.55
229.8	244.55	262.1	13.8	24.45	49.3	65	86	137.7	147.7	165	176.65
1133.6	1055.5	1339.9	1182.7	1133.1	821.1	774.8	>1740	846	484.8	524.7	890.9
2.57	2.48	3	2.67	1.93	2	1.47	2.87	3.36	2.38	2.71	3.08
<0.47	<0.47	0.66	<0.47	<0.47	<0.47	<0.47	1.13	<0.47	0.71	<0.47	<0.47
0.11	0.057	0.064	1.62	0.367	0.167	0.223	0.178	0.107	0.484	0.039	>4
174.26	140.08	138.18	190.44	42	146.53	69.12	155.73	120.84	80.47	72.26	69.52
3.06	5.83	6.77	0.84	32.22	1.92	24.31	5.98	5.14	2	2.16	2.41
12	15	13	13	131	12	31	13	12	6	5	9
2.708	3.943	2.537	2.911	4.654	1.876	1.519	2.415	3.877	2.164	2.199	3.701
6.2	12.3	2.7	2.2	20.2	39.3	<1.4	99.5	9.3	8.3	6.3	172.6
9.88	8.644	8.914	9.026	6.714	7.987	6.218	8.363	8.667	6.015	7.224	5.067
5.271	4.812	4.803	4.515	3.955	4.114	3.391	4.427	4.796	3.596	4.429	3.161
1.9425	1.9814	2.0909	2.6028	1.5472	2.2407	1.9101	2.2834	1.8597	0.4765	0.4168	0.3656
25.15	23.74	25.61	24.36	17.57	17.78	20.08	21.76	25.49	18.81	20.62	24.92
12.159	10.011	10.224	12.687	6.361	10.43	7.179	10.409	9.399	6.013	6.033	4.844
8.96	9.09	9.79	10.78	4.53	8.93	5.93	10.36	10.64	5.43	6.45	8.41
1.8821	1.7012	1.7184	1.6386	1.3726	1.5329	1.2593	1.6036	1.6961	1.2337	1.4932	1.034
0.0922	0.0862	0.065	0.0918	0.0783	0.0467	0.0867	0.0737	0.0842	0.064	0.035	0.0176
87.2	69.9	68.5	95	18.5	72.2	32.4	78.9	59.5	38.6	35.7	33.8
9.7	15.7	16.2	34.7	36.8	18.6	20.1	38	40.6	32.6	17.6	30.2
0.655	0.654	0.608	0.647	0.517	0.55	0.484	0.623	0.672	0.48	0.601	0.511
2.81	2.4	2.67	2.12	1.15	1.74	0.84	1.56	1.48	2.05	2	3.44
42.023	43.247	46.856	46.682	17.226	36.237	19.343	40.69	43.85	21.175	23.426	26.44
73.3	59.35	61.08	81.55	24.19	64.78	35.2	64.93	53.21	32.13	28.34	27.25
2.6	4.8	6.2	1.1	26.6	4.7	3.6	7.4	4.2	1.1	1	0.7
6.91	15.12	27.38	8.53	14.03	6.07	6.27	13.97	6.9	66.13	11.15	>700
20.349	16.141	16.632	21.982	5.466	17.138	8.711	18.058	13.87	8.925	8.259	7.79
108.9	123.22	150.74	147.27	107.26	89.97	47.69	122.11	163.15	160.44	172.42	200.03
0.28	0.38	0.26	0.19	0.06	0.08	0.14	0.4	0.09	0.58	0.73	1.48
8.8	12.5	11.1	13.1	29.9	10.6	33.3	11.8	11.9	4	4.5	4.5
13.585	11.439	11.472	15.251	5.927	12.255	7.57	12.16	10.177	6.38	6.244	5.418
4.79	3.15	4.17	4.15	1.46	2.07	1.57	2.85	4.6	6.45	6.92	11.64
63.4	48.7	44.4	30.6	164.3	50.8	128.1	102.9	67.6	16.3	16	41.6
2.464	2.273	2.574	2.662	1.043	2.126	1.266	2.506	2.583	1.825	1.882	2.052
1.7419	1.4717	1.5647	1.7515	1.0547	1.4885	1.1047	1.474	1.4575	0.9846	1.1144	0.8023
29.533	21.599	18.735	29.99	3.364	24.207	8.247	17.919	16.384	21.754	21.21	20.082
3167	4090	4201	4110	12887	3231	14234	3828	3804	1574	1732	2147
0.743	0.705	0.849	0.767	0.661	0.47	0.305	0.682	1.109	1.006	1.667	2.726
0.705	0.6744	0.6775	0.6543	0.5581	0.5802	0.4867	0.6346	0.6777	0.5294	0.6441	0.4982
4.904	3.808	3.824	4.212	0.941	3.458	1.875	3.768	4.269	4.613	6.482	8.102
22.5	30.9	31	30.9	281.9	25.8	306.4	29.9	27.7	11.7	12.1	16.3
1.55	2	1.61	1.84	1.54	1.72	1.5	1.98	2.31	1.93	2.57	3.7
52.07	49.89	49.56	46.01	36.8	39.46	32.28	42.3	46.21	33.8	41.98	29.24
4.488	4.351	4.241	4.281	3.583	3.861	3.2	4.256	4.504	3.415	4.244	3.421
81.1	83.7	53.4	581.7	254.5	112	117.1	55.5	96.4	151	20	1470.1
354	397	418	443	192	358	230	402	423	188	228	295
<0.2	<0.2	<0.2	<0.2	<0.2	<0.2	<0.2	<0.2	<0.2	0.23	<0.2	1.77
1.9	5.8	10.7	<0.7	9.2	35.8	19.4	10.2	<0.7	15.9	20.9	48.7
<0.002	0.002	0.004	<0.002	<0.002	<0.002	<0.002	0.003	<0.002	<0.002	0.004	0.002
0.2	0.46	0.72	0.15	0.03	0.04	0.04	1.28	0.16	0.74	0.43	0.44
0.09	0.08	0.06	1.96	0.36	0.18	0.23	0.23	0.1	0.44	0.04	9.13
2.5	5.2	5.9	0.6	29.5	1.9	25.4	5.9	4.8	1.8	2.1	2.2
6	9	2	1	19	42	<0.6	89	8	7	6	160
<0.08	<0.08	<0.08	<0.08	<0.08	<0.08	<0.08	<0.08	<0.08	<0.08	<0.08	0.1
0.006	0.013	0.004	0.015	0.014	0.008	0.028	0.005	0.006	0.017	0.003	0.015
<0.003	<0.003	<0.003	<0.003	<0.003	<0.003	<0.003	<0.003	<0.003	<0.003	<0.003	<0.003
2.62	1.57	1.81	1.47	0.92	1.6	0.66	1.48	1.97	1.62	1.71	1.99
3	4	5	<2	25	5	4	8	4	2	<2	<2
3.7	10.7	23.9	5.8	11.8	2.6	3.5	13.6	5.4	69.4	10.1	1410.8
<0.02	<0.02	<0.02	<0.02	<0.02	<0.02	<0.02	<0.02	<0.02	<0.02	<0.02	<0.02
<0.005	<0.005	<0.005	<0.005	<0.005	<0.005	<0.005	<0.005	<0.005	<0.005	<0.005	<0.005
0.07	0.2	0.14	0.03	0.02	0.03	0.02	0.2	0.02	0.46	0.59	1.26
0.7	2.3	1.8	0.4	0.5	0.4	<0.2	1.3	0.5	0.4	0.2	8.5
0.1	0.3	0.1	0.1	0.1	0.1	0.1	0.1	0.1	0.1	0.1	0.3
0.32	0.42	0.31	0.21	0.05	0.04	0.03	0.12	0.14	0.37	0.06	0.3
0.039	0.098	0.054	0.039	0.148	0.029	0.029	0.075	0.059	0.048	0.066	0.134
39	59	21	554	236	92	106	18	53	100	10	1480

D00005986	D00005987	D00005988	D00005989	D00005990	D00005991	Q311613	Q720929	Q720932	Q720934	Q720939	Q720946
TF	TF	TF	TF	TF	TF	VF	LT	MI	MI	LT	LT
K15-281	K15-281	K15-281	K15-281	K15-281	K15-281	K16-417	K16-370	K16-370	K16-370	K16-370	K15-271
183.05	184.45	199.45	212.75	227.9	251.9	96.85	98.3	160.35	189.1	276.95	174.2
183.2	184.65	199.6	212.9	228.05	252.1	96.9	98.45	160.5	189.3	277.1	174.35
533.5	1196.4	1645.7	1148.1	884	>1740	1046.4	867.3	681	1533.5	469.9	944.5
0.69	1.56	1.84	1.28	3.54	2.35	2.46	2.54	0.45	1.03	3.28	3.17
13.24	6.57	1.41	<0.47	<0.47	0.73	0.75	0.23	<0.05	<0.05	<0.05	0.12
0.16	0.126	1.208	1.051	0.07	>4	0.284	0.116	0.35	0.13	0.048	0.09
87.33	173.07	81.83	80.76	108.41	170.66	103.07	136.46	25.21	20.53	177.2	175.49
34.58	11.88	3.49	2.21	1.93	4.93	1.38	6.27	41.48	36.95	4.68	5.37
3	3	4	7	7	14	6	9	369	290	15	12
2.678	4.208	2.362	0.595	2.022	1.816	0.876	2.945	0.756	8.426	1.415	3.349
323.2	7.4	51.7	11.7	2.9	31.6	3.1	34.6	65.1	31.9	24.2	5.8
9.605	6.394	5.255	4.808	7.568	9.679	7.188	7.308	4.721	3.875	7.764	8.139
5.226	3.667	3.291	2.93	4.358	5.143	4.295	3.965	2.815	2.353	3.907	4.203
0.3627	0.5672	0.3161	0.5543	0.7917	2.2183	0.353	1.7399	1.407	1.1536	2.27	2.2866
36.79	29.12	20.88	16.26	22.35	26.03	20.52	19.88	17.94	14.99	25.63	23.59
8.85	8.535	5.269	5.115	7.549	12.09	7.093	9.227	4.599	3.728	11.343	11.208
12.22	12.22	6.93	7.14	10.65	11.03	5.11	7.88	2.83	2.31	11.89	7.89
1.9168	1.246	1.1053	0.9621	1.4757	1.8848	1.4267	1.3718	0.9718	0.8037	1.4183	1.5351
0.0265	0.0183	0.0452	0.0299	0.0524	0.1	0.061	0.0733	0.065	0.0526	0.1475	0.086
39.7	90.3	40.2	40.1	53.7	83.4	52.1	67.3	11.4	9.4	86.2	85
58.3	34.5	18.2	1.6	27.8	14	12.1	12.7	18.4	44.8	18.7	8.8
0.72	0.56	0.456	0.424	0.65	0.703	0.587	0.519	0.378	0.314	0.529	0.554
7	3.45	3.53	3.94	1.67	1.6	5.27	1.81	0.52	0.39	2.65	1.82
29.005	29.835	21.597	17.441	26.548	44.759	19.49	33.133	10.311	8.881	47.87	39.75
40.84	63.26	31.68	31.64	43.35	74.31	40.79	60.23	15.54	12.51	80.44	73.75
1.3	1.2	1.2	3.2	2.4	3.8	1.7	5.7	79.8	80.1	4.8	5.2
150.36	27.33	64.87	107.44	14.77	28.3	30.48	9.15	25.26	12.31	13.89	16.32
10.461	18.46	8.954	9.066	12.11	19.73	11.575	15.837	3.469	2.767	21.037	20.83
82.18	176.83	151.35	34.74	189.07	115.74	162.36	107.31	14.68	173.47	43.46	99.93
0.3	0.28	1.01	5.09	0.57	0.19	0.55	0.4	6.29	4.91	0.09	0.78
4.8	5.1	3.7	3.6	4.8	13	4.2	8.9	38.7	31.3	7.1	10.2
8.995	12.067	6.275	5.914	8.229	13.695	7.743	11.021	4.021	3.222	14.654	13.938
1.53	6.76	7.85	6.86	8.51	3.65	9.96	3.8	0.84	0.67	4.57	4.06
5.5	32.1	8.2	35.5	65.9	40.1	21.6	44.6	332.7	110.2	38.9	52
2.207	2.327	1.861	1.356	2.02	2.487	1.545	2.015	0.647	0.553	2.772	2.206
1.5352	1.1743	0.8596	0.8141	1.2233	1.7502	1.1428	1.2754	0.7451	0.6142	1.4456	1.5268
24.725	42.347	23.858	21.47	29.885	25.454	27.266	22.195	1.679	1.343	25.547	28.76
1964	2373	1484	1527	2169	4025	1039	2724	9214	7399	4203	3620
2.71	4.617	1.676	0.282	1.635	0.575	1.071	1.786	1.735	62.552	0.553	2.474
0.7843	0.5795	0.5079	0.4431	0.669	0.7425	0.6198	0.5312	0.3757	0.3264	0.5542	0.5877
11.196	10.04	8.424	5.979	8.107	4.032	5.605	3.504	0.342	0.283	4.347	3.959
17.9	18.2	12.6	11.7	15.2	29.5	6.1	19.3	264.8	212.6	28.2	26.4
5.53	5.2	3.96	1.87	2.26	1.64	0.95	2.01	0.39	2	2.68	1.91
52.77	35.82	31.99	27.05	42.14	53.28	40.29	37.21	25.28	20.73	36.62	41.81
5.115	3.948	3.392	2.95	4.481	4.785	4.019	3.499	2.482	2.06	3.585	3.743
1108.5	185.4	291.3	386.7	35.9	691.9	85.5	63.4	121	76.2	214.3	91.6
419	439	242	265	383	461	156	310	105	88	472	329
2.89	<0.2	0.31	4.74	0.29	0.29	<0.4	<0.4	<0.4	<0.4	<0.4	<0.4
1.4	<0.7	9	49.6	2.1	7.7	6.5	<4	53	165.9	<4	<4
0.003	<0.002	0.004	0.235	0.008	0.004	0.004	<0.003	<0.003	<0.003	<0.003	<0.003
15.91	1.49	1.66	0.35	0.38	0.77	0.8	0.2	0.02	0.04	0.03	0.12
0.17	0.14	1.48	1.29	0.05	4.65	0.26	0.15	0.06	0.07	<0.05	0.11
30.7	7.5	3.4	2.1	1.3	4.5	1.4	6.6	40	39.3	4.9	4.6
334	8	57	12	3	31	3	33	64	30	26	6
<0.08	<0.08	0.1	0.1	<0.08	<0.08	<0.08	<0.08	<0.08	<0.08	<0.08	<0.08
0.019	<0.002	0.014	0.028	0.002	0.038	0.006	0.013	0.006	<0.005	0.029	0.012
<0.003	<0.003	<0.003	<0.003	<0.003	<0.003	<0.003	<0.003	<0.003	<0.003	<0.003	<0.003
6.87	3.34	2.49	2.59	1.26	1.54	3.78	1.47	0.35	0.36	1.87	1.61
3	<2	2	2	<2	3	<2	5	59	79	5	4
147.3	11	65.7	116	13.8	27	17.9	6.3	3.8	2.9	4.5	8.7
<0.02	<0.02	<0.02	<0.02	<0.02	<0.02	<0.02	<0.02	<0.02	<0.02	<0.02	<0.02
<0.005	<0.005	<0.005	<0.005	<0.005	<0.005	<0.005	<0.005	<0.005	<0.005	<0.005	<0.005
0.2	0.05	0.82	5.23	0.36	0.11	0.42	0.22	3.93	2.17	0.05	0.49
37.9	1	2	0.3	<0.2	2.7	0.2	0.4	0.2	<0.2	1.6	0.5
1.2	0.4	0.1	0.2	0.1	0.1	0.3	0.3	0.1	0.1	0.2	0.4
0.03	<0.02	0.06	0.08	0.02	0.08	0.26	0.09	<0.04	0.06	<0.04	<0.04
1.681	0.453	0.068	0.017	0.068	0.036	0.04	0.148	1.614	>11	0.035	0.282
918	130	244	375	10	639	64	46	70	74	197	64

Q720949	Q721051	Q721071	Q721073	Q721099	Q721154	Q721155	Q721156	Q721157	Q721158	Q721160	Q721170
MI	LT	TF	MD	VF	VF	MI	LT	LT	VF	VF	VF
K15-271	K15-309	K15-287	K17-422	K15-290	K15-204	K15-204	K17-448	K17-448	K17-448	K17-448	K15-300
257.35	165.25	118.35	40.3	139.7	135.6	146.4	322.45	334	346.15	358.45	67.95
257.55	165.45	118.55	40.5	139.9	135.8	146.6	322.65	334.15	346.3	358.6	68.15
932.7	2201.4	1023.6	2944.8	5088.5	1330.9	694.5	1801.2	1842	622.4	877.7	1353.8
0.69	2.33	2.07	2.72	0.93	1.4	0.97	2.72	2.09	1.33	2.11	2.44
<0.05	0.46	0.06	0.09	1.06	0.63	0.51	<0.05	0.05	0.6	0.09	0.16
0.325	0.14	0.026	0.199	6.225	0.796	0.171	0.267	0.116	0.408	0.038	<0.018
22.19	109.04	95.45	75.55	90.02	115.38	19.85	127.81	172.97	80.4	68.78	93.84
40.11	1.22	2.43	22.97	2.11	4.2	37.31	17.39	6.53	0.71	0.65	0.88
355	8	4	28	14	14	318	136	11	5	5	6
0.897	2.224	2.649	7.012	1.083	2.763	3.169	2.135	3.13	0.837	2.613	1.48
19	8.1	0.5	7.9	32	194.1	27	168.5	24.6	6.9	6.9	1.1
3.97	8.665	5.25	5.76	6.604	7.719	3.881	8.234	10.974	7.99	8.602	8.009
2.382	4.737	3.136	3.016	3.774	5.096	2.256	4.43	5.966	4.782	5.22	4.481
1.1712	0.3956	0.2995	2.1354	0.3963	0.8727	1.107	2.0667	2.2689	0.4634	0.4969	0.5956
15.43	16.84	20.99	20.83	14.05	19.11	16.38	21.74	23.92	17.99	21.63	18.98
3.809	8.184	5.353	7.534	5.976	7.524	3.672	9.695	12.953	7.191	6.86	7.986
2.35	6.01	7.21	5.93	7.7	10.17	2.35	8.34	9.34	3.82	4.31	4.01
0.8098	1.6822	1.0697	1.0791	1.3031	1.6407	0.8014	1.6118	2.14	1.642	1.7539	1.5725
0.0525	0.0222	0.0263	0.0771	0.0352	0.0216	0.0547	0.0999	0.1059	0.0321	0.0396	0.0692
10.2	52.5	48.6	35.3	46.1	56.4	9	61.9	85.4	38.5	32.4	44.7
16.5	9.4	21.8	21.7	5.3	17.7	29.2	22.3	13.7	8.1	126.3	11.5
0.303	0.601	0.408	0.437	0.514	0.77	0.319	0.606	0.782	0.611	0.672	0.548
0.42	2.88	2.65	0.91	2.96	4.41	0.33	2.1	2.88	2.93	2.61	1.93
8.723	23.659	20.461	18.538	21.283	25.893	8.584	31.765	39.719	23.081	26.119	27.874
13.36	43.74	35.82	39.15	35.61	45.52	12.18	58.2	76.61	34.07	28.95	38.91
98.1	1.4	1.3	4.5	3.5	9.1	86.9	51.8	5.9	0.8	1.2	1.7
15.98	18.02	4	6.6	290.36	100.39	35.97	2.96	4.45	111.41	10.06	7.05
2.96	12.415	10.39	9.534	10.212	13.539	2.771	15.487	20.539	9.56	8.093	11.113
25.5	112.93	104.75	131.67	159.12	173.77	54.88	98.52	94.24	52.12	66.1	158.67
3.49	4.39	0.24	0.11	3.02	0.99	0.8	0.18	0.05	0.12	0.1	0.3
31.1	3.7	2.4	33.1	4	9.4	31.2	16	11.1	3.7	3.9	3.9
3.298	8.754	6.498	8.293	6.594	8.806	3.215	11.132	14.243	7.216	6.457	8.276
0.66	3.58	9.04	1.59	2.45	9.64	0.78	6.88	5.08	3.93	4.45	5.24
219.7	34.6	16.6	117.9	138.9	46	119.3	86.9	103.6	114.6	37.3	21.6
0.539	2.158	1.658	1.327	1.562	1.925	0.551	1.843	2.567	2.083	2.275	2.775
0.6319	1.4067	0.837	1.0646	0.9953	1.2409	0.6052	1.3996	1.8827	1.2669	1.2911	1.3452
1.555	29.199	25.109	8.36	22.565	28.979	1.408	19.275	26.929	18.689	20.166	21.686
7384	1346	1525	14168	1804	2222	7346	5614	3531	975	1022	1152
1.075	3.675	1.232	0.929	2.509	1.871	0.473	0.651	0.771	0.234	0.326	1.28
0.3187	0.6631	0.4423	0.4365	0.5456	0.781	0.3277	0.6206	0.832	0.6687	0.7496	0.6109
0.301	9.951	6.967	1.808	5.473	12.156	0.308	3.013	3.95	6.076	4.442	5.781
218	8.6	14.5	299.2	14.2	16.9	223.9	89.5	26	3.7	3.7	5.1
0.6	0.98	2.59	3.04	2.25	3.01	1.33	2.61	1.84	1.01	1.2	0.75
21.25	45.12	31.43	28.13	38.86	45.81	21.07	42.78	55.17	44.46	47.54	41.89
2.076	4.222	2.895	2.931	3.486	5.251	2.055	3.891	5.219	4.307	4.773	3.782
78.6	74.1	104.2	91.1	1254.2	275.8	218.1	197.6	142.4	82	27.2	11.3
88	192	256	232	292	389	90	337	344	109	122	128
<0.4	<0.4	<0.4	<0.4	1.13	1.29	0.4	0.89	<0.4	0.41	<0.4	<0.4
66.3	51.4	<4	<4	11.9	12	11.5	<4	<4	<4	<4	<4
<0.003	<0.003	<0.003	<0.003	0.007	0.008	<0.003	<0.003	<0.003	<0.003	<0.003	<0.003
0.02	0.51	0.05	0.06	0.87	0.6	0.5	0.04	0.05	0.61	0.09	0.16
0.05	0.17	<0.05	0.28	7.14	0.89	0.2	0.36	0.11	0.52	<0.05	<0.05
35.6	1.4	1.8	22.7	2.1	4.6	31.1	18.2	6.8	0.6	0.6	0.9
18	7	<2.2	7	32	199	31	166	28	6	8	<2.2
<0.08	<0.08	<0.08	<0.08	0.7	<0.08	<0.08	<0.08	<0.08	<0.08	<0.08	<0.08
<0.005	<0.005	<0.005	0.024	0.032	0.013	0.019	0.024	0.018	0.005	<0.005	<0.005
<0.003	<0.003	<0.003	<0.003	<0.003	<0.003	<0.003	<0.003	<0.003	<0.003	<0.003	<0.003
0.35	1.94	1.94	0.76	1.97	4.17	0.35	1.38	3.43	2.25	2.56	1.37
55	<2	<2	4	3	9	60	53	6	<2	<2	<2
1	18.2	1.4	4.6	260.6	86.1	31.9	2.1	3.3	105.3	10.2	1.8
<0.02	<0.02	<0.02	<0.02	<0.02	<0.02	<0.02	<0.02	<0.02	<0.02	<0.02	<0.02
<0.005	<0.005	<0.005	<0.005	<0.005	<0.005	<0.005	<0.005	<0.005	<0.005	<0.005	<0.005
1.53	2.95	0.07	0.07	1.63	0.59	0.26	0.06	0.03	0.07	0.05	0.19
<0.2	0.5	0.5	0.4	0.9	1	<0.2	20.5	1.1	0.7	0.5	<0.2
0.1	0.1	0.3	0.5	0.1	0.4	0.1	0.5	0.6	0.1	0.1	0.2
<0.04	0.04	0.06	<0.04	0.51	0.25	<0.04	0.05	0.04	0.19	0.04	0.08
0.675	0.151	0.162	0.377	0.075	0.142	0.211	0.065	0.373	0.032	0.048	0.042
35	29	74	72	1286	248	160	154	105	51	<4	<4

Q930095	Q930096	Q930097	Q930098	Q930099	Q930100	Q930221	Q930240	Q930243	Q930244	Q930277	Q930281
TF	VF	TF	TF	MI	TF	LT	VF	MI	VF	MI	MD
K15-235R	K15-235R	K15-235R	K15-235R	K15-235R	K15-235R	K15-232	K15-236	K15-236	K15-236	K15-286	K15-315
86.15	116.7	133.3	136.1	143.65	149.25	207.85	95	113.35	117.15	179.7	11.3
86.3	116.95	133.5	136.35	143.95	149.4	208	95.26	113.65	117.35	179.9	11.5
>1740	>1740	>1740	393.3	1536.6	>1740	2744.5	1358.8	2695.4	3071.9	1988.5	914.6
2.52	1.48	2.08	0.18	0.72	3.76	3.35	3.75	0.59	2.04	2.22	2.32
0.82	<0.47	<0.47	1.11	<0.47	<0.47	10.73	0.62	0.05	0.27	0.36	0.11
>4	0.317	0.14	0.864	0.136	0.046	0.309	0.695	0.12	0.065	0.581	0.181
71.22	75.58	131.69	34.32	20.5	117.55	149	117.82	17.85	80.93	17.98	56.12
1.57	0.7	1.91	8.04	46.58	3.1	6.48	2.45	38.39	2.55	42.21	27.35
9	7	6	4	341	11	13	11	350	9	338	27
3.716	3.982	3.859	1.124	8.141	2.409	4.884	2.691	15.78	1.071	17.374	12.831
86.7	17	15.9	33.7	42	7.1	58.4	312.8	41.9	10	1.2	18.4
6.536	5.671	6.709	3.044	3.94	8.71	8.959	9.588	3.343	5.632	3.395	5.871
4.467	3.581	3.954	1.966	2.399	5.112	4.819	6.307	2.029	3.568	2.084	3.366
0.3769	0.4177	0.6393	0.2061	1.2394	0.8621	2.2213	0.708	1.0204	0.5311	0.8703	1.5903
24.09	19.57	26.31	15.54	15.05	24.76	23.72	28.02	15.11	18.58	16.95	19.68
4.924	5.221	7.51	3.132	3.813	8.28	10.895	8.542	3.271	5.441	3.163	6.554
7.75	7.55	8.86	4.9	2.23	11.91	10.57	16.06	2.1	8.58	2.41	5.85
1.4452	1.1945	1.3675	0.638	0.8198	1.7416	1.7523	2.035	0.6822	1.1759	0.7257	1.2012
0.0838	0.0101	0.0138	0.0643	0.0559	0.0682	0.0628	0.011	0.0484	0.0298	0.0591	0.0775
35.1	37.6	64.8	15.7	9.1	58.4	73.9	55.2	8.2	40.4	8	26.6
18.9	23.7	52.6	27.1	41.7	31.2	24.3	25.5	36.5	5.7	53.6	49
0.666	0.515	0.544	0.316	0.318	0.723	0.673	0.953	0.265	0.552	0.301	0.481
3.31	2.85	2.86	1.73	0.39	3.09	2.07	13.36	0.26	3.09	0.53	0.76
25.173	20.185	25.83	11.871	8.262	28.413	43.146	22.755	7.627	21.462	9.413	16.213
27.38	29.03	52.54	15.91	12.82	46.83	64.43	47.77	10.9	32.08	10.89	29.48
1.3	<0.7	1.6	<0.7	86.8	3.1	3.9	36.5	86.7	4.4	84.2	4.8
681.58	22.15	17.73	38.71	12.43	22.21	388.68	145.17	10.67	50.29	75.23	8.34
7.975	8.446	14.755	4.206	2.843	13.5	17.74	13.766	2.419	9.206	2.529	7.391
183.57	138.53	187.53	18.56	138.54	272.37	133.2	69.55	166.83	66.39	184.12	224.59
4.01	0.67	4.02	1.03	2.57	1.47	0.17	4.46	0.87	2.35	3.96	0.77
4.7	4.1	5.3	2.1	30	5.5	11.5	5.3	30.4	4.6	34.3	31.6
4.844	5.616	9.416	3.482	3.476	9.02	11.947	9.26	2.928	6.131	2.837	6.714
11.13	9.55	10.14	1.92	0.6	9.79	3.53	37.05	0.97	7.33	0.83	1.78
17.7	91	122.1	12.1	191.1	57.9	71.4	28.6	177.5	43.4	131.1	171.7
2.351	1.757	1.931	1.039	0.534	2.18	2.572	2.765	0.456	1.588	0.57	1.186
0.9884	0.9092	1.2208	0.4805	0.6297	1.3694	1.5921	1.474	0.558	0.877	0.5354	0.9738
20.632	22.177	36.483	18.187	1.586	32.812	21.786	65.53	1.616	24.077	1.566	6.315
1567	1528	2140	804	6823	2378	3792	1733	6702	1725	8383	13845
16.161	>20	>20	4.936	6.961	7.486	0.838	16.735	14.287	1.711	5.034	1.767
0.6736	0.5342	0.5782	0.3025	0.3391	0.7564	0.6953	0.9557	0.2921	0.5438	0.3033	0.4913
9.619	7.837	7.462	4.412	0.331	8.886	4.02	36.13	0.452	7.03	0.323	3.293
8.8	11.6	17.7	5.6	208.3	19	27.5	304.1	210.8	15.4	247.6	297.5
2.89	2.87	3.82	0.64	2.32	3.63	2.46	4.83	1.76	0.51	2.75	3.72
39.87	33.97	41.78	16.6	20.33	46.26	47.03	56.11	18.67	32.43	18.24	30.59
4.515	3.647	3.889	2.119	2.214	5.046	4.493	6.278	1.827	3.662	1.968	3.135
966.2	76.7	148.5	733.5	71.5	10.7	91.7	147.3	72.2	78.3	291	100.4
232	262	315	160	79	407	426	530	80	307	100	222
1.07	<0.2	0.39	0.5	<0.2	0.49	5.33	3.18	<0.4	0.74	<0.4	<0.4
3	63.6	6.3	3.6	50.9	122.5	<4	16.9	5.6	12.9	63.4	<4
0.002	0.002	0.006	0.002	<0.002	0.008	<0.003	0.003	<0.003	0.013	<0.003	<0.003
0.75	0.05	0.12	1.11	0.03	0.42	11.7	0.71	0.06	0.3	0.36	0.12
5.27	0.32	0.18	1.07	0.1	0.05	0.34	0.71	0.11	0.1	0.7	0.22
1.6	0.5	0.7	6.7	37.7	2.8	6.6	2.7	35.6	2.7	46.4	28.6
81	17	12	33	42	7	61	321	42	10	<2.2	19
0.2	<0.08	0.1	0.1	<0.08	<0.08	<0.08	0.1	<0.08	<0.08	<0.08	<0.08
0.059	0.003	<0.002	0.054	0.01	0.002	0.009	0.005	0.021	0.008	0.043	0.018
<0.003	<0.003	<0.003	<0.003	<0.003	<0.003	<0.003	<0.003	<0.003	<0.003	<0.003	<0.003
2.35	1.89	2.38	1.31	0.24	1.95	1.73	11.93	0.28	2.42	0.51	0.59
<2	<2	<2	<2	71	3	4	35	76	4	83	5
608.9	22.2	15.7	38.2	3.8	17.3	392.2	169.7	9.9	47.1	72.8	6
<0.02	<0.02	<0.02	<0.02	<0.02	<0.02	<0.02	<0.02	<0.02	<0.02	<0.02	<0.02
<0.005	<0.005	<0.005	<0.005	<0.005	<0.005	<0.005	<0.005	<0.005	<0.005	<0.005	<0.005
3.41	0.29	3.68	0.59	0.94	0.9	0.11	4	0.38	2	2.51	0.67
2.4	0.4	0.2	1.2	<0.2	0.2	3.8	4.8	0.3	0.4	<0.2	0.2
0.2	0.3	0.2	0.8	0.2	0.2	0.2	1.8	0.2	0.3	0.3	0.4
0.02	0.02	0.02	0.07	0.02	0.03	0.23	0.05	<0.04	0.31	<0.04	<0.04
0.647	1.963	1.662	3.226	6.349	0.522	0.147	1.348	>11	0.232	3.148	1.278
962	57	49	712	62	2	64	128	59	50	284	96

Q930282	Q930290	Q930291	Q930292	Q930294	Q931941	Q931942	Q931943	Q931952	Q931973	Q931984	Q931989
VF	MI	MI	MI	VF	TF	MI	LT	MD	XT	XT	MD
K15-315	K15-315	K15-315	K15-315	K15-315	K15-235R	K15-235R	K15-235R	K15-216	K15-233	K15-282	K15-282
20.95	118.15	121.9	132.1	146.6	159.05	163.35	173.75	31.05	108	165.1	129
21.15	118.3	122.15	132.35	146.95	159.25	163.6	173.95	31.2	108.2	165.25	129.2
901.4	447.4	1413.6	247.9	1894.7	>1740	94.5	1072.4	1334	1990.3	1396.8	2104.7
1.44	0.69	1.18	0.56	0.31	2.61	0.34	2.06	1.43	2.43	2.59	3.03
0.13	<0.05	0.32	0.28	0.22	0.59	<0.47	0.5	<0.05	0.11	0.08	<0.05
0.056	0.319	0.405	0.643	1.221	3.213	0.189	0.074	0.208	0.133	0.039	0.181
95.25	20.29	21.77	23.03	76.03	113.53	20.12	104.34	69.34	180.59	171.76	97.43
1.04	43	41.63	37.71	1.85	4.1	40.78	2.05	22.53	1.6	3.76	19.69
7	361	318	293	11	9	390	10	31	11	12	25
0.76	0.606	3.838	0.684	0.879	2.125	0.531	2.451	3.123	1.528	4.066	6.262
10.4	0.8	41.6	71.5	16.5	14.8	25.1	8.3	4.5	3	4.4	1.9
6.191	3.926	4.142	4.234	5.633	6.782	3.448	6.463	5.591	9.429	8.306	5.867
3.472	2.307	2.41	2.462	3.373	4.352	2.021	3.603	2.902	4.842	4.384	3.112
0.3412	1.1771	1.2729	1.2979	0.6008	0.7894	1.078	0.4506	2.0061	2.0309	2.7113	2.4899
14.53	16.93	15.42	13.7	12.5	21.01	15.17	19.64	21.15	23.26	24.15	26.59
6.28	3.831	4.128	4.335	5.471	6.958	3.475	6.494	7.108	12.47	11.607	8.945
4.54	2.26	2.19	2.28	7.23	9.35	2.1	5.71	6.07	8.53	9.83	8.78
1.2077	0.795	0.8422	0.87	1.1522	1.4625	0.7033	1.2339	1.0524	1.7601	1.5652	1.0618
0.0298	0.0588	0.0621	0.0597	0.0347	0.0784	0.0471	0.0397	0.0774	0.0719	0.0819	0.1044
47	9.3	9.9	10.3	39	54.4	9	50.1	33	89.6	84.9	46.3
6.8	19.8	38.3	29.4	1.5	32.6	26.8	18.7	15.7	9.8	19.8	46.6
0.488	0.323	0.322	0.331	0.466	0.674	0.272	0.476	0.44	0.658	0.639	0.536
1.44	0.38	0.27	0.41	2.55	2.67	0.56	2.41	1.05	2.2	1.73	0.56
17.95	9.026	8.5	8.841	17.733	23.601	8.016	20.476	18.933	34.676	43.034	26.723
36.45	12.42	13.24	14.28	30.12	44.71	11.94	39.58	35.44	75.77	73.78	49.77
0.9	99.2	92.5	79.6	2.9	6.4	109.7	2.9	4.2	2.3	4.5	2.9
19.17	24	173.7	135.35	60.17	60.19	10.82	80.65	4.95	3.64	5.19	5.1
11.074	2.859	3.063	3.236	8.844	13.056	2.645	11.554	8.907	21.434	20.829	12.703
204.89	16.56	98.91	14.21	168.62	141.15	5.12	128.19	74.08	126.92	172.23	249.38
0.76	3.51	3.35	4.22	7.86	0.97	1.23	0.49	0.14	0.22	0.2	0.18
3.5	32.9	31.4	32.1	3.5	9.3	27.5	4.3	33.1	9.6	11.8	38.5
7.293	3.257	3.51	3.707	6.008	8.192	3.043	7.512	7.678	14.536	14.098	10.318
5.45	0.79	1.28	1.13	4.31	8.62	0.64	7.39	1.67	4.13	3.9	2.25
29.3	277.3	228.3	93	99.4	37.7	117.8	18.2	129.3	80.9	58.4	125.1
1.718	0.546	0.544	0.559	1.442	1.897	0.486	1.763	1.298	2.086	2.485	1.807
1.0469	0.6303	0.6469	0.7007	0.9127	1.0936	0.5684	1.1031	1.0152	1.7313	1.5471	1.1514
29.881	1.43	1.383	1.361	20.664	29.305	1.753	28.682	8.25	34.279	27.666	11.442
1013	8279	7442	7615	1549	2110	6818	1380	14590	3136	3909	17172
0.972	1.288	7.165	2.683	38.756	2.612	0.11	1.624	0.463	0.697	1.048	1.385
0.4989	0.3362	0.3468	0.3482	0.4944	0.6714	0.2909	0.5332	0.4209	0.6858	0.6477	0.4692
19.877	0.576	0.717	0.365	5.468	7.533	0.348	6.102	1.853	4.615	3.78	2.737
5.5	245.3	221.5	223	11.3	22.5	199.3	10.3	312.3	24.9	29.8	352.1
0.99	0.4	0.55	0.3	1.94	2.31	0.26	1.84	1.33	1.45	2.01	2.73
33.5	21.22	22.08	22.56	32.06	41.17	19.24	34.73	27.54	46	41.68	26.1
3.206	2.122	2.149	2.198	3.172	4.633	1.852	3.411	2.784	4.316	4.034	3.335
33.9	182.7	327.4	231	288.4	972.2	134.6	33.2	142.4	53.7	14.9	124.9
139	85	81	83	256	349	80	186	237	310	386	334
<0.4	<0.4	1.24	0.81	1.38	0.35	<0.2	0.23	<0.4	<0.4	<0.4	<0.4
<4	91.8	50.5	47	18.4	11.7	2.7	11.7	<4	<4	<4	<4
<0.003	<0.003	0.009	0.005	0.017	<0.002	<0.002	0.005	<0.003	<0.003	<0.003	<0.003
0.12	<0.02	0.35	0.23	0.25	0.68	0.08	0.54	0.04	0.1	0.09	0.02
0.06	0.09	0.25	0.59	1.42	3.58	0.23	0.07	0.2	0.15	<0.05	0.16
1.1	42	35.8	34.9	2.1	3.9	22.4	1.7	21.5	1	3	17.1
9	<2.2	45	71	16	13	28	7	4	<2.2	6	<2.2
<0.08	<0.08	<0.08	<0.08	0.3	0.1	<0.08	<0.08	<0.08	<0.08	<0.08	<0.08
<0.005	<0.005	0.006	0.016	0.03	0.044	0.028	0.004	0.018	0.008	0.006	0.031
<0.003	<0.003	<0.003	<0.003	<0.003	<0.003	<0.003	<0.003	<0.003	<0.003	<0.003	<0.003
1.17	0.35	0.2	0.26	1.91	2.18	0.3	1.42	0.84	1.86	1.92	0.43
<2	68	76	57	3	5	59	<2	5	<2	5	2
6.7	3.7	157.8	120	47.8	61.4	10.5	86.1	3.2	2.8	4.3	4.3
<0.02	<0.02	<0.02	<0.02	<0.02	<0.02	<0.02	<0.02	<0.02	<0.02	<0.02	<0.02
<0.005	<0.005	<0.005	<0.005	<0.005	<0.005	<0.005	<0.005	<0.005	<0.005	<0.005	<0.005
0.6	0.94	1.35	1.77	6	0.6	0.31	0.32	0.1	0.09	0.08	0.12
0.3	<0.2	1.1	0.3	0.2	0.5	<0.2	3	0.3	0.3	0.3	<0.2
0.2	0.1	0.2	0.2	0.1	0.2	0.2	0.1	0.2	0.2	0.1	0.7
<0.04	<0.04	0.05	<0.04	0.06	0.25	0.08	0.23	<0.04	0.12	<0.04	<0.04
0.07	1.23	6.499	2.608	0.528	0.489	0.05	0.058	0.177	0.058	0.08	0.573
15	113	273	161	312	961	79	14	130	15	8	100

Appendix 2.2 QA/QC Data full set

	SLV-MC basalt													
	2018	2018		2019	2019	2018				2019				
Sample	B00267984	B00267986	B00267986 lab duplicate	Q311621	Q311623	Mean	σ	% RSD	% RD IS*	Mean	σ	% RSD	% RD IS*	Mean
Rock Type	SLV-MC basalt	SLV-MC basalt	SLV-MC basalt	SLV-MC basalt	SLV-MC basalt									
Trace elements (ppm) OGL IMC-100			-											
Ba	164.70	165.60	-	156.3	153.8	165.15	0.64	0.39	1.75	155.05	1.77	1.14	-4.47	160.10
Be	0.77	0.77	-	0.79	0.74	0.77	0	0	-3.75	0.77	0.04	4.62	-3.75	0.77
Bi	<0.47	<0.47	-	<0.05	<0.05	-	-	-	-	-	-	-	-	-
Cd	0.10	0.10	-	0.102	0.103	0.1	0	2.8	-9.09	0.10	0.00	0.69	-9.09	0.10
Ce	21.97	22.34	-	20.86	20.53	22.16	0.26	1.18	2.03	20.70	0.23	1.13	-4.70	21.43
Co	49.65	48.62	-	45.47	45.82	49.14	0.73	1.48	-0.87	45.65	0.25	0.54	-7.91	47.39
Cr	229.00	225.00	-	217	215	227	2.83	1.25	-0.87	216.00	1.41	0.65	-5.68	221.50
Cs	0.09	0.07	-	0.08	0.078	0.08	0.01	16.11	0.00	0.08	0.00	1.79	0.00	0.08
Cu	54.80	52.80	-	54.7	55.5	53.8	1.41	2.63	-5.06	55.10	0.57	1.03	-2.77	54.45
Dy	3.66	3.81	-	3.542	3.633	3.73	0.11	2.86	1.36	3.59	0.06	1.79	-2.45	3.66
Er	1.85	1.92	-	1.868	1.816	1.89	0.05	2.73	0.53	1.84	0.04	2.00	-2.13	1.86
Eu	1.34	1.41	-	1.3791	1.3799	1.38	0.05	3.45	-2.13	1.38	0.00	0.04	-2.13	1.38
Ga	20.63	20.75	-	20.67	20.22	20.69	0.08	0.41	-0.86	20.45	0.32	1.56	-2.01	20.57
Gd	4.09	4.31	-	4.017	4.131	4.2	0.16	3.77	0.24	4.07	0.08	1.98	-2.86	4.14
Hf	2.55	2.74	-	2.57	2.54	2.65	0.13	5.08	2.71	2.56	0.02	0.83	-0.78	2.60
Ho	0.69	0.72	-	0.6779	0.6885	0.7	0.02	3.31	0.00	0.68	0.01	1.10	-2.86	0.69
In	0.07	0.07	-	0.063	0.063	0.07	0	2.43	0.00	0.06	0.00	0.00	-14.29	0.07
La	9.50	9.70	-	9.2	9.1	9.6	0.14	1.47	0.84	9.15	0.07	0.77	-3.89	9.38
Li	5.70	5.60	-	6	5.8	5.65	0.07	1.25	-4.07	5.90	0.14	2.40	0.17	5.78
Lu	0.23	0.24	-	0.225	0.233	0.24	0.01	3.6	9.09	0.23	0.01	2.47	4.55	0.23
Mo	3.63	3.59	-	3.37	3.45	3.61	0.03	0.78	-1.63	3.41	0.06	1.66	-7.08	3.51
Nb	8.34	8.14	-	8.115	7.934	8.24	0.14	1.69	-0.84	8.02	0.13	1.59	-3.49	8.13
Nd	14.40	14.49	-	14	13.79	14.45	0.06	0.44	-0.07	13.90	0.15	1.07	-3.87	14.17
Ni	153.40	149.50	-	149.7	146.5	151.45	2.76	1.82	-1.80	148.10	2.26	1.53	-3.97	149.78
Pb	6.68	5.91	-	5.7	5.44	6.3	0.54	8.65	9.57	5.57	0.18	3.30	-3.13	5.93
Pr	3.18	3.25	-	3.067	3.054	3.21	0.05	1.63	2.56	3.06	0.01	0.30	-2.24	3.14
Pb	5.48	5.41	-	5.54	5.85	5.45	0.05	0.91	-7.47	5.70	0.22	3.85	-3.23	5.57
Sb	0.21	0.17	-	0.17	0.18	0.19	0.03	14.89	5.56	0.18	0.01	4.04	0.00	0.18
Sc	19.80	19.80	-	20.4	20	19.8	0	0	-6.91	20.20	0.28	1.40	-5.03	20.00
Sm	3.76	4.01	-	3.763	3.652	3.88	0.17	4.46	1.57	3.71	0.08	2.12	-2.88	3.80
Sn	1.55	1.40	-	1.46	1.44	1.48	0.11	7.19	3.50	1.45	0.01	0.98	1.40	1.46
Sr	444.40	448.60	-	438.2	435.5	446.5	2.97	0.67	-2.59	436.85	1.91	0.44	-4.69	441.68
Ta	0.49	0.52	-	0.48	0.483	0.5	0.02	4.06	2.04	0.48	0.00	0.44	-2.04	0.49
Tb	0.63	0.65	-	0.5964	0.6129	0.64	0.02	2.48	1.59	0.60	0.01	1.93	-4.76	0.62
Th	0.91	0.90	-	0.834	0.834	0.91	0.01	1.09	3.41	0.83	0.00	0.00	-5.68	0.87
Ti	9157	8973	-	9043	9197	9065	130.11	1.44	-2.27	9120	108.89	1.19	-1.67	9093
Tl	0.02	0.03	-	0.017	0.022	0.02	0.01	40.86	0.00	0.02	0.00	18.13	0.00	0.02
Tm	0.25	0.26	-	0.2474	0.2514	0.26	0.01	2.65	0.00	0.25	0.00	1.13	-3.85	0.25
U	0.31	0.32	-	0.288	0.299	0.32	0.01	1.78	3.23	0.29	0.01	2.65	-6.45	0.31
V	193.50	188.50	-	190.1	193	191	3.54	1.85	-1.73	191.55	2.05	1.07	-1.45	191.28
W	0.35	0.37	-	0.39	0.34	0.36	0.01	3.93	5.88	0.37	0.04	9.69	8.82	0.36
Y	17.86	18.05	-	17.72	17.74	17.96	0.13	0.75	-1.43	17.73	0.01	0.08	-2.69	17.84
Yb	1.54	1.68	-	1.504	1.538	1.61	0.09	5.84	1.90	1.52	0.02	1.58	-3.80	1.57
Zn	108.80	105.70	-	109.7	110.3	107.25	2.19	2.04	-1.05	110.00	0.42	0.39	1.49	108.63
Zr	102.00	103.00	-	100	100	102.5	0.71	0.69	-0.78	100.00	0.00	0.00	-3.20	101.25
Trace elements (ppm) OGL IML-101														
Ag	<0.2	<0.2	<0.2	<0.4	<0.4	-	-	-	-	-	-	-	-	-
As	1	0.7	0.9	<4	<4	0.87	0.15	17.63	0.00	-	-	-	-	0.87
Au	<0.002	<0.002	<0.002	<0.003	<0.003	-	-	-	-	-	-	-	-	-
Bi	<0.02	<0.02	<0.02	<0.02	<0.02	-	-	-	-	-	-	-	-	-
Cd	0.04	0.05	0.07	0.06	0.07	0.05	0.02	28.64	-16.67	0.07	0.01	10.88	16.67	0.06
Co	36.2	34.7	35.4	37.8	37.2	35.43	0.75	2.12	-2.29	37.50	0.42	1.13	3.42	36.26
Cu	52	51	52	54	54	51.67	0.58	1.12	-1.77	54.00	0.00	0.00	2.66	52.60
Hg	<0.08	<0.08	<0.08	<0.08	<0.08	-	-	-	-	-	-	-	-	-
In	0.017	0.017	0.018	0.018	0.016	0.02	0	3.33	0.00	0.02	0.00	8.32	0.00	0.02
Ir	<0.003	<0.003	<0.003	<0.003	<0.003	-	-	-	-	-	-	-	-	-
Mo	2.91	2.9	2.9	2.97	2.96	2.9	0.01	0.2	-1.02	2.97	0.01	0.24	1.37	2.93
Ni	129	119	123	133	130	123.67	5.03	4.07	-2.47	131.50	2.12	1.61	3.71	126.80
Pb	4.8	4.5	4.7	5	4.5	4.67	0.15	3.27	-0.64	4.75	0.35	7.44	1.06	4.70
Pd	<0.02	<0.02	<0.02	<0.02	<0.02	-	-	-	-	-	-	-	-	-
Pt	<0.005	<0.005	<0.005	<0.005	<0.005	-	-	-	-	-	-	-	-	-
Sb	0.15	0.15	0.15	0.16	0.16	0.15	0	0	0.00	0.16	0.00	0.00	6.67	0.15
Se	<0.2	<0.2	<0.2	<0.2	<0.2	-	-	-	-	-	-	-	-	-
Sn	0.8	0.8	0.8	0.9	0.9	0.8	0	0	-4.76	0.90	0.00	0.00	7.14	0.84
Te	<0.02	<0.02	<0.02	<0.04	<0.04	-	-	-	-	-	-	-	-	-
Tl	0.004	0.005	0.005	0.004	0.004	0	0	12.37	-	0.00	0.00	0.00	-	0.00
Zn	83	80	82	85	85	81.67	1.53	1.87	-1.60	85.00	0.00	0.00	2.41	83.00

*LT, felsic lapillit tuff; TF, felsic tuff, VF, felsic coherent volcanic rock; MI, mafic intrusive; MD, mafic dike; XT, felsic crystal-rich tuff.

			WP-1 Watts Point dacite (Coast Plutonic Complex)											
ALL			2018	2018	2019	2019		2018				2019		
σ	% RSD	% RD IS*	B00267983	B00267985	Q311620	Q311622	Mean	σ	% RSD	% RD IS*	Mean	σ	% RSD	% RD IS*
			WP-1 dacite	WP-1 dacite	WP-1 dacite	WP-1 dacite								
5.14	3.21	-0.81		620.60	629.40	604.10	597.00	625	6.22	1	1.35	600.55	5.02	0.84
0.02	2.33	0.99		1.01	1.00	1.03	0.97	1.01	0.01	0.7	-3.81	1.00	0.04	4.24
-	-	-		<0.47	<0.47	<0.05	<0.05	-	-	-	-	-	-	-
0.00	1.61	1.75		0.05	0.05	0.05	0.06	0.05	0	1.43	-16.67	0.05	0.00	6.61
0.75	3.50	-1.31		27.33	27.52	26.61	26.42	27.43	0.13	0.49	1.03	26.52	0.13	0.51
1.79	3.77	-2.53		12.82	12.62	11.74	11.62	12.72	0.14	1.11	-0.24	11.68	0.08	0.73
5.72	2.58	-1.56		71.00	71.00	67.00	67.00	71	0	0	-1.05	67.00	0.00	0.00
0.01	8.11	12.86		0.43	0.43	0.43	0.42	0.43	0	0.33	0.00	0.42	0.01	1.51
1.00	1.84	3.13		15.00	23.30	14.60	15.40	19.15	5.87	30.65	15.08	15.00	0.57	3.77
0.09	2.59	3.95		2.35	2.41	2.30	2.33	2.38	0.04	1.87	0.42	2.31	0.02	0.92
0.04	2.09	1.90		1.34	1.35	1.33	1.38	1.34	0.01	0.58	-1.47	1.36	0.03	2.35
0.02	1.73	2.80		0.89	0.86	0.84	0.88	0.88	0.02	2.1	0.00	0.86	0.03	2.98
0.21	1.00	0.18		18.62	19.34	18.35	18.43	18.98	0.51	2.68	0.26	18.39	0.06	0.31
0.11	2.63	1.15		2.75	2.82	2.66	2.76	2.78	0.05	1.65	0.72	2.71	0.07	2.45
0.08	3.14	4.00		3.17	3.25	3.34	3.27	3.21	0.06	1.76	0.00	3.31	0.05	1.50
0.02	2.36	3.59		0.46	0.48	0.47	0.47	0.47	0.02	3.72	0.00	0.47	0.00	0.57
0.00	3.36	-7.11		0.03	0.03	0.03	0.03	0.03	0	2.11	0.00	0.03	0.00	0.91
0.24	2.54	-0.27		13.00	13.50	12.60	12.50	13.25	0.35	2.67	2.08	12.55	0.07	0.56
0.15	2.56	3.13		10.40	11.00	10.10	10.10	10.7	0.42	3.97	2.10	10.10	0.00	0.00
0.01	2.66	10.71		0.20	0.21	0.21	0.22	0.21	0.01	2.72	0.00	0.21	0.01	3.63
0.10	2.99	-1.13		0.90	0.81	0.85	0.82	0.86	0.06	7.44	-4.44	0.84	0.02	2.54
0.14	1.77	-0.08		3.57	3.54	3.43	3.33	3.55	0.02	0.54	0.85	3.38	0.07	1.95
0.29	2.02	-1.46		14.75	14.96	14.62	14.20	14.86	0.15	1	0.95	14.41	0.30	2.06
2.45	1.63	0.18		44.50	43.50	41.50	42.40	44	0.71	1.61	-1.21	41.95	0.64	1.52
0.46	7.80	17.94		7.03	7.42	6.74	6.92	7.23	0.28	3.82	2.84	6.83	0.13	1.86
0.08	2.59	2.52		3.59	3.67	3.54	3.68	3.63	0.06	1.52	0.28	3.61	0.10	2.88
0.17	3.02	2.96		22.32	21.74	21.10	22.11	22.03	0.41	1.86	-1.43	21.61	0.71	3.31
0.02	8.98	7.35		0.09	0.10	0.10	0.10	0.1	0.01	7.44	0.00	0.10	0.00	0.00
0.24	1.22	1.01		9.30	9.70	9.30	9.80	9.5	0.28	2.98	-5.28	9.55	0.35	3.70
0.13	3.42	2.32		3.01	3.11	3.00	3.09	3.06	0.08	2.52	-0.33	3.04	0.06	2.12
0.05	3.76	50.77		1.31	1.34	1.30	1.38	1.33	0.02	1.6	-4.32	1.34	0.06	4.22
5.14	1.16	-0.61		715.10	735.10	696.50	711.90	725.1	14.14	1.95	-0.29	704.20	10.89	1.55
0.02	3.13	4.89		0.21	0.22	0.22	0.21	0.22	0	1.64	0.00	0.22	0.00	2.29
0.02	3.38	2.18		0.42	0.41	0.39	0.40	0.42	0.01	1.26	5.00	0.40	0.00	1.16
0.04	4.23	1.22		2.03	2.01	1.80	2.03	2.02	0.01	0.73	2.54	1.91	0.17	8.72
89.18	0.98	1.33		3020	3072	2947	2975	3046	36.77	1.21	0.26	2961	19.80	0.67
0.01	24.51	110.00		0.14	0.16	0.17	0.14	0.15	0.01	9.49	0.00	0.15	0.03	17.45
0.01	1.99	1.14		0.20	0.20	0.20	0.21	0.2	0	1.71	0.00	0.20	0.01	3.12
0.01	4.30	9.20		0.83	0.81	0.78	0.81	0.82	0.01	1.47	2.50	0.79	0.02	2.86
2.06	1.08	2.40		88.70	88.30	83.50	86.50	88.5	0.28	0.32	0.99	85.00	2.12	2.50
0.02	5.30	20.83		0.17	0.16	0.17	0.16	0.17	0.01	4.29	6.25	0.17	0.01	4.29
0.13	0.74	-0.10		13.17	13.56	12.67	12.96	13.37	0.28	2.06	0.91	12.82	0.21	1.60
0.07	4.20	2.30		1.32	1.37	1.31	1.34	1.34	0.04	2.69	0.00	1.33	0.02	1.55
1.77	1.63	9.72		58.00	61.40	57.60	56.60	59.7	2.4	4.03	0.91	57.10	0.71	1.24
1.30	1.28	0.25		130.00	133.00	126.00	126.00	131.5	2.12	1.61	3.03	126.00	0.00	0.00
-	-	-		<0.2	<0.2	<0.4	<0.4	-	-	-	-	-	-	-
0.12	14.39	-2.30		<0.7	<0.7	<4	<4	-	-	-	-	-	-	-
-	-	-		<0.002	<0.002	<0.003	<0.003	-	-	-	-	-	-	-
-	-	-		0.02	0.02	0.02	0.02	0.02	0	0	0.00	0.02	0.00	0.00
0.01	20.11	-8.33		<0.02	<0.02	<0.05	<0.05	-	-	-	-	-	-	-
1.13	3.13	0.59		3.2	3.4	3.4	3.4	3.3	0.14	4.29	-1.49	3.40	0.00	0.00
1.20	2.28	0.29		10	11	11	11	10.5	0.71	6.73	-2.33	11.00	0.00	0.00
-	-	-		<0.08	<0.08	<0.08	<0.08	-	-	-	-	-	-	-
0.00	4.35	-15.00		0.008	0.009	0.009	0.011	0.01	0	8.32	0.00	0.01	0.00	14.14
-	-	-		<0.003	<0.003	<0.003	<0.003	-	-	-	-	-	-	-
0.03	1.04	0.17		0.62	0.53	0.52	0.65	0.58	0.06	11.07	0.00	0.59	0.09	15.71
5.08	4.00	0.75		8	8	8	8	8	0	0	0.00	8.00	0.00	0.00
0.19	4.04	0.00		3.8	2.5	2.7	2.6	3.15	0.92	29.18	8.62	2.65	0.07	2.67
-	-	-		<0.02	<0.02	<0.02	<0.02	-	-	-	-	-	-	-
-	-	-		<0.005	<0.005	<0.005	<0.005	-	-	-	-	-	-	-
0.00	3.18	3.33		0.06	0.05	0.06	0.06	0.06	0.01	12.86	0.00	0.06	0.00	0.00
-	-	-		<0.2	<0.2	<0.2	<0.2	-	-	-	-	-	-	-
0.05	5.83	1.19		1.3	1	1	0.9	1.15	0.21	18.45	9.52	0.95	0.07	7.44
-	-	-		<0.02	<0.02	<0.04	<0.04	-	-	-	-	-	-	-
0.00	11.13	-		0.019	0.019	0.032	0.021	0.02	0	0	0.00	0.03	0.01	29.35
1.90	2.29	0.30		25	24	25	25	24.5	0.71	2.89	-1.01	25.00	0.00	0.00

ALL				
Mean	σ	% RSD	% RD IS*	
-2.61	612.78	12.86	0.02	-0.63
-4.76	1.00	0.02	0.02	-4.52
-	-	-	-	-
-16.67	0.05	0.00	0.05	-14.17
-2.32	26.97	0.46	0.02	-0.66
-8.39	12.20	0.53	0.04	-4.31
-6.62	69.00	2.00	0.03	-3.83
-2.33	0.43	0.01	0.01	-0.99
-9.86	17.08	3.61	0.21	2.61
-2.53	2.34	0.04	0.02	-1.07
0.00	1.35	0.02	0.01	-0.81
-2.27	0.87	0.02	0.02	-1.16
-2.85	18.69	0.39	0.02	-1.29
-1.81	2.75	0.05	0.02	-0.46
3.12	3.26	0.06	0.02	1.48
0.00	0.47	0.01	0.02	-0.30
0.00	0.03	0.00	0.04	7.67
-3.31	12.90	0.39	0.03	-0.62
-3.63	10.40	0.37	0.04	-0.76
0.00	0.21	0.01	0.03	0.60
-6.67	0.85	0.04	0.04	-6.11
-3.98	3.47	0.09	0.03	-1.52
-2.11	14.63	0.28	0.02	-0.59
-5.81	42.98	1.13	0.03	-3.51
-2.84	7.03	0.25	0.04	-0.04
-0.28	3.62	0.06	0.02	-0.02
-3.31	21.82	0.46	0.02	-2.38
0.00	0.10	0.00	0.04	-2.50
-4.79	9.53	0.23	0.02	-5.03
-0.98	3.05	0.05	0.02	-0.65
-3.60	1.33	0.03	0.02	-4.14
-3.16	714.65	13.74	0.02	-1.72
0.00	0.22	0.00	0.01	-1.82
0.00	0.41	0.01	0.02	1.58
-3.05	1.97	0.10	0.05	-0.14
-2.53	3004	47.35	0.02	-1.14
0.00	0.15	0.02	0.10	1.00
0.00	0.20	0.00	0.02	-0.06
-1.25	0.80	0.02	0.02	0.47
-3.00	86.75	2.05	0.02	-1.00
6.25	0.17	0.01	0.03	3.13
-3.25	13.09	0.32	0.02	-1.21
-0.75	1.33	0.02	0.02	-0.52
-3.48	58.40	1.81	0.03	-1.28
-1.28	128.75	2.95	0.02	0.88
-	-	-	-	-
-	-	-	-	-
-	-	-	-	-
0.00	0.02	0.00	0.00	0.00
-	-	-	-	-
1.49	3.35	0.09	0.03	0.00
2.33	10.75	0.43	0.04	0.00
-	-	-	-	-
0.00	0.01	0.00	0.12	-7.50
-	-	-	-	-
1.72	0.58	0.06	0.10	0.00
0.00	8.00	0.00	0.00	0.00
-8.62	2.90	0.52	0.18	0.00
-	-	-	-	-
-	-	-	-	-
0.00	0.06	0.00	0.08	-4.17
-	-	-	-	-
-9.52	1.05	0.15	0.14	0.00
-	-	-	-	-
50.00	0.02	0.01	0.24	13.75
1.01	24.75	0.43	0.02	0.00

Appendix 3.1 Downhole profiles of selected metals and mass balance

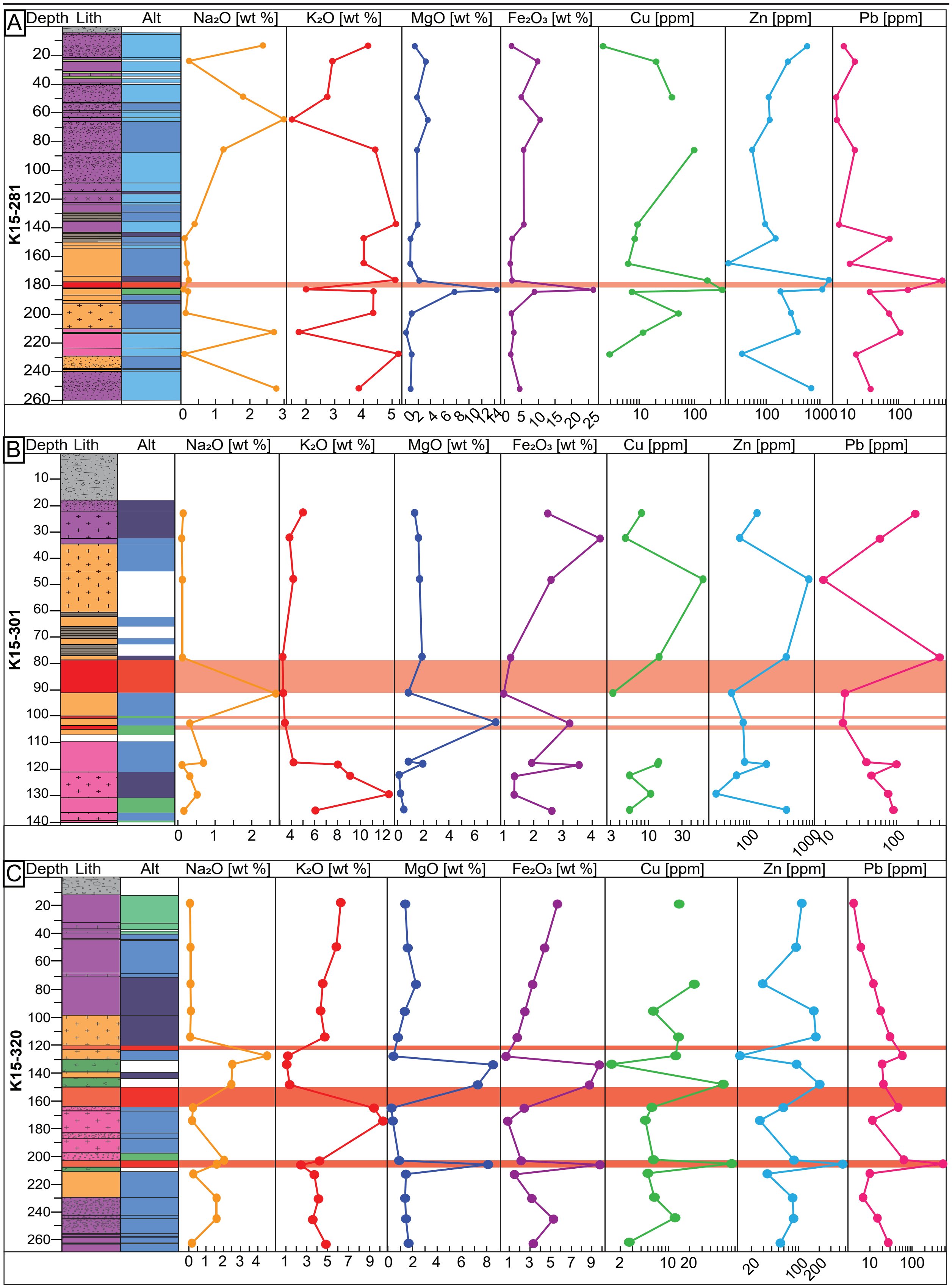
A
Depth Lith
Alt
Na₂O [wt %]
K₂O [wt %]
MgO [wt %]
Fe₂O₃ [wt %]
Cu [ppm]
Zn [ppm]
Pb [ppm]
K15-281
B
K15-301
C
K15-320

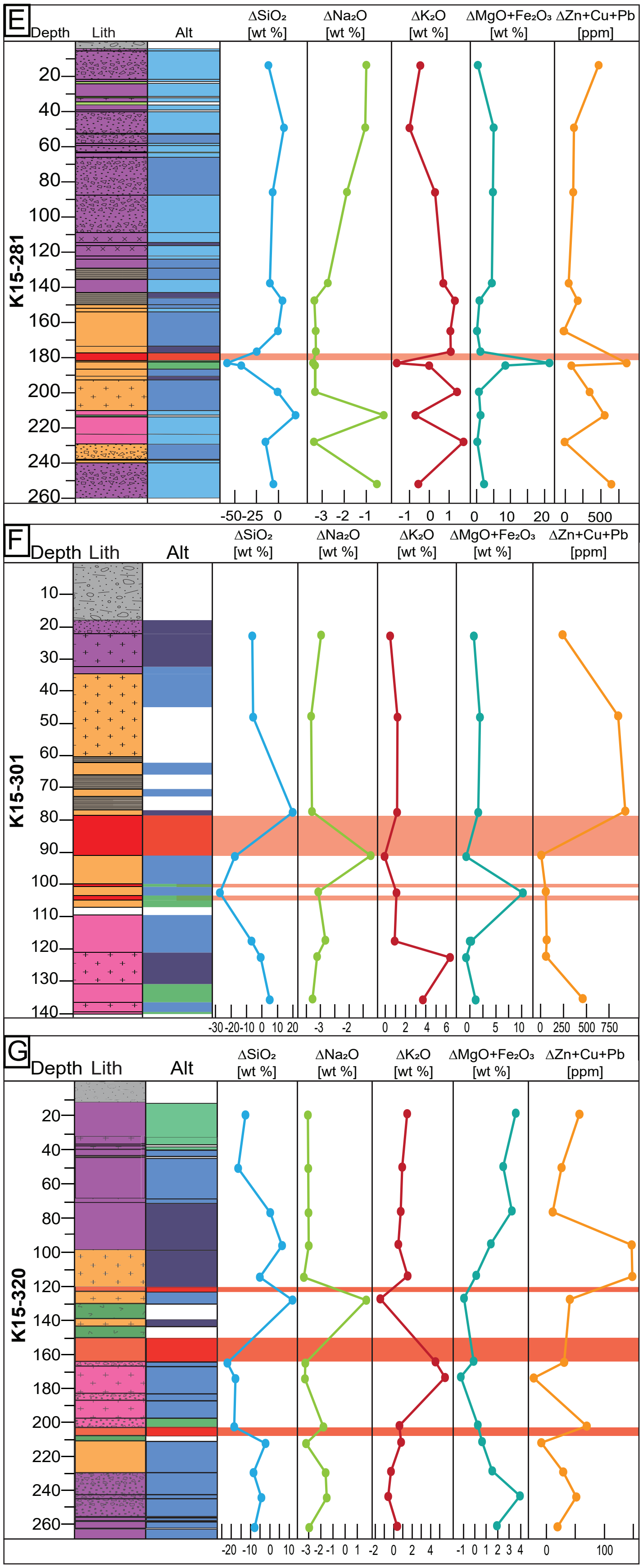

Figure A3.1Down hole profiles of drill holes in the ABM deposit. (A) Drill hole K15-281, in the western part of the ABM Zone, position of the drill hole is highlighted in the map in Figure 2A. Downhole profiles of selected elements displayed. (B) Drill hole K15-301 in the east part of the ABM Zone, 415050 mE cross section. Downhole profiles of selected elements displayed. (C) Drill hole K15-320, in the Krakatoa Zone, position of the drill hole is highlighted in the map in Figure 3.2A. Downhole profiles of selected elements displayed. (D) Drill hole K15-281, down hole profiles of mass changes of selected element displayed. (E) Drill hole K15-301, down hole profiles of mass changes of selected element displayed. (F) Drill hole K15-320, down hole profiles of mass changes of selected element displayed.

Appendix 4.1 Precursor samples used in mass balance calculations of felsic rocks

Appendix 4.1 Precursor samples used in mass balance calculations of felsic rocks

Sample Number	R9710818	R9710857	R9718957	R9719004	R9902940	R9902950	R9520451
DDH	K97-178	K97-179	K97-182	K97-187	K98-193	K98-196	K95-167
DDH_depth_FROM_m	86.5	366	124	59.3	102.9	119.5	24.3
DDH_depth_TO_m	86.6	366.1	124.1	59.4	103	119.6	24.4
Felsic_geochem_group	FA	FA	FA	FA	FA	FA	FA
Precursor_composition							
SiO2_pct	72.16	64.91	66.91	73.08	68.8	69.56	70.9
Al2O3_pct	14.63	14.98	15.64	15.03	15.82	15.18	13.05
Fe2O3_pct	1.75	5.96	5.28	1.42	2.95	1.57	0.09
CaO_pct	0.87	1.37	0.41	0.44	2.02	3	2.07
MgO_pct	0.44	1.27	2.4	0.46	0.62	0.62	1.07
Na2O_pct	3.11	3.46	4.13	3.5	2.55	3.41	2.15
K2O_pct	3.11	4.48	1.26	2.95	4.32	3.72	5.63
TiO2_pct	0.58	0.74	0.66	0.61	0.6	0.56	0.43
P2O5_pct	0.18	0.2	0.2	0.2	0.18	0.17	0.06
LOI_pct	2.48	2.27	2.18	1.9	1.58	1.2	2.2
Ba_ppm	36	104	60	40	-	-	746
Cu_ppm	5	5	10	4	-	-	5
Pb_ppm	16	2	2	5	-	-	19
Zn_ppm	2	64	131	2	-	-	34

Averaged_precursor_composition			
Felsic_geochem_group	FA	FB1	FB2
SiO2_pct	69.94	76.80	75.07
Al2O3_pct	14.54	12.03	12.57
Fe2O3_pct	2.01	1.97	1.50
CaO_pct	1.44	1.25	1.10
MgO_pct	0.76	0.25	0.54
Na2O_pct	3.11	3.65	3.34
K2O_pct	4.16	2.30	2.87
TiO2_pct	0.56	0.28	0.24
P2O5_pct	0.14	0.06	0.05
LOI_pct	1.95	1.96	1.97
Ba_ppm	426.00	2425.00	414.38
Cu_ppm	6.50	12.70	4.69
Pb_ppm	12.38	55.36	19.05
Zn_ppm	40.25	202.15	29.54

Appendix 4.1 Precursor samples used in mass balance calculations of felsic rocks

R9520452	R9520453	R9520454	R9902939	Q721158	Q721160	18MM-121	18MM-122	R9512936
K95-167	K95-167	K95-167	K98-193	K17-448	K17-448	K16-415	K16-415	K95-161
52.1	62.1	103.6	84.3	346.15	358.45	562.77	764.27	514.8
52.2	62.2	103.7	84.4	346.3	358.6	562.95	764.41	514.9
FA	FA	FA	FA	FB2	FB2	FB2	FB2	FB2
73	70.11	67.68	72.25	76.5	77	73.8	76.4	73.94
13.3	13.35	15.82	13.18	12.5	12.8	11.95	11.6	13.07
0.01	0.01	1.18	1.87	1.06	1.34	1.61	1.36	0.64
0.93	1.39	2.38	0.99	1.39	0.44	1.18	1.07	1.64
0.3	0.39	0.61	0.2	0.23	0.41	0.76	0.87	0.39
2.77	3.64	2.48	3	4.72	3.28	2.68	3.3	3.26
6.08	5.03	3.9	5.32	1.67	2.1	4.75	2.54	2.75
0.43	0.51	0.72	0.37	0.16	0.17	0.28	0.21	0.29
0.07	0.09	0.2	0.03	0.08	0.09	0.08	0.04	0.09
1.09	2.23	2.45	1.92	1.6	2.1	1.66	1.76	2.3
747	742	933	-	670	960	671	818	-
11	3	9	-	-	-	0.5	4.8	3
35	12	8	-	-	-	31.32	32	13
26	18	45	-	-	-	74.9	18.9	14

Appendix 4.1 Precursor samples used in mass balance calculations of felsic rocks

R9710677	R9710863	R9718960	R9718985	R9902934	R9902959	18MM-140	D00005989	Q930244
K97-173	K97-179	K97-181	K97-186	K98-188	K98-196	K17-449	K15-281	K15-236
95.8	483.4	20.1	15.8	148	243.8	407.8	212.75	117.15
95.9	483.5	20.2	15.9	148.1	243.9	407.97	212.9	117.35
FB2	FB2	FB2	FB2	FB2	FB2	FB1	FB1	FB1
75.19	75.61	74.58	72.36	74.37	76.02	73.1	78.8	78.5
11.69	11.93	14.02	13.89	12.85	11.93	13.75	10.45	11.9
1.55	2.04	2.05	1.75	1.29	1.79	1.5	2.74	1.67
1.84	0.77	0.17	1.09	1.62	0.89	2.21	1.15	0.38
0.28	0.87	0.55	0.47	0.56	0.56	0.44	0.09	0.21
3.71	2.15	3.43	2.83	4.09	3.25	5.25	2.7	3.01
2.03	3.72	2.54	4.61	2.07	2.76	1.76	1.75	3.4
0.3	0.15	0.28	0.31	0.28	0.21	0.3	0.25	0.29
0.03	0.01	0.07	0.02	0.01	0.05	0.11	0.02	0.04
2.46	2.15	1.86	2.08	1.87	1.79	2.04	2.43	1.42
22	33	61	80	-	-	2580	1225	3470
3	0.5	15	6	-	-	13.7	11.7	-
27	4	19	7	-	-	3.28	107.44	-
2	8	70	19	-	-	17.6	386.7	-

Appendix 4.2 Calculated mass change for samples of felsic rocks

Sample_ID	Q721156	B370175	B370176	B370177	B370178	B370188	B370189	B370190	D00005977	D00005979	D00005981	D00005982	D00005991	Q720929
DDH	K17-448	K15-320	K15-320	K15-320	K15-320	K15-320	K15-320	K15-320	K15-281	K15-281	K15-281	K15-281	K15-281	K16-370
DDH_depth_FROM_m	322.45	18.85	50.3	76.45	95.85	229.65	244.4	262	13.5	49.1	85.8	137.6	251.9	98.3
DDH_depth_TO_m	322.65	18.95	50.4	76.55	95.95	229.8	244.55	262.1	13.8	49.3	86	137.7	252.1	98.45
Rock_type*	LT	TF	TF	TF	TF	LT	LT	TF	LT	LT	TF	TF	TF	LT
Felsic_geochem_group	FA	FA	FA	FA	FA	FA	FA	FA	FA	FA	FA	FA	FA	FA
Altered_rock_composition														
SiO_2_pct	60.8	63.8	61.4	64.6	70.8	65.7	65.8	66.1	65.8	66.5	62.8	63.4	68.5	66.6
Al_2O_3_pct	14.3	16.2	16.7	13.4	13.5	15.55	14.6	15.5	16.35	12.65	14.4	15.3	15.5	12.35
Fe_2O_3_pct	8.06	5.67	4.43	3.27	2.51	3.19	5.29	3.33	2.06	4.95	5.66	5.73	4.49	6.41
CaO_pct	3.21	1.22	2.84	4.48	2.7	2.43	1.79	2.04	2.31	3.01	2.95	2.15	0.74	2.77
MgO_pct	3.73	1.4	1.6	2.27	1.36	1.39	1.46	1.67	1.47	1.83	1.83	1.91	0.81	1.65
Na_2O_pct	0.11	0.07	0.1	0.1	0.12	1.61	1.61	0.18	2.38	1.8	1.23	0.39	2.77	0.13
K_2O_pct	4.26	6.26	5.84	4.54	4.33	4.13	3.58	4.84	4.16	2.74	4.41	5.13	3.84	3.86
TiO_2_pct	0.93	0.59	0.66	0.51	0.46	0.5	0.59	0.63	0.67	0.53	0.62	0.62	0.65	0.46
P_2O_5_pct	0.21	0.17	0.19	0.17	0.15	0.15	0.19	0.21	0.22	0.16	0.21	0.21	0.22	0.15
LOI_pct	3.59	3.24	5.38	7.46	4.45	5.1	4.01	5.28	4.57	5.17	5.8	4.06	3.13	4.58
Ba_ppm	2280	1395	1290	1505	1305	1170	1090	1340	1245	849	2710	883	2570	1020
Cu_ppm	-	14.1	0.5	23.3	6	6.2	12.3	2.7	2.2	39.3	99.5	9.3	31.6	-
Pb_ppm	-	4.13	6.12	12.15	17.97	6.91	15.12	27.38	8.53	6.07	13.97	6.9	28.3	-
Zn_ppm	-	111.1	91.3	29.1	167.4	81.1	83.7	53.4	581.7	112	55.5	96.4	691.9	-
Calculated_mass_change														
SiO_2_pct_MB	-8.11	-12.67	-16.47	0.17	6.33	-8.49	-4.4	-7.92	-11.41	6.51	-6.52	-9.68	-5.67	8.49
Fe_2O_3_pct_MB	6.19	3.08	1.85	1.54	0.7	0.98	3.26	1.12	-0.18	3.68	3.71	3.44	2.2	5.54
CaO_pct_MB	1.82	-0.35	1.03	3.42	1.47	0.83	0.34	0.47	0.61	2.02	1.54	0.6	-0.75	1.82
MgO_pct_MB	3.03	0.5	0.63	1.7	0.7	0.54	0.69	0.81	0.55	1.34	1.09	1.05	0	1.18
Na_2O_pct_MB	-3	-3.05	-3.02	-3	-2.98	-1.6	-1.51	-2.94	-0.99	-1.04	-1.87	-2.74	-0.51	-2.96
K_2O_pct_MB	0.17	1.46	0.92	0.76	0.5	-0.3	-0.6	0.38	-0.46	-1.01	0.29	0.71	-0.56	0.38
TiO_2_pct_MB	0.38	-0.03	0.01	-0.01	-0.07	-0.1	0.02	0.03	0.03	0.04	0.06	0.02	0.05	-0.02
P_2O_5_pct_MB	0.07	0.01	0.02	0.04	0.02	0	0.05	0.05	0.05	0.04	0.07	0.06	0.06	0.03
Ba_ppm_MB	1892.85	826.37	697.43	1207.45	979.88	668.28	659.79	831.32	681.45	550.09	2311.03	413.35	1985.43	775.17
Cu_ppm_MB	-	6.16	-6.06	18.79	-0.04	-0.7	5.75	-3.97	-4.54	38.68	93.99	2.34	23.15	-
Pb_ppm_MB	-	-8.67	-7.05	0.81	6.98	-5.91	2.69	13.32	-4.79	-5.4	1.73	-5.82	14.18	-
Zn_ppm_MB	-	59.49	39.26	-8.67	140.09	35.6	43.13	9.86	477.18	88.52	15.8	51.38	608.96	-

Sample_ID	R9710714	R9710715	R9710716	R9710717	R9710718	R9710719	R9710720	R9710721	R9710722	R9710723	R9710724	R9710725	R9710726	R9710727
DDH	K97-174	K97-174	K97-174	K97-174	K97-174	K97-174	K97-174	K97-174	K97-174	K97-174	K97-174	K97-174	K97-174	K97-174
DDH_depth_FROM_m	230.3	240.2	246	255.5	264.8	295.3	312	330.9	341.2	349.8	356	364.1	370.5	375.8
DDH_depth_TO_m	230.4	240.3	246.1	255.6	264.9	295.4	312.1	331	341.3	349.9	356.1	364.2	370.6	375.9
Rock_type*	-	-	-	-	-	-	-	-	-	-	-	-	-	-
Felsic_geochem_group	FA1	FB2	FB2	FB2	FB2	FA1	FA1	FA1	FA1	FA1	FA1	FA1	FA2	FA1
Altered_rock_composition														
SiO_2_pct	54.06	69.65	43.86	18.53	65.9	64.31	62.18	64.7	63.27	63.59	61.49	60	69.68	61.86
Al_2O_3_pct	22.09	13.38	29.68	12.84	14.27	16.38	14.57	14.06	12.96	14.02	14.09	14.52	13.69	12.34
Fe_2O_3_pct	5.23	2.06	2.89	4.71	5.36	5.32	7.11	4.55	3.97	3.79	5.38	6.53	4.88	5.11
CaO_pct	1.82	2.45	1.63	16.34	1.67	1.28	2.81	3.41	4.57	3.66	4.55	3.31	1.22	5.67
MgO_pct	2.46	2.06	4.3	14.9	1.88	1.71	2.23	1.89	2.03	1.95	2.47	2	0.93	2.2
Na_2O_pct	1.08	0.4	0.76	0.28	0.25	0.34	0.18	0.25	0.31	0.31	0.23	1.9	2.91	2.13
K_2O_pct	5.76	3.2	8.44	2.44	4.38	5.01	4.59	4.3	3.83	4.4	4.3	3.6	2.67	2.7
TiO_2_pct	1.15	0.28	0.57	0.18	0.23	0.74	0.68	0.61	0.54	0.61	0.56	0.62	0.54	0.5
P_2O_5_pct	0.28	0.09	0.2	0.05	0.02	0.2	0.18	0.18	0.17	0.18	0.18	0.18	0.07	0.17
LOI_pct	5.15	5.75	6.67	28.52	5.4	4.26	4.51	4.98	7.9	6.98	6.07	6.11	2.84	6.55
Ba_ppm	69	51	48	72	41	71	156	78	68	56	109	78	154	155
Cu_ppm	30	6	19	2	68	27	7	40	3	7	5	48	8	5
Pb_ppm	4	2	40	72	450	2	4	4	4	2	2	4	4	4
Zn_ppm	87	42	132	181	80	65	51	53	16	25	50	26	51	26
Calculated_mass_change	-	-	-	-	-	-	-	-	-	-	-	-	-	-
SiO_2_pct_MB	-34.35	-9.53	-56.45	-56.88	-16.93	-12.84	-7.87	-3.02	1.06	-3.98	-6.47	-9.84	4.08	2.96
Fe_2O_3_pct_MB	1.44	0.30	-0.41	2.98	3.09	2.72	5.09	2.70	2.45	1.92	3.55	4.53	3.18	4.01
CaO_pct_MB	-0.24	1.27	-0.34	14.99	0.44	-0.31	1.36	2.08	3.69	2.35	3.25	1.87	-0.15	5.24
MgO_pct_MB	0.86	1.34	1.23	14.01	1.06	0.76	1.46	1.19	1.52	1.26	1.79	1.24	0.23	1.83
Na_2O_pct_MB	-2.40	-3.07	-3.13	-3.17	-3.23	-2.81	-2.93	-2.85	-2.76	-2.79	-2.87	-1.21	-0.02	-0.60
K_2O_pct_MB	-0.37	0.19	0.76	-0.43	1.04	0.28	0.42	0.28	0.13	0.40	0.27	-0.56	-1.33	-0.98
TiO_2_pct_MB	0.19	0.02	0.00	-0.07	-0.04	0.09	0.11	0.07	0.04	0.07	0.01	0.06	0.01	0.02
P_2O_5_pct_MB	0.04	0.03	0.03	-0.01	-0.04	0.03	0.04	0.04	0.05	0.04	0.04	0.04	-0.07	0.06
Ba_ppm_MB	-380.57	-376.92	-404.53	-354.31	-388.73	-362.96	-270.28	-345.32	-349.69	-367.91	-313.49	-347.87	-262.40	-243.32
Cu_ppm_MB	13.25	1.21	3.62	-2.48	55.54	17.47	0.49	34.88	-3.13	0.76	-1.34	41.58	2.00	-0.61
Pb_ppm_MB	-9.74	-16.61	-1.53	52.08	378.40	-10.60	-8.38	-8.24	-7.89	-10.30	-10.31	-8.37	-8.13	-7.66
Zn_ppm_MB	17.03	5.99	22.46	143.90	37.05	17.46	10.66	14.57	-22.29	-14.32	11.36	-14.21	13.93	-9.61

*LT, felsic lapillit tuff; TF, felsic tuff, VF, felsic coherent volcanic rock; XT, felsic crystal-rich tuff.

Q720939	Q720946	Q721157	Q930221	Q931973	Q931984	B370156	B370183	B370184	B370185	D00005990	Q930100	Q931941	Q721099	Q721154	Q930294	B370159
K16-370	K15-271	K17-448	K15-232	K15-233	K15-282	K15-301	K15-320	K15-320	K15-320	K15-281	K15-235R	K15-235R	K15-290	K15-204	K15-315	K15-301
276.95	174.2	334	207.85	108	165.1	22.65	165	174.3	202.65	227.9	149.25	159.05	139.7	135.6	146.6	91.25
277.1	174.35	334.15	208	108.2	165.25	22.8	165.2	174.4	202.75	228.05	149.4	159.25	139.9	135.8	146.95	91.4
LT	LT	LT	LT	XT	XT	LT	TF	VF	TF	TF	TF	TF	VF	VF	VF	TF
FA	FA	FA	FA	FA	FA	FA	FB1	FB1	FB1	FB1	FB1	FB1	FB1	FB1	FB1	FB1
62.5	65.4	64	62.5	65.3	64.2	68.7	68	70.2	69.4	68.9	68.5	71.9	74	68.4	72	69
15.9	14.25	14.4	15	15.05	15.4	15.7	16.15	15.45	15.45	14.4	16.4	14.55	11.45	13.8	10.4	15.1
7.96	4.48	5.35	5.11	3.15	4.53	2.48	2.45	0.85	2.15	1.82	2.34	2.46	1.45	5.83	2.01	0.97
0.3	2.94	3.79	2.88	2.27	3.09	1.48	0.3	0.87	1.99	2.71	0.89	1.94	1.59	0.2	3.18	2.98
2.79	0.98	0.8	1.72	1.33	1.77	1.31	0.28	0.39	0.91	0.97	1.08	0.91	0.11	0.25	0.07	0.82
0.25	0.51	2.76	0.19	1.23	0.09	0.14	0.24	0.19	2.05	0.09	0.14	0.43	0.33	0.22	0.34	2.65
3.21	3.89	3.52	4.69	4.82	5.54	5	9.44	10.3	4.23	5.22	7.07	4.9	8.36	9.59	8.53	3.29
0.68	0.53	0.61	0.62	0.53	0.65	0.57	0.39	0.37	0.36	0.34	0.39	0.34	0.28	0.34	0.26	0.36
0.21	0.18	0.18	0.18	0.17	0.18	0.19	0.05	0.04	0.04	0.04	0.05	0.05	0.02	0.05	0.03	0.04
4.21	4.15	3.36	4.77	4.7	5.95	3.87	1.83	1.55	3.58	4.06	2.82	3.57	1.28	3.07	3.25	4.21
851	999	1970	3030	2150	1540	1400	9210	1055	6960	906	1760	1910	5370	1520	1815	7720
-	-	-	-	-	-	8.1	5.7	4.6	6	2.9	7.1	14.8	-	-	-	3.2
-	-	-	-	-	-	182.21	46.98	11.49	63.76	14.77	22.21	60.19	-	-	-	18.87
-	-	-	-	-	-	131.5	59.1	26.4	84.9	35.9	10.7	972.2	-	-	-	51.9
-12.77	-3.19	-5.3	-9.34	-6.84	-9.31	-6.3	-22.05	-17.86	-18.51	-14.83	-22.48	-12.85	6.29	-12.67	12.09	-17.54
5.27	2.56	3.4	2.95	1.04	2.27	0.29	0.27	-0.95	0.11	-0.05	0.16	0.49	-0.04	3.68	0.79	-0.83
-1.17	1.56	2.39	1.35	0.75	1.48	-0.07	-0.8	-0.32	0.59	1.34	-0.35	0.65	0.72	-0.85	2.82	1.45
1.79	0.24	0.05	0.91	0.52	0.91	0.45	-0.38	-0.28	0.15	0.25	0.23	0.19	-0.47	-0.37	-0.51	0.09
-2.88	-2.59	-0.32	-2.92	-1.92	-3.02	-2.98	-3.26	-3.29	-1.78	-3.37	-3.34	-3.08	-3.09	-3.25	-3.04	-1.24
-1.23	-0.19	-0.61	0.38	0.49	1.07	0.47	4.53	5.57	0.62	1.74	2.6	1.42	6.37	5.92	7.5	-0.08
0.06	-0.02	0.05	0.04	-0.05	0.05	-0.04	0.06	0.06	0.05	0.05	0.05	0.05	0.06	0.06	0.07	0.05
0.05	0.04	0.04	0.03	0.02	0.03	0.03	-0.02	-0.02	-0.02	-0.02	-0.02	-0.01	-0.03	-0.01	-0.02	-0.02
352.4	593.59	1563.65	2511.81	1651.66	1028.36	870.88	6752.54	434.53	5244.85	366.97	925.79	1227.27	5477.81	961.38	1771.58	6009.72
-	-	-	-	-	-	1	0	-0.69	0.45	-1.9	1.01	8.36	-	-	-	-1.77
-	-	-	-	-	-	156.41	18.12	-9.13	33.45	-5.58	-1.45	33.57	-	-	-	-2.76
-	-	-	-	-	-	81.56	12.54	-12.01	35.65	-2.14	-25.3	807.45	-	-	-	9.75

R9710732	R9710733	R9710734	R9710735	R9710736	R9710737	R9710739	R9710740	R9710742	R9710744	R9710745	R9710746	R9710749	R9710750	R9710751	R9710752	R9710753
K97-175	K97-175	K97-175	K97-175	K97-175	K97-175	K97-175	K97-175	K97-175	K97-175	K97-175	K97-175	K97-175	K97-175	K97-175	K97-175	K97-175
131.5	143.3	149.2	172.9	183.1	196.6	216.6	223.5	242.7	256.7	267.8	281.3	298.1	310.8	327	339.1	346.7
131.6	143.4	149.3	173	183.2	196.7	216.7	223.6	242.8	256.8	267.9	281.4	298.2	310.9	327.1	339.2	346.8
-	-	-	-	-	-	-	-	-	-	-	-	-	-	-	-	-
FA1	FA1	FA1	FA1	FA1	FA1	FA1	FA1	FA1	FA1	FA1	FA1	FA1	FA1	FA1	FA1	FB2
67.63	68.66	61.38	61.63	66.65	64.18	69.02	73.2	63.61	64.62	68.94	63.22	75.48	67.87	71.83	62.65	74.66
14.02	14.42	14.14	16.13	14.72	15.35	14.23	13.64	15.25	14.59	13.88	15.15	13.48	17.17	13.85	20.63	14.1
5.15	3.71	5.55	5.32	4.3	5.28	4.61	2.18	4.82	4.73	3.93	5.23	1.6	2.3	2.41	2.65	1.83
1.77	1.69	3.35	2.19	2.01	2.25	1	1.07	2.24	2.56	1.48	2.79	0.37	1.1	1.69	0.76	0.2
1.3	0.95	1.76	1.61	0.69	1.44	0.97	0.55	1.51	1.34	0.97	1.42	0.66	0.97	0.87	1.08	0.83
0.09	1.69	0.15	0.1	1.65	0.11	0.1	2.73	0.14	2.01	0.99	0.82	0.15	0.25	0.1	0.21	0.11
2.25	4.07	4.92	5.92	4.44	6.19	5.73	3.11	6.09	4.42	5.28	4.98	4.76	5.86	4.55	7.03	4.86
0.83	0.5	0.6	0.68	0.5	0.62	0.47	0.43	0.67	0.62	0.47	0.64	0.61	0.58	0.46	0.81	0.23
0.18	0.14	0.18	0.21	0.12	0.2	0.14	0.11	0.2	0.2	0.07	0.18	0.17	0.17	0.14	0.25	0.01
6.44	3.81	7.07	5.57	4.38	4.09	3.08	2.51	4.88	4.21	3.39	4.78	2.23	3.46	3.36	3.48	2.92
131	119	243	103	83	58	59	49	62	77	97	79	55	47	52	46	29
5	3	6	4	7	4	8	6	8	9	5	3	1	4	4	5	3
2	9	5	2	20	2	48	43	4	2	2	4	5	4	51	14	39
67	24	30	41	37	35	24	69	29	8	12	5	2	7	29	13	9
-	-	-	-	-	-	-	-	-	-	-	-	-	-	-	-	-
0.21	-0.69	-6.81	-14.37	-4.09	-9.13	0.60	8.11	-9.28	-5.53	2.29	-9.25	11.49	-12.45	5.49	-25.78	-8.41
3.33	1.73	3.70	2.79	2.24	2.99	2.70	0.32	2.59	2.71	2.11	3.01	-0.28	-0.06	0.52	-0.14	0.00
0.39	0.26	2.00	0.53	0.54	0.69	-0.42	-0.30	0.69	1.11	0.11	1.24	-1.04	-0.51	0.33	-0.91	-0.85
0.59	0.20	1.05	0.69	-0.08	0.60	0.23	-0.18	0.68	0.57	0.25	0.60	-0.05	0.06	0.15	0.00	0.15
-3.02	-1.40	-2.95	-3.02	-1.48	-3.00	-3.01	-0.20	-2.98	-1.11	-2.07	-2.32	-2.95	-2.90	-3.00	-2.96	-3.35
-1.83	-0.06	0.90	1.17	0.22	1.70	1.69	-0.85	1.64	0.24	1.37	0.62	0.97	0.80	0.61	0.79	1.52
0.30	-0.06	0.05	0.05	-0.07	0.02	-0.08	-0.11	0.07	0.05	-0.07	0.05	0.09	-0.07	-0.08	0.01	-0.04
0.04	0.00	0.04	0.05	-0.03	0.05	0.00	-0.03	0.05	0.06	-0.07	0.03	0.04	0.00	0.00	0.03	-0.05
-290.11	-305.98	-176.06	-333.13	-343.99	-371.05	-365.70	-373.75	-366.87	-349.24	-324.36	-350.16	-366.66	-386.19	-371.40	-393.57	-399.00
-1.31	-3.47	-0.33	-2.89	0.42	-2.71	1.68	-0.10	1.13	2.47	-1.26	-3.62	-5.42	-3.11	-2.30	-2.98	-1.76
-10.30	-3.30	-7.23	-10.57	7.39	-10.48	36.68	33.47	-8.56	-10.38	-10.28	-8.54	-6.98	-8.99	41.18	-2.51	16.32
29.25	-16.04	-9.39	-3.28	-3.69	-7.09	-15.72	33.32	-12.59	-32.28	-27.68	-35.45	-38.09	-34.32	-9.80	-31.09	-25.48

B370161	B370162	B370163	D00005989	Q930244	B370179	B370180	B370187	D00005983	D00005984	D00005985	D00005986	D00005987	D00005988	Q930095	Q930096
K15-301	K15-301	K15-301	K15-281	K15-236	K15-320	K15-320	K15-320	K15-281	K15-281	K15-281	K15-281	K15-281	K15-281	K15-235R	K15-235R
117.6	122.7	135.85	212.75	117.15	114.45	127.95	212.45	147.5	164.8	176.55	183.05	184.45	199.45	86.15	116.7
117.7	122.8	136	212.9	117.35	114.55	128.05	212.55	147.7	165	176.65	183.2	184.65	199.6	86.3	116.95
TF	VF	TF	TF	VF	TF	VF	TF	TF	TF	TF	TF	TF	TF	TF	VF
FB1	FB1	FB1	FB1	FB1	FB2	FB2	FB2	FB2	FB2	FB2	FB2	FB2	FB2	FB2	FB2
76.2	73.1	74.4	78.8	78.5	76.3	76.2	74.9	77.7	76.8	65.6	27.6	50.1	76.1	73.7	57.2
14.05	12.4	11.7	10.45	11.9	13.75	11.05	12.95	12.25	12.95	16.45	21.7	19.5	12.9	15.55	12.7
1.93	1.34	2.62	2.74	1.67	1.77	0.68	1.5	2.22	1.67	2.21	26.4	8.86	2.02	1.86	3.14
0.63	0.68	1	1.15	0.38	0.42	3.68	1.68	0.59	0.37	2.46	0.13	1.98	0.18	0.55	7.07
0.82	0.1	0.47	0.09	0.21	0.8	0.44	1.45	0.79	0.76	2.17	14.35	7.71	0.98	1.28	4.6
0.69	0.32	0.16	2.7	3.01	0.08	4.54	0.26	0.1	0.16	0.22	0.07	0.2	0.13	0.22	0.24
4.18	9.09	6.07	1.75	3.4	4.73	1.2	3.73	4.01	4.01	5.11	2	4.35	4.34	4.82	3.89
0.33	0.27	0.27	0.25	0.29	0.26	0.2	0.28	0.25	0.28	0.33	0.35	0.38	0.23	0.27	0.26
0.03	0.03	0.02	0.02	0.04	0.02	0.01	0.07	0.08	0.07	0.04	0.03	0.06	0.03	0.04	0.04
2.81	1.2	2.2	2.43	1.42	2.53	3.59	4.14	2.82	2.69	5.3	8.3	7.32	2.46	2.73	12.05
2120	3130	5190	1225	3470	1800	2040	769	549	572	977	604	1425	1670	1835	3030
14.1	5.5	5.5	11.7	-	13.8	12.6	5	8.3	6.3	172.6	323.2	7.4	51.7	86.7	17
37.73	44.29	90.18	107.44	-	29.99	59.09	9.97	66.13	11.15	-	150.36	27.33	64.87	681.58	22.15
83.5	62.2	384.1	386.7	-	179.7	13.4	34.1	151	20	1470.1	1108.5	185.4	291.3	966.2	76.7
-6.79	-0.85	4.99	19.86	7.98	-5.21	11.74	-2.25	4.78	-0.41	-24.86	-59.04	-42.71	-0.8	-15.4	-18.36
0.09	-0.28	1.18	1.66	0.13	-0.02	-0.86	-0.18	0.64	-0.02	0.05	13.67	4.08	0.33	-0.13	1.47
-0.47	-0.34	0.05	0.36	-0.63	-0.65	3.16	0.6	-0.42	-0.67	0.85	-0.95	0.25	-0.85	-0.58	5.98
0.14	-0.49	-0.09	-0.49	-0.37	0.14	-0.09	0.81	0.22	0.14	1.07	7.73	4.38	0.36	0.44	3.96
-2.83	-3.12	-3.28	-0.2	-0.26	-3.38	1.72	-3.2	-3.35	-3.29	-3.28	-3.41	-3.32	-3.32	-3.27	-3.21
0.92	6.4	3.71	-0.71	0.77	1.51	-1.46	0.8	1.3	1.07	1.09	-1.66	-0.01	1.41	1.08	1.03
0.05	0.03	0.04	0.06	0.06	-0.01	-0.02	0.03	0.01	0.03	0.01	-0.04	0	-0.02	-0.03	0.01
-0.03	-0.02	-0.03	-0.03	-0.01	-0.04	-0.04	0.01	0.03	0.01	-0.02	-0.04	-0.02	-0.02	-0.02	-0.01
1474.18	2752.02	5158.06	1050.48	3245.1	1222.71	1898.65	322.49	139.16	131.03	322.61	-74.57	494.85	1204.44	1060.32	2577.87
8.19	1.14	1.48	9.65	-	8.19	9.91	0.42	4.09	1.69	127.62	183.02	0.34	46	65.74	12.41
15.31	26.46	78.52	110.91	-	8.96	48.81	-8.8	49.45	-7.65	-	68.72	-0.85	44.8	533.16	3.46
41.29	29.62	379.67	432.22	-	130.97	-18.25	-0.37	121.63	-14.07	1091.26	609.41	86.15	250.69	748.51	42.5

R9710754	R9710755	R9710756	R9710757	R9710758	R9710759	R9710760	R9710762	R9710763	R9710764	R9710765	R9710766	R9710768	R9710769	R9710770	R9710771
K97-175	K97-175	K97-175	K97-175	K97-175	K97-175	K97-175	K97-175	K97-175	K97-175	K97-175	K97-176	K97-176	K97-176	K97-176	K97-176
364	380.3	397.1	405.6	418.7	431.2	438.4	448.6	460.7	467.4	480	22.7	36.2	46.3	55.9	63.4
364.1	380.4	397.2	405.7	418.8	431.3	438.5	448.7	460.8	467.5	480.1	22.8	36.3	46.4	56	63.5
-	-	-	-	-	-	-	-	-	-	-	-	-	-	-	-
FB2	FB2	FB2	FB2	FB2	FB1	FA1	FA1	FA1	FA1	FA1	FB2	FB2	FB2	FB2	FA1
75.95	75.19	70.55	73.02	73.91	69.76	63.5	64.05	63.18	63.02	65.54	72.43	71.54	69.56	67.27	61.95
12.51	13.1	13.61	14.39	13.77	15.6	17.32	13.06	15.02	13.39	13.18	13.28	13.71	13.94	12.73	14.98
1.98	1.76	1.57	2.13	2.15	2.25	2.72	6.71	4.34	4.86	4.9	1.52	1.57	2.31	2.77	4.51
0.75	1.37	3.16	0.21	0.62	1.53	2.11	2.84	2.53	4.07	3.63	1.98	2.16	1.63	3.44	2.91
0.52	0.28	0.95	1.07	0.75	0.75	1.8	1.79	1.72	1.74	1.49	1.3	1.26	1.64	1.7	1.86
0.15	1.42	0.1	0.1	0.1	0.1	0.14	0.18	0.18	0.18	0.18	0.18	0.37	0.14	0.93	0.2
4.03	3.59	4.78	4.94	4.07	4.17	6.03	4.53	4.98	4.42	3.94	4.78	4.8	5.19	3.85	5.21
0.2	0.23	0.3	0.23	0.21	0.43	0.74	0.58	0.66	0.57	0.55	0.28	0.28	0.34	0.28	0.62
0.01	0.01	0.02	0.01	0.01	0.14	0.21	0.18	0.21	0.17	0.17	0.12	0.11	0.14	0.12	0.18
2.99	2.85	4.19	2.75	3.33	4.48	4.78	5	6.09	6.17	5.86	3.66	3.93	4.11	6.05	6.34
47	61	141	161	139	227	89	138	110	107	80	134	132	85	112	66
5	5	1	30	6	5	5	5	5	5	3	1	1	0.5	3	3
20	27	27	43	28	15	10	2	5	15	11	2	4	7	46	13
10	8	5	24	15	6	29	21	50	50	47	2	2	20	24	35
-	-	-	-	-	-	-	-	-	-	-	-	-	-	-	-
1.36	-2.81	-9.81	-11.18	-7.49	-18.77	-16.62	1.38	-8.77	-1.49	2.38	-6.40	-9.37	-12.24	-8.54	-9.80
0.35	0.05	-0.19	0.22	0.33	0.18	0.28	5.46	2.19	3.27	3.40	-0.20	-0.20	0.45	1.10	2.37
-0.28	0.29	1.89	-0.85	-0.46	0.20	0.33	1.72	1.01	2.98	2.56	0.85	0.95	0.44	2.37	1.38
-0.07	-0.33	0.28	0.34	0.09	0.01	0.75	1.23	0.90	1.13	0.88	0.64	0.56	0.89	1.09	1.04
-3.30	-2.08	-3.36	-3.36	-3.36	-3.37	-2.99	-2.91	-2.93	-2.91	-2.91	-3.28	-3.11	-3.32	-2.53	-2.91
1.23	0.63	1.60	1.50	0.90	0.54	0.90	0.88	0.66	0.64	0.18	1.71	1.58	1.86	0.98	0.89
-0.04	-0.02	0.03	-0.04	-0.05	0.10	0.06	0.08	0.07	0.05	0.04	0.02	0.01	0.06	0.03	0.04
-0.04	-0.04	-0.04	-0.05	-0.05	0.06	0.03	0.06	0.06	0.04	0.04	0.06	0.05	0.07	0.06	0.03
-377.60	-366.28	-294.50	-284.07	-297.84	-241.75	-351.27	-272.32	-319.49	-309.78	-337.72	-297.89	-303.71	-348.15	-314.16	-361.92
0.59	0.37	-3.51	21.80	1.05	-0.40	-2.30	-0.93	-1.66	-1.07	-3.19	-3.49	-3.52	-3.99	-1.47	-3.59
1.63	7.45	6.48	19.12	7.10	-6.39	-3.98	-10.15	-7.53	3.92	-0.24	-16.60	-14.82	-12.17	26.99	0.25
-23.45	-25.83	-28.89	-12.52	-19.80	-28.67	-15.90	-16.86	8.16	14.06	11.61	-31.62	-31.68	-15.46	-9.78	-6.27

Q930097	Q930098	Q931943	Q311613	Q721051	Q721071	Q721170	Q930240	Q930282	B370157	B370158	B370160	Q721158	Q721160	17MM-007	17MM-031
K15-235R	K15-235R	K15-235R	K16-417	K15-309	K15-287	K15-300	K15-236	K15-315	K15-301	K15-301	K15-301	K17-448	K17-448	K15-299	K15-301
133.3	136.1	173.75	96.85	165.25	118.35	67.95	95	20.95	47.9	77.55	102.55	346.15	358.45	66.35	30.13
133.5	136.35	173.95	96.9	165.45	118.55	68.15	95.26	21.15	48.05	77.65	102.7	346.3	358.6	66.54	34.36
TF	TF	LT	VF	MS	MI	VF	VF	VF	LT	TF	TF	VF	VF	-	-
FB2	FB2	FB2	FB2	FB2	FB2	FB2	FB2	FB2	FB2	FB2	FB2	FB2	FB2	FA2	FA2
56.5	71.1	77.2	75.7	76.1	71.5	77.6	64.1	77.8	71.6	76.9	41.8	76.5	77	68.2	69.3
16.55	8.02	12.75	12.3	12.9	13.05	12.7	17.95	10.9	13	10.2	11	12.5	12.8	15	11.85
2.71	9.74	2.36	1.3	1.04	4.2	0.95	4.16	0.94	2.59	1.21	3.23	1.06	1.34	3.64	4.27
3.63	0.86	0.12	0.67	0.95	0.45	0.51	0.45	0.78	2.04	1.98	11.15	1.39	0.44	1.72	2.81
3.36	5.85	0.97	0.45	0.52	3.09	0.48	0.75	0.33	1.7	1.89	7.66	0.23	0.41	1.21	1.61
0.12	0.02	0.21	0.24	0.43	0.12	0.21	6.91	0.27	0.12	0.12	0.32	4.72	3.28	1.58	0.1
5.12	0.43	4.03	8.16	4.22	3.61	7.21	2.03	8.06	4.16	3.23	3.43	1.67	2.1	4.29	3.83
0.33	0.15	0.22	0.18	0.22	0.24	0.2	0.3	0.16	0.26	0.14	0.21	0.16	0.17	0.6	0.43
0.03	0.02	0.03	0.03	-	0.03	0.09	0.04	0.03	0.07	0.02	0.02	0.08	0.09	0.17	0.18
8.01	3.73	2.8	1.52	2.8	3.07	1.45	2.36	1.15	4.08	4.28	19.25	1.6	2.1	4.16	5.65
-	275	1135	1200	2300	1255	1475	9990	875	1075	1930	1155	670	960	1905	981
15.9	33.7	8.3	-	-	-	-	-	-	59.2	14.3	0.5	-	-	24.7	4.8
17.73	38.71	80.65	-	-	-	-	-	-	9.42	400.53	17.67	-	-	10.58	58.33
148.5	733.5	33.2	-	-	-	-	-	-	865.8	381.5	79.4	-	-	198.6	69.8
														-	-
-32.08	36.53	1.16	2.41	-0.8	-6.09	1.85	-30.1	14.79	-5.73	19.84	-27.22	1.98	0.66	-3.82	15.11
0.42	13.65	0.69	-0.31	-0.62	2.41	-0.7	1.28	-0.55	0.87	-0.15	2.06	-0.57	-0.32	1.52	3.23
1.73	0.32	-0.91	-0.34	-0.1	-0.6	-0.52	-0.71	-0.13	0.95	1.41	11.73	0.37	-0.6	0.22	2.01
1.96	8.59	0.36	-0.13	-0.09	2.39	-0.12	-0.07	-0.21	1.05	1.74	8.17	-0.36	-0.19	0.41	1.21
-3.36	-3.42	-3.24	-3.2	-3.03	-3.33	-3.24	1.4	-3.14	-3.33	-3.3	-3.08	1.3	-0.22	-1.58	-2.99
1.07	-2.15	1.16	5.53	1.29	0.66	4.32	-1.4	6.48	1.2	1.16	1.1	-1.14	-0.76	0.00	0.54
0.01	-0.01	-0.03	-0.06	-0.03	-0.01	-0.05	-0.04	-0.06	0.01	-0.07	-0.01	-0.08	-0.08	0.02	-0.04
-0.03	-0.02	-0.02	-0.02	-0.05	-0.03	0.04	-0.03	-0.02	0.01	-0.03	-0.03	0.03	0.03	0.02	0.08
-	6.67	695.5	803	1819.1	785.47	1036.85	6579.71	585.44	615.86	1956.55	896.62	249.71	519.05	1421.04	777.99
7.65	48.45	3.76	-	-	-	-	-	-	52.88	13.21	-3.87	-	-	17.45	-0.61
-5.01	42.26	61.12	-	-	-	-	-	-	-9.37	475.72	1.73	-	-	-2.12	59.21
79.42	1117.57	-0.74	-	-	-	-	-	-	804.7	437.22	57.33	-	-	152.31	45.42

R9710772	R9710773	R9710775	R9710776	R9710777	R9710778	R9710779	R9710780	R9710781	R9710782	R9710783	R9710784	R9710785	R9710786	R9710787	R9710788
K97-176	K97-176	K97-176	K97-176	K97-176	K97-176	K97-176	K97-176	K97-176	K97-176	K97-176	K97-176	K97-176	K97-176	K97-176	K97-176
78.2	90.3	102.5	110.5	126.9	135	154.6	172.7	184.8	197.2	201.8	207.6	217.3	222.5	226.3	251.7
78.3	90.4	102.6	110.6	127	135.1	154.7	172.8	184.9	197.3	201.9	207.7	217.4	222.6	226.4	251.8
-	-	-	-	-	-	-	-	-	-	-	-	-	-	-	-
FA1	FA1	FA1	FA1	FA1	FA1	FA1	FA1	FA1	FB2	FB2	FB2	FB2	FB2	FB2	FA1
65.37	66.48	63.88	62.18	66.36	65.01	66.63	61.22	61.22	60.97	67.84	75.13	73.58	73.31	76.98	67.25
14.02	15.18	14.3	14.18	14.55	14	13.71	15.21	15.81	17.67	10.28	10.67	12.53	14.97	13.52	13.52
4.96	4.78	5.17	5.92	4.61	4.73	4.53	5.42	5.86	3.02	1.91	2.06	2.41	2.23	1.86	3.84
2.1	1.45	2.33	2.8	1.78	2.27	2.35	3	3.05	3.35	5.44	2.18	1.37	0.15	0.09	2.68
1.47	1.54	1.67	2.07	1.49	1.5	1.29	1.65	2.34	2.56	3.52	1.62	1.37	0.68	0.34	1.64
0.14	1.51	1.7	0.28	0.17	0.1	0.6	0.2	0.28	1.1	0.34	0.11	0.17	0.15	0.27	0.23
4.86	4.07	4.34	5.13	4.94	4.94	4.34	4.73	4.78	4.86	2.76	3.32	3.76	4.65	4.01	4.48
0.6	0.63	0.58	0.58	0.56	0.49	0.5	0.62	0.67	0.34	0.2	0.21	0.28	0.23	0.2	0.58
0.18	0.2	0.17	0.18	0.15	0.12	0.2	0.2	0.2	0.07	0.05	0.09	0.07	0.03	0.02	0.18
5.44	3.89	4.65	5.4	4.42	4.94	4.13	5.53	4.59	5.23	7.32	3.84	3.91	3.15	2.3	4.55
57	73	71	70	62	66	70	72	165	105	73	61	53	45	70	131
4	4	4	6	4	5	34	33	21	4	1	8	5	10	11	21
48	8	6	4	20	70	17	13	6	25	7	2	27	59	33	32
370	45	24	21	18	37	759	23	72	126	28	45	14	9	5	42
-	-	-	-	-	-	-	-	-	-	-	-	-	-	-	-
-2.13	-6.25	-4.97	-6.17	-3.61	-2.41	0.74	-11.40	-13.63	-31.62	8.01	13.57	-1.14	-13.41	-3.39	2.40
3.14	2.57	3.25	4.06	2.60	2.91	2.80	3.17	3.38	0.51	0.70	0.79	0.78	0.24	0.09	2.12
0.74	-0.05	0.93	1.43	0.34	0.92	1.05	1.43	1.36	1.36	5.63	1.54	0.35	-0.90	-0.95	1.44
0.76	0.71	0.94	1.36	0.73	0.80	0.61	0.82	1.39	1.23	3.71	1.32	0.78	-0.02	-0.28	1.00
-2.96	-1.66	-1.38	-2.82	-2.94	-3.01	-2.47	-2.92	-2.85	-2.66	-3.03	-3.32	-3.28	-3.32	-3.20	-2.86
0.88	-0.26	0.25	1.10	0.77	0.97	0.44	0.36	0.23	0.64	0.56	1.09	0.95	1.09	0.91	0.66
0.06	0.04	0.03	0.03	0.00	-0.06	-0.03	0.03	0.05	0.00	0.00	0.00	0.04	-0.05	-0.06	0.06
0.04	0.05	0.03	0.04	0.01	-0.02	0.07	0.05	0.04	0.00	0.01	0.05	0.02	-0.03	-0.04	0.05
-366.87	-356.06	-353.79	-354.20	-364.03	-357.44	-351.74	-357.15	-274.22	-350.10	-335.51	-352.94	-371.65	-387.06	-359.73	-285.08
-2.35	-2.67	-2.43	-0.35	-2.50	-1.31	29.57	25.05	12.82	-1.59	-3.21	5.00	0.58	3.97	5.80	16.09
37.42	-4.71	-6.27	-8.27	7.62	60.34	5.66	0.06	-6.86	-0.68	-9.92	-16.13	8.63	31.11	12.23	22.05
343.57	2.86	-15.84	-18.71	-22.26	-1.81	764.90	-18.26	25.98	56.23	0.77	19.57	-19.45	-25.95	-28.86	4.93

17MM-033	17MM-034	17MM-061	17MM-062	17MM-074	17MM-075	17MM-077	18MM-115	18MM-116	18MM-117	18MM-119	18MM-121	18MM-122	18MM-123
K15-301	K15-301	K16-372	K16-372	K15-302	K16-372	K16-372	K16-415	K16-415	K16-415	K16-415	K16-415	K16-415	K16-415
118.37	128.51	103.45	585	175.31	62.22	401.11	22.65	93.78	106.92	309.47	562.77	764.27	812.33
118.57	131	106.22	587.25	175.52	62.42	401.32	22.82	93.99	107.08	309.63	562.95	764.41	812.5
-	-	-	-	-	-	-	-	-	-	-	-	-	-
FB1	FB1	FA2	FB2	FB2	FA2	FA2	FB2	FB2	FB2	FB2	FB2	FB2	FA2
59.3	67.2	70.8	74.8	75.3	66.3	65.6	72.6	77.1	74.5	75.9	73.8	76.4	68.1
21	17.25	13.2	12.8	12.1	20.2	15.4	13.75	11.35	11.8	12.25	11.95	11.6	15.95
3.55	1.33	1.69	3.18	1.35	1.96	5.8	2.02	0.72	2.09	1.43	1.61	1.36	2.81
1.18	0.16	2.67	0.26	1.15	0.45	2.2	0.94	0.08	1.18	0.63	1.18	1.07	0.77
1.95	0.21	1.18	1.19	0.66	1.1	1.98	0.82	0.04	1.2	0.48	0.76	0.87	0.7
0.11	0.52	0.14	4.68	0.43	0.12	3.55	2.35	0.31	0.06	0.13	2.68	3.3	7.13
8.02	12.45	6.67	2.33	7.38	7.26	2.39	3.99	9.35	5.17	7.29	4.75	2.54	1.55
0.54	0.35	0.49	0.31	0.24	0.68	0.64	0.29	0.32	0.33	0.23	0.28	0.21	0.5
0.07	0.05	0.15	0.08	0.07	0.21	0.2	0.11	0.06	0.08	0.06	0.08	0.04	0.16
4.19	1.05	3.66	0.88	1.62	3.04	3.61	2.27	0.65	2.83	1.91	1.66	1.76	0.79
3490	-	1450	509	806	2790	2290	2070	4210	702	541	671	818	731
13.6	10.9	4.9	2.7	17.8	0.5	11	5	4.6	1.4	1.6	0.5	4.8	4.9
99.41	76.01	8.23	14.61	93.81	2.84	9.51	16.14	15.44	35.78	8.34	31.32	32	4.88
185.6	29.5	32.1	61.3	860.6	87.1	98.5	49.6	8.9	50.8	41.4	74.9	18.9	29.2
-	-	-	-	-	-	-	-	-	-	-	-	-	-
-39.51	-26.02	8.06	-1.50	3.28	-22.21	-7.99	-8.59	10.45	4.41	2.93	2.68	7.85	-7.85
0.49	-0.67	-0.15	1.49	-0.23	-0.60	3.47	0.21	-0.84	0.59	-0.17	0.06	-0.16	0.55
-0.32	-0.91	1.50	-0.77	0.17	-1.12	0.63	-0.17	-0.94	0.23	-0.38	0.21	0.13	-0.74
0.57	-0.44	0.54	0.58	0.09	0.03	1.11	0.16	-0.55	0.68	-0.10	0.21	0.35	-0.12
-3.38	-3.07	-2.95	1.15	-3.00	-3.02	0.24	-1.30	-3.10	-3.38	-3.31	-0.63	0.13	3.39
1.98	6.26	3.19	-0.53	4.85	1.06	-1.91	0.83	7.55	2.69	4.67	2.18	-0.07	-2.75
0.08	0.01	-0.02	0.06	0.00	-0.07	0.04	0.02	0.11	0.11	-0.01	0.05	-0.02	-0.11
-0.01	-0.02	0.02	0.02	0.02	0.01	0.05	0.05	0.01	0.03	0.01	0.03	-0.01	0.00
1666.76	-	1171.60	75.59	413.47	1582.75	1736.66	1469.85	4243.51	323.86	130.94	281.81	462.63	240.55
3.71	3.52	-1.10	-1.78	14.08	-6.14	3.89	0.14	0.66	-2.94	-2.79	-3.91	0.77	-2.03
41.09	36.97	-3.31	-4.13	79.09	-10.33	-3.39	-3.72	-1.37	19.67	-9.92	14.50	16.23	-7.93
77.72	-11.99	-4.88	26.76	861.64	22.46	52.77	11.89	-23.64	20.67	9.02	45.37	-13.01	-13.62

R9710789	R9710790	R9710791	R9710792	R9710793	R9710794	R9710795	R9710796	R9710797	R9710798	R9710799	R9710800	R9710801	R9710802
K97-176	K97-176	K97-176	K97-176	K97-176	K97-176	K97-176	K97-176	K97-177	K97-177	K97-177	K97-177	K97-177	K97-177
271.3	288.6	310.9	320.1	327.6	337	345.7	351.6	10	14.7	18.9	23.7	30.5	34.1
271.4	288.7	311	320.2	327.7	337.1	345.8	351.7	10.1	14.8	19	23.8	30.6	34.2
-	-	-	-	-	-	-	-	-	-	-	-	-	-
FA1	FA1	FA1	FA1	FA1	FA1	FA1	FB2	FB2	FB2	FB2	FB2	FB2	FB2
60.68	63.49	66	61.99	61.65	56.63	63.45	73.01	72.62	70.29	60.06	46.04	69.83	75.11
15.5	13.86	16.19	14.81	16.15	14.85	16.45	13.18	16.04	10.52	14.63	8.17	11.89	12.73
4.59	5.75	4.38	4.19	5.9	5.53	3.54	1.91	1.26	2.97	5.01	8.18	1.73	2.42
3.91	2.55	0.88	3.43	2.28	4.92	2.36	1.58	0.05	3.18	3.57	11.01	4.82	0.83
1.85	1.84	1.38	2.17	1.63	2.52	1.44	1.14	1.1	2.05	2.47	4.9	0.6	0.74
1.37	0.25	0.37	0.37	1.19	0.25	0.93	0.83	0.15	0.05	0.02	0.21	0.09	0.02
4.53	4.3	4.76	4.55	4.75	4.53	4.82	3.84	5.65	3.93	5.51	3.09	4.21	4.36
0.64	0.58	0.68	0.62	0.68	0.56	0.68	0.28	0.36	0.18	0.33	0.14	0.28	0.3
0.21	0.18	0.2	0.18	0.2	0.21	0.2	0.14	0.02	0.01	0.02	0.02	0.05	0.03
5.4	6.21	4.76	7.28	4.38	8.8	4.8	3.5	2.54	6.46	7.4	16.87	5.53	3.18
129	112	162	62	82	75	77	46	27	30	50	27	41	45
22	8	14	6	80	20	20	4	8	7	21	30	3	9
19	5	10	6	35	10	17	27	260	12	7	7	18	46
136	57	50	33	41	38	19	639	78	58	36	53	4	17
-	-	-	-	-	-	-	-	-	-	-	-	-	-
-13.01	-3.32	-10.65	-9.07	-14.42	-14.48	-13.84	-5.33	-18.07	9.05	-23.38	-4.12	-1.13	-0.79
2.30	4.03	1.93	2.11	3.30	3.41	1.12	0.19	-0.65	1.91	2.67	10.96	0.19	0.75
2.23	1.23	-0.65	1.93	0.61	3.38	0.64	0.48	-0.99	2.77	2.04	15.93	4.07	-0.21
0.97	1.17	0.48	1.37	0.71	1.71	0.51	0.49	0.27	1.86	1.53	6.95	0.04	0.14
-1.82	-2.85	-2.78	-2.75	-2.04	-2.86	-2.29	-2.66	-3.33	-3.39	-3.43	-3.12	-3.35	-3.43
0.09	0.35	0.11	0.30	0.11	0.27	0.10	0.84	1.61	1.88	1.92	1.94	1.63	1.49
0.04	0.04	0.05	0.04	0.05	-0.02	0.04	0.02	0.04	-0.03	0.04	-0.03	0.05	0.05
0.05	0.05	0.04	0.03	0.04	0.06	0.03	0.08	-0.04	-0.04	-0.04	-0.02	0.00	-0.02
-304.96	-308.48	-280.47	-365.12	-352.16	-352.55	-357.92	-380.96	-403.70	-389.00	-381.88	-383.30	-381.49	-380.40
14.14	1.89	6.08	-0.61	65.54	13.09	11.18	-0.62	1.84	3.94	13.63	41.78	-1.26	4.46
5.45	-7.13	-3.39	-6.48	19.14	-2.58	2.65	7.29	185.52	-4.13	-12.47	-7.71	0.56	26.99
87.36	19.56	4.67	-7.84	-3.33	-3.03	-23.45	576.68	27.69	35.88	-2.54	48.13	-29.28	-16.71

18MM-128	18MM-129	18MM-130	18MM-131	18MM-133	18MM-134	18MM-135	18MM-138	18MM-139	18MM-140	18MM-141	18MM-143	R9512893	R9512894
K15-326	K15-326	K15-326	K15-326	K15-326	K15-326	K15-328	K15-328	K15-328	K17-449	K17-449	K17-449	K95-161	K95-161
141.43	146.78	209.91	289.26	393.13	433.17	76.26	170.64	215.48	407.8	525.54	748.86	17.2	46.5
141.59	146.97	210.11	289.41	394	433.44	76.45	170.78	215.6	407.97	525.7	749	17.3	46.6
-	-	-	-	-	-	-	-	-	-	-	-	-	-
FB1	FB1	FA2	FB2	FA2	FA2	FB2	FA2	FB2	FB1	FB2	FB2	FB2	FB1
74.5	75.3	69.4	75.3	66.3	69.5	74	69.1	80.8	73.1	75	68.6	43.78	71.32
12.45	12.45	15.4	13.35	15.55	14.2	14.6	14.05	10.15	13.75	12.3	15.55	18.11	12.24
0.85	2.02	1.67	2.25	4.84	3.01	2.32	4.4	1.95	1.5	2.17	1.09	3.77	1.84
0.79	0.94	1.47	0.91	2.2	1.76	0.42	1.23	0.55	2.21	1.18	2.43	6.77	1.9
0.29	0.55	0.94	0.66	1.48	1.5	1.89	1.22	0.64	0.44	0.42	0.57	4.59	0.49
0.29	2.26	0.1	0.07	0.18	0.21	0.18	0.32	0.14	5.25	4.43	7.16	0.12	0.35
8.32	3.28	5.66	4.52	4.64	4.59	4.37	5.35	3.16	1.76	1.74	1.2	6.65	7.47
0.3	0.29	0.48	0.23	0.57	0.43	0.25	0.52	0.23	0.3	0.25	0.19	0.42	0.32
0.04	0.03	0.14	0.03	0.18	0.13	0.04	0.17	0.06	0.11	0.04	0.07	0.06	0.05
1.74	2.56	3.78	3.28	4.24	4.38	3.5	3.39	2.12	2.04	1.42	2.96	12.81	1.54
1835	751	2030	2040	1595	568	1170	3720	3880	2580	1580	869	-	-
2.7	2.6	6.7	6.7	10.8	4.6	12.3	1.6	4.3	13.7	61.9	69.9	2	10
8.94	26.03	19.29	15.73	23.11	23.48	24.36	4.97	6.95	3.28	2.17	6.13	165	27
12.6	30.8	100.4	18.1	79.5	40.7	143	127.6	53.1	17.6	11.9	27.3	165	54
-	-	-	-	-	-	-	-	-	-	-	-	-	-
0.27	1.07	-4.40	-4.06	-7.93	1.24	-11.26	1.59	25.14	-8.14	1.70	-19.52	-44.62	-1.71
-0.78	0.40	-0.43	0.48	2.52	1.07	0.36	2.55	0.78	-0.27	0.58	-0.76	0.98	0.25
-0.23	-0.08	-0.05	-0.17	0.61	0.36	-0.67	-0.17	-0.35	0.99	0.18	0.94	3.67	0.92
-0.30	-0.04	0.13	0.03	0.62	0.77	1.03	0.50	0.20	-0.19	-0.17	-0.13	2.59	-0.09
-3.16	-1.16	-3.01	-3.38	-2.94	-2.89	-3.29	-2.78	-3.27	1.36	1.08	2.35	-3.36	-3.09
5.59	0.49	1.18	1.44	0.18	0.54	0.94	1.37	1.10	-1.21	-1.04	-1.85	1.80	4.86
0.06	0.05	-0.11	-0.03	-0.03	-0.12	-0.03	-0.03	0.04	0.03	0.01	-0.09	0.05	0.08
-0.01	-0.02	-0.01	-0.03	0.02	-0.01	-0.02	0.03	0.02	0.05	-0.01	0.00	-0.01	0.00
1430.13	334.30	1491.12	1498.34	1065.77	155.75	583.70	3424.70	4386.25	1936.67	1191.83	278.46	-	-
-1.71	-1.81	-0.17	1.88	3.60	-1.79	6.17	-4.84	0.89	8.10	58.90	52.14	-3.05	5.85
-9.45	7.82	5.84	-3.66	9.24	11.67	2.51	-7.23	-9.87	-15.49	-16.27	-13.53	96.18	9.27
-20.78	-2.38	54.57	-16.45	34.10	1.43	89.76	91.83	32.33	-17.40	-21.34	-11.42	81.16	22.01

R9710803	R9710804	R9710805	R9710807	R9710808	R9710809	R9710810	R9710814	R9710815	R9710816	R9710817	R9710818	R9710819	R9710820
K97-177	K97-177	K97-177	K97-177	K97-177	K97-177	K97-177	K97-178	K97-178	K97-178	K97-178	K97-178	K97-178	K97-178
38	39.8	46.7	58.9	59.9	63.7	68.2	37.4	48.2	55.1	73.2	86.5	89.6	104.4
38.1	39.9	46.8	59	60	63.8	68.3	37.5	48.3	55.2	73.3	86.6	89.7	104.5
-	-	-	-	-	-	-	-	-	-	-	-	-	-
FB2	FB2	FB2	FA1	FB2	FB2	FB2	FA1	FA1	FA1	FB2	FA1	FA1	FB2
29.63	75.18	71.37	64.73	62.54	74.72	74.68	64.2	62.56	58.52	75.77	72.16	65.76	68.88
17.57	12.96	13.88	16.17	10.84	12.85	13.68	14.34	16.1	18.38	13.68	14.63	14.1	15.48
9.39	2	2.58	3.8	2.61	2.16	2.21	4.21	5.01	5.76	2.5	1.75	3.5	3.09
10.6	0.81	1.24	1.23	5.46	0.87	0.37	2.83	2.38	1.84	0.11	0.87	3.02	0.72
5.98	0.95	1.14	1.71	3.58	0.87	0.82	1.65	1.45	1.28	0.4	0.44	1.48	0.97
0.25	0.05	0.03	0.1	0.1	0.03	0.07	0.1	1.27	2.25	0.05	3.11	0.17	2.73
6.73	4.46	5.05	5.65	3.79	4.44	4.5	4.82	5	5.36	3.27	3.11	5.78	4.5
0.34	0.23	0.23	0.68	0.23	0.25	0.28	0.52	0.69	0.79	0.28	0.58	0.5	0.37
0.09	0.02	0.01	0.21	0.05	0.05	0.05	0.17	0.21	0.23	0.05	0.18	0.15	0.1
16.67	3.06	4.01	4.86	9.63	3.3	3	6.15	4.76	5.11	3.58	2.48	4.67	2.55
62	41	37	26	19	15	24	127	64	89	43	36	45	45
88	4	6	7	2	2	5	3	6	9	2	5	5	4
15	15	27	50	2	16	14	5	2	4	21	16	102	5
73	20	37	77	92	10	27	33	9	17	3	2	6	8
-	-	-	-	-	-	-	-	-	-	-	-	-	-
-53.82	-2.04	-10.33	-11.72	-2.44	-1.86	-6.34	-4.83	-13.43	-23.64	-5.34	1.79	-2.11	-19.05
5.09	0.30	0.70	1.41	1.39	0.48	0.39	2.26	2.52	2.55	0.66	-0.27	1.60	0.87
6.56	-0.24	0.09	-0.34	5.31	-0.18	-0.69	1.43	0.71	0.01	-0.93	-0.58	1.67	-0.44
3.69	0.33	0.44	0.78	3.56	0.26	0.16	0.91	0.55	0.25	-0.23	-0.32	0.76	0.19
-3.27	-3.40	-3.42	-3.02	-3.33	-3.42	-3.38	-3.01	-1.96	-1.33	-3.40	-0.02	-2.93	-1.23
2.00	1.51	1.76	0.92	1.58	1.53	1.32	0.72	0.35	0.08	0.19	-1.07	1.80	0.84
0.00	-0.02	-0.04	0.05	0.02	0.00	0.01	-0.04	0.06	0.06	0.01	0.01	-0.05	0.05
0.01	-0.03	-0.05	0.05	0.00	-0.01	-0.01	0.03	0.05	0.04	-0.01	0.04	0.01	0.03
-380.48	-385.07	-391.34	-402.62	-402.83	-410.20	-402.81	-297.20	-368.19	-355.58	-385.33	-390.21	-379.58	-388.30
58.60	-0.55	1.00	-0.20	-2.12	-2.48	0.16	-3.46	-1.08	0.62	-2.60	-1.53	-1.34	-1.19
-7.75	-3.92	5.99	32.60	-16.17	-2.82	-5.61	-7.30	-10.57	-9.21	0.83	3.53	92.83	-14.43
18.78	-14.09	0.04	29.01	73.30	-23.72	-8.67	-6.78	-32.12	-26.80	-30.75	-38.26	-34.06	-27.01

R9512895	R9512896	R9512898	R9512899	R9512900	R9512901	R9512902	R9512904	R9512905	R9512906	R9512907	R9512908	R9512909	R9512910	R9512911	R9512912
K95-161	K95-161	K95-161	K95-161	K95-161	K95-161	K95-161	K95-161	K95-161	K95-161	K95-161	K95-161	K95-161	K95-161	K95-161	K95-161
51.7	62.7	82.9	102.8	114.9	120.4	131.6	148.2	154.7	159.1	167	173.1	178.1	189.4	194.2	199.7
51.8	62.8	83	102.9	115	120.5	131.7	148.3	154.8	159.2	167.1	173.2	178.2	189.5	194.3	199.8
-	-	-	-	-	-	-	-	-	-	-	-	-	-	-	-
FB1	FB2	FB1	FB2	FB2	FB2	FA2	FA2	FA2	FA2	FA2	FA2	FA2	FA2	FA2	FA2
68.16	68.99	74.16	77.97	58.11	76.4	65.59	65.04	62.08	65.01	69.75	64.56	72.85	66.36	55.01	64.69
12.57	14.66	12.76	12.2	14.18	13.03	13.84	13.89	14.79	15.19	13.87	13	12.53	14.79	12.39	14.16
2.59	2.81	1.31	0.58	0.67	1.34	1.31	1.02	1.06	1.2	0.96	0.99	1.54	1.11	2.04	1.25
3.64	0.99	1.26	0.22	1.08	0.17	2.14	2.19	3.13	2.43	1.28	2.19	1.28	1.14	1.98	1.4
0.76	1.56	1.06	0.81	10.05	0.72	1.89	1.49	1.71	1.42	1.07	2.4	0.87	2.14	5.45	2.07
0.01	0.14	0.09	0.19	0.11	0.19	0.26	1.43	1.53	0.76	2.83	2.6	0.14	3.73	0.01	2.61
4.23	5.41	4.81	4.01	1.78	4.18	4.57	3.85	4.23	5	3.37	2.98	4.29	2.09	1.8	2.71
0.34	0.33	0.3	0.19	0.33	0.28	0.6	0.68	0.68	0.64	0.46	0.53	0.55	0.66	0.57	0.68
0.05	0.04	0.03	0.03	0.09	0.07	0.19	0.2	0.18	0.16	0.14	0.17	0.07	0.18	0.17	0.19
3.32	3.43	2.99	2.31	6.73	2.74	4.33	5.08	5.43	4.75	2.6	4.25	2.76	3.18	7.35	3.64
-	-	-	-	-	-	-	-	-	-	-	-	-	-	-	-
7	3	3	86	13	5	4	11	76	26	204	10	34	231	6	32
65	69	16	54	383	8	2	2	2	2	2	2	2	8	2	2
103	14	7	2380	3030	20	49	71	36	40	76	107	41	82	116	75
-	-	-	-	-	-	-	-	-	-	-	-	-	-	-	-
-6.80	-15.82	-1.90	5.39	-23.47	-1.25	-1.02	-1.84	-8.90	-7.70	3.20	2.28	14.62	-4.69	-5.37	-3.50
0.95	0.77	-0.35	-1.04	-1.04	-0.34	-0.63	-0.94	-0.97	-0.86	-1.00	-0.90	-0.22	-0.92	0.39	-0.72
2.61	-0.18	0.21	-0.80	-0.07	-0.87	0.81	0.85	1.64	0.88	-0.10	1.01	0.04	-0.32	0.88	0.00
0.17	0.74	0.45	0.24	8.33	0.10	1.22	0.80	0.92	0.60	0.36	1.92	0.25	1.34	5.64	1.36
-3.44	-3.33	-3.36	-3.25	-3.35	-3.26	-2.84	-1.61	-1.60	-2.38	-0.14	-0.20	-2.95	0.56	-3.10	-0.43
1.41	1.82	1.92	1.31	-1.24	1.22	0.64	-0.13	0.00	0.62	-0.63	-0.83	0.82	-2.11	-2.05	-1.38
0.09	0.04	0.05	-0.05	0.05	0.02	0.07	0.15	0.10	0.05	-0.08	0.03	0.07	0.08	0.10	0.13
0.00	-0.02	-0.02	-0.02	0.03	0.01	0.06	0.07	0.03	0.01	0.00	0.05	-0.06	0.03	0.06	0.05
-	-	-	-	-	-	-	-	-	-	-	-	-	-	-	-
2.57	-1.86	-1.48	84.28	7.10	0.39	-2.30	5.02	68.23	18.39	207.41	4.69	32.96	220.65	0.54	26.37
46.59	40.75	-2.71	37.22	321.45	-10.76	-10.27	-10.28	-10.41	-10.46	-10.28	-10.14	-10.05	-4.51	-10.03	-10.32
69.62	-21.49	-26.61	2421.76	2655.84	-14.19	11.24	34.09	-4.85	-1.95	39.44	79.46	7.34	40.38	95.91	36.78

R9710821	R9710822	R9710824	R9710825	R9710826	R9710827	R9710828	R9710829	R9710831	R9710832	R9710833	R9710834	R9710835	R9710836	R9710837	R9710844
K97-178	K97-178	K97-178	K97-178	K97-178	K97-178	K97-178	K97-178	K97-178	K97-178	K97-178	K97-178	K97-178	K97-178	K97-178	K97-179
121.5	130.2	144.7	157.2	171.3	173.1	180.7	203.8	225.9	237.4	244.6	262.3	294.6	325.9	344.4	141.7
121.6	130.3	144.8	157.3	171.4	173.2	180.8	203.9	226	237.5	244.7	262.4	294.7	326	344.5	141.8
-	-	-	-	-	-	-	-	-	-	-	-	-	-	-	-
FA1	FA1	FB2	FA1	FA1	FA1	FA1	FA1	FA1	FA1	FB2	FB2	FB2	FA1	FA1	FA1
67.01	68.88	73.58	64.01	65.34	63.18	66.69	71.79	67.73	64.5	72.37	68.75	71.48	67.3	62.68	70.08
14.86	14.36	11.44	14.65	14.69	16.01	13.63	12.81	13.86	14.86	14.01	15.6	12.67	16.95	16.04	12.6
4.44	2.04	1.91	4.51	4.07	4.38	4.32	1.63	4.8	5.32	2.73	2.77	2.05	1.72	4.98	2.88
1.12	2.45	2.81	2.69	2.63	2.57	2.52	2.31	2.3	2.44	1.19	1.82	2.88	1.34	2.41	3.07
1.21	1.32	0.77	1.57	1.25	1.45	1.21	0.58	0.75	1.13	0.76	0.82	0.87	1.29	0.94	0.5
0.1	0.15	0.95	0.25	2.32	1.96	1.08	3.22	1.51	0.15	0.12	0.01	0.1	0.27	0.15	2.96
6.05	5.44	3.74	5.63	3.93	4.78	4.3	3.08	4.13	5.53	4.84	5.09	4.34	5.46	6.05	1.87
0.64	0.44	0.25	0.61	0.62	0.63	0.55	0.38	0.57	0.61	0.31	0.34	0.21	0.67	0.68	0.47
0.2	0.15	0.1	0.18	0.18	0.2	0.17	0.05	0.18	0.28	0.11	0.11	0.01	0.18	0.23	0.05
3.66	4.19	3.92	5.44	4.25	4.3	4.84	3.31	3.71	4.73	3.18	4.11	4.76	4.21	5.17	4.9
70	115	41	55	69	77	213	52	53	58	36	49	48	43	102	124
6	1	4	3	6	1	6	1	7	7	3	3	5	2	4	5
2	9	21	8	36	11	8	11	2	99	2	14	26	2	27	2
17	11	4	13	41	29	14	1	11	42	1	19	20	36	23	27
-	-	-	-	-	-	-	-	-	-	-	-	-	-	-	-
-4.36	-0.18	5.90	-6.40	-5.25	-12.55	1.22	11.56	1.13	-6.81	-10.03	-19.58	-4.04	-12.20	-13.11	10.95
2.34	0.06	0.46	2.47	2.02	1.97	2.60	-0.16	3.03	3.20	0.81	0.60	0.40	-0.53	2.51	1.32
-0.35	1.04	2.06	1.23	1.16	0.89	1.25	1.18	0.97	0.95	0.04	0.44	1.83	-0.29	0.74	2.10
0.42	0.58	0.25	0.80	0.48	0.56	0.53	-0.10	0.03	0.34	0.09	0.07	0.27	0.35	0.09	-0.18
-3.01	-2.96	-2.40	-2.86	-0.81	-1.33	-1.96	0.55	-1.52	-2.96	-3.34	-3.44	-3.35	-2.88	-2.97	0.31
1.76	1.35	1.29	1.43	-0.27	0.18	0.42	-0.67	0.17	1.25	1.53	1.28	1.49	0.52	1.32	-2.01
0.06	-0.12	0.03	0.04	0.05	0.01	0.02	-0.13	0.03	0.03	0.03	0.03	-0.04	0.01	0.05	-0.02
0.05	0.01	0.06	0.04	0.03	0.04	0.04	-0.09	0.05	0.13	0.04	0.03	-0.04	0.01	0.06	-0.09
-357.49	-309.53	-379.78	-371.40	-357.69	-356.05	-198.72	-366.96	-370.39	-369.23	-392.55	-385.36	-377.21	-389.10	-333.52	-282.87
-0.63	-5.49	-0.04	-3.52	-0.56	-5.59	-0.10	-5.36	0.85	0.35	-1.74	-2.02	0.53	-4.78	-2.87	-0.73
-10.42	-3.26	4.61	-4.43	23.27	-2.38	-3.84	0.11	-10.28	84.52	-16.69	-7.20	7.34	-10.66	12.11	-10.07
-23.61	-29.11	-29.11	-27.34	0.34	-13.91	-25.31	-39.11	-28.71	0.86	-32.61	-18.18	-13.65	-9.36	-19.40	-9.09

R9512913	R9512914	R9512915	R9512916	R9512917	R9512918	R9512919	R9512920	R9512922	R9512923	R9512925	R9512926	R9512927	R9512928	R9512929	R9512930
K95-161	K95-161	K95-161	K95-161	K95-161	K95-161	K95-161	K95-161	K95-161	K95-161	K95-161	K95-161	K95-161	K95-161	K95-161	K95-161
210.8	221.2	232.2	251.9	261.2	269.5	282.5	291.7	319.1	331.1	362.2	373	378	390	409.8	425.8
210.9	221.3	232.3	252	261.3	269.6	282.6	291.8	319.2	331.2	362.3	373.1	378.1	390.1	409.9	425.9
-	-	-	-	-	-	-	-	-	-	-	-	-	-	-	-
FA2	FA2	FA2	FA2	FA2	FA2	FA2	FA2	FA2	FA2	FA2	FA2	FA2	FA2	FB2	FB2
66.99	64.11	67.47	68.64	67.31	64.99	71.41	66.55	61.6	68.08	66.48	62.93	69.11	62.1	72.37	56.33
12.6	14.22	12.86	13.52	13.17	13.89	13.3	13.34	12.51	15.08	13.96	15.56	11.33	13.38	11.85	12.12
1.34	1.47	0.64	0.84	0.3	1.17	0.96	0.95	1.3	0.01	1.17	1	0.64	0.75	0.85	1.37
2.32	2.03	4.98	2.84	4.77	2.61	1.23	2.81	4.65	1.39	2.43	2.5	3.22	4.44	1.98	7.44
1.91	2.44	0.45	1.24	0.37	1.75	1.04	1.73	1.53	1.29	1.62	2.2	1.49	2.26	1.33	2.79
2.85	0.51	5.77	2.46	4.69	0.65	2.27	0.43	2.59	0.19	1.41	0.32	0.11	1.09	1.03	0.22
2.68	5.25	1.15	3.62	1.95	4.86	3.77	4.66	2.86	5.14	2.23	3.14	3.11	3.93	3.48	3.99
0.56	0.7	0.5	0.54	0.48	0.64	0.49	0.58	0.61	0.73	0.62	0.5	0.48	0.62	0.28	0.25
0.17	0.19	0.15	0.17	0.15	0.19	0.08	0.18	0.18	0.21	0.19	0.16	0.15	0.19	0.1	0.11
3.34	3.69	4.01	3.69	4.64	4.33	2.53	5.02	7.08	3.59	4.33	6.2	6.69	5.81	3.99	7.36
-	-	-	-	-	-	-	-	-	-	-	-	-	-	-	-
3	2	44	3	80	5	3	4	18	23	8	9	5	11	6	43
12	2	8	2	14	2	2	2	2	2	2	2	2	2	29	11
94	273	20	35	21	29	18	17	27	40	79	52	30	75	43	53
-	-	-	-	-	-	-	-	-	-	-	-	-	-	-	-
7.38	-4.37	6.36	3.90	4.39	-1.89	8.15	2.61	1.67	-4.28	-0.68	-11.12	18.77	-2.44	1.82	-16.55
-0.46	-0.50	-1.28	-1.10	-1.68	-0.78	-0.96	-0.97	-0.50	-2.00	-0.79	-1.07	-1.19	-1.19	-0.74	-0.22
1.24	0.63	4.19	1.61	3.82	1.29	-0.10	1.62	3.96	-0.10	1.09	0.89	2.69	3.38	1.07	6.70
1.44	1.73	-0.25	0.57	-0.35	1.07	0.38	1.12	1.02	0.48	0.93	1.29	1.15	1.69	0.82	2.30
0.18	-2.59	3.42	-0.46	2.07	-2.43	-0.63	-2.64	-0.10	-2.93	-1.64	-2.81	-2.97	-1.92	-2.35	-3.22
-1.07	1.21	-2.86	-0.27	-2.01	0.93	-0.04	0.92	-0.84	0.79	-1.84	-1.23	-0.17	0.11	0.87	1.32
0.08	0.15	0.00	0.02	-0.03	0.11	-0.03	0.07	0.14	0.14	0.08	-0.10	0.05	0.11	0.05	0.01
0.05	0.05	0.03	0.04	0.02	0.06	-0.06	0.05	0.07	0.06	0.05	0.01	0.05	0.06	0.05	0.06
-	-	-	-	-	-	-	-	-	-	-	-	-	-	-	-
-3.04	-4.45	43.26	-3.27	81.84	-1.26	-3.22	-2.14	14.43	15.68	1.83	1.91	-0.08	5.46	1.94	40.22
1.48	-10.33	-3.33	-10.22	3.09	-10.28	-10.19	-10.19	-10.05	-10.45	-10.29	-10.51	-9.81	-10.20	12.31	-7.07
68.25	238.96	-17.63	-2.60	-17.06	-9.89	-20.57	-21.72	-8.86	-1.67	42.05	8.35	-1.74	41.27	12.16	21.52

R9710848	R9710849	R9710850	R9710851	R9710852	R9710853	R9710854	R9710857	R9710859	R9710860	R9710861	R9710862	R9710863	R9710865	R9718940	R9718941
K97-179	K97-179	K97-179	K97-179	K97-179	K97-179	K97-179	K97-179	K97-179	K97-179	K97-179	K97-179	K97-179	K97-179	K97-182	K97-182
253.4	270.7	285.3	293.1	301.4	309	327.6	366	397.9	430.4	452.8	471.7	483.4	496.3	8.2	20.4
253.5	270.8	285.4	293.2	301.5	309.1	327.7	366.1	398	430.5	452.9	471.8	483.5	496.4	8.3	20.5
-	-	-	-	-	-	-	-	-	-	-	-	-	-	-	-
FA1	FA1	FB2	FA1	FA1	FA1	FA1	FA1	FA1	FA1	FA1	FA1	FB2	FA1	FA1	FA1
62.38	66.48	73.62	64.05	63.13	65.55	68.26	64.91	64.34	68.94	67.41	65.47	75.61	69.77	66.33	67.72
16.5	14.02	12.56	14.59	14.77	14.42	12.71	14.98	16.31	13.8	13.97	15.38	11.93	12.56	14.73	15.42
3.47	4.32	1.92	5.36	5.38	4.65	5.03	5.96	4.48	3.71	3.21	4.42	2.04	5.25	4.19	4.88
3.04	2.81	1.63	2.17	2.56	2.55	2.49	1.37	1.28	1.65	2.58	0.98	0.77	0.57	2	0.98
1.39	1.24	1.13	1.79	1.74	1.11	0.94	1.27	1.34	0.69	1.24	2.15	0.87	1.78	1.9	1.4
0.14	0.56	0.47	1.38	0.09	2.3	2.03	3.46	2.67	2.95	0.85	1.69	2.15	1.09	2	0.52
6.01	5.03	4.34	4.88	5.53	3.99	3.83	4.48	5.46	3.67	5.46	5.73	3.72	5.67	3.19	4.88
0.56	0.44	0.23	0.6	0.6	0.5	0.5	0.74	0.7	0.5	0.44	0.6	0.15	0.6	0.57	0.6
0.18	0.14	0.11	0.18	0.18	0.14	0.14	0.2	0.21	0.15	0.12	0.18	0.01	0.17	0.2	0.2
5.61	4.13	3.28	4.38	5.05	3.89	3.45	2.27	2.64	3.1	3.83	2.64	2.15	2.19	3.16	2.42
63	109	146	85	79	86	104	104	96	33	47	50	33	71	33	197
2	6	6	3	13	7	3	5	0.5	2	0.5	5	0.5	0.5	62	26
32	5	16	2	4	56	11	2	15	2	2	2	4	7	18	516
25	28	15	27	49	44	45	64	43	7	5	27	8	40	275	89
-	-	-	-	-	-	-	-	-	-	-	-	-	-	-	-
-14.96	-0.98	-1.28	-6.10	-7.78	-3.83	8.17	-6.92	-12.57	2.71	0.24	-8.03	4.72	10.85	-4.45	-6.07
1.05	2.47	0.29	3.33	3.29	2.68	3.75	3.78	1.99	1.90	1.33	2.17	0.51	4.07	2.13	2.59
1.24	1.47	0.60	0.72	1.08	1.13	1.41	-0.11	-0.30	0.30	1.24	-0.52	-0.22	-0.78	0.53	-0.52
0.46	0.52	0.54	1.02	0.95	0.36	0.31	0.47	0.43	-0.03	0.53	1.27	0.32	1.30	1.11	0.56
-2.99	-2.53	-2.98	-1.73	-3.02	-0.79	-0.79	0.25	-0.73	0.00	-2.22	-1.51	-1.18	-1.85	-1.13	-2.62
1.13	1.05	1.53	0.70	1.28	-0.14	0.22	0.19	0.71	-0.30	1.52	1.25	1.10	2.40	-1.01	0.44
-0.07	-0.11	-0.02	0.03	0.03	-0.06	0.01	0.15	0.06	-0.04	-0.11	0.00	-0.09	0.13	0.00	0.00
0.02	0.00	0.06	0.04	0.03	0.00	0.02	0.05	0.04	0.01	-0.02	0.03	-0.04	0.05	0.05	0.04
-370.47	-312.93	-278.59	-341.27	-348.21	-339.26	-307.00	-325.03	-340.40	-391.22	-377.07	-378.72	-390.07	-343.79	-393.42	-240.20
-4.74	-0.28	1.57	-3.51	6.30	0.56	-3.07	-1.65	-6.05	-4.39	-5.98	-1.77	-3.91	-5.92	54.72	18.02
15.83	-7.19	-2.46	-10.38	-8.44	44.11	0.21	-10.43	1.00	-10.27	-10.29	-10.48	-14.27	-4.27	5.40	474.30
-18.21	-11.20	-18.48	-13.34	8.00	4.13	11.24	21.89	-1.91	-32.87	-35.04	-14.72	-25.07	6.07	231.27	43.69

R9512931	R9512932	R9512936	R9512939	R9512940	R9512941	R9512942	R9512943	R9515413	R9515414	R9515415	R9515416	R9515417	R9515418	R9515420	R9515421
K95-161	K95-161	K95-161	K95-161	K95-161	K95-161	K95-161	K95-161	K95-081	K95-081	K95-081	K95-081	K95-081	K95-081	K95-081	K95-149
437.8	457	514.8	539.4	84.3	161.4	285.8	429.4	12.4	18.4	44.2	53.8	65.5	76.4	15.4	5.6
437.9	457.1	514.9	539.5	84.4	161.5	285.9	429.5	12.5	18.5	44.3	53.9	65.6	76.5	15.5	5.7
-	-	-	-	-	-	-	-	-	-	-	-	-	-	-	-
FB2	FB2	FB2	FB2	FB1	FA2	FA2	FB2	FB1	FB1	FB1	FB1	FB1	FB1	FA2	FA2
68.64	75.11	73.94	67.25	75.97	63.47	67.37	74.13	64.6	74.18	61.61	71.4	67.09	67.18	68.94	70.79
15.57	11.77	13.07	15.5	12.78	13.15	13.1	13.5	18.6	12.25	17.44	13.4	13.49	12.28	12.39	12.8
0.68	0.39	0.64	0.29	0.15	1.19	0.01	0.57	1.33	1.38	0.65	0.34	1.43	4.07	0.74	1.1
2.27	2.63	1.64	2.68	0.69	4.06	2.98	0.41	1.2	1.02	3.39	1.22	1.11	0.95	2.73	1.36
0.27	0.3	0.39	0.74	0.2	1.9	1.77	1.3	1.05	0.27	0.73	0.62	0.23	0.38	1.4	1.14
5.61	2.69	3.26	5.72	5.03	0.3	2.04	0.11	0.01	0.01	0.01	0.01	0.16	0.01	2.67	1.22
1.96	2.43	2.75	2.49	1.55	4.69	3.74	4.66	7.86	7.92	10.24	8.18	9.55	6.84	3.23	4.19
0.2	0.26	0.29	0.28	0.35	0.6	0.56	0.25	0.49	0.32	0.44	0.34	0.35	0.33	0.56	0.58
0.06	0.07	0.09	0.1	0.04	0.17	0.15	0.08	0.05	0.05	0.07	0.05	0.04	0.05	0.17	0.17
2.79	3.02	2.3	2.74	1.25	5.31	4.7	2.61	3.55	1.88	4.26	2.36	1.74	3.4	4.07	2.89
-	-	-	-	-	-	-	-	1612	1321	1661	3634	20347	14820	1158	1767
5	12	3	3	6	32	58	5	12	20	11	9	9	17	26	76
4	6	13	32	30	2	47	2	10	16	5	32	1140	304	20	2
17	10	14	55	4260	63	28	24	121	97	181	81	296	1210	70	87
-	-	-	-	-	-	-	-	-	-	-	-	-	-	-	-
-19.56	5.27	-3.85	-20.44	-0.23	0.25	4.85	-5.94	-31.34	1.17	-30.59	-7.99	-12.45	-6.19	10.98	10.49
-1.09	-1.22	-1.02	-1.40	-1.49	-0.69	-2.00	-1.11	-0.74	-0.22	-1.17	-1.32	-0.30	2.53	-1.14	-0.76
0.80	1.78	0.55	1.15	-0.35	3.05	1.87	-0.65	-0.22	0.02	1.42	0.12	0.01	-0.06	1.76	0.10
-0.38	-0.27	-0.22	0.01	-0.40	1.34	1.20	0.62	0.12	-0.32	-0.07	-0.01	-0.38	-0.21	0.88	0.53
1.09	-0.57	-0.31	1.20	1.51	-2.78	-0.84	-3.35	-3.44	-3.44	-3.44	-3.44	-3.30	-3.44	0.03	-1.72
-1.24	-0.22	-0.17	-0.80	-1.30	1.02	-0.01	1.52	2.50	5.31	4.57	4.86	6.09	4.19	-0.37	0.60
-0.08	0.03	0.03	-0.02	0.10	0.10	0.06	-0.01	0.09	0.08	0.07	0.07	0.08	0.09	0.09	0.09
-0.01	0.02	0.03	0.03	-0.01	0.04	0.02	0.02	-0.02	0.00	0.00	-0.01	-0.02	0.00	0.06	0.05
-	-	-	-	-	-	-	-	665.88	932.33	773.80	2988.31	18558.35	14764.20	933.28	1581.70
-0.40	8.39	-1.55	-2.00	1.47	28.89	57.89	0.22	3.68	16.11	3.50	4.02	3.96	12.99	24.02	79.85
-15.26	-12.08	-5.97	7.49	11.05	-10.16	39.80	-16.63	-11.72	-2.05	-14.88	11.56	1045.10	293.08	11.10	-10.10
-19.77	-22.82	-20.03	11.15	4161.77	29.43	-9.16	-11.14	48.36	66.15	97.11	42.57	242.65	1206.62	41.92	58.60

R9718943	R9718944	R9718945	R9718946	R9718947	R9718948	R9718949	R9718950	R9718951	R9718952	R9718953	R9718954	R9718955	R9718956	R9718957	R9718958
K97-182	K97-182	K97-182	K97-182	K97-182	K97-182	K97-182	K97-182	K97-182	K97-182	K97-182	K97-182	K97-182	K97-182	K97-182	K97-182
32.5	35.5	52	58	64	70.3	76	82.5	88.4	94.4	100.8	106.4	111.7	117.7	124	130
32.6	35.6	52.1	58.1	64.1	70.4	76.1	82.6	88.5	94.5	100.9	106.5	111.8	117.8	124.1	130.1
-	-	-	-	-	-	-	-	-	-	-	-	-	-	-	-
FA1	FB2	FB2	FB2	FB2	FB2	FA1	FA1	FA1	FA1	FA1	FA1	FA1	FA1	FA1	FA1
66.84	60.29	66.69	73.06	62.93	53.06	66.12	68.05	62.97	67.76	67.44	66.54	66.52	64.16	66.91	67.06
11.93	10.15	11.6	11.84	10.57	16.77	14.93	14.35	16.48	14.14	13.94	13.68	15.27	15.35	15.64	15.55
4.23	16.43	8.61	5.05	13.72	13.31	5.19	3.92	6.46	5.21	4.32	6.17	4.53	6.32	5.28	5.05
3.48	0.6	0.6	0.49	0.8	0.83	1.83	1.72	0.76	0.49	2.41	1.92	1.5	1.25	0.41	0.81
2.57	3.97	4.67	3.1	5.17	3.75	1.5	1.34	3.27	3.03	1.83	2.3	1.84	2.61	2.4	2.52
0.07	0.01	0.05	0.1	0.12	0.15	0.09	0.02	0.18	1.96	1.25	2.3	2.71	2.81	4.13	2.92
3.67	1.99	1.92	2.72	0.85	4.82	5.11	4.78	4.73	4.21	3.56	2.3	2.77	1.94	1.26	2.03
0.38	0.23	0.21	0.2	0.2	0.3	0.57	0.51	0.68	0.58	0.54	0.54	0.6	0.64	0.66	0.61
0.12	0.05	0.05	0.05	0.05	0.07	0.15	0.18	0.18	0.2	0.15	0.15	0.2	0.21	0.2	0.2
5.98	5.94	4.17	2.96	4.65	5.76	3.61	4.28	3.55	1.78	3.79	3.55	3.29	2.78	2.18	2.78
80	31	34	44	70	64	239	172	305	770	273	233	189	166	60	80
11	296	198	18	135	2833	52	94	57	61	30	9	2	331	10	3
35	18	2844	15	77	1296	79	40	85	8	6	15	6	196	2	20
54	439	11910	275	542	3989	256	63	359	348	116	193	50	1007	131	57
-	-	-	-	-	-	-	-	-	-	-	-	-	-	-	-
11.54	-0.29	-2.69	2.61	-0.12	-35.23	-5.53	-0.97	-14.37	-0.25	0.42	0.80	-6.59	-9.15	-7.72	-7.22
3.15	18.73	7.70	3.73	14.70	8.35	3.05	1.96	3.69	3.35	2.50	4.55	2.31	3.98	2.90	2.71
2.80	-0.29	-0.38	-0.51	-0.08	-0.41	0.34	0.30	-0.77	-0.94	1.07	0.60	-0.01	-0.26	-1.06	-0.69
2.37	4.33	4.47	2.70	5.56	2.22	0.70	0.60	2.12	2.35	1.15	1.68	0.99	1.71	1.47	1.60
-3.02	-3.44	-3.39	-3.34	-3.31	-3.34	-3.02	-3.09	-2.95	-1.09	-1.80	-0.66	-0.53	-0.45	0.73	-0.38
0.31	-0.35	-0.74	0.07	-1.81	0.79	0.81	0.68	0.01	0.17	-0.45	-1.72	-1.53	-2.33	-2.99	-2.27
-0.10	0.04	-0.02	-0.03	-0.01	-0.02	-0.01	-0.05	0.04	0.03	0.00	0.01	0.01	0.04	0.05	0.01
0.00	0.01	0.00	0.00	0.01	0.00	0.00	0.04	0.02	0.06	0.01	0.02	0.05	0.06	0.04	0.04
-328.47	-386.45	-388.00	-378.12	-341.54	-376.86	-193.18	-251.68	-156.84	365.98	-141.18	-178.29	-245.99	-268.72	-370.21	-351.18
6.91	362.60	210.39	14.70	156.31	2121.72	44.15	88.77	43.80	56.24	24.80	3.07	-4.60	307.11	2.80	-3.69
30.29	3.83	3067.21	-2.55	73.19	954.15	64.58	28.16	62.64	-4.15	-6.12	3.57	-6.66	173.33	-10.52	6.33
25.58	510.84	12888.67	258.81	611.85	2960.22	209.13	23.60	276.57	317.68	80.77	164.93	7.37	913.85	81.57	13.06

R9515422	R9515423	R9515425	R9515426	R9515427	R9515428	R9515429	R9515430	R9515431	R9515432	R9515433	R9515434	R9515435	R9515436	R9515437	R9515438
K95-149	K95-149	K95-149	K95-149	K95-149	K95-149	K95-149	K95-149	K95-149	K95-149	K95-149	K95-149	K95-149	K95-149	K95-149	K95-149
13.4	20.5	38.6	46.1	58.1	67.2	75.9	84.9	100.3	103.8	115.8	126.5	134.8	147	164.2	189.9
13.5	20.6	38.7	46.2	58.2	67.3	76	85	100.4	103.9	115.9	126.6	134.9	147.1	164.3	190
-	-	-	-	-	-	-	-	-	-	-	-	-	-	-	-
FA1	FA2	FA2	FA2	FA2	FA2	FA2	FA1	FA2	FA2	FA2	FA2	FA2	FA2	FB2	FB2
69.71	74.43	73.82	69.82	75.9	64.98	62.21	69.49	67.87	68.08	62.46	64.9	62.95	60.7	69.25	55.26
12.9	11.53	11.47	11.28	11.61	15.16	13.9	13.96	13.17	14.78	13.77	14.18	13.67	11.48	10.27	21.68
0.89	0.58	1.3	0.74	0.5	2.5	0.89	0.93	0.01	1.27	3.17	0.04	0.7	0.7	0.92	4.03
1.77	1.65	1.65	3.09	1.27	2.97	3.84	1.91	3.05	1.33	3.94	3.06	3.91	5.79	3.74	0.85
0.77	0.68	0.89	1.44	0.43	1.44	1.89	1.1	1.46	1.06	2.17	1.97	2.32	3.22	2.67	2.32
3.64	2.62	1.78	2.08	3.02	1.74	0.21	1.37	1.83	0.39	0.01	0.51	0.13	0.1	0.01	0.09
2.67	2.65	2.85	2.58	2.36	4.19	4.81	4.08	3.54	5.37	4.96	4.67	4.71	3.71	2.9	7.36
0.73	0.48	0.54	0.52	0.38	0.62	0.68	0.49	0.57	0.61	0.58	0.69	0.64	0.49	0.24	0.5
0.1	0.15	0.15	0.16	0.1	0.18	0.2	0.13	0.18	0.2	0.18	0.23	0.21	0.16	0.05	0.05
3.12	3.26	3.22	5.49	2.55	4.19	6.23	3.7	5.29	3.07	5.68	5.61	6.91	8.97	5.27	5.64
1294	1136	1800	1626	2208	1356	1082	1123	859	1139	737	802	711	648	1236	7708
18	5	190	3	23	18	58	39	3	9	8	6	7	8	1380	18
2	2	2	23	8	2	2	2	2	2	11	47	2	2	239	68
61	93	78	66	33	43	38	23	58	49	71	127	43	65	2520	40
-	-	-	-	-	-	-	-	-	-	-	-	-	-	-	-
8.65	23.94	23.66	20.08	25.14	-7.60	-4.85	2.45	5.01	-2.95	-3.97	-3.38	-2.97	6.96	9.82	-42.97
-1.00	-1.28	-0.36	-1.05	-1.38	0.39	-1.08	-1.04	-2.00	-0.76	1.34	-1.97	-1.26	-1.12	-0.51	0.70
0.55	0.64	0.65	2.54	0.15	1.41	2.58	0.55	1.93	-0.13	2.72	1.70	2.72	5.89	3.55	-0.54
0.11	0.10	0.37	1.09	-0.22	0.62	1.22	0.38	0.85	0.28	1.53	1.26	1.71	3.32	2.68	0.75
0.99	0.20	-0.85	-0.43	0.67	-1.44	-2.89	-1.68	-1.09	-2.73	-3.10	-2.59	-2.97	-2.98	-3.44	-3.40
-1.15	-0.82	-0.55	-0.84	-1.21	-0.14	0.87	0.09	-0.25	1.12	1.08	0.63	0.85	0.54	0.73	1.45
0.26	0.04	0.12	0.11	-0.09	0.03	0.15	-0.05	0.06	0.04	0.05	0.14	0.12	0.06	0.05	0.04
-0.03	0.05	0.05	0.06	-0.02	0.03	0.07	-0.01	0.06	0.05	0.05	0.09	0.08	0.06	0.01	-0.03
1032.87	1006.92	1856.35	1670.45	2339.92	874.87	706.10	743.95	522.59	694.78	352.41	396.57	330.44	394.93	1089.82	4049.82
13.79	-0.19	234.41	-2.63	22.31	10.77	54.19	34.13	-3.19	2.36	1.95	-0.35	0.95	3.63	1686.75	6.01
-10.12	-9.85	-9.84	17.28	-2.35	-10.46	-10.28	-10.29	-10.17	-10.41	-0.76	35.83	-10.25	-9.84	274.40	20.98
28.52	77.06	58.65	44.85	1.09	1.00	-0.49	-16.29	23.80	7.97	34.74	90.01	5.50	42.10	3054.73	-10.29

R9718959	R9718960	R9718961	R9718962	R9718963	R9718964	R9718965	R9718966	R9718967	R9718968	R9718971	R9718972	R9718974	R9718976	R9718977	R9718978
K97-182	K97-181	K97-181	K97-181	K97-181	K97-181	K97-181	K97-181	K97-181	K97-181	K97-181	K97-181	K97-181	K97-181	K97-181	K97-181
134.9	20.1	26.1	32.5	38.5	45	51	53.2	57.4	64	74.9	78	95.9	107.7	111.8	115.9
135	20.2	26.2	32.6	38.6	45.1	51.1	53.3	57.5	64.1	75	78.1	96	107.8	111.9	116
-	-	-	-	-	-	-	-	-	-	-	-	-	-	-	-
FA1	FB2	FB2	FA1	FB1	FB1	FA1	FA1	FB1	FB2	FB2	FA1	FA1	FA1	FA1	FB2
63.41	74.58	69.3	64.13	69.73	70.26	69.94	66.77	73.26	70.98	71.62	65.65	65.2	64.91	59.93	79.26
13.9	14.02	14.18	16.35	14.39	13.92	16.21	15.39	13.28	14.06	14	15.23	15.13	14.27	15.18	11.77
5.36	2.05	3.06	3.42	2	2.67	1.74	3.42	3.66	3.65	1.84	3.38	3.35	8.15	9.92	1.24
3.34	0.17	1.98	2.31	2.15	1.75	1.16	2.13	0.86	0.51	1.45	2.03	2.01	0.43	1.08	0.23
1.76	0.55	1.71	1.89	1.66	1.49	1.34	1.6	0.86	1.46	1.27	1.7	1.74	4.19	3.7	0.56
1.75	3.43	0.34	0.25	0.31	0.74	0.02	0.07	0.07	0.01	0.1	1.21	1.26	0.07	0.09	1.24
3.45	2.54	4.07	4.8	4.19	3.89	5.05	4.8	4.28	4.88	4.9	4.69	4.63	2.83	3.43	2.89
0.57	0.28	0.3	0.63	0.43	0.4	0.5	0.63	0.34	0.25	0.3	0.62	0.62	0.57	0.63	0.23
0.2	0.07	0.09	0.21	0.15	0.14	0.17	0.23	0.02	0.1	0.1	0.23	0.2	0.17	0.2	0.07
4.05	1.86	4.21	4.92	4.65	4.05	3.47	3.82	2.77	3.81	3.2	4.01	4.88	3.9	5.05	1.87
88	61	38	34	43	31	53	69	60	38	58	55	54	72	94	112
27	15	18	9	6	8	7	7	31	6	4	7	6	29	7	6
10	19	51	35	33	50	22	26	2	54	22	21	21	19	8	51
62	70	34	58	50	78	23	60	14	9	24	12	11	195	123	29
-	-	-	-	-	-	-	-	-	-	-	-	-	-	-	-
-3.60	-8.10	-13.54	-12.90	-14.06	-11.52	-7.19	-6.84	-5.62	-11.51	-10.66	-7.25	-7.27	-3.79	-12.52	9.71
3.60	0.20	1.08	1.03	0.11	0.78	-0.45	1.22	1.83	1.63	0.02	1.22	1.21	6.30	7.50	-0.31
2.05	-0.88	0.73	0.61	0.85	0.55	-0.40	0.57	-0.21	-0.57	0.27	0.50	0.49	-1.00	-0.41	-0.78
1.08	-0.10	0.92	0.92	0.86	0.75	0.44	0.75	0.22	0.71	0.55	0.86	0.91	3.51	2.78	0.00
-1.28	-0.37	-3.15	-2.89	-3.18	-2.78	-3.09	-3.04	-3.38	-3.44	-3.36	-1.95	-1.90	-3.04	-3.02	-2.12
-0.55	-0.54	0.79	0.11	0.84	0.69	0.37	0.37	1.23	1.55	1.58	0.32	0.29	-1.28	-0.88	0.27
0.03	0.01	0.02	0.00	0.13	0.12	-0.12	0.03	0.08	-0.02	0.02	0.03	0.03	0.02	0.04	0.00
0.07	0.01	0.03	0.04	0.08	0.07	0.01	0.07	-0.04	0.04	0.04	0.08	0.05	0.03	0.05	0.02
-333.93	-370.13	-391.16	-395.76	-387.28	-396.86	-378.45	-360.79	-368.03	-390.87	-372.75	-373.48	-374.09	-352.62	-335.94	-305.13
21.75	9.03	11.54	1.51	0.81	2.80	-0.22	0.12	24.94	0.93	-0.84	0.18	-0.73	23.06	0.21	1.98
-1.91	-1.43	26.78	18.76	10.37	26.72	7.36	12.20	-16.60	29.85	1.29	7.68	7.81	6.99	-4.71	36.04
24.62	29.33	-3.33	11.34	10.22	37.01	-19.61	16.45	-20.24	-25.46	-11.94	-28.79	-29.68	158.49	77.59	-2.50

R9520451	R9520452	R9520453	R9520454	R9520455	R9520456	R9520457	R9520458	R9520459	R9520460	R9520461	R9520462	R9520464	R9520465	R9520466	R9710636
K95-167	K95-167	K95-167	K95-167	K95-170	K95-170	K95-170	K95-170	K95-170	K95-170	K95-170	K95-170	K95-170	K95-170	K95-170	K97-172
24.3	52.1	62.1	103.6	201.1	226.8	250.2	286.8	305.3	331	350.8	378.3	405.7	423.3	440.7	22.4
24.4	52.2	62.2	103.7	201.2	226.9	250.3	286.9	305.4	331.1	350.9	378.4	405.8	423.4	440.8	22.5
-	-	-	-	-	-	-	-	-	-	-	-	-	-	-	-
FA2	FA2	FA2	FA2	FB2	FA1	FA1	FB2	FA1	FA1	FA1	FA1	FA1	FA1	FA1	FA1
70.9	73	70.11	67.68	74.05	68.51	67.76	70.96	63.5	66.89	67.4	68.25	67.09	65.69	66.28	62.58
13.05	13.3	13.35	15.82	12.87	14.86	14.16	13.09	15.83	12.99	13.42	13.33	13.49	13.67	14.59	15.76
0.09	0.01	0.01	1.18	0.39	0.54	0.41	0.61	0.92	0.01	2.46	1.02	1.16	0.5	0.76	4.53
2.07	0.93	1.39	2.38	1.56	1.58	1.75	2.08	2.13	3.28	2.52	2.67	2.81	3.86	2.49	2.66
1.07	0.3	0.39	0.61	0.52	0.75	0.65	0.81	1.7	1.41	0.97	0.87	1.09	0.63	1	1.75
2.15	2.77	3.64	2.48	3.15	3.18	5.82	1.07	0.28	0.66	3.02	1.51	1.35	5.08	2.4	0.75
5.63	6.08	5.03	3.9	2.58	4.14	2.01	4.26	6.23	5.13	3.41	4.11	4.43	1.9	4.12	4.98
0.43	0.43	0.51	0.72	0.32	0.52	0.44	0.32	0.58	0.49	0.5	0.58	0.55	0.46	0.65	0.67
0.06	0.07	0.09	0.2	0.13	0.15	0.14	0.13	0.17	0.16	0.16	0.15	0.16	0.14	0.18	0.2
2.2	1.09	2.23	2.45	2.9	3.48	2.86	3.98	5.37	5.19	3.13	3.77	3.99	4.03	3.13	4.46
746	747	742	933	869	912	374	980	904	1277	347	439	527	674	805	49
5	11	3	9	6	4	14	6	3	5	9	7	8	8	9	28
19	35	12	8	21	9	7	2	10	42	6	36	19	8	35	7
34	26	18	45	11	18	27	13	20	28	98	63	70	38	148	37
-	-	-	-	-	-	-	-	-	-	-	-	-	-	-	-
9.07	9.88	6.44	-7.72	-2.63	-2.89	-0.35	-6.82	-11.60	4.95	3.10	4.52	2.39	-0.05	-3.87	-12.19
-1.91	-2.00	-2.00	-0.92	-1.26	-1.48	-1.59	-1.05	-1.16	-2.00	0.66	-0.90	-0.76	-1.48	-1.25	2.17
0.86	-0.43	0.07	0.75	0.50	0.10	0.35	0.97	0.51	2.23	1.29	1.47	1.59	2.66	1.04	1.01
0.43	-0.43	-0.34	-0.20	-0.09	-0.03	-0.09	0.18	0.80	0.82	0.29	0.19	0.41	-0.09	0.24	0.85
-0.71	-0.08	0.86	-0.83	-0.37	0.00	2.87	-2.42	-2.85	-2.37	0.16	-1.46	-1.65	2.30	-0.72	-2.42
2.11	2.48	1.32	-0.58	-0.30	-0.11	-2.10	1.27	1.56	1.58	-0.47	0.32	0.61	-2.14	-0.06	0.43
-0.09	-0.09	-0.01	0.10	0.07	-0.06	-0.11	0.06	-0.03	-0.02	-0.02	0.07	0.03	-0.08	0.08	0.05
-0.08	-0.07	-0.05	0.04	0.07	0.00	0.00	0.07	0.01	0.04	0.03	0.02	0.03	0.01	0.04	0.04
405.38	390.85	382.34	431.73	424.92	466.58	-41.87	517.37	404.54	1003.73	-49.95	52.97	142.16	291.07	376.44	-380.78
-0.93	5.53	-3.23	1.77	1.43	-2.59	7.88	1.33	-3.74	-0.90	3.25	1.14	2.12	2.01	2.47	19.34
8.80	25.90	0.70	-5.02	2.05	-3.57	-5.19	-16.57	-3.19	34.65	-5.87	26.90	8.11	-3.86	22.51	-5.92
-2.36	-11.82	-20.64	1.12	-22.76	-22.63	-12.52	-21.01	-21.88	-8.90	65.96	28.49	35.22	0.18	107.28	-6.11

R9718979	R9718980	R9718981	R9718982	R9718983	R9718984	R9718985	R9718986	R9718987	R9718988	R9718990	R9718991	R9718992	R9718993	R9718994	R9718995
K97-181	K97-181	K97-181	K97-181	K97-181	K97-186	K97-186	K97-186	K97-186	K97-186	K97-186	K97-186	K97-186	K97-187	K97-187	K97-187
120.2	92	89.6	124	129.9	13.1	15.8	21	26.7	32.5	41.9	46.4	48.9	7.9	16.4	18.4
120.3	92.1	89.7	124.1	130	13.2	15.9	21.1	26.8	32.6	42	46.5	49	8	16.5	18.5
-	-	-	-	-	-	-	-	-	-	-	-	-	-	-	-
FA1	FA1	FB2	FA1	FA1	FB2	FB2	FB2	FB2	FB2	FA1	FA1	FA1	FA1	FA1	FA1
68.5	66.87	74.05	66.13	60.66	70.3	72.36	70.13	73.91	73.41	64.3	67.41	64.91	64.09	62.9	71.22
13.39	15.35	13.59	15.39	16.07	14.97	13.89	14.52	12.57	13.67	14.77	14.5	17.45	15.64	18.95	14.97
4.5	3.83	1.84	5.19	8.22	2.32	1.75	1.76	1.97	1.37	3.67	3.39	3.35	3.58	2.1	1.85
1.25	1.11	0.95	0.82	0.51	1.04	1.09	0.79	0.25	1.4	2.98	2.41	1.52	2.6	1.8	1.52
2.83	1.53	0.75	2.98	4.78	1.09	0.47	0.49	0.33	1.41	2.06	1.61	1.65	1.8	1.67	0.87
0.07	0.01	1.78	0.12	0.1	1.5	2.83	0.2	0.15	0.12	0.88	0.34	0.25	0.12	0.2	0.31
3.75	5.71	3.83	4.17	3.73	4.76	4.61	8.89	7.76	3.96	3.65	3.93	4.92	4.96	5.8	4.32
0.52	0.62	0.3	0.62	0.67	0.34	0.31	0.33	0.28	0.23	0.6	0.56	0.69	0.64	0.6	0.46
0.15	0.17	0.1	0.18	0.18	0.02	0.02	0.03	0.02	0.01	0.23	0.2	0.25	0.25	0.18	0.1
4.36	4.01	2.25	3.72	4.3	3.03	2.08	1.84	1.67	3.75	5.84	4.57	4.09	5.63	4.88	3.88
115	80	126	137	151	124	80	150	126	62	67	39	48	62	54	49
11	8	2	9	3	7	6	5	7	29	10	15	12	11	6	5
118	33	2	2	7	10	7	35	116	50	32	11	4	10	17	18
153	25	4	53	72	39	19	45	206	14	103	91	45	196	220	10
-	-	-	-	-	-	-	-	-	-	-	-	-	-	-	-
4.46	-6.58	-6.47	-7.45	-15.04	-15.94	-9.48	-14.26	-1.04	-7.46	-6.63	-2.33	-15.84	-10.34	-21.67	-0.75
2.88	1.62	0.07	2.90	5.43	0.31	-0.05	-0.11	0.33	-0.38	1.61	1.39	0.78	1.32	-0.40	-0.21
-0.09	-0.39	-0.15	-0.67	-0.98	-0.16	-0.04	-0.35	-0.78	0.26	1.49	0.97	-0.18	0.98	-0.06	0.03
2.31	0.69	0.10	2.05	3.56	0.32	-0.17	-0.17	-0.26	0.70	1.27	0.85	0.61	0.91	0.52	0.08
-3.03	-3.10	-1.80	-3.00	-3.02	-2.19	-0.88	-3.27	-3.30	-3.34	-2.24	-2.77	-2.90	-3.00	-2.96	-2.81
-0.09	1.25	0.72	-0.22	-0.79	1.18	1.35	4.88	4.95	0.82	-0.57	-0.22	-0.06	0.45	0.29	0.03
0.00	0.02	0.03	0.02	0.04	0.04	0.04	0.04	0.03	-0.03	0.03	0.00	0.01	0.03	-0.10	-0.12
0.02	0.02	0.04	0.03	0.02	-0.04	-0.04	-0.03	-0.03	-0.04	0.08	0.06	0.06	0.09	-0.01	-0.05
-301.09	-350.20	-308.20	-296.53	-289.34	-320.64	-352.40	-294.87	-298.73	-367.81	-360.03	-386.88	-385.99	-368.35	-384.56	-378.40
5.45	1.08	-2.59	2.01	-3.78	1.45	1.00	-0.10	2.57	22.26	3.35	8.55	3.50	3.73	-1.90	-1.64
115.79	18.89	-16.64	-10.48	-6.04	-10.08	-12.15	11.85	97.65	27.54	19.13	-1.34	-9.04	-3.08	0.67	5.11
125.93	-16.56	-29.81	9.84	24.91	-0.72	-16.30	5.49	172.75	-20.62	61.17	51.02	-2.74	142.01	128.59	-30.53

R9710637	R9710639	R9710640	R9710641	R9710643	R9710644	R9710645	R9710648	R9710649	R9710650	R9710651	R9710652	R9710653	R9710654	R9710655	R9710656
K97-172	K97-172	K97-172	K97-172	K97-172	K97-172	K97-172	K97-172	K97-172	K97-172	K97-172	K97-172	K97-172	K97-172	K97-172	K97-172
42.8	54.5	61.9	70.6	76.3	81.1	83.8	97	108.5	127.5	139.9	151.4	162.9	171.8	183.8	197.3
42.9	54.6	62	70.7	76.4	81.2	83.9	97.1	108.6	127.6	140	151.5	163	171.9	183.9	197.4
-	-	-	-	-	-	-	-	-	-	-	-	-	-	-	-
FB2	FA1	FA1	FA1	FA1	FA1	FA1	FA1	FA1	FA1	FA1	FA1	FA1	FB2	FB2	FB2
72.9	66.44	69.33	64.94	60.16	45.58	63.15	66.36	66.61	67.22	65.51	65.51	57.22	72.9	73.83	77.36
14.42	15.51	13.8	14.85	15.8	19.46	14.75	14.3	14.14	13.17	14.47	15.48	16.4	13.13	13.38	13.39
2.21	4.17	3.41	4.34	3.81	10.46	4.61	5.26	4.11	4.01	4.21	4.01	5.55	2	2.06	1.19
0.43	1.59	1.92	2.19	3.65	4.19	3.08	1.79	2.23	2.25	2.41	1.92	3.42	1.28	0.89	0.18
1.3	0.97	1.25	1.16	1.66	3.57	1.86	1.44	1.35	1.37	1.32	1.29	2.25	1.37	0.95	0.58
0.28	2.18	2.14	3.51	3.95	0.43	0.77	1.99	0.28	0.18	0.6	1.47	0.34	0.18	0.15	0.2
5.07	4.38	3.86	3.25	3.09	6.13	4.53	3.9	4.57	5.13	4.65	4.03	5.07	3.67	3.89	3.98
0.28	0.66	0.56	0.62	0.64	0.89	0.61	0.6	0.57	0.51	0.55	0.66	0.69	0.3	0.28	0.27
0.11	0.18	0.17	0.18	0.2	0.25	0.18	0.17	0.15	0.11	0.15	0.18	0.2	0.07	0.07	0.07
2.53	3.03	3.15	3.61	5.98	7.69	5.73	3.17	5.05	4.53	5.11	4.84	6.69	4.46	3.74	2.4
110	108	158	78	110	94	92	159	167	157	145	55	32	25	30	43
19	50	6	54	9	57	29	75	30	59	86	10	8	10	3	3
40	18	2	172	13	4	6	10	10	11	8	20	4	18	13	4
11	52	33	668	237	183	18	79	82	55	41	44	30	58	12	14
-	-	-	-	-	-	-	-	-	-	-	-	-	-	-	-
-11.42	-7.64	3.12	-6.34	-14.57	-35.88	-7.68	-2.45	-1.43	4.29	-4.10	-8.39	-19.20	-5.17	-5.60	-2.33
0.29	1.90	1.59	2.24	1.50	5.81	2.54	3.34	2.22	2.42	2.22	1.76	2.91	0.28	0.30	-0.52
-0.65	0.05	0.58	0.70	1.92	1.69	1.59	0.38	0.85	1.04	0.98	0.36	1.59	0.20	-0.19	-0.86
0.54	0.15	0.56	0.37	0.77	1.91	1.07	0.70	0.63	0.75	0.56	0.45	1.23	0.72	0.30	-0.05
-3.20	-1.06	-0.85	0.33	0.53	-2.79	-2.35	-1.09	-2.82	-2.91	-2.51	-1.73	-2.81	-3.28	-3.31	-3.26
1.60	-0.06	-0.10	-0.98	-1.32	0.42	0.30	-0.20	0.54	1.50	0.51	-0.38	0.33	0.70	0.84	0.92
0.00	0.05	0.03	0.04	0.02	0.10	0.04	0.05	0.02	0.00	-0.01	0.06	0.05	0.04	0.02	0.01
0.04	0.03	0.04	0.03	0.04	0.04	0.03	0.03	0.01	-0.02	0.01	0.03	0.03	0.01	0.01	0.01
-328.88	-324.73	-259.49	-349.61	-324.75	-355.75	-335.29	-264.29	-254.23	-252.62	-280.26	-374.33	-397.62	-400.93	-396.67	-384.47
12.15	40.38	-0.18	46.39	1.78	36.10	22.09	69.78	24.36	58.65	79.94	2.90	0.59	5.15	-1.62	-1.62
16.42	4.50	-10.27	156.08	-0.41	-9.39	-6.46	-2.20	-2.09	-0.23	-4.33	6.42	-8.83	-1.24	-6.26	-14.73
-23.91	8.51	-5.47	613.97	177.90	96.52	-22.50	40.10	44.09	20.49	0.96	1.09	-13.65	22.08	-22.22	-20.35

R9718996	R9718997	R9718998	R9718999	R9719000	R9719001	R9719002	R9719003	R9719004	R9719005	R9719006	R9719012	R9719015	R9719019	R9719022	R9719024
K97-187	K97-187	K97-187	K97-187	K97-187	K97-187	K97-187	K97-187	K97-187	K97-187	K97-187	K97-182	K97-182	K97-182	K97-182	K97-182
20.9	26.5	32.7	36.8	39.7	45.5	51.8	56.6	59.3	62.9	64.6	16.5	38.4	43.2	47.3	66.2
21	26.6	32.8	36.9	39.8	45.6	51.9	56.7	59.4	63	64.7	17.5	38.9	44.9	48.8	67.7
-	-	-	-	-	-	-	-	-	-	-	-	-	-	-	-
FA1	FA1	FA1	FA1	FA1	FA1	FA1	FA1	FA1	FB2	FB1	FA1	FB2	FB2	FB2	FB2
67.7	65.97	68	66.23	64.58	62.02	66.15	63.91	73.08	65.68	69.84	62.81	55.27	51.81	61.65	50.31
16.48	13.27	15.98	16.13	14.4	18	15.07	16.45	15.03	9.01	13.43	14.8	11.71	9.51	12.97	13.14
1.72	5.03	3.35	4.38	4.38	5.76	3.42	4.23	1.42	9.48	2.19	6.21	16.87	23.12	11.73	17.5
2	3.2	1.4	0.98	3.15	1.14	2.43	1.5	0.44	2.82	2.83	2.06	1.16	1.21	0.68	2.11
1.58	1.62	1.15	1.11	1.77	1.57	1.52	1.54	0.46	0.79	1.19	2.63	4.28	3.79	5.73	6.46
0.07	0.01	0.15	0.09	0.03	0.21	0.15	0.1	3.5	0.01	0.81	0.15	0.1	0.41	0.01	0.1
4.94	3.95	4.96	4.94	4.48	5.3	4.63	5.3	2.95	3.25	4.4	4.48	1.96	0.61	2.03	1.29
0.51	0.56	0.68	0.66	0.5	0.75	0.63	0.68	0.61	0.21	0.34	0.6	0.21	0.15	0.25	0.23
0.17	0.18	0.21	0.25	0.18	0.25	0.23	0.21	0.2	0.07	0.11	0.23	0.07	0.05	0.09	0.07
4.17	5.46	3.52	4.63	5.38	4.28	4.71	5.3	1.9	7.86	4.19	4.53	6.3	6.4	4.55	6.11
66	64	67	66	70	56	61	51	40	28	59	-	-	-	-	-
3	16	7	16	6	10	4	7	4	48	4	92	285	2700	97	5430
5	4	2	6	5	7	22	117	5	33	8	49	970	1680	309	338
94	38	48	53	47	72	49	174	2	6	0.5	385	6210	11400	370	1150
-	-	-	-	-	-	-	-	-	-	-	-	-	-	-	-
-10.20	2.36	-8.05	-10.23	-4.72	-19.83	-6.10	-13.44	0.77	16.70	-9.60	-8.22	-15.64	-6.48	-15.22	-26.86
-0.49	3.50	1.04	1.94	2.42	2.65	1.29	1.73	-0.63	11.60	0.41	4.09	16.49	28.96	9.74	15.12
0.32	2.06	-0.17	-0.56	1.74	-0.52	0.90	-0.12	-1.02	2.91	1.62	0.58	0.22	0.57	-0.37	0.99
0.63	1.01	0.28	0.24	1.03	0.51	0.71	0.60	-0.32	0.51	0.52	1.82	4.01	4.42	4.97	5.59
-3.05	-3.10	-2.97	-3.03	-3.08	-2.94	-2.96	-3.02	0.28	-3.43	-2.69	-2.96	-3.34	-2.91	-3.44	-3.35
0.20	0.17	0.35	0.29	0.36	0.12	0.30	0.52	-1.31	1.72	1.30	0.24	-0.72	-2.02	-0.85	-1.59
-0.11	0.05	0.05	0.03	-0.06	0.04	0.04	0.04	0.03	0.05	0.07	0.03	-0.02	-0.05	0.00	-0.03
0.01	0.05	0.05	0.08	0.04	0.06	0.08	0.04	0.05	0.04	0.05	0.08	0.02	0.01	0.03	0.01
-367.75	-355.86	-365.02	-366.49	-355.30	-380.75	-367.13	-380.91	-387.29	-385.78	-369.60	-	-	-	-	-
-3.85	11.04	-0.13	7.93	-0.44	1.58	-2.64	-0.31	-2.63	62.61	-0.69	83.91	301.88	3568.83	89.69	5196.56
-7.96	-7.99	-10.55	-6.97	-7.33	-6.72	8.86	91.07	-7.54	27.61	-10.99	35.78	1024.06	2204.87	281.36	305.25
42.71	1.40	3.44	7.54	7.22	17.92	7.04	113.59	-38.31	-25.13	-33.04	338.08	6640.96	15053.61	325.53	1067.99

R9710657	R9710658	R9710659	R9710660	R9710661	R9710662	R9710663	R9710664	R9710665	R9710666	R9710669	R9710670	R9710671	R9710673	R9710674	R9710675
K97-172	K97-172	K97-172	K97-172	K97-172	K97-172	K97-172	K97-172	K97-172	K97-172	K97-173	K97-173	K97-173	K97-173	K97-173	K97-173
207.2	209.3	222.3	234.2	245.8	254.2	258.7	264.2	274.4	294.9	9	42.8	53.6	70.3	80.8	87.2
207.3	209.4	222.4	234.3	245.9	254.3	258.8	264.3	274.5	295	9.1	42.9	53.7	70.4	80.9	87.3
-	-	-	-	-	-	-	-	-	-	-	-	-	-	-	-
FB2	FB2	FB2	FA1	FA1	FA1	FA1	FB2	FB2	FB2	FA1	FA1	FA1	FA1	FB2	FB2
73.72	73.83	69.83	60.93	64.75	63.68	61.75	70.45	71.83	70.77	72.11	62.38	62.02	63.38	64.18	66.69
13.03	14.22	12.94	15.02	13.65	15.31	16.79	12.59	13.35	13.03	12.82	15.82	14.22	14.92	16.69	16.53
3.65	2.48	1.88	4.73	7.9	5.03	5.03	2.79	2.27	2.08	5.63	5.55	5.28	4.76	2.15	1.07
0.15	0.1	2.46	4.28	1.3	2.09	2.35	2.44	1.96	2.07	0.28	1.82	2.81	2.86	0.69	0.38
0.67	0.76	1.98	1.77	2.13	1.9	2.01	1.42	1.16	1.32	1.07	1.29	1.86	0.93	0.5	0.47
0.1	0.1	0.14	1.87	3.86	1.82	1.91	1.61	1.29	1.26	0.12	0.05	0.09	1.26	0.49	0.5
3.97	4.3	4.05	3.56	1.53	4.09	4.8	3.36	3.86	3.75	3.68	4.23	4.78	4.51	12.88	12.67
0.28	0.23	0.31	0.62	0.56	0.62	0.72	0.27	0.28	0.28	0.87	0.68	0.61	0.62	0.21	0.23
0.05	0.02	0.07	0.18	0.15	0.18	0.21	0.12	0.14	0.11	0.18	0.2	0.18	0.18	0.02	0.02
3.69	3.28	5.51	6.09	3.35	4.26	3.79	3.86	3.2	4.34	2.8	6.9	7	5.53	1.85	1.12
18	24	30	131	67	115	132	48	50	49	85	84	57	83	33	36
10	15	5	22	165	17	15	5	4	1	22	7	4	5	4	2
20	42	6	6	2	6	5	65	2	5	2	2	2	17	4	9
12	17	18	37	211	64	71	129	16	12	40	61	35	25	7	6
-	-	-	-	-	-	-	-	-	-	-	-	-	-	-	-
-3.84	-9.70	-7.13	-10.94	-0.95	-9.45	-16.45	-4.62	-7.33	-6.69	11.86	-12.59	-6.51	-8.16	-26.65	-24.27
1.89	0.56	0.19	2.57	6.41	2.77	2.35	1.15	0.50	0.37	4.38	3.09	3.39	2.63	-0.02	-0.82
-0.89	-0.94	1.36	2.70	-0.06	0.54	0.59	1.41	0.82	0.97	-1.13	0.23	1.43	1.35	-0.51	-0.74
0.05	0.08	1.33	0.95	1.51	1.04	0.98	0.82	0.50	0.68	0.45	0.42	1.14	0.14	-0.22	-0.24
-3.35	-3.36	-3.31	-1.30	1.00	-1.38	-1.45	-1.84	-2.23	-2.23	-2.97	-3.06	-3.02	-1.88	-3.08	-3.07
1.01	0.98	1.12	-0.72	-2.53	-0.28	-0.01	0.54	0.82	0.80	0.01	-0.27	0.73	0.23	6.89	6.82
0.02	-0.04	0.06	0.04	0.03	0.02	0.06	0.02	0.02	0.02	0.42	0.06	0.06	0.04	-0.09	-0.07
-0.01	-0.04	0.01	0.03	0.02	0.03	0.04	0.07	0.08	0.05	0.06	0.04	0.04	0.03	-0.04	-0.04
-407.50	-403.65	-395.71	-299.15	-354.61	-316.76	-311.66	-376.90	-377.75	-377.56	-329.57	-348.78	-367.70	-345.09	-400.00	-397.48
5.22	8.84	0.43	14.80	169.30	9.65	6.49	0.56	-0.67	-3.47	18.46	-0.06	-2.41	-1.63	-1.42	-2.91
0.83	18.68	-12.66	-6.57	-10.24	-6.68	-8.04	46.49	-16.61	-13.66	-10.11	-10.54	-10.33	4.20	-15.47	-11.64
-21.92	-18.47	-16.01	-4.42	184.56	20.55	21.25	95.44	-18.43	-21.92	5.13	15.83	-4.45	-15.88	-28.23	-28.94

R9719028	R9902916	R9902917	R9902918	R9902920	R9902921	R9902922	R9902925	R9902926	R9902927	R9902928	R9902929	R9902930	R9902933	R9902934	R9902935
K97-182	K98-188	K98-188	K98-188	K98-188	K98-188	K98-188	K98-188	K98-188	K98-188	K98-188	K98-188	K98-188	K98-188	K98-188	K98-188
72.6	28.2	35.7	43.7	52.7	62.3	70.3	75.6	80.6	83.3	92.8	107.8	117.5	144.8	148	162.2
74.1	28.3	35.8	43.8	52.8	62.4	70.4	75.7	80.7	83.4	92.9	107.9	117.6	144.9	148.1	162.3
-	-	-	-	-	-	-	-	-	-	-	-	-	-	-	-
FA1	FA2	FA2	FA1	FB2	FB2	FA1	FA1	FB2	FB2	FB2	FB2	FB2	FA1	FB2	FA1
69.05	66.76	64.41	67.98	71.15	74.97	50.24	47.61	72.91	73.59	72.84	73.23	71.62	58.86	74.37	70.69
14.06	14.85	15.8	14.64	11.06	11.85	22.43	21.72	11.9	12.3	12.44	12.26	11.57	18.1	12.85	13.68
5.4	5.07	6.03	3.84	3.26	2.45	7.8	10.9	2.49	3.19	2.64	1.64	2.34	6.98	1.29	3.77
0.86	2.33	2	3	3.32	1.62	0.62	0.3	1.37	1.21	1.12	0.81	1.28	2.25	1.62	2.21
0.87	1.33	0.81	0.88	1.96	0.82	1.86	1.71	1.12	1.33	0.95	0.75	3.75	1.87	0.56	1.29
0.34	1.94	0.75	0.47	0.18	0.66	0.2	1.89	0.21	0.31	0.5	0.23	0.21	0.43	4.09	1.69
4.48	3.68	4.13	4.46	4.13	4.07	8.02	6.8	4.96	5.13	6.26	7.32	4.92	5.59	2.07	3.05
0.49	0.66	0.67	0.58	0.21	0.23	0.82	1	0.23	0.23	0.25	0.23	0.21	0.7	0.28	0.52
0.2	0.2	0.18	0.17	0.07	0.05	0.2	0.14	0.07	0.05	0.09	0.07	0.07	0.18	0.01	0.15
3.56	2.29	4.38	3.05	3.01	2	6.55	5.13	2.98	2.27	1.95	2.01	3.47	3.83	1.87	2.18
-	-	-	-	-	-	-	-	-	-	-	-	-	-	-	-
392	-	-	-	-	-	-	-	-	-	-	-	-	-	-	-
143	-	-	-	-	-	-	-	-	-	-	-	-	-	-	-
1680	-	-	-	-	-	-	-	-	-	-	-	-	-	-	-
-	-	-	-	-	-	-	-	-	-	-	-	-	-	-	-
1.48	-4.56	-10.65	-2.41	5.92	4.58	-37.37	-38.06	2.06	0.25	-1.35	0.13	2.86	-22.65	-2.21	5.21
3.58	2.96	3.54	1.81	2.07	0.96	3.05	5.29	1.00	1.63	1.03	0.05	0.91	3.60	-0.37	2.00
-0.55	0.84	0.40	1.54	2.75	0.69	-1.04	-1.24	0.42	0.21	0.10	-0.20	0.36	0.37	0.56	0.91
0.14	0.54	-0.02	0.11	1.64	0.28	0.44	0.38	0.59	0.77	0.37	0.17	3.48	0.74	-0.05	0.61
-2.76	-1.21	-2.42	-2.64	-3.24	-2.75	-2.98	-1.84	-3.23	-3.13	-2.94	-3.21	-3.22	-2.76	0.56	-1.31
0.47	-0.56	-0.36	0.27	1.88	1.50	1.04	0.39	2.42	2.43	3.51	4.69	2.53	0.33	-0.80	-0.92
-0.06	0.08	0.05	0.01	-0.01	0.00	-0.03	0.11	0.00	-0.01	0.01	-0.01	-0.02	0.00	0.03	-0.01
0.06	0.05	0.02	0.03	0.03	0.00	-0.01	-0.05	0.02	0.00	0.04	0.02	0.02	0.00	-0.04	0.02
-	-	-	-	-	-	-	-	-	-	-	-	-	-	-	-
398.98	-	-	-	-	-	-	-	-	-	-	-	-	-	-	-
135.54	-	-	-	-	-	-	-	-	-	-	-	-	-	-	-
1697.54	-	-	-	-	-	-	-	-	-	-	-	-	-	-	-

R9710676	R9710677	R9710680	R9710681	R9710682	R9710683	R9710684	R9710685	R9710686	R9710687	R9710688	R9710689	R9710690	R9710694	R9710696	R9710697
K97-173	K97-173	K97-173	K97-173	K97-173	K97-173	K97-173	K97-173	K97-173	K97-173	K97-173	K97-173	K97-173	K97-174	K97-174	K97-174
90.4	95.8	121.2	138	146.6	160.8	181.6	226.7	251.4	260.6	269.5	273.5	280.5	41.2	64.9	69.5
90.5	95.9	121.3	138.1	146.7	160.9	181.7	226.8	251.5	260.7	269.6	273.6	280.6	41.3	65	69.6
-	-	-	-	-	-	-	-	-	-	-	-	-	-	-	-
FA1	FB2	FB2	FA1	FA1	FA1	FA1	FB1	FA1	FB2	FB2	FB2	FB2	FA1	FB2	FA1
64.19	75.19	74.01	65.43	62.36	62.36	65.79	67.19	57.59	75.05	74.23	70.55	75.69	53.27	69.3	70.2
16	11.69	13.06	15.15	14.27	16.95	15.22	6.63	12.26	13.1	11.98	13.84	13	11.39	13.15	14.27
2.73	1.55	1.75	3.97	3.66	3.08	2.68	1.12	6.63	1.86	4.05	2.25	2.24	3.52	1.94	2.04
2.66	1.84	0.34	2.03	4.67	2.4	2.17	10.72	5	0.31	0.1	1.8	0.1	12.14	3.17	1.75
1.5	0.28	0.76	1.28	1.62	1.74	1.75	0.57	2.65	0.28	1.05	1.52	0.81	1.22	1.24	1.24
0.1	3.71	0.1	0.11	0.09	0.1	0.14	0.02	0.05	0.2	0.18	0.18	0.18	0.95	0.52	0.93
6.65	2.03	7.03	6.26	5.63	6.86	5.69	2.22	4.25	6.34	4.46	5.09	4.36	3.36	5.07	4.96
0.52	0.3	0.28	0.51	0.56	0.68	0.66	0.18	0.49	0.21	0.25	0.28	0.23	0.46	0.28	0.54
0.15	0.03	0.01	0.15	0.17	0.2	0.18	0.07	0.25	0.01	0.01	0.01	0.01	0.15	0.1	0.15
4.65	2.46	1.84	4.07	6.03	4.57	4.65	9.73	8.55	2.26	3.33	4.09	2.96	12.3	4.65	3.55
31	22	86	102	85	90	66	23	34	76	51	35	55	119	89	86
2	3	2	3	5	3	8	4	6	4	10	3	3	7	3	2
8	27	2	20	7	9	10	13	80	9	907	29	31	13	41	4
5	2	3	4	4	2	5	2	321	1	1847	6	13	4	4	5
-	-	-	-	-	-	-	-	-	-	-	-	-	-	-	-
-11.59	5.90	-3.72	-7.13	-6.39	-16.43	-7.08	52.50	-1.62	-2.94	2.94	-10.89	-1.77	-1.92	-8.72	1.60
0.47	0.03	0.05	1.80	1.72	0.63	0.55	0.49	5.86	0.15	2.62	0.41	0.53	2.49	0.22	0.07
0.98	0.95	-0.70	0.51	3.32	0.62	0.63	19.32	4.49	-0.73	-0.92	0.61	-0.93	14.06	2.00	0.34
0.60	-0.29	0.14	0.47	0.89	0.73	0.91	0.49	2.38	-0.33	0.51	0.79	0.19	0.80	0.59	0.50
-3.02	0.55	-3.35	-3.00	-3.02	-3.02	-2.98	-3.41	-3.05	-3.26	-3.26	-3.28	-3.27	-1.90	-2.95	-2.16
1.88	-0.64	3.95	1.85	1.57	1.72	1.27	1.39	0.88	3.27	1.86	1.81	1.40	0.13	2.03	0.89
-0.09	0.08	0.02	-0.07	0.01	0.02	0.07	0.10	0.02	-0.04	0.02	0.01	-0.02	0.02	0.02	-0.01
-0.01	-0.02	-0.04	0.00	0.03	0.03	0.03	0.08	0.15	-0.04	-0.04	-0.05	-0.04	0.05	0.04	0.01
-397.82	-401.20	-342.01	-328.08	-339.37	-348.78	-362.93	-381.23	-385.67	-351.87	-371.31	-393.06	-371.64	-274.05	-339.71	-338.35
-4.68	-1.21	-2.51	-3.62	-1.40	-3.93	1.14	3.16	0.62	-0.59	6.07	-1.71	-1.53	2.44	-1.57	-4.46
-5.10	10.58	-16.56	6.82	-5.24	-4.65	-2.82	6.19	82.53	-9.84	934.38	7.88	11.52	4.22	20.75	-8.30
-35.71	-31.36	-30.62	-36.41	-36.17	-38.53	-35.47	-29.72	340.54	-32.55	1906.89	-28.06	-20.93	-35.14	-29.68	-35.15

R9902936	R9902937	R9902938	R9902939	R9902940	R9902941	R9902942	R9902944	R9902945	R9902946	R9902949	R9902950	R9902951	R9902952	R9902953	R9902955
K98-188	K98-193	K98-193	K98-193	K98-193	K98-193	K98-193	K98-193	K98-193	K98-196	K98-196	K98-196	K98-196	K98-196	K98-196	K98-196
172.8	25.6	58.6	84.3	102.9	107.1	126.1	141.8	172.4	43	100.1	119.5	141.9	154.4	178.8	207.9
172.9	25.7	58.7	84.4	103	107.2	126.2	141.9	172.5	43.1	100.2	119.6	142	154.5	178.9	208
-	-	-	-	-	-	-	-	-	-	-	-	-	-	-	-
FA1	FA2	FA2	FA2	FA1	FA1	FA2	FA1	FA1	FA2	FA2	FA1	FA1	FA1	FA1	FA1
64.76	55.27	69.91	72.25	68.8	65.8	65.11	62.99	52.79	61.61	71.91	69.56	67.97	68.23	70.22	66.48
14.39	11.17	13.27	13.18	15.82	14.76	17.04	15.03	22.87	10.85	12.88	15.18	16.04	15.5	15.32	16.8
7.42	5.57	4.13	1.87	2.95	5.78	3.7	3.63	6.65	6.44	3.09	1.57	2.58	2.85	1.85	3.36
0.7	10	0.89	0.99	2.02	3.34	2.56	4.23	0.82	5.46	0.93	3	1.39	2.54	2.71	1.48
0.93	3	0.68	0.2	0.62	1.32	1.35	0.79	2.29	2.31	0.43	0.62	0.91	1.01	0.5	1.15
0.86	0.28	1.84	3	2.55	1.16	0.64	2.4	0.18	0.14	4.38	3.41	1.78	1.1	1.69	0.62
4.25	4.9	6.53	5.32	4.32	4.9	5.25	4.63	8.43	4.4	2.46	3.72	5.42	5.07	4.57	5.38
0.63	0.4	0.4	0.37	0.6	0.61	0.72	0.75	0.92	0.49	0.34	0.56	0.6	0.54	0.55	0.69
0.2	0.07	0.05	0.03	0.18	0.17	0.18	0.2	0.2	0.09	0.01	0.17	0.18	0.17	0.18	0.18
5.32	8.09	1.51	1.92	1.58	1.62	2.6	4.57	3.91	7.13	2.61	1.2	2.22	2.49	1.74	2.97
-	-	-	-	-	-	-	-	-	-	-	-	-	-	-	-
-	-	-	-	-	-	-	-	-	-	-	-	-	-	-	-
-	-	-	-	-	-	-	-	-	-	-	-	-	-	-	-
-	-	-	-	-	-	-	-	-	-	-	-	-	-	-	-
-	-	-	-	-	-	-	-	-	-	-	-	-	-	-	-
-4.49	2.02	6.68	9.78	-6.69	-5.11	-14.37	-8.99	-36.37	12.64	11.26	-3.30	-8.31	-5.92	-3.28	-12.39
5.49	5.24	2.52	0.06	0.70	3.69	1.15	1.50	2.22	6.62	1.48	-0.50	0.33	0.67	-0.25	0.90
-0.74	11.58	-0.47	-0.35	0.41	1.85	0.74	2.65	-0.92	5.88	-0.39	1.43	-0.18	0.94	1.13	-0.16
0.18	3.14	-0.02	-0.54	-0.19	0.54	0.39	0.00	0.69	2.33	-0.28	-0.17	0.06	0.19	-0.29	0.23
-2.24	-2.74	-1.09	0.20	-0.76	-1.97	-2.56	-0.79	-2.99	-2.92	1.84	0.16	-1.50	-2.08	-1.50	-2.57
0.13	2.22	2.99	1.71	-0.19	0.66	0.32	0.32	1.20	1.73	-1.39	-0.60	0.75	0.59	0.17	0.49
0.07	-0.04	-0.13	-0.16	-0.01	0.04	0.05	0.16	0.02	0.09	-0.18	-0.03	-0.02	-0.06	-0.04	0.03
0.06	-0.05	-0.09	-0.11	0.02	0.02	0.01	0.05	-0.02	-0.02	-0.13	0.02	0.02	0.02	0.03	0.01
-	-	-	-	-	-	-	-	-	-	-	-	-	-	-	-
-	-	-	-	-	-	-	-	-	-	-	-	-	-	-	-
-	-	-	-	-	-	-	-	-	-	-	-	-	-	-	-
-	-	-	-	-	-	-	-	-	-	-	-	-	-	-	-

R9710698	R9710699	R9710700	R9710701	R9710703	R9710705	R9710706	R9710708	R9710709	R9710710	R9710711	R9710712	R9710713
K97-174	K97-174	K97-174	K97-174	K97-174	K97-174	K97-174	K97-174	K97-174	K97-174	K97-174	K97-174	K97-174
80.4	93.8	97.1	117.8	127.4	145.1	156.7	168.6	179.7	187.4	204.3	214.2	221.2
80.5	93.9	97.2	117.9	127.5	145.2	156.8	168.7	179.8	187.5	204.4	214.3	221.3
-	-	-	-	-	-	-	-	-	-	-	-	-
FA1	FA1	FA1	FA1	FA1	FA1	FA1	FA1	FA1	FA1	FA1	FA1	FA1
69.65	66.04	60.56	65.04	63.06	64.26	64.83	62.88	66.19	67.25	67.33	59.29	64.41
15.3	15.11	15.48	13.42	14.72	14.47	15.59	16.42	14.4	15.72	12.69	15.65	13.4
2.8	4.5	5.36	4.23	3.92	4.84	4.44	4.92	4.94	3.27	6.76	4.9	4.51
0.94	1.7	2.89	3.13	4	3.53	1.65	2.03	2.4	1.88	1.79	4.05	4.01
0.97	1.55	1.87	1.88	1.23	1.9	1.69	1.34	1.09	1	1.83	2.42	2.22
1.57	0.18	0.23	0.23	1.87	0.27	0.28	1.38	0.7	0.95	0.95	0.92	0.47
4.61	5.42	5.53	4.84	4.44	4.92	5.19	4.8	4.3	4.46	3.21	3.75	3.54
0.62	0.63	0.66	0.55	0.62	0.62	0.51	0.68	0.58	0.63	0.5	0.68	0.57
0.15	0.2	0.2	0.15	0.18	0.18	0.15	0.18	0.15	0.18	0.15	0.2	0.18
3.17	4.28	6.11	5.46	5.01	4.69	4.94	4.9	4.8	4.34	3.8	6.76	4.88
55	94	126	66	139	74	81	139	84	60	94	70	127
5	6	10	4	5	8	6	27	51	6	169	25	26
7	2	2	2	28	37	5	9	16	7	7	4	4
14	19	90	13	20	203	77	26	28	27	3591	44	71
-	-	-	-	-	-	-	-	-	-	-	-	-
-3.74	-6.38	-13.05	0.54	-7.64	-5.35	-9.46	-14.25	-3.09	-7.72	7.22	-14.84	-0.03
0.65	2.32	3.03	2.58	1.86	2.86	2.13	2.35	2.98	1.02	5.74	2.55	2.89
-0.55	0.19	1.27	1.95	2.51	2.11	0.10	0.36	0.98	0.30	0.61	2.32	2.91
0.16	0.73	1.00	1.28	0.45	1.15	0.81	0.43	0.34	0.16	1.34	1.49	1.65
-1.62	-2.94	-2.89	-2.86	-1.26	-2.84	-2.85	-1.89	-2.40	-2.23	-2.02	-2.25	-2.60
0.22	1.05	1.03	1.08	0.22	0.78	0.68	0.09	0.18	-0.04	-0.48	-0.68	-0.32
0.02	0.04	0.06	0.03	0.05	0.06	-0.09	0.04	0.02	0.02	0.01	0.07	0.05
0.00	0.05	0.04	0.02	0.03	0.04	0.00	0.02	0.01	0.02	0.03	0.04	0.05
-373.72	-335.52	-307.62	-354.47	-288.67	-351.62	-350.44	-302.88	-341.16	-370.49	-318.27	-360.95	-288.16
-1.75	-0.72	2.90	-2.17	-1.56	1.54	-0.90	17.41	45.01	-0.95	187.19	16.73	21.72
-5.72	-10.45	-10.50	-10.21	15.29	24.81	-7.71	-4.40	3.78	-5.90	-4.35	-8.66	-8.03
-26.94	-21.96	44.31	-26.16	-20.49	163.78	31.58	-17.22	-11.97	-15.27	4075.29	0.64	36.81

R9902956	R9902957	R9902959	R9902960	R9902961	R9902962	R9902963	R9902964	R9902965	R9902966	R9902968	R9902970	R9902971
K98-196	K98-196	K98-196	K98-196	K98-196	K98-196	K98-196	K98-196	K98-196	K98-196	K98-196	K98-196	K98-196
223.5	229.5	243.8	248.3	253.6	255.9	258.5	260.3	264.7	270.4	287.3	298	305
223.6	229.6	243.9	248.4	253.7	256	258.6	260.4	264.8	270.5	287.4	298.1	305.1
-	-	-	-	-	-	-	-	-	-	-	-	-
FB2	FA1	FB2	FB2	FB2	FA1	FA1	FA1	FA1	FA1	FA1	FA1	FA1
68.83	61.18	76.02	75.9	76.41	33.06	46.58	28.42	66.52	68.54	71.13	69.72	57.04
11.4	14.44	11.93	12.52	11.89	19.81	26.96	19.44	7.01	14.36	13.68	14.3	8.56
5.59	10.34	1.79	2.05	1.39	21.78	6.92	21.29	10.6	3.05	1.58	1.47	10.26
3.45	0.46	0.89	0.17	0.55	0.6	0.31	2.66	1.98	1.66	0.74	1.62	6.4
2.08	4.11	0.56	1.45	1	9.44	2.63	11.65	3.01	1.2	0.64	0.43	2.73
0.11	0.12	3.25	0.05	1.7	0.36	0.18	0.18	0.55	0.57	2.68	4.38	2.06
4.19	3.74	2.76	4.9	3.98	6.01	9.35	3.92	1.91	4.69	3.63	2.88	0.93
0.21	0.55	0.21	0.23	0.21	0.76	1.32	1	0.31	0.54	0.47	0.54	0.34
0.05	0.15	0.05	0.1	0.05	0.23	0.1	0.15	0.1	0.17	0.15	0.15	0.1
3	3.65	1.79	2.19	1.9	4.71	4.53	7.44	2.25	2.55	3.01	3.38	5.88
-	-	-	-	-	-	-	-	-	-	-	-	-
-	-	-	-	-	-	-	-	-	-	-	-	-
-	-	-	-	-	-	-	-	-	-	-	-	-
-	-	-	-	-	-	-	-	-	-	-	-	-
-	-	-	-	-	-	-	-	-	-	-	-	-
0.94	-8.32	5.15	1.25	5.83	-45.67	-44.81	-48.68	68.07	-0.53	5.68	0.97	26.97
4.53	8.41	0.25	0.42	-0.17	13.98	1.72	13.92	19.98	1.08	-0.33	-0.51	15.42
2.78	-0.98	-0.09	-0.86	-0.45	-1.00	-1.28	0.55	2.67	0.24	-0.66	0.20	9.43
1.70	3.38	0.00	0.86	0.46	6.17	0.66	7.95	5.48	0.45	-0.08	-0.32	3.88
-3.33	-2.99	-0.02	-3.40	-1.65	-2.84	-3.01	-2.97	-1.97	-2.53	-0.26	1.35	0.39
1.80	-0.40	0.09	2.10	1.39	0.25	0.88	-1.23	-0.20	0.59	-0.30	-1.23	-2.58
-0.01	-0.01	-0.02	-0.01	-0.02	-0.01	0.15	0.18	0.08	-0.02	-0.06	-0.02	0.01
0.00	0.01	0.00	0.05	0.00	0.03	-0.09	-0.03	0.06	0.03	0.02	0.01	0.03
-	-	-	-	-	-	-	-	-	-	-	-	-
-	-	-	-	-	-	-	-	-	-	-	-	-
-	-	-	-	-	-	-	-	-	-	-	-	-
-	-	-	-	-	-	-	-	-	-	-	-	-

Appendix 5.1 Results of electron probe microanalyzer analysis of white mica

Point_ID	D00005981-1-10	D00005981-1-7-C	D00005981-3-7	D00005981-3-8	D00005981-4-13
Alteration assemblage	Mod wm ± chl	Mod wm ± chl	Mod wm ± chl	Mod wm ± chl	Mod wm ± chl
Microprobe analysis (wt %)					
SiO_2	51.402	55.591	54.733	49.297	51.270
TiO_2	30.465	31.877	32.171	28.948	29.275
Al_2O_3	3.165	3.250	2.616	2.651	3.367
FeO	2.172	2.317	2.127	1.948	2.161
MnO	0.004	0.017	-	0.004	0.003
ZnO	0.536	0.606	0.565	0.505	0.602
MgO	-	0.002	0.013	-	0.017
CaO	-	0.007	-	0.011	0.016
SrO	0.008	0.003	0.006	0.010	0.007
Na_2O	0.047	0.057	0.065	0.154	0.140
K_2O	3.230	2.353	2.451	8.875	7.704
BaO	1.028	0.432	0.971	1.120	0.917
F	0.010	0.080	0.062	-	-
Cl	0.016	0.001	0.008	0.016	0.000
Total	92.083	96.593	95.788	93.539	95.479
Atoms per formula units					
Si(IV)	3.40	3.47	3.44	3.34	3.38
Al (IV)	0.60	0.53	0.56	0.66	0.62
Al (VI)	1.770	1.813	1.820	1.645	1.650
Al total	2.373	2.344	2.382	2.309	2.273
Sr	0.000	0.001	-	0.000	0.000
Ba	0.014	0.015	0.014	0.013	0.016
Zn	-	0.000	0.001	-	0.001
Fe^{2+}	0.175	0.170	0.137	0.150	0.185
Mg	0.214	0.216	0.199	0.197	0.212
Mn	-	0.000	-	0.001	0.001
Ca	0.001	0.000	0.000	0.001	0.000
Na	0.006	0.007	0.008	0.020	0.018
K	0.272	0.187	0.196	0.766	0.647
Ti	0.051	0.020	0.046	0.057	0.045
F	0.002	0.016	0.012	-	-
Cl	0.002	0.000	0.001	0.002	0.000
Calculated T[1]	114.9	94.0	100.7	249.3	212.1

[1] Calculated after Battaglia (2004). Formula: T(°C) = 267.95x + 31.5 where x = K+|Fe-Mg|

D00005981-4-14	D00005981-4-4	D00005981-4-7	D00005981-5-5	D00005981-5-6	D00005981-6-10
Mod wm ± chl	Mod wm ± chl	Mod wm ± chl	Mod wm ± chl	Mod wm ± chl	Mod wm ± chl
51.856	51.477	51.706	52.391	51.843	51.083
29.174	30.074	29.722	28.785	29.191	30.289
3.149	2.952	2.721	3.157	3.049	2.812
2.180	1.984	2.177	2.177	2.197	1.978
0.002	-	0.002	0.044	0.030	0.042
0.685	0.580	0.639	0.616	0.630	0.541
0.005	0.039	-	-	0.014	-
0.019	0.004	0.016	0.001	-	0.015
0.006	0.035	0.005	0.009	0.013	-
0.137	0.124	0.151	0.135	0.141	0.204
7.826	7.927	7.581	7.615	7.904	7.882
0.453	0.763	1.122	0.480	0.721	0.775
-	-	-	0.053	-	-
0.007	0.003	0.000	0.012	0.008	0.009
95.499	95.962	95.842	95.475	95.741	95.630
3.41	3.37	3.38	3.44	3.40	3.35
0.59	0.63	0.62	0.56	0.60	0.65
1.672	1.692	1.666	1.664	1.658	1.695
2.262	2.321	2.288	2.226	2.257	2.343
0.000	-	0.000	0.002	0.001	0.002
0.018	0.015	0.016	0.016	0.016	0.014
0.000	0.002	-	-	0.001	-
0.173	0.162	0.149	0.173	0.167	0.154
0.214	0.194	0.212	0.213	0.215	0.194
0.001	0.000	0.001	0.000	-	0.001
0.000	0.002	0.000	0.001	0.001	-
0.017	0.016	0.019	0.017	0.018	0.026
0.657	0.662	0.632	0.637	0.661	0.660
0.022	0.038	0.055	0.024	0.036	0.038
-	-	-	0.011	-	-
0.001	0.000	0.000	0.001	0.001	0.001
218.3	217.5	217.7	212.9	221.5	218.8

D00005981-6-11	D00005981-6-12-C	D00005981-6-15	D00005981-6-16	D00005981-7-10	D00005981-7-11
Mod wm ± chl	Mod wm ± chl	Mod wm ± chl	Mod wm ± chl	Mod wm ± chl	Mod wm ± chl
51.493	51.523	51.226	50.932	51.335	49.499
29.560	29.839	29.344	29.116	29.531	29.292
3.039	2.281	2.668	3.023	3.239	3.974
2.125	2.156	1.977	2.041	2.042	1.934
0.049	-	0.015	-	0.002	-
0.596	0.578	0.476	0.539	0.657	0.585
-	0.010	0.020	0.019	-	-
-	0.013	0.010	0.011	0.007	0.009
0.001	0.003	0.026	0.017	0.093	0.032
0.124	0.121	0.217	0.193	0.140	0.160
7.511	7.998	7.443	7.559	7.793	8.418
1.143	1.132	0.695	1.149	0.827	0.852
-	-	-	-	0.009	-
-	0.024	0.015	0.009	0.005	-
95.641	95.678	94.132	94.608	95.680	94.755
3.38	3.37	3.40	3.38	3.37	3.32
0.62	0.63	0.60	0.62	0.63	0.68
1.660	1.675	1.696	1.654	1.663	1.635
2.284	2.302	2.296	2.276	2.288	2.315
0.002	-	0.001	-	0.000	-
0.015	0.015	0.012	0.014	0.017	0.015
-	0.000	0.001	0.001	-	-
0.167	0.125	0.148	0.168	0.178	0.223
0.208	0.210	0.196	0.202	0.200	0.193
-	0.001	0.001	0.001	0.000	0.001
0.000	0.000	0.002	0.001	0.007	0.002
0.016	0.015	0.028	0.025	0.018	0.021
0.628	0.668	0.630	0.640	0.653	0.720
0.056	0.056	0.035	0.057	0.041	0.043
-	-	-	-	0.002	-
-	0.003	0.002	0.001	0.001	-
210.8	233.4	213.1	212.0	212.5	232.4

D00005981-7-5	D00005981-7-6	D00005981-8.1-10	D00005981-8.1-13	D00005981-8.1-6	D00005981-8.1-7
Mod wm ± chl	Mod wm ± chl	Mod wm ± chl	Mod wm ± chl	Mod wm ± chl	Mod wm ± chl
52.384	52.591	51.576	51.591	50.868	53.102
29.197	30.006	30.498	30.009	28.862	28.389
3.125	3.082	2.344	2.693	3.016	3.258
2.206	2.066	2.026	1.963	2.081	2.437
0.026	0.018	0.030	0.006	-	0.020
0.663	0.697	0.630	0.636	0.686	0.322
-	0.004	0.026	-	-	-
0.009	0.019	0.004	0.003	0.014	-
0.064	0.048	0.005	0.008	0.008	0.008
0.116	0.158	0.135	0.129	0.159	0.094
8.007	7.364	7.595	7.931	8.205	7.694
0.438	0.358	1.126	1.006	0.425	0.288
0.032	0.005	-	-	0.025	-
0.003	-	-	0.006	0.007	0.008
96.270	96.416	95.995	95.981	94.356	95.620
3.42	3.41	3.36	3.37	3.41	3.47
0.58	0.59	0.64	0.63	0.59	0.53
1.665	1.704	1.698	1.682	1.672	1.657
2.246	2.293	2.340	2.311	2.261	2.187
0.001	0.001	0.001	0.000	0.001	0.001
0.017	0.018	0.016	0.016	0.017	0.008
-	0.000	0.001	-	0.001	-
0.171	0.167	0.128	0.147	0.155	0.178
0.215	0.200	0.197	0.191	0.215	0.237
0.000	0.001	0.000	0.000	-	-
0.004	0.003	0.000	0.001	0.000	0.001
0.015	0.020	0.017	0.016	0.018	0.012
0.667	0.609	0.631	0.661	0.698	0.641
0.022	0.017	0.055	0.049	0.021	0.014
0.007	0.001	-	-	-	-
0.000	-	-	0.001	0.001	0.001
221.9	203.5	219.0	220.4	234.6	219.3

D00005981-8.1-9	D00005981-8-11-C	D00005981-8-12	D00005981-8-15	D00005981-8-2	D00005981-8-9
Mod wm ± chl	Mod wm ± chl	Mod wm ± chl	Mod wm ± chl	Mod wm ± chl	Mod wm ± chl
52.247	49.212	52.549	52.034	52.040	50.760
28.716	29.533	29.383	29.254	29.701	28.912
3.069	2.396	3.183	2.824	3.225	3.277
2.344	1.704	2.293	2.200	2.042	2.055
-	0.008	0.030	0.022	0.030	0.007
0.648	0.637	0.698	0.673	0.634	0.611
-	-	-	0.011	-	0.004
0.013	0.002	0.020	-	0.011	0.004
0.001	0.005	0.008	0.005	0.019	0.023
0.108	0.150	0.116	0.138	0.145	0.224
7.702	7.784	7.523	8.341	7.698	7.397
0.317	1.071	0.368	0.422	0.297	1.018
0.005	0.015	-	-	-	-
0.001	0.002	-	0.006	-	0.017
95.171	92.519	96.171	95.930	95.842	94.309
3.44	3.34	3.42	3.41	3.41	3.38
0.56	0.66	0.58	0.59	0.59	0.62
1.669	1.699	1.681	1.672	1.699	1.649
2.228	2.361	2.256	2.261	2.292	2.269
-	0.000	0.001	0.001	0.001	0.000
0.017	0.017	0.018	0.017	0.016	0.016
-	-	-	0.001	-	0.000
0.169	0.136	0.173	0.155	0.177	0.183
0.230	0.172	0.223	0.215	0.199	0.204
0.001	0.000	0.001	-	0.001	0.000
0.000	0.000	0.001	0.000	0.001	0.002
0.014	0.020	0.015	0.018	0.018	0.029
0.647	0.673	0.625	0.698	0.643	0.628
0.016	0.055	0.018	0.021	0.015	0.051
0.001	0.003	-	-	-	-
0.000	0.000	-	0.001	-	0.002
221.2	221.7	212.3	234.6	209.9	205.6

D00005985-1-14	D00005985-1-15	D00005985-1-4	D00005985-1-6	D00005985-1-9	D00005985-2-11
Per wm	Per wm	Per wm	Per wm	Per wm	Per wm
51.742	50.383	50.294	51.026	52.293	49.037
31.717	32.863	33.042	33.432	31.618	31.251
1.163	0.749	0.734	0.774	1.351	0.913
2.192	1.688	1.728	1.617	2.102	1.842
0.009	0.030	0.003	0.029	0.005	0.013
0.152	0.144	0.153	0.197	0.159	0.139
-	-	-	-	0.008	-
0.016	-	0.011	0.014	0.009	0.025
0.005	0.001	0.006	0.000	-	0.004
0.416	0.510	0.539	0.498	0.423	0.369
7.903	8.156	8.056	8.345	7.903	9.324
0.187	0.390	0.388	0.432	0.201	0.443
0.117	0.159	0.009	0.072	0.114	0.185
0.010	0.007	0.001	-	0.007	0.010
95.629	95.080	94.964	96.436	96.193	93.555
3.35	3.29	3.28	3.28	3.37	3.29
0.65	0.71	0.72	0.72	0.63	0.71
1.774	1.814	1.825	1.821	1.769	1.753
2.422	2.527	2.542	2.536	2.400	2.468
0.000	0.001	0.000	0.001	0.000	0.001
0.004	0.004	0.004	0.005	0.004	0.004
-	-	-	-	0.000	-
0.063	0.041	0.040	0.042	0.073	0.051
0.212	0.164	0.168	0.155	0.202	0.184
0.001	-	0.001	0.001	0.000	0.001
0.000	0.000	0.000	0.000	-	0.000
0.052	0.065	0.068	0.062	0.053	0.048
0.653	0.679	0.671	0.685	0.649	0.797
0.009	0.019	0.019	0.021	0.010	0.022
0.024	0.033	0.002	0.015	0.023	0.039
0.001	0.001	0.000	-	0.001	0.001
246.4	246.4	245.6	245.5	240.1	280.6

D00005985-2-14	D00005985-2-15	D00005985-2-9	D00005985-3-1	D00005985-3-10	D00005985-3-11
Per wm	Per wm	Per wm	Per wm	Per wm	Per wm
50.331	51.291	51.101	52.091	50.730	51.538
32.262	33.346	33.229	31.874	31.749	32.386
0.848	0.794	0.872	1.169	1.301	1.102
1.860	1.756	1.744	2.084	1.901	1.968
-	0.020	0.018	0.043	0.009	0.001
0.168	0.187	0.161	0.168	0.223	0.222
-	-	0.016	-	0.006	0.034
0.015	-	-	0.009	0.005	0.011
0.006	0.006	0.004	-	0.003	0.005
0.441	0.451	0.517	0.394	0.455	0.444
7.951	8.422	8.435	8.002	7.679	8.175
0.393	0.384	0.425	0.327	0.135	0.122
0.130	0.100	0.060	0.126	0.113	0.120
-	0.001	0.000	0.001	0.011	0.007
94.405	96.758	96.582	96.288	94.320	96.135
3.30	3.29	3.29	3.35	3.33	3.33
0.70	0.71	0.71	0.65	0.67	0.67
1.800	1.813	1.807	1.771	1.794	1.793
2.496	2.522	2.520	2.418	2.460	2.465
-	0.001	0.001	0.002	0.000	0.000
0.004	0.005	0.004	0.004	0.006	0.006
-	-	0.001	-	0.000	0.002
0.047	0.043	0.047	0.063	0.072	0.060
0.182	0.168	0.167	0.200	0.186	0.189
0.001	-	-	0.000	0.000	0.001
0.000	0.000	0.000	-	0.000	0.000
0.056	0.056	0.064	0.049	0.058	0.056
0.666	0.689	0.692	0.657	0.644	0.673
0.019	0.019	0.021	0.016	0.007	0.006
0.027	0.020	0.012	0.026	0.023	0.025
-	0.000	0.000	0.000	0.001	0.001
246.2	249.8	249.2	244.3	234.8	246.8

D00005985-3-13	D00005985-3-5	D00005985-4-11	D00005985-4-16	D00005985-4-17	D00005985-4-9
Per wm	Per wm	Per wm	Per wm	Per wm	Per wm
50.054	50.875	48.803	50.567	47.379	50.640
32.370	33.558	31.014	32.956	30.997	32.297
0.835	0.776	1.019	0.707	1.107	0.876
1.646	1.604	1.907	1.758	1.799	1.828
-	-	0.007	0.026	-	0.016
0.136	0.146	0.147	0.141	0.203	0.139
0.007	-	0.009	-	-	0.033
0.015	0.003	0.014	0.019	0.019	0.012
0.007	0.022	0.001	0.008	0.009	0.009
0.466	0.452	0.346	0.451	0.406	0.509
8.528	7.867	10.006	8.348	9.640	7.418
0.429	0.491	0.470	0.414	0.498	0.466
0.019	0.110	0.163	0.132	0.094	0.156
-	0.011	0.025	0.000	0.021	0.018
94.512	95.915	93.931	95.527	92.172	94.417
3.29	3.28	3.28	3.29	3.24	3.31
0.71	0.72	0.72	0.71	0.76	0.69
1.806	1.832	1.728	1.810	1.743	1.804
2.511	2.551	2.453	2.524	2.500	2.490
-	-	0.000	0.001	-	0.001
0.004	0.004	0.004	0.004	0.005	0.004
0.000	-	0.000	-	-	0.002
0.046	0.042	0.057	0.038	0.063	0.048
0.162	0.154	0.191	0.170	0.184	0.178
0.001	0.000	0.001	0.001	0.001	0.001
0.000	0.002	0.000	0.001	0.001	0.001
0.059	0.057	0.045	0.057	0.054	0.065
0.716	0.647	0.857	0.692	0.842	0.619
0.021	0.024	0.024	0.020	0.026	0.023
0.004	0.022	0.035	0.027	0.020	0.032
-	0.001	0.003	0.000	0.002	0.002
254.3	235.0	296.8	252.3	289.2	232.3

D00005985-5-10-C	D00005985-5-13	D00005985-5-5	D00005985-5-7	D00005985-6-10	D00005985-6-13
Per wm	Per wm	Per wm	Per wm	Per wm	Per wm
49.929	51.557	51.440	51.793	50.751	52.133
33.627	32.326	30.875	31.775	33.179	32.935
0.718	1.267	1.169	1.152	0.744	1.149
1.468	1.852	2.286	2.045	1.672	1.947
0.030	0.011	0.004	0.014	0.016	0.014
0.194	0.211	0.202	0.148	0.147	0.172
0.013	-	-	0.016	-	-
-	0.010	-	0.014	0.020	-
0.008	0.007	0.004	0.004	0.005	0.018
0.505	0.442	0.370	0.473	0.487	0.404
7.804	8.302	8.203	7.751	8.632	7.914
0.417	0.152	0.187	0.391	0.452	0.323
0.106	0.129	0.084	0.168	0.070	0.160
0.005	-	0.007	-	0.002	-
94.824	96.266	94.831	95.744	96.177	97.169
3.26	3.33	3.37	3.35	3.28	3.32
0.74	0.67	0.63	0.65	0.72	0.68
1.848	1.790	1.753	1.770	1.810	1.796
2.588	2.460	2.383	2.421	2.528	2.474
0.001	0.000	0.000	0.001	0.001	0.001
0.005	0.005	0.005	0.004	0.004	0.004
0.001	-	-	0.001	-	-
0.039	0.068	0.064	0.062	0.040	0.061
0.143	0.178	0.223	0.197	0.161	0.185
-	0.001	-	0.001	0.001	-
0.001	0.000	0.000	0.000	0.000	0.001
0.064	0.055	0.047	0.059	0.061	0.050
0.650	0.684	0.685	0.639	0.712	0.643
0.020	0.007	0.009	0.019	0.022	0.015
0.022	0.026	0.017	0.034	0.014	0.032
0.001	-	0.001	-	0.000	-
233.4	244.2	257.8	238.9	254.7	237.0

D00005985-6-14	D00005985-6-7	D00005985-7-12	D00005985-7-14	D00005985-7-5	D00005985-8-11
Per wm	Per wm	Per wm	Per wm	Per wm	Per wm
51.130	51.485	52.602	50.645	51.612	49.651
32.310	33.185	32.751	32.115	32.469	32.788
0.957	0.826	0.795	0.992	1.172	1.087
1.929	1.771	2.069	1.839	1.928	1.664
-	0.024	0.011	0.028	0.011	0.022
0.121	0.238	0.111	0.138	0.158	0.220
-	-	-	0.010	0.013	0.013
-	-	0.000	-	-	0.014
0.002	0.000	0.011	0.004	-	0.014
0.461	0.451	0.621	0.444	0.401	0.513
8.359	8.659	7.390	8.577	7.978	8.101
0.338	0.420	0.273	0.302	0.130	0.318
0.115	0.066	0.155	0.153	0.083	0.093
0.010	0.003	0.011	0.004	0.002	0.017
95.732	97.128	96.800	95.251	95.957	94.515
3.32	3.30	3.35	3.31	3.33	3.27
0.68	0.70	0.65	0.69	0.67	0.73
1.788	1.802	1.803	1.783	1.803	1.812
2.470	2.505	2.456	2.474	2.471	2.544
-	0.001	0.000	0.001	0.000	0.001
0.003	0.006	0.003	0.004	0.004	0.006
-	-	-	0.000	0.001	0.001
0.052	0.044	0.042	0.054	0.063	0.060
0.187	0.169	0.196	0.179	0.186	0.163
-	-	0.000	-	-	0.001
0.000	0.000	0.001	0.000	-	0.001
0.058	0.056	0.077	0.056	0.050	0.065
0.692	0.707	0.600	0.715	0.657	0.680
0.016	0.020	0.013	0.015	0.006	0.016
0.024	0.013	0.031	0.032	0.017	0.019
0.001	0.000	0.001	0.000	0.000	0.002
252.9	254.5	233.5	256.6	240.3	241.5

D00005985-8-4	D00005985-8-9	D00005986-10-18	D00005986-10-8	D00005986-2-2	D00005986-2-9
Per wm	Per wm	Per chl - min	Per chl - min	Per chl - min	Per chl - min
51.055	51.330	50.134	49.141	51.561	51.217
32.011	32.000	30.771	30.777	32.286	31.257
0.957	1.321	2.770	2.556	2.538	2.349
2.025	1.897	2.184	2.045	2.006	2.193
0.019	0.049	0.023	0.022	0.023	0.009
0.138	0.184	0.252	0.310	0.262	0.223
-	0.022	0.001	0.042	-	0.018
0.003	0.016	0.016	-	0.014	0.003
0.011	0.021	0.009	0.023	0.001	0.020
0.398	0.492	0.532	0.479	0.589	0.494
8.136	8.286	7.454	7.480	7.814	6.948
0.292	0.129	0.341	0.418	0.355	0.243
0.078	0.119	0.028	0.200	0.064	0.184
0.002	0.024	0.004	0.006	-	0.010
95.125	95.890	94.519	93.499	97.513	95.168
3.33	3.33	3.32	3.29	3.31	3.34
0.67	0.67	0.68	0.71	0.69	0.66
1.788	1.779	1.718	1.720	1.744	1.744
2.459	2.448	2.400	2.429	2.439	2.403
0.001	0.002	0.001	0.001	0.001	0.000
0.004	0.005	0.007	0.008	0.007	0.006
-	0.001	0.000	0.002	-	0.001
0.052	0.072	0.153	0.143	0.136	0.128
0.197	0.184	0.215	0.204	0.192	0.213
0.000	0.001	0.001	-	0.001	0.000
0.001	0.001	0.001	0.002	0.000	0.001
0.050	0.062	0.068	0.062	0.073	0.062
0.677	0.686	0.629	0.639	0.639	0.578
0.014	0.006	0.017	0.021	0.017	0.012
0.016	0.024	0.006	0.042	0.013	0.038
0.000	0.003	0.000	0.001	-	0.001
251.6	245.3	216.8	219.1	217.6	209.2

D00005986-4-3	D00005986-5-12	Q721080-1-3	Q721080-4-3	Q721080-4-7	Q721080-8-5	Q721080-9-9
Per chl - min	Per chl - min	Per chl - min	Per chl - min	Per chl - min	Per chl - min	Per chl - min
51.145	35.817	36.926	37.264	35.524	48.048	39.675
30.906	16.651	13.877	14.436	15.164	34.767	20.370
2.436	18.739	17.284	17.565	18.649	1.489	16.282
2.246	12.023	15.182	14.020	14.028	0.636	9.833
-	0.011	0.011	0.032	0.023	0.053	0.026
0.235	0.114	0.095	0.108	0.078	0.367	0.009
0.045	0.084	0.205	0.112	0.074	0.020	0.257
-	0.051	0.076	0.090	0.049	-	0.010
0.012	0.007	0.092	0.001	0.033	0.017	0.076
0.505	0.189	0.137	0.233	0.130	1.005	0.049
7.188	9.211	7.615	8.853	6.533	7.298	3.113
0.219	1.191	0.675	1.223	1.096	0.033	0.197
0.111	0.449	0.635	0.423	0.306	-	0.419
0.008	0.015	0.027	0.009	0.033	0.002	0.011
95.056	94.552	92.837	94.369	91.720	93.735	90.327
3.35	2.75	2.84	2.84	2.77	3.19	2.97
0.65	1.25	1.16	1.16	1.23	0.81	1.03
1.733	0.253	0.102	0.139	0.166	1.918	0.767
2.384	1.505	1.259	1.297	1.394	2.724	1.797
-	0.000	0.000	0.001	0.001	0.002	0.001
0.006	0.003	0.003	0.003	0.002	0.010	0.000
0.002	0.005	0.012	0.006	0.004	0.001	0.014
0.133	1.202	1.113	1.120	1.217	0.083	1.019
0.219	1.375	1.743	1.594	1.632	0.063	1.097
-	0.003	0.005	0.006	0.003	-	0.001
0.001	0.001	0.008	0.000	0.003	0.001	0.006
0.064	0.028	0.020	0.034	0.020	0.130	0.007
0.600	0.901	0.748	0.861	0.650	0.619	0.297
0.011	0.069	0.039	0.070	0.064	0.002	0.011
0.023	0.109	0.155	0.102	0.075	-	0.099
0.001	0.002	0.004	0.001	0.004	0.000	0.001
215.3	319.3	400.7	389.2	316.9	202.6	132.1

Q930216-1-13	Q930216-12-4	Q930216-13-13	Q930216-1-7	Q930216-3-4	Q930216-4-5	Q930216-9-11
Per chl - min	Per chl - min	Per chl - min	Per chl - min	Per chl - min	Per chl - min	Per chl - min
35.055	33.105	36.315	35.453	37.595	37.303	51.332
15.994	16.738	15.944	15.498	15.282	15.018	29.632
20.373	21.125	18.734	18.238	18.489	18.811	1.611
11.180	11.257	11.256	11.848	12.514	12.591	2.667
-	0.018	0.006	0.005	-	0.016	0.022
0.898	0.659	0.964	1.114	0.370	0.452	1.799
0.081	0.039	0.111	0.127	0.091	0.126	0.007
0.069	0.102	0.111	0.085	0.114	0.094	-
0.023	0.048	0.026	0.032	0.153	0.006	0.002
0.119	0.099	0.282	0.286	0.286	0.254	0.418
8.200	6.216	8.234	7.680	8.463	8.345	7.208
0.357	0.496	0.546	0.326	0.415	0.456	0.205
0.449	0.080	0.115	0.039	0.322	0.337	0.081
0.041	0.053	0.037	0.045	0.027	0.031	0.018
92.839	90.035	92.681	90.776	94.121	93.840	95.002
2.77	2.68	2.85	2.83	2.88	2.87	3.39
1.23	1.32	1.15	1.17	1.12	1.13	0.61
0.259	0.284	0.317	0.294	0.259	0.236	1.697
1.489	1.599	1.472	1.460	1.379	1.363	2.306
-	0.001	0.000	0.000	-	0.001	0.001
0.028	0.021	0.030	0.035	0.011	0.014	0.047
0.005	0.002	0.006	0.007	0.005	0.007	0.000
1.346	1.433	1.227	1.219	1.184	1.212	0.089
1.317	1.361	1.315	1.412	1.429	1.446	0.263
0.005	0.007	0.007	0.006	0.007	0.006	-
0.002	0.004	0.002	0.003	0.013	0.000	0.000
0.018	0.016	0.043	0.044	0.042	0.038	0.054
0.827	0.643	0.823	0.783	0.827	0.820	0.607
0.021	0.030	0.032	0.020	0.024	0.026	0.010
0.112	0.021	0.028	0.010	0.078	0.082	0.017
0.005	0.007	0.005	0.006	0.004	0.004	0.002
260.8	223.0	275.4	292.9	318.6	313.9	240.7

Q930216-9-3-C Per chl - min	Q930216-9-8 Per chl - min	Q930221-10-3 Mod wm ± chl	Q930221-10-9 Mod wm ± chl	Q930221-11-10 Mod wm ± chl	Q930221-11-11 Mod wm ± chl	Q930221-11-5 Mod wm ± chl
35.317	49.957	36.811	50.923	57.494	40.022	50.030
16.874	30.879	16.953	32.564	29.973	17.929	31.883
18.755	2.187	17.390	2.207	1.980	14.798	2.347
10.290	2.186	11.814	1.455	1.226	10.767	1.629
-	0.019	0.035	0.007	0.035	0.002	0.040
1.494	1.637	0.107	0.589	0.557	0.088	0.779
0.180	-	0.054	-	0.016	0.027	0.004
0.119	0.013	0.131	0.003	-	0.098	0.015
0.058	0.002	0.004	0.005	0.025	0.021	0.010
0.309	0.572	0.089	0.506	0.555	0.022	0.318
8.269	7.635	9.208	8.324	7.736	8.786	8.018
0.816	0.221	0.547	0.162	0.225	0.148	0.283
0.366	-	0.111	-	-	0.679	-
0.040	-	0.003	-	0.009	0.011	0.003
92.887	95.308	93.257	96.745	99.831	93.398	95.359
2.78	3.32	2.83	3.30	3.56	2.99	3.30
1.22	0.68	1.17	0.70	0.44	1.01	0.70
0.345	1.731	0.371	1.789	1.752	0.568	1.774
1.565	2.415	1.538	2.488	2.189	1.578	2.477
-	0.001	0.002	0.000	0.001	0.000	0.002
0.046	0.043	0.003	0.015	0.014	0.003	0.020
0.010	-	0.003	-	0.001	0.001	0.000
1.234	0.121	1.119	0.120	0.103	0.924	0.129
1.207	0.216	1.356	0.141	0.113	1.199	0.160
0.008	0.001	0.009	0.000	-	0.006	0.001
0.005	0.000	0.000	0.000	0.002	0.002	0.001
0.047	0.074	0.013	0.064	0.067	0.003	0.041
0.830	0.646	0.904	0.688	0.612	0.837	0.674
0.048	0.011	0.032	0.008	0.010	0.008	0.014
0.091	-	0.027	-	-	0.160	-
0.005	-	0.000	-	0.001	0.001	0.000
261.2	230.1	337.0	221.6	198.2	329.4	220.4

Q930221-11-7	Q930221-11-9	Q930221-1-4	Q930221-1-5	Q930221-1-7	Q930221-2-11	Q930221-2-7-C
Mod wm ± chl	Mod wm ± chl	Mod wm ± chl	Mod wm ± chl	Mod wm ± chl	Mod wm ± chl	Mod wm ± chl
51.895	53.089	51.216	49.929	50.415	49.978	50.509
31.738	30.693	31.205	31.977	32.439	32.608	32.376
2.410	1.919	2.204	2.566	1.998	2.062	2.188
1.734	1.824	1.804	1.346	1.388	1.223	1.482
0.025	0.029	0.028	0.023	0.012	0.016	0.039
0.649	0.380	0.419	0.592	0.575	0.668	0.623
-	-	-	-	-	-	0.013
0.008	0.010	0.019	0.004	0.014	0.010	0.007
0.001	0.028	0.056	0.001	0.004	0.004	0.005
0.432	0.281	0.325	0.568	0.556	0.481	0.523
7.839	8.061	8.624	8.121	8.005	8.002	7.653
0.222	0.345	0.157	0.496	0.321	0.236	0.129
-	0.097	-	-	-	-	-
0.006	0.007	0.011	0.013	0.007	0.007	0.007
96.959	96.763	96.068	95.636	95.734	95.295	95.554
3.35	3.41	3.35	3.29	3.30	3.29	3.31
0.65	0.59	0.65	0.71	0.70	0.71	0.69
1.764	1.740	1.752	1.767	1.796	1.815	1.802
2.414	2.326	2.404	2.481	2.500	2.528	2.497
0.001	0.001	0.001	0.001	0.000	0.001	0.001
0.016	0.010	0.011	0.015	0.015	0.017	0.016
-	-	-	-	-	-	0.001
0.130	0.103	0.120	0.141	0.109	0.113	0.120
0.167	0.175	0.176	0.132	0.135	0.120	0.145
0.000	0.001	0.001	0.000	0.001	0.001	0.000
0.000	0.002	0.004	0.000	0.000	0.000	0.000
0.054	0.035	0.041	0.072	0.070	0.061	0.066
0.645	0.661	0.719	0.682	0.668	0.671	0.639
0.011	0.017	0.008	0.025	0.016	0.012	0.006
-	0.020	-	-	-	-	-
0.001	0.001	0.001	0.001	0.001	0.001	0.001
214.3	227.9	239.0	216.7	217.4	213.1	209.3

Q930221-2-9	Q930221-4-12	Q930221-4-9	Q930221-5-3	Q930221-5-4-C	Q930221-5-6	Q930221-6-11
Mod wm ± chl	Mod wm ± chl	Mod wm ± chl	Mod wm ± chl	Mod wm ± chl	Mod wm ± chl	Mod wm ± chl
51.219	49.318	54.405	50.433	51.292	50.982	45.439
32.234	32.255	30.830	32.423	32.714	31.964	29.268
2.221	2.468	0.839	2.648	1.970	2.484	7.992
1.586	1.400	1.669	1.451	1.477	1.613	2.185
0.022	0.033	0.030	0.009	0.005	0.041	0.029
0.686	0.595	0.139	0.614	0.612	0.597	0.473
-	-	-	0.008	0.037	0.006	0.010
0.008	0.010	-	0.009	0.016	0.001	0.009
0.025	0.018	0.278	0.022	0.008	0.033	0.034
0.520	0.559	0.314	0.494	0.436	0.395	0.302
7.917	7.754	4.433	7.759	8.234	8.093	6.211
0.272	0.242	0.025	0.387	0.271	0.224	0.240
-	-	0.251	-	-	-	-
0.006	0.010	0.022	0.006	0.001	0.006	0.019
96.716	94.662	93.235	96.263	97.073	96.439	92.211
3.32	3.27	3.51	3.29	3.31	3.32	3.18
0.68	0.73	0.49	0.71	0.69	0.68	0.82
1.780	1.794	1.856	1.778	1.795	1.768	1.587
2.461	2.522	2.345	2.490	2.487	2.451	2.411
0.001	0.001	0.001	0.000	0.000	0.002	0.001
0.017	0.015	0.004	0.016	0.015	0.015	0.013
-	-	-	0.000	0.002	0.000	0.001
0.120	0.137	0.045	0.144	0.106	0.135	0.467
0.153	0.138	0.161	0.141	0.142	0.156	0.228
0.000	0.001	-	0.000	0.001	0.000	0.001
0.002	0.001	0.019	0.002	0.001	0.002	0.003
0.065	0.072	0.039	0.062	0.055	0.050	0.041
0.654	0.656	0.365	0.645	0.677	0.672	0.554
0.013	0.012	0.001	0.019	0.013	0.011	0.013
-	-	0.051	-	-	-	-
0.001	0.001	0.002	0.001	0.000	0.001	0.002
215.6	207.7	160.2	205.2	222.6	217.2	244.1

Q930221-6-12-C	Q930221-6-6	Q930221-6-8	Q930221-8-10	Q930221-8-5	Q930221-9-10	Q930221-9-12
Mod wm ± chl	Mod wm ± chl	Mod wm ± chl	Mod wm ± chl	Mod wm ± chl	Mod wm ± chl	Mod wm ± chl
50.374	52.082	49.968	50.495	49.977	50.433	49.917
31.959	30.471	32.210	32.803	31.858	32.468	31.881
2.246	2.553	2.252	2.333	2.444	2.355	2.755
1.596	1.920	1.602	1.414	1.610	1.547	1.414
0.045	0.027	0.016	0.028	0.010	0.030	-
0.531	0.651	0.873	0.608	0.614	0.537	0.595
-	-	-	0.003	0.029	-	-
0.006	0.002	0.021	0.010	0.015	-	0.013
0.008	0.008	0.002	0.006	0.014	0.005	0.012
0.409	0.422	0.334	0.446	0.304	0.329	0.546
7.368	7.859	7.932	8.455	8.061	8.241	7.763
0.226	0.226	0.344	0.228	0.381	0.123	0.424
-	-	-	-	-	-	-
0.024	0.002	0.005	-	0.008	0.003	-
94.792	96.223	95.559	96.829	95.325	96.071	95.320
3.32	3.39	3.28	3.28	3.30	3.30	3.29
0.68	0.61	0.72	0.72	0.70	0.70	0.71
1.796	1.727	1.780	1.788	1.772	1.796	1.767
2.480	2.337	2.495	2.510	2.476	2.500	2.477
0.002	0.001	0.001	0.001	0.000	0.001	-
0.014	0.017	0.022	0.015	0.016	0.014	0.015
-	-	-	0.000	0.001	-	-
0.124	0.139	0.124	0.127	0.135	0.129	0.152
0.157	0.186	0.157	0.137	0.158	0.151	0.139
0.000	0.000	0.001	0.001	0.001	-	0.001
0.001	0.001	0.000	0.000	0.001	0.000	0.001
0.052	0.053	0.043	0.056	0.039	0.042	0.070
0.619	0.652	0.665	0.700	0.678	0.687	0.653
0.011	0.011	0.017	0.011	0.019	0.006	0.021
-	-	-	-	-	-	-
0.003	0.000	0.001	-	0.001	0.000	-
206.1	219.0	218.6	221.9	219.5	221.4	209.9

Q930221-9-13	Q930221-9-3	Q930221-9-5	Q931973-10-10	Q931973-10-11	Q931973-10-7	Q931973-12-10
Mod wm ± chl	Mod wm ± chl	Mod wm ± chl	Mod wm ± chl	Mod wm ± chl	Mod wm ± chl	Mod wm ± chl
51.005	38.642	37.673	51.637	51.074	51.891	51.715
33.123	20.527	17.637	29.438	30.924	30.038	29.567
2.119	15.283	16.621	3.156	2.237	3.326	3.335
1.300	9.120	11.470	1.908	1.377	1.809	1.828
0.018	-	0.004	0.005	0.027	0.015	0.014
0.530	0.088	0.204	0.484	0.354	0.438	0.441
-	0.028	0.057	0.020	0.011	0.003	0.032
-	0.081	0.121	-	-	0.013	-
0.009	0.037	0.026	0.009	0.201	0.018	0.042
0.564	0.058	0.066	0.052	0.114	0.152	0.295
8.012	7.106	8.700	7.579	6.369	7.214	6.632
0.321	0.868	0.192	0.836	0.368	1.161	1.198
-	0.301	0.144	-	-	-	0.053
0.003	0.009	0.012	0.009	0.037	0.001	0.030
97.004	92.148	92.927	95.133	93.093	96.079	95.182
3.29	2.90	2.88	3.40	3.39	3.38	3.39
0.71	1.10	1.12	0.60	0.61	0.62	0.61
1.807	0.719	0.468	1.682	1.806	1.680	1.672
2.517	1.817	1.589	2.283	2.418	2.304	2.283
0.001	-	0.000	0.000	0.001	0.001	0.001
0.013	0.003	0.006	0.012	0.009	0.011	0.011
-	0.002	0.003	0.001	0.001	0.000	0.002
0.114	0.960	1.062	0.174	0.124	0.181	0.183
0.125	1.021	1.307	0.187	0.136	0.175	0.179
-	0.005	0.008	-	-	0.001	-
0.001	0.003	0.002	0.001	0.014	0.001	0.003
0.071	0.008	0.010	0.007	0.015	0.019	0.037
0.659	0.681	0.848	0.636	0.539	0.599	0.554
0.016	0.049	0.011	0.041	0.018	0.057	0.059
-	0.071	0.035	-	-	-	0.011
0.000	0.001	0.002	0.001	0.004	0.000	0.003
211.0	230.3	324.3	205.6	179.1	193.4	181.1

Q931973-12-2	Q931973-5-10	Q931973-5-8	Q931973-5-9	Q931973-6-4	Q931973-6-6	Q931973-7-10-C
Mod wm ± chl	Mod wm ± chl	Mod wm ± chl	Mod wm ± chl	Mod wm ± chl	Mod wm ± chl	Mod wm ± chl
51.122	49.815	52.131	51.857	51.758	50.220	51.488
29.924	32.983	28.871	29.524	29.299	32.682	28.801
3.282	1.440	3.473	3.012	3.164	1.195	3.428
1.865	0.782	2.173	1.795	1.996	1.040	2.115
0.000	0.011	0.029	0.024	0.009	0.042	0.034
0.436	0.323	0.385	0.414	0.442	0.310	0.447
-	-	-	-	0.046	0.053	-
0.004	-	0.006	0.003	0.014	0.022	0.022
0.005	0.217	-	0.048	0.027	0.481	0.019
0.126	0.178	0.127	0.108	0.128	0.264	0.089
7.753	7.419	8.034	7.767	7.539	7.391	7.976
1.106	0.201	0.737	0.926	0.411	0.072	0.889
0.041	-	0.018	-	-	0.057	0.015
0.011	0.017	-	0.008	0.011	0.079	-
95.675	93.386	95.984	95.486	94.844	93.908	95.323
3.35	3.31	3.41	3.40	3.42	3.31	3.40
0.65	0.69	0.59	0.60	0.58	0.69	0.60
1.669	1.884	1.642	1.681	1.696	1.855	1.639
2.314	2.579	2.228	2.281	2.279	2.541	2.240
0.000	0.000	0.001	0.001	0.000	0.002	0.001
0.011	0.008	0.010	0.011	0.011	0.008	0.012
-	-	-	-	0.002	0.003	-
0.180	0.080	0.190	0.165	0.175	0.066	0.189
0.182	0.077	0.212	0.175	0.196	0.102	0.208
0.000	-	0.000	0.000	0.001	0.001	0.001
0.000	0.015	-	0.003	0.002	0.034	0.001
0.016	0.023	0.016	0.014	0.016	0.034	0.011
0.649	0.628	0.671	0.650	0.635	0.622	0.672
0.055	0.010	0.036	0.046	0.020	0.004	0.044
0.009	-	0.004	-	-	0.012	0.003
0.001	0.002	-	0.001	0.001	0.009	-
206.0	200.4	217.2	208.3	207.4	207.9	216.5

Q931973-7-5	Q931973-7-8	Q931973-7-9	Q931973-8-6	Q931973-8-7-C	Q931973-9-5	Q931984-10-12-C
Mod wm ± chl	Mod wm ± chl	Mod wm ± chl	Mod wm ± chl	Mod wm ± chl	Mod wm ± chl	Mod wm ± chl
51.988	52.185	51.902	51.576	50.139	51.339	51.505
29.028	29.565	29.670	29.421	28.280	28.697	27.527
3.223	3.183	3.211	3.259	3.314	3.449	4.189
2.016	1.896	1.875	1.903	1.866	2.175	2.052
0.013	0.026	0.029	0.011	0.000	0.016	0.005
0.483	0.461	0.400	0.420	0.546	0.423	0.215
-	-	0.000	-	0.012	-	0.001
0.006	0.012	0.009	0.011	0.004	0.017	0.012
0.002	-	0.006	0.003	0.032	0.036	0.021
0.094	0.128	0.098	0.107	0.102	0.194	0.105
7.948	7.939	7.788	7.655	7.578	7.522	7.254
0.701	0.528	1.093	1.172	0.805	0.764	0.566
-	-	0.035	0.002	-	0.018	0.033
0.004	0.002	-	0.005	0.008	0.004	0.016
95.506	95.925	96.116	95.545	92.686	94.654	93.501
3.42	3.42	3.38	3.38	3.40	3.40	3.45
0.58	0.58	0.62	0.62	0.60	0.60	0.55
1.669	1.696	1.665	1.659	1.660	1.645	1.631
2.250	2.280	2.280	2.275	2.260	2.242	2.176
0.000	0.001	0.001	0.000	0.000	0.001	0.000
0.012	0.012	0.010	0.011	0.015	0.011	0.006
-	-	0.000	-	0.001	-	0.000
0.177	0.174	0.175	0.179	0.188	0.191	0.235
0.198	0.185	0.182	0.186	0.189	0.215	0.205
0.000	0.001	0.000	0.001	0.000	0.001	0.001
0.000	-	0.000	0.000	0.002	0.003	0.002
0.012	0.016	0.012	0.014	0.013	0.025	0.014
0.667	0.663	0.648	0.641	0.655	0.636	0.621
0.035	0.026	0.054	0.058	0.041	0.038	0.029
-	-	0.007	0.000	-	0.004	0.007
0.000	0.000	-	0.001	0.001	0.000	0.002
215.6	212.0	207.0	205.1	207.3	208.3	205.8

Q931984-10-8 Mod wm ± chl	Q931984-1-6 Mod wm ± chl	Q931984-1-8 Mod wm ± chl	Q931984-3.2-11 Mod wm ± chl	Q931984-3.2-7 Mod wm ± chl	Q931984-3.2-9 Mod wm ± chl	Q931984-3-13 Mod wm ± chl
51.228	50.329	51.292	50.972	50.314	50.134	52.099
27.664	27.105	27.757	28.069	29.466	29.920	27.770
4.613	4.759	4.854	4.668	4.238	4.192	4.090
2.003	1.880	1.973	2.010	1.790	2.659	2.073
-	0.040	0.007	0.035	0.029	0.019	0.052
0.187	0.180	0.122	0.132	0.200	0.095	0.234
0.007	-	-	-	0.004	0.009	-
0.028	0.003	0.004	0.019	0.025	0.018	0.006
0.074	0.025	0.013	0.006	0.004	0.144	0.020
0.085	0.161	0.220	0.177	0.213	0.117	0.084
8.032	7.152	6.568	7.425	8.010	5.826	7.582
0.982	1.200	1.202	1.113	0.762	0.219	0.427
-	-	-	-	-	0.051	0.027
0.002	0.012	0.019	0.007	0.004	0.031	0.001
94.905	92.846	94.031	94.633	95.059	93.434	94.465
3.42	3.42	3.42	3.40	3.35	3.34	3.46
0.58	0.58	0.58	0.60	0.65	0.66	0.54
1.589	1.589	1.604	1.599	1.657	1.689	1.637
2.174	2.170	2.182	2.204	2.310	2.349	2.175
-	0.002	0.000	0.001	0.001	0.001	0.002
0.005	0.005	0.003	0.003	0.005	0.002	0.006
0.000	-	-	-	0.000	0.000	-
0.257	0.270	0.271	0.260	0.236	0.234	0.227
0.199	0.190	0.196	0.200	0.178	0.264	0.205
0.002	0.000	0.000	0.001	0.001	0.001	0.000
0.005	0.002	0.001	0.000	0.000	0.010	0.001
0.011	0.021	0.028	0.023	0.027	0.015	0.011
0.683	0.620	0.559	0.631	0.680	0.495	0.643
0.049	0.061	0.060	0.056	0.038	0.011	0.021
-	-	-	-	-	0.011	0.006
0.000	0.001	0.002	0.001	0.000	0.004	0.000
230.1	219.0	201.3	216.7	229.2	172.3	209.6

Q931984-3-14	Q931984-3-17	Q931984-3-18	Q931984-3-19-C	Q931984-4-10-C	Q931984-4-15	Q931984-5-8
Mod wm ± chl	Mod wm ± chl	Mod wm ± chl	Mod wm ± chl	Mod wm ± chl	Mod wm ± chl	Mod wm ± chl
52.462	53.165	51.763	52.144	53.230	51.976	51.844
28.000	28.162	27.691	27.552	27.917	27.863	28.864
4.027	4.077	4.544	4.618	4.225	4.390	3.858
2.106	2.186	2.141	2.030	2.136	2.123	2.212
0.013	0.063	-	0.002	0.019	0.014	0.008
0.220	0.219	0.166	0.104	0.225	0.174	0.222
-	0.008	-	0.024	0.024	-	-
0.005	0.029	0.028	0.007	0.007	0.015	0.001
0.032	0.020	0.037	0.025	0.011	0.009	0.006
0.126	0.150	0.142	0.109	0.120	0.122	0.248
7.805	8.017	7.439	7.246	7.756	7.628	8.605
0.534	0.280	1.033	1.129	0.612	0.682	0.817
0.054	0.021	-	-	0.077	-	0.032
0.000	0.010	-	0.024	0.003	0.000	0.003
95.384	96.407	94.984	95.014	96.362	94.996	96.720
3.45	3.47	3.43	3.45	3.47	3.44	3.39
0.55	0.53	0.57	0.55	0.53	0.56	0.61
1.628	1.631	1.595	1.595	1.614	1.617	1.611
2.173	2.164	2.163	2.147	2.144	2.175	2.223
0.000	0.002	-	0.000	0.001	0.001	0.000
0.006	0.006	0.004	0.003	0.006	0.005	0.006
-	0.000	-	0.001	0.001	-	-
0.222	0.222	0.252	0.255	0.230	0.243	0.211
0.207	0.213	0.212	0.200	0.208	0.210	0.215
0.000	0.002	0.002	0.000	0.000	0.001	0.000
0.002	0.001	0.003	0.002	0.001	0.001	0.000
0.016	0.019	0.018	0.014	0.015	0.016	0.031
0.656	0.667	0.629	0.611	0.645	0.644	0.717
0.026	0.014	0.052	0.056	0.030	0.034	0.040
0.011	0.004	-	-	0.016	-	0.007
0.000	0.001	-	0.003	0.000	0.000	0.000
211.2	212.8	210.8	210.1	210.4	213.2	224.9

Q931984-5-9	Q931984-6-5-C	Q931984-6-6	Q931984-7.1-4	Q931984-7.1-6	Q931984-7-12	Q931984-9-5
Mod wm ± chl	Mod wm ± chl	Mod wm ± chl	Mod wm ± chl	Mod wm ± chl	Mod wm ± chl	Mod wm ± chl
51.396	51.105	51.956	49.850	45.219	52.985	52.766
27.519	28.084	27.692	24.950	25.950	28.111	28.736
4.669	4.901	4.336	7.042	9.664	4.154	4.191
2.044	2.007	2.065	3.415	4.658	2.119	2.101
0.039	0.028	0.007	0.027	-	-	0.002
0.166	0.227	0.223	0.606	0.020	0.177	0.253
-	0.033	-	-	0.023	-	0.001
0.002	0.020	0.021	0.021	0.035	0.012	0.017
0.003	0.040	0.016	0.316	0.192	0.008	0.015
0.123	0.242	0.125	0.204	0.133	0.088	0.082
7.861	7.019	7.863	7.697	5.078	7.518	7.811
1.020	0.741	0.376	0.008	0.291	0.708	0.520
-	-	0.010	0.065	0.150	0.035	-
0.007	0.020	0.007	0.050	0.019	0.006	0.004
94.849	94.467	94.697	94.251	91.432	95.921	96.499
3.42	3.41	3.46	3.41	3.20	3.46	3.44
0.58	0.59	0.54	0.59	0.80	0.54	0.56
1.585	1.617	1.626	1.427	1.357	1.626	1.644
2.161	2.208	2.170	2.013	2.161	2.164	2.206
0.002	0.001	0.000	0.001	-	-	0.000
0.004	0.006	0.006	0.016	0.001	0.005	0.006
-	0.002	-	-	0.001	-	0.000
0.260	0.273	0.241	0.403	0.571	0.227	0.228
0.203	0.200	0.205	0.349	0.491	0.206	0.204
0.000	0.001	0.001	0.001	0.002	0.001	0.001
0.000	0.003	0.001	0.023	0.015	0.001	0.001
0.016	0.031	0.016	0.027	0.018	0.011	0.010
0.668	0.597	0.667	0.672	0.458	0.626	0.649
0.051	0.037	0.019	0.000	0.015	0.035	0.025
-	-	0.002	0.014	0.034	0.007	-
0.001	0.002	0.001	0.006	0.002	0.001	0.000
225.8	211.3	220.0	226.3	175.7	204.9	211.9

Q931984-9-6	Q931984-9-8	Q931984-9-9
Mod wm ± chl	Mod wm ± chl	Mod wm ± chl
52.242	51.959	52.277
27.992	28.033	28.182
4.162	4.569	3.997
2.033	1.979	2.085
0.022	0.001	0.012
0.217	0.106	0.265
-	-	0.004
0.027	-	0.013
0.013	0.008	0.004
0.160	0.112	0.120
7.833	7.686	7.717
0.384	1.096	0.578
-	-	-
0.007	0.004	0.017
95.092	95.553	95.271
3.46	3.42	3.45
0.54	0.58	0.55
1.638	1.589	1.636
2.182	2.174	2.190
0.001	-	0.000
0.006	0.005	0.007
-	0.000	0.000
0.230	0.257	0.220
0.200	0.199	0.205
0.002	0.002	0.001
0.001	0.005	0.000
0.021	0.011	0.015
0.661	0.683	0.649
0.019	0.049	0.029
-	-	-
0.001	0.000	0.002
216.6	230.1	209.5

Appendix 5.2 Results of electron probe microanalyzer analysis of carbonate minerals

Point_ID[1]	D00005981-1-11	D00005981-1-5	D00005981-4-2	D00005981-5-1	D00005981-5-10
Alteration assemblage	Mod wm ± chl	Mod wm ± chl	Mod wm ± chl	Mod wm ± chl	Mod wm ± chl
Microprobe analysis (wt %)					
FeO	18.146	17.560	17.979	14.465	17.603
BaO	0.000	0.035	0.000	0.020	0.013
CaO	28.248	28.171	28.422	28.309	28.118
SrO	0.086	0.098	0.147	0.107	0.107
MgO	9.283	9.499	9.776	12.050	9.373
MnO	0.660	0.666	0.685	0.995	0.650
ZnO	0.000	0.002	0.000	0.025	0.012
CO2	43.627	43.967	43.007	44.029	44.124
Total	100.003	99.998	99.999	100.000	100.000
Atoms per formula units					
Fe^{2+}	0.254	0.245	0.253	0.200	0.245
Ba	0.000	0.000	0.000	0.000	0.000
Ca	0.507	0.504	0.513	0.501	0.502
Sr	0.001	0.001	0.001	0.001	0.001
Mg	0.232	0.236	0.245	0.297	0.233
Mn	0.009	0.009	0.010	0.014	0.009
Zn	0.000	0.000	0.000	0.000	0.000
C	1.00	1.00	0.99	0.99	1.00

[1] If point id is the same, C at the end stands for core of the grains, R stands for the rim of the grain.

Point_ID[1]	Q930221-4-2	Q930221-4-4	Q930221-4-5	Q930221-4-7	Q930221-5-15-C
Alteration assemblage	Mod wm ± chl	Mod wm ± chl	Mod wm ± chl	Mod wm ± chl	Mod wm ± chl
Microprobe analysis (wt %)					
FeO	41.125	41.009	41.432	41.770	15.906
BaO	0.058	0.034	0.051	0.095	0.000
CaO	2.003	3.385	3.985	2.058	28.326
SrO	0.000	0.000	0.000	0.000	0.081
MgO	9.831	9.373	10.964	9.868	10.719
MnO	0.502	0.686	0.382	0.744	0.734
ZnO	0.000	0.000	0.000	0.018	0.009
CO2	46.507	45.581	43.209	45.524	44.225
Total	99.999	99.999	99.998	99.999	100.000
Atoms per formula units					
Fe^{2+}	0.578	0.581	0.599	0.593	0.220
Ba	0.000	0.000	0.000	0.001	0.000
Ca	0.036	0.061	0.074	0.037	0.503
Sr	0.000	0.000	0.000	0.000	0.001
Mg	0.246	0.237	0.283	0.250	0.265
Mn	0.007	0.010	0.006	0.011	0.010
Zn	0.000	0.000	0.000	0.000	0.000
C	1.07	1.06	1.02	1.05	1.00

[1] If point id is the same, C at the end stands for core of the grains, R stands for the rim of the grain.

D00005981-5-2	D00005981-5-3	D00005981-5-9	D00005981-7-12	D00005981-7-16	D00005981-8-1
Mod wm ± chl	Mod wm ± chl	Mod wm ± chl	Mod wm ± chl	Mod wm ± chl	Mod wm ± chl
14.674	17.287	14.775	17.771	17.989	18.059
0.000	0.000	0.000	0.012	0.000	0.000
28.582	28.237	28.592	28.372	28.272	28.392
0.138	0.123	0.155	0.117	0.136	0.060
11.765	10.191	11.065	9.402	9.405	9.601
0.994	0.618	0.984	0.752	0.710	0.663
0.006	0.013	0.025	0.031	0.004	0.032
43.884	43.573	44.435	43.545	43.512	43.229
100.001	100.002	100.000	100.002	100.000	99.999
0.203	0.242	0.204	0.249	0.252	0.254
0.000	0.000	0.000	0.000	0.000	0.000
0.507	0.506	0.506	0.510	0.508	0.511
0.001	0.001	0.001	0.001	0.001	0.001
0.290	0.254	0.272	0.235	0.235	0.241
0.014	0.009	0.014	0.011	0.010	0.009
0.000	0.000	0.000	0.000	0.000	0.000
0.99	0.99	1.00	1.00	1.00	0.99

Q930221-5-15-R	Q930221-5-2	Q930221-6-3	Q930221-6-5	Q930221-8-11	Q930221-8-14
Mod wm ± chl	Mod wm ± chl	Mod wm ± chl	Mod wm ± chl	Mod wm ± chl	Mod wm ± chl
6.381	43.888	42.507	41.989	18.077	42.737
0.176	0.043	0.052	0.093	0.036	0.017
34.365	2.058	3.525	4.089	28.429	3.346
0.108	0.050	0.031	0.096	0.036	0.036
11.820	9.613	10.339	10.414	9.229	10.127
0.882	0.486	0.552	0.512	0.665	0.476
0.004	0.004	0.007	0.000	0.038	0.000
46.265	43.859	42.987	42.813	43.492	43.295
100.001	100.001	100.000	100.001	100.002	99.999
0.086	0.635	0.618	0.611	0.254	0.619
0.001	0.000	0.000	0.001	0.000	0.000
0.591	0.038	0.066	0.076	0.511	0.062
0.001	0.001	0.000	0.001	0.000	0.000
0.283	0.248	0.268	0.270	0.231	0.262
0.012	0.007	0.008	0.008	0.009	0.007
0.000	0.000	0.000	0.000	0.000	0.000
1.01	1.04	1.02	1.02	1.00	1.02

D00005985-1-11	D00005985-2-7	D00005985-2-8	D00005985-8-1	D00005985-8-3	D00005985-8-6
Per wm	Per wm	Per wm	Per wm	Per wm	Per wm
6.519	11.576	8.880	12.339	6.419	11.568
0.062	0.023	0.000	0.000	0.012	0.000
29.440	28.844	28.542	28.894	29.599	29.819
0.062	0.046	0.000	0.048	0.000	0.000
16.592	13.230	13.881	12.877	16.483	12.732
1.479	1.455	1.182	1.319	1.456	1.317
0.000	0.016	0.024	0.064	0.000	0.049
45.859	44.808	47.540	44.476	46.050	44.543
99.999	99.998	99.999	100.001	99.999	99.999
0.087	0.158	0.118	0.169	0.085	0.158
0.000	0.000	0.000	0.000	0.000	0.000
0.503	0.504	0.484	0.507	0.504	0.523
0.001	0.000	0.000	0.000	0.000	0.000
0.394	0.322	0.328	0.315	0.391	0.311
0.020	0.020	0.016	0.018	0.020	0.018
0.000	0.000	0.000	0.001	0.000	0.001
1.00	1.00	1.03	0.99	1.00	0.99

Q930221-8-1-C	Q930221-8-1-R	Q930221-8-2	Q930221-8-3	Q930221-8-6	Q930221-8-7
Mod wm ± chl	Mod wm ± chl	Mod wm ± chl	Mod wm ± chl	Mod wm ± chl	Mod wm ± chl
42.799	42.924	17.806	41.055	10.630	16.958
0.074	0.065	0.000	0.077	0.009	0.000
3.702	1.634	28.601	4.926	30.170	28.318
0.000	0.000	0.078	0.000	0.073	0.047
10.436	9.588	9.873	10.631	13.908	10.087
0.379	0.381	0.622	0.447	0.520	0.606
0.000	0.010	0.021	0.026	0.007	0.054
42.650	45.460	43.014	42.879	44.683	43.934
99.998	99.999	100.000	99.998	100.000	100.001
0.624	0.610	0.251	0.595	0.145	0.236
0.001	0.000	0.000	0.001	0.000	0.000
0.069	0.030	0.516	0.092	0.526	0.505
0.000	0.000	0.001	0.000	0.001	0.000
0.271	0.243	0.248	0.275	0.337	0.251
0.006	0.005	0.009	0.007	0.007	0.009
0.000	0.000	0.000	0.000	0.000	0.001
1.01	1.06	0.99	1.02	0.99	1.00

D00005986-10-17	D00005986-10-24	D00005986-10-5	D00005986-10-7	D00005986-6-5	Q721071-4-2
Per chl - min	Per chl - min	Per chl - min	Per chl - min	Per chl - min	Per chl - bar
48.515	43.584	50.421	48.710	43.415	37.413
0.000	0.119	0.013	0.009	0.042	0.000
0.477	1.202	0.452	0.247	0.759	0.724
0.000	0.000	0.000	0.000	0.000	0.005
9.430	6.707	7.458	8.908	11.387	6.761
0.154	0.174	0.151	0.250	0.206	2.924
0.002	0.000	0.028	0.000	0.016	0.007
41.461	48.318	41.503	41.890	44.272	52.204
99.999	99.997	100.000	99.999	99.999	100.000
0.722	0.608	0.756	0.724	0.622	0.501
0.000	0.001	0.000	0.000	0.000	0.000
0.009	0.021	0.009	0.005	0.014	0.012
0.000	0.000	0.000	0.000	0.000	0.000
0.250	0.167	0.199	0.236	0.291	0.162
0.002	0.002	0.002	0.004	0.003	0.040
0.000	0.000	0.000	0.000	0.000	0.000
1.01	1.10	1.02	1.02	1.04	1.14

Q930221-9-1	Q930221-9-2-R	Q930221-9-4	Q931973-10-5	Q931973-12-1	Q931973-12-9
Mod wm ± chl	Mod wm ± chl	Mod wm ± chl	Mod wm ± chl	Mod wm ± chl	Mod wm ± chl
44.056	6.089	43.528	19.159	18.923	19.065
0.074	0.165	0.000	0.039	0.000	0.052
3.135	34.972	2.120	28.249	28.345	28.775
0.000	0.133	0.000	0.114	0.148	0.154
9.706	11.921	9.754	8.578	8.606	8.085
0.507	0.954	0.668	0.634	0.680	0.797
0.000	0.000	0.000	0.009	0.000	0.016
42.565	45.768	43.965	43.218	43.336	43.053
100.001	100.001	100.001	100.000	100.001	99.997
0.645	0.082	0.628	0.270	0.267	0.270
0.001	0.001	0.000	0.000	0.000	0.000
0.059	0.604	0.039	0.511	0.512	0.522
0.000	0.001	0.000	0.001	0.001	0.002
0.253	0.286	0.251	0.216	0.216	0.204
0.008	0.013	0.010	0.009	0.010	0.011
0.000	0.000	0.000	0.000	0.000	0.000
1.02	1.01	1.04	1.00	1.00	1.00

Q721080-14-14	Q721080-1-5	Q721080-5-1	Q721080-7-1	Q930216-1-6	Q930216-1-8	Q930216-2-3	Q930216-2-6
Per chl - min	Per chl - min	Per chl - min	Per chl - min	Per chl - min	Per chl - min	Per chl - min	Per chl - min
36.727	34.636	38.381	35.982	12.968	10.594	10.829	12.776
0.000	0.000	0.000	0.067	0.000	0.000	0.023	0.000
0.311	0.886	0.244	0.380	27.901	28.451	29.303	28.420
0.002	0.000	0.000	0.022	0.013	0.011	0.046	0.052
17.458	16.382	15.626	18.205	11.344	14.447	14.063	12.307
1.731	4.126	2.322	1.675	3.185	0.294	0.270	2.151
0.111	0.020	0.071	0.103	0.030	0.025	0.022	0.000
43.674	44.032	43.384	43.567	44.598	46.184	45.443	44.312
100.001	100.000	100.002	100.001	100.001	100.001	99.999	100.000
0.518	0.488	0.547	0.507	0.179	0.142	0.146	0.176
0.000	0.000	0.000	0.000	0.000	0.000	0.000	0.000
0.006	0.016	0.004	0.007	0.492	0.488	0.507	0.501
0.000	0.000	0.000	0.000	0.000	0.000	0.000	0.000
0.439	0.411	0.397	0.457	0.279	0.345	0.339	0.302
0.025	0.059	0.033	0.024	0.044	0.004	0.004	0.030
0.001	0.000	0.001	0.001	0.000	0.000	0.000	0.000
1.01	1.01	1.01	1.00	1.00	1.01	1.00	1.00

Q931-973-2-4	Q931973-5-3	Q931973-5-5	Q931973-7-4	Q931973-9-6	Q931973-9-7	Q931984-10-10	Q931984-10-7
Mod wm ± chl	Mod wm ± chl	Mod wm ± chl	Mod wm ± chl	Mod wm ± chl	Mod wm ± chl	Mod wm ± chl	Mod wm ± chl
17.474	18.897	50.343	16.350	18.448	17.380	20.192	20.535
0.000	0.019	0.077	0.018	0.041	0.025	0.041	0.014
28.655	28.489	3.331	28.555	28.523	28.948	28.155	28.106
0.116	0.107	0.000	0.142	0.086	0.104	0.072	0.050
9.342	8.608	3.802	9.832	8.434	9.456	7.497	6.769
0.741	0.616	0.317	0.883	0.783	0.792	1.313	1.221
0.018	0.049	0.001	0.009	0.000	0.040	0.000	0.000
43.657	43.214	42.171	44.212	43.692	43.255	42.761	43.331
99.998	99.999	99.999	100.001	100.001	100.000	100.001	100.001
0.245	0.267	0.757	0.227	0.259	0.244	0.288	0.291
0.000	0.000	0.001	0.000	0.000	0.000	0.000	0.000
0.514	0.515	0.064	0.509	0.513	0.521	0.514	0.511
0.001	0.001	0.000	0.001	0.001	0.001	0.001	0.000
0.233	0.217	0.102	0.244	0.211	0.237	0.190	0.171
0.011	0.009	0.005	0.012	0.011	0.011	0.019	0.018
0.000	0.001	0.000	0.000	0.000	0.000	0.000	0.000
1.00	1.00	1.04	1.00	1.00	0.99	0.99	1.00

Q930216-2-7	Q930216-4-1	Q930216-4-2	Q930216-4-6	Q930216-7-5-C	Q930216-7-5-R	Q930221-10-10
Per chl - min	Per chl - min	Per chl - min	Per chl - min	Per chl - min	Per chl - min	Mod wm ± chl
20.282	41.099	51.564	10.600	10.398	10.493	18.111
0.926	0.012	0.123	0.009	0.000	0.038	0.000
0.045	0.290	4.200	29.353	29.234	29.215	28.568
0.000	0.017	0.071	0.000	0.041	0.030	0.000
13.464	13.528	1.544	15.064	14.919	15.127	9.637
0.087	1.135	0.738	0.176	0.122	0.138	0.637
0.085	0.181	0.000	0.009	0.029	0.046	0.004
65.655	43.739	41.763	44.813	45.276	44.913	43.080
100.000	100.001	100.000	100.002	100.002	100.000	100.001
0.235	0.588	0.786	0.144	0.140	0.142	0.255
0.005	0.000	0.001	0.000	0.000	0.000	0.000
0.001	0.005	0.082	0.509	0.505	0.506	0.515
0.000	0.000	0.001	0.000	0.000	0.000	0.000
0.278	0.345	0.042	0.364	0.359	0.365	0.242
0.001	0.016	0.011	0.002	0.002	0.002	0.009
0.001	0.002	0.000	0.000	0.000	0.001	0.000
1.24	1.02	1.04	0.99	1.00	0.99	0.99

Q931984-3-15	Q931984-3-16	Q931984-3-23	Q931984-4-11	Q931984-5-6	Q931984-5-7	Q931984-6-4
Mod wm ± chl	Mod wm ± chl	Mod wm ± chl	Mod wm ± chl	Mod wm ± chl	Mod wm ± chl	Mod wm ± chl
19.330	20.675	15.222	18.097	49.215	12.612	19.605
0.007	0.000	0.044	0.025	0.000	0.020	0.041
28.116	28.253	33.551	29.408	1.137	30.702	28.059
0.007	0.042	0.092	0.020	0.000	0.066	0.017
7.571	7.314	5.977	8.227	6.451	8.228	8.087
1.756	1.253	1.669	1.344	2.146	3.719	1.191
0.042	0.008	0.000	0.033	0.015	0.000	0.000
43.172	42.462	43.443	42.845	41.071	44.661	43.010
100.001	99.999	99.998	99.999	99.998	100.000	99.999
0.274	0.296	0.215	0.256	0.744	0.175	0.278
0.000	0.000	0.000	0.000	0.000	0.000	0.000
0.511	0.517	0.607	0.534	0.022	0.546	0.510
0.000	0.000	0.001	0.000	0.000	0.001	0.000
0.191	0.186	0.150	0.208	0.174	0.203	0.204
0.025	0.018	0.024	0.019	0.033	0.052	0.017
0.001	0.000	0.000	0.000	0.000	0.000	0.000
1.00	0.99	1.00	0.99	1.01	1.01	1.00

Q930221-11-2	Q930221-1-3	Q930221-1-6	Q930221-2-10	Q930221-2-6	Q930221-2-8-C	Q930221-2-8-R
Mod wm ± chl	Mod wm ± chl	Mod wm ± chl	Mod wm ± chl	Mod wm ± chl	Mod wm ± chl	Mod wm ± chl
17.851	32.683	18.243	41.682	41.989	18.476	15.900
0.000	0.022	0.000	0.077	0.039	0.035	0.018
28.476	6.684	28.480	3.507	2.788	28.458	28.609
0.123	0.000	0.063	0.000	0.005	0.068	0.074
9.957	15.175	9.302	10.486	9.856	9.470	10.484
0.629	0.396	0.685	0.506	0.506	0.648	0.681
0.033	0.001	0.042	0.000	0.006	0.009	0.024
42.934	45.087	43.199	43.839	44.810	42.836	44.211
100.000	99.999	100.000	100.000	99.999	100.000	100.001
0.251	0.454	0.257	0.600	0.600	0.261	0.220
0.000	0.000	0.000	0.001	0.000	0.000	0.000
0.514	0.119	0.514	0.065	0.051	0.515	0.508
0.001	0.000	0.001	0.000	0.000	0.001	0.001
0.250	0.376	0.233	0.269	0.251	0.238	0.259
0.009	0.006	0.010	0.007	0.007	0.009	0.010
0.000	0.000	0.001	0.000	0.000	0.000	0.000
0.99	1.02	0.99	1.03	1.05	0.99	1.00

Q931984-7-11	Q931984-9-7-C	Q931984-9-7-R
Mod wm ± chl	Mod wm ± chl	Mod wm ± chl
1.128	1.039	1.261
0.254	0.000	0.039
48.982	54.967	54.567
0.033	0.110	0.191
0.328	0.252	0.317
0.779	0.596	0.202
0.000	0.019	0.015
48.514	43.051	43.408
100.001	100.000	100.000
0.015	0.015	0.018
0.002	0.000	0.000
0.841	0.991	0.981
0.000	0.001	0.002
0.008	0.006	0.008
0.011	0.008	0.003
0.000	0.000	0.000
1.06	0.99	0.99

Appendix 5.3 Results of electron microprobe mycroanalyzer analysis of chlorite

Point_ID	D005986-1-11	D005986-1-8	D005986-2-7	D005986-4-5	D005986-5-9	D005986-6-10-c
Alteration assemblage	Per chl - min	Per chl - min	Per chl - min	Per chl - min	Per chl - min	Per chl - min
Microprobe analysis (wt %)						
SiO_2	25.37	25.63	24.45	24.91	25.79	25.46
TiO_2	0.05	0.07	0.10	0.07	0.06	0.03
Al_2O_3	20.37	19.84	21.26	20.78	19.98	19.91
Cr_2O_3	0.01	0.00	0.00	-	0.00	-
V_2O_3	-	0.00	0.02	0.00	-	-
FeO	23.44	23.02	25.10	23.79	23.46	23.49
MnO	0.08	0.08	0.09	0.08	0.08	0.07
ZnO	0.13	0.11	0.13	0.17	0.17	0.15
MgO	15.81	16.26	14.32	15.55	16.33	15.67
CaO	-	0.00	0.03	0.02	0.01	0.04
SrO	-	-	0.02	0.02	0.02	0.02
Na_2O	0.01	0.01	0.04	0.08	-	0.06
K_2O	0.04	-	0.01	0.03	-	0.01
BaO	-	-	-	-	0.00	-
F	0.01	0.01	0.02	0.01	0.01	0.01
Cl	-	-	-	-	-	-
Total	85.17	84.79	85.36	85.33	85.74	84.72
Atoms per formula units						
Si(IV)	2.73	2.76	2.65	2.68	2.75	2.75
Al (IV)	1.27	1.24	1.35	1.32	1.25	1.25
Al (VI)	1.31	1.28	1.36	1.32	1.27	1.29
Al total	2.58	2.52	2.72	2.64	2.51	2.54
Fe^{2+}	2.11	2.07	2.27	2.14	2.09	2.12
Ba	0.00	0.00	0.00	0.00	0.00	0.00
Sr	0.00	0.00	0.00	0.00	0.00	0.00
Cr	0.00	0.00	0.00	0.00	0.00	0.00
V	0.00	0.00	0.00	0.00	0.00	0.00
Zn	0.01	0.01	0.01	0.01	0.01	0.01
Mg	2.53	2.61	2.31	2.50	2.60	2.53
Mn	0.01	0.01	0.01	0.01	0.01	0.01
Ca	0.00	0.00	0.00	0.00	0.00	0.00
Na	0.00	0.00	0.01	0.02	0.00	0.01
K	0.00	0.00	0.00	0.00	0.00	0.00
Ti	0.00	0.00	0.00	0.00	0.00	0.00
F	0.00	0.00	0.00	0.00	0.00	0.00
Cl	0.00	0.00	0.00	0.00	0.00	0.00
T (C) K&M[1]	321.27	313.90	341.13	331.62	315.43	316.11
T (C) Cath[2]	347.40	337.49	372.86	362.24	339.40	339.26
T (C) Jw[3]	336.31	326.50	361.50	351.00	328.40	328.25
T(C) Z&F[4]	276.94	271.46	289.83	286.00	272.38	271.30

[1] Calculated after Cathelineau (1988). Formula: T(°C) = -61.92 + 321.98(Al^{IV})

[2] Calculated after Kranidiotis & MacLean (1987). Formula: T(°C) = 106(Al^{IV})$_{corrected}$ + 18, where Al(^{IV})$_{corrected}$ = (Al^{IV})$_{sample}$ ± 0.7 Fe/(Fe+Mg).

[3] Calculated after Jowett (1991). Formula: T(°C) = 318.5(Al^{IV})$_C$ - 68.7, where Al(IV)$_C$ = Al(^{IV})$_M$ + 0.1 Fe/(Fe+Mg).

[4] Calculated after Zang & Fyfe (1995). Formula: T(°C) = 106.2(Al^{IV})$_{corrected}$ + 17.5, where Al(^{IV})$_{corrected}$ = (Al^{IV})$_{sample}$ ± 0.88 [Fe/(Fe+Mg) - 0.34].

D005986-6-4-c	D005986-8-10	D005986-8-14	D005986-9-22	D005986-9-23	Q721071-1-4	Q721071-1-5-C	Q721071-1-6
Per chl - min	Per chl - min	Per chl - min	Per chl - min	Per chl - min	Per chl - bar	Per chl - bar	Per chl - bar
24.39	25.51	24.98	25.02	24.83	24.56	26.18	26.13
0.00	0.06	0.03	0.05	0.05	0.09	0.05	0.06
21.79	20.21	20.67	20.63	20.78	20.60	20.88	20.73
0.01	-	0.00	-	-	0.00	0.00	0.01
-	-	0.00	0.02	-	0.03	0.00	0.02
23.70	23.57	24.45	23.68	24.55	25.19	23.80	23.27
0.07	0.08	0.07	0.09	0.08	0.41	0.39	0.39
0.15	0.15	0.13	0.14	0.08	0.05	0.03	0.07
15.42	15.93	15.26	15.20	14.84	14.10	14.53	14.57
0.01	0.03	0.00	0.01	0.02	0.01	0.03	0.03
0.02	0.03	-	0.01	0.00	0.03	0.01	-
0.00	0.05	0.01	0.01	0.09	0.01	0.00	0.02
0.01	0.01	0.00	0.02	0.03	0.01	0.01	0.01
0.01	-	0.02	0.01	-	-	0.02	-
0.01	0.03	-	0.03	0.02	0.01	0.01	0.01
-	-	-	-	-	-	-	-
85.38	85.42	85.40	84.73	85.14	84.88	85.70	85.15
2.62	2.74	2.69	2.71	2.69	2.68	2.79	2.80
1.38	1.26	1.31	1.29	1.31	1.32	1.21	1.20
1.38	1.29	1.32	1.34	1.34	1.33	1.41	1.42
2.76	2.55	2.63	2.63	2.65	2.65	2.62	2.62
2.13	2.11	2.20	2.14	2.22	2.30	2.12	2.09
0.00	0.00	0.00	0.00	0.00	0.00	0.00	0.00
0.00	0.00	0.00	0.00	0.00	0.00	0.00	0.00
0.00	0.00	0.00	0.00	0.00	0.00	0.00	0.00
0.00	0.00	0.00	0.00	0.00	0.00	0.00	0.00
0.01	0.01	0.01	0.01	0.01	0.00	0.00	0.01
2.47	2.55	2.45	2.45	2.39	2.30	2.31	2.33
0.01	0.01	0.01	0.01	0.01	0.04	0.04	0.04
0.00	0.00	0.00	0.00	0.00	0.00	0.00	0.00
0.00	0.01	0.00	0.00	0.02	0.00	0.00	0.00
0.00	0.00	0.00	0.00	0.00	0.00	0.00	0.00
0.00	0.00	0.00	0.00	0.00	0.00	0.00	0.00
0.00	0.00	0.00	0.00	0.00	0.00	0.00	0.00
0.00	0.01	0.00	0.00	0.00	0.00	0.00	0.00
344.96	319.79	330.37	326.27	332.10	334.48	309.87	307.37
382.35	345.21	359.05	353.60	360.76	362.23	327.29	324.21
370.89	334.14	347.83	342.44	349.53	350.98	316.41	313.36
299.16	275.53	282.82	279.87	283.20	282.38	261.35	259.90

Q721071-2-8	Q721071-2-9	Q721071-3-10	Q721071-3-5	Q721071-4-11	Q721071-5-2	Q721071-5-3	Q721071-5-5
Per chl - bar	Per chl - bar	Per chl - bar	Per chl - bar	Per chl - bar	Per chl - bar	Per chl - bar	Per chl - bar
26.32	25.60	25.00	25.01	24.79	25.26	24.27	25.31
0.04	0.09	0.06	0.08	0.05	0.08	0.08	0.06
21.09	20.65	20.32	20.17	20.27	20.15	19.45	20.25
0.00	-	-	-	0.01	-	-	0.01
0.03	0.01	0.02	0.00	0.03	0.02	0.02	0.03
23.66	23.86	24.71	24.53	24.49	24.67	25.37	24.93
0.38	0.40	0.42	0.41	0.41	0.40	0.42	0.39
0.05	0.06	0.04	0.07	0.04	0.05	0.07	0.05
14.03	15.21	14.63	14.48	13.98	15.03	14.52	14.81
0.02	0.01	0.02	0.01	0.01	0.02	0.04	0.01
0.01	-	0.01	-	-	0.02	-	0.02
-	0.05	0.02	0.00	0.01	0.03	-	0.05
0.07	0.01	0.01	-	0.01	0.00	0.00	0.01
0.01	0.01	-	0.05	-	0.02	0.00	-
0.00	0.00	0.01	0.00	0.01	-	0.00	0.03
-	-	-	-	-	-	-	-
85.53	85.80	85.06	84.63	83.87	85.60	83.87	85.79
2.81	2.74	2.72	2.73	2.73	2.73	2.69	2.73
1.19	1.26	1.28	1.27	1.27	1.27	1.31	1.27
1.46	1.34	1.32	1.32	1.36	1.29	1.23	1.30
2.65	2.60	2.60	2.59	2.63	2.56	2.54	2.57
2.11	2.13	2.24	2.24	2.25	2.23	2.35	2.25
0.00	0.00	0.00	0.00	0.00	0.00	0.00	0.00
0.00	0.00	0.00	0.00	0.00	0.00	0.00	0.00
0.00	0.00	0.00	0.00	0.00	0.00	0.00	0.00
0.00	0.00	0.00	0.00	0.00	0.00	0.00	0.00
0.00	0.00	0.00	0.01	0.00	0.00	0.01	0.00
2.23	2.43	2.37	2.36	2.29	2.42	2.40	2.38
0.03	0.04	0.04	0.04	0.04	0.04	0.04	0.04
0.00	0.00	0.00	0.00	0.00	0.00	0.00	0.00
0.00	0.01	0.00	0.00	0.00	0.01	0.00	0.01
0.01	0.00	0.00	0.00	0.00	0.00	0.00	0.00
0.00	0.00	0.00	0.00	0.00	0.00	0.00	0.00
0.00	0.00	0.00	0.00	0.00	0.00	0.00	0.00
0.00	0.00	0.00	0.00	0.00	0.00	0.00	0.01
306.43	320.08	326.41	323.47	324.55	323.65	332.56	323.93
321.24	344.01	351.55	346.99	347.70	348.17	359.93	347.87
310.43	332.95	340.41	335.91	336.61	337.07	348.71	336.77
256.67	273.38	276.63	273.56	273.26	275.08	281.38	274.29

Q721071-7-8	Q721071-8-10	Q721071-8-6	Q721080-12-1	Q721080-12-5	Q721080-14-5	Q721080-2-11	Q721080-2-2
Per chl - bar	Per chl - bar	Per chl - bar	Per chl - min	Per chl - min	Per chl - min	Per chl - min	Per chl - min
25.51	25.14	24.70	27.25	28.48	28.95	25.74	25.20
0.08	0.06	0.05	0.01	0.00	0.01	0.07	0.05
19.96	20.24	20.55	16.52	15.39	15.53	20.12	20.71
0.01	0.00	0.00	0.00	0.00	0.01	-	-
0.04	0.04	0.03	0.00	-	0.02	0.00	-
24.15	24.10	24.86	28.24	31.55	26.42	22.36	22.32
0.42	0.37	0.41	0.05	0.01	0.03	0.21	0.25
0.08	0.04	0.06	0.14	0.01	0.08	0.08	0.13
15.08	14.90	14.21	12.02	8.88	12.99	16.55	16.42
0.02	0.01	0.01	0.11	0.21	0.16	0.05	0.01
0.03	0.02	-	0.02	0.01	0.01	-	0.02
0.00	0.02	0.01	0.09	0.19	0.07	0.07	-
0.02	0.01	0.01	0.07	0.11	0.05	0.01	0.00
0.00	-	0.00	-	0.02	0.00	0.05	0.00
0.00	0.01	0.00	0.02	0.01	0.01	0.02	-
-	-	-	-	-	-	-	-
85.18	84.80	84.69	84.37	84.66	84.29	85.14	84.92
2.76	2.73	2.70	3.04	3.21	3.19	2.75	2.70
1.24	1.27	1.30	0.96	0.79	0.81	1.25	1.30
1.30	1.32	1.34	1.20	1.25	1.20	1.29	1.32
2.54	2.59	2.64	2.17	2.04	2.01	2.54	2.62
2.18	2.19	2.27	2.63	2.97	2.43	2.00	2.00
0.00	0.00	0.00	0.00	0.00	0.00	0.00	0.00
0.00	0.00	0.00	0.00	0.00	0.00	0.00	0.00
0.00	0.00	0.00	0.00	0.00	0.00	0.00	0.00
0.00	0.00	0.00	0.00	0.00	0.00	0.00	0.00
0.01	0.00	0.00	0.00	0.00	0.00	0.01	0.01
2.43	2.41	2.31	2.00	1.49	2.13	2.64	2.63
0.04	0.03	0.04	0.00	0.00	0.00	0.02	0.02
0.00	0.00	0.00	0.01	0.03	0.02	0.01	0.00
0.00	0.00	0.00	0.02	0.04	0.01	0.01	0.00
0.00	0.00	0.00	0.01	0.02	0.01	0.00	0.00
0.00	0.00	0.00	0.00	0.00	0.00	0.00	0.00
0.00	0.00	0.00	0.00	0.00	0.00	0.00	0.00
0.00	0.00	0.00	0.00	0.00	0.00	0.00	0.00
316.72	322.51	330.98	264.66	235.40	230.27	314.26	325.17
338.33	346.85	357.49	248.55	193.14	200.34	339.33	355.74
327.33	335.76	346.30	238.50	183.67	190.80	328.33	344.56
269.16	274.54	279.74	201.00	155.34	172.52	273.75	284.44

Q721080-3-6	Q721080-3-8	Q721080-4-8	Q721080-4-9	Q721080-5-2	Q721080-5-4	Q721080-9-8	Q930216-12-3
Per chl - min	Per chl - min	Per chl - min	Per chl - min	Per chl - min	Per chl - min	Per chl - min	Per chl - min
25.42	25.49	25.46	25.56	25.85	25.48	26.32	25.34
0.08	0.03	0.09	0.05	0.06	0.06	0.05	0.02
20.47	20.54	20.31	20.13	20.83	20.82	18.49	19.71
0.01	-	0.00	-	0.00	-	0.01	-
0.01	0.01	-	-	0.01	0.02	0.01	-
21.16	22.12	22.59	22.61	21.84	21.63	23.38	24.79
0.22	0.16	0.21	0.20	0.24	0.16	0.16	0.23
0.14	0.17	0.25	0.12	0.16	0.18	0.09	0.17
16.98	16.60	16.84	16.52	17.24	17.11	16.66	14.80
0.01	0.02	0.02	0.01	0.02	0.00	0.02	0.02
0.02	0.02	-	0.01	0.03	0.01	0.02	0.02
0.01	0.07	0.01	0.03	0.06	0.03	0.01	0.04
0.01	0.01	-	0.01	0.03	0.01	0.01	0.04
-	0.02	-	-	-	-	-	0.00
-	0.03	0.01	0.01	0.01	0.00	0.01	0.01
-	-	-	-	-	-	-	-
84.34	85.09	85.59	85.07	86.24	85.32	85.07	84.98
2.73	2.72	2.71	2.74	2.72	2.71	2.83	2.76
1.27	1.28	1.29	1.26	1.28	1.29	1.17	1.24
1.32	1.31	1.27	1.28	1.30	1.31	1.18	1.28
2.59	2.59	2.55	2.54	2.58	2.61	2.35	2.53
1.90	1.98	2.01	2.03	1.92	1.92	2.10	2.25
0.00	0.00	0.00	0.00	0.00	0.00	0.00	0.00
0.00	0.00	0.00	0.00	0.00	0.00	0.00	0.00
0.00	0.00	0.00	0.00	0.00	0.00	0.00	0.00
0.00	0.00	0.00	0.00	0.00	0.00	0.00	0.00
0.01	0.01	0.02	0.01	0.00	0.00	0.00	0.00
2.72	2.65	2.68	2.64	2.71	2.71	2.67	2.40
0.02	0.01	0.02	0.02	0.02	0.01	0.01	0.02
0.00	0.00	0.00	0.00	0.00	0.00	0.00	0.00
0.00	0.01	0.00	0.01	0.01	0.01	0.00	0.01
0.00	0.00	0.00	0.00	0.00	0.00	0.00	0.01
0.00	0.00	0.00	0.00	0.00	0.00	0.00	0.00
0.00	0.00	0.00	0.00	0.00	0.00	0.00	0.00
0.00	0.01	0.00	0.00	0.00	0.00	0.00	0.00
318.06	320.04	322.30	317.31	319.90	322.84	297.91	317.90
347.32	348.49	351.74	343.60	349.66	354.19	313.47	337.79
336.23	337.39	340.60	332.55	338.55	343.03	302.73	326.80
280.86	280.11	282.10	276.27	282.03	285.07	255.82	266.87

Q930216-1-3	Q930216-13-12	Q930216-13-2	Q930216-13-6	Q930216-13-8	Q930216-1-5	Q930216-3-2	Q930216-3-7
Per chl - min	Per chl - min	Per chl - min	Per chl - min	Per chl - min	Per chl - min	Per chl - min	Per chl - min
25.18	25.06	25.06	25.28	25.70	24.96	25.00	25.17
0.02	0.00	0.04	0.02	0.05	0.02	0.01	0.01
19.55	19.75	19.95	19.49	19.37	19.79	20.17	19.73
0.00	-	-	-	0.00	0.00	-	-
-	0.01	0.00	-	-	-	0.01	-
25.07	25.07	25.59	24.87	24.62	25.35	25.66	24.54
0.19	0.20	0.22	0.20	0.20	0.21	0.20	0.17
0.15	0.13	0.13	0.18	0.21	0.15	0.13	0.08
14.41	14.51	14.02	14.66	14.75	14.24	14.30	14.99
0.01	0.02	0.05	0.01	0.04	0.02	0.05	0.01
0.02	-	-	-	-	0.02	-	0.03
0.03	0.02	0.04	0.03	0.06	0.05	0.06	0.04
0.01	0.06	0.07	0.13	0.26	0.02	0.06	0.10
-	-	-	0.01	0.01	0.00	0.03	-
0.07	0.01	0.02	0.01	0.02	0.01	0.01	0.01
-	-	-	-	-	-	-	-
84.46	84.60	84.97	84.65	85.08	84.61	85.45	84.63
2.76	2.74	2.74	2.76	3.63	2.74	2.72	2.74
1.24	1.26	1.26	1.24	0.37	1.26	1.28	1.26
1.28	1.29	1.31	1.27	1.87	1.29	1.30	1.28
2.52	2.55	2.57	2.51	2.24	2.56	2.58	2.53
2.30	2.29	2.34	2.27	2.54	2.32	2.33	2.24
0.00	0.00	0.00	0.00	0.00	0.00	0.00	0.00
0.00	0.00	0.00	0.00	0.00	0.00	0.00	0.00
0.00	0.00	0.00	0.00	0.00	0.00	0.00	0.00
0.00	0.00	0.00	0.00	0.00	0.00	0.00	0.00
0.00	0.00	0.00	0.00	0.00	0.00	0.00	0.00
2.35	2.37	2.28	2.39	0.71	2.33	2.32	2.44
0.02	0.02	0.02	0.02	0.00	0.02	0.02	0.02
0.00	0.00	0.01	0.00	0.07	0.00	0.01	0.00
0.01	0.00	0.01	0.01	0.04	0.01	0.01	0.01
0.00	0.01	0.01	0.02	0.05	0.00	0.01	0.01
0.00	0.00	0.00	0.00	0.00	0.00	0.00	0.00
0.00	0.00	0.00	0.00	0.00	0.00	0.00	0.00
0.01	0.00	0.00	0.00	0.01	0.00	0.00	0.00
323.11	317.79	321.41	323.25	316.57	153.81	327.61	319.89
345.04	338.68	343.31	344.56	336.48	56.34	351.66	342.52
333.98	327.68	332.26	333.50	325.51	48.31	340.53	331.48
271.11	268.33	270.67	270.21	266.59	54.35	275.30	271.41

Q930216-4.1-2-C	Q930216-4.1-4	Q930216-4.1-9	Q930216-4-4	Q930216-8-4	Q930216-9-10	Q930216-9-9	Q930221-5-1
Per chl - min	Per chl - min	Per chl - min	Per chl - min	Per chl - min	Per chl - min	Per chl - min	Mod wm ± chl
25.30	25.20	25.34	26.00	24.72	24.68	25.28	34.94
0.02	0.05	0.02	0.03	0.00	0.04	0.04	-
20.09	19.94	19.84	19.28	20.19	20.24	19.51	18.26
-	0.01	-	-	-	0.00	-	0.00
0.01	0.00	0.01	0.00	-	0.01	-	0.01
25.21	24.75	24.58	23.95	25.51	25.43	25.84	29.26
0.22	0.22	0.21	0.20	0.23	0.20	0.21	0.01
0.18	0.19	0.18	0.12	0.15	0.18	0.15	-
14.71	14.05	14.80	15.78	14.04	14.05	13.83	4.61
0.02	0.01	0.01	0.03	0.02	0.03	0.03	0.59
-	0.03	0.02	0.03	0.03	0.01	0.03	0.02
0.04	-	0.01	0.08	0.01	0.02	0.01	0.19
0.08	0.24	0.13	0.06	0.09	0.05	0.34	0.38
0.02	0.03	0.04	-	0.01	0.03	0.02	0.03
0.03	0.01	0.00	0.02	-	0.02	0.02	0.07
-	-	-	-	-	-	-	-
85.69	84.49	84.99	85.33	84.77	84.75	85.10	88.13
2.73	2.76	2.75	2.80	2.71	2.70	2.77	3.63
1.27	1.24	1.25	1.20	1.29	1.30	1.23	0.37
1.29	1.33	1.29	1.24	1.31	1.32	1.28	1.87
2.56	2.57	2.54	2.45	2.61	2.61	2.52	2.24
2.28	2.27	2.23	2.16	2.34	2.33	2.36	2.54
0.00	0.00	0.00	0.00	0.00	0.00	0.00	0.00
0.00	0.00	0.00	0.00	0.00	0.00	0.00	0.00
0.00	0.00	0.00	0.00	0.00	0.00	0.00	0.00
0.00	0.00	0.00	0.00	0.00	0.00	0.00	0.00
0.00	0.00	0.00	0.00	0.00	0.00	0.00	0.00
2.37	2.29	2.40	2.53	2.29	2.29	2.26	0.71
0.02	0.02	0.02	0.02	0.02	0.02	0.02	0.00
0.00	0.00	0.00	0.00	0.00	0.00	0.00	0.07
0.01	0.00	0.00	0.02	0.00	0.00	0.00	0.04
0.01	0.03	0.02	0.01	0.01	0.01	0.05	0.05
0.00	0.00	0.00	0.00	0.00	0.00	0.00	0.00
0.00	0.00	0.00	0.00	0.00	0.00	0.00	0.00
0.01	0.00	0.00	0.00	0.00	0.00	0.00	0.01
306.96	323.09	318.01	317.95	329.44	330.26	317.30	153.81
325.01	346.09	337.59	339.16	354.08	355.45	334.87	56.34
314.15	335.01	326.61	328.16	342.92	344.27	323.91	48.31
261.61	272.69	266.44	268.85	276.60	277.59	263.27	54.35

Q930221-5-12-C	Q931984-1-10
Mod wm ± chl	Mod wm ± chl
35.38	39.72
0.02	0.03
18.57	24.84
-	0.01
0.00	0.01
27.08	12.32
0.00	0.04
-	0.00
4.66	4.16
0.64	0.06
0.02	0.01
0.24	0.54
0.37	3.72
0.01	0.09
0.06	0.04
-	-
86.76	84.80
3.69	3.89
0.31	0.11
1.96	2.76
2.28	2.87
2.36	1.01
0.00	0.00
0.00	0.00
0.00	0.00
0.00	0.00
0.00	0.00
0.72	0.61
0.00	0.00
0.07	0.01
0.05	0.10
0.05	0.46
0.00	0.00
0.00	0.00
0.01	0.01
141.56	87.80
39.46	-
31.61	-
44.65	14.41

Appendix 6.1 Results of short-wave infrared analysis

Sample_id	B00267967	B00267968	B00267969	B00267970	B00267971	B00267972
DH_id	K15-200	K15-200	K15-200	K15-200	K15-200	K15-200
From_m	124.8	129.95	139.5	160.3	163.8	168.65
To_m	125	130.15	139.8	160.5	164	168.8
Lithology[1]	LT	LT	TF	TF	TF	TF
Alteration assemblage	Mod ser ± chl	-	Mod ser ± chl	Mod ser ± chl	-	Chl-carb-act
2200P[2] (nm)	2210.4	2207.71	2208.05	2217.94	2214.87	2199.05
2200D[2]	0.338	0.423	0.29	0.208	0.207	0.388
2255P (nm)	-	-	-	2241.11	-	-
2255D	-	-	-	0.123	-	-

Sample_id	Q930228	Q930229	Q930230	Q930231	Q930232	D00005977
DH_id	K15-274	K15-274	K15-274	K15-274	K15-274	K15-281
From_m	76.75	86.65	96.2	116.55	127.2	13.5
To_m	76.9	86.7	96.3	116.75	127.4	13.8
Lithology[1]	TF	MS	MS	MI	MI	LT
Alteration assemblage	Mod ser ± chl	-	Mod ser ± chl	Chl-carb-act	-	Mod ser ± chl
2200P (nm)	2212.95	2226.61	2218.62	2220.36	-	2213.82
2200D	0.0833	0.127	0.0835	0.211	-	0.29
2255P (nm)	2253.91	2257.9	2253.99	-	2255.72	-
2255D	0.098	0.122	0.08	-	0.215	-

Sample_id	Q931851	Q931852	Q931853	Q931854	Q721169	Q721170
DH_id	K15-299	K15-299	K15-299	K15-299	K15-300	K15-300
From_m	16.59	66.35	145.68	164.16	49.55	67.95
To_m	16.78	66.54	145.84	164.4	49.8	68.15
Lithology[1]	-	-	-	-	TF	VF
Alteration assemblage	-	-	-	-	Mod ser ± chl	Mod ser ± chl
2200P (nm)	2221	2207.89	2222.47	2215.88	2221.02	2215.7
2200D	0.058	0.463	0.189	0.516	0.257	0.329
2255P (nm)	2251.32	-	2253.28	-	-	-
2255D	0.117	-	0.248	-	-	-

Sample_id	B357979	B357980	B357981	B357982	B357983	B357984
DH_id	K16-358	K16-358	K16-358	K16-358	K16-358	K16-358
From_m	121.5	131.55	152.9	156	163.2	171.15
To_m	121.65	131.65	153	156.15	163.35	171.3
Lithology[1]	TF	TF	TF	TF	TF	TF
Alteration assemblage	Mod ser ± chl	Per ser	Mod ser ± chl	Per chl	Per ser	Chl-carb-act
2200P (nm)	2207.15	2204.06	2214.03	2222.57	2214.56	-
2200D	0.274	0.314	0.282	0.0678	0.223	-
2255P (nm)	-	-	-	2252.5	-	2252.47
2255D	-	-	-	0.124	-	0.206

[1] LT=Felsic lapilli tuff, XT=Felsic crystal-rich tuff, TF=Felsic Tuff, VF=Coherent felsic volcanic, MI=Mafic intrusive, MD=Mafic dyke, MDS=Mudstone

[2] P = peak, D = depth

B00267973	B00267974	Q721151	Q721152	Q721153	Q721154	Q721155	Q311619
K15-200	K15-200	K15-204	K15-204	K15-204	K15-204	K15-204	K15-206
173.5	192.45	112.53	116	117.6	135.6	146.4	204.15
173.7	192.65	112.62	116.17	117.69	135.8	146.6	204.35
MI	LT	MS	MS	MS	VF	MI	VF
Chl-carb-act	Mod ser ± chl	-	-	-	Mod ser ± chl	Chl-carb-act	Mod ser ± chl
2224.96	2209.72	2206.1	2220.3	2207.02	2217.05	2225.77	2199.77
0.15	0.301	0.0602	0.0647	0.103	0.31	0.13	0.081
2253.14	-	2240.95	2250.52	2251.48	2240.73	2249.79	2241.87
0.218	-	0.0481	0.0642	0.0965	0.174	0.169	0.0427

D00005978	D00005979	D00005980	D00005981	D00005982	D00005983	D00005984	D00005985
K15-281	K15-281	K15-281	K15-281	K15-281	K15-281	K15-281	K15-281
24.3	49.1	64.9	85.8	137.6	147.5	164.8	176.55
24.45	49.3	65	86	137.7	147.7	165	176.65
TF	LT	MI	TF	TF	TF	TF	TF
-	Mod ser ± chl	Per chl	Mod ser ± chl	Mod ser ± chl	Per ser	Per ser	Per ser
2210.75	2207.27	2205.48	2213.8	2212.63	2211.15	2205.92	2207.61
0.161	0.223	0.0964	0.315	0.211	0.22	0.186	0.311
2256.81	-	2256.81	2240.69	2242.9	2241.15	2240.68	2240.84
0.136	-	0.103	0.207	0.128	0.089	0.0572	0.134

Q721171	Q721172	Q721173	Q721174	Q721175	B370156	B370157	B370158
K15-300	K15-300	K15-300	K15-300	K15-300	K15-301	K15-301	K15-301
71.65	78.9	89.85	120.1	150.05	22.65	47.9	77.55
71.85	79.05	90.05	120.3	150.25	22.8	48.05	77.65
VF	MD	VF	XT	LT	LT	LT	TF
-	-	Mod ser ± chl	Mod ser ± chl	Mod ser ± chl	Mod ser ± chl	Per ser	Per ser
2208.85	2224.2	2210.33	2209.7	2214.77	2210.81	2210.74	2210.72
0.402	0.167	0.373	0.229	0.278	0.342	0.345	0.204
-	-	-	-	-	2241.26	-	-
-	-	-	-	-	0.141	-	-

B357985	B357986	B357987	B357988	B357989	B370153	B370154	B370155
K16-358	K16-358	K16-358	K16-358	K16-358	K16-358	K16-358	K16-358
193.5	215	226.2	235.35	255.7	271.7	286.1	321.9
193.7	215.15	226.3	235.5	255.8	271.85	286.25	322.05
MI	MI	MI	MI	TF	LT	LT	LT
Chl-carb-act	-	Chl-carb-act	Chl-carb-act	Per ser	Mod ser ± chl	Mod ser ± chl	Per ser
-	2225.57	2222.81	-	2207.99	2207.91	2203.28	2205.52
-	0.112	0.161	-	0.177	0.221	0.16	0.327
2254.23	2251.73	2249.13	2252	-	-	2247.54	-
0.188	0.149	0.157	0.223	-	-	0.0884	-

Q931951	Q931952	Q931953	Q931954	Q931955	Q931956	Q931957	Q931958
K15-216	K15-216	K15-216	K15-216	K15-216	K15-216	K15-216	K15-216
15.6	31.05	37.9	58.55	71.65	91.4	113.5	131.55
15.8	31.2	38	58.7	71.85	91.55	113.7	131.75
LT	MD	LT	LT	LT	LT	XT	LT
Mod ser ± chl	-	Mod ser ± chl	-	Mod ser ± chl	-	Mod ser ± chl	Mod ser ± chl
2218.6	2214.47	2216.46	2213.69	2214.5	2215.84	2218.02	2217.65
0.341	0.0941	0.18	0.32	0.212	0.26	0.281	0.327
-	2253.69	-	-	-	-	-	-
-	0.0891	-	-	-	-	-	-

D00005986	D00005987	D00005988	D00005989	D00005990	D00005991	Q931980	Q931981
K15-281	K15-281	K15-281	K15-281	K15-281	K15-281	K15-282	K15-282
183.05	184.45	199.45	212.75	227.9	251.9	77.15	95.9
183.2	184.65	199.6	212.9	228.05	252.1	77.35	96.1
TF	TF	TF	TF	TF	TF	VF	XT
Per chl	Mod ser ± chl	Per ser	Per ser	Mod ser ± chl	Mod ser ± chl	Mod ser ± chl	Mod ser ± chl
2225.71	2218.9	2210.59	2197.54	2216.44	2218.57	2220.47	2218.64
0.0683	0.117	0.374	0.243	0.289	0.213	0.393	0.372
2252.04	2254.1	-	2243.28	2240.95	2241.28	-	-
0.126	0.139	-	0.0596	0.164	0.139	-	-

B370159	B370160	B370161	B370162	B370163	Q931876	Q931877	Q931878
K15-301	K15-301	K15-301	K15-301	K15-301	K15-301	K15-301	K15-301
91.25	102.55	117.6	122.7	135.85	30.13	72.36	118.37
91.4	102.7	117.7	122.8	136	34.36	72.54	118.57
TF	TF	TF	VF	TF	-	-	-
Mod ser ± chl	Mod ser ± chl	Mod ser ± chl	Per ser	Per chl	-	-	-
2210	2211.22	2213.79	2214.41	2221.01	2208.01	2212.23	2216.48
0.325	0.147	0.288	0.158	0.304	0.327	0.226	0.384
-	2241.26	-	2242.97	2243.12	-	2251.57	-
-	0.067	-	0.0632	0.23	-	0.117	-

Q720924	Q720925	Q720926	Q720927	Q720928	Q720929	Q720930	Q720931
K16-370	K16-370	K16-370	K16-370	K16-370	K16-370	K16-370	K16-370
42.7	64.5	75.7	84.95	87.95	98.3	111.05	129.85
42.9	64.65	75.85	85.1	88.1	98.45	111.25	130
VF	LT	LT	TF	MD	LT	LT	LT
Mod ser ± chl	Mod ser ± chl	Mod ser ± chl	Mod ser ± chl	-	Mod ser ± chl	Mod ser ± chl	-
2215.99	2211.25	2214.64	2211.47	2211.94	2208.43	2199.96	2210.95
0.269	0.272	0.269	0.176	0.291	0.172	0.351	0.2
-	-	-	2241	-	-	-	-
-	-	-	0.0967	-	-	-	-

Q931959	Q931960	Q931961	Q931962	Q931963	Q931964	Q931965	Q931966
K15-216	K15-216	K15-216	K15-216	K15-216	K15-216	K15-216	K15-216
141.45	148.05	167.19	174.1	184.45	199.45	216.8	224
141.6	148.2	167.27	174.15	184.6	199.65	217	244.2
LT	-	MS	MS	LT	MI	LT	LT
Mod ser ± chl	Per chl	-	-	Per ser	-	Mod ser ± chl	Mod ser ± chl
2206.27	2206.25	-	2227.04	2214.28	-	2207.85	2207.11
0.348	0.0935	-	0.0591	0.26	-	0.29	0.19
-	2250.07	2268.7	2258.17	-	2252.85	-	2241.63
-	0.037	0.202	0.0578	-	0.164	-	0.097

Q931982	Q931983	Q931984	Q931985	Q931986	Q931987	Q931988	Q931989
K15-282	K15-282	K15-282	K15-282	K15-282	K15-282	K15-282	K15-282
119.7	134.4	165.1	195.65	213.9	270.45	330.95	129
119.9	134.6	165.25	195.8	214.05	270.65	331.15	129.2
XT	LT	XT	LT	TF	MI	MI	MD
Mod ser ± chl	-	Mod ser ± chl	Per ser	Per ser	Chl-carb-act	Chl-carb-act	-
2222.18	2214.92	2218.19	2210.53	2206.51	-	-	2222.14
0.36	0.318	0.352	0.339	0.231	-	-	0.102
-	-	-	-	-	2253.87	2254.6	2249.42
-	-	-	-	-	0.179	0.182	0.0726

Q931879	Q721051	Q721052	Q721053	Q721054	Q721055	Q721056	Q721057
K15-301	K15-309	K15-309	K15-309	K15-309	K15-309	K15-309	K15-309
128.51	165.25	174	196.65	211.6	214.65	217.8	224.74
131	165.45	174.2	196.8	211.8	214.9	217.93	224.78
-	MS	LT	MI	MI	LT	MS	MS
-	Per ser	-	Chl-carb-act	-	Mod ser ± chl	-	-
2217.64	2204.88	2212.61	-	2222.33	2216.87	2227.09	2219.3
0.345	0.19	0.227	-	0.163	0.33	0.0801	0.115
-	-	-	2253.39	2250.63	-	2257.59	2241.24
-	-	-	0.247	0.154	-	0.0835	0.114

Q720932	Q720933	Q720934	Q720935	Q720936	Q720937	Q720938	Q720939
K16-370	K16-370	K16-370	K16-370	K16-370	K16-370	K16-370	K16-370
160.35	176.8	189.1	211.6	247.3	255.4	269.1	276.95
160.5	176.95	189.3	211.75	247.5	255.6	269.3	277.1
MI	MI	MI	MI	LT	LT	LT	LT
Chl-carb-act	-	Chl-carb-act	Chl-carb-act	Mod ser ± chl	-	Per chl	-
-	2220.64	2227.12	-	2207.36	2203.71	2206.07	2205.76
-	0.11	0.0791	-	0.163	0.157	0.166	0.189
2254.29	2253.08	2250.29	2254.01	2240.93	2246.81	2251.93	2255.51
0.119	0.132	0.142	0.223	0.0701	0.0678	0.0973	0.117

Q931967	Q930209	Q930210	Q930211	Q930212	Q930213	Q930214	Q930216
K15-216	K15-232	K15-232	K15-232	K15-232	K15-232	K15-232	K15-232
231.5	29.5	61.1	76.1	75.2	106.15	123.8	142.08
231.65	29.75	61.3	76.3	75.4	106.4	123.95	142.16
LT	LT	XT	TF	TF	TF	-	-
-	Mod ser ± chl	Mod ser ± chl	Mod ser ± chl	Mod ser ± chl	Mod ser ± chl	Per chl	Per chl
2212.28	2212.74	2212.35	2215.79	2220.15	2209.05	2205.51	2210.85
0.182	0.362	0.183	0.324	0.156	0.349	0.0701	0.0401
2251.55	-	-	-	2247.75	-	2247.08	2249.84
0.0986	-	-	-	0.123	-	0.0442	0.101

Q930266	Q930267	Q930268	Q930269	Q930270	Q930271	Q930272	Q930273
K15-286	K15-286	K15-286	K15-286	K15-286	K15-286	K15-286	K15-286
41.6	48.2	70.15	88.8	105.6	127.08	132.71	142.11
41.8	48.4	70.35	89	105.8	127.15	132.81	142.2
MD	TF	LT	LT	LT	-	MS	MS
-	Mod ser ± chl	Mod ser ± chl	Mod ser ± chl	-	Per chl	-	-
2218.36	2218.13	2206.41	2201.56	2205.27	2216.66	2224.79	2209.45
0.0634	0.261	0.236	0.232	0.162	0.0673	0.0743	0.0917
2252.18	2240.93	-	-	2241.22	-	2245.3	2243.63
0.0792	0.173	-	-	0.0541	-	0.0804	0.0968

Q721058	Q721059	Q721060	Q721061	Q721062	Q721063	Q930281	Q930282
K15-309	K15-309	K15-309	K15-309	K15-309	K15-309	K15-315	K15-315
226.25	227	229.1	242.25	268.15	296.7	11.3	20.95
226.34	227.1	229.18	242.4	268.3	296.9	11.5	21.15
MS	MS	MS	MI	LT	LT	MD	VF
-	-	-	Chl-carb-act	Mod ser ± chl	Mod ser ± chl	Chl-carb-act	Mod ser ± chl
2225.82	2218.41	2216.75	-	2203.82	2208.87	2220.63	2223.82
0.0813	0.049	0.056	-	0.129	0.211	0.0914	0.238
2266.65	-	2251.58	2256.37	2255.99	-	2245.51	-
0.0782	-	0.0589	0.184	0.0704	-	0.061	-

Q931883	Q931884	Q931885	Q931886	Q931887	Q931898	Q931899	Q931900
K16-372	K16-372	K16-372	K16-372	K16-372	K16-372	K16-372	K16-372
27.14	103.45	585	364.96	301.6	62.22	172.72	401.11
29.77	106.22	587.25	365.14	301.79	62.42	172.93	401.32
-	-	-	-	-	-	-	-
-	-	-	-	-	-	-	-
2227.11	2216.75	2224.1	2219.15	-	2209.91	2216.22	2211.3
0.0856	0.319	0.146	0.436	-	0.4	0.512	0.248
2249.71	-	2249.61	-	2255.51	-	-	2243.45
0.246	-	0.136	-	0.104	-	-	0.165

Q930217	Q930218	Q930219	Q930220	Q930221	Q930222	Q931968	Q931969
K15-232	K15-232	K15-232	K15-232	K15-232	K15-232	K15-233	K15-233
160.85	155.5	172.8	181.2	207.85	187.1	29.85	35.75
160.9	155.6	172.95	181.4	208	187.3	30	35.9
MS	MS	TF	TF	LT	VF	MD	XT
Per chl	-	Mod ser ± chl	Mod ser ± chl	Mod ser ± chl	-	-	Mod ser ± chl
-	-	2197.23	2209.95	2206.39	2203.82	2218.74	2218.07
-	-	0.179	0.27	0.249	0.235	0.0467	0.296
2256.08	2268.39	-	-	-	2241.37	2256.67	-
0.155	0.0708	-	-	-	0.0734	0.101	-

Q930274	Q930276	Q930277	Q930278	Q930279	Q930280	Q721064	Q721065
K15-286	K15-286	K15-286	K15-286	K15-286	K15-286	K15-287	K15-287
153.7	169.5	179.7	184.75	111.55	154.7	37.9	49.3
153.9	169.7	179.9	184.9	111.7	154.9	38.15	49.38
LT	TF	MI	MI	MDS	MI	LT	MS
Per ser	Mod ser ± chl	Chl-carb-act	-	Mod ser ± chl	Chl-carb-act	Per ser	-
2218.17	2214.29	2220.39	-	2201.73	2208.25	2212.59	-
0.207	0.294	0.175	-	0.124	0.0821	0.223	-
-	-	2242.95	2250.8	2241.68	2252.39	-	2256.54
-	-	0.14	0.131	0.0589	0.171	-	0.0383

Q930283	Q930284	Q930285	Q930286	Q930287	Q930288	Q930290	Q930291
K15-315	K15-315	K15-315	K15-315	K15-315	K15-315	K15-315	K15-315
35	46.7	75	93.85	103.35	107.25	118.15	121.9
35.2	46.85	75.2	94.1	103.4	107.45	118.3	122.15
MD	TF	LT	LT	MS	LT	MI	MI
-	Mod ser ± chl	Per ser	-	-	Per ser	-	-
2219.07	2218.6	2210.64	2215.66	2220.56	2221.81	-	-
0.0956	0.225	0.161	0.238	0.0933	0.26	-	-
2249.62	-	-	2240.77	2262.23	-	2252.49	2255.73
0.0928	-	-	0.112	0.0863	-	0.163	0.159

Q930078	Q930079	Q930080	Q930081	Q930082	Q930083	Q930084	Q930085
K16-406	K16-406	K16-406	K16-406	K16-406	K16-406	K16-406	K16-406
19.35	26.5	67.85	95	133.8	168.4	191.35	237.15
19.45	26.65	68	95.25	133.95	168.55	191.55	237.3
LT	MDS	LT	LT	LT	LT	LT	LT
Mod ser ± chl	-	Mod ser ± chl	Mod ser ± chl	Mod ser ± chl	Mod ser ± chl	Per ser	Mod ser ± chl
2216.72	2216	2216.59	2216.39	2218.09	2217.92	2212.9	2211.89
0.334	0.114	0.345	0.249	0.331	0.274	0.249	0.238
-	2244.57	-	-	-	-	-	-
-	0.0696	-	-	-	-	-	-

Q931970	Q931971	Q931972	Q931973	Q931974	Q931975	Q931976	Q931977
K15-233	K15-233	K15-233	K15-233	K15-233	K15-233	K15-233	K15-233
53.4	75.55	95.15	108	150.85	168.55	174.33	181.9
53.6	75.75	95.35	108.2	151	168.7	174.31	182
LT	LT	MDS	XT	LT	-	-	TF
Per ser	Mod ser ± chl	Mod ser ± chl	Mod ser ± chl	Mod ser ± chl	Per chl	Per chl	Mod ser ± chl
2216.26	2212.53	2216.31	2214.24	2207.99	2201.88	2208.23	2207.77
0.244	0.245	0.153	0.355	0.308	0.148	0.0426	0.34
-	-	-	-	-	2247.93	2257.73	-
-	-	-	-	-	0.124	0.0268	-

Q721066	Q721067	Q721068	Q721069	Q721070	Q721071	Q721072	D00005956
K15-287	K15-287	K15-287	K15-287	K15-287	K15-287	K15-287	K15-289
58.1	66.65	70.45	79.58	98.9	118.35	123.1	15.1
58.3	66.72	70.65	79.65	99.15	118.55	123.3	15.3
TF	MS	LT	MS	TF	MI	LT	LT
Per ser	-	Per ser	-	Mod ser ± chl	Chl-carb-act	Mod ser ± chl	Mod ser ± chl
2221.76	2216.82	2209.63	2220.4	2212.84	2216.1	2207.93	2210.02
0.276	0.0583	0.287	0.186	0.218	0.2	0.268	0.255
-	2243.61	-	-	-	-	-	-
-	0.0626	-	-	-	-	-	-

Q930292	Q930293	Q930294	Q930295	Q930296	Q930297	Q930298	Q930299
K15-315	K15-315	K15-315	K15-315	K15-315	K15-315	K15-315	K15-315
132.1	139.96	146.6	151.6	176.75	181.26	182.39	187.75
132.35	140	146.95	151.7	177	181.34	182.46	187.95
MI	MS	VF	VF	LT	MS	MS	LT
Chl-carb-act	-	Mod ser ± chl	-	Per ser	-	-	Per ser
-	2220.54	2208.82	2216.56	2210.04	2227.25	2218.4	2211.03
-	0.0443	0.0603	0.0999	0.246	0.101	0.0513	0.219
2252.02	2254.39	-	2243.88	-	-	2257.73	-
0.136	0.0506	-	0.0725	-	-	0.065	-

Q930086	Q930087	Q930088	B358001	B358002	B358003	B358004	B358006
K16-406	K16-406	K16-406	K16-415	K16-415	K16-415	K16-415	K16-415
256.85	267.95	292.7	22.65	93.78	106.92	261.8	309.47
257	268.1	292.85	22.82	93.99	107.08	261.93	309.63
TF	TF	TF	-	-	-	-	-
Mod ser ± chl	-	Mod ser ± chl	-	-	-	-	-
2224.52	2217.22	2214.59	2218.65	2211.35	2217.77	2216.02	2216.98
0.0464	0.323	0.368	0.485	0.065	0.484	0.429	0.496
2254.26	-	-	-	2240.54	-	2241.02	-
0.115	-	-	-	0.0392	-	0.286	-

Q931978	Q930093	Q930094	Q930095	Q930096	Q930097	Q930098	Q930099
K15-233	K15-235R	K15-235R	K15-235R	K15-235R	K15-235R	K15-235R	K15-235R
201.75	10.5	37.65	86.15	116.7	133.3	136.1	143.65
202	10.65	37.8	86.3	116.95	133.5	136.35	143.95
MI	LT	TF	TF	VF	TF	TF	MI
Chl-carb-act	Mod ser ± chl	Mod ser ± chl	Per ser	Mod ser ± chl	Mod ser ± chl	Per chl	Chl-carb-act
-	2210.02	2210.66	2220.18	2227.33	2223.11	2216.61	2217.96
-	0.28	0.37	0.361	0.0488	0.114	0.299	0.224
2252.92	-	-	-	2249.82	2249.81	2241.03	2243.39
0.274	-	-	-	0.128	0.203	0.179	0.138

D00005957	D00005958	D00005959	D00005960	D00005961	D00005962	D00005963	D00005964
K15-289	K15-289	K15-289	K15-289	K15-289	K15-289	K15-289	K15-289
38.7	53.4	61.4	79.8	108.85	129.1	152.25	171.65
38.9	53.5	61.6	80	109	129.3	152.45	171.85
TF	TF	MD	LT	TF	VF	TF	LT
Mod ser ± chl	Mod ser ± chl	Mod ser ± chl	Mod ser ± chl	Mod ser ± chl	Mod ser ± chl	Mod ser ± chl	Mod ser ± chl
2220.27	2204.5	2204.13	2214.72	2218.14	2212.74	2209.82	2206.51
0.294	0.242	0.0964	0.314	0.247	0.1	0.143	0.223
-	-	2256.7	-	-	2245.24	2241.23	2240.95
-	-	0.0523	-	-	0.0762	0.0578	0.0789

Q930300	B370164	B370165	B370166	B370167	B370168	B370169	B370170
K15-315	K15-316	K15-316	K15-316	K15-316	K15-316	K15-316	K15-316
207.35	39.6	51.85	55.65	63.05	82.6	103.6	118.05
207.55	39.7	52	55.75	63.2	82.7	103.7	118.2
LT	MI	MI	MI	VF	VF	TF	TF
-	Chl-carb-act	Chl-carb-act	Chl-carb-act	Mod ser ± chl	-	Mod ser ± chl	Mod ser ± chl
2208.56	-	2222.17	-	2220.57	2217.1	2217.17	2211.54
0.178	-	0.0972	-	0.302	0.107	0.425	0.0622
-	2255.57	2249.5	2251.79	-	-	-	2244.22
-	0.173	0.139	0.205	-	-	-	0.0241

B358007	B358008	B358009	B358010	Q311612	Q311613	Q311614	Q311615
K16-415	K16-415	K16-415	K16-415	K16-417	K16-417	K16-417	K16-417
349.31	562.77	764.27	812.33	74.45	96.85	137.85	242.3
349.54	562.95	764.41	812.5	74.6	96.9	137.95	242.4
-	-	-	-	TF	VF	XT	MS
-	-	-	-	Mod ser ± chl	Mod ser ± chl	Mod ser ± chl	Mod ser ± chl
2218.3	2221.01	2222.23	2217.16	2215.09	2217.94	2214.27	2216.85
0.312	0.392	0.442	0.33	0.213	0.285	0.241	0.0321
-	-	-	2240.69	-	-	-	2247.71
-	-	-	0.197	-	-	-	0.0297

Q930100	Q931941	Q931942	Q931943	Q930233	Q930234	Q930235	Q930236
K15-235R	K15-235R	K15-235R	K15-235R	K15-236	K15-236	K15-236	K15-236
149.25	159.05	163.35	173.75	24.1	32.1	51.15	70.5
149.4	159.25	163.6	173.95	24.2	32.25	51.3	70.7
TF	TF	VF	LT	LT	LT	TF	LT
Mod ser ± chl	-	Chl-carb-act	Per ser	Mod ser ± chl	Mod ser ± chl	Mod ser ± chl	Mod ser ± chl
-	2207.35	2214.17	2209.17	2212.75	2207.15	2210.26	2211.26
-	0.281	0.347	0.21	0.0608	0.169	0.174	0.247
2256.13	2241.16	-	2241.58	2253.21	-	2243.18	-
0.187	0.141	-	0.116	0.038	-	0.0525	-

D00005965	D00005966	D00005967	D00005968	D00005969	A00348391	A00348392	A00348393
K15-289	K15-289	K15-289	K15-289	K15-289	K15-290	K15-290	K15-290
187.45	196.15	215.9	219.15	231.1	32.2	55.8	68
187.6	196.25	216.05	219.3	231.2	32.4	56	68.2
TF	TF	LT	LT	LT	LT	LT	MDS
Per ser	Mod ser ± chl	Per chl	-	-	Mod ser ± chl	Per ser	Mod ser ± chl
2205.78	2214.49	2214.59	2216.43	2217.85	2212.27	2207.64	2225.99
0.089	0.301	0.172	0.313	0.325	0.275	0.281	0.235
-	-	2249.18	2240.7	2240.7	-	-	2241.39
-	-	0.118	0.21	0.234	-	-	0.234

B370171	B370172	B370173	B370174	B370175	B370176	B370177	B370178
K15-316	K15-316	K15-316	K15-316	K15-320	K15-320	K15-320	K15-320
127.55	149.4	165.9	178.9	18.85	50.3	76.45	95.85
127.65	149.55	166	179.05	18.95	50.4	76.55	95.95
LT	LT	MI	VF	TF	TF	TF	TF
Per ser	Mod ser ± chl	-	Per ser	Mod ser ± chl	Mod ser ± chl	Per ser	-
2205.92	2204.59	2205.75	2210.02	2222.12	2217.79	2213.24	2206.19
0.302	0.164	0.13	0.319	0.319	0.263	0.393	0.307
-	-	2241.69	-	2240.57	-	-	-
-	-	0.056	-	0.225	-	-	-

Q311616	Q311617	Q311618	Q721073	Q721074	Q721075	Q721076	Q721077
K16-417	K16-417	K16-417	K17-422	K17-422	K17-422	K17-422	K17-422
248.81	285.4	276.45	40.3	52.55	114.45	148.85	145.75
248.9	285.5	276.55	40.5	52.7	114.65	149	145.95
MS	MS	LT	MD	LT	XT	-	-
-	-	-	-	Mod ser ± chl	Mod ser ± chl	Per chl	Per chl
2208.21	2203.67	2220.74	2222.78	2210.89	2216.16	2224.38	2211.06
0.0533	0.0349	0.0564	0.0441	0.363	0.209	0.0343	0.25
2245.58	-	-	2255.48	2241.47	-	2241.26	-
0.0314	-	-	0.0731	0.209	-	0.0373	-

Q930237	Q930238	Q930239	Q930240	Q930241	Q930242	Q930243	Q930244
K15-236	K15-236	K15-236	K15-236	K15-236	K15-236	K15-236	K15-236
81.88	82.3	86.33	95	96.73	110.6	113.35	117.15
81.95	82.45	86.42	95.26	96.82	110.65	113.65	117.35
MS	MS	MS	VF	VF	MS	MD	VF
-	-	-	Mod ser ± chl	-	-	Chl-carb-act	Mod ser ± chl
2212.42	2222.5	2224.71	2205.07	2222.64	2218.94	2224.45	2205.92
0.0529	0.0762	0.0349	0.0556	0.101	0.0416	0.0875	0.219
2247.84	2247.28	2268.87	2245.73	-	2241.03	2252.07	-
0.0527	0.0666	0.0363	0.0239	-	0.0408	0.101	-

A00348394	A00348395	A00348396	A00348397	A00348398	A00348399	A00348400	Q721099
K15-290	K15-290	K15-290	K15-290	K15-290	K15-290	K15-290	K15-290
73.65	78.92	82.48	84.91	90.7	117.3	133.8	139.7
73.7	79	82.58	84.98	90.9	117.45	134	139.9
TF	MS	MS	MS	MI	MI	TF	VF
Per ser	-	-	-	Chl-carb-act	Chl-carb-act	Mod ser ± chl	Mod ser ± chl
2211.02	2207.82	2218.68	2224.49	2215.74	-	2220.87	2219.64
0.147	0.0386	0.118	0.0923	0.0884	-	0.167	0.241
-	2249.1	2251.85	2251.78	2252.93	2252.1	2249.21	2240.57
-	0.0397	0.124	0.0727	0.0845	0.257	0.117	0.151

B370179	B370180	B370181	B370182	B370183	B370184	B370185	B370186
K15-320	K15-320	K15-320	K15-320	K15-320	K15-320	K15-320	K15-320
114.45	127.95	134	148.4	165	174.3	202.65	205.5
114.55	128.05	134.15	148.5	165.2	174.4	202.75	205.65
TF	VF	MI	MI	TF	VF	TF	MI
Per ser	Mod ser ± chl	Chl-carb-act	Chl-carb-act	Mod ser ± chl	Mod ser ± chl	Per chl	Chl-carb-act
2212.7	2220.44	-	-	2218.54	2218.09	2216.75	2227.16
0.191	0.151	-	-	0.224	0.294	0.259	0.073
-	-	2251.06	2255.41	2245	-	2241.32	2251.52
-	-	0.19	0.246	0.136	-	0.169	0.101

Q721078	Q721079	Q721080	Q721081	Q721082	Q721083	Q721084	Q311201
K17-422	K17-422	K17-422	K17-422	K17-422	K17-422	K17-422	K17-439
147.25	152.3	160.9	166.55	182.25	195.4	208.45	23.61
147.31	152.43	160.95	166.7	182.4	195.55	208.6	23.77
-	TF	-	TF	LT	TF	LT	-
Per chl	Mod ser ± chl	Per chl	Per chl	Mod ser ± chl	Per ser	Mod ser ± chl	-
2226.17	2212.48	2208	2203.42	2212.28	2210.98	2207.13	2208.72
0.045	0.182	0.063	0.178	0.317	0.324	0.245	0.127
2257.98	-	2260.1	2259.14	2241.05	-	-	2253.13
0.0902	-	0.0937	0.134	0.15	-	-	0.186

Q930245	Q931944	Q931945	Q931946	Q931947	Q931948	Q931949	B370196
K15-236	K15-240	K15-240	K15-240	K15-240	K15-240	K15-240	K15-244
123.8	42	55.1	69	74.45	83.1	107.45	35.3
124	42.3	55.4	69.25	74.65	83.3	107.65	35.45
MI	LT	LT	TF	TF	LT	MI	TF
Chl-carb-act	Per ser	Per ser	-	Chl-carb-act	Mod ser ± chl	Chl-carb-act	Mod ser ± chl
2219.44	2207.13	2216.68	2218.2	2217.34	2209.27	-	2210.2
0.0894	0.185	0.359	0.109	0.162	0.231	-	0.262
2248.89	-	-	2252.16	2247.91	-	2252.44	-
0.0954	-	-	0.134	0.169	-	0.24	-

B357954	B357955	B357956	B357957	B357958	B357959	B357960	B357961
K15-293	K15-293	K15-293	K15-293	K15-293	K15-293	K15-293	K15-293
33.9	43.7	53.2	55.75	66.5	80.45	91.55	106.6
34	43.9	53.5	55.95	66.65	80.6	91.7	106.8
MI	LT	MI	LT	LT	LT	XT	MI
Mod ser ± chl	-	Mod ser ± chl	-	Mod ser ± chl	Mod ser ± chl	Mod ser ± chl	-
2220.27	2212.45	2206.99	2206.13	2210.11	2212.9	2217	2218.53
0.247	0.253	0.184	0.316	0.403	0.396	0.185	0.111
-	-	2249.78	2240.54	-	-	2245.39	2249.87
-	-	0.0924	0.14	-	-	0.141	0.101

B370187	B370188	B370189	B370190	B358013	B358014	B358015	B358016
K15-320	K15-320	K15-320	K15-320	K15-326	K15-326	K15-326	K15-326
212.45	229.65	244.4	262	95.99	121.68	141.43	146.78
212.55	229.8	244.55	262.1	96.18	121.84	141.59	146.97
TF	LT	LT	TF	-	-	-	-
Mod ser ± chl	Mod ser ± chl	Mod ser ± chl	Mod ser ± chl	-	-	-	-
2208.24	2203.9	2206.61	2208.06	2210.87	2218.35	2211.23	2217.22
0.282	0.234	0.171	0.291	0.331	0.178	0.232	0.406
-	2240.93	2243.44	-	-	2243.19	-	-
-	0.11	0.0861	-	-	0.104	-	-

Q311202	Q311203	Q311204	Q721156	Q721157	Q721158	Q721159	Q721160
K17-439	K17-439	K17-439	K17-448	K17-448	K17-448	K17-448	K17-448
52.41	70.5	99.3	322.45	334	346.15	349.7	358.45
52.61	70.78	99.49	322.65	334.15	346.3	349.85	358.6
-	-	-	LT	LT	VF	MDS	VF
-	-	-	Mod ser ± chl	Mod ser ± chl	Mod ser ± chl	-	Mod ser ± chl
-	2224.94	2225.44	2220.19	2214.63	2218.13	2216.39	2212.43
-	0.0732	0.115	0.226	0.135	0.312	0.0869	0.334
2257.83	2254.27	2258.91	-	-	2240.93	2256.08	-
0.134	0.142	0.143	-	-	0.188	0.099	-

B370197	B370198	B370199	B370200	Q930076	Q930077	B370191	B370192
K15-244	K15-244	K15-244	K15-244	K15-244	K15-244	K15-251	K15-251
48.35	78.85	86.15	72.65	100.35	117.3	15	33.3
48.5	79	86.25	72.75	100.45	117.4	15.1	33.45
TF	TF	TF	TF	VF	VF	TF	MI
Mod ser ± chl	Mod ser ± chl	Per ser	Mod ser ± chl	Mod ser ± chl	-	Per ser	Chl-carb-act
2209.98	2210.94	2217.7	2209.14	2208.89	2215.58	2209.27	2224.34
0.215	0.285	0.358	0.246	0.18	0.365	0.325	0.147
-	-	-	-	2240.9	-	-	2250.25
-	-	-	-	0.0618	-	-	0.244

B357962	B357963	B357964	B357965	B357966	B357967	B357968	B357969
K15-293	K15-293	K15-293	K15-293	K15-293	K15-293	K15-293	K15-293
116.6	134.15	149.9	151.55	168.8	186.95	197.05	210.25
116.85	134.3	150.05	151.7	168.95	187.15	197.2	210.4
XT	TF	TF	TF	TF	TF	TF	LT
-	Per ser	Per ser	-	Mod ser ± chl	Mod ser ± chl	Per ser	Mod ser ± chl
2215.2	2204.36	-	2212.16	2211.04	2207.05	2205.68	2210.26
0.104	0.17	-	0.235	0.174	0.257	0.0798	0.23
2249.66	2241.03	2255.88	-	-	-	-	-
0.0875	0.0496	0.0795	-	-	-	-	-

B358017	B358018	B358019	B358021	B358022	Q930089	Q930090	Q930091
K15-326	K15-326	K15-326	K15-326	K15-326	K15-326	K15-326	K15-326
209.91	289.26	328.65	393.13	433.17	269.15	299.1	313.8
210.11	289.41	328.83	394	433.44	269.35	299.3	313.95
-	-	-	-	-	LT	TF	TF
-	-	-	-	-	-	-	-
2214.02	2212.73	-	2207.17	2210.89	2203.91	2214.58	-
0.491	0.411	-	0.252	0.421	0.318	0.355	-
-	-	2253.24	2240.83	-	-	-	2250.05
-	-	0.307	0.136	-	-	-	0.182

B358028	B358029	B358030	B358031	B358011	B358012	Q311605	Q311606
K17-449	K17-449	K17-449	K17-449	K18-469	K18-469	K18-484	K18-484
407.8	525.54	745.86	748.86	300.96	441.88	20.85	37.1
407.97	525.7	746	749	302.39	442.27	21	37.25
-	-	-	-	-	-	VF	TF
-	-	-	-	-	-	Mod ser ± chl	Mod ser ± chl
2216.88	2216.65	2216.65	2218.22	2206.87	2206.81	2206.1	2220.48
0.427	0.428	0.317	0.374	0.459	0.442	0.137	0.295
-	-	-	-	-	-	-	-
-	-	-	-	-	-	-	-

B370193	B370194	B370195	D00005970	D00005971	D00005972	D00005973	D00005974
K15-251	K15-251	K15-251	K15-260	K15-260	K15-260	K15-260	K15-260
50.85	57.35	78.75	57	94.4	120.4	134.7	195.55
50.95	57.45	78.85	57.2	94.5	120.6	134.85	195.65
MI	TF	TF	LT	LT	TF	TF	MI
-	Mod ser ± chl	Mod ser ± chl	Mod ser ± chl	Per ser	Per ser	Mod ser ± chl	Chl-carb-act
-	2218.58	2216.35	2209.96	2212.62	2214.44	2210.16	2208.37
-	0.237	0.16	0.244	0.242	0.319	0.281	0.33
2254.34	2240.78	2243.62	-	-	-	-	-
0.163	0.16	0.0718	-	-	-	-	-

B357970	Q930246	Q930247	Q930248	Q930249	Q930250	Q930251	Q930252
K15-293	K15-294	K15-294	K15-294	K15-294	K15-294	K15-294	K15-294
223.3	30.9	53.2	71.8	85.6	88.65	102.4	117.65
223.5	31.15	53.45	72	85.85	88.96	102.65	117.95
LT	XT	MD	LT	LT	XT	XT	XT
Mod ser ± chl	-	-	-	-	-	-	-
2216.67	2209.36	2199.94	2207.71	2224.46	2209.16	2209.74	2210.52
0.203	0.0289	0.0154	0.112	0.0341	0.0496	0.111	0.234
2241.23	2256.43	2259.38	2244.56	2251.85	2254.07	2252.38	-
0.124	0.0783	0.042	0.0386	0.0629	0.0917	0.0981	-

Q930092	B357951	B357952	B357953	D00005992	D00005993	D00005994	D00005995
K15-326	K15-327	K15-327	K15-327	K15-327	K15-327	K15-327	K15-327
380.05	178.2	190.5	213.6	19.85	43.7	57.95	68.6
380.25	178.35	190.65	213.7	20	43.85	58.1	68.75
TF	TF	LT	TF	MI	TF	MI	TF
-	-	Mod ser ± chl	Mod ser ± chl	Mod ser ± chl	Per ser	Chl-carb-act	Mod ser ± chl
2212.68	2220.23	2223.68	2222.27	-	2214.58	2199.54	-
0.269	0.117	0.119	0.161	-	0.195	0.226	-
-	2251.41	2245.61	-	2257.68	-	2241.33	2253.01
-	0.105	0.0857	-	0.115	-	0.0621	0.223

Q311607	Q311608	Q311609	Q311610	Q311611	Q721176	Q721177	Q721178
K18-484	K18-484	K18-484	K18-484	K18-484	K18-486	K18-486	K18-486
61.7	84.85	101.6	118.25	134.1	6.4	15.7	23.55
61.85	84.95	101.8	118.45	134.25	6.6	15.8	23.75
LT	TF	LT	TF	TF	MI	LT	LT
Mod ser ± chl	Mod ser ± chl	Mod ser ± chl	Mod ser ± chl	Mod ser ± chl	Chl-carb-act	Per ser	Mod ser ± chl
2217.64	2210.94	2214.53	2217.11	2218.44	-	2210.93	2212.24
0.314	0.178	0.229	0.0917	0.225	-	0.209	0.198
-	-	-	-	-	2249.67	-	2241.64
-	-	-	-	-	0.117	-	0.0947

D00005975	D00005976	B00267975	B00267976	B00267977	B00267978	B00267979	B00267980
K15-260	K15-260	K15-265	K15-265	K15-265	K15-265	K15-265	K15-265
203.05	215.35	45.6	78.05	137.15	177.9	212.35	218.05
203.2	215.5	45.8	78.35	137.45	178.1	212.5	218.3
TF	MI	MI	TF	LT	LT	TF	MI
Mod ser ± chl	Chl-carb-act	-	Mod ser ± chl	Per ser	-	Mod ser ± chl	Chl-carb-act
2205.88	2208.14	2208.23	2209.96	2205.49	2209.99	2210.19	-
0.196	0.218	0.211	0.331	0.263	0.185	0.305	-
-	-	-	-	-	2249.14	-	2253.86
-	-	-	-	-	0.0977	-	0.173

Q930253	Q930254	Q930255	Q930256	Q930257	Q930258	Q930259	Q930260
K15-294	K15-294	K15-294	K15-294	K15-294	K15-294	K15-294	K15-294
123.2	133.45	146.7	156.1	169.3	181.3	197.4	208.95
123.4	133.7	146.9	156.3	169.5	181.5	197.6	209.15
XT	TF	LT	MD	LT	MD	TF	MD
-	-	-	-	-	-	-	-
2212.45	2214.11	2208.78	2207.31	2208.21	2218.59	2209.91	2206.73
0.0831	0.284	0.106	0.0572	0.311	0.0324	0.144	0.113
2250	-	2246.12	2251.09	2241.02	2260.33	2240.87	2254.53
0.121	-	0.057	0.105	0.131	0.0722	0.0604	0.0918

D00005996	D00005997	D00005998	D00005999	D00006000	B358023	B358024	B358025
K15-327	K15-327	K15-327	K15-327	K15-327	K15-328	K15-328	K15-328
101.7	118.4	131.7	152.55	159.9	76.26	118.71	147.41
101.9	118.6	131.85	152.7	160	76.45	118.88	147.54
TF	TF	MD	MI	TF	-	-	-
Mod ser ± chl	Mod ser ± chl	Mod ser ± chl	Mod ser ± chl	-	-	-	-
2217.91	-	-	2207.31	2214.43	2209.09	2216.16	2214.83
0.201	-	-	0.312	0.277	0.339	0.163	0.194
-	2253.18	2258.04	-	-	-	2241.13	2241.39
-	0.161	0.103	-	-	-	0.117	0.146

Q721179	Q721180	Q721181	Q721182	Q721183	Q721184	Q721185	Q721186
K18-486	K18-486	K18-486	K18-486	K18-486	K18-486	K18-486	K18-486
37.3	38.75	42.75	46.5	59.25	96.25	102.55	165.3
37.5	38.8	42.95	46.58	59.5	96.45	102.7	165.45
TF	LT	LT	LT	XT	TF	TF	TF
Mod ser ± chl	-	-	-	Per chl	Mod ser ± chl	-	Per chl
2214.58	2212.86	2212.29	-	2207.77	2208.12	2205.83	2222.62
0.225	0.159	0.188	-	0.0483	0.31	0.217	0.0433
-	-	2241.19	2256.01	2255.14	-	-	2256.7
-	-	0.0798	0.126	0.152	-	-	0.0918

B00267981	B00267982	Q720940	Q720941	Q720942	Q720943	Q720944	Q720945
K15-265	K15-265	K15-271	K15-271	K15-271	K15-271	K15-271	K15-271
259.7	282.55	40.25	61.35	82.7	99	143.65	168.75
260	282.85	40.45	61.55	82.95	99.25	143.95	168.95
MI	LT	LT	TF	LT	MD	LT	LT
-	Mod ser ± chl	Mod ser ± chl	Mod ser ± chl	Mod ser ± chl	-	Mod ser ± chl	-
-	2214.33	2218.07	2217.84	2220.52	2226.1	2208.12	2203.54
-	0.248	0.378	0.226	0.335	0.0589	0.247	0.396
2253.28	-	-	-	-	2257.96	-	-
0.258	-	-	-	-	0.115	-	-

Q930261	Q930262	Q930263	Q930264	Q930265	B357990	B357991	B357992
K15-294	K15-294	K15-294	K15-294	K15-294	K15-295	K15-295	K15-295
220.15	230.35	231.33	249.85	262.05	22	45.3	61.85
220.4	230.5	231.37	250.05	262.25	22.2	45.45	61.95
XT	-	-	TF	LT	TF	TF	TF
-	Per chl	Per chl	-	-	Mod ser ± chl	Mod ser ± chl	Mod ser ± chl
2209.22	-	-	2208.92	2205.68	2216.35	2211.98	2214.2
0.262	-	-	0.172	0.252	0.259	0.214	0.309
2243.31	2249.75	2255.97	2241.19	2240.99	-	-	-
0.13	0.113	0.127	0.0948	0.104	-	-	-

B358026	B358027	Q721161	Q721162	Q721163	Q721164	Q721165	Q721166
K15-328	K15-328	K16-350	K16-350	K16-350	K16-350	K16-350	K16-350
170.64	215.48	22.95	34.75	47.95	88.9	110.1	129.6
170.78	215.6	23.15	34.8	48.15	89.1	110.18	129.8
-	-	TF	-	LT	MI	-	MI
-	-	Per ser	Per chl	Per ser	Chl-carb-act	Per chl	Chl-carb-act
2220.36	2207.82	2207.38	2197.84	2201.73	-	2220.38	2226.27
0.263	0.366	0.239	0.0706	0.3	-	0.16	0.124
-	-	-	2257.16	-	2251.09	2246.95	2249.38
-	-	-	0.0704	-	0.139	0.115	0.148

Q721187	Q721188	Q721189	Q721190	Q721191	Q721192	Q311601	Q311602
K18-486	K18-486	K18-486	K18-486	K18-486	K18-486	K18-487	K18-487
185.9	202.35	214.8	236	245	139.8	207.1	246.2
186.05	202.55	215	236.15	245.15	140	207.25	246.35
TF	XT	MI	XT	MI	XT	TF	TF
Mod ser ± chl	Mod ser ± chl	Chl-carb-act	Mod ser ± chl	Chl-carb-act	Mod ser ± chl	Per chl	Mod ser ± chl
2214.33	2214.61	-	2224.02	2203.52	2212.49	2203.77	2207.59
0.166	0.177	-	0.235	0.0164	0.24	0.203	0.194
2252.42	-	2252.48	-	2250.39	2246.64	2249.96	2252.8
0.183	-	0.134	-	0.089	0.163	0.168	0.167

Q720946	Q720947	Q720948	Q720949	Q720950	Q930223	Q930224	Q930225
K15-271	K15-271	K15-271	K15-271	K15-271	K15-274	K15-274	K15-274
174.2	200.25	234.5	257.35	9.25	41.72	47.05	61.7
174.35	200.4	234.7	257.55	9.5	41.8	47.2	61.85
LT	LT	LT	MI	MD	TF	TF	MS
Mod ser ± chl	Per ser	Per ser	Chl-carb-act	-	-	Mod ser ± chl	-
2198.07	2208.65	2210.09	-	-	2215.23	2207.38	2222.41
0.291	0.28	0.304	-	-	0.0319	0.28	0.089
-	-	-	2255.84	2260.02	2240.99	-	-
-	-	-	0.203	0.146	0.0181	-	-

B357993	B357994	B357995	B357996	B357997	B357998	B357999	B358000
K15-295	K15-295	K15-295	K15-295	K15-295	K15-295	K15-295	K15-295
80.5	99.9	109	130.4	148.55	175.35	180.9	184.25
80.65	100.05	109.1	130.5	148.65	175.5	181	184.4
MI	LT	MD	TF	TF	MI	MI	MI
-	Mod ser ± chl	Mod ser ± chl	Per ser	Mod ser ± chl	Per chl	Chl-carb-act	-
2216.7	2210.76	2208.03	2204.17	2210.33	2216.53	-	2226.64
0.152	0.273	0.28	0.278	0.0298	0.209	-	0.102
2250.78	2240.78	-	-	2252.54	2247.63	2250.88	2253.38
0.0881	0.155	-	-	0.0883	0.154	0.205	0.141

Q721167	Q721168	B357971	B357972	B357973	B357974	B357975	B357976
K16-350	K16-350	K16-358	K16-358	K16-358	K16-358	K16-358	K16-358
192.9	215.8	13.9	25.25	30.2	51.9	57.6	73.8
193.15	216	14	25.45	30.35	52	57.8	73.95
TF	TF	XT	TF	MI	MI	TF	TF
Mod ser ± chl	Per ser	Mod ser ± chl	Mod ser ± chl	-	-	Mod ser ± chl	Per ser
2198.25	2205.61	2219.06	2217.76	2216.89	2222.32	2216.05	2216.69
0.323	0.246	0.156	0.326	0.378	0.355	0.243	0.303
-	-	2243.8	2240.69	-	-	-	-
-	-	0.115	0.222	-	-	-	-

Q311603	Q311604	Q721193	Q721194	Q721195	Q721196	Q721197	Q721198
K18-487	K18-487	K18-487	K18-487	K18-487	K18-487	K18-487	K18-487
304.45	341.35	29.55	51.25	77.2	94	106.2	125.75
304.6	341.5	29.75	51.4	77.45	94.2	106.4	125.9
LT	LT	LT	-	TF	TF	TF	XT
Mod ser ± chl	Mod ser ± chl	Mod ser ± chl	Per chl	Mod ser ± chl	Per chl	Mod ser ± chl	Mod ser ± chl
2218.84	2209.91	2216.36	2222.39	2214.04	2220.34	2220.35	2212.39
0.33	0.141	0.249	0.0448	0.0905	0.0883	0.178	0.179
-	2249.9	-	2257.51	2255.97	2253.38	-	2241.08
-	0.103	-	0.0685	0.091	0.126	-	0.104

Q930226	Q930227
K15-274	K15-274
70.55	73.2
70.7	73.4
TF	TF
Mod ser ± chl	-
2214.7	2220.59
0.183	0.0807
-	-
-	-

B370151	B370152
K15-295	K15-295
188.3	200.3
188.4	200.5
TF	VF
Per ser	Per ser
2221.59	2219.23
0.316	0.426
-	-
-	-

B357977	B357978
K16-358	K16-358
85.8	98.05
86	98.2
TF	TF
Mod ser ± chl	Mod ser ± chl
2209.54	2215.85
0.152	0.218
-	-
-	-

Q721199	Q721200
K18-487	K18-487
148.2	183.4
148.4	183.55
LT	TF
Mod ser ± chl	Mod ser ± chl
2208.29	2210.83
0.158	0.227
2252.96	2241
0.0979	0.118

Appendix 6.2 QA/QC data for SWIR analysis

Standard	MUN-Pyr-001	MUN-Pyr-002	MUN-Pyr-003	MUN-Pyr-004	MUN-Pyr-005	MUN-Pyr-006
1410P[1] (nm)	1408.35	1407.9	1408.26	1408.03	1407.88	1408.32
1410D[1]	0.871	0.875	0.822	0.851	0.849	0.837
2200P (nm)	2186.91	2193.1	2195.22	2189.09	2193.77	2193.07
2200D	0.787	0.765	0.694	0.712	0.718	0.729
2255P (nm)	2243.81	-	-	-	-	2241.37
2255D	0.478	-	-	-	-	0.229

Standard	MUN-Pyr-021	MUN-Pyr-022	MUN-Pyr-023	MUN-Pyr-024	MUN-Pyr-025	MUN-Pyr-026
1410P (nm)	1408.03	1407.82	1407.96	1407.87	1407.83	1407.98
1410D	0.861	0.849	0.86	0.854	0.86	0.861
2200P (nm)	2191.32	2194.87	2190.99	2191.48	2189.54	2195.15
2200D	0.767	0.745	0.765	0.768	0.747	0.74
2255P (nm)	-	-	2241.01	-	2240.72	2240.59
2255D	-	-	0.225	-	0.166	0.138

Standard	MUN-Pyr-041	MUN-Pyr-042	MUN-Pyr-043	MUN-Pyr-044	MUN-Pyr-045	MUN-Pyr-046
1410P (nm)	1408.09	1408	1408.33	1408.1	1408.21	1408.07
1410D	0.86	0.863	0.273	0.851	0.856	0.863
2200P (nm)	2196.11	2191.18	2196.82	2191.77	2193.75	2195.29
2200D	0.749	0.765	0.355	0.735	0.751	0.772
2255P (nm)	-	2241.17	2241.34	-	2240.93	-
2255D	-	0.192	0.0431	-	0.17	-

Standard	MUN-Pyr-061	MUN-Pyr-062	MUN-Pyr-063	MUN-Pyr-064	MUN-Pyr-065	MUN-Pyr-066
1410P (nm)	1408.19	1408.02	1408.18	1408.09	1408.21	1408.06
1410D	0.852	0.854	0.843	0.854	0.854	0.852
2200P (nm)	2191.63	2194.1	2193.23	2195.44	2191.23	2190.14
2200D	0.723	0.745	0.707	0.721	0.73	0.73
2255P (nm)	-	2241.02	-	-	2240.57	-
2255D	-	0.201	-	-	0.168	-

Standard	Mean	Standard Deviation
1410P (nm)	1407.99	0.27
1410D	0.85	0.01
2200P (nm)	2192.48	1.89
2200D	0.74	0.02
2255P (nm)	2241.55	0.94
2255D	0.23	0.10

[1] P = peak, D = depth

MUN-Pyr-007	MUN-Pyr-008	MUN-Pyr-009	MUN-Pyr-010	MUN-Pyr-011	MUN-Pyr-012	MUN-Pyr-013
1408.06	1408.23	1408.02	1407.99	1407.2	1407.72	1407.98
0.85	0.853	0.848	0.862	0.859	0.86	0.862
2193.46	2195.28	2193.57	2191.41	2191.7	2191.36	2193.19
0.725	0.73	0.728	0.77	0.754	0.751	0.765
2241.46	2241.13	2241.19	2241.08	-	2240.81	-
0.169	0.212	0.178	0.22	-	0.158	-

MUN-Pyr-027	MUN-Pyr-028	MUN-Pyr-029	MUN-Pyr-030	MUN-Pyr-031	MUN-Pyr-032	MUN-Pyr-033
1407.08	1407.75	1408.13	1408.07	1407.89	1407.97	1407.94
0.86	0.861	0.856	0.851	0.854	0.858	0.859
2191.61	2191.83	2189.57	2194.73	2195.16	2194.71	2193.51
0.759	0.745	0.736	0.748	0.724	0.749	0.763
-	-	-	-	-	-	-
-	-	-	-	-	-	-

MUN-Pyr-047	MUN-Pyr-048	MUN-Pyr-049	MUN-Pyr-050	MUN-Pyr-051	MUN-Pyr-052	MUN-Pyr-053
1408.11	1408.18	1408.04	1408.21	1408.15	1408.19	1408.25
0.858	0.847	0.861	0.859	0.848	0.852	0.854
2196.94	2195.19	2190.46	2194.98	2193.43	2191.59	2193
0.748	0.729	0.75	0.747	0.736	0.743	0.747
-	-	-	-	-	-	-
-	-	-	-	-	-	-

MUN-Pyr-067	MUN-Pyr-068	MUN-Pyr-069	MUN-Pyr-070	MUN-Pyr-071	MUN-Pyr-072	MUN-Pyr-073
1407.79	1408.1	1408.27	1408.14	1408.14	1408.07	1408.17
0.854	0.853	0.854	0.855	0.855	0.854	0.845
2195.44	2194.89	2195.2	2193.71	2187.44	2195.34	2193.58
0.727	0.735	0.731	0.733	0.739	0.725	0.727
-	-	-	-	-	-	-
-	-	-	-	-	-	-

MUN-Pyr-014	MUN-Pyr-015	MUN-Pyr-016	MUN-Pyr-017	MUN-Pyr-018	MUN-Pyr-019	MUN-Pyr-020
1407.93	1408.2	1408.15	1408.1	1408.09	1408	1407.47
0.856	0.856	0.859	0.857	0.857	0.855	0.852
2193.26	2193.38	2192.78	2191.07	2191.42	2193.24	2193.28
0.758	0.765	0.75	0.752	0.736	0.754	0.753
-	-	-	-	-	-	-
-	-	-	-	-	-	-

MUN-Pyr-034	MUN-Pyr-035	MUN-Pyr-036	MUN-Pyr-037	MUN-Pyr-038	MUN-Pyr-039	MUN-Pyr-040
1407.74	1408.06	1408.08	1408.1	1408.12	1407.97	1408.03
0.86	0.86	0.862	0.862	0.862	0.863	0.864
2190	2191.2	2193.43	2192.02	2189.05	2192.07	2192.23
0.762	0.743	0.753	0.758	0.765	0.769	0.764
-	2241.06	2240.99	-	-	-	-
-	0.116	0.13	-	-	-	-

MUN-Pyr-054	MUN-Pyr-055	MUN-Pyr-056	MUN-Pyr-057	MUN-Pyr-058	MUN-Pyr-059	MUN-Pyr-060
1407.8	1408.12	1408.14	1408.23	1408.08	1408.2	1408.01
0.861	0.853	0.855	0.851	0.853	0.855	0.854
2195.16	2190.26	2194.93	2193.48	2190.4	2193.32	2189.31
0.766	0.728	0.737	0.726	0.734	0.751	0.749
-	2241.38	-	2240.66	-	-	-
-	0.15	-	0.16	-	-	-

MUN-Pyr-074
1408.19
0.847
2193.1
0.737
-
-

Appendix 7.1 Parameters for numeric models of element distribution created in Leapfrog 2021.2

Element	Total sill	Base range	Alpha	Nugget	Accuracy
Ag	10,000	60	3	0	0.08
As	50,000	60	3	0	2
Au	1	60	3	0	0.001
Ba	5,000	50	3	0	20
Bi	2,000	60	3	0	0.04
Co	8,000	60	3	0	0.2
Cu	1	60	3	0	0.002
Ni	300	60	3	0	0.3
Pb	2	60	3	0	0.002
Sb	60,000	60	3	0	0.8
Se	30,000	60	3	0	0.2
Zn	10	60	3	0	0.002
Magnetic susceptibility	1,000	60	3	0	0.02

Appendix 8.1 List of samples for EPMA analysis of sulfide minerals

TS_id	DH_id	From_m	To_m	Zone	Assemblage
A00348395	K15-290	78.92	79	ABM	Assemblage 1
B00232695	K15-319	188	188.05	KKT	Assemblage 1
B00233308	K15-321	237.89	237.96	KKT	Assemblage 1
B00264518	K15-200	151.12	151.2	ABM	Assemblage 3
B00265159a	K15-292	239.65	239.71	KKT	Assemblage 2
B00266543	K15-229	63.58	63.63	ABM	Assemblage 1
B00266564	K15-231	54.04	54.11	ABM	Assemblage 1
B00266575	K15-231	63.09	63.14	ABM	Assemblage 2
B00266585	K15-231	71	71.06	ABM	Assemblage 1
B00269601	K15-299	115.94	116	ABM	Assemblage 1
B00291152	K15-339	165.25	165.3	KKT	Assemblage 1
B00291157	K15-339	171	171.05	KKT	Assemblage 2
Q721151	K15-204	112.53	112.62	ABM	Assemblage 2
Q721165	K16-350	110.1	110.18	KKT	Assemblage 3
Q930238	K15-236	82.3	82.45	ABM	Assemblage 2
Q930239	K15-236	86.33	86.42	ABM	Assemblage 1
Q930271	K15-286	127.08	127.15	ABM	Assemblage 3

Appendix 8.2 Results of electron probe microanalyzer analysis of pyrite

Spot_id	A348395-1-1-8	A348395-1-1-9	A348395-2-1-11	A348395-2-1-12	A348395-2-1-13	A348395-2-2-14
TS_id	A348395	A348395	A348395	A348395	A348395	A348395
Assemblage	Assemblage 1	Assemblage 1	Assemblage 1	Assemblage 1	Assemblage 1	Assemblage 1
S wt%	54.00	53.88	53.84	53.82	53.74	53.80
Fe wt%	45.71	46.00	46.05	46.01	46.21	46.16
Cu wt%	bdl	bdl	0.03	0.03	bdl	bdl
Zn wt%	0.03	0.03	bdl	bdl	bdl	bdl
Pb wt%	0.03	0.02	bdl	0.11	0.01	0.01
As wt%	0.21	0.06	0.05	bdl	0.01	bdl
Co wt%	0.02	0.02	0.03	0.02	0.03	0.01
Sb wt%	bdl	bdl	bdl	bdl	bdl	bdl
Total wt%	100.00	100.00	100.00	99.99	100.00	100.00
S_apfu	2.000	2.000	2.000	2.000	2.000	2.000
Fe_apfu	0.972	0.980	0.982	0.982	0.987	0.985
Cu_apfu	-	-	-	-	-	-
Zn_apfu	-	-	-	-	-	-
Pb_apfu	-	-	-	0.001	-	-
As_apfu	-	-	-	-	-	-
Co_apfu	0.000	0.000	0.001	0.000	0.001	-
Sb_apfu	-	-	-	-	-	-

Spot_id	B266585-8-1-27	B266585-8-3-15	B266585-8-3-18	B266585-8-3-2	B291152-1-1-13	B291152-1-1-15*
TS_id	B266585	B266585	B266585	B266585	B291152	B291152
Assemblage	Assemblage 1	Assemblage 1	Assemblage 1	Assemblage 1	Assemblage 1	Assemblage 1
S wt%	53.87	53.94	53.79	53.94	53.03	51.46
Fe wt%	46.07	45.98	46.00	45.99	46.09	44.25
Cu wt%	bdl	0.01	0.03	bdl	0.01	3.77
Zn wt%	bdl	bdl	0.05	bdl	0.04	0.44
Pb wt%	bdl	bdl	0.01	0.03	0.05	bdl
As wt%	0.04	0.05	bdl	0.01	0.77	0.05
Co wt%	0.02	0.02	0.02	0.02	0.02	0.02
Sb wt%	bdl	bdl	0.08	bdl	bdl	bdl
Total wt%	100.00	100.00	99.98	100.00	100.00	100.00
S_apfu	2.000	2.000	2.000	2.000	2.000	2.000
Fe_apfu	0.982	0.979	0.982	0.979	0.998	0.987
Cu_apfu	-	-	-	-	-	0.074
Zn_apfu	-	-	-	-	-	0.008
Pb_apfu	-	-	-	-	-	-
As_apfu	-	-	-	-	0.012	-
Co_apfu	0.000	0.000	0.000	0.000	0.000	0.000
Sb_apfu	-	-	-	-	-	-

* notes analyses of spots with likely inclusions

A348395-3-1-21	A348395-3-1-24	A348395-8-1-20	A348395-8-1-21	A348395-8-3-13	A348395-8-3-14
A348395	A348395	A348395	A348395	A348395	A348395
Assemblage 1	Assemblage 1	Assemblage 1	Assemblage 1	Assemblage 1	Assemblage 1
53.77	53.68	53.73	53.73	53.64	53.78
46.15	46.23	45.91	46.26	46.03	46.15
0.01	0.02	0.04	bdl	bdl	0.01
0.01	bdl	bdl	bdl	0.12	bdl
bdl	bdl	bdl	bdl	0.03	bdl
0.03	0.04	0.29	bdl	0.17	0.01
0.02	0.01	bdl	0.01	0.01	0.03
0.01	0.01	0.02	bdl	bdl	bdl
100.00	100.00	100.00	100.00	100.00	99.99
2.000	2.000	2.000	2.000	2.000	2.000
0.985	0.989	0.981	0.988	0.985	0.985
-	-	-	-	-	-
-	-	-	-	-	-
-	-	-	-	-	-
-	-	0.005	-	-	-
-	-	-	-	-	0.001
-	-	-	-	-	-

B291152-1-1-16	B291152-2-1-10	B291152-2-1-13	B291152-2-1-14	B291152-3-1-15	B291152-3-1-16
B291152	B291152	B291152	B291152	B291152	B291152
Assemblage 1	Assemblage 1	Assemblage 1	Assemblage 1	Assemblage 1	Assemblage 1
53.91	53.72	53.95	53.84	53.72	53.67
45.94	46.26	45.99	46.08	46.18	46.03
bdl	0.01	bdl	bdl	0.01	0.16
0.13	bdl	bdl	bdl	bdl	0.02
bdl	bdl	0.01	0.01	bdl	0.04
bdl	bdl	0.03	0.03	0.04	0.05
0.02	0.02	0.03	0.03	0.04	0.04
bdl	bdl	bdl	bdl	bdl	bdl
100.00	100.00	100.00	100.00	100.00	100.00
2.000	2.000	2.000	2.000	2.000	2.000
0.979	0.989	0.979	0.983	0.987	0.985
-	-	-	-	-	0.003
-	-	-	-	-	-
-	-	-	-	-	-
-	-	-	-	-	-
0.000	-	0.001	0.001	0.001	0.001
-	-	-	-	-	-

A348395-8-3-18	B232695-1-1-16	B232695-1-1-20	B232695-1-1-7	B232695-2-1-15	B232695-3-1-19
A348395	B232695	B232695	B232695	B232695	B232695
Assemblage 1	Assemblage 1	Assemblage 1	Assemblage 1	Assemblage 1	Assemblage 1
53.96	53.68	53.49	53.61	53.60	53.17
45.97	46.15	46.35	46.33	46.31	46.78
0.01	0.02	0.07	bdl	bdl	bdl
bdl	0.04	bdl	bdl	0.04	bdl
0.03	0.01	0.04	bdl	bdl	0.02
0.01	0.05	0.02	0.01	0.02	bdl
0.02	0.05	0.03	0.05	0.04	0.02
bdl	bdl	bdl	bdl	bdl	0.01
100.00	100.00	100.00	100.00	100.00	99.99
2.000	2.000	2.000	2.000	2.000	2.000
0.978	0.987	0.995	0.992	0.992	1.010
-	-	-	-	-	-
-	-	-	-	-	-
-	-	-	-	-	-
-	-	-	-	-	-
0.000	0.001	0.001	0.001	0.001	-
-	-	-	-	-	-

B291152-3-1-18	B291152-4-1-13	B291152-4-1-6	B291152-4-2-20	B291152-4-2-21	B291152-4-2-23
B291152	B291152	B291152	B291152	B291152	B291152
Assemblage 1	Assemblage 1	Assemblage 1	Assemblage 1	Assemblage 1	Assemblage 1
53.90	53.80	53.70	53.77	53.82	53.59
45.99	46.05	46.09	46.18	45.97	46.20
bdl	bdl	bdl	0.02	0.12	0.01
bdl	0.07	0.13	bdl	0.03	0.01
0.04	bdl	bdl	bdl	bdl	bdl
0.05	0.04	0.04	bdl	0.03	0.13
0.02	0.04	0.04	0.03	0.04	0.04
bdl	bdl	bdl	bdl	bdl	bdl
100.00	100.00	100.00	100.00	100.00	99.99
2.000	2.000	2.000	2.000	2.000	2.000
0.980	0.983	0.986	0.986	0.981	0.990
-	-	-	-	0.002	-
-	-	-	-	-	-
-	-	-	-	-	-
-	-	-	-	-	-
0.000	0.001	0.001	0.001	0.001	0.001
-	-	-	-	-	-

B232695-3-1-20	B232695-5-1-23	B232695-5-1-24	B232695-7-1-13	B232695-7-1-14	B232695-7-1-15
B232695	B232695	B232695	B232695	B232695	B232695
Assemblage 1	Assemblage 1	Assemblage 1	Assemblage 1	Assemblage 1	Assemblage 1
53.74	53.64	53.48	53.89	53.61	53.73
46.21	46.21	46.06	45.95	46.26	46.23
bdl	bdl	0.10	bdl	0.01	bdl
bdl	0.02	0.26	0.05	bdl	bdl
bdl	0.01	bdl	bdl	0.01	0.01
bdl	0.07	0.06	0.06	0.04	bdl
0.04	0.05	0.04	0.06	0.06	0.02
bdl	bdl	bdl	bdl	0.01	bdl
100.00	100.00	100.00	100.00	100.00	100.00
2.000	2.000	2.000	2.000	2.000	2.000
0.987	0.989	0.989	0.979	0.991	0.988
-	-	0.002	-	-	-
-	-	-	-	-	-
-	-	-	-	-	-
-	-	-	-	-	-
0.001	0.001	0.001	0.001	0.001	0.000
-	-	-	-	-	-

B291152-6-1-12	B291152-6-1-15	B291152-6-1-18	B291152-7-1-7	B291152-7-1-9	B291157-11-1-6
B291152	B291152	B291152	B291152	B291152	B291157
Assemblage 1	Assemblage 1	Assemblage 1	Assemblage 1	Assemblage 1	Assemblage 2
53.79	53.88	53.77	53.65	53.78	53.68
46.00	46.03	45.91	46.26	46.14	46.19
0.12	bdl	0.21	0.03	0.01	bdl
0.06	bdl	bdl	bdl	0.04	bdl
bdl	0.01	0.04	bdl	bdl	0.01
0.01	0.05	0.05	0.02	bdl	0.05
0.03	0.02	0.03	0.03	0.02	0.08
bdl	bdl	bdl	0.01	bdl	bdl
100.00	99.99	100.00	100.00	100.00	100.00
2.000	2.000	2.000	2.000	2.000	2.000
0.982	0.981	0.980	0.990	0.985	0.988
0.002	-	0.004	-	-	-
-	-	-	-	-	-
-	-	-	-	-	-
-	-	-	-	-	-
0.001	0.000	0.001	0.001	0.000	0.002
-	-	-	-	-	-

B232695-8-1-12	B232695-8-1-13	B232695-8-1-16	B232695-9-1-10	B232695-9-1-15	B232695-9-1-16
B232695	B232695	B232695	B232695	B232695	B232695
Assemblage 1	Assemblage 1	Assemblage 1	Assemblage 1	Assemblage 1	Assemblage 1
53.65	53.84	53.84	53.69	53.78	53.53
46.16	46.13	46.07	46.25	46.14	46.42
0.01	bdl	bdl	0.01	bdl	bdl
0.08	bdl	bdl	bdl	bdl	0.03
0.01	bdl	0.03	0.03	0.02	bdl
0.05	bdl	0.05	bdl	0.02	bdl
0.03	0.04	0.02	0.02	0.03	0.02
bdl	bdl	bdl	bdl	bdl	bdl
100.00	100.00	100.00	100.00	99.99	100.00
2.000	2.000	2.000	2.000	2.000	2.000
0.988	0.984	0.982	0.989	0.985	0.996
-	-	-	-	-	-
-	-	-	-	-	-
-	-	-	-	-	-
-	-	-	-	-	-
0.001	0.001	0.000	0.000	0.001	0.000
-	-	-	-	-	-

B291157-11-1-7	B291157-2-1-11	B291157-2-1-15	B291157-4-1-12	B291157-4-1-13	B291157-5-1-1
B291157	B291157	B291157	B291157	B291157	B291157
Assemblage 2	Assemblage 2	Assemblage 2	Assemblage 2	Assemblage 2	Assemblage 2
53.69	53.56	53.87	53.68	53.74	53.74
46.13	46.27	46.00	46.11	46.13	46.08
bdl	bdl	bdl	0.01	bdl	bdl
0.03	bdl	bdl	bdl	bdl	bdl
bdl	bdl	0.03	bdl	bdl	0.03
0.08	0.11	0.03	0.13	0.04	0.03
0.07	0.05	0.07	0.07	0.09	0.13
bdl	0.01	bdl	0.01	bdl	bdl
100.00	100.00	100.00	100.00	100.00	100.00
2.000	2.000	2.000	2.000	2.000	2.000
0.986	0.992	0.980	0.986	0.985	0.984
-	-	-	-	-	-
-	-	-	-	-	-
-	-	-	-	-	-
-	-	-	-	-	-
0.001	0.001	0.001	0.001	0.002	0.003
-	-	-	-	-	-

B232695-9-1-17	B233308-1-1-12	B233308-1-1-9	B233308-2-1-13	B233308-2-1-15	B233308-2-1-16
B232695	B233308	B233308	B233308	B233308	B233308
Assemblage 1	Assemblage 1	Assemblage 1	Assemblage 1	Assemblage 1	Assemblage 1
53.65	53.76	53.68	53.36	53.50	53.75
45.92	46.14	46.23	46.46	46.33	46.09
bdl	bdl	bdl	bdl	bdl	bdl
0.37	0.03	0.01	0.05	0.08	0.10
0.02	0.05	0.02	0.06	0.05	0.02
0.01	bdl	0.03	0.03	0.01	0.02
0.03	0.02	0.03	0.03	0.02	0.01
bdl	bdl	bdl	bdl	bdl	bdl
100.00	100.00	100.00	100.00	99.99	100.00
2.000	2.000	2.000	2.000	2.000	2.000
0.983	0.985	0.989	1.000	0.994	0.985
-	-	-	-	-	-
0.007	-	-	-	-	-
-	-	-	-	-	-
-	-	-	-	-	-
0.001	0.000	0.001	0.001	-	-
-	-	-	-	-	-

B291157-5-1-16	B291157-5-1-2	B291157-5-2-11	B291157-5-2-9	B291157-6-39	Q721151-1-1-12
B291157	B291157	B291157	B291157	B291157	Q721151
Assemblage 2	Assemblage 2	Assemblage 2	Assemblage 2	Assemblage 2	Assemblage 2
53.69	53.87	53.68	53.71	53.82	53.36
46.11	45.94	45.80	45.83	45.81	46.22
bdl	bdl	bdl	bdl	bdl	0.01
bdl	0.03	0.43	0.28	0.19	bdl
bdl	0.02	bdl	0.01	bdl	0.24
0.09	0.04	bdl	0.06	0.05	bdl
0.11	0.09	0.08	0.11	0.13	0.16
bdl	bdl	bdl	bdl	bdl	bdl
100.00	100.00	100.00	100.00	100.00	100.00
2.000	2.000	2.000	2.000	2.000	2.000
0.986	0.979	0.979	0.980	0.977	0.995
-	-	-	-	-	-
-	-	0.008	-	-	-
-	-	-	-	-	0.001
-	-	-	-	-	-
0.002	0.002	0.002	0.002	0.003	0.003
-	-	-	-	-	-

B233308-3-1-10	B233308-3-1-11	B233308-3-1-9	B233308-4-1-12	B233308-4-1-13	B233308-4-1-14
B233308	B233308	B233308	B233308	B233308	B233308
Assemblage 1	Assemblage 1	Assemblage 1	Assemblage 1	Assemblage 1	Assemblage 1
53.67	53.89	53.82	54.05	53.73	53.77
46.31	46.00	45.94	45.74	46.19	46.11
bdl	bdl	bdl	bdl	bdl	bdl
bdl	0.07	0.15	0.13	bdl	bdl
bdl	bdl	0.05	0.04	0.01	0.10
bdl	0.01	0.01	0.03	0.06	bdl
0.02	0.02	0.03	bdl	0.01	0.02
bdl	bdl	bdl	bdl	bdl	bdl
100.00	99.99	100.00	99.99	100.00	100.00
2.000	2.000	2.000	2.000	2.000	2.000
0.991	0.980	0.980	0.971	0.987	0.985
-	-	-	-	-	-
-	-	-	-	-	-
-	-	-	-	-	0.001
-	-	-	-	-	-
-	0.000	0.001	-	-	-
-	-	-	-	-	-

Q721151-1-1-7*	Q721151-2-1-10	Q721151-2-1-7	Q721151-2-1-8	Q721151-3-1-20	Q721151-3-1-21
Q721151	Q721151	Q721151	Q721151	Q721151	Q721151
Assemblage 2	Assemblage 2	Assemblage 2	Assemblage 2	Assemblage 2	Assemblage 2
45.94	53.56	53.57	53.64	53.30	52.78
39.39	46.34	46.27	46.18	45.91	46.75
12.94	0.01	0.02	bdl	0.05	bdl
bdl	bdl	bdl	bdl	0.01	bdl
1.52	0.01	bdl	bdl	bdl	bdl
0.01	bdl	bdl	bdl	bdl	bdl
0.17	0.07	0.13	0.17	0.73	0.46
bdl	bdl	0.01	bdl	bdl	bdl
99.97	100.00	100.00	100.00	100.00	100.00
2.000	2.000	2.000	2.000	2.000	2.000
0.984	0.993	0.992	0.988	0.989	1.017
0.284	-	-	-	-	-
-	-	-	-	-	-
0.010	-	-	-	-	-
-	-	-	-	-	-
0.004	0.001	0.003	0.003	0.015	0.010
-	-	-	-	-	-

B233308-4-1-15*	B233308-5-1-1	B233308-5-1-10	B233308-5-1-12	B233308-7-1-15	B233308-7-1-16
B233308	B233308	B233308	B233308	B233308	B233308
Assemblage 1	Assemblage 1	Assemblage 1	Assemblage 1	Assemblage 1	Assemblage 1
53.24	53.62	53.68	53.57	53.53	53.76
45.19	45.66	46.20	46.22	46.09	46.06
bdl	0.09	0.01	0.02	0.03	bdl
bdl	0.39	0.08	0.04	bdl	bdl
1.46	0.15	0.02	0.08	0.04	bdl
0.09	0.07	bdl	0.04	0.28	0.14
0.02	0.02	0.03	0.03	0.03	0.03
bdl	bdl	bdl	bdl	bdl	bdl
100.00	100.00	100.00	100.00	100.00	100.00
2.000	2.000	2.000	2.000	2.000	2.000
0.975	0.978	0.988	0.991	0.988	0.984
-	0.002	-	-	-	-
-	0.007	-	-	-	-
0.008	0.001	-	0.000	-	-
-	-	-	-	0.004	-
0.000	0.000	0.001	0.001	0.001	0.001
-	-	-	-	-	-

Q721151-6-2-10	Q721151-6-2-11	Q721151-6-2-12	Q721151-6-2-13	Q721151-6-2-4	Q721151-6-2-8
Q721151	Q721151	Q721151	Q721151	Q721151	Q721151
Assemblage 2	Assemblage 2	Assemblage 2	Assemblage 2	Assemblage 2	Assemblage 2
53.74	53.57	53.56	53.32	53.73	53.53
46.06	46.29	46.27	46.12	46.14	46.08
0.01	0.03	0.01	0.03	0.02	0.01
0.03	bdl	bdl	bdl	0.01	bdl
0.03	0.02	0.00	0.17	0.03	0.12
bdl	bdl	0.03	0.10	0.03	bdl
0.12	0.07	0.12	0.25	0.05	0.26
0.01	bdl	0.01	bdl	bdl	bdl
100.00	99.99	99.99	99.98	100.00	100.00
2.000	2.000	2.000	2.000	2.000	2.000
0.984	0.992	0.992	0.993	0.986	0.988
-	-	-	-	-	-
-	-	-	-	-	-
-	-	-	0.001	-	0.001
-	-	-	-	-	-
0.002	0.001	0.002	0.005	0.001	0.005
-	-	-	-	-	-

B233308-7-1-17	B233308-7-1-18	B233308-7-1-7	B265159A-1-1-12	B265159A-3-2-15	B265159A-3-2-24
B233308	B233308	B233308	B265159A	B265159A	B265159A
Assemblage 1	Assemblage 1	Assemblage 1	Assemblage 2	Assemblage 2	Assemblage 2
53.87	53.59	52.42	53.55	53.58	53.58
45.97	46.14	47.42	46.21	45.97	45.96
bdl	0.02	0.04	0.06	bdl	0.22
0.10	0.01	bdl	0.04	0.40	0.02
bdl	0.15	0.07	bdl	0.02	0.03
0.03	0.05	0.03	0.08	bdl	0.11
0.03	0.03	0.01	0.06	0.03	0.07
bdl	bdl	bdl	bdl	bdl	bdl
100.00	99.99	100.00	99.99	100.00	99.99
2.000	2.000	2.000	2.000	2.000	2.000
0.980	0.989	1.039	0.991	0.985	0.985
-	-	-	-	-	0.004
-	-	-	-	0.007	-
-	0.001	0.000	-	-	-
-	-	-	-	-	-
0.001	0.001	-	0.001	0.001	0.001
-	-	-	-	-	-

Q721151-6-2-9	Q721165-5-1-2	Q721165-1-1-1	Q721165-1-1-8	Q721165-1-1-9	Q721165-4-1-18
Q721151	Q721165	Q721165	Q721165	Q721165	Q721165
Assemblage 2	Assemblage 2	Assemblage 3	Assemblage 3	Assemblage 3	Assemblage 3
53.56	53.12	53.86	53.99	54.05	53.71
46.33	46.13	46.02	45.76	45.67	46.21
bdl	0.01	bdl	0.01	bdl	0.01
bdl	bdl	0.03	0.15	0.21	bdl
0.03	0.23	0.04	bdl	bdl	0.03
bdl	bdl	0.01	0.04	0.03	0.02
0.07	0.06	0.02	0.04	0.03	0.02
bdl	0.39	0.01	bdl	bdl	bdl
100.00	99.93	99.99	100.00	100.00	100.00
2.000	2.000	2.000	2.000	2.000	2.000
0.993	0.997	0.981	0.973	0.970	0.988
-	-	-	-	-	-
-	-	-	-	-	-
-	0.001	-	-	-	-
0.000	-	-	-	-	-
0.001	0.001	0.000	0.001	0.001	0.000
-	0.004	-	-	-	-

B265159A-3-3-12	B265159A-3-3-14	B265159A-3-3-15	B265159A-4-1-11	B265159A-4-1-8	B265159A-9-1-14
B265159A	B265159A	B265159A	B265159A	B265159A	B265159A
Assemblage 2	Assemblage 2	Assemblage 2	Assemblage 2	Assemblage 2	Assemblage 2
53.63	53.55	51.85	53.16	53.38	53.88
46.17	46.37	47.91	46.23	46.41	45.91
bdl	bdl	0.01	bdl	0.01	0.01
bdl	bdl	bdl	0.55	0.03	bdl
bdl	0.02	0.04	bdl	0.03	bdl
0.09	bdl	0.05	bdl	0.09	0.15
0.11	0.04	0.12	0.05	0.05	0.04
bdl	bdl	0.02	bdl	0.01	bdl
100.00	100.00	100.00	100.00	100.00	100.00
2.000	2.000	2.000	2.000	2.000	2.000
0.988	0.994	1.061	0.999	0.998	0.978
-	-	-	-	-	-
-	-	-	0.010	-	-
-	-	-	-	-	-
-	-	-	-	-	-
0.002	0.001	0.002	0.001	0.001	0.001
-	-	-	-	-	-

Q721165-5-1-1	Q721165-5-1-10	Q721165-6-1-24	Q721165-6-1-7	Q721165-7-1-14	Q721165-7-1-15
Q721165	Q721165	Q721165	Q721165	Q721165	Q721165
Assemblage 3	Assemblage 3	Assemblage 3	Assemblage 3	Assemblage 3	Assemblage 3
53.76	53.79	53.80	53.77	53.68	53.66
46.21	46.16	46.18	46.05	46.22	46.27
bdl	bdl	bdl	bdl	bdl	0.01
bdl	bdl	bdl	0.10	0.04	bdl
bdl	bdl	bdl	bdl	bdl	bdl
bdl	0.04	bdl	0.04	0.03	0.02
0.03	0.01	0.02	0.03	0.02	0.02
bdl	bdl	bdl	bdl	bdl	0.01
100.00	100.00	100.00	100.00	100.00	100.00
2.000	2.000	2.000	2.000	2.000	2.000
0.987	0.985	0.985	0.983	0.989	0.990
-	-	-	-	-	-
-	-	-	-	-	-
-	-	-	-	-	-
-	-	-	-	-	-
0.001	-	0.000	0.001	0.000	0.000
-	-	-	-	-	-

B265159A-9-1-5	B265159A-9-1-9	B266543-1-2-10	B266543-1-2-6	B266543-1-2-9	B266543-2-1-14
B265159A	B265159A	B266543	B266543	B266543	B266543
Assemblage 2	Assemblage 2	Assemblage 1	Assemblage 1	Assemblage 1	Assemblage 1
53.15	53.67	53.67	53.70	53.92	53.82
46.04	46.09	46.20	46.26	45.82	46.11
0.25	0.04	0.03	bdl	0.05	bdl
bdl	0.01	0.02	bdl	0.05	0.01
0.12	bdl	bdl	bdl	bdl	bdl
0.36	0.14	0.04	bdl	0.12	0.03
0.08	0.05	0.03	0.04	0.02	0.03
bdl	bdl	bdl	bdl	bdl	bdl
100.00	100.00	100.00	100.00	99.99	99.99
2.000	2.000	2.000	2.000	2.000	2.000
0.995	0.986	0.988	0.989	0.976	0.984
0.005	-	-	-	-	-
-	-	-	-	-	-
0.001	-	-	-	-	-
0.006	-	-	-	-	-
0.002	0.001	0.001	0.001	-	0.001
-	-	-	-	-	-

Q721165-7-2-23	Q721165-7-2-24	Q721165-7-2-5	Q930238-1-1-26	Q930238-1-3-21	Q930238-1-3-22
Q721165	Q721165	Q721165	Q930238	Q930238	Q930238
Assemblage 3	Assemblage 3	Assemblage 3	Assemblage 2	Assemblage 2	Assemblage 2
53.92	53.56	53.58	53.76	53.32	53.66
46.05	46.27	46.10	45.86	45.64	46.21
bdl	0.01	0.02	0.02	bdl	0.01
bdl	0.11	bdl	0.02	bdl	bdl
bdl	0.03	0.05	0.16	bdl	0.03
0.01	bdl	0.23	bdl	0.38	bdl
0.02	0.01	0.02	0.07	0.62	0.09
bdl	bdl	bdl	0.05	0.01	bdl
100.00	100.00	100.00	99.95	99.98	100.00
2.000	2.000	2.000	2.000	2.000	2.000
0.981	0.992	0.988	0.979	0.983	0.989
-	-	-	-	-	-
-	-	-	-	-	-
-	-	-	0.001	-	-
-	-	0.004	-	0.006	-
-	-	-	0.002	0.013	0.002
-	-	-	-	-	-

B266543-2-1-5	B266543-3-1-6	B266543-3-1-7	B266543-3-1-8	B266543-3-2-13	B266543-3-2-16	B266543-4-2-15
B266543	B266543	B266543	B266543	B266543	B266543	B266543
Assemblage 1	Assemblage 1	Assemblage 1	Assemblage 1	Assemblage 1	Assemblage 1	Assemblage 1
54.06	53.83	53.83	53.80	53.80	53.75	53.87
45.86	46.15	46.14	46.16	46.13	46.18	46.07
bdl	bdl	0.01	bdl	bdl	0.01	bdl
bdl	bdl	bdl	0.01	bdl	0.01	bdl
0.05	bdl	bdl	bdl	0.01	0.02	bdl
bdl	bdl	bdl	bdl	0.03	bdl	0.03
0.02	0.02	0.03	0.02	0.02	0.02	0.02
bdl	bdl	bdl	bdl	bdl	bdl	bdl
100.00	100.00	100.00	99.99	100.00	99.99	100.00
2.000	2.000	2.000	2.000	2.000	2.000	2.000
0.974	0.984	0.984	0.985	0.984	0.986	0.982
-	-	-	-	-	-	-
-	-	-	-	-	-	-
-	-	-	-	-	-	-
-	-	-	-	-	-	-
0.000	-	0.001	0.000	0.000	0.000	0.000
-	-	-	-	-	-	-

Q930238-2-1-12	Q930238-2-2-10	Q930238-2-2-4	Q930238-3-1-17	Q930238-3-1-18	Q930238-3-2-11	Q930238-3-2-12
Q930238	Q930238	Q930238	Q930238	Q930238	Q930238	Q930238
Assemblage 2	Assemblage 2	Assemblage 2	Assemblage 2	Assemblage 2	Assemblage 2	Assemblage 2
53.88	53.95	53.58	53.04	53.52	52.68	53.51
45.74	45.68	46.22	46.81	46.38	46.87	46.14
0.02	bdl	0.02	0.04	0.02	0.01	0.01
bdl	bdl	bdl	bdl	bdl	0.06	bdl
bdl	0.02	0.03	0.02	0.01	bdl	0.03
0.05	0.13	bdl	bdl	bdl	0.09	0.07
0.31	0.21	0.13	0.08	0.06	0.28	0.25
bdl	bdl	0.02	bdl	bdl	0.01	bdl
100.00	100.00	100.00	100.00	100.00	100.00	100.00
2.000	2.000	2.000	2.000	2.000	2.000	2.000
0.975	0.972	0.990	1.013	0.995	1.022	0.990
-	-	-	-	-	-	-
-	-	-	-	-	-	-
-	-	-	-	-	-	-
-	-	-	-	-	-	-
0.006	0.004	0.003	0.002	0.001	0.006	0.005
-	-	-	-	-	-	-

B266543-4-2-16	B266543-5-1-10	B266543-5-1-14	B266543-5-1-16	B266543-6-1-11	B266543-6-1-12
B266543	B266543	B266543	B266543	B266543	B266543
Assemblage 1	Assemblage 1	Assemblage 1	Assemblage 1	Assemblage 1	Assemblage 1
53.65	53.54	53.58	53.78	53.85	53.78
46.30	45.19	46.17	46.01	46.09	46.16
0.01	0.75	0.04	0.04	bdl	bdl
bdl	bdl	0.03	bdl	bdl	0.02
bdl	bdl	0.02	0.04	0.01	bdl
0.01	0.42	0.13	0.10	0.03	0.01
0.02	0.01	0.02	0.01	0.03	0.02
bdl	0.07	bdl	0.03	bdl	bdl
99.99	99.99	99.99	100.00	100.00	100.00
2.000	2.000	2.000	2.000	2.000	2.000
0.991	0.969	0.989	0.982	0.983	0.986
-	0.014	-	-	-	-
-	-	-	-	-	-
-	-	-	-	-	-
-	0.007	-	-	-	-
0.000	-	0.000	-	0.001	0.000
-	-	-	-	-	-

Q930238-4-1-17	Q930238-4-1-2	Q930238-4-2-8*	Q930238-6-8	Q930239-1-1-11	Q930239-1-2-12
Q930238	Q930238	Q930238	Q930238	Q930239	Q930239
Assemblage 2	Assemblage 2	Assemblage 2	Assemblage 2	Assemblage 1	Assemblage 1
53.79	53.27	49.39	53.26	53.99	53.82
46.14	46.44	41.03	43.94	45.83	46.06
0.02	0.12	7.68	0.23	0.01	bdl
bdl	0.05	0.00	0.02	0.10	0.02
bdl	0.03	0.04	0.05	bdl	bdl
bdl	bdl	0.30	0.12	0.02	0.07
0.05	0.08	1.54	2.38	0.04	0.03
bdl	bdl	bdl	bdl	bdl	bdl
100.00	100.00	99.97	99.99	99.99	100.00
2.000	2.000	2.000	2.000	2.000	2.000
0.985	1.001	0.954	0.947	0.974	0.983
-	0.002	0.157	0.004	-	-
-	-	-	-	-	-
-	-	-	-	-	-
-	-	0.005	-	-	-
0.001	0.002	0.034	0.049	0.001	0.001
-	-	-	-	-	-

2665575-10-1-13	2665575-1-1-11	2665575-1-1-12	2665575-2-1-14	2665575-2-1-15	2665575-2-1-16
B266575	B266575	B266575	B266575	B266575	B266575
Assemblage 2	Assemblage 2	Assemblage 2	Assemblage 2	Assemblage 2	Assemblage 2
53.74	53.90	54.06	53.70	53.99	53.80
45.54	46.03	45.83	46.18	45.92	46.16
0.03	bdl	bdl	bdl	0.01	0.01
0.48	bdl	0.07	0.02	bdl	0.01
0.02	bdl	bdl	0.01	bdl	bdl
0.10	0.01	bdl	0.04	0.03	bdl
0.09	0.06	0.04	0.05	0.05	0.02
bdl	bdl	bdl	bdl	bdl	bdl
100.00	100.00	100.00	100.00	100.00	100.00
2.000	2.000	2.000	2.000	2.000	2.000
0.973	0.980	0.973	0.987	0.977	0.985
-	-	-	-	-	-
0.009	-	-	-	-	-
-	-	-	-	-	-
-	-	-	-	-	-
0.002	0.001	0.001	0.001	0.001	0.000
-	-	-	-	-	-

Q930239-1-2-8	Q930239-1-2-9	Q930239-2-1-11	Q930239-2-1-6	Q930239-3-1-16	Q930239-3-1-17
Q930239	Q930239	Q930239	Q930239	Q930239	Q930239
Assemblage 1	Assemblage 1	Assemblage 1	Assemblage 1	Assemblage 1	Assemblage 1
53.85	53.81	53.99	53.95	53.83	53.76
45.96	46.15	45.94	45.99	45.94	46.10
bdl	bdl	bdl	bdl	bdl	bdl
0.11	bdl	0.03	bdl	0.15	0.10
bdl	bdl	bdl	bdl	bdl	bdl
0.05	bdl	0.02	0.04	0.04	0.03
0.03	0.03	0.02	0.02	0.03	0.01
bdl	bdl	bdl	bdl	bdl	bdl
100.00	100.00	100.00	100.00	100.00	100.00
2.000	2.000	2.000	2.000	2.000	2.000
0.980	0.985	0.977	0.979	0.980	0.985
-	-	-	-	-	-
-	-	-	-	-	-
-	-	-	-	-	-
-	-	-	-	-	-
0.001	0.001	0.000	-	0.001	-
-	-	-	-	-	-

2665575-2-1-17	2665575-2-2-13	2665575-2-2-14	2665575-2-2-15	2665575-4-1-14	2665575-4-1-23
B266575	B266575	B266575	B266575	B266575	B266575
Assemblage 2	Assemblage 2	Assemblage 2	Assemblage 2	Assemblage 2	Assemblage 2
53.72	53.63	53.29	53.79	53.53	54.28
46.17	46.29	45.83	46.10	46.19	45.51
0.01	0.01	bdl	0.01	0.03	0.04
0.03	bdl	bdl	bdl	0.01	bdl
0.02	0.01	bdl	bdl	0.13	0.03
bdl	0.01	0.73	0.04	bdl	0.03
0.05	0.04	0.04	0.06	0.03	0.11
bdl	bdl	0.12	bdl	0.01	bdl
100.00	100.00	100.00	100.00	99.91	100.00
2.000	2.000	2.000	2.000	2.000	2.000
0.987	0.991	0.987	0.984	0.991	0.963
-	-	-	-	-	-
-	-	-	-	-	-
-	-	-	-	0.001	-
-	-	0.012	-	-	-
0.001	0.001	0.001	0.001	0.001	0.002
-	-	0.001	-	-	-

Q930239-3-1-8*	Q930239-3-2-11	Q930239-3-2-15	Q930239-3-3-5	Q930239-3-3-7*	Q930239-3-3-8*
Q930239	Q930239	Q930239	Q930239	Q930239	Q930239
Assemblage 1	Assemblage 1	Assemblage 1	Assemblage 1	Assemblage 1	Assemblage 1
49.69	53.97	53.71	53.90	49.30	52.47
41.33	45.98	45.80	45.66	41.24	43.63
0.03	bdl	bdl	bdl	0.02	0.02
0.03	bdl	bdl	0.29	bdl	bdl
8.06	bdl	0.39	0.13	9.33	3.73
0.80	0.03	0.07	bdl	0.07	0.09
0.02	0.02	0.03	0.02	0.03	0.02
0.05	bdl	bdl	bdl	bdl	0.04
100.00	100.00	100.00	100.00	100.00	100.00
2.000	2.000	2.000	2.000	2.000	2.000
0.955	0.978	0.979	0.973	0.960	0.955
-	-	-	-	-	-
-	-	-	-	-	-
0.050	-	0.002	0.001	0.059	0.022
0.014	-	-	-	-	-
-	-	0.001	0.000	0.001	-
-	-	-	-	-	-

2665575-4-1-24	2665575-4-1-3	2665575-4-1-5	B266585-1-1-10	B266585-1-1-9	B266585-2-1-11
B266575	B266575	B266575	B266585	B266585	B266585
Assemblage 2	Assemblage 2	Assemblage 2	Assemblage 1	Assemblage 1	Assemblage 1
53.79	53.73	53.80	53.58	53.91	53.65
45.97	46.12	46.03	45.91	46.02	45.97
0.02	0.06	bdl	bdl	bdl	bdl
bdl	bdl	bdl	0.46	0.05	0.30
bdl	bdl	bdl	0.01	bdl	0.02
0.11	0.03	0.04	0.02	bdl	0.03
0.11	0.06	0.13	0.02	0.02	0.02
bdl	bdl	bdl	bdl	bdl	bdl
100.00	100.00	100.00	99.99	100.00	99.99
2.000	2.000	2.000	2.000	2.000	2.000
0.981	0.985	0.982	0.984	0.980	0.984
-	-	-	-	-	-
-	-	-	0.008	-	0.005
-	-	-	-	-	-
-	-	-	-	-	-
0.002	0.001	0.003	0.000	-	0.000
-	-	-	-	-	-

Q930239-3-4-12	Q930239-3-4-5	Q930239-3-6-19	Q930239-3-6-21	Q930239-9-1-15	Q930239-9-1-16
Q930239	Q930239	Q930239	Q930239	Q930239	Q930239
Assemblage 1	Assemblage 1	Assemblage 1	Assemblage 1	Assemblage 1	Assemblage 1
53.89	53.74	53.57	53.95	53.90	53.87
46.05	46.10	45.51	45.74	45.94	46.10
bdl	bdl	0.04	0.08	0.01	bdl
bdl	0.07	0.03	0.16	0.08	bdl
bdl	bdl	0.14	bdl	0.02	bdl
0.05	0.06	0.38	0.03	bdl	bdl
0.02	0.03	0.03	0.02	0.03	0.02
bdl	bdl	0.28	bdl	0.02	bdl
100.00	100.00	99.97	99.99	100.00	100.00
2.000	2.000	2.000	2.000	2.000	2.000
0.981	0.985	0.975	0.973	0.979	0.983
-	-	-	0.002	-	-
-	-	-	-	-	-
-	-	0.001	-	-	-
-	-	0.006	-	-	-
-	0.001	0.001	-	0.001	0.000
-	-	0.003	-	-	-

B266585-2-1-6	B266585-2-1-7	B266585-6-1-1	B266585-6-1-12	B266585-6-1-5	B266585-7-1-19
B266585	B266585	B266585	B266585	B266585	B266585
Assemblage 1	Assemblage 1	Assemblage 1	Assemblage 1	Assemblage 1	Assemblage 1
53.25	53.40	53.64	53.75	53.76	53.86
45.95	46.03	46.06	46.19	46.12	46.02
bdl	bdl	bdl	bdl	bdl	bdl
0.16	bdl	0.24	0.02	0.06	bdl
0.01	bdl	0.03	bdl	0.02	0.03
0.61	0.52	bdl	0.02	0.01	0.06
0.02	0.03	0.03	0.02	0.03	0.03
bdl	0.01	bdl	bdl	bdl	bdl
100.00	100.00	100.00	100.00	100.00	100.00
2.000	2.000	2.000	2.000	2.000	2.000
0.991	0.990	0.986	0.986	0.985	0.981
-	-	-	-	-	-
-	-	-	-	-	-
-	-	-	-	-	-
0.010	0.008	-	-	-	-
-	0.001	0.001	0.000	0.001	0.001
-	-	-	-	-	-

Q930239-9-1-18*	Q930239-9-1-3	Q930271-1-1-1	Q930271-1-1-4	Q930271-5-1-1	Q930271-6-1-1
Q930239	Q930239	Q930239	Q930271	Q930271	Q930271
Assemblage 1	Assemblage 1	Assemblage 1	Assemblage 3	Assemblage 3	Assemblage 3
53.80	53.22	54.19	53.64	53.52	53.74
46.11	45.09	45.68	46.19	45.76	46.08
bdl	0.01	bdl	0.02	0.02	0.01
0.02	0.12	0.05	bdl	0.56	bdl
bdl	1.50	bdl	0.05	bdl	0.03
0.05	0.04	0.04	bdl	0.04	bdl
0.02	0.02	0.03	0.07	0.09	0.13
bdl	bdl	bdl	0.02	0.01	bdl
99.99	100.00	100.00	99.99	100.00	99.99
2.000	2.000	2.000	2.000	2.000	2.000
0.984	0.973	0.968	0.989	0.982	0.985
-	-	-	-	-	-
-	-	-	-	0.010	-
-	0.009	-	-	-	-
-	-	-	-	-	-
-	0.000	0.001	0.001	0.002	0.003
-	-	-	-	-	-

Appendix 8.3 Results of electron probe microanalyzer analysis of arsenopyrite

Spot_id	A348395-3-1-25	A348395-3-1-13	A348395-8-1-14	A348395-4-1-7	A348395-2-2-12	A348395-2-1-7
TS_id	A348395	A348395	A348395	A348395	A348395	A348395
Assemblage	Assemblage 1	Assemblage 1	Assemblage 1	Assemblage 1	Assemblage 1	Assemblage 1
S wt%	20.18	19.13	19.98	20.61	19.49	20.42
Fe wt%	34.95	35.69	35.32	35.32	35.56	36.02
Cu wt%	0.30	0.23	bdl	0.33	bdl	bdl
Zn wt%	0.12	0.18	1.26	0.50	0.48	0.11
Pb wt%	1.77	0.09	0.07	0.06	0.06	0.06
As wt%	41.38	43.50	43.19	43.18	43.49	42.75
Co wt%	0.01	0.01	0.02	0.01	0.01	0.02
Sb wt%	1.27	1.16	0.18	bdl	0.91	0.62
Total wt%	100.00	99.99	100.00	100.01	100.00	100.01
S_apfu	1.000	1.000	1.000	1.000	1.000	1.000
Fe_apfu	0.994	1.071	1.015	0.984	1.047	1.013
Cu_apfu	0.008	0.006	-	0.008	-	-
Zn_apfu	-	-	0.031	0.012	0.012	-
Pb_apfu	0.014	-	-	-	-	-
As_apfu	0.877	0.973	0.925	0.896	0.955	0.896
Co_apfu	0.000	-	0.001	0.000	0.000	0.001
Sb_apfu	0.018	0.017	0.003	-	0.013	0.009

Spot_id	B266543-6-1-1	B266585-7-1-24	B266585-8-3-11	B266585-6-1-2	B266585-8-1-26	B266585-1-1-2
TS_id	B266543	B266585	B266585	B266585	B266585	B266585
Assemblage	Assemblage 1	Assemblage 1	Assemblage 1	Assemblage 1	Assemblage 1	Assemblage 1
S wt%	20.74	20.19	20.89	20.54	20.65	20.30
Fe wt%	35.53	35.58	35.36	36.28	36.09	36.20
Cu wt%	0.45	bdl	bdl	bdl	bdl	bdl
Zn wt%	0.90	bdl	bdl	0.19	0.03	bdl
Pb wt%	0.04	1.37	0.55	0.10	0.10	0.04
As wt%	42.32	41.79	43.06	41.60	42.58	43.45
Co wt%	0.02	0.02	0.02	0.03	0.02	0.03
Sb wt%	bdl	1.06	0.13	1.28	0.54	bdl
Total wt%	100.01	100.01	100.01	100.00	100.01	100.01
S_apfu	1.000	1.000	1.000	1.000	1.000	1.000
Fe_apfu	0.983	1.011	0.972	1.014	1.003	1.024
Cu_apfu	0.011	-	-	-	-	-
Zn_apfu	0.021	-	-	-	-	-
Pb_apfu	-	0.010	0.004	-	-	-
As_apfu	0.873	0.886	0.882	0.867	0.882	0.916
Co_apfu	0.001	0.000	0.001	0.001	0.001	0.001
Sb_apfu	-	0.015	0.002	0.018	0.007	-

* notes analyses of spots with likely inclusions

A348395-4-1-9	A348395-8-1-8	A348395-4-2-12	A348395-4-2-10	A348395-2-2-8	B232695-5-1-10
A348395	A348395	A348395	A348395	A348395	B232695
Assemblage 1	Assemblage 1	Assemblage 1	Assemblage 1	Assemblage 1	Assemblage 1
20.35	19.47	19.36	19.33	20.35	19.67
34.56	35.78	35.73	35.80	35.06	34.92
0.05	0.01	0.04	0.12	0.03	0.12
2.35	bdl	0.15	0.06	2.00	0.24
0.05	0.04	0.04	0.01	bdl	1.36
42.64	44.33	42.55	42.77	41.98	43.08
0.02	0.02	0.02	0.02	0.02	0.12
bdl	0.34	2.12	1.89	0.56	0.49
100.02	100.00	100.00	100.00	100.00	100.00
1.000	1.000	1.000	1.000	1.000	1.000
0.975	1.055	1.060	1.063	0.989	1.019
-	-	-	0.003	-	0.003
0.057	-	-	-	0.048	-
-	-	-	-	-	0.011
0.896	0.974	0.941	0.947	0.882	0.937
0.001	0.001	0.001	0.000	0.000	0.003
-	0.005	0.031	0.028	0.008	0.007

B266585-8-1-25	B291152-6-1-8	B291152-1-1-2	B291152-7-1-5	B291152-7-1-2	B291152-2-1-6
B266585	B291152	B291152	B291152	B291152	B291152
Assemblage 1	Assemblage 1	Assemblage 1	Assemblage 1	Assemblage 1	Assemblage 1
20.97	21.44	20.86	20.43	20.26	20.29
36.40	35.60	35.15	35.65	35.79	35.55
0.01	0.21	0.01	0.49	0.10	0.01
bdl	1.40	1.23	0.29	0.17	0.22
0.03	0.20	0.09	0.08	0.07	0.06
41.01	40.96	41.31	43.02	42.66	42.51
0.02	0.03	0.01	0.01	0.02	0.02
1.61	0.16	1.34	0.04	0.94	1.34
100.05	100.00	100.00	100.00	100.00	100.00
1.000	1.000	1.000	1.000	1.000	1.000
0.996	0.953	0.968	1.002	1.014	1.006
-	0.005	-	0.012	0.002	-
-	0.032	0.029	-	-	-
-	0.001	-	-	-	-
0.836	0.817	0.848	0.901	0.901	0.897
0.000	0.001	0.000	0.000	0.001	0.001
0.022	0.002	0.018	-	0.013	0.019

B232695-5-1-22	B232695-3-1-2	B232695-2-1-1	B232695-3-1-12	B232695-2-1-2	B233308-5-1-6	B233308-4-1-1
B232695	B232695	B232695	B232695	B232695	B233308	B233308
Assemblage 1	Assemblage 1	Assemblage 1	Assemblage 1	Assemblage 1	Assemblage 1	Assemblage 1
20.07	20.46	19.60	20.12	20.25	20.90	20.56
35.73	35.66	34.65	36.27	35.65	36.34	35.71
0.03	bdl	bdl	bdl	bdl	bdl	bdl
0.21	0.14	1.53	0.01	0.47	bdl	bdl
0.40	0.11	0.09	0.06	0.04	0.52	0.11
43.06	42.54	43.29	42.67	43.21	41.93	42.72
0.07	0.02	0.03	0.05	0.02	0.01	0.03
0.43	1.07	0.80	0.82	0.37	0.33	0.92
100.00	100.00	100.00	100.00	100.00	100.04	100.05
1.000	1.000	1.000	1.000	1.000	1.000	1.000
1.022	1.000	1.015	1.035	1.011	0.998	0.997
-	-	-	-	-	-	-
-	-	0.038	-	0.011	-	-
0.003	0.001	-	-	-	0.004	0.001
0.918	0.889	0.945	0.908	0.913	0.857	0.888
0.002	0.000	0.001	0.001	0.001	0.000	0.001
0.006	0.015	0.012	0.012	0.005	0.005	0.013

B291152-4-1-14	B291152-4-2-9	B291152-2-1-2	B291157-2-1-1	B291157-2-1-4	Q930238-4-1-6	Q930238-4-1-1
B291152	B291152	B291152	B291157	B291157	Q930238	Q930238
Assemblage 1	Assemblage 1	Assemblage 1	Assemblage 2	Assemblage 2	Assemblage 2	Assemblage 2
20.58	20.47	20.75	20.00	20.22	20.16	20.81
34.58	35.89	35.82	34.40	35.30	34.58	36.32
0.04	0.05	bdl	bdl	bdl	0.18	bdl
1.84	bdl	bdl	1.53	bdl	0.47	bdl
0.04	0.01	0.01	0.05	0.03	0.06	0.04
42.18	43.55	42.18	43.37	43.94	43.28	42.80
0.03	0.03	0.02	0.23	0.35	1.28	0.03
0.70	0.03	1.22	0.43	0.16	bdl	bdl
100.00	100.03	100.00	100.01	100.00	100.00	100.00
1.000	1.000	1.000	1.000	1.000	1.000	1.000
0.965	1.006	0.991	0.987	1.002	0.985	1.002
-	-	-	-	-	0.005	-
0.044	-	-	0.037	-	0.011	-
-	-	-	-	-	-	-
0.877	0.909	0.870	0.928	0.930	0.919	0.880
0.001	0.001	0.001	0.006	0.010	0.034	0.001
0.010	-	0.017	0.006	0.002	-	-

B233308-7-1-6	B233308-4-1-6	B233308-7-1-9	B233308-7-1-1	B233308-5-1-9	B265159A-3-2-10*
B233308	B233308	B233308	B233308	B233308	B265159A
Assemblage 1	Assemblage 1	Assemblage 1	Assemblage 1	Assemblage 1	Assemblage 2
20.97	21.23	21.25	22.26	20.92	24.31
36.61	36.22	36.21	37.03	36.46	33.43
bdl	0.01	bdl	bdl	bdl	0.07
bdl	bdl	0.05	bdl	0.08	4.91
0.06	0.06	0.02	0.01	bdl	0.42
41.28	40.89	41.07	40.32	42.01	36.58
0.02	0.02	0.02	0.02	0.02	0.10
1.07	1.63	1.37	0.43	0.50	0.18
100.01	100.05	100.00	100.06	100.00	99.99
1.000	1.000	1.000	1.000	1.000	1.000
1.002	0.980	0.978	0.955	1.000	0.790
-	-	-	-	-	0.001
-	-	-	-	-	0.099
-	-	-	-	-	0.003
0.842	0.823	0.827	0.774	0.859	0.644
0.001	0.000	0.001	0.000	0.001	0.002
0.014	0.022	0.018	0.005	0.007	0.002

Q930238-3-1-2	Q930238-4-2-10	Q930238-3-1-1	Q930238-4-1-12	Q930239-2-1-10	Q930239-9-1-1
Q930238	Q930238	Q930238	Q930238	Q930239	Q930239
Assemblage 2	Assemblage 2	Assemblage 2	Assemblage 2	Assemblage 1	Assemblage 1
21.26	21.88	20.74	21.73	20.65	20.49
34.29	34.28	36.09	35.95	35.97	35.58
0.04	0.06	0.01	0.04	bdl	bdl
bdl	bdl	bdl	bdl	bdl	0.09
0.03	0.01	bdl	bdl	0.16	0.06
42.23	41.51	43.09	41.87	43.23	43.77
2.17	2.27	0.07	0.47	0.01	0.03
bdl	bdl	bdl	bdl	bdl	bdl
100.02	100.00	100.01	100.06	100.02	100.01
1.000	1.000	1.000	1.000	1.000	1.000
0.926	0.899	0.999	0.950	1.000	0.997
-	0.001	-	-	-	-
-	-	-	-	-	-
-	-	-	-	0.001	-
0.850	0.811	0.889	0.823	0.895	0.914
0.056	0.056	0.002	0.012	0.000	0.001
-	-	-	-	-	-

B265159A-3-2-26	B265159A-4-1-20	B265159A-9-1-16	B265159A-9-1-4	B265159A-9-1-12	B266543-5-1-1
B265159A	B265159A	B265159A	B265159A	B265159A	B266543
Assemblage 2	Assemblage 2	Assemblage 2	Assemblage 2	Assemblage 2	Assemblage 1
20.10	20.74	19.49	20.43	20.94	20.91
35.21	35.94	35.52	35.49	36.16	36.44
0.08	0.01	0.40	0.83	0.46	0.02
0.47	0.09	bdl	bdl	0.02	bdl
0.09	0.08	0.08	0.08	0.07	0.06
43.54	41.83	43.23	42.83	41.79	42.56
0.16	0.09	0.08	0.15	0.13	0.01
0.36	1.22	1.21	0.24	0.43	0.02
100.00	100.00	100.00	100.05	100.00	100.03
1.000	1.000	1.000	1.000	1.000	1.000
1.006	0.995	1.046	0.998	0.991	1.000
0.002	-	0.010	0.021	0.011	-
0.012	-	-	-	-	-
-	-	-	-	-	-
0.927	0.863	0.949	0.896	0.854	0.870
0.004	0.002	0.002	0.004	0.003	0.000
0.005	0.017	0.018	0.003	0.006	-

Q930239-3-6-20	Q930239-3-6-15	Q930239-2-1-1
Q930239	Q930239	Q930239
Assemblage 1	Assemblage 1	Assemblage 1
20.82	20.58	20.69
34.88	35.79	35.81
bdl	bdl	bdl
1.80	0.15	0.01
0.03	0.03	0.01
42.48	43.46	43.43
0.02	0.02	0.02
bdl	bdl	0.01
100.02	100.02	100.00
1.000	1.000	1.000
0.962	0.998	0.993
-	-	-
0.042	-	-
-	-	-
0.873	0.903	0.898
0.000	0.000	0.001
-	-	-

Appendix 8.4 Results of electron probe microanalyzer analysis of pyrrhotite

Spot_id	B232695-1-1-19	B264518-4-1-5	B264518-6-1-17	B264518-2-2-17	B264518-6-1-14
TS_id	B232695	B264518	B264518	B264518	B264518
Assemblage	Assemblage 1	Assemblage 3	Assemblage 3	Assemblage 3	Assemblage 3
S wt%	39.63	39.76	40.06	39.97	39.68
Fe wt%	60.16	59.72	59.63	59.76	60.05
Zn wt%	bdl	0.32	0.12	0.10	0.07
Pb wt%	0.11	0.13	0.11	0.08	0.11
Cu wt%	0.02	bdl	bdl	bdl	0.01
Co wt%	0.08	0.07	0.08	0.08	0.09
Total wt%	100.00	100.00	99.99	100.00	100.00
S_apfu	1.000	1.000	1.000	1.000	1.000
Fe_apfu	0.871	0.862	0.854	0.858	0.869
Zn_apfu	-	-	-	-	-
Pb_apfu	-	-	-	-	-
Cu_apfu	-	-	-	-	-
Co_apfu	0.001	0.001	0.001	0.001	0.001

Spot_id	Q721151-6-1-15	Q721151-3-1-17	Q721151-1-1-13	Q721151-2-1-12	Q721151-2-1-14
TS_id	Q721151	Q721151	Q721151	Q721151	Q721151
Assemblage	Assemblage 2	Assemblage 2	Assemblage 2	Assemblage 2	Assemblage 2
S wt%	39.91	39.65	39.73	39.89	39.67
Fe wt%	59.42	59.64	59.48	59.54	59.74
Zn wt%	0.12	0.08	0.05	bdl	bdl
Pb wt%	0.14	0.14	0.13	0.10	0.11
Cu wt%	bdl	0.02	0.18	0.07	0.04
Co wt%	0.41	0.47	0.43	0.40	0.43
Total wt%	100.00	99.99	100.00	100.00	99.99
S_apfu	1.000	1.000	1.000	1.000	1.000
Fe_apfu	0.855	0.864	0.859	0.857	0.865
Zn_apfu	-	-	-	-	-
Pb_apfu	0.001	0.001	0.001	-	-
Cu_apfu	-	-	0.002	0.001	-
Co_apfu	0.006	0.006	0.006	0.005	0.006

* notes analyses of spots with likely inclusions

B264518-9-1-11	B264518-3-2-4	B264518-9-1-17	B264518-6-1-5	B264518-1-1-17	B264518-9-1-6
B264518	B264518	B264518	B264518	B264518	B264518
Assemblage 3	Assemblage 3	Assemblage 3	Assemblage 3	Assemblage 3	Assemblage 3
39.82	39.86	39.68	39.76	40.05	39.58
59.93	59.80	60.26	60.02	59.61	60.19
0.05	bdl	bdl	bdl	bdl	bdl
0.11	0.12	0.02	0.12	0.24	0.14
bdl	0.13	0.04	0.02	bdl	bdl
0.09	0.08	bdl	0.08	0.09	0.09
100.00	99.99	100.00	100.00	99.98	100.00
1.000	1.000	1.000	1.000	1.000	1.000
0.864	0.861	0.872	0.867	0.854	0.873
-	-	-	-	-	-
-	-	-	-	0.001	0.001
-	0.002	-	-	-	-
0.001	0.001	-	0.001	0.001	0.001

Q721151-3-1-11	Q721151-3-1-19	Q721151-6-1-22	Q721151-2-1-15	Q721151-6-1-20	Q721151-6-1-21
Q721151	Q721151	Q721151	Q721151	Q721151	Q721151
Assemblage 2	Assemblage 2	Assemblage 2	Assemblage 2	Assemblage 2	Assemblage 2
39.75	39.91	40.16	39.67	40.22	39.95
59.66	59.51	59.40	59.73	58.76	59.60
bdl	bdl	bdl	bdl	bdl	bdl
0.13	0.11	0.05	0.14	0.62	0.06
0.03	0.02	0.02	0.01	bdl	bdl
0.41	0.44	0.38	0.45	0.37	0.39
99.98	99.99	100.00	100.00	99.97	99.99
1.000	1.000	1.000	1.000	1.000	1.000
0.862	0.856	0.849	0.864	0.839	0.857
-	-	-	-	-	-
-	-	-	0.001	0.002	-
-	-	-	-	-	-
0.006	0.006	0.005	0.006	0.005	0.005

B264518-9-1-9	B264518-7-1-13	B264518-1-1-12	B264518-2-1-9	B264518-7-1-6	B264518-2-2-15
B264518	B264518	B264518	B264518	B264518	B264518
Assemblage 3	Assemblage 3	Assemblage 3	Assemblage 3	Assemblage 3	Assemblage 3
39.66	39.82	39.94	39.73	39.78	39.67
60.13	59.97	59.86	60.06	60.05	60.15
bdl	bdl	bdl	bdl	bdl	bdl
0.11	0.11	0.10	0.10	0.09	0.09
bdl	bdl	bdl	bdl	bdl	bdl
0.10	0.09	0.08	0.09	0.08	0.09
100.00	99.99	99.98	99.98	100.00	100.00
1.000	1.000	1.000	1.000	1.000	1.000
0.870	0.865	0.860	0.868	0.867	0.871
-	-	-	-	-	-
-	-	-	-	-	-
-	-	-	-	-	-
0.001	0.001	0.001	0.001	0.001	0.001

Q721151-6-1-14	Q721151-6-1-18	Q721165-7-1-16	Q721165-7-1-1	Q930238-5-1-23	Q930238-1-1-15
Q721151	Q721151	Q721165	Q721165	Q930238	Q930238
Assemblage 2	Assemblage 2	Assemblage 3	Assemblage 3	Assemblage 2	Assemblage 2
39.67	39.70	39.68	39.63	39.85	40.06
59.77	59.72	60.10	60.15	58.72	59.57
bdl	0.01	bdl	bdl	0.61	0.08
0.12	0.10	0.11	0.12	0.69	0.18
bdl	0.02	0.02	0.01	bdl	0.01
0.44	0.42	0.08	0.09	0.09	0.09
100.00	99.97	99.99	100.00	99.97	100.00
1.000	1.000	1.000	1.000	1.000	1.000
0.865	0.864	0.870	0.871	0.846	0.854
-	-	-	-	0.008	-
-	-	-	-	0.003	0.001
-	-	-	-	-	-
0.006	0.006	0.001	0.001	0.001	0.001

B264518-4-1-7	B264518-2-1-8	B264518-9-1-18	B264518-1-1-4	B265159A-1-1-13	B265159A-4-1-5
B264518	B264518	B264518	B264518	B265159A	B265159A
Assemblage 3	Assemblage 3	Assemblage 3	Assemblage 3	Assemblage 2	Assemblage 2
39.62	39.96	39.67	39.74	39.91	39.75
60.18	59.86	60.08	60.03	59.66	59.91
bdl	bdl	bdl	bdl	0.17	0.09
0.11	0.10	0.10	0.12	0.15	0.13
bdl	bdl	0.04	0.01	0.01	0.01
0.09	0.08	0.09	0.09	0.10	0.09
100.00	100.00	99.99	100.00	100.00	99.98
1.000	1.000	1.000	1.000	1.000	1.000
0.872	0.860	0.869	0.867	0.858	0.865
-	-	-	-	-	-
-	-	-	-	0.001	-
-	-	-	-	-	-
0.001	0.001	0.001	0.001	0.001	0.001

Q930238-1-1-24	Q930238-4-2-11	Q930238-3-1-13	Q930238-3-2-13	Q930238-6-3	Q930238-2-1-4
Q930238	Q930238	Q930238	Q930238	Q930238	Q930238
Assemblage 2	Assemblage 2	Assemblage 2	Assemblage 2	Assemblage 2	Assemblage 2
39.87	39.78	39.75	39.90	39.91	39.91
59.77	59.97	59.85	59.82	59.86	59.87
0.06	bdl	bdl	bdl	bdl	bdl
0.13	0.14	0.30	0.15	0.13	0.12
0.04	0.02	0.01	bdl	bdl	bdl
0.10	0.09	0.09	0.10	0.10	0.09
99.98	100.00	100.00	99.97	100.00	99.99
1.000	1.000	1.000	1.000	1.000	1.000
0.861	0.865	0.864	0.861	0.861	0.861
-	-	-	-	-	-
0.001	0.001	0.001	0.001	-	-
-	-	-	-	-	-
0.001	0.001	0.001	0.001	0.001	0.001

B265159A-1-1-15	B265159A-4-1-1	B265159A-3-3-13	B265159A-1-1-5	B265159A-3-3-11	B265159A-4-1-12
B265159A	B265159A	B265159A	B265159A	B265159A	B265159A
Assemblage 2	Assemblage 2	Assemblage 2	Assemblage 2	Assemblage 2	Assemblage 2
39.58	39.99	39.89	39.79	39.72	39.69
59.55	59.76	59.81	59.94	60.08	60.04
bdl	bdl	bdl	bdl	bdl	0.02
0.20	0.13	0.17	0.13	0.11	0.15
0.56	0.04	0.02	0.02	bdl	0.01
0.09	0.09	0.09	0.10	0.09	0.09
99.98	100.00	99.99	99.97	100.00	100.00
1.000	1.000	1.000	1.000	1.000	1.000
0.864	0.858	0.861	0.865	0.868	0.868
-	-	-	-	-	-
0.001	0.001	0.001	0.001	-	0.001
0.007	-	-	-	-	-
0.001	0.001	0.001	0.001	0.001	0.001

Q930238-2-1-15	Q930238-1-3-17	Q930238-5-1-24	Q930238-1-3-23	Q930238-3-1-11	Q930238-5-1-19
Q930238	Q930238	Q930238	Q930238	Q930238	Q930238
Assemblage 2	Assemblage 2	Assemblage 2	Assemblage 2	Assemblage 2	Assemblage 2
39.85	39.69	40.25	39.79	39.93	39.62
59.75	60.10	59.41	59.90	59.80	59.97
bdl	bdl	bdl	bdl	0.02	0.01
0.28	0.11	0.24	0.22	0.11	0.32
0.01	0.01	bdl	bdl	0.04	bdl
0.09	0.09	0.10	0.08	0.09	0.09
99.98	99.99	100.00	99.99	100.00	100.00
1.000	1.000	1.000	1.000	1.000	1.000
0.861	0.869	0.847	0.864	0.860	0.869
-	-	-	-	-	-
0.001	-	0.001	0.001	-	0.001
-	-	-	-	-	-
0.001	0.001	0.001	0.001	0.001	0.001

B266575-2-1-13	B2665575-5-1-25	B266575-4-1-13	B266575-1-1-10	B266575-4-1-6	B291157-6-1-34
B266575	B266575	B266575	B266575	B266575	B291157
Assemblage 2	Assemblage 2	Assemblage 2	Assemblage 2	Assemblage 2	Assemblage 2
40.08	40.00	39.83	40.68	40.08	39.62
59.65	59.80	59.97	59.01	59.68	60.05
bdl	bdl	bdl	0.03	0.02	0.09
0.15	0.12	0.11	0.17	0.14	0.12
bdl	bdl	bdl	bdl	bdl	0.02
0.09	0.09	0.09	0.08	0.08	0.09
99.98	100.00	100.00	99.98	100.00	100.00
1.000	1.000	1.000	1.000	1.000	1.000
0.854	0.858	0.864	0.833	0.855	0.870
-	-	-	-	-	-
0.001	-	-	0.001	0.001	-
-	-	-	-	-	-
0.001	0.001	0.001	0.001	0.001	0.001

Q930238-3-2-10	Q930721-1-1-17	Q930721-6-1-20	Q930721-1-1-16*	Q930721-5-1-18	Q930721-7-1-4
Q930238	Q930271	Q930271	Q930271	Q930271	Q930271
Assemblage 2	Assemblage 3	Assemblage 3	Assemblage 3	Assemblage 3	Assemblage 3
40.12	39.83	39.80	47.69	39.53	39.98
59.61	59.28	59.54	51.72	59.81	59.76
0.01	0.46	0.33	0.29	bdl	bdl
0.14	0.14	0.15	0.15	0.29	0.10
bdl	0.17	0.04	0.02	0.24	0.04
0.11	0.12	0.13	0.11	0.12	0.12
99.99	100.00	99.99	99.98	99.99	100.00
1.000	1.000	1.000	1.000	1.000	1.000
0.853	0.854	0.859	0.623	0.869	0.858
-	0.006	-	-	-	-
0.001	0.001	0.001	0.000	0.001	-
-	0.002	-	-	0.003	-
0.001	0.002	0.002	0.001	0.002	0.002

B291157-4-1-14	B291157-5-1-6	B291157-5-1-17	B291157-4-1-5	B291157-4-1-1*
B291157	B291157	B291157	B291157	B291157
Assemblage 2	Assemblage 2	Assemblage 2	Assemblage 2	Assemblage 2
39.88	39.83	39.75	40.06	42.02
59.87	59.94	60.05	59.84	57.15
bdl	bdl	bdl	bdl	bdl
0.13	0.13	0.11	0.01	0.75
bdl	bdl	0.01	0.10	0.02
0.10	0.09	0.09	bdl	0.03
99.98	99.99	100.00	100.00	99.98
1.000	1.000	1.000	1.000	1.000
0.862	0.864	0.867	0.858	0.781
-	-	-	-	-
0.001	0.001	-	-	0.003
-	-	-	0.001	-
0.001	0.001	0.001	0.000	0.000

Q930721-6-1-17	Q930721-5-1-19	Q930721-7-1-6	Q930721-7-1-5
Q930271	Q930271	Q930271	Q930271
Assemblage 3	Assemblage 3	Assemblage 3	Assemblage 3
39.54	39.89	39.71	40.00
60.19	59.85	60.02	59.64
bdl	bdl	0.04	0.02
0.12	0.12	0.10	0.16
0.03	0.01	bdl	0.05
0.13	0.13	0.12	0.12
100.00	100.00	100.00	100.00
1.000	1.000	1.000	1.000
0.874	0.861	0.868	0.856
-	-	-	-
-	-	-	0.001
-	-	-	0.001
0.002	0.002	0.002	0.002

Appendix 8.5 Results of electron probe microanalyzer analysis of sphalerite

Spot_id	A348395-1-1-10	A348395-1-1-11	A348395-2-1-15	A348395-2-1-17	A348395-2-2-13
TS_id	A348395	A348395	A348395	A348395	A348395
Assemblage	Assemblage 1	Assemblage 1	Assemblage 1	Assemblage 1	Assemblage 1
S wt%	32.65	32.55	32.85	32.69	32.67
Fe wt%	2.51	2.48	2.99	2.24	2.50
Zn wt%	64.49	64.61	63.78	64.74	64.43
Cd wt%	0.36	0.34	0.38	0.33	0.38
Hg wt%	bdl	bdl	bdl	bdl	bdl
Total wt%	100.00	99.98	100.00	100.00	99.97
S_apfu	1.000	1.000	1.000	1.000	1.000
Fe_apfu	0.044	0.044	0.052	0.039	0.044
Zn_apfu	0.969	0.973	0.952	0.971	0.967
Cd_apfu	0.003	0.003	0.003	0.003	0.003
Hg_apfu	-	-	-	-	-

Spot_id	Q721151-3-1-10	Q930721-1-1-8	Q930721-5-1-12	Q930721-5-1-17	Q930721-5-1-3
TS_id	Q721151	Q930271	Q930271	Q930271	Q930271
Assemblage	Assemblage 2	Assemblage 3	Assemblage 3	Assemblage 3	Assemblage 3
S wt%	33.28	33.38	33.39	33.46	33.50
Fe wt%	10.39	9.86	10.46	9.98	10.17
Zn wt%	55.87	56.20	55.52	55.97	55.78
Cd wt%	0.46	0.45	0.46	0.45	0.45
Hg wt%	bdl	0.02	0.02	bdl	bdl
Total wt%	100.00	99.90	99.85	99.85	99.90
S_apfu	1.000	1.000	1.000	1.000	1.000
Fe_apfu	0.179	0.170	0.180	0.171	0.174
Zn_apfu	0.823	0.826	0.815	0.820	0.816
Cd_apfu	0.004	0.004	0.004	0.004	0.004
Hg_apfu	-	-	-	-	-

Spot_id	B291152-7-1-10	B291152-7-1-4	B291157-11-1-9	B291157-2-1-12	B291157-2-1-16
TS_id	B291152	B291152	B291157	B291157	B291157
Assemblage	Assemblage 1	Assemblage 1	Assemblage 2	Assemblage 2	Assemblage 2
S wt%	33.62	33.65	33.63	33.52	33.28
Fe wt%	10.14	10.77	9.01	8.26	8.66
Zn wt%	55.95	55.28	57.04	57.89	57.76
Cd wt%	0.29	0.30	0.33	0.32	0.30
Hg wt%	bdl	bdl	bdl	bdl	bdl
Total wt%	100.00	100.00	100.00	100.00	100.00
S_apfu	1.000	1.000	1.000	1.000	1.000
Fe_apfu	0.173	0.184	0.154	0.142	0.149
Zn_apfu	0.816	0.806	0.832	0.847	0.851
Cd_apfu	0.002	0.003	0.003	0.003	0.003
Hg_apfu	-	-	-	-	-

A348395-2-2-16	A348395-3-1-22	A348395-4-1-10	A348395-4-1-8	A348395-8-1-12	A348395-8-1-2
A348395	A348395	A348395	A348395	A348395	A348395
Assemblage 1	Assemblage 1	Assemblage 1	Assemblage 1	Assemblage 1	Assemblage 1
32.74	32.71	32.64	32.87	32.80	32.88
3.86	1.48	2.49	1.83	1.74	1.81
63.05	65.44	64.53	64.96	65.12	64.96
0.34	0.37	0.34	0.33	0.34	0.35
bdl	bdl	bdl	0.01	bdl	bdl
100.00	100.00	100.00	100.00	100.00	100.00
1.000	1.000	1.000	1.000	1.000	1.000
0.068	0.026	0.044	0.032	0.030	0.032
0.944	0.981	0.969	0.969	0.973	0.969
0.003	0.003	0.003	0.003	0.003	0.003
-	-	-	-	-	-

B264518-1-1-16	B264518-1-1-3	B264518-1-1-8	B264518-2-1-5	B264518-2-1-6	B264518-2-2-16
B264518	B264518	B264518	B264518	B264518	B264518
Assemblage 3	Assemblage 3	Assemblage 3	Assemblage 3	Assemblage 3	Assemblage 3
33.12	33.26	32.91	33.62	33.86	33.38
11.52	11.05	12.30	10.60	12.33	10.83
54.92	55.29	54.35	55.36	53.33	55.40
0.39	0.39	0.42	0.39	0.38	0.39
bdl	bdl	bdl	bdl	bdl	bdl
99.95	99.99	99.98	99.97	99.90	100.00
1.000	1.000	1.000	1.000	1.000	1.000
0.200	0.191	0.214	0.181	0.209	0.186
0.813	0.815	0.810	0.807	0.772	0.814
0.003	0.003	0.004	0.003	0.003	0.003
-	-	-	-	-	-

B291157-4-1-15	B291157-4-1-6	B291157-5-1-14	B291157-5-1-19	B291157-5-2-10	B291157-5-2-13
B291157	B291157	B291157	B291157	B291157	B291157
Assemblage 2	Assemblage 2	Assemblage 2	Assemblage 2	Assemblage 2	Assemblage 2
33.43	33.57	33.67	33.00	33.57	33.66
8.91	9.28	8.87	9.31	8.53	8.85
57.32	56.81	57.12	57.34	57.57	57.12
0.33	0.33	0.33	0.35	0.33	0.33
bdl	0.02	0.01	bdl	bdl	bdl
99.98	100.00	100.00	100.00	100.00	99.96
1.000	1.000	1.000	1.000	1.000	1.000
0.153	0.159	0.151	0.162	0.146	0.151
0.841	0.830	0.832	0.852	0.841	0.832
0.003	0.003	0.003	0.003	0.003	0.003
-	-	-	-	-	-

A348395-8-3-15	A348395-8-3-7	A348395-1-1-12	A348395-1-1-2	B233308-1-1-10	B233308-1-1-3
A348395	A348395	A348395	A348395	B233308	B233308
Assemblage 1	Assemblage 1	Assemblage 1	Assemblage 1	Assemblage 1	Assemblage 1
32.69	32.91	33.24	33.20	33.01	33.11
2.34	2.00	3.57	3.61	8.05	8.12
64.61	64.70	63.20	63.19	58.65	58.46
0.36	0.39	bdl	bdl	0.29	0.29
bdl	bdl	bdl	bdl	bdl	bdl
100.00	100.00	100.00	100.00	100.00	99.98
1.000	1.000	1.000	1.000	1.000	1.000
0.041	0.035	0.062	0.062	0.140	0.141
0.969	0.964	0.932	0.933	0.871	0.866
0.003	0.003	-	-	0.002	0.002
-	-	-	-	-	-

B264518-2-2-6	B264518-2-2-7	B264518-3-2-17	B264518-4-1-10	B264518-4-1-11	B264518-6-1-15
B264518	B264518	B264518	B264518	B264518	B264518
Assemblage 3	Assemblage 3	Assemblage 3	Assemblage 3	Assemblage 3	Assemblage 3
33.28	33.03	33.66	33.74	33.69	33.51
11.34	12.73	10.38	10.07	9.46	10.08
54.91	53.77	55.55	55.77	56.46	55.95
0.41	0.42	0.39	0.37	0.36	0.38
0.04	bdl	bdl	bdl	bdl	bdl
99.99	99.95	99.99	99.95	99.97	99.93
1.000	1.000	1.000	1.000	1.000	1.000
0.196	0.221	0.177	0.171	0.161	0.173
0.809	0.798	0.809	0.810	0.822	0.819
0.004	0.004	0.003	0.003	0.003	0.003
-	-	-	-	-	-

B291157-6-1-32	B291157-6-1-33	Q721165-1-1-10	Q721165-1-1-2	Q721165-4-1-8	Q721165-5-1-4
B291157	B291157	Q721165	Q721165	Q721165	Q721165
Assemblage 2	Assemblage 2	Assemblage 3	Assemblage 3	Assemblage 3	Assemblage 3
33.88	33.60	33.66	33.69	33.67	33.89
9.59	9.58	9.58	7.73	10.12	10.72
56.21	56.43	56.34	58.08	55.69	54.97
0.32	0.33	0.39	0.50	0.44	0.37
bdl	bdl	bdl	bdl	bdl	bdl
100.00	99.94	99.96	100.00	99.91	99.96
1.000	1.000	1.000	1.000	1.000	1.000
0.163	0.164	0.163	0.132	0.173	0.182
0.814	0.823	0.821	0.845	0.811	0.795
0.003	0.003	0.003	0.004	0.004	0.003
-	-	-	-	-	-

B233308-2-1-14	B233308-2-1-5	B233308-3-1-12	B233308-3-1-14	B233308-3-1-6	B233308-4-1-3	B233308-4-1-5
B233308	B233308	B233308	B233308	B233308	B233308	B233308
Assemblage 1	Assemblage 1	Assemblage 1	Assemblage 1	Assemblage 1	Assemblage 1	Assemblage 1
33.19	35.00	32.97	33.12	32.72	32.95	33.07
8.18	9.27	7.94	8.07	8.05	8.46	8.16
58.36	55.45	58.81	58.51	58.97	58.33	58.49
0.26	0.27	0.28	0.29	0.26	0.26	0.27
bdl	bdl	bdl	bdl	bdl	bdl	bdl
100.00	100.00	100.00	100.00	100.00	100.00	100.00
1.000	1.000	1.000	1.000	1.000	1.000	1.000
0.141	0.152	0.138	0.140	0.141	0.147	0.142
0.862	0.777	0.875	0.866	0.884	0.868	0.867
0.002	0.002	0.002	0.003	0.002	0.002	0.002
-	-	-	-	-	-	-

B264518-6-1-16	B232695-2-1-16	B232695-2-1-3	B232695-3-1-18	B232695-3-1-21	B232695-5-1-21	B232695-7-1-11
B264518	B232695	B232695	B232695	B232695	B232695	B232695
Assemblage 3	Assemblage 1	Assemblage 1	Assemblage 1	Assemblage 1	Assemblage 1	Assemblage 1
33.68	33.54	33.51	33.54	33.56	33.63	33.58
10.68	8.94	9.14	7.79	8.90	9.30	8.95
55.18	57.23	57.06	58.38	57.21	56.79	57.20
0.37	0.29	0.28	0.30	0.32	0.28	0.27
0.03	bdl	bdl	bdl	0.01	bdl	bdl
99.94	100.00	100.00	100.00	100.00	100.00	100.00
1.000	1.000	1.000	1.000	1.000	1.000	1.000
0.182	0.153	0.157	0.133	0.152	0.159	0.153
0.803	0.837	0.835	0.854	0.836	0.828	0.835
0.003	0.002	0.002	0.003	0.003	0.002	0.002
-	-	-	-	-	-	-

Q721165-5-1-5	Q721165-6-1-22	Q721165-6-1-26	Q721165-6-1-6	Q721165-7-1-5	Q721165-7-2-3	Q930238-3-2-1
Q721165	Q721165	Q721165	Q721165	Q721165	Q721165	Q930238
Assemblage 3	Assemblage 3	Assemblage 3	Assemblage 3	Assemblage 3	Assemblage 3	Assemblage 2
33.83	33.60	33.70	33.56	33.70	33.63	34.03
10.35	9.97	10.21	10.00	10.30	10.45	10.69
55.39	56.01	55.65	56.02	55.49	55.44	54.83
0.41	0.41	0.43	0.41	0.40	0.43	0.41
bdl	bdl	0.02	bdl	bdl	bdl	0.01
99.98	99.98	100.00	99.98	99.89	99.96	99.98
1.000	1.000	1.000	1.000	1.000	1.000	1.000
0.176	0.170	0.174	0.171	0.175	0.178	0.180
0.803	0.818	0.810	0.818	0.807	0.808	0.790
0.003	0.003	0.004	0.003	0.003	0.004	0.003
-	-	-	-	-	-	-

B233308-4-1-9	B233308-5-1-14	B233308-5-1-2	B233308-5-1-5	B233308-7-1-12	B233308-7-1-5
B233308	B233308	B233308	B233308	B233308	B233308
Assemblage 1	Assemblage 1	Assemblage 1	Assemblage 1	Assemblage 1	Assemblage 1
33.33	33.22	33.23	33.06	33.18	33.02
8.18	8.91	8.92	8.92	8.28	8.16
58.21	57.56	57.60	57.67	58.24	58.54
0.28	0.29	0.25	0.31	0.28	0.27
bdl	0.01	bdl	0.04	0.01	bdl
99.99	100.00	100.00	100.00	100.00	100.00
1.000	1.000	1.000	1.000	1.000	1.000
0.141	0.154	0.154	0.155	0.143	0.142
0.857	0.850	0.850	0.855	0.861	0.869
0.002	0.003	0.002	0.003	0.002	0.002
-	-	-	-	-	-

B232695-7-1-8	B232695-8-1-14	B232695-9-1-14	B232695-9-1-6	B232695-9-1-9	B266543-2-1-12
B232695	B232695	B232695	B232695	B232695	B266543
Assemblage 1	Assemblage 1	Assemblage 1	Assemblage 1	Assemblage 1	Assemblage 1
33.49	33.46	33.40	33.74	33.30	33.19
8.95	8.66	7.32	8.20	7.71	2.50
57.25	57.61	59.00	57.71	58.69	63.75
0.28	0.28	0.29	0.30	0.30	0.56
0.03	bdl	bdl	bdl	bdl	0.01
100.00	100.00	100.00	99.96	100.00	100.00
1.000	1.000	1.000	1.000	1.000	1.000
0.153	0.149	0.126	0.139	0.133	0.043
0.838	0.844	0.866	0.839	0.864	0.942
0.002	0.002	0.002	0.003	0.003	0.005
-	-	-	-	-	-

Q930238-4-1-18	Q930238-4-1-8	Q930238-4-2-12	Q930238-6-2	Q930238-6-4	Q930239-1-1-12
Q930238	Q930238	Q930238	Q930238	Q930238	Q930239
Assemblage 2	Assemblage 2	Assemblage 2	Assemblage 2	Assemblage 2	Assemblage 1
33.83	34.01	34.14	33.72	33.67	33.27
10.47	9.89	10.23	9.53	9.62	4.35
55.29	55.71	55.16	56.32	56.28	61.79
0.41	0.39	0.47	0.42	0.40	0.39
bdl	bdl	bdl	0.01	bdl	0.20
100.00	100.00	100.00	100.00	99.98	100.00
1.000	1.000	1.000	1.000	1.000	1.000
0.178	0.167	0.172	0.162	0.164	0.075
0.801	0.803	0.792	0.819	0.820	0.911
0.003	0.003	0.004	0.004	0.003	0.003
-	-	-	-	-	0.001

B265159A-1-1-14	B265159A-1-1-16	B265159A-1-1-7	B265159A-3-2-12	B265159A-4-1-3	B265159A-4-1-7
B265159A	B265159A	B265159A	B265159A	B265159A	B265159A
Assemblage 2	Assemblage 2	Assemblage 2	Assemblage 2	Assemblage 2	Assemblage 2
33.20	32.55	33.41	33.61	33.17	33.03
8.95	9.25	9.64	9.28	8.55	10.42
57.50	57.86	56.63	56.80	57.93	56.20
0.31	0.32	0.33	0.31	0.32	0.31
0.03	0.02	bdl	bdl	0.03	0.04
100.00	100.00	100.00	100.00	100.00	100.00
1.000	1.000	1.000	1.000	1.000	1.000
0.155	0.163	0.166	0.158	0.148	0.181
0.849	0.872	0.831	0.829	0.856	0.834
0.003	0.003	0.003	0.003	0.003	0.003
-	-	-	-	-	-

B266543-2-1-2	B266543-2-1-4	B266543-3-1-2	B266543-3-2-15	B266543-3-2-9	B266543-6-1-7
B266543	B266543	B266543	B266543	B266543	B266543
Assemblage 1	Assemblage 1	Assemblage 1	Assemblage 1	Assemblage 1	Assemblage 1
32.88	33.24	33.07	33.21	33.17	33.51
2.82	2.49	2.66	2.06	2.01	2.89
63.73	63.68	63.70	64.18	64.25	63.03
0.55	0.57	0.58	0.55	0.57	0.54
0.02	bdl	bdl	bdl	bdl	0.02
100.00	99.98	100.00	100.00	100.00	100.00
1.000	1.000	1.000	1.000	1.000	1.000
0.049	0.043	0.046	0.036	0.035	0.049
0.951	0.939	0.945	0.948	0.950	0.922
0.005	0.005	0.005	0.005	0.005	0.005
-	-	-	-	-	-

Q930239-1-1-3	Q930239-1-2-10	Q930239-1-2-11	Q930239-2-1-12	Q930239-2-1-8	Q930239-3-1-6
Q930239	Q930239	Q930239	Q930239	Q930239	Q930239
Assemblage 1	Assemblage 1	Assemblage 1	Assemblage 1	Assemblage 1	Assemblage 1
33.18	33.10	33.09	34.20	33.19	33.29
4.26	4.63	4.95	5.98	4.21	3.61
61.96	61.68	61.33	59.28	61.94	62.49
0.42	0.41	0.44	0.42	0.42	0.43
0.17	0.18	0.19	0.13	0.24	0.17
100.00	100.00	100.00	100.00	100.00	100.00
1.000	1.000	1.000	1.000	1.000	1.000
0.074	0.080	0.086	0.100	0.073	0.062
0.916	0.914	0.909	0.850	0.915	0.920
0.004	0.004	0.004	0.003	0.004	0.004
-	-	-	-	0.001	-

B266585-1-1-3	B266585-2-1-13	B266585-2-1-14	B266585-2-1-5	B266585-6-1-10	B266585-6-1-11
B266585	B266585	B266585	B266585	B266585	B266585
Assemblage 1	Assemblage 1	Assemblage 1	Assemblage 1	Assemblage 1	Assemblage 1
32.93	32.98	32.90	32.96	32.67	32.86
3.61	3.74	4.20	3.95	4.14	3.80
62.92	62.75	62.34	62.58	62.74	62.88
0.39	0.40	0.37	0.39	0.33	0.32
0.15	0.13	0.18	0.13	0.11	0.15
100.00	100.00	99.99	100.00	100.00	100.00
1.000	1.000	1.000	1.000	1.000	1.000
0.063	0.065	0.073	0.069	0.073	0.066
0.937	0.933	0.929	0.931	0.942	0.938
0.003	0.003	0.003	0.003	0.003	0.003
-	-	-	-	-	-

B266543-6-1-9	B266575-10-14	B266575-10-8	B266575-2-1-10	B266575-2-1-8	B266575-4-1-7
B266543	B266575	B266575	B266575	B266575	B266575
Assemblage 1	Assemblage 2	Assemblage 2	Assemblage 2	Assemblage 2	Assemblage 2
33.55	33.39	33.73	33.87	33.65	33.61
3.50	10.29	10.26	10.80	10.09	10.67
62.40	55.93	55.61	54.95	55.86	55.30
0.55	0.40	0.40	0.39	0.40	0.41
bdl	bdl	bdl	bdl	bdl	0.01
100.00	100.00	100.00	100.00	99.99	100.00
1.000	1.000	1.000	1.000	1.000	1.000
0.060	0.177	0.175	0.183	0.172	0.182
0.912	0.821	0.809	0.796	0.814	0.807
0.005	0.003	0.003	0.003	0.003	0.004
-	-	-	-	-	-

Q930239-3-2-9	Q930239-3-4-13	Q930239-3-4-4	Q930239-6-1-8	Q930239-9-1-17	Q930239-9-1-2
Q930239	Q930239	Q930239	Q930239	Q930239	Q930239
Assemblage 1	Assemblage 1	Assemblage 1	Assemblage 1	Assemblage 1	Assemblage 1
33.34	33.49	33.21	33.00	37.11	33.09
3.87	3.90	3.97	3.60	8.98	3.54
62.20	61.95	62.24	62.78	53.37	62.84
0.44	0.45	0.41	0.45	0.39	0.40
0.15	0.21	0.17	0.18	0.16	0.13
100.00	99.99	100.00	100.00	100.00	100.00
1.000	1.000	1.000	1.000	1.000	1.000
0.067	0.067	0.069	0.063	0.139	0.061
0.915	0.907	0.919	0.933	0.705	0.931
0.004	0.004	0.004	0.004	0.003	0.003
-	0.001	-	-	-	-

B266585-7-1-14	B266585-7-1-20	B266585-8-1-23	B266585-8-1-24	B266585-8-3-19	B264518-7-1-5
B266585	B266585	B266585	B266585	B266585	B264518
Assemblage 1	Assemblage 1	Assemblage 1	Assemblage 1	Assemblage 1	Assemblage 3
32.95	32.82	32.98	33.13	33.14	33.69
3.32	3.21	3.76	3.71	3.41	11.42
63.16	63.45	62.75	62.62	62.85	54.89
0.36	0.36	0.35	0.38	0.38	bdl
0.15	0.15	0.17	0.16	0.18	bdl
99.94	100.00	100.00	100.00	99.96	100.00
1.000	1.000	1.000	1.000	1.000	1.000
0.058	0.056	0.065	0.064	0.059	0.195
0.940	0.948	0.933	0.927	0.930	0.799
0.003	0.003	0.003	0.003	0.003	-
-	-	-	-	-	-

B266575-5-1-11	B291152-1-1-6	B291152-3-1-10	B291152-3-1-8	B291152-4-1-12	B291152-6-1-14
B266575	B291152	B291152	B291152	B291152	B291152
Assemblage 2	Assemblage 1	Assemblage 1	Assemblage 1	Assemblage 1	Assemblage 1
33.60	33.64	33.77	33.91	33.67	33.68
11.00	7.28	9.83	9.90	10.00	10.08
55.00	58.79	56.15	55.89	56.05	55.90
0.40	0.28	0.26	0.30	0.28	0.31
bdl	bdl	bdl	bdl	bdl	0.03
100.00	100.00	100.00	100.00	100.00	100.00
1.000	1.000	1.000	1.000	1.000	1.000
0.188	0.124	0.167	0.168	0.170	0.172
0.803	0.857	0.815	0.808	0.816	0.814
0.003	0.002	0.002	0.003	0.002	0.003
-	-	-	-	-	-

Q930239-9-1-5
Q930239
Assemblage 1
34.05
7.42
57.97
0.39
0.15
99.98
1.000
0.125
0.835
0.003
-

Appendix 8.6 Results of electron probe microanalyzer analysis of chalcopyrite

Spot_id	A348395-3-1-23	A348395-4-1-13	A348395-3-1-27	A348395-8-1-18	A348395-2-1-16
TS_id	A348395	A348395	A348395	A348395	A348395
Assemblage	Assemblage 1	Assemblage 1	Assemblage 1	Assemblage 1	Assemblage 1
S wt%	34.59	35.05	34.52	34.83	34.65
Fe wt%	31.03	30.48	31.07	30.89	30.86
Cu wt%	34.23	34.27	34.25	34.09	34.27
Zn wt%	bdl	bdl	bdl	0.03	0.07
Pb wt%	0.06	0.06	0.03	0.03	0.02
Ag wt%	bdl	0.01	bdl	0.02	0.01
Bi wt%	0.09	0.11	0.13	0.12	0.12
Total wt%	100.00	99.98	100.00	100.00	100.00
S_apfu	2.000	2.000	2.000	2.000	2.000
Fe_apfu	1.030	0.998	1.033	1.018	1.023
Cu_apfu	0.999	0.987	1.001	0.987	0.998
Zn_apfu	-	-	-	-	-
Pb_apfu	0.001	0.001	-	-	-
Ag_apfu	-	-	-	-	-
Bi_apfu	-	-	0.001	0.001	-

Spot_id	B291152-1-1-4	B291152-4-1-15	B291152-4-2-22	B291152-6-1-13	B291152-4-2-24
TS_id	B291152	B291152	B291152	B291152	B291152
Assemblage	Assemblage 1	Assemblage 1	Assemblage 1	Assemblage 1	Assemblage 1
S wt%	35.35	34.94	34.95	34.77	35.15
Fe wt%	31.06	31.25	30.87	30.88	30.76
Cu wt%	33.43	33.69	34.01	34.14	33.95
Zn wt%	0.01	bdl	0.02	bdl	bdl
Pb wt%	0.02	0.01	0.01	bdl	bdl
Ag wt%	0.03	0.03	0.02	0.03	0.03
Bi wt%	0.11	0.08	0.12	0.14	0.11
Total wt%	100.00	100.00	100.00	99.96	100.00
S_apfu	2.000	2.000	2.000	2.000	2.000
Fe_apfu	1.009	1.027	1.014	1.020	1.005
Cu_apfu	0.954	0.973	0.982	0.991	0.975
Zn_apfu	-	-	-	-	-
Pb_apfu	-	-	-	-	-
Ag_apfu	-	-	-	-	-
Bi_apfu	-	-	-	0.001	-

* notes analyses of spots with likely inclusions

A348395-8-1-22	A348395-4-1-6	A348395-2-1-14	A348395-4-2-7	B232695-5-1-8*	B232695-5-1-20
A348395	A348395	A348395	A348395	B232695	B232695
Assemblage 1	Assemblage 1	Assemblage 1	Assemblage 1	Assemblage 1	Assemblage 1
34.87	35.11	34.86	34.91	35.47	34.98
30.65	30.62	30.56	30.50	36.97	31.05
34.18	34.13	34.03	34.44	26.92	33.53
0.14	bdl	0.41	bdl	0.02	0.24
0.01	bdl	bdl	bdl	0.44	0.05
0.03	0.01	bdl	0.02	0.05	0.03
0.11	0.12	0.13	0.13	0.13	0.12
100.00	100.00	100.00	100.00	100.00	100.00
2.000	2.000	2.000	2.000	2.000	2.000
1.009	1.001	1.007	1.003	1.197	1.019
0.989	0.981	0.985	0.995	0.766	0.967
-	-	0.012	-	-	-
-	-	-	-	0.004	0.000
-	-	-	-	-	-
-	0.001	0.001	0.001	0.001	0.001

B291157-11-1-1	B291157-11-1-8	B291157-6-1-35	B291157-4-1-16	Q721151-1-1-4	Q721151-6-2-17
B291157	B291157	B291157	B291157	Q721151	Q721151
Assemblage 2	Assemblage 2	Assemblage 2	Assemblage 2	Assemblage 2	Assemblage 2
35.16	35.48	35.03	34.98	34.59	36.42
30.63	30.27	30.64	30.78	31.12	32.53
34.12	34.20	33.95	34.19	33.16	30.80
bdl	bdl	0.31	0.02	bdl	bdl
0.04	0.02	0.02	bdl	0.40	0.11
0.05	0.04	0.03	0.02	0.05	0.02
0.01	bdl	0.02	bdl	0.68	0.12
100.00	100.00	100.00	100.00	100.00	100.00
2.000	2.000	2.000	2.000	2.000	2.000
1.000	0.979	1.004	1.010	1.033	1.026
0.979	0.973	0.978	0.986	0.967	0.853
-	-	-	-	-	-
-	-	-	-	0.004	0.001
-	-	-	-	-	-
-	-	-	-	0.006	0.001

B232695-1-1-17	B232695-8-1-8	B232695-7-1-10	B232695-1-1-11	B232695-7-1-9	B232695-8-1-15
B232695	B232695	B232695	B232695	B232695	B232695
Assemblage 1	Assemblage 1	Assemblage 1	Assemblage 1	Assemblage 1	Assemblage 1
34.81	34.84	34.94	34.78	34.95	34.70
30.93	30.99	30.93	30.83	30.86	30.74
33.94	33.93	33.98	34.13	33.67	33.67
0.11	0.07	bdl	bdl	0.36	0.75
0.04	0.01	0.01	0.16	bdl	bdl
0.04	0.05	0.02	0.02	0.02	0.04
0.14	0.10	0.12	0.09	0.13	0.11
100.00	100.00	100.00	100.00	100.00	100.00
2.000	2.000	2.000	2.000	2.000	2.000
1.020	1.021	1.016	1.018	1.014	1.017
0.984	0.983	0.981	0.990	0.972	0.979
-	-	-	-	0.010	0.021
-	-	-	0.001	-	-
-	-	-	-	-	-
0.001	-	-	-	0.001	-

Q721151-3-1-22	Q721151-2-1-11	Q721151-1-1-8	Q721151-6-1-16	Q721151-6-1-17	Q721151-2-1-13
Q721151	Q721151	Q721151	Q721151	Q721151	Q721151
Assemblage 2	Assemblage 2	Assemblage 2	Assemblage 2	Assemblage 2	Assemblage 2
34.81	34.62	35.05	34.85	35.02	34.51
32.09	31.00	30.71	30.83	31.15	31.24
32.78	34.19	34.00	34.11	33.67	34.07
bdl	bdl	0.03	bdl	bdl	0.03
0.04	0.04	0.03	0.04	0.03	0.02
0.04	0.02	0.02	0.03	0.01	0.03
0.25	0.13	0.15	0.15	0.12	0.08
100.00	100.00	99.99	100.00	100.00	100.00
2.000	2.000	2.000	2.000	2.000	2.000
1.059	1.028	1.006	1.015	1.021	1.039
0.950	0.996	0.979	0.988	0.970	0.996
-	-	-	-	-	-
-	-	-	-	-	-
-	-	-	-	-	-
0.002	0.001	0.001	0.001	-	-

B232695-1-1-18	B264518-2-1-4	B264518-3-2-18	B264518-2-1-17	B264518-6-1-4	B264518-9-1-4	B264518-3-2-3
B232695	B264518	B264518	B264518	B264518	B264518	B264518
Assemblage 1	Assemblage 3	Assemblage 3	Assemblage 3	Assemblage 3	Assemblage 3	Assemblage 3
34.73	34.89	34.82	35.01	34.94	34.65	35.00
31.11	30.97	30.86	30.59	31.02	31.69	30.81
33.99	34.01	34.19	34.09	33.97	33.59	34.04
bdl	0.05	0.04	0.20	bdl	bdl	0.09
bdl	0.03	0.02	0.02	0.01	0.01	bdl
0.03	0.04	0.05	0.05	0.05	0.04	0.05
0.14	bdl	0.02	0.04	0.01	0.03	0.02
100.00	100.00	100.00	100.00	100.00	100.00	100.00
2.000	2.000	2.000	2.000	2.000	2.000	2.000
1.028	1.019	1.018	1.003	1.019	1.050	1.011
0.988	0.984	0.991	0.983	0.981	0.978	0.981
-	-	-	-	-	-	-
-	-	-	-	-	-	-
-	-	-	-	-	-	-
0.001	-	-	-	-	-	-

Q721151-6-2-14	Q721151-6-2-2	Q721151-6-2-16	Q721151-3-1-18	Q721165-6-1-10	Q721165-7-1-4	Q721165-7-1-11
Q721151	Q721151	Q721151	Q721151	Q721165	Q721165	Q721165
Assemblage 2	Assemblage 2	Assemblage 2	Assemblage 2	Assemblage 3	Assemblage 3	Assemblage 3
34.75	34.84	34.65	34.77	34.94	34.93	35.05
30.72	30.95	30.94	30.89	30.51	30.39	31.36
34.34	34.05	34.22	34.11	33.78	33.79	33.40
0.04	bdl	bdl	0.09	0.61	0.73	0.04
0.02	0.02	0.01	0.01	0.04	0.04	0.04
0.03	0.02	0.03	0.03	0.06	0.12	0.11
0.10	0.12	0.15	0.11	0.02	bdl	bdl
100.00	100.00	100.00	100.00	99.96	100.00	100.00
2.000	2.000	2.000	2.000	2.000	2.000	2.000
1.015	1.020	1.025	1.020	1.003	0.999	1.027
0.997	0.986	0.996	0.990	0.976	0.976	0.962
-	-	-	-	0.017	0.021	-
-	-	-	-	0.000	-	-
-	-	-	-	0.001	0.002	0.002
-	0.001	0.001	-	-	-	-

B264518-2-1-15	B265159A-1-1-11	B265159A-9-1-15*	B265159A-9-1-2*	B265159A-4-1-2	B265159A-3-2-27
B264518	B265159A	B265159A	B265159A	B265159A	B265159A
Assemblage 3	Assemblage 2	Assemblage 2	Assemblage 2	Assemblage 2	Assemblage 2
34.75	35.06	39.37	39.09	34.80	35.15
31.53	30.73	33.62	33.47	30.80	30.59
33.64	33.93	26.77	26.88	33.93	33.86
0.01	bdl	bdl	0.34	0.21	0.11
bdl	0.05	0.03	0.03	0.03	bdl
0.07	0.09	0.07	0.06	0.12	0.12
bdl	0.15	0.14	0.13	0.10	0.13
100.00	100.00	100.00	100.00	100.00	99.97
2.000	2.000	2.000	2.000	2.000	2.000
1.041	1.006	0.981	0.983	1.016	0.999
0.977	0.976	0.686	0.694	0.984	0.972
-	-	-	0.009	-	-
-	0.000	-	-	-	-
0.001	0.001	0.001	0.001	0.002	0.002
-	0.001	0.001	0.001	-	0.001

Q721165-4-1-11	Q721165-4-1-7	Q721165-6-1-15	Q721165-7-2-6	Q721165-7-1-6	Q721165-7-2-22
Q721165	Q721165	Q721165	Q721165	Q721165	Q721165
Assemblage 3	Assemblage 3	Assemblage 3	Assemblage 3	Assemblage 3	Assemblage 3
35.00	35.17	34.98	35.03	35.22	34.97
30.92	30.59	30.85	30.93	30.80	30.64
33.86	34.02	34.02	33.88	33.87	34.26
bdl	0.07	0.09	bdl	bdl	bdl
0.03	0.02	0.01	0.01	bdl	bdl
0.15	0.14	0.06	0.14	0.11	0.12
0.03	bdl	bdl	bdl	bdl	bdl
100.00	100.00	100.00	100.00	100.00	100.00
2.000	2.000	2.000	2.000	2.000	2.000
1.014	0.998	1.013	1.014	1.004	1.006
0.976	0.976	0.981	0.976	0.970	0.989
-	-	-	-	-	-
-	-	-	-	-	-
0.003	0.002	0.001	0.002	0.002	0.002
-	-	-	-	-	-

B265159A-3-2-11	B265159A-1-1-6	B265159A-4-1-9	B266543-5-1-12	B266543-3-2-6	B266543-6-1-14
B265159A	B265159A	B265159A	B266543	B266543	B266543
Assemblage 2	Assemblage 2	Assemblage 2	Assemblage 1	Assemblage 1	Assemblage 1
35.22	34.97	34.92	/	34.88	35.17
30.42	30.85	30.86	30.31	30.55	29.76
33.79	34.00	33.90	34.06	34.38	34.82
0.34	bdl	0.09	0.22	0.02	0.06
bdl	bdl	bdl	0.06	0.04	0.04
0.11	0.08	0.10	0.01	0.02	0.02
0.12	0.11	0.14	0.12	0.11	0.13
100.00	100.00	100.00	100.00	100.00	99.99
2.000	2.000	2.000	2.000	2.000	2.000
0.992	1.013	1.015	0.988	1.006	0.972
0.968	0.981	0.979	0.976	0.995	0.999
0.009	-	-	-	-	-
-	-	-	0.001	-	-
0.002	0.001	0.002	-	-	-
0.001	-	0.001	0.001	-	0.001

Q721165-6-1-23	Q930238-4-2-9	Q930238-5-1-20	Q930238-4-1-17	Q930238-4-2-14	Q930238-4-1-7
Q721165	Q930238	Q930238	Q930238	Q930238	Q930238
Assemblage 3	Assemblage 2	Assemblage 2	Assemblage 2	Assemblage 2	Assemblage 2
34.86	35.02	35.06	35.15	35.11	35.00
30.91	30.83	30.74	30.40	30.96	30.86
34.15	34.03	34.03	33.90	33.76	34.03
bdl	bdl	bdl	0.47	0.10	0.04
bdl	0.05	0.03	0.02	0.02	0.02
0.08	0.06	0.14	0.05	0.05	0.06
bdl	0.02	bdl	0.02	bdl	bdl
100.00	100.00	100.00	100.00	100.00	100.00
2.000	2.000	2.000	2.000	2.000	2.000
1.018	1.011	1.007	0.993	1.012	1.012
0.988	0.981	0.979	0.973	0.970	0.981
-	-	-	0.013	-	-
-	0.000	-	-	-	-
0.001	0.001	0.002	-	-	-
-	-	-	-	-	-

B266543-2-1-13	B266543-3-2-14	B266543-1-2-5*	B266543-1-2-12	B266543-6-1-13	B266575-2-1-3
B266543	B266543	B266543	B266543	B266543	B266575
Assemblage 1	Assemblage 1	Assemblage 1	Assemblage 1	Assemblage 1	Assemblage 2
34.85	34.99	37.04	35.10	35.65	35.19
30.78	30.35	29.54	29.87	29.97	31.02
34.24	34.50	33.22	34.83	34.28	33.61
bdl	bdl	0.05	0.01	bdl	0.12
0.02	0.01	0.01	bdl	bdl	0.03
0.01	0.01	0.01	0.07	0.01	0.02
0.10	0.13	0.15	0.11	0.09	0.01
100.00	99.99	100.00	100.00	100.00	100.00
2.000	2.000	2.000	2.000	2.000	2.000
1.014	0.996	0.916	0.977	0.965	1.012
0.991	0.995	0.905	1.001	0.970	0.964
-	-	-	-	-	-
-	-	-	-	-	-
-	-	-	0.001	-	-
-	0.001	0.001	-	-	-

Q930238-3-2-9	Q930238-2-2-8	Q930238-6-1	Q930238-3-1-16	Q930238-6-7	Q930238-2-2-9
Q930238	Q930238	Q930238	Q930238	Q930238	Q930238
Assemblage 2	Assemblage 2	Assemblage 2	Assemblage 2	Assemblage 2	Assemblage 2
35.06	35.32	35.17	35.28	35.11	35.24
31.02	30.90	30.96	30.80	30.83	30.87
33.85	33.66	33.81	33.86	33.35	33.78
bdl	bdl	bdl	bdl	0.63	bdl
0.01	bdl	bdl	bdl	bdl	bdl
0.06	0.08	0.05	0.06	0.06	0.09
bdl	0.02	bdl	bdl	bdl	0.02
100.00	99.98	100.00	100.00	99.99	100.00
2.000	2.000	2.000	2.000	2.000	2.000
1.016	1.004	1.011	1.002	1.008	1.006
0.974	0.961	0.970	0.969	0.958	0.967
-	-	-	-	0.018	-
-	-	-	-	-	-
0.001	0.001	-	0.001	0.001	0.002
-	-	-	-	-	-

B266575-2-2-2	B266575-5-1-15	B266575-5-1-10	B266575-2-1-11	B266575-5-1-10	B266575-4-1-8
B266575	B266575	B266575	B266575	B266575	B266575
Assemblage 2	Assemblage 2	Assemblage 2	Assemblage 2	Assemblage 2	Assemblage 2
35.02	35.12	34.95	35.25	35.14	35.17
31.03	30.76	30.83	30.65	30.68	30.96
33.88	33.67	34.12	34.06	33.81	33.83
bdl	0.41	0.06	bdl	0.33	bdl
0.03	0.02	0.01	0.01	bdl	bdl
0.03	0.02	0.04	0.01	0.03	0.01
0.02	bdl	bdl	0.01	0.01	0.02
100.00	100.00	100.00	100.00	100.00	99.98
2.000	2.000	2.000	2.000	2.000	2.000
1.017	1.006	1.013	0.998	1.003	1.011
0.976	0.968	0.985	0.975	0.971	0.971
-	0.011	-	-	-	-
-	-	-	-	-	-
-	-	-	-	-	-
-	-	-	-	-	-

Q930239-3-1-12	Q930239-6-1-18	Q930239-3-2-3	Q930239-6-1-6	Q930271-7-1-3	Q930271-6-1-18
Q930239	Q930239	Q930239	Q930239	Q930271	Q930271
Assemblage 1	Assemblage 1	Assemblage 1	Assemblage 1	Assemblage 3	Assemblage 3
35.15	34.99	34.91	34.91	34.90	35.05
30.44	30.70	30.66	30.96	30.79	30.67
34.34	34.27	34.38	34.05	34.01	34.07
bdl	bdl	bdl	0.07	bdl	0.01
0.05	0.03	0.03	bdl	0.05	0.03
0.01	0.01	bdl	0.02	0.08	0.08
0.01	bdl	0.01	bdl	0.16	0.09
100.00	100.00	100.00	100.00	100.00	100.00
2.000	2.000	2.000	2.000	2.000	2.000
0.994	1.008	1.008	1.018	1.013	1.005
0.986	0.988	0.994	0.984	0.983	0.981
-	-	-	-	-	-
0.000	-	-	-	0.000	-
-	-	-	-	0.001	0.001
-	-	-	-	0.001	-

B266575-5-1-9	B291152-6-1-17	B291152-3-1-5	B291152-2-1-9	B291152-2-1-12	B291152-7-1-11
B266575	B291152	B291152	B291152	B291152	B291152
Assemblage 2	Assemblage 1	Assemblage 1	Assemblage 1	Assemblage 1	Assemblage 1
34.79	34.94	34.95	35.56	34.96	35.08
31.04	30.74	30.71	30.18	30.77	30.87
34.04	34.09	34.17	33.97	34.10	33.84
0.11	0.02	bdl	0.12	bdl	0.02
bdl	0.05	0.04	0.03	0.04	0.03
0.01	0.03	0.01	0.04	0.06	0.04
bdl	0.13	0.12	0.09	0.06	0.12
100.00	100.00	100.00	100.00	100.00	100.00
2.000	2.000	2.000	2.000	2.000	2.000
1.024	1.010	1.009	0.974	1.011	1.010
0.987	0.985	0.987	0.964	0.984	0.973
-	-	-	-	-	-
-	0.000	-	-	-	-
-	-	-	-	0.001	-
-	0.001	-	-	-	0.001

Q930271-7-1-9	Q930271-5-1-16	Q930271-1-1-2	Q930271-5-1-20	Q930271-1-1-7	Q930271-6-1-16
Q930271	Q930271	Q930271	Q930271	Q930271	Q930271
Assemblage 3	Assemblage 3	Assemblage 3	Assemblage 3	Assemblage 3	Assemblage 3
34.90	34.91	34.84	34.93	35.02	34.75
30.71	30.78	30.88	30.76	30.85	30.90
34.18	34.11	34.04	34.08	33.92	34.16
bdl	bdl	bdl	0.02	bdl	bdl
0.02	0.02	0.01	0.01	bdl	bdl
0.06	0.08	0.09	0.06	0.07	0.06
0.13	0.10	0.13	0.13	0.13	0.12
100.00	100.00	100.00	100.00	100.00	100.00
2.000	2.000	2.000	2.000	2.000	2.000
1.010	1.012	1.018	1.011	1.012	1.021
0.988	0.986	0.986	0.984	0.977	0.992
-	-	-	-	-	-
-	-	-	-	-	-
0.001	0.001	0.002	0.001	0.001	0.001
0.001	-	0.001	0.001	0.001	0.001

B291152-1-1-17	B291152-7-1-12
B291152	B291152
Assemblage 1	Assemblage 1
34.95	35.03
30.61	30.80
34.25	33.95
0.03	0.07
0.02	0.02
0.01	0.04
0.10	0.10
99.97	100.00
2.000	2.000
1.006	1.009
0.989	0.978
-	-
-	-
-	-
-	-

Q930271-1-1-15	Q930271-6-1-2
Q930271	Q930271
Assemblage 3	Assemblage 3
35.11	34.98
30.74	30.92
33.97	33.93
bdl	0.01
bdl	bdl
0.06	0.05
0.12	0.10
100.00	100.00
2.000	2.000
1.005	1.015
0.976	0.979
-	-
-	-
0.001	-
-	-

Appendix 8.7 Results of electron probe microanalyzer analysis of galena

Spot_id	A348395-1-1-1	A348395-2-1-18	A348395-2-1-8	A348395-2-2-11	A348395-2-2-15	A348395-3-1-15
TS_id	A348395	A348395	A348395	A348395	A348395	A348395
Assemblage 1	Assemblage 1	Assemblage 1	Assemblage 1	Assemblage 1	Assemblage 1	Assemblage 1
S wt%	13.48	13.47	13.35	13.51	13.43	13.40
Fe wt%	0.08	1.00	0.31	0.07	0.09	0.07
Zn wt%	bdl	bdl	0.31	0.05	bdl	0.12
Cu wt%	bdl	0.01	bdl	bdl	bdl	0.09
Pb wt%	86.18	85.29	85.73	85.95	86.05	86.13
Ag wt%	bdl	bdl	bdl	bdl	bdl	bdl
Sb wt%	0.03	0.03	0.05	0.14	0.16	bdl
Bi wt%	0.16	0.14	0.17	0.20	0.11	0.14
Hg wt%	bdl	bdl	bdl	bdl	bdl	bdl
Se wt%	0.08	0.06	0.09	0.09	0.16	0.04
Total wt%	100.00	100.00	100.00	100.00	100.00	100.00
S_apfu	0.998	0.998	0.997	0.997	0.995	0.999
Fe_apfu	0.003	0.042	0.013	0.003	0.004	0.003
Zn_apfu	-	-	-	-	-	-
Cu_apfu	-	-	-	-	-	0.003
Pb_apfu	0.987	0.978	0.991	0.982	0.986	0.993
Ag_apfu	-	-	-	-	-	-
Sb_apfu	0.001	0.001	0.001	0.003	0.003	0.000
Bi_apfu	-	-	-	-	-	-
Hg_apfu	0.000	0.000	0.000	0.000	0.000	0.000
Se_apfu	-	-	-	-	-	-

Spot_id	B266585-1-1-1	B266585-7-1-1	B266585-7-1-21	B266585-7-1-6	B266585-8-1-15	B266585-8-1-16
TS_id	B266585	B266585	B266585	B266585	B266585	B266585
Assemblage 1	Assemblage 1	Assemblage 1	Assemblage 1	Assemblage 1	Assemblage 1	Assemblage 1
S wt%	13.66	13.65	13.56	13.67	13.25	13.54
Fe wt%	0.29	0.07	0.39	0.14	0.43	0.20
Zn wt%	0.27	bdl	0.18	bdl	2.45	0.18
Cu wt%	bdl	bdl	bdl	bdl	bdl	bdl
Pb wt%	85.01	85.36	84.74	85.52	83.03	85.61
Ag wt%	0.19	0.32	0.38	0.16	0.21	0.09
Sb wt%	0.39	0.48	0.59	0.37	0.40	0.25
Bi wt%	0.13	0.11	0.12	0.07	0.18	0.14
Hg wt%	bdl	bdl	bdl	bdl	bdl	bdl
Se wt%	0.05	0.01	0.04	0.06	0.04	bdl
Total wt%	100.00	100.00	100.00	100.00	100.00	100.00
S_apfu	0.998	1.000	0.999	0.998	0.999	1.000
Fe_apfu	0.012	0.003	0.016	0.006	0.019	0.008
Zn_apfu	-	-	-	-	0.091	-
Cu_apfu	-	-	-	-	-	-
Pb_apfu	0.961	0.968	0.966	0.966	0.969	0.978
Ag_apfu	0.004	0.007	0.008	0.003	0.005	-
Sb_apfu	0.008	0.009	0.011	0.007	0.008	0.005
Bi_apfu	-	-	-	-	-	-
Hg_apfu	0.000	0.000	0.000	0.000	0.000	0.000
Se_apfu	-	-	-	-	-	-

A348395-3-1-19	A348395-4-1-14	A348395-4-2-11	A348395-8-1-19	A348395-8-3-19	A348395-8-3-20	B232695-1-1-4
A348395	A348395	A348395	A348395	A348395	A348395	B232695
Assemblage 1	Assemblage 1	Assemblage 1	Assemblage 1	Assemblage 1	Assemblage 1	Assemblage 1
13.39	13.43	13.49	13.32	13.44	13.39	13.07
0.05	0.08	0.04	0.12	0.62	0.63	0.39
bdl	0.09	0.05	bdl	0.17	0.41	0.51
bdl	0.44	bdl	bdl	bdl	0.15	0.17
86.18	85.76	86.07	86.35	85.61	85.24	85.26
bdl	bdl	bdl	bdl	bdl	bdl	bdl
0.02	bdl	0.02	0.01	0.01	bdl	0.08
0.13	0.20	0.26	0.15	0.15	0.15	0.20
bdl	bdl	bdl	bdl	bdl	bdl	bdl
0.22	bdl	0.06	0.04	bdl	0.04	0.32
100.00	100.00	100.00	100.00	100.00	100.00	100.00
0.993	1.000	0.998	0.999	1.000	0.999	0.990
-	0.003	-	0.005	0.027	0.027	0.017
-	-	-	-	-	-	0.019
-	0.016	-	-	-	0.005	0.006
0.989	0.988	0.985	1.002	0.986	0.984	0.999
-	-	-	-	-	-	-
0.000	0.000	0.000	0.000	0.000	0.000	0.002
-	-	0.003	-	-	-	-
0.000	0.000	0.000	0.000	0.000	0.000	0.000
-	-	-	-	-	-	0.010

B266585-8-1-18	B266585-8-1-28	B266585-8-3-17	B266585-8-3-6	B291152-3-1-19	B291152-1-1-14	B291152-1-1-5
B266585	B266585	B266585	B266585	B291152	B291152	B291152
Assemblage 1	Assemblage 1	Assemblage 1	Assemblage 1	Assemblage 1	Assemblage 1	Assemblage 1
13.54	13.45	13.56	13.56	21.23	13.34	13.26
0.19	1.00	0.96	0.53	9.97	0.31	1.03
bdl	0.02	bdl	bdl	bdl	0.08	bdl
bdl	bdl	bdl	bdl	bdl	bdl	0.08
85.95	85.23	84.88	85.59	68.72	85.77	85.09
bdl	bdl	0.12	bdl	bdl	bdl	bdl
0.07	0.14	0.34	0.12	0.09	0.05	0.08
0.18	0.09	0.11	0.17	-	0.23	0.19
bdl	bdl	bdl	bdl	-	bdl	bdl
0.06	0.07	0.02	0.03	-	0.21	0.26
100.00	100.00	100.00	100.00	100.00	100.00	100.00
0.998	0.998	0.999	0.999	1.000	0.994	0.992
0.008	0.043	0.041	0.022	0.270	0.013	0.044
-	-	-	-	-	-	-
-	-	-	-	-	-	0.003
0.980	0.979	0.968	0.976	0.501	0.989	0.985
-	-	0.003	-	-	-	-
0.001	0.003	0.007	0.002	0.001	0.001	0.002
-	-	-	-	-	-	-
0.000	0.000	0.000	0.000	-	0.000	0.000
-	-	-	-	-	-	0.008

B232695-1-1-9	B232695-2-1-6	B232695-3-1-16	B232695-3-1-17	B232695-3-1-7	B232695-5-1-17	B232695-5-1-26
B232695	B232695	B232695	B232695	B232695	B232695	B232695
Assemblage 1	Assemblage 1	Assemblage 1	Assemblage 1	Assemblage 1	Assemblage 1	Assemblage 1
13.28	13.29	13.29	13.37	13.20	13.22	13.05
0.52	0.25	0.23	0.08	0.66	1.14	0.76
bdl	0.09	bdl	bdl	0.11	0.12	0.69
bdl	bdl	bdl	bdl	0.01	bdl	0.58
85.63	85.77	85.90	85.83	85.54	85.08	84.48
bdl	bdl	bdl	0.02	bdl	bdl	bdl
0.06	0.08	0.07	0.13	0.07	0.06	0.07
0.18	0.23	0.20	0.26	0.19	0.18	0.27
bdl	bdl	bdl	bdl	bdl	bdl	bdl
0.33	0.29	0.31	0.31	0.23	0.20	0.09
100.00	100.00	100.00	100.00	100.00	100.00	100.00
0.990	0.991	0.991	0.991	0.993	0.994	0.997
0.022	0.011	0.010	0.003	0.028	0.049	0.033
-	-	-	-	-	-	0.026
-	-	-	-	-	-	0.022
0.988	0.990	0.991	0.984	0.996	0.990	0.999
-	-	-	-	-	-	-
0.001	0.002	0.001	0.002	0.001	0.001	0.001
-	-	-	0.003	-	-	0.003
0.000	0.000	0.000	0.000	0.000	0.000	0.000
0.010	0.009	0.009	0.009	-	-	-

B291152-2-1-1	B291152-2-1-15	B291152-4-1-5	B291152-4-2-13	B291152-4-2-13	B291152-4-2-4	B291152-5-1-1
B291152	B291152	B291152	B291152	B291152	B291152	B291152
Assemblage 1	Assemblage 1	Assemblage 1	Assemblage 1	Assemblage 1	Assemblage 1	Assemblage 1
13.42	13.21	13.19	13.11	17.83	13.30	13.35
0.21	0.77	0.58	1.65	0.44	1.01	0.14
bdl	bdl	0.23	bdl	0.02	bdl	bdl
bdl	bdl	0.06	0.13	1.53	0.46	0.01
85.78	85.55	85.42	84.75	61.11	84.82	85.84
bdl	bdl	bdl	bdl	0.03	bdl	bdl
0.13	0.06	0.08	bdl	18.75	0.04	0.17
0.23	0.18	0.20	0.19	0.20	0.18	0.24
bdl	bdl	bdl	bdl	bdl	bdl	bdl
0.22	0.23	0.23	0.16	0.09	0.20	0.25
100.00	100.00	100.00	100.00	100.00	100.00	100.00
0.993	0.993	0.993	0.995	0.998	0.994	0.992
0.009	0.033	0.025	0.072	0.014	0.043	0.006
-	-	-	-	-	-	-
-	-	-	0.005	0.042	0.017	-
0.982	0.995	0.995	0.995	0.529	0.981	0.987
-	-	-	-	-	-	-
0.002	0.001	0.002	0.000	0.276	0.001	0.003
-	-	-	-	-	-	-
0.000	0.000	0.000	0.000	0.000	0.000	0.000
-	-	-	-	-	-	-

B232695-7-1-5	B232695-7-1-7	B232695-8-1-10	B232695-8-1-17	B232695-8-1-4	B232695-9-1-13	B232695-9-1-5
B232695	B232695	B232695	B232695	B232695	B232695	B232695
Assemblage 1	Assemblage 1	Assemblage 1	Assemblage 1	Assemblage 1	Assemblage 1	Assemblage 1
13.37	13.19	13.64	13.37	13.21	13.42	13.42
0.18	0.52	0.27	0.51	0.55	0.13	0.40
bdl	0.23	0.19	0.01	0.23	bdl	bdl
0.01	bdl	bdl	0.01	0.06	bdl	bdl
85.87	85.46	85.22	85.56	85.36	85.39	86.03
bdl	bdl	0.06	bdl	bdl	0.26	bdl
0.05	0.03	0.20	0.03	0.06	0.32	bdl
0.23	0.27	0.18	0.22	0.23	0.24	bdl
bdl	bdl	bdl	bdl	bdl	bdl	bdl
0.29	0.31	0.23	0.28	0.31	0.24	0.16
100.00	100.00	100.00	100.00	100.00	100.00	100.00
0.991	0.991	0.993	0.991	0.991	0.993	0.995
0.008	0.022	0.011	0.022	0.024	0.005	0.017
-	-	-	-	-	-	-
-	-	-	-	-	-	-
0.985	0.993	0.960	0.982	0.991	0.977	0.987
-	-	-	-	-	0.006	-
0.001	0.001	0.004	0.001	0.001	0.006	0.000
-	0.003	-	-	-	-	-
0.000	0.000	0.000	0.000	0.000	0.000	0.000
0.009	0.009	-	0.009	0.009	-	-

B291152-5-1-14	B291152-5-1-20	B291152-6-1-10	B291152-7-1-1	B291157-11-1-10	B291157-11-1-3	B291157-11-1-4
B291152	B291152	B291152	B291152	B291157	B291157	B291157
Assemblage 1	Assemblage 1	Assemblage 1	Assemblage 1	Assemblage 2	Assemblage 2	Assemblage 2
13.31	13.31	13.22	13.41	13.02	13.03	13.04
1.17	0.66	0.57	0.74	0.03	0.48	0.09
bdl	bdl	bdl	bdl	bdl	bdl	bdl
bdl	0.01	0.76	bdl	bdl	0.02	0.01
84.95	85.49	85.05	85.52	85.92	85.63	85.71
bdl	0.02	bdl	bdl	0.05	bdl	0.05
0.21	0.11	0.11	0.08	0.10	0.03	0.12
0.19	0.14	0.16	0.00	0.28	0.29	0.35
bdl	bdl	bdl	bdl	bdl	bdl	bdl
0.16	0.26	0.14	0.26	0.60	0.52	0.63
100.00	100.00	100.00	100.00	100.00	100.00	100.00
0.995	0.992	0.996	0.992	0.982	0.984	0.981
0.050	0.028	0.025	0.031	-	0.021	0.004
-	-	-	-	-	-	-
-	-	0.028	-	-	-	-
0.982	0.986	0.991	0.979	1.002	1.001	0.997
-	-	-	-	-	-	-
0.004	0.002	0.002	0.001	0.002	0.001	0.002
-	-	-	-	0.003	0.003	0.004
0.000	0.000	0.000	0.000	0.000	0.000	0.000
-	0.008	-	0.008	0.018	0.016	0.019

B233308-1-1-1	B233308-1-1-4	B233308-2-1-1	B233308-2-1-17	B233308-3-1-1	B233308-3-1-13	B233308-4-1-10
B233308	B233308	B233308	B233308	B233308	B233308	B233308
Assemblage 1	Assemblage 1	Assemblage 1	Assemblage 1	Assemblage 1	Assemblage 1	Assemblage 1
13.61	13.36	13.78	13.41	13.54	13.60	13.51
0.10	0.09	0.05	0.07	0.34	0.13	0.24
bdl	0.04	bdl	0.20	0.04	bdl	0.01
bdl	bdl	bdl	bdl	bdl	bdl	0.01
85.79	86.33	85.32	86.13	85.85	85.53	86.13
0.10	0.00	0.32	bdl	bdl	0.21	bdl
0.22	0.07	0.44	0.03	0.08	0.35	0.01
0.13	0.10	0.08	0.16	0.13	0.18	0.07
bdl	bdl	bdl	bdl	bdl	bdl	bdl
0.04	bdl	0.02	bdl	0.03	bdl	0.03
100.00	100.00	100.00	100.00	100.00	100.00	100.00
0.999	1.000	0.999	1.000	0.999	1.000	0.999
0.004	0.004	-	0.003	0.014	0.006	0.010
-	-	-	-	-	-	-
-	-	-	-	-	-	-
0.974	1.000	0.957	0.994	0.980	0.973	0.985
0.002	-	0.007	-	-	0.005	-
0.004	0.001	0.008	0.001	0.001	0.007	0.000
-	-	-	-	-	-	-
0.000	0.000	0.000	0.000	0.000	0.000	0.000
-	-	-	-	-	-	-

B291157-11-1-5	B291157-2-1-13	B291157-2-1-14	B291157-4-1-10	B291157-4-1-11	B291157-4-1-18	B291157-5-1-15
B291157	B291157	B291157	B291157	B291157	B291157	B291157
Assemblage 2	Assemblage 2	Assemblage 2	Assemblage 2	Assemblage 2	Assemblage 2	Assemblage 2
13.11	12.99	13.12	13.19	13.12	13.07	13.23
0.08	0.10	0.38	0.10	0.13	0.65	0.12
bdl	0.79	0.19	bdl	bdl	0.41	bdl
0.01	bdl	bdl	bdl	0.01	0.15	bdl
85.75	85.02	85.29	85.53	85.67	84.84	85.61
0.01	0.01	0.02	0.04	0.05	bdl	0.03
0.04	0.03	0.05	0.14	0.06	0.02	0.05
0.34	0.38	0.37	0.43	0.39	0.39	0.34
bdl	bdl	bdl	bdl	bdl	bdl	bdl
0.65	0.66	0.59	0.56	0.57	0.46	0.61
100.00	100.00	100.00	100.00	100.00	100.00	100.00
0.980	0.980	0.982	0.983	0.983	0.986	0.982
0.003	0.004	0.016	0.004	0.005	0.028	0.005
-	0.029	-	-	-	-	-
-	-	-	-	-	0.006	-
0.992	0.992	0.988	0.986	0.993	0.990	0.983
-	-	-	-	-	-	-
0.001	0.001	0.001	0.003	0.001	0.000	0.001
0.004	0.004	0.004	0.005	0.005	0.004	0.004
0.000	0.000	0.000	0.000	0.000	0.000	0.000
0.020	0.020	0.018	0.017	0.017	0.014	0.018

B233308-4-1-11	B233308-4-1-16	B233308-5-1-13	B233308-7-1-14	B233308-7-1-19	B264518-2-2-1	B264518-7-1-3
B233308	B233308	B233308	B233308	B233308	B264518	B264518
Assemblage 1	Assemblage 1	Assemblage 1	Assemblage 1	Assemblage 1	Assemblage 3	Assemblage 3
13.49	13.44	13.61	13.51	13.64	8.50	10.43
0.09	1.11	0.79	0.45	0.87	2.24	1.03
bdl	bdl	bdl	bdl	bdl	0.98	bdl
bdl	bdl	bdl	bdl	0.01	bdl	bdl
86.08	85.18	85.43	85.76	85.27	79.06	82.19
bdl	0.02	bdl	bdl	bdl	0.21	0.25
0.07	0.13	0.02	0.10	0.05	0.01	0.01
0.16	0.05	0.14	0.18	0.12	0.79	0.81
bdl	bdl	bdl	bdl	bdl	bdl	bdl
0.11	0.07	0.02	bdl	0.03	8.21	5.27
100.00	100.00	100.00	100.00	100.00	100.00	100.00
0.997	0.998	0.999	1.000	0.999	0.718	0.830
0.004	0.047	0.033	0.019	0.037	0.109	0.047
-	-	-	-	-	0.041	-
-	-	-	-	-	-	-
0.984	0.978	0.971	0.982	0.967	1.034	1.011
-	-	-	-	-	0.005	0.006
0.001	0.002	0.000	0.002	0.001	0.000	0.000
-	-	-	-	-	0.010	0.010
0.000	0.000	0.000	0.000	0.000	0.000	0.000
-	-	-	-	-	0.282	0.170

B291157-5-1-18	B291157-5-2-1	B291157-5-2-12	B291157-5-2-4	B291157-6-1-36	Q721151-2-1-2	Q721151-2-1-3
B291157	B291157	B291157	B291157	B291157	Q721151	Q721151
Assemblage 2	Assemblage 2	Assemblage 2	Assemblage 2	Assemblage 2	Assemblage 2	Assemblage 2
13.08	13.10	13.16	13.21	13.22	3.19	4.67
0.21	0.47	0.04	0.06	0.25	1.06	1.32
0.76	bdl	bdl	bdl	bdl	bdl	bdl
0.01	bdl	bdl	bdl	0.19	bdl	bdl
84.98	85.48	85.76	85.60	85.64	73.27	73.90
0.02	bdl	0.06	0.04	0.04	0.84	1.08
0.05	0.05	0.09	0.03	0.21	bdl	bdl
0.34	0.36	0.30	0.36	bdl	2.51	2.95
bdl	bdl	bdl	bdl	bdl	bdl	bdl
0.55	0.54	0.59	0.70	0.46	19.13	16.08
100.00	100.00	100.00	100.00	100.00	100.00	100.00
0.983	0.983	0.982	0.979	0.986	0.291	0.417
0.009	0.020	-	-	0.011	0.055	0.067
0.028	-	-	-	-	-	-
-	-	-	-	0.007	-	-
0.988	0.993	0.990	0.981	0.988	1.035	1.021
-	-	-	-	-	0.023	0.029
0.001	0.001	0.002	0.001	0.004	0.000	0.000
0.004	0.004	0.003	0.004	-	0.035	0.040
0.000	0.000	0.000	0.000	0.000	0.000	0.000
0.017	0.017	0.018	0.021	0.014	0.709	0.583

B264518-1-1-5	B264518-1-1-7	B264518-2-1-1	B264518-2-1-3	B264518-2-2-1	B265159A-1-1-1
B264518	B264518	B264518	B264518	B264518	B265159A
Assemblage 3	Assemblage 3	Assemblage 3	Assemblage 3	Assemblage 3	Assemblage 2
9.71	10.33	8.05	8.37	8.63	12.92
0.96	0.91	2.43	2.62	2.22	1.75
bdl	0.37	bdl	bdl	0.91	bdl
0.66	bdl	bdl	bdl	0.01	0.02
80.66	81.22	78.59	78.97	78.45	84.44
0.24	0.23	0.23	0.18	0.21	bdl
bdl	bdl	bdl	bdl	bdl	bdl
1.01	1.07	0.89	0.92	0.86	0.31
bdl	bdl	bdl	bdl	bdl	bdl
6.75	5.85	9.80	8.93	8.71	0.55
100.00	100.00	100.00	100.00	100.00	100.00
0.780	0.813	0.669	0.698	0.709	0.983
0.044	0.041	0.116	0.126	0.105	0.076
0.000	0.014	0.000	0.000	0.037	-
0.026	0.000	0.000	0.000	0.001	-
1.002	0.989	1.011	1.019	0.998	0.994
0.006	0.005	0.006	0.005	0.005	-
0.000	0.000	0.000	0.000	0.000	0.000
0.012	0.013	0.011	0.012	0.011	0.004
0.000	0.000	0.000	0.000	0.000	0.000
0.220	0.187	0.331	0.302	0.291	0.017

Q721151-3-1-8	Q721151-6-1-1	Q721151-6-1-19	Q721151-6-1-5	Q721151-6-2-6	Q721165-5-1-6
Q721151	Q721151	Q721151	Q721151	Q721151	Q721165
Assemblage 2	Assemblage 2	Assemblage 2	Assemblage 2	Assemblage 2	Assemblage 2
3.45	2.31	1.87	2.67	6.76	12.22
0.78	0.54	0.44	0.86	3.50	0.52
bdl	bdl	bdl	bdl	bdl	0.12
0.03	bdl	0.01	bdl	0.23	bdl
74.29	72.94	73.04	73.14	72.55	84.20
0.67	0.84	0.65	0.73	1.31	bdl
bdl	bdl	bdl	bdl	bdl	0.02
2.19	2.48	2.08	2.19	3.53	0.25
bdl	bdl	bdl	bdl	bdl	bdl
18.58	20.88	21.91	20.41	12.11	2.67
100.00	100.00	100.00	100.00	100.00	100.00
0.314	0.214	0.174	0.244	0.579	0.929
0.041	0.029	0.023	0.045	0.172	0.024
-	-	-	-	-	-
-	-	-	-	0.010	-
1.045	1.046	1.050	1.033	0.961	0.996
0.018	0.023	0.018	0.020	0.033	-
0.000	0.000	0.000	0.000	0.000	0.001
0.031	0.035	0.030	0.031	0.046	-
0.000	0.000	0.000	0.000	0.000	0.000
0.686	0.786	0.826	0.756	0.421	0.071

B265159A-1-1-10	B265159A-1-1-9	B265159A-3-2-13	B265159A-3-2-14	B265159A-3-2-17	B265159A-3-2-18
B265159A	B265159A	B265159A	B265159A	B265159A	B265159A
Assemblage 2	Assemblage 2	Assemblage 2	Assemblage 2	Assemblage 2	Assemblage 2
13.25	13.25	12.73	12.98	14.88	13.20
0.14	0.32	0.49	0.28	1.24	0.09
0.09	bdl	3.60	1.31	0.52	0.06
0.13	bdl	0.07	0.18	3.34	0.22
85.55	85.60	82.21	84.13	65.43	84.82
0.01	0.04	0.02	0.14	7.75	bdl
0.04	0.04	0.03	0.17	6.35	1.04
0.34	0.30	0.30	0.31	0.22	0.28
bdl	bdl	bdl	bdl	bdl	bdl
0.46	0.45	0.56	0.49	0.28	0.29
100.00	100.00	100.00	100.00	100.00	100.00
0.986	0.986	0.982	0.985	0.993	0.991
0.006	0.014	0.022	0.012	0.048	0.004
-	-	0.136	0.049	0.017	-
0.005	-	0.003	0.007	0.109	0.008
0.985	0.986	0.982	0.987	0.675	0.985
-	-	-	0.003	0.154	-
0.001	0.001	0.001	0.003	0.112	0.021
0.004	0.003	0.004	0.004	-	0.003
0.000	0.000	0.000	0.000	0.000	0.000
0.014	0.014	0.018	0.015	0.007	0.009

Q721165-6-1-1	Q721165-7-1-17	Q721165-4-1-1	Q721165-5-1-6	Q721165-6-1-25	Q721165-7-1-17
Q721165	Q721165	Q721165	Q721165	Q721165	Q721165
Assemblage 2	Assemblage 2	Assemblage 2	Assemblage 2	Assemblage 2	Assemblage 2
12.77	12.51	13.16	12.23	13.08	12.78
0.31	0.49	0.10	0.55	0.06	0.82
0.62	1.42	bdl	bdl	0.06	0.84
0.02	0.42	0.01	0.01	0.01	0.17
85.01	83.57	85.21	84.73	85.13	83.74
bdl	0.07	0.15	bdl	0.13	0.03
0.03	0.09	0.16	0.07	0.17	0.06
0.24	0.22	0.35	0.13	0.39	0.40
bdl	bdl	bdl	bdl	bdl	bdl
1.01	1.21	0.86	2.29	0.98	1.17
100.00	100.00	100.00	100.00	100.00	100.00
0.969	0.962	0.974	0.918	0.970	0.964
0.014	0.022	0.004	0.023	0.003	0.035
0.023	0.054	0.000	0.004	0.002	0.031
-	0.016	0.001	0.000	0.000	0.006
0.998	0.995	0.976	0.979	0.977	0.978
-	-	0.003	0.000	0.003	0.001
0.001	0.002	0.003	0.000	0.003	0.001
-	-	0.004	0.003	0.004	0.005
0.000	0.000	0.000	0.000	0.000	0.000
0.031	0.038	0.026	0.082	0.030	0.036

B265159A-3-3-10	B265159A-3-3-6	B265159A-4-1-10	B265159A-4-1-4	B265159A-4-1-6	B265159A-9-1-13	B265159A-9-1-17
B265159A	B265159A	B265159A	B265159A	B265159A	B265159A	B265159A
Assemblage 2	Assemblage 2	Assemblage 2	Assemblage 2	Assemblage 2	Assemblage 2	Assemblage 2
13.24	13.24	12.90	13.23	13.37	13.00	12.83
0.77	0.80	0.20	0.08	0.33	1.19	1.85
bdl	bdl	1.40	bdl	0.10	bdl	bdl
bdl	0.23	bdl	0.10	0.02	0.94	0.42
85.41	84.92	84.50	85.10	85.67	84.20	83.97
bdl	0.06	0.01	0.06	bdl	bdl	0.01
0.01	0.07	0.02	0.23	0.02	0.01	bdl
0.37	0.37	0.43	0.60	0.29	0.23	0.35
bdl	bdl	bdl	bdl	bdl	bdl	bdl
0.19	0.30	0.55	0.60	0.21	0.43	0.57
100.00	100.00	100.00	100.00	100.00	100.00	100.00
0.994	0.991	0.983	0.982	0.994	0.987	0.982
0.033	0.034	0.009	0.003	0.014	0.052	0.081
-	-	0.052	-	-	-	-
-	0.009	-	0.004	-	0.035	0.016
0.992	0.983	0.996	0.977	0.985	0.989	0.995
-	-	-	-	-	-	-
0.000	0.001	0.000	0.004	0.000	0.000	0.000
0.004	0.004	0.005	0.007	0.003	-	0.004
0.000	0.000	0.000	0.000	0.000	0.000	0.000
-	0.009	0.017	0.018	-	0.013	0.018

Q721165-7-1-7	gal-Q721165-7-2-19	gal-Q721165-7-2-2	gal-Q721165-7-2-	gal-Q721165-7-2-	Q930239-1-1-10	Q930239-1-1-4
Q721165	Q721165	Q721165	Q721165	Q721165	Q930239	Q930239
Assemblage 2	Assemblage 2	Assemblage 2	Assemblage 2	Assemblage 2	Assemblage 1	Assemblage 1
12.86	13.15	12.99	13.02	13.13	11.83	11.71
0.15	0.24	0.29	0.19	0.06	0.92	1.11
0.24	bdl	bdl	bdl	bdl	1.60	2.46
0.14	0.01	0.02	bdl	bdl	0.01	bdl
84.77	85.11	85.17	85.10	85.19	83.00	82.10
0.08	0.01	0.05	0.09	0.07	bdl	bdl
0.11	0.03	0.06	0.12	0.10	0.03	0.06
0.35	0.36	0.35	0.37	0.46	0.26	0.18
bdl	bdl	bdl	bdl	bdl	bdl	bdl
1.32	1.09	1.07	1.09	0.99	2.36	2.39
100.00	100.00	100.00	100.00	100.00	100.00	100.00
0.960	0.968	0.968	0.967	0.970	0.925	0.923
0.006	0.010	0.012	0.008	0.002	0.041	0.050
0.009	0.000	0.000	0.000	0.000	0.061	0.095
0.005	0.000	0.001	0.000	0.000	-	-
0.980	0.969	0.981	0.978	0.974	1.005	1.002
0.002	0.000	0.001	0.002	0.002	-	-
0.002	0.001	0.001	0.002	0.002	0.001	0.001
0.004	0.004	0.004	0.004	0.005	0.003	-
0.000	0.000	0.000	0.000	0.000	0.000	0.000
0.040	0.032	0.032	0.033	0.030	0.075	0.077

B266543-1-2-11	B266543-1-2-4	B266543-2-1-1	B266543-2-1-11	B266543-3-1-1	B266543-3-2-12	B266543-4-1-1
B266543	B266543	B266543	B266543	B266543	B266543	B266543
Assemblage 1	Assemblage 1	Assemblage 1	Assemblage 1	Assemblage 1	Assemblage 1	Assemblage 1
13.42	13.26	13.28	13.49	13.34	13.37	13.32
0.03	0.27	0.24	0.05	0.20	0.10	0.06
bdl	bdl	bdl	bdl	bdl	bdl	bdl
bdl	bdl	bdl	bdl	0.01	bdl	bdl
85.59	85.42	85.52	86.15	85.61	85.63	85.73
0.11	0.11	0.06	0.09	0.04	0.10	0.07
0.04	0.03	bdl	bdl	bdl	bdl	bdl
0.54	0.61	0.60	bdl	0.59	0.53	0.57
bdl	bdl	bdl	bdl	bdl	bdl	bdl
0.28	0.30	0.30	0.22	0.21	0.28	0.25
100.00	100.00	100.00	100.00	100.00	100.00	100.00
0.992	0.991	0.991	0.994	0.994	0.992	0.993
-	0.012	0.010	-	0.009	0.004	-
-	-	-	-	-	-	-
-	-	-	-	-	-	-
0.979	0.988	0.988	0.981	0.986	0.983	0.988
0.002	0.003	-	-	-	-	-
0.001	0.001	0.000	0.000	0.000	0.000	0.000
0.006	0.007	0.007	-	0.007	0.006	0.007
0.000	0.000	0.000	0.000	0.000	0.000	0.000
0.008	0.009	0.009	-	-	0.008	-

Q930239-1-2-7	Q930239-2-1-9	Q930239-3-1-14	Q930239-3-1-18	Q930239-3-2-14	Q930239-3-2-4	Q930239-3-3-3
Q930239	Q930239	Q930239	Q930239	Q930239	Q930239	Q930239
Assemblage 1	Assemblage 1	Assemblage 1	Assemblage 1	Assemblage 1	Assemblage 1	Assemblage 1
12.02	12.20	12.33	12.44	12.53	12.46	12.34
1.47	0.98	0.13	0.38	0.06	0.17	0.70
0.52	0.51	0.04	bdl	bdl	bdl	bdl
bdl	bdl	bdl	0.02	0.08	0.01	bdl
83.46	83.96	85.35	85.13	85.56	85.44	84.71
bdl	bdl	bdl	0.02	bdl	bdl	bdl
0.04	0.03	0.02	0.10	0.01	0.03	bdl
0.22	0.26	0.24	0.17	0.21	0.16	0.16
bdl	bdl	bdl	bdl	bdl	bdl	bdl
2.26	2.06	1.89	1.75	1.56	1.73	2.08
100.00	100.00	100.00	100.00	100.00	100.00	100.00
0.929	0.936	0.941	0.946	0.952	0.947	0.936
0.065	0.043	0.006	0.016	-	0.008	0.031
0.020	0.019	-	-	-	-	-
-	-	-	-	0.003	-	-
0.998	0.997	1.008	1.002	1.006	1.005	0.994
-	-	-	-	-	-	-
0.001	0.001	0.000	0.002	0.000	0.001	0.000
-	0.003	-	-	-	-	-
0.000	0.000	0.000	0.000	0.000	0.000	0.000
0.071	0.064	0.059	0.054	0.048	0.053	0.064

B266543-5-1-13	B266543-5-1-6	B266543-6-1-10	B266543-6-1-5	B266575-2-2-1	B266575-5-1-17	B266575-5-1-2
B266543	B266543	B266543	B266543	B266575	B266575	B266575
Assemblage 1	Assemblage 1	Assemblage 1	Assemblage 1	Assemblage 2	Assemblage 2	Assemblage 2
13.26	13.31	13.45	13.27	11.00	9.86	9.66
0.08	0.25	0.06	0.09	0.76	1.96	1.84
bdl	bdl	bdl	bdl	bdl	bdl	bdl
bdl	bdl	bdl	0.04	0.14	0.03	0.10
85.82	85.59	85.81	85.79	80.75	79.37	79.34
0.03	0.02	0.04	0.05	0.50	0.53	0.47
bdl	bdl	bdl	bdl	bdl	0.17	0.19
0.52	0.56	0.46	0.53	2.37	1.84	1.74
bdl	bdl	bdl	bdl	bdl	bdl	bdl
0.28	0.26	0.19	0.23	4.48	6.24	6.66
100.00	100.00	100.00	100.00	100.00	100.00	100.00
0.991	0.992	0.994	0.993	0.858	0.795	0.781
0.003	0.011	-	0.004	0.034	0.091	0.085
-	-	-	-	-	-	-
-	-	-	-	0.006	-	0.004
0.992	0.987	0.981	0.994	0.975	0.991	0.993
-	-	-	-	0.012	0.013	0.011
0.000	0.000	0.000	0.000	0.000	0.004	0.004
0.006	0.006	0.005	0.006	0.028	0.023	0.022
0.000	0.000	0.000	0.000	0.000	0.000	0.000
0.009	0.008	-	-	0.142	0.205	0.219

Q930239-3-3-6	Q930239-3-3-9	Q930239-3-4-8	Q930239-6-1-9	Q930239-9-1-11	Q930239-9-1-12	Q930239-9-1-8
Q930239	Q930239	Q930239	Q930239	Q930239	Q930239	Q930239
Assemblage 1	Assemblage 1	Assemblage 1	Assemblage 1	Assemblage 1	Assemblage 1	Assemblage 1
12.18	12.36	12.21	12.60	12.60	12.68	12.49
1.05	0.39	0.08	0.46	0.17	0.21	0.63
bdl	bdl	bdl	bdl	bdl	bdl	bdl
0.06	0.02	bdl	0.01	bdl	bdl	bdl
84.47	85.03	85.29	84.95	85.37	85.36	85.02
bdl	bdl	bdl	bdl	bdl	bdl	bdl
bdl	bdl	bdl	0.04	0.06	0.06	0.06
0.22	0.13	0.19	0.14	0.23	0.17	0.18
bdl	bdl	bdl	bdl	bdl	bdl	bdl
2.00	2.07	2.23	1.79	1.58	1.53	1.62
100.00	100.00	100.00	100.00	100.00	100.00	100.00
0.937	0.936	0.931	0.946	0.951	0.953	0.950
0.046	0.017	0.004	0.020	0.007	0.009	0.028
-	-	-	-	-	-	-
-	-	-	-	-	-	-
1.006	0.997	1.006	0.986	0.998	0.993	1.000
-	-	-	-	-	-	-
0.000	0.000	0.000	0.001	0.001	0.001	0.001
-	-	-	-	-	-	-
0.000	0.000	0.000	0.000	0.000	0.000	0.000
0.063	0.064	0.069	0.054	0.049	0.047	0.050

Q930238-1-3-24	Q930238-2-1-16	Q930238-2-1-17	Q930238-3-2-4
Q930238	Q930238	Q930238	Q930238
Assemblage 2	Assemblage 2	Assemblage 2	Assemblage 2
11.48	11.74	11.35	9.71
1.09	1.18	0.83	1.35
bdl	0.10	bdl	bdl
0.03	0.75	0.43	0.02
81.16	78.62	80.79	79.58
0.34	1.27	0.65	0.52
0.53	0.91	0.28	bdl
1.29	1.10	1.18	1.74
bdl	bdl	bdl	bdl
4.08	4.34	4.50	7.09
100.00	100.00	100.00	100.00
0.874	0.870	0.861	0.771
0.048	0.050	0.036	0.062
0.000	0.003	0.000	0.000
0.001	0.027	0.016	0.001
0.956	0.901	0.949	0.979
0.008	0.028	0.015	0.012
0.011	0.018	0.006	0.000
0.015	0.012	0.014	0.021
0.000	0.000	0.000	0.000
0.126	0.130	0.139	0.229

Q930271-7-1-19	Q930271-7-1-3	Q930271-7-1-6
Q930271	Q930271	Q930271
Assemblage 3	Assemblage 3	Assemblage 3
11.24	11.38	14.32
3.85	1.13	5.75
bdl	bdl	0.03
bdl	0.04	0.08
72.32	77.79	71.72
1.68	1.61	1.14
bdl	bdl	bdl
4.53	4.14	3.19
bdl	bdl	bdl
6.38	3.90	3.76
100.00	100.00	100.00
0.813	0.878	0.904
0.160	0.050	0.208
-	-	-
-	-	0.003
0.809	0.928	0.700
0.036	0.037	0.021
0.000	0.000	0.000
0.050	0.049	0.031
0.000	0.000	0.000
0.187	0.122	0.096

Appendix 8.8 Results of electron probe microanalyzer analysis of sulfosalts

Spot_id	A348395-2-2-1	A348395-2-2-2	A348395-4-2-2	A348395-8-1-1	A348395-8-3-10	A348395-8-3-16
Mineral	tennantite	tennantite	tennantite	tennantite	tennantite	tennantite
TS_id	A348395	A348395	A348395	A348395	A348395	A348395
Assemblage	Assemblage 1	Assemblage 1	Assemblage 1	Assemblage 1	Assemblage 1	Assemblage 1
S wt%	27.07	27.14	26.79	27.17	27.21	27.16
Fe wt%	5.08	4.64	4.30	4.77	4.85	5.08
Zn wt%	3.02	2.92	3.92	3.40	3.15	3.31
Cu wt%	40.21	39.72	39.98	40.73	40.70	40.26
Pb wt%	0.14	0.02	0.09	0.10	0.09	0.11
Ag wt%	2.01	2.30	1.83	1.63	1.59	1.69
As wt%	13.37	11.37	11.73	13.85	13.14	13.33
Co wt%	0.01	0.01	bdl	0.01	0.01	0.01
Ni wt%	bdl	bdl	0.04	0.06	0.07	0.03
Sb wt%	9.10	11.87	11.33	8.27	9.18	9.02
Bi wt%	bdl	bdl	bdl	bdl	bdl	bdl
Se wt%	bdl	bdl	bdl	0.01	bdl	bdl
Total wt%	100.00	100.00	100.00	100.00	100.00	100.00
S_apfu	13.000	13.000	13.000	13.000	13.000	13.000
Fe_apfu	1.400	1.275	1.197	1.309	1.330	1.396
Zn_apfu	0.712	0.686	0.932	0.799	0.739	0.776
Cu_apfu	9.743	9.598	9.790	9.833	9.811	9.721
Pb_apfu	-	-	-	-	-	-
Ag_apfu	0.287	0.327	0.264	0.232	0.226	0.240
As_apfu	2.748	2.331	2.436	2.835	2.687	2.729
Co_apfu	-	-	-	-	-	-
Ni_apfu	-	-	-	-	-	-
Sb_apfu	1.150	1.497	1.448	1.042	1.155	1.137
Bi_apfu	-	-	-	-	-	-
Se_apfu	-	-	-	0.003	-	-

Spot_id	B266543-1-2-1	B266543-1-2-2	B266543-1-2-3	B266543-1-2-8	B266543-3-2-10	B266543-3-2-4
Mineral	tennantite	tennantite	tennantite	tennantite	tennantite	tennantite
TS_id	B266543	B266543	B266543	B266543	B266543	B266543
Assemblage	Assemblage 1	Assemblage 1	Assemblage 1	Assemblage 1	Assemblage 1	Assemblage 1
S wt%	27.99	27.93	27.97	27.92	27.97	27.75
Fe wt%	5.47	5.29	5.46	5.68	5.20	5.40
Zn wt%	2.40	2.62	2.27	2.34	2.69	2.54
Cu wt%	42.09	42.21	42.23	41.79	42.10	42.46
Pb wt%	0.06	0.08	0.05	0.09	0.07	0.06
Ag wt%	1.30	1.19	1.39	1.40	1.32	1.19
As wt%	17.54	17.21	17.43	17.48	17.58	17.42
Co wt%	bdl	0.02	0.02	0.01	0.01	bdl
Ni wt%	bdl	0.01	bdl	bdl	0.01	bdl
Sb wt%	3.13	3.45	3.16	3.26	3.07	3.17
Bi wt%	bdl	bdl	bdl	bdl	bdl	bdl
Se wt%	0.01	bdl	0.02	0.02	bdl	bdl
Total wt%	100.00	100.00	100.00	100.00	100.00	100.00
S_apfu	13.000	13.000	13.000	13.000	13.000	13.000
Fe_apfu	1.460	1.414	1.457	1.519	1.387	1.451
Zn_apfu	0.547	0.598	0.519	0.534	0.613	0.583
Cu_apfu	9.864	9.913	9.904	9.816	9.873	10.035
Pb_apfu	-	-	-	-	-	-
Ag_apfu	0.180	0.165	0.193	0.194	0.182	0.166
As_apfu	3.486	3.429	3.467	3.483	3.497	3.492
Co_apfu	-	-	-	-	-	-
Ni_apfu	-	-	-	-	-	-
Sb_apfu	0.383	0.423	0.387	0.399	0.375	0.391
Bi_apfu	-	-	-	-	-	-
Se_apfu	0.002	-	0.004	0.003	-	-

A348395-3-1-26	A348395-3-1-5	A348395-4-1-1	A348395-4-1-11	A348395-4-1-3	A348395-4-1-5	A348395-4-2-1
tetrahedrite	tetrahedrite	tetrahedrite	tetrahedrite	tetrahedrite	tetrahedrite	tetrahedrite
A348395	A348395	A348395	A348395	A348395	A348395	A348395
Assemblage 1	Assemblage 1	Assemblage 1	Assemblage 1	Assemblage 1	Assemblage 1	Assemblage 1
25.52	25.48	26.12	24.97	26.23	26.13	26.10
2.62	2.67	3.34	2.61	3.32	3.42	3.25
4.85	4.81	4.23	4.71	4.02	4.14	4.37
36.90	37.19	38.24	34.07	38.27	38.91	38.59
0.08	0.05	0.14	0.05	0.02	0.03	0.05
3.80	3.53	2.89	6.49	2.95	2.51	2.85
3.95	4.20	7.87	1.63	7.93	8.09	7.58
bdl	0.01	bdl	0.02	0.01	bdl	bdl
bdl	bdl	bdl	0.02	bdl	bdl	0.02
22.21	22.06	17.18	25.42	17.25	16.77	17.20
bdl	bdl	bdl	bdl	bdl	bdl	bdl
0.06	bdl	bdl	bdl	bdl	bdl	bdl
100.00	100.00	100.00	100.00	100.00	100.00	100.00
13.000	13.000	13.000	13.000	13.000	13.000	13.000
0.765	0.782	0.953	0.779	0.944	0.976	0.928
1.212	1.203	1.032	1.202	0.978	1.010	1.067
9.483	9.575	9.602	8.950	9.569	9.766	9.700
-	-	-	-	-	-	-
0.575	0.536	0.428	1.005	0.435	0.371	0.422
0.861	0.917	1.677	0.364	1.682	1.722	1.615
-	-	-	-	-	-	-
-	-	-	-	-	-	-
2.980	2.965	2.252	3.485	2.251	2.197	2.256
-	-	-	-	-	-	-
0.013	-	-	-	-	-	-

B266543-4-1-12	B266543-4-1-17	B266543-4-1-3	B266543-4-1-4	B266543-5-1-11	B266543-5-1-15	B266543-5-1-16
tennantite	tennantite	tennantite	tennantite	tennantite	tennantite	tennantite
B266543	B266543	B266543	B266543	B266543	B266543	B266543
Assemblage 1	Assemblage 1	Assemblage 1	Assemblage 1	Assemblage 1	Assemblage 1	Assemblage 1
27.91	28.03	28.10	28.32	28.15	28.08	27.84
5.39	5.31	5.28	5.30	5.31	5.25	5.10
2.54	2.45	2.43	2.40	2.49	2.51	2.67
42.11	42.20	42.08	41.76	42.05	41.99	41.86
0.07	0.05	0.10	0.22	0.08	0.09	0.06
1.21	1.20	1.19	1.21	1.24	1.28	1.37
17.47	17.53	17.56	17.26	17.42	17.56	16.67
bdl	bdl	bdl	bdl	bdl	0.01	0.02
bdl	bdl	0.02	bdl	bdl	bdl	bdl
3.29	3.23	3.23	3.46	3.23	3.22	4.42
bdl	bdl	bdl	bdl	bdl	bdl	bdl
bdl	bdl	bdl	0.06	0.03	bdl	bdl
100.00	100.00	99.97	99.99	100.00	100.00	100.00
13.000	13.000	13.000	13.000	13.000	13.000	13.000
1.441	1.414	1.402	1.396	1.409	1.396	1.366
0.580	0.558	0.552	0.541	0.565	0.571	0.610
9.894	9.876	9.822	9.670	9.798	9.809	9.861
-	-	-	0.016	-	-	-
0.168	0.165	0.164	0.165	0.170	0.176	0.190
3.482	3.480	3.477	3.389	3.442	3.480	3.332
-	-	-	-	-	-	-
-	-	-	-	-	-	-
0.404	0.394	0.393	0.418	0.393	0.393	0.544
-	-	-	-	-	-	-
-	-	-	0.011	0.005	-	-

A348395-4-2-13	A348395-4-2-5	A348395-8-1-13	A348395-8-1-4	A348395-8-1-7	A348395-8-3-17	B232695-5-1-3
tetrahedrite	tetrahedrite	tetrahedrite	tetrahedrite	tetrahedrite	tetrahedrite	freibergite
A348395	A348395	A348395	A348395	A348395	A348395	B232695
Assemblage 1	Assemblage 1	Assemblage 1	Assemblage 1	Assemblage 1	Assemblage 1	Assemblage 1
24.51	24.37	24.93	25.08	25.13	24.88	21.91
3.18	3.41	3.48	3.05	3.12	3.93	5.71
4.21	3.92	3.88	4.37	3.83	4.21	0.46
33.55	32.02	34.76	35.52	35.23	33.48	18.73
0.08	0.05	0.09	0.06	0.07	0.04	4.01
7.12	8.59	5.60	4.87	5.22	6.27	23.64
1.50	0.89	2.52	2.81	2.65	1.83	0.05
bdl	bdl	bdl	0.01	bdl	0.01	0.01
bdl	bdl	bdl	0.01	bdl	0.05	0.01
25.86	26.75	24.69	24.20	24.73	25.28	25.39
bdl	bdl	bdl	bdl	bdl	bdl	bdl
bdl	bdl	0.06	0.02	bdl	0.01	0.06
100.00	100.00	100.00	100.00	100.00	100.00	100.00
13.000	13.000	13.000	13.000	13.000	13.000	13.000
0.968	1.045	1.040	0.909	0.927	1.179	1.945
1.094	1.026	0.992	1.112	0.972	1.079	0.133
8.979	8.618	9.143	9.289	9.193	8.825	5.607
-	-	-	-	-	-	0.368
1.122	1.363	0.868	0.750	0.803	0.974	4.168
0.339	0.203	0.562	0.624	0.587	0.410	-
-	-	-	-	-	-	-
-	-	-	-	-	-	-
3.612	3.758	3.390	3.303	3.368	3.478	3.967
-	-	-	-	-	-	-
-	-	0.012	0.005	-	0.001	0.015

B266543-6-1-6	B266543-6-1-8	B266575-9-1-1	B266575-9-1-2	B266575-10-1-5	B291152-4-2-3	B291152-4-2-5
tennantite	tennantite	bournonite	bournonite	gudmubdlite	boulangerite	boulangerite
B266543	B266543	B266575	B266575	B266575	B291152	B291152
Assemblage 1	Assemblage 1	Assemblage 2	Assemblage 2	Assemblage 2	Assemblage 1	Assemblage 1
27.93	27.94	17.17	17.11	15.48	17.96	17.83
5.48	5.44	0.10	0.16	27.24	0.97	0.45
2.37	2.78	bdl	bdl	bdl	bdl	bdl
42.20	41.78	0.91	0.87	0.01	1.31	1.43
0.09	0.07	50.14	50.26	1.77	61.26	61.19
1.23	1.24	bdl	bdl	bdl	bdl	bdl
17.41	17.46	bdl	bdl	bdl	0.01	0.06
0.01	0.01	bdl	bdl	bdl	bdl	bdl
0.02	0.02	bdl	bdl	bdl	bdl	bdl
3.27	3.22	20.72	20.73	54.36	18.41	18.94
bdl	bdl	8.84	8.68	0.85	bdl	bdl
bdl	0.05	2.13	2.19	0.29	0.08	0.10
100.00	100.00	100.00	100.00	100.00	100.00	100.00
13.000	13.000	3.000	3.000	1.000	11.000	11.000
1.463	1.453	0.010	0.016	1.010	0.341	0.159
0.540	0.633	-	-	-	-	-
9.910	9.810	0.080	0.077	0.000	0.405	0.444
-	-	1.356	1.363	0.018	5.805	5.842
0.171	0.171	-	-	-	-	-
3.468	3.477	-	-	-	-	-
-	-	-	-	-	-	-
-	-	-	-	-	-	-
0.401	0.395	0.953	0.957	0.925	2.970	3.078
-	-	0.237	0.233	-	-	-
-	0.009	0.151	0.156	0.008	0.021	0.024

B232695-5-1-4	B233308-2-1-18	B233308-2-1-2	B233308-2-1-3	B233308-7-1-10	B233308-7-1-20	B265159A-3-2-16
tetrahedrite	tetrahedrite	tetrahedrite	tetrahedrite	tetrahedrite	tetrahedrite	bournonite
B232695	B233308	B233308	B233308	B233308	B233308	B265159A
Assemblage 1	Assemblage 1	Assemblage 1	Assemblage 1	Assemblage 1	Assemblage 1	Assemblage 2
22.99	22.88	23.43	23.47	23.19	22.01	16.48
6.20	5.32	5.33	4.97	5.60	5.05	3.48
0.61	0.99	1.39	1.31	0.84	1.32	0.59
21.77	21.62	23.19	23.36	21.97	17.75	7.91
0.61	0.10	0.14	0.10	0.08	0.04	38.44
21.45	22.48	19.70	19.72	21.93	27.56	12.80
0.04	0.06	0.02	0.08	0.07	0.04	bdl
0.01	0.02	0.01	0.02	bdl	0.01	bdl
bdl	0.01	bdl	0.01	bdl	bdl	bdl
26.28	26.51	26.74	26.97	26.32	26.22	19.85
bdl	bdl	bdl	bdl	bdl	bdl	0.25
0.04	bdl	0.04	bdl	bdl	bdl	0.20
100.00	100.00	100.00	100.00	100.00	100.00	100.00
13.000	13.000	13.000	13.000	13.000	13.000	3.000
2.014	1.734	1.699	1.580	1.803	1.714	0.363
0.170	0.275	0.379	0.355	0.230	0.382	0.053
6.210	6.197	6.492	6.528	6.211	5.291	0.726
0.053	-	-	-	-	-	1.082
3.604	3.796	3.248	3.246	3.654	4.840	0.692
-	-	-	-	-	-	0.000
-	-	-	-	-	-	0.000
-	-	-	-	-	-	0.000
3.913	3.966	3.906	3.934	3.885	4.079	0.951
-	-	-	-	-	-	-
0.010	-	0.009	-	-	-	0.014

B291152-6-1-16	B291157-6-1-1	B291157-11-1-11	B291157-6-1-37	B291157-6-1-38	B291157-11-1-12	Q721165-4-1-17
boulangerite	boulangerite	freibergite	freibergite	freibergite	menenghinite	tetrahedrite
B291152	B291157	B291157	B291157	B291157	B291157	Q721165
Assemblage 1	Assemblage 2	Assemblage 2	Assemblage 2	Assemblage 2	Assemblage 2	Assemblage 3
17.80	19.13	23.05	20.69	20.73	18.42	21.50
1.19	0.41	5.32	5.31	4.53	4.67	5.84
bdl	bdl	0.75	0.59	0.76	0.50	1.59
1.58	1.07	20.48	14.26	16.96	12.84	16.39
60.37	50.37	1.07	4.93	15.92	24.87	bdl
bdl	2.06	22.94	29.65	18.59	19.05	28.82
bdl	0.03	0.14	0.08	0.05	0.07	bdl
bdl	bdl	0.01	0.01	bdl	bdl	bdl
bdl	bdl	bdl	bdl	bdl	0.02	bdl
18.87	26.69	26.25	24.39	22.40	19.40	26.11
0.17	bdl	bdl	bdl	bdl	bdl	bdl
0.03	0.25	bdl	0.08	0.06	0.16	bdl
100.00	100.00	100.00	100.00	100.00	100.00	100.25
11.000	11.000	13.000	13.000	13.000	14.000	13.000
0.421	0.135	1.723	1.917	1.631	2.038	2.027
-	-	0.206	0.181	0.234	0.185	0.472
0.491	0.309	5.830	4.519	5.365	4.924	4.999
5.771	4.481	0.093	0.479	1.544	2.925	-
-	0.351	3.846	5.536	3.466	4.304	5.179
-	-	-	-	-	-	-
-	-	-	-	-	-	-
-	-	-	-	-	-	-
3.070	4.042	3.899	4.036	3.699	3.884	4.157
-	-	-	-	-	-	-
0.008	0.058	0.001	0.021	0.016	0.050	-

B265159A-4-1-13	B265159A-4-1-14	B265159A-4-1-15	B265159A-3-3-16	B265159A-3-3-5	B265159A-4-1-17
discrasite	discrasite	discrasite	freibergite	freibergite	freibergite
B265159A	B265159A	B265159A	B265159A	B265159A	B265159A
Assemblage 2	Assemblage 2	Assemblage 2	Assemblage 2	Assemblage 2	Assemblage 2
bdl	bdl	bdl	20.87	20.07	21.30
0.03	0.05	0.04	6.58	8.38	5.46
bdl	0.10	bdl	0.52	0.69	0.36
0.07	0.13	0.12	13.20	10.68	15.48
0.06	0.02	0.09	12.70	0.07	2.71
72.28	68.57	67.97	24.16	17.51	29.18
bdl	0.07	0.05	0.06	0.16	0.09
0.02	bdl	0.02	0.01	0.38	bdl
0.04	0.04	bdl	0.03	7.46	bdl
19.20	18.40	19.59	21.84	34.61	25.38
bdl	bdl	bdl	bdl	bdl	bdl
0.01	bdl	bdl	0.01	bdl	0.05
91.71	87.41	87.90	99.99	100.00	100.00
0.000	0.000	0.000	13.000	13.000	13.000
0.001	0.001	0.001	2.353	3.117	1.913
-	-	-	0.160	0.219	-
0.002	0.003	0.003	4.148	3.491	4.768
-	-	-	1.225	-	0.256
1.000	1.000	1.000	4.473	3.372	5.294
-	-	-	-	-	-
-	-	-	-	0.132	-
-	-	-	-	2.640	-
0.235	0.238	0.255	3.582	5.904	4.079
-	-	-	-	-	-
0.000	-	-	0.002	-	0.013

Q721165-4-1-3	Q721165-4-1-6	Q930238-2-1-1	Q930238-2-1-14	Q930239-3-1-1	Q930239-3-1-13
tetrahedrite	tetrahedrite	freibergite	freibergite	tennantite	tennantite
Q721165	Q721165	Q930238	Q930238	Q930239	Q930239
Assemblage 3	Assemblage 3	Assemblage 2	Assemblage 2	Assemblage 1	Assemblage 1
21.92	21.38	19.16	20.97	26.87	26.80
5.65	5.31	4.52	6.29	5.49	5.51
0.92	0.96	0.45	0.54	2.00	2.06
16.26	16.49	13.68	15.21	40.26	40.10
0.09	bdl	20.24	9.30	0.03	0.04
29.06	28.78	21.31	24.30	2.00	2.08
0.11	bdl	0.02	0.07	12.00	11.81
0.01	bdl	bdl	bdl	0.01	0.01
bdl	bdl	bdl	0.02	0.02	0.01
25.97	25.88	20.62	23.29	11.18	11.42
bdl	bdl	bdl	bdl	bdl	bdl
bdl	bdl	bdl	bdl	0.12	0.15
100.00	98.86	100.00	100.00	99.97	99.97
13.000	13.000	13.000	13.000	13.000	13.000
1.924	1.854	1.759	2.237	1.524	1.534
0.269	0.287	0.149	0.165	0.474	0.489
4.867	5.059	4.682	4.757	9.830	9.813
-	-	2.125	0.892	-	-
5.123	5.201	4.296	4.477	0.287	0.299
-	-	-	-	2.485	2.451
-	-	-	-	-	-
-	-	-	-	-	-
4.056	4.144	3.684	3.802	1.424	1.459
-	-	-	-	-	-
-	0.002	-	-	0.024	0.029

B265159A-4-1-19	B265159A-3-2-20	B265159A-4-1-18	B265159A-3-2-19	B265159A-3-3-1	B265159A-3-3-17
gudmubdlite	menenghinite	menenghinite	tetrahedrite	tetrahedrite	ullmannite
B265159A	B265159A	B265159A	B265159A	B265159A	B265159A
Assemblage 2	Assemblage 2	Assemblage 2	Assemblage 2	Assemblage 2	Assemblage 2
14.97	19.04	15.13	22.62	22.30	8.93
27.15	7.31	1.95	9.80	8.78	6.92
0.00	2.17	0.19	0.97	0.52	0.14
0.00	6.92	5.38	13.07	15.54	3.08
0.08	35.83	56.15	0.80	0.49	0.10
0.02	15.34	11.70	28.82	26.92	4.57
0.42	0.08	0.01	0.09	0.11	0.45
0.04	0.01	bdl	0.01	0.03	0.66
0.18	bdl	0.03	0.02	0.20	12.91
57.12	13.22	9.14	23.78	25.11	62.24
bdl	bdl	bdl	bdl	bdl	bdl
0.01	0.07	0.31	0.01	bdl	bdl
100.00	100.00	100.00	100.00	100.00	100.00
1.000	14.000	24.000	13.000	13.000	1.000
1.042	3.087	1.778	3.235	2.937	0.445
-	0.782	-	0.272	0.148	-
0.000	2.568	4.308	3.788	4.570	0.174
-	4.075	13.780	0.071	0.044	-
-	3.351	5.517	4.923	4.664	0.152
0.012	-	-	-	-	0.021
-	-	-	-	-	0.040
-	-	-	-	-	0.789
1.005	2.559	3.818	3.599	3.855	1.836
-	-	-	-	-	-
0.000	0.022	0.198	0.002	-	-

Q930239-3-2-5	Q930239-3-1-5	Q930239-3-2-12	Q930239-3-2-13	Q930239-3-2-6	B265159A-3-3-4
tennantite	tetrahedrite	tetrahedrite	tetrahedrite	tetrahedrite	ullmannite
Q930239	Q930239	Q930239	Q930239	Q930239	B265159A
Assemblage 1	Assemblage 1	Assemblage 1	Assemblage 1	Assemblage 1	Assemblage 2
27.01	29.63	26.47	26.24	25.83	15.37
5.46	7.79	5.01	4.85	4.21	1.58
2.09	2.45	2.42	2.61	3.04	0.53
40.26	35.79	38.77	38.04	35.84	0.30
0.07	0.07	bdl	0.06	0.05	0.09
2.04	2.28	2.75	2.92	4.29	0.51
12.35	8.18	8.88	7.65	4.35	0.37
0.01	0.01	bdl	0.01	bdl	0.88
bdl	0.03	bdl	0.01	bdl	24.93
10.61	13.70	15.64	17.46	22.25	55.45
bdl	bdl	bdl	bdl	bdl	bdl
0.10	0.06	0.05	0.10	0.11	bdl
100.00	100.00	100.00	99.95	99.98	100.00
13.000	13.000	13.000	13.000	13.000	1.000
1.508	1.963	1.413	1.379	1.217	0.059
0.494	0.528	0.584	0.634	0.750	0.017
9.777	7.922	9.608	9.509	9.102	0.010
-	-	-	-	-	-
0.292	0.298	0.401	0.430	0.642	0.010
2.543	1.536	1.867	1.622	0.938	0.010
-	-	-	-	-	0.031
-	-	-	-	-	0.886
1.345	1.582	2.023	2.277	2.949	0.950
-	-	-	-	-	-
0.020	0.012	0.010	0.021	0.023	-

Appendix 9.1 Results of laser ablation inductively coupled plasma mass spectrometry of sulfide minerals

Spot_id		B264518-1-2	B264518-1-3	B264518-1-4	B264518-2-1	B264518-2-1
TS_id		B264518	B264518	B264518	B264518	B264518
Min		sph	cpy	po	gal	gal
Assemblage	Average detection limit	Assemblage 3	Assemblage 3	Assemblage 3	Assemblage 3	Assemblage 3
Mn_ppm_m55	0.899	499.103	bdl	1.153	bdl	7.527
Fe_ppm_m57	29.364	34915.325	-	-	bdl	144.136
Co_ppm_m59	2.210	9.878	bdl	39.538	bdl	bdl
Ni_ppm_m60	3.029	bdl	bdl	58.251	bdl	bdl
Cu_ppm_m65	0.849	214.832	-	bdl	bdl	48.179
Zn_ppm_m66	3.233	-	1741.659	4.042	bdl	466.933
Ga_ppm_m69	0.202	0.075	bdl	bdl	bdl	bdl
Ge_ppm_m72	0.714	0.173	0.894	bdl	bdl	bdl
As_ppm_m75	4.752	0.139	bdl	bdl	bdl	0.356
Se_ppm_m77	1.812	154.775	606.852	623.388	59028.734	79515.791
Ag_ppm_m109	0.098	1.800	369.483	1.668	4936.540	4790.867
Cd_ppm_m111	0.345	1484.776	5.943	bdl	8.661	5.486
In_ppm_m115	0.040	0.432	0.560	bdl	bdl	bdl
Sn_ppm_m118	0.138	0.101	34.683	bdl	4.859	9.111
Sb_ppm_m121	0.134	0.257	4.105	0.122	89.953	67.142
Te_ppm_m125	0.196	bdl	bdl	bdl	bdl	bdl
Au_ppm_m197	0.026	bdl	0.123	bdl	bdl	bdl
Tl_ppm_m205	0.006	0.015	bdl	0.011	103.088	114.838
Pb_ppm_m208	0.360	67.509	3.285	3.487	-	-
Bi_ppm_m209	0.024	1.246	0.646	0.940	7412.258	7317.451
Hg202_ppm	0.110	2.753	bdl	bdl	bdl	bdl

Spot_id	B291152-4-3	B291152-4-4	B291152-4-5	B291152-4-6	B291157-1-1	B291157-1-2
TS_id	B291152	B291152	B291152	B291152	B291157	B291157
Min	py	cpy	sph	gal	py	py
Assemblage	Assemblage 1	Assemblage 1	Assemblage 1	Assemblage 1	Assemblage 2	Assemblage 2
Mn_ppm_m55	1.274	134.464	40.332	13.318	14.833	1.107
Fe_ppm_m57	-	-	26468.670	176162.039	-	-
Co_ppm_m59	111.737	20.257	bdl	57.330	1723.754	1949.683
Ni_ppm_m60	34.281	13.435	bdl	14.486	27.793	242.394
Cu_ppm_m65	6.501	-	263.415	27.869	5140.665	307.583
Zn_ppm_m66	9.620	15424.122	-	11.678	21231.515	10.957
Ga_ppm_m69	bdl	24.419	4.135	0.525	0.961	bdl
Ge_ppm_m72	1.591	bdl	0.229	bdl	0.961	1.134
As_ppm_m75	954.946	848.908	8.078	65436.511	251.772	868.861
Se_ppm_m77	20.778	4722.222	13.074	3123.274	964.284	55.673
Ag_ppm_m109	bdl	7477.239	5.786	1222.523	141.441	36.158
Cd_ppm_m111	bdl	86.940	932.995	7.819	56.630	0.220
In_ppm_m115	bdl	bdl	0.299	0.550	bdl	bdl
Sn_ppm_m118	bdl	980.861	0.868	168.804	40.995	0.512
Sb_ppm_m121	4.487	6114.466	4.017	1971.080	758.281	63.238
Te_ppm_m125	bdl	bdl	bdl	0.176	bdl	bdl
Au_ppm_m197	bdl	0.420	bdl	5.915	0.745	0.019
Tl_ppm_m205	0.009	354.507	0.177	189.860	25.382	2.738
Pb_ppm_m208	21.865	-	1.939	-	428.638	196.974
Bi_ppm_m209	0.419	888.252	0.013	545.709	7.031	3.195
Hg202_ppm	bdl	4.353	8.427	bdl	1.781	bdl

B264518-2-2	B264518-2-3	B264518-3-1	B264518-3-2	B264518-4-1	B264518-4-1	B264518-4-2
B264518	B264518	B264518	B264518	B264518	B264518	B264518
po	sph	po	cpy	gal	gal	po
Assemblage 3	Assemblage 3	Assemblage 3	Assemblage 3	Assemblage 3	Assemblage 3	Assemblage 3
117.646	507.274	13817.626	bdl	bdl	bdl	bdl
-	36187.991	-	-	bdl	bdl	-
38.659	9.217	27.195	bdl	bdl	bdl	46.650
49.494	bdl	38.453	bdl	bdl	bdl	54.697
bdl	349.802	34699.488	-	bdl	bdl	bdl
2.012	-	4382.817	1588.774	bdl	bdl	5.568
bdl	19.779	13.168	bdl	8.812	6.287	bdl
bdl	0.256	bdl	bdl	bdl	bdl	bdl
bdl	0.206	bdl	bdl	bdl	bdl	bdl
498.330	245.118	452.623	638.291	65889.833	77772.443	518.009
0.535	3.222	74.552	436.412	4347.082	5038.032	5.931
bdl	1343.884	5.003	7.239	4.378	4.026	bdl
bdl	0.544	bdl	0.614	bdl	bdl	bdl
0.177	0.500	7.643	31.999	1.842	1.988	bdl
bdl	0.640	5.105	5.324	57.086	50.677	0.864
bdl	bdl	bdl	bdl	0.516	bdl	bdl
bdl	bdl	bdl	bdl	bdl	bdl	bdl
bdl	0.502	0.400	0.191	117.421	121.613	0.063
1.799	2.135	123.476	5.766	-	-	24.225
0.119	0.097	3.079	0.697	7017.109	7688.692	3.759
bdl	2.947	bdl	bdl	bdl	bdl	bdl

B291157-1-3	B291157-1-4	B291157-1-5	B291157-1-6	B291157-1-7	B291157-1-8	B291157-2-1
B291157	B291157	B291157	B291157	B291157	B291157	B291157
gal	po	cpy	sph	py	py	gal
Assemblage 2	Assemblage 2	Assemblage 2	Assemblage 2	Assemblage 2	Assemblage 2	Assemblage 2
bdl	bdl	9.255	72.540	43.368	0.969	bdl
bdl	-	-	39341.991	-	-	bdl
bdl	bdl	bdl	1.356	2301.127	1186.127	bdl
bdl	45.560	bdl	bdl	49.240	75.003	bdl
bdl	0.857	-	42.032	1250.895	bdl	0.989
bdl	3.952	2334.609	-	61.072	25.147	13.880
bdl	bdl	9.728	1.176	bdl	bdl	bdl
bdl	0.976	5.217	0.210	0.774	1.062	bdl
33.517	15.353	23.844	1.739	1229.241	646.709	18.859
4560.304	47.040	36.704	29.694	161.243	46.913	6939.884
2346.799	7.902	296.137	2.219	42.305	bdl	2281.795
16.880	bdl	9.601	1251.763	0.527	bdl	10.370
0.253	bdl	3.852	1.607	bdl	bdl	0.299
82.044	bdl	534.037	0.156	0.524	bdl	108.521
890.199	8.993	36.633	0.158	153.165	bdl	844.813
bdl	bdl	bdl	bdl	bdl	bdl	bdl
bdl	bdl	1.245	bdl	0.152	bdl	bdl
92.494	0.466	1.471	0.001	5.624	0.027	83.335
-	86.43	83.138	2.768	993.688	6.468	-
2122.133	30.420	0.340	bdl	2.985	bdl	2082.576
bdl	bdl	0.416	10.142	bdl	bdl	bdl

B264518-4-3	B264518-5-1	B264518-5-2	B264518-5-3	B264518-5-3	B266543-1-1	B266543-1-2
B264518	B264518	B264518	B264518	B264518	B266543	B266543
sph	cpy	po	sph	sph	gal	sph
Assemblage 3	Assemblage 3	Assemblage 3	Assemblage 3	Assemblage 3	Assemblage 1	Assemblage 1
524.875	1.401	4.937	712.824	836.029	bdl	46.352
34472.658	-	-	34915.325	36387.191	bdl	9083.262
9.935	bdl	48.324	9.377	8.500	bdl	bdl
bdl	bdl	75.891	bdl	bdl	bdl	bdl
226.040	-	4.541	19.148	7.496	12.931	13.443
-	2123.874	34.308	-	-	bdl	-
0.089	0.256	0.316	0.132	0.155	bdl	8.379
0.176	bdl	1.153	0.221	0.178	bdl	bdl
0.182	0.438	bdl	0.153	0.144	141.936	bdl
207.650	771.360	723.689	232.862	436.661	bdl	19.972
3.086	353.714	5.108	0.763	0.688	2867.368	0.230
1399.518	8.214	bdl	1445.398	1442.508	43.740	1623.188
0.488	0.601	bdl	0.519	0.538	0.038	1.644
0.023	28.951	bdl	bdl	0.037	7.123	0.142
0.532	3.617	0.864	0.033	bdl	508.918	0.126
bdl	bdl	bdl	bdl	bdl	bdl	bdl
0.090	bdl	bdl	bdl	bdl	bdl	bdl
0.007	0.075	0.159	bdl	bdl	126.760	0.003
1.681	4.626	11.995	1.357	0.198	-	0.394
0.165	0.492	1.631	0.008	0.011	3843.243	bdl
2.755	0.185	0.195	2.668	2.661	bdl	23.130

B291157-2-2	B291157-2-3	B291157-2-4	B291157-2-5	B291157-2-6	B291157-2-7	B291157-2-8
B291157	B291157	B291157	B291157	B291157	B291157	B291157
py	py	cpy	po	sph	py	py
Assemblage 2	Assemblage 2	Assemblage 2	Assemblage 2	Assemblage 2	Assemblage 2	Assemblage 2
1.130	7.451	15.865	1.638	91.397	2.676	19.608
-	-	-	-	31982.659	-	-
1439.251	1730.029	41.496	bdl	1.857	1780.236	1175.667
37.311	84.394	9.006	70.053	bdl	90.105	83.759
4.198	959.591	-	1944.885	10.228	2.999	68.542
28.021	99.332	2047.431	229.918	-	20.297	14.909
bdl	bdl	24.432	0.830	1.323	bdl	bdl
1.620	1.523	0.982	bdl	0.224	1.216	2.066
705.949	798.759	78.531	10.367	1.044	908.354	744.456
67.290	3104.245	47.159	28.821	41.775	67.036	63.291
0.200	1005.732	577.604	32.726	4.024	0.208	0.271
bdl	5.203	5.791	0.634	1114.124	bdl	bdl
bdl	bdl	2.731	bdl	1.649	bdl	bdl
bdl	25.645	439.710	125.069	0.145	bdl	2.337
3.539	672.996	105.417	34.230	1.564	0.273	0.777
bdl	bdl	bdl	bdl	bdl	bdl	bdl
bdl	0.324	0.482	0.614	0.008	bdl	bdl
0.045	40.331	2.924	1.628	0.008	0.014	bdl
52.918	373955.901	23.131	156.991	1.791	1.035	21.167
0.232	856.792	0.336	0.641	bdl	bdl	0.065
bdl	0.250	0.226	bdl	7.875	bdl	bdl

B266543-1-3	B266543-1-4	B266543-1-5	B266543-1-6	B266543-1-7	B266543-2-1	B266543-2-2
B266543	B266543	B266543	B266543	B266543	B266543	B266543
py	ten-tet	cpy	py	ten-tet	cpy	py
Assemblage 1	Assemblage 1	Assemblage 1	Assemblage 1	Assemblage 1	Assemblage 1	Assemblage 1
8.604	bdl	bdl	bdl	5.505	bdl	5.071
-	419111.240	-	-	55232.065	-	-
302.049	70.541	bdl	77.096	bdl	16.682	7.182
bdl	bdl	bdl	bdl	bdl	bdl	bdl
96.210	-	-	32.937	-	-	5295.860
56695.906	112027.833	988.072	25.994	116434.725	821.074	1494.152
3.714	bdl	28.987	bdl	bdl	35.133	bdl
1.192	2.511	2.266	1.176	bdl	2.389	1.282
337.414	305899.572	7.684	259.745	287604.143	180.027	2247.307
87.108	225.926	41.389	23.975	276.852	49.259	49.308
9.787	bdl	14.846	bdl	15436.564	18.398	76.753
180.582	bdl	3.615	bdl	803.984	3.185	5.770
bdl	0.248	bdl	bdl	0.246	bdl	bdl
0.219	0.090	171.365	bdl	bdl	229.303	10.091
4.289	42046.390	1.789	0.191	36686.797	4.907	38.466
bdl	bdl	bdl	bdl	bdl	bdl	bdl
0.160	0.456	0.438	bdl	bdl	0.292	1.210
0.876	bdl	0.126	0.036	0.045	0.291	0.180
44.373	234.938	2.658	8.939	bdl	91.039	4437.299
0.588	214.183	0.179	bdl	199.857	0.967	23.447
1.617	164.454	0.243	bdl	83.566	0.358	0.224

B291157-3-1	B291157-3-2	B291157-3-3	B291157-3-4	B291157-3-5	B291157-3-6	B291157-4-1
B291157	B291157	B291157	B291157	B291157	B291157	B291157
gal	po	cpy	py	sph	py	py
Assemblage 2	Assemblage 2	Assemblage 2	Assemblage 2	Assemblage 2	Assemblage 2	Assemblage 2
bdl	4.683	415.142	348.324	96.049	bdl	7.266
bdl	-	-	-	33144.659	-	-
bdl	bdl	bdl	1757.225	bdl	1903.660	4.665
bdl	50.890	bdl	64.215	bdl	75.130	48.352
bdl	50.550	-	574.041	573.974	bdl	23.561
13.326	6304.790	3284980.324	747.234	-	24.788	334.100
bdl	0.928	12.216	0.142	1.392	bdl	1.962
bdl	bdl	1.554	0.735	bdl	bdl	1.696
24.051	17.278	9.674	739.519	bdl	952.785	12.342
6877.648	94.587	343.639	104.744	34.877	75.543	76.622
2084.216	13.410	486.837	46.934	9.286	bdl	3.512
8.082	13.074	7391.147	1.454	1084.500	bdl	0.907
0.164	bdl	11.629	bdl	1.641	bdl	bdl
70.489	58.113	367.876	1.680	3.477	bdl	13.707
817.091	18.275	25.037	51.287	5.732	0.627	17.753
bdl	bdl	bdl	bdl	bdl	bdl	bdl
bdl	bdl	1.353	0.432	0.009	bdl	bdl
88.289	0.614	bdl	6.771	bdl	bdl	1.743
-	711.457	18.304	199.326	2.575	26.636	58.798
1964.263	2.183	0.127	1.763	0.014	0.216	0.216
bdl	bdl	64.223	0.211	9.283	bdl	bdl

B266543-2-3	B266543-2-4	B266543-2-5	B266543-2-6	B266543-3-1	B266543-3-2	B266543-3-3
B266543	B266543	B266543	B266543	B266543	B266543	B266543
gal	py	sph	py	gal	py	ten-tet
Assemblage 1	Assemblage 1	Assemblage 1	Assemblage 1	Assemblage 1	Assemblage 1	Assemblage 1
bdl	15.598	33.033	3.389	bdl	88.205	6.792
bdl	-	8074.506	-	bdl	-	56183.561
bdl	1.394	bdl	39.499	bdl	1.669	bdl
bdl	bdl	bdl	4.228	bdl	13.606	bdl
bdl	16.902	33.024	5.461	bdl	18.982	-
8.795	51.374	-	27.222	bdl	31.316	93704.440
bdl	0.431	8.670	0.698	bdl	bdl	0.523
bdl	1.160	0.220	1.389	bdl	1.027	0.864
29.291	356.513	1.621	222.821	111.860	954.946	190052.916
3039.517	5.674	20.333	24.374	3516.814	15.743	201.574
2088.096	3.898	0.314	0.123	2436.790	1.949	12671.953
29.745	bdl	1553.188	bdl	34.828	bdl	548.328
bdl	bdl	1.632	bdl	bdl	bdl	0.137
3.331	0.233	0.103	0.094	10.117	bdl	0.180
27.426	3.695	0.194	bdl	108.036	80.494	27990.667
bdl	bdl	bdl	bdl	bdl	bdl	bdl
bdl	0.192	bdl	0.041	bdl	0.161	bdl
339.047	0.932	0.004	0.030	bdl	5.454	0.136
-	136.977	0.640	57.878	-	133.762	6.409
3862.888	0.650	0.010	0.119	4099.107	0.109	144.628
bdl	0.112	23.333	bdl	bdl	1.414	66.898

B291157-4-2	B291157-4-3	B291157-4-4	B291157-4-5	B291157-4-6	Q721165-1-1	Q721165-1-3
B291157	B291157	B291157	B291157	B291157	Q721165	Q721165
po	cpy	py	sph	py	gal	py
Assemblage 2	Assemblage 2	Assemblage 2	Assemblage 2	Assemblage 2	Assemblage 3	Assemblage 3
bdl	bdl	6.736	91.523	24.913	bdl	bdl
-	-	-	32480.659	-	bdl	-
3.975	bdl	1414.147	0.957	763.556	bdl	40.165
45.687	bdl	65.611	bdl	43.276	bdl	25.889
1962.020	-	239.898	23.491	3726.982	2.722	1.028
185.012	2115.610	13.113	-	9933.188	3.208	8.981
5.267	3.408	bdl	0.935	0.751	bdl	bdl
1.682	bdl	1.437	0.245	1.336	bdl	0.692
11.848	18.552	849.114	bdl	2665.823	0.723	445.785
84.430	90.370	58.403	25.282	451.353	10869.214	82.399
21.791	433.661	2.331	2.127	37.914	7262.699	0.095
1.514	5.936	bdl	1167.590	22.412	28.978	bdl
bdl	2.630	bdl	1.587	bdl	bdl	bdl
1465.450	568.865	37.268	0.951	20.529	5.401	bdl
12.358	1.825	4.525	0.374	145.042	4757.816	bdl
bdl	bdl	bdl	bdl	bdl	0.148	bdl
bdl	0.194	bdl	bdl	1.009	0.045	bdl
1.203	bdl	0.070	0.004	7.770	34.186	bdl
19.580	6.349	5.409	0.145	278.703	-	2.146
0.238	bdl	0.185	bdl	19.292	2128.226	bdl
bdl	0.444	bdl	9.104	1.086	bdl	bdl

B266543-3-4	B266543-3-5	B266543-3-6	B266543-3-7	B266543-4-1	B266543-4-2	B266543-4-3
B266543	B266543	B266543	B266543	B266543	B266543	B266543
cpy	py	ten-tet	ten-tet	gal	py	sph
Assemblage 1	Assemblage 1	Assemblage 1	Assemblage 1	Assemblage 1	Assemblage 1	Assemblage 1
13.693	33.527	9.284	6.299	0.480	15.622	29.431
-	-	56410.107	126866.105	802.227	-	9400.172
bdl	bdl	bdl	bdl	1.744	58.931	bdl
bdl	6.323	bdl	bdl	bdl	6.669	bdl
-	52.785	-	-	5.759	9.534	32.480
76772.697	159.649	111795.891	83730.948	10.093	27.836	-
9.053	bdl	17192.691	10.465	bdl	0.386	8.864
bdl	1.335	bdl	bdl	0.421	1.266	0.191
191004.278	1037.071	221008.782	165171.133	9.222	157.884	0.724
126.852	12.227	216.667	137.778	2621.601	22.536	21.019
10556.681	6.834	13331.131	11924.229	2099.230	5.065	0.096
565.544	bdl	601.697	527.668	49.019	bdl	1728.019
bdl	bdl	bdl	bdl	0.019	bdl	1.629
119.955	bdl	2.024	92.211	5.678	bdl	1.009
28534.175	29.361	36762.284	28081.252	251.001	0.891	bdl
bdl	bdl	bdl	bdl	bdl	bdl	bdl
0.186	2.540	0.502	0.078	0.009	0.137	bdl
7.964	16.621	bdl	4.856	84.995	0.271	0.005
56.899	983.923	257.698	26.210	-	34.148	bdl
141.117	6.753	160.888	137.464	3107.525	1.125	bdl
124.312	1.346	90.784	99.937	bdl	bdl	19.900

Q721165-1-4	Q721165-2-1	Q721165-2-2	Q721165-2-3	Q721165-2-4	Q721165-2-5	Q721165-3-1
Q721165	Q721165	Q721165	Q721165	Q721165	Q721165	Q721165
cpy	gal	cpy	py	sph	gal	gal
Assemblage 3	Assemblage 3	Assemblage 3	Assemblage 3	Assemblage 3	Assemblage 3	Assemblage 3
2.618	bdl	bdl	1.200	608.478	bdl	bdl
-	bdl	-	-	38290.658	bdl	bdl
bdl	bdl	bdl	18.179	bdl	bdl	bdl
65.757	bdl	bdl	20.051	bdl	bdl	bdl
-	bdl	-	11.224	86.867	bdl	1.797
2320.146	bdl	2402.787	13.831	-	3.916	3.115
0.287	bdl	bdl	bdl	0.259	bdl	bdl
1.388	bdl	0.877	1.019	0.176	bdl	0.663
182.101	0.895	bdl	455.165	bdl	bdl	0.948
162.315	11035.583	146.741	336.452	69.544	10721.510	10901.085
1391.750	4087.571	1196.465	94.188	2.930	5177.944	7423.990
7.696	12.577	8.915	4.136	1512.231	11.655	23.940
1.336	0.052	0.912	bdl	0.873	bdl	bdl
26.992	8.674	20.897	0.114	bdl	9.502	4.400
27.013	2083.992	2.075	51.635	0.073	3047.341	4806.374
bdl	0.150	bdl	bdl	bdl	bdl	bdl
1.569	bdl	2.541	0.110	bdl	bdl	bdl
1.195	45.876	0.007	0.077	bdl	46.622	47.450
1743.208	-	6.483	14758.323	0.521	-	-
1.663	2105.255	0.072	39.799	bdl	2111.654	2215.709
0.673	bdl	1.548	bdl	19.013	bdl	bdl

B266543-4-4	B266543-4-5	B266543-4-6	B266543-4-7	B291152-1-1	B291152-1-2	B291152-1-3
B266543	B266543	B266543	B266543	B291152	B291152	B291152
py	cpy	py	gal	gal	sph	cpy
Assemblage 1	Assemblage 1	Assemblage 1	Assemblage 1	Assemblage 1	Assemblage 1	Assemblage 1
307.635	bdl	0.649	bdl	bdl	45.180	bdl
-	-	-	2945.746	270289.427	28477.253	-
54.707	bdl	43.301	2.421	25.164	bdl	bdl
14.539	bdl	14.939	bdl	29.198	bdl	bdl
54.605	-	5.807	147.735	149203.302	151.134	-
290.643	1203.777	21.696	5.928	18935.428	-	19946.985
8.690	41777.409	0.149	bdl	2.701	4.212	17.193
1.277	bdl	0.936	bdl	bdl	0.191	bdl
636.631	12.807	406.807	21.696	232.489	160.401	14.344
727.232	58.148	26.292	3733.963	2684.480	11.015	42.963
405.228	95.040	0.901	3094.348	1470.668	2.334	217.430
8.092	2.238	bdl	59.431	77.954	1012.802	69.725
bdl	bdl	bdl	bdl	1.691	0.315	bdl
2.625	167.693	bdl	8.391	592.821	0.210	835.608
76.536	5.435	0.389	289.216	991.348	1.221	6.643
bdl	bdl	bdl	bdl	bdl	bdl	bdl
0.417	1.360	0.008	bdl	0.238	0.009	0.402
22.977	0.282	0.086	155.475	158.031	bdl	0.355
142122.186	125.545	28.296	-	-	0.606	4.537
694.039	2.493	0.091	4555.547	547.627	0.008	bdl
0.893	0.643	bdl	bdl	bdl	10.418	1.379

Q721165-3-2	Q721165-3-3	Q721165-3-4	Q721165-3-5	Q721165-3-6	Q721165-3-7	Q930238-1-1
Q721165	Q721165	Q721165	Q721165	Q721165	Q721165	Q930238
cpy	sph	py	py	po	py	po
Assemblage 3	Assemblage 3	Assemblage 3	Assemblage 3	Assemblage 3	Assemblage 3	Assemblage 2
bdl	586.226	0.512	1.615	1.615	bdl	6.828
-	37017.991	-	-	-	-	-
bdl	bdl	49.160	14.518	bdl	44.558	242.874
bdl	bdl	25.255	10.990	120.055	13.198	bdl
-	145.712	bdl	1139.514	bdl	0.942	342.711
2080.488	-	9.538	969.968	7.365	165.254	57479.567
0.370	0.136	bdl	124.433	bdl	bdl	0.632
0.744	0.147	0.803	1.259	bdl	0.932	1.105
bdl	bdl	463.063	4023.418	bdl	515.886	19.401
135.335	43.001	97.254	126.963	221.550	76.178	628.467
970.924	5.057	0.559	45.497	0.774	bdl	36.558
7.079	1506.451	bdl	4.469	bdl	0.900	213.446
1.038	0.835	bdl	bdl	bdl	bdl	bdl
30.547	bdl	bdl	0.695	bdl	bdl	107.382
4.777	0.200	bdl	765.823	1.137	bdl	45.833
bdl	bdl	bdl	bdl	bdl	bdl	bdl
1.013	bdl	bdl	0.475	bdl	bdl	bdl
0.190	0.005	bdl	0.045	0.029	bdl	1.965
10.526	0.900	111.716	2281.366	4.075	4.586	640.899
0.099	bdl	bdl	2.874	bdl	bdl	30.402
0.603	18.561	bdl	bdl	bdl	bdl	2.329

B291152-1-4	B291152-1-5	B291152-1-6	B291152-1-7	B291152-2-1	B291152-2-2	B291152-2-3
B291152	B291152	B291152	B291152	B291152	B291152	B291152
py	py	gal	py	py	py	cpy
Assemblage 1	Assemblage 1	Assemblage 1	Assemblage 1	Assemblage 1	Assemblage 1	Assemblage 1
2451.470	56.240	26.343	0.985	341.283	0.721	bdl
-	-	176441.881	-	-	-	-
210.167	48.370	32.854	72.238	24.502	99.697	bdl
47.086	32.013	13.048	18.274	28.945	39.616	bdl
1516.818	4593.790	3728.001	8.234	1291.462	1.994	-
139.181	79.825	94.899	17.398	65.497	17.193	1911.199
0.371	0.460	bdl	0.238	0.130	bdl	26.080
0.958	1.186	bdl	1.048	0.867	1.436	1.776
4214.496	2801.175	569.123	8658.178	3151.322	772.870	12.148
87.907	11.907	3199.332	33.565	17.502	21.977	49.630
103.883	17.085	1172.433	19.918	46.533	0.713	247.044
0.495	0.734	10.177	1.049	0.277	bdl	7.059
bdl	bdl	0.665	bdl	bdl	bdl	bdl
1.694	17.642	212.105	0.254	1.200	0.174	1297.478
311.420	482.965	1151.911	126.679	195.957	0.284	1.600
bdl	bdl	bdl	bdl	bdl	bdl	bdl
1.442	0.734	0.103	0.417	0.373	bdl	0.527
14.602	55.403	186.873	1.018	109.517	bdl	0.077
578.778	302.251	-	3086.817	420.579	1.736	2.012
7.503	0.769	544.025	4.064	1.313	0.013	bdl
1.338	4.986	bdl	bdl	8.356	bdl	0.526

Q930238-1-2	Q930238-1-3	Q930238-1-4	Q930238-1-5	Q930238-2-1	Q930238-2-2	Q930238-2-3
Q930238	Q930238	Q930238	Q930238	Q930238	Q930238	Q930238
py	sph	cpy	sph	cpy	po	py
Assemblage 2	Assemblage 2	Assemblage 2	Assemblage 2	Assemblage 2	Assemblage 2	Assemblage 2
0.992	60.345	bdl	86.117	bdl	8.996	0.934
-	99599.976	-	35191.992	-	-	-
3305.256	751.970	6.916	37.245	5.032	166.518	805.395
20.559	bdl	bdl	bdl	bdl	bdl	bdl
549.194	511.393	-	45.862	-	1.542	19.363
12394.032	-	4132.051	-	1671.415	4.311	8.209
0.257	0.219	bdl	0.099	0.226	bdl	bdl
1.831	0.557	1.049	0.202	bdl	bdl	0.903
937.975	227.444	31.697	1.552	282.257	91.329	522.304
555.463	260.876	660.225	141.468	340.714	264.718	245.673
45.018	19.138	539.097	5.162	536.346	7.264	1.461
34.485	1517.289	14.782	1367.366	7.391	bdl	bdl
bdl	1.418	2.302	1.838	1.831	bdl	bdl
3.784	0.496	28.661	0.069	25.396	bdl	bdl
135.759	18.115	7.116	2.239	19.173	1.741	7.821
bdl	bdl	bdl	bdl	bdl	bdl	bdl
0.263	0.064	bdl	bdl	0.088	bdl	0.374
1.965	1.307	0.220	0.075	1.293	0.385	0.401
552.702	1060.854	7.174	1.398	101.240	1046.606	54.800
88.443	17.416	3.163	0.319	5.147	12.990	11.829
0.325	8.636	0.211	8.238	0.207	0.180	bdl

B291152-2-4	B291152-2-5	B291152-3-2	B291152-3-3	B291152-3-4	B291152-3-5	B291152-3-6
B291152	B291152	B291152	B291152	B291152	B291152	B291152
sph	po	py	po	cpy	py	sph
Assemblage 1	Assemblage 1	Assemblage 1	Assemblage 1	Assemblage 1	Assemblage 1	Assemblage 1
49.475	1.250	0.937	1.418	8.763	235.533	49.453
24625.236	-	-	-	-	-	23562.918
bdl	bdl	87.235	bdl	37.177	19.855	bdl
bdl	bdl	18.274	bdl	43.141	10.404	bdl
9.519	3380.336	bdl	890.155	-	1742.173	83.920
-	2926.901	12.076	196.082	3339.960	85.965	-
5.115	21.465	bdl	20.722	21.844	0.253	5.118
bdl	1.335	0.968	2.022	2.542	1.096	0.150
bdl	9.358	594.613	23.301	424.454	604.799	1.274
15.963	33.405	14.305	42.995	38.056	22.296	14.844
0.532	2747.309	bdl	14.166	253.636	15.625	2.901
942.126	10.940	bdl	1.956	11.363	0.420	907.971
0.305	bdl	bdl	bdl	bdl	bdl	0.298
0.304	88.915	bdl	719.784	861.721	15.101	1.281
0.145	2639.155	bdl	14.251	98.888	58.061	1.484
bdl	bdl	bdl	bdl	bdl	bdl	bdl
bdl	bdl	bdl	bdl	0.314	0.249	0.007
0.003	0.829	bdl	0.910	4.565	8.332	0.016
0.189	143.408	1.904	27.974	152.710	5594.855	1.071
bdl	0.260	0.088	0.065	0.960	3.939	bdl
9.289	bdl	bdl	0.164	0.387	0.211	8.898

Q930238-2-4	Q930238-2-5	Q930238-2-6	Q930238-3-1	Q930238-3-2	Q930238-3-3	Q930238-3-4
Q930238	Q930238	Q930238	Q930238	Q930238	Q930238	Q930238
aspy	aspy	aspy	po	py	cpy	sph
Assemblage 2	Assemblage 2	Assemblage 2	Assemblage 2	Assemblage 2	Assemblage 2	Assemblage 2
283.734	4.429	10149.842	bdl	163.782	87.259	29.670
-	-	-	-	-	-	125606.637
34098.526	69870.598	589.925	175.095	619.212	1478.584	15836.939
37.945	6.218	bdl	bdl	bdl	bdl	3.424
64686.701	bdl	119948.849	bdl	161.931	-	3423.297
289.194	5.389	156272.572	bdl	30.356	132225.623	-
bdl	0.362	bdl	bdl	bdl	bdl	bdl
1.153	0.817	1.019	1.182	0.927	bdl	0.506
-	-	913.291	27.152	222.646	665.807	133790.738
1053.793	848.113	162.513	384.063	28.313	611.239	1708.824
144.474	2.690	217.110	2.698	34.323	581.271	110.730
1.654	bdl	633.669	bdl	bdl	373.367	1513.676
bdl	0.320	bdl	bdl	bdl	2.433	2.027
26.530	bdl	18.255	bdl	0.141	37.876	1.541
373.049	114.293	28.486	1.857	25.179	85.652	71.255
bdl	bdl	bdl	bdl	bdl	bdl	bdl
11.630	0.031	0.338	bdl	0.600	0.282	bdl
6.771	0.355	1.820	0.422	1.110	4.153	5.453
1587.549	133.472	328.093	496.844	134.648	1092.857	11701.536
189.600	11.055	17.744	18.794	29.905	89.127	153.741
0.433	0.222	3.881	bdl	0.058	1.254	9.010

B291152-4-1	B291152-4-2
B291152	B291152
aspy	aspy
Assemblage 1	Assemblage 1
1970.789	14.420
-	-
105.189	61.466
76.165	22.809
92.743	1612.160
30.497	3008.772
0.297	1.337
0.873	0.968
-	15151.812
495.476	56.740
121.053	91.005
1.169	9.591
bdl	bdl
6.210	7.127
11018.474	216.411
bdl	bdl
17.146	0.377
11.381	3.651
81028.939	11639.871
66.903	8.504
0.285	0.174

Q930238-3-5
Q930238
py
Assemblage 2
bdl
-
69243.018
105.334
3.427
7.005
bdl
bdl
702493.671
1904.445
0.287
bdl
0.435
bdl
34.056
bdl
0.102
bdl
5.057
0.907
0.272